

**A COMPARISON OF LIQUIDS PRODUCED FROM COAL BY RAPID  
AND SLOW HEATING PYROLYSIS EXPERIMENTS<sup>1</sup>**

M. Rashid Khan  
Texaco Research Center, Texaco Inc.,  
P.O. Box 509, Beacon, NY 12508

M. A. Serio  
Advanced Fuel Research, Inc.  
87 Church Street  
East Hartford, CT 06108

R. Malhotra  
SRI International  
Menlo Park, CA

P. R. Solomon  
Advanced Fuel Research, Inc.  
87 Church Street  
East Hartford, CT 06108

It is well-known that the quality and yield of pyrolysis liquids depend strongly on the conditions at which coal is devolatilized. However, quantifications in pyrolysis yield and quality and the trade-off relations in them are not well-known and are currently being developed under the mild gasification program. In this study, selected Argonne coal samples were devolatilized in fixed-bed and entrained-flow reactors. The liquid products were characterized by a number of techniques including field ionization mass spectroscopy (FIMS), Fourier transform infrared spectroscopy (FTIR), elemental analysis and nuclear magnetic resonance spectroscopy (NMR). The quality and yield trade-off relationships as well as the characteristics of the liquids generated in the diverse processing conditions are presented.

## INTRODUCTION

Mild gasification is defined as the devolatilization of coal at relatively "mild" conditions of temperature and pressure aimed at producing a high-quality (as defined by relatively high H/C ratio) liquid product which can be used with little or no upgrading (1). One approach that has been taken is to allow the tars to undergo some secondary reactions while percolating through a packed bed (2). Relatively few studies have addressed in a systematic way how this process influences the composition and quality of tar produced, and we are aware of only a few previous studies (2-4) where a comparison has been made to rapid heating rate tars produced from the same coal.

---

<sup>1</sup> A portion of the work described in this study was performed at Morgantown Energy Technology Center.

In the present study, we compared tars which were produced at the US DOE in a slow heating, fixed bed system with those produced at Advanced Fuel Research, Inc. (AFR) in rapid heating, entrained flow reactor system. Tars produced from these coals by slow heating in vacuum in the inlet of the SRI Field Ionization Mass Spectrum (FIMS) provide an additional point for comparing the effect of reaction severity on the nature of the evolved tars. The tars were subsequently analyzed by a variety of techniques. The study was done on tar samples produced primarily from the Argonne Premium Coal Samples.

#### EXPERIMENTAL

**Tar Preparation** - Bulk samples of the Argonne coals were obtained from Karl Vorres and sieved to produce +200, 200X325 and -325 mesh size fractions. The -325 mesh size fraction was sent to METC and pyrolysis experiments were done in the Slow Heating Rate Organic Devolatilization Reactor (SHRODR) described previously (2,4). A thick bed (3.8 cm) of coal was heated at 12.5 °C/min to a final temperature of 650°C and held for 60 min. However, tar evolution from the reactor was essentially complete during non-isothermal heating and 5-10 min of the initial heat-treatment. The tars were taken off overhead using a water cooled condenser. The experiments were done without sweep gas. Samples of the 200 X 325 mesh size fraction of each coal were subjected to pyrolysis in AFR's entrained flow reactor system, described elsewhere (6). The experiments were done with a maximum reactor temperature of 700°C. The heating rate has been estimated to be 5000 - 10000°C/s while the time at final temperature is approximately 0.5 s (7). The entire effluent from the reactor system is collected in a polyethylene bag which is secured on a plexiglass manifold covered with aluminum foil. The tars form an aerosol and collect on the walls of the bag and the foil liner. The tars used in the present study were scraped from the foil liner.

**Tar Analysis** - The tars were analyzed by FT-IR at AFR using a KBr pellet method. A quantitative analysis technique has been developed at AFR using a Nicolet 7199 FT-IR. The techniques, which are described in previous publications (8,9) have been used to determine quantitative concentrations of the hydroxyl, aliphatic and aromatic hydrogen, and aliphatic and aromatic carbon for a wide number of coals, lignins, chars, tars, coal liquefaction products, oil shales, coal extracts and jet fuels. Qualitative information is also obtained concerning the types of ether linkages (oxygen linked to an aliphatic or aromatic carbon), carbonyl contents, the distribution of aromatic hydrogen (whether 1,2 or more adjacent hydrogens on a ring) and the forms of aliphatic hydrogen (methyl or methylene).

The tars were analyzed by Field Ionization Mass Spectrometry (FIMS) at SRI International. FIMS has proven to be an invaluable technique for the analysis of complex mixtures, particularly fossil fuels (9). The technique of field ionization consists of passing the vaporized material of interest through a very high electric field, typically about 1 MV/cm. Field ionization is unique in its ability to produce unfragmented molecular ions from almost all classes of compounds. The sample is vaporized by gradually heating the samples while continuously collecting mass spectral data. The pyrolysis tars studied evolved below 200°C (under vacuum) and presumably did not undergo any thermal reaction during FIMS analysis. If desired, the samples can be heated to temperatures as high as 500°C and the coals themselves were pyrolyzed in the inlet by heating them at 3°/min to 500°C. Mass analysis was performed by a medium resolution 60° magnetic sector analyzer, which has a maximum range up to 2000 daltons. The tars were also characterized by elemental analysis at METC and by NMR performed at the University of North Dakota Mineral and Energy

Research Laboratory. The NMR spectra were analyzed by a technique used by Clutter et al (12) to identify the key structural parameters of the tars.

## RESULTS AND DISCUSSION

**FIMS Analysis** - A summary of the FIMS results is given in Table 1. In general, the tars produced from the slow-heating fixed bed reactor has low average molecular weights and narrow molecular weight distributions. A comparison is made of FIMS spectra from the three experiments for three of the coals in Figs 1-3. The overall MW profiles of the tars formed by in-situ pyrolysis in the FIMS and the entrained-flow reactor are similar to each other. In both cases, the tars represent primary products of pyrolysis with little secondary reactions. Consistent with the lower N content of the SHRODR tars, FI-mass spectra of these liquids show a lower abundance of odd-mass peaks. In-situ pyrolysis tars appear to have relatively greater amounts of low molecular weight materials than the EFR tars. This difference is perhaps due to differences in the sampling efficiency. It is interesting to note that both SHRODR and FIMS tars are richer in simple phenols like cresols and catechols than the EFR tars which contained larger amounts of poly-phenols. In the case of in-situ FIMS of coals, these peaks evolved only at higher temperatures (>350°C) and represent thermal fragments from a large matrix. Again, differences in the methods for collecting tars in the various experiments may be partly responsible.

**FT-IR Analysis** - A comparison of the results from FT-IR analysis of the EFR and SHRODR tars is given in Table 2 (data provided in relative units). These analyses were done with the KBr pellet method. Because of the high volatility of the SHRODR liquids, the results on the fixed bed samples are not as reliable as for the EFR tars. The SHRODR liquids will be repeated using a liquid cell for verification. The FT-IR analysis of the tars from slow heating and rapid heating indicates that the former liquids were more aliphatic (less aromatic), lower in oxygen content, lower in heteroatom content, and the aromatic rings are less substituted. These indicators are consistent with the concept behind mild gasification, which stresses the fact that higher quality liquids can be produced from fixed-bed or moving-bed systems, although in lower yields (1,2).

**Elemental Analysis** - A comparison of the H/C (atomic) ratios of the pyrolysis liquids generated in the fixed-bed and entrained-flow reactors for several coals are shown in Fig. 4. The H/C (atomic) ratio of the parent coals are also shown in this figure. For all coals, the H/C of the fixed-bed liquids were significantly higher than the corresponding tar generated in the entrained-flow reactor(s). The Arkwright coal sample utilized in previous studies showed similar differences. The Arkwright (Pittsburgh seam) coal was also pyrolyzed at METC's entrained-flow reactor (also known as Advanced Gasification Facility, AGF; performed at 650 °C, nominal residence time 2 sec, 100 psig He). The H/C of the tar generated in the AGF is remarkably similar to that produced at BNL, as reported previously (4). Detailed elemental analyses are continuing.

**NMR Results** - A comparison of the NMR results (Fig. 5) obtained in two reactors demonstrate that the fixed-bed liquids are significantly less aromatic (as defined by carbon or proton aromaticity) than the tars generated in the entrained flow reactor. Furthermore, the fixed-bed reactor produces liquids with more mono- and di-aromatics while the tar formed in the entrained flow reactor are enriched in tri-aromatics and other larger molecules.

Results of this study confirm that rapid heating rate processes increase the yield of tar (Table 3) at the expense of tar quality (Fig. 1-4). Similar trade-off between tar yield and tar quality was reported by Khan (2,4) when comparing results from SHRODR experiments on Pittsburgh No. 8 coal with fluidized bed experiments by Tyler (10). A comparison was also made between the SHRODR tars and tars produced in an entrained flow reactor at Brookhaven National Lab (BNL) where differences similar to those found in the present study were reported (2).

The results of this study are consistent with the limited data reported by Peters and Bertling (3) who compared tars generated in a rapid- and slowly heated reactors. The tar yield in the fluid-bed was higher than the liquid generated in the fixed bed reactor. However, no elemental, NMR or FT-IR analyses of tars were provided. They proposed that in the slow heating process, the longer residence time of the tar leads to condensation and decomposition of the pitch to yield primarily coke, with some formation of light gases and light oils. Majumder et al (13), in contrast, attributed lower tar yield in a fixed bed reactor to the polymerization reactions alone and argued that "cracking" of tars is not significant. One can propose that the differences in the yield and composition of tar between the two experiments are a result of both cracking processes (which remove high molecular weight products as light oils), and repolymerization processes (which deliver high molecular weight products as coke). The relative importance of these two processes depends on the coal type, bed geometry, particle size, and heating rate in a complex way which is currently not well understood. Serio (11) investigated homogeneous cracking reactions of tars produced at low temperature and low residence time in a gas-swept fixed-bed reactor. The changes in the molecular weight distribution between the rapidly heated and slowly heated tars are consistent with a thermal cracking process which would produce primarily lower molecular weight material.

**ACKNOWLEDGEMENTS:** Funding for this work was provided by the US Dept of Energy, Morgantown Energy Technology Center. Comments by Dr. R. Johnson on this study are appreciated.

#### REFERENCES

1. Khan, M. R., and Kurata, T. "The Feasibility of Mild Gasification of Coal: Research Needs," DOE/METC-85/4019, DE85013625, 1985, pg. 80.
2. Khan, M. R. Fuel Sci. & Tech. Intl, 5 (2), pp 185-231. Also, Khan, M.R., Proc. of the Seventh Annual Gasification and Gas Stream Cleanup Systems Contractors review meeting, DOE/METC-87/6079, vol. 1, p. 170, (1987).
3. Peters, W., and Bertling, H., Fuel, 44, 317, (1965).
4. Khan, M.R., Proc. 1987 Int. Conf. on Coal Science, J.A. Moulijn et al., editors, Elsevier, Amsterdam, pp. 647-651.
5. Solomon, P.R., Hamblen, D.G., Carangelo, R.M., Krause, J.L., Ninetheenth Symposium (International) on Combustion; The Combustion Institute, Pittsburgh, PA, p. 1139, (1982).
6. Serio, M.A., Hamblen, D.G., Markham, J.R., Solomon, P.R., Energy Fuels, 1, 138, (1987).
7. Solomon, P.R., Coal Structure, Advances in Chemistry Series, 192, 95, (1981).
8. Solomon, P.R., Hamblen, D.G., and Carangelo, R.M., ACS Symposium Series, 205, Coal and Coal Products: Analytical Characterization Techniques, American Chemical Society, Washington, DC (1982), Pg. 77.
9. St. John, G.A., Buttrill, S.E., Jr., and Anbar, M., "Field Ionization and Field Desorption Mass Spectroscopy Applied to Coal Research", in Organic

- Chemistry of Coal, (Ed. J. Larsen), ACS Symposium Series, 71, 1978, p.223.
10. Tyler, R.J., Fuel, 50 (4), 218, (1980).
  11. Serio, M.A., Ph.D. Thesis, Dept. of Chemical Eng., Massachusetts Institute of Technology, Cambridge, MA, (1984).
  12. Clutter, D.R., Petrakis, L. Strenger, R.L., Jr., and Jensen, R.K., Anal. Chem., 44, 1395 (1972).
  13. Majumder et al, Fuel, 52, 11 (1973).

TABLE 1 - RESULTS FROM FIMS ANALYSIS OF TARS

COAL	SHRODR		IN-SITU FIMS		EPR	
	<u>Wt. Av. MW</u>	<u>MW Range</u>	<u>Wt. Av. MW</u>	<u>MW Range</u>	<u>Wt. Av. MW</u>	<u>MW Range</u>
Pocahontas	-	-	426	100 - 700	566	200 - 900
Upper Freeport	324	100 - 500	526	100 - 900	536	100 - 900
Pitts. No. 8	326	100 - 500	497	100 - 900	484	150 - 800
Lewiston-Stockton	-	-	546	100 - 900	478	150 - 750
Utah Blind Canyon	331	120 - 600	524	100 - 900	493	130 - 850
Wyodak	-	-	527	100 - 850	504	100 - 800

TABLE 2 - SOME RESULTS FROM FR-IR ANALYSIS OF TARS FROM THE TWO REACTORS

<u>COAL</u>	<u>SHRODR</u>			<u>EFR</u>		
	$H_{ar}/H_{tot}$	$H_{oh}$	C=O	$H_{ar}/H_{tot}$	$H_{oh}$	C=O
Pocahontas	.41	.27	(32.3)	.43	.13	6.7
Upper Freeport	.25	.18	8.6	.40	.23	9.3
Pitts. No. 8	.24	.18	5.7	.37	.29	9.1
Lewiston-Stockton	.23	.14	9.8	.37	.33	12.7
Utah Blind Canyon	.13	.19	5.7	.28	.32	13.0
Wyodak	.15	.19	14.5	.30	.35	20.3

TABLE 3 - COMPARISON OF TAR YIELDS FROM VARIOUS REACTORS

(Yield on dry-ash-free-basis)

<u>COAL</u>	<u>SHRODR</u>	<u>EFR</u>
Pocahontas	8	10
Upper Freeport	14	22
Pitts. No. 8	19	30
Lewiston-Stockton	13	17
Utah Blind Canyon	20	26
Wyodak	12	13

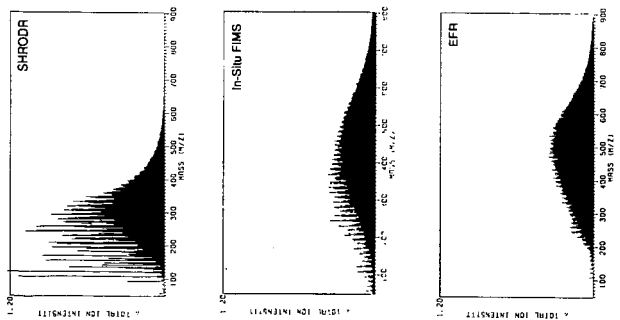


Fig. 1 - FIMS Spectra from  
Upper Freeport Coal

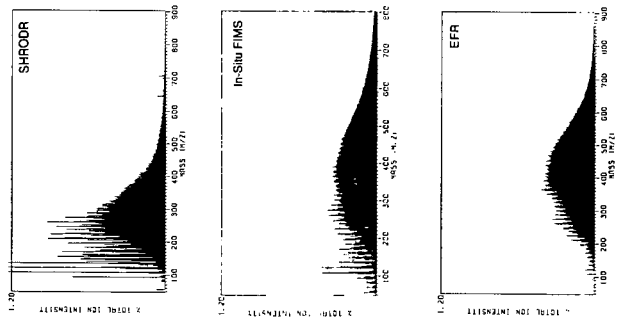


Fig. 2 - FIMS Spectra from  
Pittsburgh No. 8 Coal

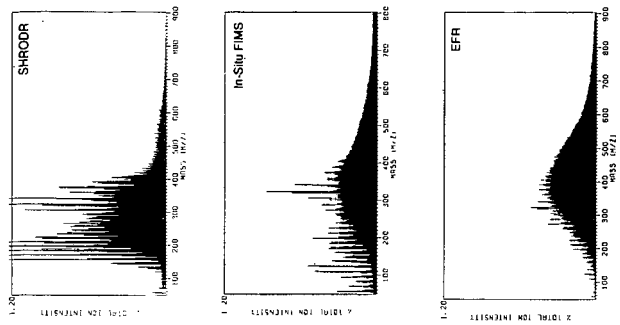
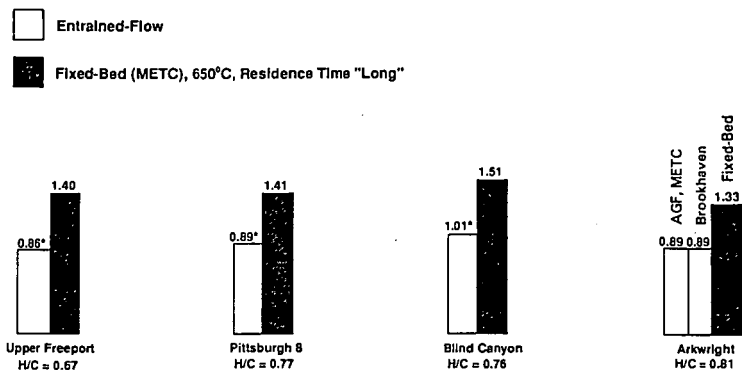


Fig. 3 - FIMS Spectra from  
Utah Blind Canyon Coal

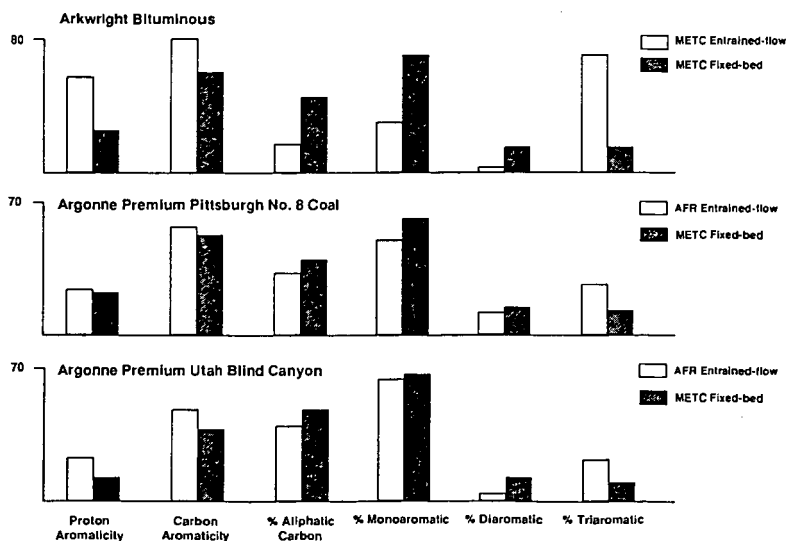
Fig. 4 - Comparison of H/C of Coal Pyrolysis Liquids Generated in Fixed-Bed and Entrained-Flow Reactors



\* Data from Entrained Flow Reactor Unit of Advanced Fuel Research

CB9-991-3 AA5

Fig. 5 - Influence of Processing Conditions on the characteristics of Pyrolysis Liquids (average structural properties)



CB9-0869-3 AA5



## Coal volatiles post pyrolysis in a two staged reactor

Laurent JULIEN and Radwan KHALIFEH

Laboratoire de Chimie Physique de la Combustion  
Université de Poitiers - UA 872 au CNRS  
F 86800 St Julien l'Ars - FRANCE

### INTRODUCTION

The aim of this paper is to present some new results about volatiles post pyrolysis of the low rank, french, Gardanne coal. Direct pyrolysis of this peculiar coal has been earlier described, with special consideration of light gases release (1)(2) and solid evolution (3)(4). Focusing now on volatiles transformation, we use a two staged reactor where volatiles, produced in the first stage, undergo post pyrolysis in the second stage. After a first study where second stage temperature was kept close to first stage temperature (5), one observation is enlarged here to a wider second stage temperature range.

Compared to other coal tar pyrolysis studies where products are collected at the end of experiments (6)(7)(8)(9), one experimental device is designed as to follow light gases flow rates during post pyrolysis experiments as a function of volatiles production temperature in first stage and of post pyrolysis temperature in second stage.

### EXPERIMENTAL

The Gardanne, or Provence, french coal studied here is a low rank one, from Upper Cretaceous, with following characteristics :

Prox. anal. (wt %) - Moisture : 9.6, Ash : 7.4, VM : 45.1

Ult. anal. (wt %, daf) - C : 74.9, H : 5.3, O : 11.3, N : 2.0, S : 5.4

The two staged reactor has been already described (2)(5). It is composed of two stainless steel cylindrical stages series connected and independently heated. Coal sample of 10 g were placed as a thin bed in middle of first stage, supported by carborundum particles deposited on the steel grid present at the bottom of each stage. Carborundum particles also filled second stage as to ensure thermal equilibrium. Coal particles were sized between 0.4 mm and 0.5 mm so that coal bed was formed, on an average, of four particles layers. Carrier gas was  $N_2$  which entered first stage with  $33 \text{ cm}^3\text{min}^{-1}$  flowrate. Gaseous effluent was cooled in two successive traps and, after partial condensation, introduced into GC for analysis.

For each experiment, once the reactor was filled and fitted as above described, second stage was heated up to the predetermined  $T_2$  value while  $N_2$  flowed across the whole reactor and first stage remained at ambient temperature. When the predetermined  $T_2$  value was

reached, it was held constant and first stage began to be heated at  $3^{\circ}\text{C min}^{-1}$  heating rate : temperature  $T_1$  of first stage was then measured at the same time that gases were introduced in GC.

## RESULTS AND DISCUSSION

### General features and results presentation

In one stage experiments, it was found that among the nine gases studied, four were largely predominant ( $\text{CO}$ ,  $\text{CO}_2$ ,  $\text{H}_2$ ,  $\text{CH}_4$ ) and five appeared as minor gases ( $\text{C}_2\text{H}_4$ ,  $\text{C}_2\text{H}_6$ ,  $\text{C}_3\text{H}_6$ ,  $\text{C}_3\text{H}_8$ ,  $\text{H}_2\text{S}$ ). For the last three gases, flow rate which was already very low in one stage experiments became lower in two stages experiments and rapidly undetectable with increasing  $T_2$  values. In sake of illustrating  $T_2$  influence upon gases flow rate, results are presented as flow rate v.s.  $T_2$  curves for  $\text{CH}_4$ ,  $\text{H}_2$ ,  $\text{CO}$ ,  $\text{CO}_2$ ,  $\text{C}_2\text{H}_4$  and  $\text{C}_2\text{H}_6$  (fig. 1 to 6) and as flow rate v.s.  $T_1$  curves for  $\text{C}_3\text{H}_6$ ,  $\text{C}_3\text{H}_8$  and  $\text{H}_2\text{S}$  (fig. 7 to 9).

When flow rates are plotted against second stage temperature for different  $T_1$  values, post pyrolysis of volatiles, main purpose of these experiments, is only concerned by  $T_2$  values higher than  $T_1$ . However results for  $T_2$  lower than  $T_1$  are also quoted : they show how volatiles cooling in second stage may influence gases flow rates, keeping in mind that this cooling always maintain volatiles above  $600^{\circ}\text{C}$ .

Increasing first stage temperature,  $T_1$  became equal to  $T_2$  and situation occurred where volatiles were kept in second stage at their production temperature in first stage. Compared to one stage experiments, two stages experiments lead thus to increase residence time of volatiles at their production temperature, giving indication upon residence time influence on gases flow rate.

Although main purpose of this study was volatiles post pyrolysis on an, as possible, inert solid, when second stage temperature exceeded  $700^{\circ}\text{C}$ , coke was found in second stage, deposited on carborundum particles and internal reactor walls. In conditions described in experimental part, and taking into account that apparatus was not conveniently suitable for quantitative solid recuperation, coke traces are observed at  $800^{\circ}\text{C}$  and averaged weights of 40 mg and 500 mg respectively measured at  $900^{\circ}\text{C}$  and  $1000^{\circ}\text{C}$ .

### Carbon dioxide

Before coke deposition,  $T_2$  rise has a positive effect on  $\text{CO}_2$  flow rate (fig. 1). With coke present in second stage, at  $T_2$  higher than  $800^{\circ}\text{C}$ , two different effects are observed according to first stage temperature range : the effect of  $T_2$  rise is positive for low values of  $T_1$  ( $500$  to  $600^{\circ}\text{C}$ ) and negative for higher  $T_1$  values. Cooling volatiles from  $700^{\circ}\text{C}$  and  $800^{\circ}\text{C}$  to lower temperatures decreases  $\text{CO}_2$  flow rate.

Volatiles are assumed to contain  $\text{CO}_2$  precursors which require for decomposition temperatures higher than their production temperature in first stage. Decomposition into  $\text{CO}_2$  is also enhanced by longer residence time, as we observed positive effect of residence time upon  $\text{CO}_2$  flow rate at  $700^\circ\text{C}$  and  $800^\circ\text{C}$ . These decomposition reactions appear to be reversed when cooling volatiles from  $700^\circ\text{C}$  and  $800^\circ\text{C}$  to lower temperature. Above  $800^\circ\text{C}$ ,  $T_2$  value,  $\text{CO}_2$  flow rate increase is related to reaction with deposited coke, this reaction being less complete when volatile are produced at low  $T_1$  ( $500^\circ\text{C}$  to  $600^\circ\text{C}$ ).

#### Carbon monoxide

In absence of coke, CO flow rate is little changed by post pyrolysis temperature rise. Compared to one stage experiments, two stages experiments lead to CO flow rate decrease of about 25 % for 600 to 800 common values of  $T_1$  and  $T_2$ . Inversely cooling volatiles from  $600^\circ\text{C}$  to  $700^\circ\text{C}$  increases CO flow rate (fig. 2). In presence of coke, CO flow rate increases with  $T_2$  rise, for all  $T_1$  values and this increase is more important the lower the volatiles production temperature  $T_1$ .

These results do not allow definitive conclusions about predominance of CO production or consumption reactions involatiles below  $800^\circ\text{C}$ : we may only conclude to existence of such reactions from decrease of CO flow rate for higher residence time and from CO increase when cooling volatiles. At higher temperature of second stage, when coke is deposited, CO flow rate increase is partly ascribed to reaction of  $\text{CO}_2$  with coke, what explains also  $\text{CO}_2$  flow rate decreases observed on figure 1. Other part of CO production increase is assumed to reaction between coke and water produced in primary pyrolysis and present in volatiles released below  $600^\circ\text{C}$ .

#### Hydrogen

Variations of  $\text{H}_2$  flow rate with second stage temperature seem qualitatively like CO ones, with  $\text{H}_2$  flow rate about twice CO one (fig. 3). Below  $800^\circ\text{C}$ , effect of  $T_2$  rise is weakly positive, effect of residence time is negative except for  $800^\circ\text{C}$  where it becomes unappreciable and cooling volatiles decreases  $\text{H}_2$  flow rate. Above  $800^\circ\text{C}$ ,  $T_2$  has positive effect upon  $\text{H}_2$  flow rate and this effect is more important when volatiles are produced below  $600^\circ\text{C}$  than when produced above  $600^\circ\text{C}$ .

In absence of coke,  $\text{H}_2$  flow rate variations result from competition between  $\text{H}_2$  producing and  $\text{H}_2$  consuming reactions which may be mainly hydrocarbons cracking, deshydrogenation and aromatisation of  $\text{H}_2$  production and hydrocracking for  $\text{H}_2$  consumption. From our observations, in this competition  $\text{H}_2$  producing reactions would be favoured by higher post pyrolysis temperature while  $\text{H}_2$  consuming ones would be promoted by longer residence time and lower temperature. In presence of coke (at the end of experiment), as for CO,  $\text{H}_2$  flow rate increase may be partly ascribed to water reaction with coke, forming simultaneously CO and

H<sub>2</sub>, when volatiles are produced below 600°C and contain thus quantity of water. For T<sub>1</sub> value above 600°C, volatiles do not contain more water and H<sub>2</sub> production is only related to aromatisation and cokefaction.

#### Methane

CH<sub>4</sub> flow rates are in the range of H<sub>2</sub> ones, but evolution with T<sub>2</sub> is quite different (fig. 4). Up to 650°C T<sub>1</sub> value, CH<sub>4</sub> flow rate show two maxima, for T<sub>2</sub> values of 700°C and 850°C, and a minimum between 750°C and 950°C. For T<sub>1</sub> higher than 650°C, CH<sub>4</sub> flow rate decreases when T<sub>2</sub> varies from 800°C to 1000°C. Cooling volatiles from 700°C and 800°C to lower temperature in second stage decreases CH<sub>4</sub> flow rate and residence time has positive effect upon this flow rate, of 60 % at 700°C and 480 % at 800°C.

CH<sub>4</sub> production in second stage is ascribed to cracking and hydrocracking reactions below 800°C T<sub>2</sub> value and to cokefaction above 800°C. Parallel to cracking and hydrocracking reactions, aromatisation occurs when T<sub>2</sub> rises above 700°C, decreasing thus CH<sub>4</sub> flow rate after the maximum shown at 700°C. Above 800°C, cokefaction occurs and releases CH<sub>4</sub>, what increases CH<sub>4</sub> flow rate till maximum at 950°C, above which temperature cokefaction does not release more CH<sub>4</sub>. CH<sub>4</sub> precursors chemical groups appear to be different for cracking reactions and cokefaction, as first maximum related to cracking reactions increases for higher T<sub>1</sub> values and second maximum, related to cokefaction, decreases for higher T<sub>1</sub> values.

#### C<sub>2</sub> hydrocarbons

C<sub>2</sub>H<sub>4</sub> flow rate evolution looks like CH<sub>4</sub> one when T<sub>2</sub> increases with two maxima, at 700°C and 950°C, for T<sub>1</sub> lower than 700°C and with a rapid decrease for T<sub>1</sub> higher than 700°C (fig. 5). Maximum at 700°C is assumed to result from competition between cracking and deshydrogenation reactions, predominant below 700°C, and aromatisation reactions which prevail above 700°C.

C<sub>2</sub>H<sub>6</sub> evolution is different from C<sub>2</sub>H<sub>4</sub> one, specially by shifting of maximum flow rate to higher T<sub>2</sub> values when T<sub>1</sub> increases (fig. 6). Assuming that C<sub>2</sub>H<sub>6</sub> decomposition reaction is the same, very probably deshydrogenation, for all T<sub>1</sub> values, maximum shifting is ascribed to difference in chemical nature of C<sub>2</sub>H<sub>6</sub> precursors when volatiles production temperature varies.

#### C<sub>3</sub> hydrocarbons and hydrogen sulfide

C<sub>3</sub> hydrocarbons and hydrogen sulfide rapidly disappear from volatiles when second stage temperature increases (fig. 7, 8, 9). For C<sub>3</sub> hydrocarbons, it is evident that disappearance is related to numerous consumption reactions like cracking, deshydrogenation and aromatisation. H<sub>2</sub>S is known to decompose in the temperature range of second stage operating.

## CONCLUSION

The above experiments of coal volatiles post pyrolysis in a two staged reactor give informations upon respective influence of pyrolysis and post pyrolysis temperatures on light gases production. Such two stages experiments allow to relate light gases production to volatiles composition and to distinguish between temperature ranges where solid coke is, or not, deposited. Results confirm influence of residence time upon post pyrolysis reactions and go further in details of peculiar effects. Slow cooling of volatiles, in temperature range where they remain reactive, modify gaseous flow rates, indicating thus volatiles evolution between reacting place and analysis inlet.

## REFERENCES

- 1- JULIEN L., BERTHO C., VANTELON J.P., GOUDEAU J.C., Proc. 1986 Int. Congress on Renewable Energy Sources, Madrid, 1986.
2. BERTHO C., Thesis, Poitiers, France, 1987.
3. TEKELY P., NICOLE D., DELPUECH J.J., JULIEN L., BERTHO C., Energy and Fuel, 1987, 1, 121.
4. JULIEN L., BERTHO C., TEKELY P., NICOLE D., DELPUECH J.J., Fuel Proc. Techn. 1988, 20, 349.
5. JULIEN L., BERTHO C., Fuel, Submitted for publication 1989.
6. CYPRES R., ACS Fuel Chem. Div. Preprints, 1981, 26-44.
7. CYPRES R., Royal Soc. of Chemistry, Autumn meeting, Leeds UK, 1981.
8. SERIO MA, PETERS WA, SAWADA K., HOWARD J.B., Proc. Int. Conf. on Coal Sc., Pittsburgh, USA, 1983, 533.
9. SERIO MA, PETERS WA, SAWADA K., HOWARD J.B., A.C.S. Fuel Chem. Div. Preprint 1984, 29, 65.

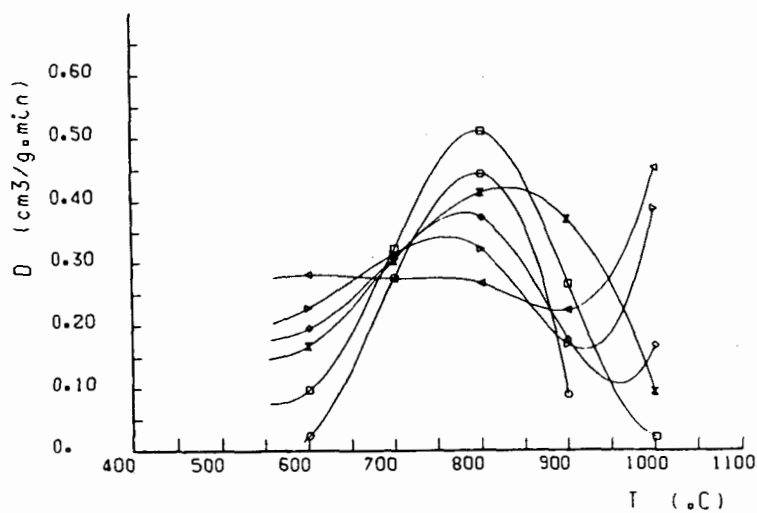


FIG 1 CO<sub>2</sub> FLOW RATE VS SECOND STAGE TEMPERATURE  
FIRST STAGE TEMPERATURE:  
◄ 500°C, ▤ 550°C, ○ 600°C, X 650°C, □ 700°C, ○ 800°C

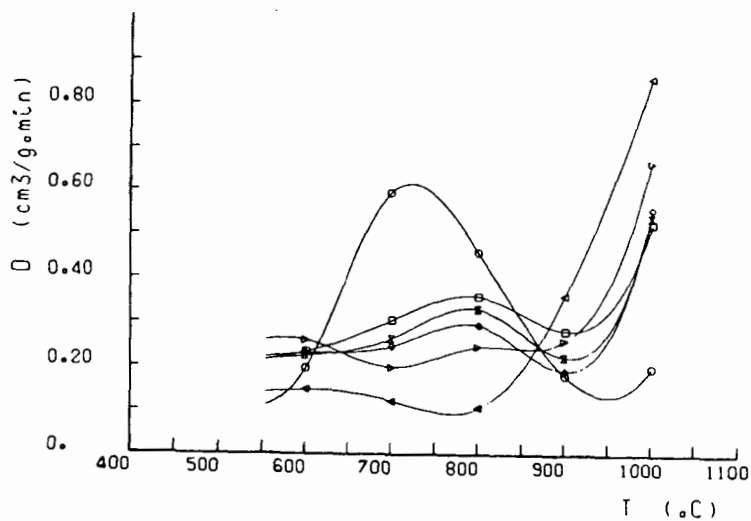


FIG 2. CO FLOW RATE VS SECOND STAGE TEMPERATURE  
FIRST STAGE TEMPERATURE:  
◄ 500°C, ▤ 550°C, ○ 600°C, X 650°C, □ 700°C, ○ 800°C

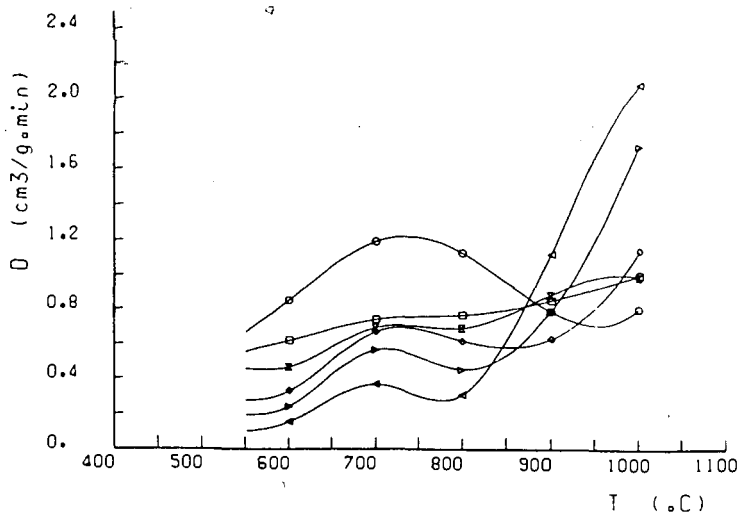


FIG 3 H<sub>2</sub> FLOW RATE VS SECOND STAGE TEMPERATURE  
FIRST STAGE TEMPERATURE:  
◄ 500°C, ▹ 550°C, ○ 600°C, ⋈ 650°C, □ 700°C, ○ 800°C

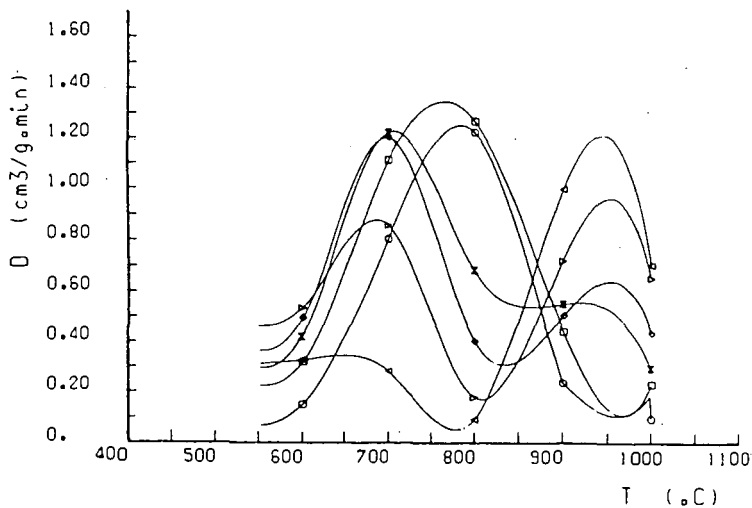


FIG 4 CH<sub>4</sub> FLOW RATE VS SECOND STAGE TEMPERATURE  
FIRST STAGE TEMPERATURE:  
◄ 500°C, ▹ 550°C, ○ 600°C, ⋈ 650°C, □ 700°C, ○ 800°C

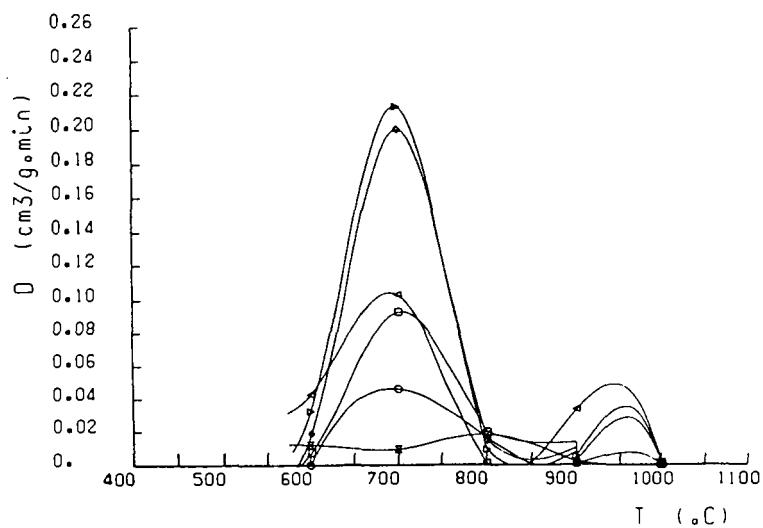


FIG 5  $C_2H_4$  FLOW RATE VS SECOND STAGE TEMPERATURE  
FIRST STAGE TEMPERATURE :  
◻ 500°C, ▴ 550°C, ◊ 600°C, ⋈ 650°C, □ 700°C, ○ 800°C

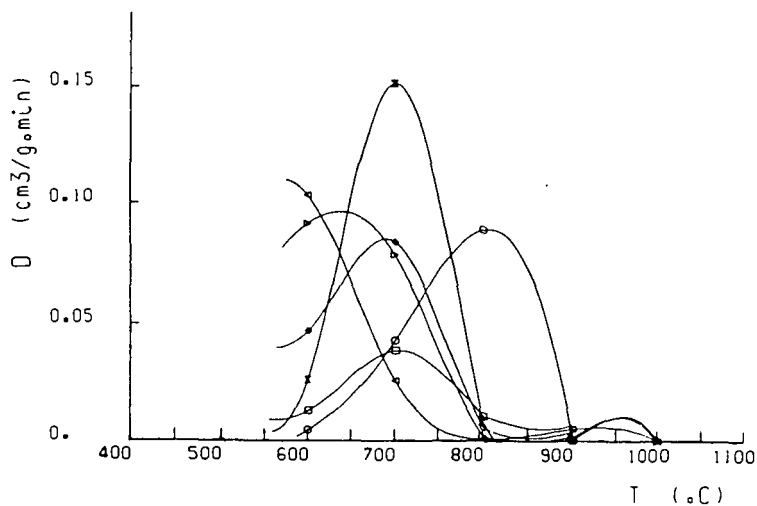


FIG 6  $C_2H_6$  FLOW RATE VS SECOND STAGE TEMPERATURE  
FIRST STAGE TEMPERATURE :  
◻ 500°C, ▴ 550°C, ◊ 600°C, ⋈ 650°C, □ 700°C, ○ 800°C



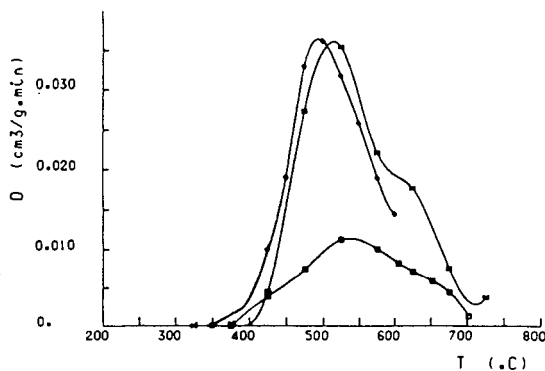


FIG 7 C<sub>3</sub>H<sub>6</sub> FLOW RATE VS FIRST STAGE TEMPERATURE  
SECOND STAGE TEMPERATURE  
○ 600°C, □ 700°C, ONE STAGE IN-4

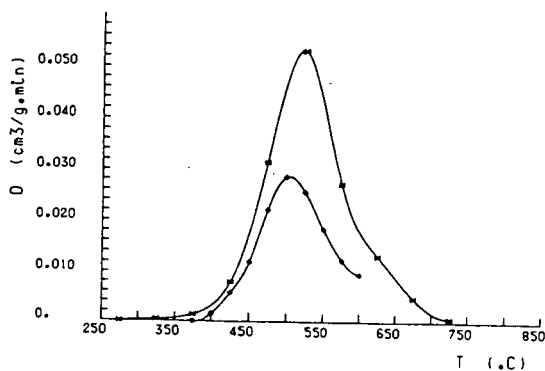


FIG 8 C<sub>3</sub>H<sub>6</sub> FLOW RATE VS FIRST STAGE TEMPERATURE  
SECOND STAGE TEMPERATURE  
○ 600°C, □ 700°C, ONE STAGE IN-4

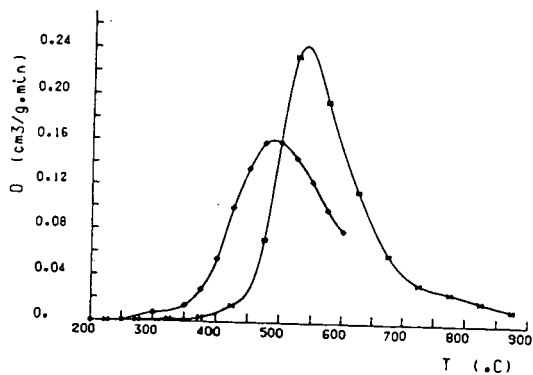


FIG 9 H<sub>2</sub> FLOW RATE VS FIRST STAGE TEMPERATURE  
SECOND STAGE TEMPERATURE  
○ 600°C, □ 700°C, ONE STAGE IN-4

## A NOVEL METHOD FOR FLASH PYROLYSIS OF COAL

Kouichi Miura, Kazuhiro Mae, Tomonori Yoshimura  
and Kenji Hashimoto\*

Research Laboratory of Carbonaceous Resources  
Conversion Technology,

\*Department of Chemical Engineering, Kyoto University  
Kyoto 606, Japan

### Introduction

Flash pyrolysis of coal is a promising process for producing chemicals such as benzene, toluene and xylene (BTX). But, the yield of liquid products including BTX (tar) is limited because of low hydrogen to carbon ratio in coal. It is necessary to supply hydrogen to coal efficiently for increasing the tar yield. Hydropyrolysis is one of the means to supply hydrogen to coal. This is, however, realized under only severe reaction conditions: high hydrogen pressure, high temperature and long residence time.

Recently, several attempts have been made to supply atomic hydrogen or radicals from super critical steam<sup>1,2)</sup> or solvents<sup>3)</sup> to coal. This paper presents a new efficient method for increasing both the conversion and the tar yield in which the coal swollen by solvents was pyrolyzed in a flash mode in an inert and a hydrogen atmospheres. We will show drastic increase of coal conversion and tar yield are brought about by a physical effect and effective hydrogen transfer from/via tetralin.

### Experimental

#### Sample Preparation

A Japanese coal, Taiheiyo coal, was used as a raw coal. Its properties are given in Table 1. The coal was ground and the particles less than 74  $\mu\text{m}$  were used. The coal was dried in vacuo at 110 °C for 1 h before use.

The coal particles were mixed with tetralin by the ratio of 10 to 6 by weight, then heated to the temperatures between 25 and 350 °C under the 1 MPa of nitrogen. By this treatment coal particles were swollen, and tetralin was retained in the coal matrix. This sample is abbreviated to tetralin treated coal (TTC).

The tetralin treated coal was degassed at 70 °C in vacuo for 1 h to completely remove the retained tetralin (vacuum dried coal; VDC). When the swelling is irreversible, swollen but tetralin free coal is obtained. This sample was pyrolyzed to examine the physical effect of swelling on the pyrolysis. Several partially degassed samples were also prepared to examine the effect of the amount of tetralin retained on the pyrolysis.

Char produced under a high temperature pyrolysis of Taiheiyo coal, this is not pyrolyzed further, was also treated by tetralin in the same manner as was employed to prepare TTC. This sample was pyrolyzed

to obtain the yield of each component from tetralin. This result was utilized to estimate the contribution of pyrolysis of tetralin on the product yields from TTC. Thus, four kind of samples were prepared from the Taiheiyo coal.

#### Flash pyrolysis of samples

Samples prepared above were pyrolyzed in an inert and high-pressure hydrogen atmospheres. Pyrolysis in the inert gas of atmospheric pressure was performed using a Curie-point pyrolyzer (Japan Analytical Ind., JHP-2S). About 2 mg of sample were wrapped in a ferromagnetic foil, and heated up to a temperature between 650 to 920 °C at the rate of 3000 °C/s by induction heating coil to be pyrolyzed rapidly. The products were immediately cooled down by the inert gas of high flow rate. Then, the tar was trapped completely by the silica wool placed just below the foil. The inorganic gases and hydrocarbon gases were led to gas chromatograph and analyzed. On the other hand, the pyrolysis under high pressure was performed using a specially designed Curie-point pyrolyzer. This reactor consisted of high pressure vessel and a quartz reactor as shown in Fig. 1. This was designed to keep the inner and outer pressure of the reactor same. About 5 mg of sample were pyrolyzed at 764 °C under 0.1 to 7.5 MPa of hydrogen. Produced tar was again trapped by the silica wool, but producted gases were collected in a gas holder once. Then a part of gas was introduced to a gas chromatograph to be analyzed. The column used was Porapak Q. The yields of char and tar were measured from the weight changes of the foil and the reactor. The same experiment was performed several times to check the reproducibility of experiment.

#### Analysis of structure change of coal by swelling

The swelling ratio, elemental composition, the pore volume and the surface area were measured to examine the change of coal structure by swelling. The swelling ratio of tetralin-treated coal was measured by volumetric method<sup>6,7</sup>. The pore volume and surface area of raw coal and TTC were calculated from the adsorption isotherm of CO<sub>2</sub> measured at 0 °C. Furthermore, to estimate the interaction between coal surface and tetralin, the thermal desorption curve of tetralin from the TTC was measured under the heating rate of 5 °C/min using a thermobalance (Shimadzu Co. Ltd., TGA 50).

### RESULTS AND DISCUSSION

#### Effect of pretreatment temperature on product distribution

Figure 2 shows the change of swelling ratio of TTC and VDC against swelling temperature. Taiheiyo coal began to swell by tetralin at 70 °C, and the swelling ratio reached 1.34 at above 170 °C. Taiheiyo coal swollen at below 100 °C shrank reversibly to its original state by vacuum drying, but the coal swollen at above 100 °C did not shrink completely, and the swelling at 250 °C was almost irreversible. At 250 °C, the coal structure was expected to change as mentioned in earlier works<sup>6,7</sup>. The micropore volume and the internal surface area of VDC of coal swollen at 250 °C were larger than those of raw coal

as shown in Table 2.

Figure 3 shows the curves of the thermal desorption of tetralin from TTC. Since tetralin desorbs at higher temperatures from the coal treated above 100 °C as compared with that treated at 25 °C, the interaction between coal and tetralin is stronger for the coals treated above 100 °C. Coals treated by tetralin at several temperatures were pyrolyzed at 764 °C under 0.1 MPa of He. The product yield of each component of treated coal,  $Y_i$ , was represented based on daf coal excluding the yield from the pyrolysis of tetralin. The yield,  $Y_i$ , is defined by

$$Y_i = \{(\text{Yield from TTC}) - w(\text{Yield from solvent})\} / (1 - w) \quad (1)$$

where  $w$  is the weight fraction of tetralin in TTC.

Figure 4 shows the tar yield against the swelling temperature. The tar yield was same as that of raw coal at the swelling temperature of 25 °C, but it reached about 1.5 times larger than that of raw coal at 100 to 250 °C. This result and Figure 3 show only the tetralin retained strongly by coal is effective to increase the tar yield.

The tar yield decreased at the swelling temperature of 350 °C, because the coal was almost decomposed during the treatment at this temperature. From above results, the swelling temperature was decided to be 250 °C.

#### Effect of the amount of tetralin in the coal

The effect of the amount of tetralin retained in the coal on the tar yield was examined at the pyrolysis temperature of 764 °C. The amount of tetralin was varied by changing the vacuum drying time of TTC prepared at 250 °C. Figure 5 shows the tar yield during the flash pyrolysis against the amount of tetralin retained in the coal. The sample of zero tetralin content was completely dried one (VDC). Even a trace of tetralin was not detected in this sample, judging from the mass balance during the vacuum drying and the FTIR measurements. Since the VDC is still swollen by 30 %, this coal has much larger pore volume than the raw coal. The tar yield of the VDC was about 4 wt.% larger than that of raw coal. This means that the pore enlargement by swelling increases the tar yield. This is just a physical effect. On the other hand, the gradual increase of the tar yield with the increase of tetralin content is the chemical effect produced by tetralin. These are discussed in more detail in relation to the yields of the other products in the next section. The tar yield of the coal treated at 25 °C is almost same as that of raw coal as stated earlier.

#### Flash Pyrolysis in an Inert Atmosphere

Figure 6 shows the char yields of TTC, VDC and raw coal against the pyrolysis temperature. The char yield of TTC is lower than that of raw coal at all the temperature by 4 to 10 wt.%. The char yield of VDC is also 4wt.% lower than that of raw coal. These results show the swelling of coal by tetralin is effective to increase the conversion

of coal into gas and liquid. This effect was brought about from the pore enlargement and the tetralin retained strongly in the coal as stated earlier.

Figure 7 shows the tar yield. The tar yield of TTC increased drastically up to 30 wt.% daf at the pyrolysis temperature of 764 °C, which was 1.5 times larger than that of raw coal. This indicates the effectiveness of the proposed method for increasing the liquid product. The tar yield of TTC at 920 °C, however, was almost equal to that of raw coal. The trend of tar yield of TTC with the temperature is similar to that of the H<sub>2</sub> yield from the pyrolysis of tetralin. On the other hand, the tar yield of vacuum dried coal increased by 4 wt.% irrespective of pyrolysis temperature, as compared with that of raw coal. Figures 8 and 9 show the yields of other products. The inorganic gas (IOG) yield was nearly equal between three samples. The hydrocarbon gas (HCG) yield and the total yields of benzene, toluene and xylene (BTX) were nearly equal at the temperatures lower than 764 °C. These yields of TTC at 920 °C, however, were larger than those of the other two samples. The H<sub>2</sub> yield of TTC was smaller than that of raw coal at temperatures lower than 800 °C, but exceeded that of raw coal at 920 °C. The H<sub>2</sub> yield of VDC was almost same as that of raw coal at all temperatures.

The physical effect and the effect of hydrogen donability of tetralin are summarized from above results as follows: The increase of micropore caused by tetralin pretreatment facilitated the escape of the tar vapor, which would be stabilized as char, from coal particles. Then the tar yield of VDC was increased at all the temperatures. On the other hand, the effect of hydrogen donability from the tetralin to coal depends on the pyrolysis temperature.

The conversion of coal to volatile matter is expected to increase when hydrogen atom is supplied timely to the reactive fragments of coal which would be stabilized as char without hydrogen supply. At both 670 and 764 °C, the char yield of TTC was smaller than that of VDC. So, hydrogen atom was effectively transferred from tetralin to the coal fragments at these temperatures. This is substantiated by the small H<sub>2</sub> yield and large tar yield of TTC at these temperatures. This indicates that the rates of the dehydrogenation of tetralin and the formation of coal fragments matched well at these temperatures. Then the mechanism of the pyrolysis of TTC is schematically represented as given in Fig. 10.

On the other hand, the char yield of TTC was almost same as that of VDC at 920 °C. So, tetralin did not contribute to increase the conversion of coal at this temperature, but contributed to increase the yields of light hydrocarbons as shown in Fig. 8. This was supposed to be brought about by the radicals produced by the decomposition reaction of tetralin, which was prevailing over the hydrogenation reaction at this temperature. The radicals were very reactive, and decomposed primary pyrolysis products of coal, though the reaction mechanism is not clear now.

#### Pyrolysis in hydrogen atmospheres

It has been reported that the yield of volatile matter during flash pyrolysis decreases with increasing hydrogen pressure<sup>8-10</sup>. This is said to be because the escape of tar vapor from coal particles is suppressed under pressurized conditions. The flash hydrolypyrolysis of TTC, however, is, as it were, liquefaction within the pore space. Therefore, the increase of tar yield is expected under pressurized hydrogen.

Figure 11 shows the hydrogen pressure dependency of the char yields of TTC, VDC and raw coal at the pyrolysis temperature of 764 °C. The char yield of VDC was smaller than that of raw coal by 2 to 4 wt.%. This was considered to be brought about by the pore enlargement. The char yield of TTC was smaller than that of VDC and tended to decrease with increasing hydrogen pressure. This means that the tetralin treatment is more effective for the pyrolysis in high pressure hydrogen. This is because molecular hydrogen is expected to be transferred to the reactive coal fragments via tetralin as is transferred in coal liquefaction. The char yields of both VDC and raw coal did not decrease with increasing hydrogen pressure contrary to previous works<sup>8-10</sup>. We examined the effect of hydrogen flow rate on the char yield, and found that the char yield increases significantly with increasing pressure under low hydrogen flow rate as reported previously. The increase of char yield was suppressed with increasing hydrogen flow rate. So, our experiments were all performed under high hydrogen flow rate. This is the reason that our char yield did not decrease with increasing hydrogen pressure.

Figure 12 shows the tar yields corresponding to Fig. 11. The tar yield of TTC increased with the increase of hydrogen pressure, and reached up to 38 wt.% at 5 MPa, which was 1.8 times larger than that of raw coal. This clearly shows that proposed method is effective for increasing the tar yield as well as the coal conversion, especially in high pressure hydrogen atmospheres. Both tar yields of VDC and raw coal decreased with increasing hydrogen pressure. This was due to the decomposition of tar to lighter hydrocarbons under high hydrogen pressure.

#### CONCLUSION

A novel flash pyrolysis method of coal was developed for drastically increasing the tar yield, in which the coal swollen by solvents was pyrolyzed in a flash mode. The tar yield was increased by the factor of 1.5 for the flash pyrolysis, and by the factor of 1.8 for the flash hydrolypyrolysis. The increase of tar yield is brought about by the pore enlargement caused by swelling and by the effective hydrogen transfer from/via tetralin.

#### ACKNOWLEDGMENT

This work was performed in the framework of the "Priority-Area Research" and "Japan-Canada Joint Academic Research Program" which was sponsored by the Ministry of Education, Culture and Science of Japan.

# REFERENCES

1. Graff, R.A. and Brandes, S.D., Energy & Fuels, 1, 84(1987)
2. Khan, M.R., Chen, W.Y. and Suuberg, E., Energy & Fuels, 3, 223(1989)
3. Hutteringer, K.J. and Sperling, R.E., Proc. 1987 International Conference on Coal Science, Oct.(Mauustrich) p.699
4. Nelson, J.R., Mahajan, O.P. and Walker, P.L., Fuel, 59, 831(1980)
5. Green, T.K., Kovac, J. and Larsen, J.W., Fuel, 63, 935(1984)
6. Medeiros, D. and Peterson, E.E., Fuel, 58, 531(1979)
7. Brenner, D., Fuel, 62, 1347(1983)
8. Anthony, D.B., Howard, J.B., Hottel, H.C. and Meissner, H.P., Fuel, 55, 121(1976)
9. Gavaras, G.R., Coal Pyrolysis, Coal Science and Technology 4 Elsevier, New York, 1982
10. Wantzl, W., Fuel Processing Technology, 20, 317(1988)

Table 1 Properties of Coal

	Proximate Analysis (wt%)			Elemental Analysis (wt% daf)			
	FC	VM	ASH	C	H	N	S+O
Raw coal	43.2	45.8	11.0	74.5	6.0	1.3	18.20
Treated coal	-	-	11.0	72.7	5.9	1.5	19.90

Table 2 Change of Pore Volume and Surface Area during Swelling

Coal	Solvent	Temp. (°C)	Pore Volume (cc/g)	Surface Area (m <sup>2</sup> /g)
Taiheiyō	Raw	-	0.039	108.2
	Tetralin	100	0.039	102.4
		170	0.040	102.5
		250	0.061	152.9

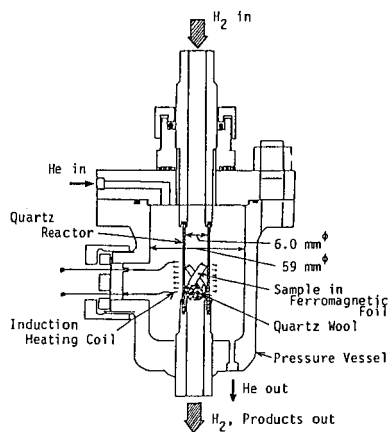


Fig.1 Schematic of a high pressure Curie-point pyrolyzer

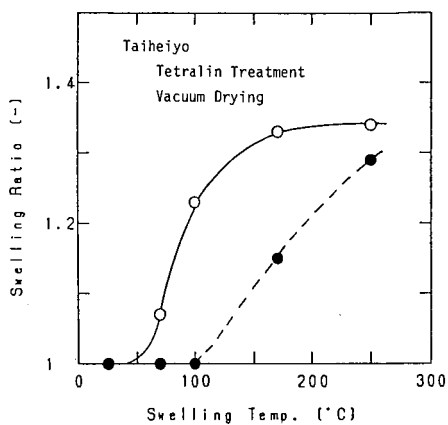


Fig.2 Change of the swelling ratio of tetralin treated coal and vacuum dried coal with the pretreatment temperature

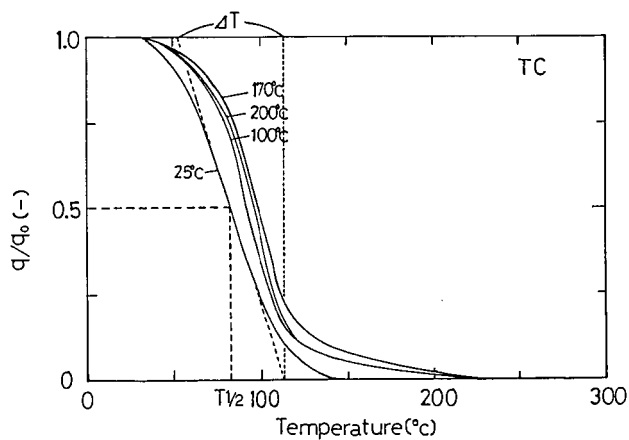


Fig.3 Thermal desorption curves of tetralin from the coal treated with tetralin at different temperatures



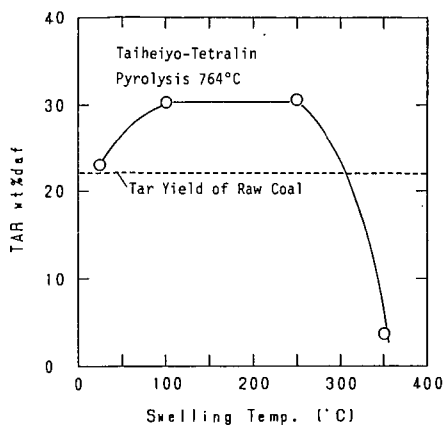


Fig.4 Effect of the pretreatment temperature on the tar yield during the pyrolysis of tetralin treated coal

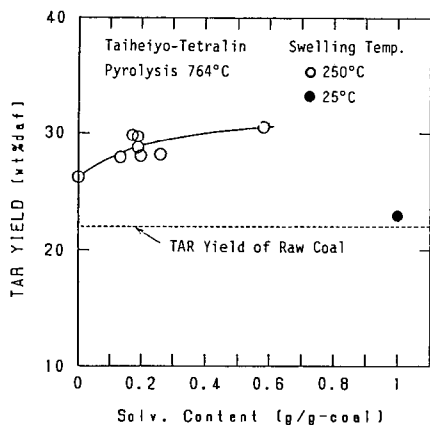


Fig.5 Effect of the amount of solvent remaining in the coal on the tar yield

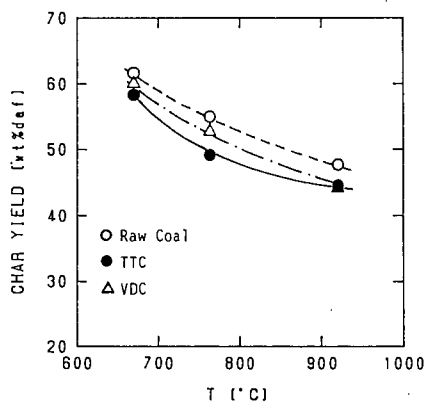


Fig.6 Effect of the pyrolysis temperature on the char yield during the pyrolysis for coal, tetralin treated coal and vacuum dried coal

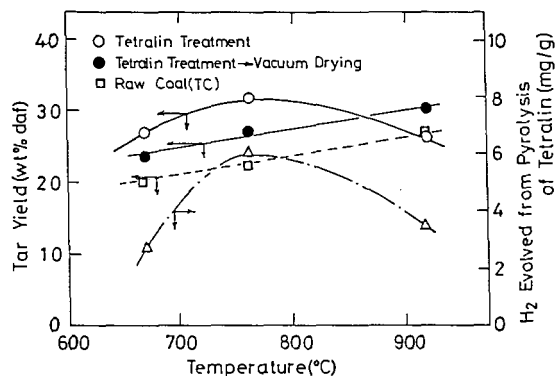


Fig.7 Effect of the pyrolysis temperature on the tar yield during the pyrolysis for coal, tetralin treated coal and vacuum dried coal

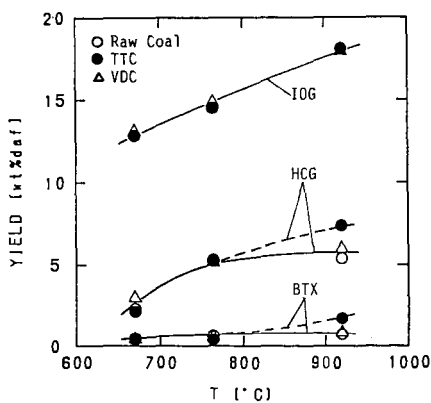


Fig.8 Effect of the pyrolysis temperature on the IOG, HCG and BTX yields during the pyrolysis for coal, tetralin treated coal and vacuum dried coal

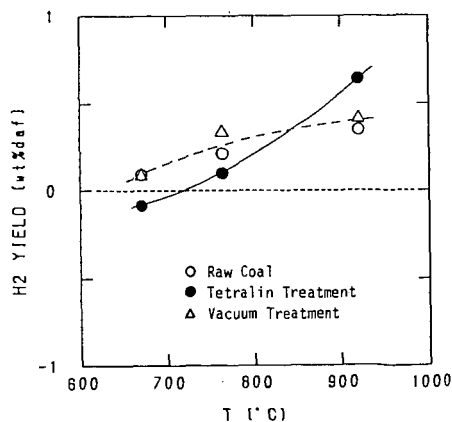


Fig.9 Effect of the pyrolysis temperature on the H<sub>2</sub> yield during the pyrolysis for coal, tetralin treated coal and vacuum dried coal

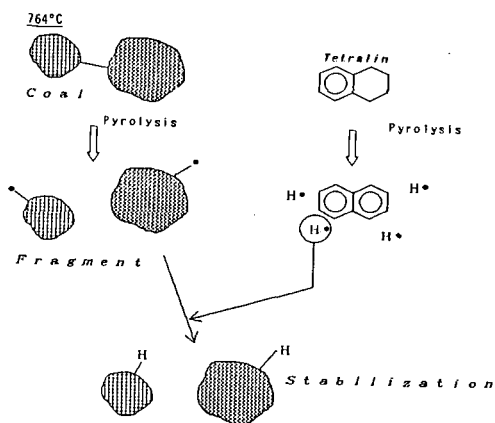


Fig.10 Presumed mechanism of pyrolysis of tetralin treated coal at temperatures lower than 764 °C

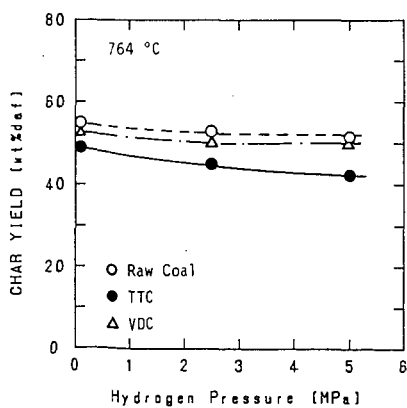


Fig.11 Change of the char yield during the pyrolysis with increasing hydrogen pressure

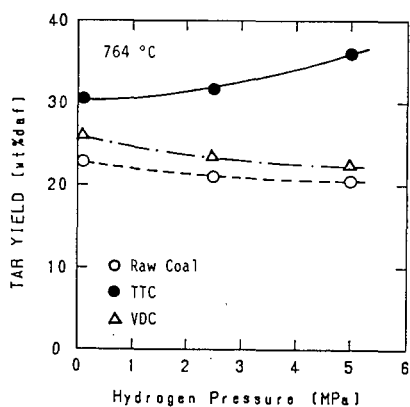


Fig.12 Change of the tar yield during the pyrolysis with increasing hydrogen pressure

THE ANALYSIS OF VOLATILE COMPONENTS FROM  
PYROLYZED GASIFIER CARBON-RICH SOLID SAMPLES

Vincent P. Nero and Mitri S. Najjar

Texaco Inc.  
Beacon, New York, 12508

ABSTRACT

Samples of carbon-rich solid products, taken during the processing of coal in a Texaco Coal Gasifier, have been analyzed by flash-pyrolysis using the electrically-heated grid technique. Gas chromatography and mass spectrometry data were obtained on the composition of the gases and tars evolved.

SAMPLE PREPARATION

The coal gasifier solid products, consisting approximately of 51.2% carbonaceous material, 47.1% ash, and 1.7% water by weight, were pyrolyzed using a heated grid apparatus, which was similar to a procedure used by other workers.(1,2) The pyrolyzer consisted basically of two layers of wire mesh mounted between two electrodes, with a thin uniform layer of gasifier solid sample weighing about 50 mg placed between the two wire mesh screens. The sample was heated under vacuum for six seconds to a peak temperature of 1350°C. The heating rate was estimated to be in the order to 2000°C/s. The reaction products, consisting of gases, tars, and char were collected.

The gases were analyzed on-line by gas chromatography. The gases consisted of 0.5% hydrogen, 1.8% methane, 1.7% water, 0.2% ethylene, 1.0% carbon monoxide, 0.6% ethane, 0.3% propylene, 0.9% carbon dioxide, and 0.7% other olefins based upon the weight relative to the initial sample.

The tars, materials collected on filter paper at the reactor exit or condensed on other reactor surfaces at room temperature, were analyzed by mass spectrometry.

ANALYSIS OF TARS BY MASS SPECTROMETRY

The tar samples were analyzed by both direct insertion probe and direct exposure probe mass spectrometry, using a VG Analytical 7070HS instrument. The mass spectrometer was operated under the following electron impact conditions: 200 uA trap current, 70 eV electron energy, 4 kV accelerating voltage, 1200 resolution (10% valley), and a 250°C source temperature. Masses were magnetically scanned from 20 to 800 daltons, and subsequently from 25 to 300 daltons every four seconds.

For the direct insertion probe analysis, a 100 ug sample of tar was fractionally sublimed from a shallow (4 mm) quartz cup which was attached to the probe and positioned in the source just short of the electron beam. The probe temperature was controlled by both a water cooling line and an electrical heating element. The sample was initially heated from 20°C to 50°C in the first minute, and then increased by 50°C every 30 seconds, to a final temperature of 450°C for five minutes.

During the direct exposure probe analysis, the tar was dissolved in methylene chloride and then deposited onto a platinum emitter filament. After the evaporation of the solvent, the direct exposure probe was positioned in the source so that the sample was in actual contact with the electron beam. A current was ramped from 0 to 1.2 A in 50 seconds to flash vaporize the sample.

#### MASS SPECTROMETRY RESULTS

Approximately 75% of the tar sublimed from the quartz direct insertion probe cup into the mass spectrometer source. This was determined by weighing the probe cup after the analysis. Although the initial mass scanning range was from 25 to 800 daltons, few ions were observed above a mass of 250 daltons, even at the higher probe temperatures. The upper mass limit was then reduced to 300 daltons.

When using the second introduction technique, the emitter coil on the direct exposure probe was burnt clean. Although this technique generally allows better detection for high molecular weight molecules, again only an upper mass range of approximately 250 daltons was observed.(3)

A total ion chromatogram for a tar sublimation reveals that the tar was composed of a fairly uniform distribution of materials over the entire temperature range. (Figure 1) Each time the temperature was incremented by 50°C, there was a corresponding increase in total ion intensity which would then fall off after about 15 seconds. This periodic tendency continued even at the highest probe temperature of 450°C. There was still about 15% of the tar remaining after about five minutes at this temperature, although the ion intensity dropped off to only a few percent of this maximum level.

The mass spectra indicate mainly the presence of relatively simple hydrocarbons. The most prominent types of hydrocarbons observed were alkenes, dienes and some alkylated phenols. No substituted cycloalkanes, benzenes, polynuclear aromatics, or common biomarkers such as dicyclic terpanes, were observed. The major fragmentation series at 27, 41, 55, 69, 83, 97, and 111, having the empirical formula  $C_nH_{n-1}$ , and the relative abundance of these peaks, represents the strong presence of alkenes. The fragmentation series 67, 81, 95, 109, 123, 137, 151, and 165,

having the empirical formula  $C_nH_{2n-3}$ , and the relative abundance of these peaks, represents the presence of dienes. Alkenes and dienes were prominent throughout the entire chromatogram, especially being dominant below 150°C. (Figure 2) The alkylated phenol fragmentation was represented in the 135, 149, and 163 series. The alkylphenols were most intense at about 250°C. (Figure 3) Peaks representing paraffinic molecules, having an empirical formula  $C_nH_{2n+1}$ , end very quickly at about 85 daltons indicating that this series probably only represents the alkylated regions in the parent molecules.

#### CONCLUSION

Overall the mass spectra indicate that the tars generally contained only relatively light alkenes, dienes, and alkylphenols. These components are somewhat less complex than materials typically associated with coal pyrolysis.(4) This simpler distribution is actually the result of a double pyrolysis. The coal was first pyrolyzed in a coal gasifier, and then the selected carbon-rich products were pyrolyzed in the screen-heater reactor.

#### REFERENCES

1. Anthony, D. B., Howard, J. B., Meissner, H. P. and Hottel, H. C. Rev. Sci. Instr. 45, 992 (1974).
2. Anthony, D. B., Howard, J. B., Meissner, H. P. Fifteenth Symposium (International) on Combustion, Tokyo, The Combustion Institute, 1975, 1303.
3. Traldi, P., Org. Mass Spectrom. 17, 245 (1982).
4. Miller, D. J. and Hawthorne, S. B., ACS Div. Fuel Chem. Preprints, 32(4), 10-13 (1987).

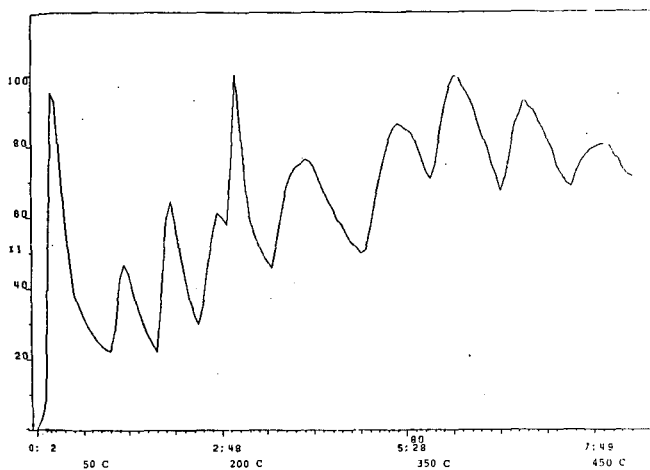


FIGURE 1. Total Ion Chromatogram of Tar

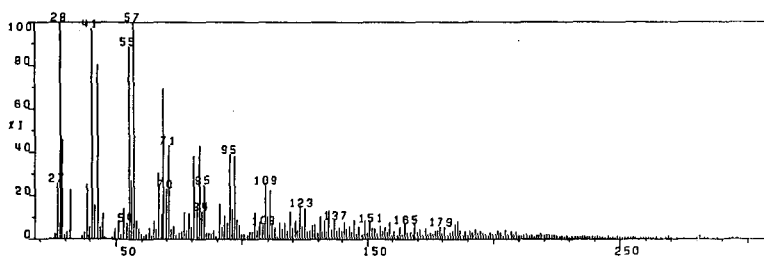


FIGURE 2. Mass Spectrum at 100°C

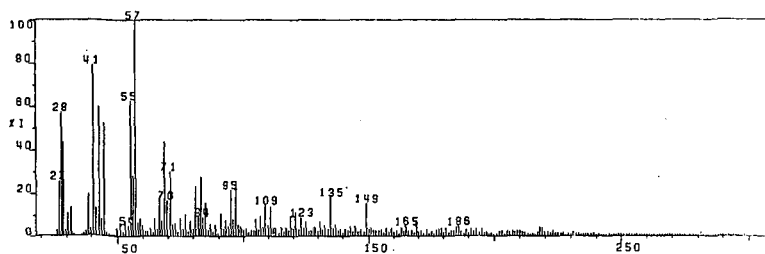


FIGURE 3. Mass Spectrum at 250°C

# INFLUENCE OF HYDROGEN SULPHIDE PRETREATMENT ON HYDROPYROLYSIS OF A BITUMINOUS COAL

Li Baoqing

Université Libre de Bruxelles, Faculté des Sciences Appliquées,  
Service de Chimie Générale et Carbochimie, 1050 Bruxelles, Belgium

## Abstract

The influence of 5%  $H_2S/H_2$  pretreatment of a bituminous Beringen Belgian coal on HyPy is studied in a thermobalance. The presence of  $H_2S$  does not improve the total oil yield, but increases the oil evolution rate. Thus, HyPy can be performed at a temperature 60°C lower in  $H_2S/H_2$ -HyPy than in normal HyPy, resulting in an increase in the efficiency of hydrogen utilization. Sulphur is added to coal during  $H_2S/H_2$  pretreatment stage and is removed in the following HyPy stage, indicating that  $H_2S$  does not act as a real catalyst. A kinetic analysis shows that the activation energy in the initial stage of oil formation in  $H_2S/H_2$ -HyPy is remarkably reduced as compared with that in  $H_2$ -HyPy. It is suggested that  $H_2S$  acts as a hydrogen donor to improve hydrogen transfer and to generate the active sulphur radicals for easier saturation of free radicals formed pyrolytically.

## Introduction

Hydrogen pretreatment of coal was reported to be effective in improving both the yield and the quality of the oil in the following hydropyrolysis (HyPy) (1). It is still interesting to find a way to accelerate the rate of oil formation at low temperature in order to increase the hydrogen utilization efficiency due to the decrease in the formation of light hydrocarbon gases.

It is known that  $H_2S$  can act as a hydrogen transfer catalyst and appears to be a hydrogen donor (2-5). The activation energy for hydrogen transfer and the temperature necessary to promote effective hydrogen transfer are bound to decrease (6,7). The reaction between  $H_2S$  and free radicals formed pyrolytically is much faster than that between  $H_2$  and radicals, even with the addition of only a small amount of  $H_2S$  under lower temperature (8). According to several reports on coal liquefaction (9-11), 5%  $H_2S$  in  $H_2$  seems to be enough effective to obtain the highest catalytic activity.

The purpose of this paper is to examine the influence of coal pretreatment with 5%  $H_2S$  in  $H_2$  on HyPy using a thermogravimetry study. The comparison between the pretreatment under  $H_2$  and  $H_2S/H_2$  at 673 K and 3 MPa is investigated in detail while the effects of  $H_2S/H_2$  pretreatment at other temperatures are simply compared. A kinetic analysis is attempted to obtain further information for the explanation of the  $H_2S$  function.

## Experimental

A two-pin thermobalance with a sample of 0.1 g is used in this study. The apparatus has been described elsewhere (12). The on-line



gas analysis is carried out by gas chromatography with a methanizer using Ni as a catalyst for the quantitative detection of gas components  $\text{CH}_4$ ,  $\text{C}_2\text{H}_4$ ,  $\text{C}_2\text{H}_6$ , CO and  $\text{CO}_2$ .

Hydrogen pretreatment ( $\text{H}_2\text{P}$ ) and  $\text{H}_2\text{S}/\text{H}_2$  pretreatment ( $\text{H}_2\text{S}/\text{H}_2\text{P}$ ) are performed under 3 MPa with a gas flow rate of 1 l/min and a heating rate of 5 K/min up to 673 K (or at other temperatures) for 30 min. In the  $\text{H}_2\text{P}$ -HyPy process, HyPy is run up to 1100 K directly after pretreatment, while in the  $\text{H}_2\text{S}/\text{H}_2\text{P}$ -HyPy process, the reactor is first evacuated to remove  $\text{H}_2\text{S}$  for later analysis of the gas, HyPy is then operated under 3 MPa and a heating rate of 5 K/min with a gas flow rate of 1 l/min.

A bituminous Berigen Belgian coal is ground to less than 90  $\mu\text{m}$  for this study. Its characteristics are given in Table 1.

The content of combustible sulphur in the pretreated coal and char is analysed by means of Carlo Erba Elemental Analyser (Model 1106) with a paropok column (1/4" X 0.8 m).

The data on gas composition obtained by G.C. is corrected in order to eliminate the influence of the time-lag in getting product gases to G.C.. The oil yield is given by carbon balance. The carbon content in char at various temperatures is analysed in our laboratory (13). The carbon content in oil is found to be  $84 \pm 2\%$ .

### Kinetic analysis

The thermal decomposition of coal can be described as:

$$\frac{dx}{dt} = A \exp(-E/RT) (1-x)^n \quad (1)$$

Assuming first order for the rate of mass loss at a constant heating rate, we obtain:

$$\frac{dx}{dT} = \frac{A}{m} \exp(-E/RT) (1-x) \quad (2)$$

where  $m$  is the heating rate,  $x$  the decomposed fraction (on the decomposable basis, here based on the weight loss at 913 K at which oil evolution is ended) and  $A$ ,  $E$  and  $R$  are the usual Arrhenius equation terms. The integration of equation (2), by using the integral approximation method (14), gives

$$\ln(-\ln(1-x)/T^2) = \ln\left(\frac{AR}{mE}\right) / (1+2RT/E) - E/RT \quad (3)$$

Since  $2RT/E$  is much less than unity at moderate temperature and high activation energies, the value of  $(1+2RT/E)$  is assumed constant. Thus, the kinetic parameters from equation (3) can be determined by plotting  $\ln(-\ln(1-x)/T^2)$  versus  $1/T$ . For low activation energy, the value of  $2RT/E$  can not be negligible. Equation (3) can be rewritten as:

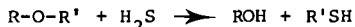
$$\ln(-\ln(1-x)/T^2) + \ln(1+2RT/E) = \ln\frac{AR}{mE} - E/RT \quad (4)$$

A more accurate value of  $E$  is obtained by using the first approximate  $E$  and plotting  $\ln(-\ln(1-x)/T^2) + \ln(1+2RT/E)$  versus  $1/T$ .

## Results and Discussion

### 1. Comparison of $H_2P$ -HyPy and $H_2S/H_2P$ -HyPy

The influence of pretreatment with 5%  $H_2S/H_2$  on HyPy under 3 MPa and 5 K/min at 673 K for 30 min is first studied to compare the results obtained in  $H_2P$ -HyPy under same conditions. Figure 1 shows the comparison in yields of char, oil and gas. The conversion in  $H_2S/H_2P$ -HyPy is about 4% (wt%) higher than that in  $H_2P$ -HyPy. Before 880 K the higher conversion is mainly attributed to the higher oil yield while after 880 K it comes from the difference in gas yield. Figure 2 and 3 show the yields of  $CH_4$ ,  $C_2H_6$ , CO and  $CO_2$ . Before 1100 K the  $CH_4$  yield is lower in  $H_2S/H_2P$ -HyPy than that in  $H_2P$ -HyPy, which may relate to the higher oil yield at lower temperature in  $H_2S/H_2P$ -HyPy because  $H_2S$  can change the route of cleavage of some bonds. Surprisingly, it is found that at higher temperatures, the difference in gas yield, which leads to higher conversion in  $H_2S/H_2P$ -HyPy, results from the increasing CO yield with an increase in temperature. In  $H_2P$ -HyPy, like HyPy, the evolution of CO is ended at about 1000 K. The reason why CO enhances with increasing temperature and more CO is formed might be that  $H_2S$  reacts with ether groups to form phenolic hydroxyl groups according to the following reaction (10):



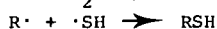
Then, hydroxyl groups decompose to CO at higher temperature (15,16).

Figure 4 shows the comparison of oil evolution rates in  $H_2P$ -HyPy and  $H_2S/H_2P$ -HyPy. It is clear that although the maximum oil yield is same in these two processes, the oil yield formed during the pretreatment stage is higher and the oil reaches the maximum yield more quickly in  $H_2S/H_2P$ -HyPy. This demonstrates that the reactions between  $H_2S$  and free radicals formed pyrolytically are much faster than that between  $H_2$  and radicals. It is also observed that the oil evolution ends about 60°C earlier in  $H_2S/H_2P$ -HyPy as compared with  $H_2P$ -HyPy. Figure 5 gives the comparison of hydrogen utilization in  $H_2P$ -HyPy and  $H_2S/H_2P$ -HyPy. For the same oil yield, a high amount of total hydrogen in gaseous compounds means more hydrogen being consumed in the formation of hydrocarbon gases. One important factor in the economics of the coal hydrogenation process is the hydrogen consumption. For this reason, it is desirable that the formation of gaseous products which consume more  $H_2$  be minimized while liquids are maximized. Thus, using  $H_2S$  pretreatment, HyPy can be performed at lower temperature, resulting in an increase in the efficiency of hydrogen utilization due to the decrease in the formation of light hydrocarbon gases. The study (17) on the reaction of  $H_2S$  with model compounds also found that the addition of  $H_2S$  reduced reductant consumption as much as three-fold whilst maintaining high oil yield levels when the reaction temperature was reduced by 60°C.

Table 2 gives the comparison of combustible sulphur content in  $H_2S/H_2$  pretreated coal,  $H_2$  pretreated coal and chars obtained in  $H_2S/H_2P$ -HyPy and HyPy. After  $H_2S/H_2$  pretreatment the sulphur content in pretreated coal increases from 0.42% to 1.11% as compared with that in  $H_2$  pretreated coal, showing that  $H_2S$  does not act as a real

catalyst. However, the sulphur content in char in  $H_2S/H_2$ P-HyPy is almost the same as that in HyPy. This implies that the additional sulphur in  $H_2S/H_2$  pretreatment stage will be removed in the following HyPy stage, leaving the sulphur content in char unchanged. Thus, it is suggested that  $H_2S$  acts as a hydrogen donor to improve the hydrogen transfer and the reactions between  $H_2S$  and coal follow free radical chain mechanism, involving the active sulphur radicals  $\cdot SH$  as intermediate as follows:

in  $H_2S/H_2$  pretreatment stage,



in the following HyPy stage,



Figure 6 gives the comparison of kinetic curves in  $H_2$ P-HyPy and  $H_2S/H_2$ P-HyPy. Table 3 lists the kinetic parameters. HyPy can be roughly divided into three stages: the pyrolytic stage at temperature below 750 K; hydrogenation in temperatures ranging from 750 to 850 K; and the hydrocracking stage at higher temperatures. In the pyrolytic stage the free radicals are mainly saturated by internal hydrogen while at the hydrogenation stage they are stabilized by gaseous hydrogen. The presence of  $H_2S$  decreases the apparent activation energy as much as four-fold in the pyrolytic stage as compared with that in the absence of  $H_2S$ , while it has no effect on the apparent activation energy in higher temperature stages. It is known that the bond energy of  $H_2$  is greater than that of most C-H bonds whereas that for  $H_2S$  is not (18). According to data on the relative bond strengths most C-S bonds are cleaved much more rapidly than almost all C-C bonds (5). Thus, the saturation of free radicals by  $H_2S$  and the cleavage of the saturated radicals are much faster at the low temperature stage in  $H_2S/H_2$ P-HyPy than that in  $H_2$ P-HyPy.

It should be noted that HyPy in fixed-bed reactor, due to the slow rate of hydrogen diffusion and without solvent, seems to be more subject to mass transfer limitation (1). During  $H_2S/H_2$  pretreatment stage, a considerable amount of oil is produced, which results in a decrease in agglomeration ability. Therefore, more  $H_2$  will penetrate the coal to saturate the free radicals in the following HyPy stage, leading to an increase in oil evolution rate.

The  $H_2S/H_2$  pretreatment of coal can be easier performed because  $H_2S$  is generated within the process. The problem is whether the sulphur content in oil will be increased, which leads to an additional cost in the treatment of oil. The studies (5,10) in coal liquefaction using  $H_2S/H_2$  showed a very small increase in total sulphur in liquids and a very large increase in total sulphur in the residue. It might be possible to obtain the same quality of oil in  $H_2S/H_2$ P-HyPy as in  $H_2$ P-HyPy, but this needs to be proved.

## 2. Influence of different pretreatment temperature

Figure 7 shows the influence of  $H_2S/H_2$  pretreatment temperature

ranging from 573 to 723 K under 3 MPa for 30 min on oil yield. The oil yield obtained in  $H_2S/H_2P-HyPy$  indicates the same tendency as in  $H_2P-HyPy$ (1). After 623 K, the oil yields in  $H_2S/H_2P-HyPy$  and  $H_2P-HyPy$  are higher than that in  $HyPy$ . The same oil yield produced in  $H_2S/H_2P-HyPy$  and  $H_2P-HyPy$  shows that the presence of  $H_2S$  does not improve oil yield. However, the oil yield obtained during  $H_2S/H_2$  pretreatment stage is much higher than that obtained during  $H_2$  pretreatment stage. In  $H_2P$  at 673 K, little oil is produced while in  $H_2S/H_2P$  at the same temperature about 25% of total oil in  $H_2S/H_2P-HyPy$  is already formed. This further demonstrates that  $H_2S$  can reduce the activation energy for hydrogen transfer and the temperature necessary to promote effective hydrogen transfer.

### References

1. Cyprés, R. and Li Baoqing, Fuel Process. Technol. 20, 337 (1988).
2. Stenberg, V. I., Ogawa, T., Willson, W. G. and Miller, D., Fuel 62, 1487 (1983).
3. Stenberg, V. I., Baltisberger, R. J., Ogawa, T., Raman, K. and Woolsey, N. F., ACS Div. Fuel Chem. preprints 27(3-4), 22 (1982).
4. Baldwin, R. M. and Vincignerra, S., Fuel 62, 498 (1983).
5. Trewhella, M. J. and Grint, A., Fuel 66, 1315 (1987).
6. Hirschon, A. S. and Laine, R. M., Fuel 64, 911 (1985).
7. Hirschon, A. S., Sundback, K. and Laine, R. M., Fuel 64, 772 (1985).
8. Cassidy, P. J., Chemitech. 13, 562 (1983).
9. Sweeny, P. G., Stenberg, V. I., Hei, R. D. and Montano, P. A., Fuel 66, 532 (1987).
10. Gao, J-S. and Oelert, H. H., J. Fuel Chem. and Technol.(China) 12, 41 (1984).
11. Baldwin, R. M., Proc. Int. Conf. Coal Sci., Pittsburgh, 98 (1983).
12. Ghodsi, M. and Neumann-Tilte, C., Thermochimica Acta 62, 1 (1983).
13. Planchon, D., Ph.D. thesis in Univ. Libre de Bruxelles, Belgium, (1987).
14. Lee, T. V. and Beck, S. R., AIChE J. 30, 517 (1984).
15. Cyprés, R. and Bettens, B., Tetrahedron 31, 353 (1975).
16. Cyprés, R. and Bettens, B., Tetrahedron 31, 359 (1975).
17. Sondreal, E. A., Wilson, W. G. and Stenberg, V.I., Fuel 61, 925 (1982).
18. Pitts, W. S., Tarrer, A. R., Guin, J. A. and Prather, J. W., ACS Div. Fuel Chem. preprints 22(2), 214 (1977).

Table 1. Beringen Coal Analysis

Proximate Analysis(wt%, as received)		Ultimate Analysis(wt%,daf)	
Moisture	1.49	C	84.74
Ash	4.72	H	4.86
Volatile Matter	34.52	N	1.70
		O+S(by difference)	8.70

Table 2. Combustible sulphur Contents in Pretreated Coal and Char

Coal	Pretreated Coal 3 MPa,673 K,30 min		Char 3 MPa,1073 K		
	H <sub>2</sub> P	H <sub>2</sub> S/H <sub>2</sub> P	HyPy	H <sub>2</sub> S/H <sub>2</sub> P-HyPy	
S(wt%,daf)	1.17	0.42	1.11	0.12	0.18

Table 3. Comparison of Kinetic Parameters in H<sub>2</sub>S/H<sub>2</sub>P-HyPy and H<sub>2</sub>P-HyPy under 3 MPa and 5 K/min. Pretreatment: 3 MPa, 673 K

Process	Tem. Range (K)	Ea° (KJ/mol)	A (1/min)	Coef. Correlation
H <sub>2</sub> P-HyPy	673-750	79.99	7.58x10 <sup>6</sup>	0.979
	750-850	43.08	45.71	0.980
	850-913	74.31	5.10x10 <sup>3</sup>	0.991
H <sub>2</sub> S/H <sub>2</sub> P-HyPy	673-750	20.17	0.71	0.977
	750-850	43.08	45.71	0.980
	850-913	74.31	5.10x10 <sup>3</sup>	0.991

- Apparent activation energy obtained by  $\ln(-\ln(1-x)/T^2) + \ln(1+2RT/E)$  versus  $1/T$ .

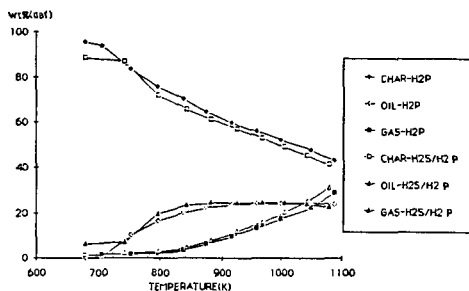


FIG 1 COMPARISON BETWEEN H<sub>2</sub>P-HyPy AND 5% H<sub>2</sub>S/H<sub>2</sub> P-HyPy IN YIELDS OF CHAR,OIL AND GAS. PRETREATMENT: 3 MPa, 673 K, 30 min

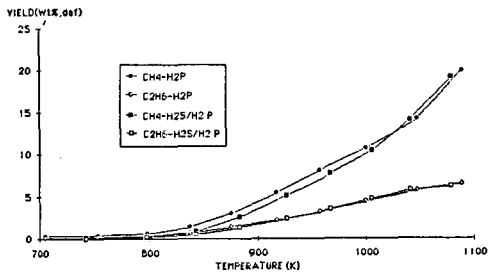


FIG 2 COMPARISON ON YIELDS OF CH<sub>4</sub> AND C<sub>2</sub>H<sub>6</sub> BETWEEN H<sub>2</sub>P AND 5% H<sub>2</sub>S/H<sub>2</sub> P PRETREATMENT CONDITION: 3 MPa, 673 K, 30 min

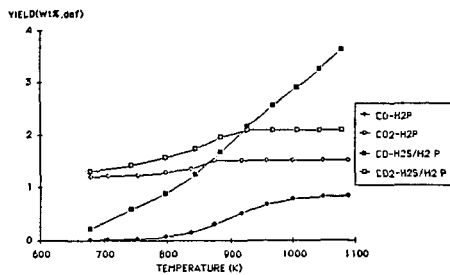


FIG 3 COMPARISON ON YIELDS OF CO AND CO<sub>2</sub> BETWEEN H<sub>2</sub>P AND 5% H<sub>2</sub>S/H<sub>2</sub> P PRETREATMENT CONDITION: 3 MPa, 673 K, 30 min

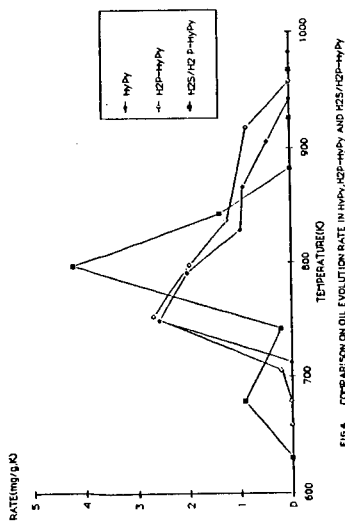


FIG 4 COMPARISON OF OIL EVOLUTION RATE IN H<sub>2</sub>P-H<sub>2</sub>P, H<sub>2</sub>P-H<sub>2</sub>P, AND H<sub>2</sub>S/H<sub>2</sub>P-H<sub>2</sub>P AT 3 MPa, 5 K/min, 673 K, 30 min

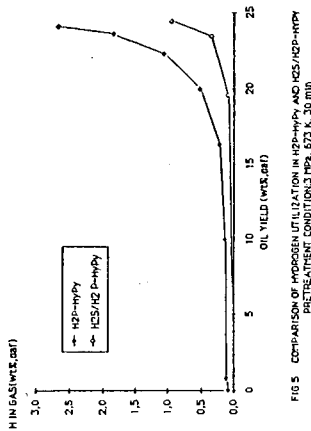


FIG 5 COMPARISON OF HYDROGEN UTILIZATION IN H<sub>2</sub>P-H<sub>2</sub>P AND H<sub>2</sub>S/H<sub>2</sub>P-H<sub>2</sub>P PRETREATMENT CONDITIONS 3 MPa, 673 K, 30 min

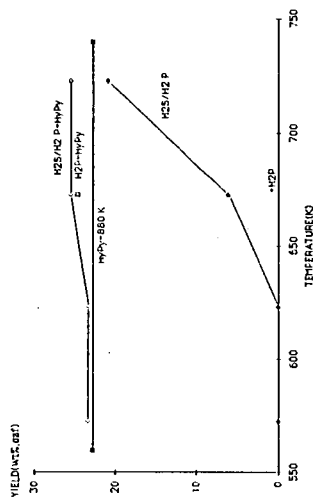


FIGURE 7 INFLUENCE OF PRETREATMENT TEMPERATURE ON OIL YIELD PRETREATMENT: 36 H<sub>2</sub>S/H<sub>2</sub>P, 3 MPa, 5 K/min, 30 min

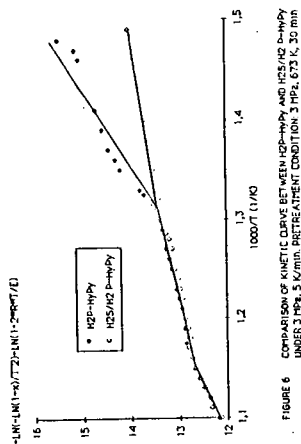


FIGURE 6 COMPARISON OF KINETIC CURVE BETWEEN H<sub>2</sub>P-H<sub>2</sub>P AND H<sub>2</sub>S/H<sub>2</sub>P-H<sub>2</sub>P UNDER 3 MPa, 5 K/min, PRETREATMENT CONDITION 3 MPa, 673 K, 30 min

## **Influence of Reactor Configuration/Type on the Composition of Mild Gasification Liquids\***

**M. Rashid Khan**  
Texaco Research Center, Texaco Inc.  
P.O. Box 509, Beacon, NY 12508

**Kalkunte S. Seshadri**  
EG&G Washington, Morgantown, WV 26505

### **INTRODUCTION**

Yield, quality, and the composition of coal liquids produced by devolatilization depend on the reactor configuration, pyrolysis temperature, and on the coal type used. In this investigation a fixed-bed, a fluidized-bed, and an entrained-flow reactor were used in which Pittsburgh No. 8, Illinois No. 6, and Montana Rosebud coals were pyrolyzed. In addition to the above-mentioned reactor configurations, the liquid produced in the fixed-bed reactor was passed through a reactor tube maintained at 500°C and then the sample was collected to investigate the effects of heat treatment on liquid composition/quality. Vapor phase reactions occurring in the pyrolysis liquids are an important consideration keeping in mind that in a mild gasification process, liquid may experience some hot or high-temperature surfaces.

The goals of this study were (a) to understand the chemical reactions induced in the thermal (tube) reactor and (b) to compare compositional differences of coal liquids produced in a fixed-, fluidized-, and entrained-flow reactors. To this end, devolatilization products were separated using gravity-flow liquid chromatography according to chemical functionality. Subsequently, the first fraction which contained mainly neutral aromatic compounds and the third fraction which was composed of phenolic compounds were analyzed using FIMS.

### **EXPERIMENTAL**

The experimental procedure for coal pyrolysis liquid in a fixed-bed reactor is described by Khan (1). In this configuration liquids were generated at 500°C from the Pittsburgh No. 8 and Montana Rosebud coals. In a separate experiment, coal liquids thus generated were passed through a reactor tube (modified configuration) maintained at 500°C before the final collection. In addition, coal liquids from the pyrolysis of Illinois No. 6 coal in a fixed- and a fluidized-bed reactor at 500°C, of Pittsburgh No. 8 coal in a fixed-bed and an entrained-flow reactor at 650°C, and finally, of Pittsburgh No. 8 coal in an entrained-flow reactor at a reactor temperature of 850°C are included in this study. All experiments were performed in an inert atmosphere.

Open column liquid chromatographic (LC) separation was carried out on silica column with sequential elution of the sample with solvents of different polarity (2,3). Field ionization mass spectral data were obtained at SRI International (Menlo Park, California). Data in the tabular form spread over 14 columns contained relative intensity for each mass number. For each spectrum the relative intensities were normalized to 10,000. Details of instrumentation and data acquisition procedure are described by St. John, et al. (4). Data were reduced to identify homologous

\*Work reported here was performed at Morgantown Energy Technology Center



series in each column and their relative concentration was expressed in mole percent of given fraction or of the total sample. Proton NMR spectra of the Pittsburgh No. 8 coal liquid from the fixed-bed and entrained-flow reactor (reactor temperature 850°C) were obtained at The Energy and Mineral Research Center in Grand Forks, North Dakota, from which average molecular parameters were derived (5). Elemental analysis for these samples were obtained in our laboratory.

## RESULTS AND DISCUSSION

### Comparison of Coal Liquids Produced in the Fixed-Bed and the Modified Fixed-Bed Reactors

The relative quantities of chromatographic fractions in Pittsburgh No. 8 and Montana Rosebud coal liquids produced in the fixed-bed reactor and in the modified configuration are given in Table 1. The separation results suggest certain gross compositional changes in liquids produced in the modified configuration relative to the raw liquids. The relative weight percent of the residue, which is mainly asphaltenes like materials are less abundant in the liquids produced in the modified reactor, whereas that of fraction 3 is higher than in the raw liquid. These two observations suggest that heavier polar compounds with multifunctional groups are cracked producing simple phenols. On the other hand, FIMS data for the first and the third fractions give details of certain chemical reactions induced in the tube reactor.

In our LC separation the first fraction is composed of alkanes, cycloalkanes, olefins, and neutral aromatic compounds whereas, the third fraction is made up of simple phenolic compounds. FIMS data for these two fractions were reduced to identify homologous series in compound class types mentioned above, using the procedure described by Whitehurst, et al. (6). Results are given in Tables 2 and 3.

According to the separation results one of the reactions in the modified fixed-bed reactor is the formation of simple phenols from heavier polar compounds. FIMS results agree with this conclusion; more importantly, they suggest that two parallel reactions are taking place involving phenols. One is the deoxygenation of simple phenolic compounds such as phenols, naphthols, and others; the other is the formation of hydroxy hydroaromatic and aromatic compounds with three or more condensed rings and hydroxy indenenes and benzofurans. Results of elemental analysis (Table 4), however, indicate that there is a decrease in elemental oxygen upon thermal treatment. The decrease in elemental oxygen is consistent with the separation as well as FIMS results. When simple phenols are deoxygenated, the decrease in the weight percent of oxygen is much larger than the percentage increase in elemental oxygen when heavier phenols are formed.

FIMS data for the first LC fraction were obtained without any further separation. Nevertheless, with the aid of certain definite compositional information, which are, that the first fraction of coal liquids produced in fixed-bed reactors contain about 15 weight percent of olefins and saturated compounds, that mono- and di-aromatic compounds are the two major ring systems in this fraction, and that in the present sample not more than two homologous series constitute each column of FIMS data, it was possible to identify all series with reasonable certainty. To illustrate the identification of series in a given column, Column 10 is taken as the example in which are included alkanes, naphthalenes, dibenzothiophenes, binaphthyls, and phenolic compounds. The distribution of relative intensity of molecular ions as a function of carbon number suggest that only two series contribute to this column. The contribution of one series, whose parent compound begins with  $m/e = 128$  to the total relative intensity in the column was 75 percent. Since phe-

nolic compounds were not eluted into this fraction, there are only two possible assignments to the parent compound; an alkane or an aromatic compound. Coal liquids contain mainly higher alkanes at a much lower concentration than aromatics. Therefore, the series beginning with  $m/e = 128$  was assigned to naphthalenes and the other series to alkanes. In a similar manner, homologous series in the other columns were identified. The results suggest that alkanes and cyclic alkanes are cracked in the modified configuration of the fixed-bed reactor, while neutral aromatic compounds are practically unchanged, with the exception of naphthalene. A large increase in the concentration of naphthalene is probably due to its formation from cracking of larger molecules or deoxygenation of naphthols. These possible reactions do not explain why a concentration increase was observed only for naphthalene and not for other aromatic compounds commonly found in fixed-bed samples.

The influence of modified reactor configuration on tar and char yield, gas composition and elemental composition of tar and char are presented in Table 4. In the modified reactor, the tar yield is decreased and the total gas yield is increased. In gaseous products, the increase in the level of  $C_1$ - $C_8$  alkanes is significant. These observations are consistent with some of the reactions induced in the modified reactor, identified based on FIMS data. Cracking of saturated compounds, including alkanes and cyclic alkanes would enhance the total gas production, in particular those of short-chain hydrocarbons.

#### Compositional Comparison of Pittsburgh No. 8 Coal Liquids Produced in the Entrained-Flow Reactor and the Fixed-Bed Reactor

A primary objective of this comparison was to assess whether coal tars produced in the entrained-flow reactor at elevated temperatures can serve as feedstocks for high energy density fuels. To this end, the first fraction of the LC separation of entrained-flow reactor liquid was analyzed using FIMS, data were reduced and finally, specific chemical structures were assigned to parent members of homologous series. The separation and mass spectral results along with those for the fixed-bed sample are given in Tables 5 and 6, respectively. The pyrolysis temperature in the fixed-bed reactor was 500°C; although the entrained-flow reactor was heated to 850°C, the particle temperature was much less, but at least 100°-150°C higher than 500°C.

Results included in Table 6 are presented in a different format in Figure 1 to highlight the difference in the naphthenic carbon content in the two samples. The first column of this figure contains names of identified compounds along with their structures. In the next two columns, the total number of carbon atoms and naphthenic carbons, respectively, contributed by each structure to the LC fraction-1 of fixed-bed liquid are given. The other two columns contain the same information for the entrained-flow reactor sample. The total number of carbons contributed by aromatic compounds and cyclic alkanes were obtained assuming that on the average that each structure is substituted with three carbon atom side chains. The average number of carbon atoms in normal and branched alkanes was assumed to be 20.

Elemental analysis indicated that the fixed-bed sample was hydrogen rich relative to the EFR sample. According to average molecular parameters derived from the proton NMR spectra, the EFR sample was more aromatic, contained less naphthenic carbons, had a higher concentration of polycyclic aromatic compounds, and the aromatic structures were substituted with shorter alkyl chains relative to the fixed-bed sample. These gross structural features are in agreement with the results of elemental analysis. FIMS results, on the other hand, gave details of structural changes.

Two important compositional differences were reduced concentration of monoaromatic and increased concentration of polycyclic aromatic compounds in the EFR sample relative to the fixed-bed sample. Tetralin, a monoaromatic compound, was probably first changed to butyl benzene and eventually to volatile BTX. Side chains in alkyl benzenes were severely cracked. Elevated temperatures favor ring condensation reactions and in this process certain hydroaromatic compounds were formed. Therefore, EFR samples also contain reasonable amounts of naphthenic carbons, although tetralins and octahydronaphthalenes were substantially depleted at elevated temperatures. However, the total population of naphthenic carbons in the first fraction of fixed-bed sample was higher than in the EFR sample. Also the weight percent of first fraction in the total fixed-bed sample was about 50 percent higher than in the EFR sample. Therefore, coal liquids produced in a fixed-bed reactor have a definite edge as a high energy density fuel feedstock over the EFR liquids.

#### Compositional Comparison of Coal Liquids Produced from a Fixed-Bed, Fluidized-Bed, and Entrained-Flow Reactors

Coal liquids produced from Pittsburgh No. 8 coal in the fixed-bed and entrained-flow reactors at 650°C and from Illinois No. 6 coal in the fixed-bed and in the fluidized-bed reactors at 500°C were separated using LC and the results are given in Table 7. Unlike for the previously discussed samples, field ionization mass spectral data were obtained for the total sample. Therefore, assignments of chemical structure to the parent compound of each homologous series is based solely on m/e values. Despite this limitation, assignments appear to be reasonable. Results are presented in Tables 8 and 9.

A survey of the composition of fluidized-bed and entrained-flow reactor samples relative to the composition of fixed-bed liquids suggest that cracking of simple hydroaromatic compounds such as tetralins, deoxygenation of simple phenolic compounds, and ring fusion are the reactions induced by rapid pyrolysis both at moderate and elevated temperatures. The ring fusion reaction results in neutral polycyclic aromatic, polycyclic hydroaromatic, and oxygen-containing polycyclic aromatic compounds.

#### SUMMARY AND CONCLUSIONS

Coal pyrolysis liquids produced by slow heating at moderate temperatures in fixed-bed and modified fixed-bed reactors and by rapid pyrolysis at moderate or elevated temperatures in fluidized-bed or entrained-flow reactors were separated by adsorption chromatography. Pertinent fractions thus generated and total liquids in some cases were analyzed using field ionization mass spectroscopy. The mass spectral data were deconvoluted and each homologous series was associated with a chemical structure. In data analyses for fractions, it was possible to assign definite chemical structures to the parent compound of each series. Identification of components in the total sample is tentative, nevertheless reasonable.

The thrust of this study was to understand compositional differences among coal liquids produced in different reactor configuration and to decide the best configuration for the production of high energy density fuels. In the modified fixed-bed reactor the primary pyrolysis liquid was post-heated to 500°C to understand the influence of heat treatment on liquid quality.

Separation and FIMS results have shown that slow pyrolysis in the modified fixed-bed reactor and rapid pyrolysis both at moderate and elevated temperatures induce

some common reactions, in particular deoxygenation of phenolic compounds and cracking of heavier polar compounds.

Rapid pyrolysis depletes the concentration of simple hydroaromatic compounds and alkyl benzenes, and reduces the length of alkyl side chains on aromatic structures. Ring condensation is another reaction induced during rapid pyrolysis and results in polycyclic aromatic, polycyclic hydroaromatic, and oxygen-containing polycyclic aromatic compounds.

Based on compositional data for liquids produced in different reactor configurations, mild gasification liquids produced in the fixed-bed reactor appear to be the suitable feedstock for high energy density fuels.

**ACKNOWLEDGEMENT:** Funding for this work was provided by the US Dept of Energy, Morgantown Energy Technology Center.

#### REFERENCES

- 1(a). Khan, M. R., Fuel Science and Technology International, **5(2)**, 185, 1987.
- 1(b). Khan, M. R., Proceedings, International Conference on Coal Science, Elsevier, p. 647, 1987.
2. Farcasiu, M., Fuel, **56(1)**, 9, (1977).
3. Seshadri, K. S., and D. Cronauer, Fuel, **62(12)**, 1436, 1983.
4. St. John, G. A., S. E. Buttrill, Jr., and M. Anbar, Organic Chemistry of Coal (Ed. J. Larsen), ACS Symposium Series **71**, 223, (1978).
5. Clutter, D. R., L. Petrakis, R. L. Stenger, Jr., and R. K. Jensen, Anal. Chem., **44(8)**, 1395, (1972).
6. Whitehurst, D. D., S. E. Buttrill, Jr., F. J. Derbyshire, M. Farcasiu, G. A. Odoerfer, and L. R. Rudmik, Fuel, **61**, 994, (1982).

TABLE 1. Fractions of Coal Liquids Produced in Fixed-Bed and in the Modified Configuration from Pittsburgh No. 8 and Montana Rosebud Coals

Fraction No.	Weight-Percent in Sample			
	A	B	C	D
1	42.8	42.6	42.8	46.1
2	13.8	4.9	7.5	6.2
3	14.8	24.7	12.1	23.0
4	1.0	2.1	1.4	0.6
5	8.5	12.4	4.3	4.7
6	6.3	7.1	2.5	6.2
Residue	12.8	6.2	27.1	13.5

A -- Pittsburgh No. 8 Fixed-Bed (FB) Reactor  
 B -- Pittsburgh No. 8 Modified FB Reactor  
 C -- Montana Rosebud FB Reactor  
 D -- Montana Rosebud Modified FB Reactor

TABLE 2. Composition of LC Fraction-1 of Montana Rosebud and Pittsburgh No. 8 Coal Liquids Produced in Fixed-Bed and Modified Fixed-Bed Reactors

Compound	MR	MRM	PGH	PGHM
<u>Alkanes and Cyclic Alkanes</u>				
Alkanes, Normal and Branched	4.54	2.10	6.45	4.36
Monocyclic Alkanes	2.39	0.66	3.81	2.69
Tetracyclic Alkanes	2.93	2.07	4.15	2.85
Pentacyclic Alkanes			1.76	0.46
<u>Aromatics</u>				
Benzenes	9.45	9.98	9.43	10.23
Naphthalenes	15.82	19.34	9.63	12.94
Tetralins	12.51	13.76	4.96	4.29
Acenaphthenes/Biphenyls	13.24	13.63	12.59	14.29
Fluorenes	11.87	10.99	9.41	10.53
Anthracenes/Phenanthrenes	11.45	11.08	12.66	12.04
Dibenzothiophenes	0.92	1.12	2.78	1.64
Octahydroanthracenes	8.20	9.72	4.68	4.69
Fluoranthenes	2.80	1.79	8.41	10.52
Dihdropyrenes	--	--	0.74	0.72
Tetrahydro Fluoranthenes	0.80	0.81	1.59	1.44
Chrysenes	3.02	2.89	6.97	6.25

TABLE 3. Composition of LC Fraction-3 of Pittsburgh No. 8 and Montana Rosebud Coal Liquids Produced in Fixed-Bed and Modified Fixed-Bed Reactors (Mole Percent)

Compound	PGH	PGHM	MR	MRM
2-Indenols	3.1	7.0	5.8	7.2
Unidentified	3.8	3.4	2.9	3.0
Hydroxybenzofurans	7.4	11.1	10.9	10.7
Hydroxypyrenes	6.2	4.9	4.7	2.7
Phenols	31.9	27.8	26.1	24.7
Hydroxyphenylnaphthalenes	3.6	4.1	3.2	5.5
Catechols	2.4	1.0	--	--
Phenanthrols	5.2	6.7	7.3	8.3
1-Hydroxy 9,10-Dihydroanthracenes	8.0	9.1	9.48	10.34
Hydroxypentacenes	1.5	1.4	0.74	0.38
Hydroxybiphenyls	10.9	8.5	11.6	9.8
9-Hydroxytetrahydroanthracenes	1.8	1.9	0.2	3.0
Naphthols	9.9	8.2	15.9	12.4
9,10-Dihydroxytetrahydroanthracenes	2.1	3.7	1.3	2.0
Unidentified	1.7	0	--	--

PGH -- Pittsburgh No. 8 Liquid Produced in the FB Reactor  
PGHM -- Pittsburgh No. 8 Liquid Produced in the Modified FB Reactor  
MR -- Montana Rosebud Liquid Produced in the FB Reactor  
MRM -- Montana Rosebud Liquid Produced in the Modified FB Reactor

TABLE 4. Influence of Fixed-Bed Reactor Configuration on Product Composition (Pittsburgh No. 8 Coal)  
(All Data on Dry Coal Basis)

	Fixed-Bed Reactor	Modified Fixed-Bed Reactor
Wt Sample (g)	50.0	50.0
Total Gas (l)/100 g Dry Coal	10.0	12.5
Char (Wt %)	71.2	72.0
Tar (Wt %)	18.0	9.0
<u>Gas Composition (Vol %)</u>		
H <sub>2</sub>	10.51	8.29
CO	4.54	4.46
CO <sub>2</sub>	6.81	7.43
H <sub>2</sub> S	6.58	5.78
COS	0.16	0.23
H <sub>2</sub> O	0.03	0.08
CH <sub>4</sub>	48.32	43.22
C <sub>2</sub> H <sub>4</sub>	1.52	1.79
C <sub>2</sub> H <sub>6</sub>	9.91	10.80
C <sub>1</sub> -C <sub>8</sub>	71.10	73.69
<u>Tar Composition (Wt %)</u>		
C	77.62	81.68
H	8.93	8.69
S	0.74	0.93
N	0.94	0.86
O	11.77	7.84
H/C (atomic)	1.38	1.28
Btu/lb	14,926	15,626
<u>Char Composition (as received, Wt %)</u>		
C	78.56	78.73
H	2.89	2.86
N	1.76	1.73
S	1.66	1.71
Ash	10.51	10.77
VM	10.61	11.26
H <sub>2</sub> O	0.30	0.81
H/C	0.44	0.44
O (By Difference)	15.13	14.97
Btu/lb	13,121	13,101

TABLE 5. Fractions of Pittsburgh No. 8 Coal Liquids  
in Fixed-Bed and Entrained-Flow Reactors

Fraction No.	Fixed-Bed	Entrained-Flow Reactor
1	42.8	33.1
2	13.8	3.5
3	14.8	26.5
4	1.0	9.1
5	8.5	8.6
6	6.3	14.0
Residue	12.8	5.2

TABLE 6. Composition in Mole Percent of LC Fraction-1  
of Fixed-Bed and Entrained-Flow Reactor  
Liquids Generated From Pittsburgh No. 8 Coal

Compound	Fixed-Bed	Entrained-Flow
Tetralins	5.0	1.0
Pyrenes/Fluoranthenes	8.4	12.0
Cyclic alkanes	1.8	2.0
Benzenes	4.1	0.9
Dihdropyrenes	9.3	7.4
Tetracyclic alkanes	0.7	4.2
Phenanthrenes	--	9.6
Tetrahydropyrenes	1.6	5.6
Octahydronaphthalenes	12.7	--
Acenaphthylenes	9.4	7.1
Hexahydropyrenes	3.0	--
Octahydrobenzanthracenes	--	6.9
Acenaphthenes	12.6	6.1
Monocyclic alkanes	3.8	--
Benzopyrenes	--	9.3
Naphthalenes	9.6	8.3
Alkanes	6.4	7.5
Binaphthyls	--	0.5
Indenes	4.7	1.8
Chrysenes	6.9	8.3
Unknown	--	1.4

TABLE 7. Fractions of Fixed-Bed and Fluid-Bed (Illinois No. 6) and Fixed-Bed and Entrained-Flow Reactor (Pittsburgh No. 8) Liquids

Fraction No.	Weight Percent in			
	Fixed-Bed Illinois No. 6 500°C	Fluid-Bed Illinois No. 6 500°C	Fixed-Bed Pittsburgh No. 8 650°C	Entrained-Flow Reactor Pittsburgh No. 8 650°C
1	28.6	12.9	39.2	4.7
2	4.6	5.0	14.3	10.3
3	23.8	20.0	14.3	28.3
4	19.7	23.2	5.3	30.0
5	14.1	37.8	9.0	11.4
6	11.29	0.0	5.5	6.2
Residue	9.0	1.1	17.9	9.0

TABLE 8. Relative Weight Percent of Neutral Aromatic and Phenolic Compounds in 500°C Fixed-Bed and Fluid-Bed Liquids (Illinois No. 6 Coal)

Compound	Fixed-Bed	Fluid-Bed
Benzenes	6.1	--
Phenols	11.4	3.6
Catechols/Hydroquinones	--	1.6
Indenes	7.7	--
Naphthalenes	4.5	8.8
Tetralins	7.2	3.8
Benzo thiophenes	--	3.1
Naphthols	--	3.7
Acenaphthenes/Biphenyls	10.5	7.5
Fluorenes	9.1	9.7
Hydroxybiphenyls	7.7	--
Octahydronaphthalenes	10.8	--
Anthracenes/Phenanthrenes	--	7.9
Octahydrophenanthrenes	4.5	4.6
Hexylbenzenes	5.1	--
Pyrenes	--	8.6
Dihdropyrenes	--	8.6
Hydroxytetralins	9.3	--
Benzopyrenes	--	2.7
Binaphthyls	1.75	2.6
Chrysenes	--	6.2
Hydroxypentacenes	--	4.2
Dibenzopyrenes	--	2.5
Pentacenes	--	3.1
Dihydrobenzopyrenes	--	2.7



TABLE 9. Composition of Fixed-Bed and Entrained-Flow  
Reactor Liquids Generated from Pittsburgh  
No. 8 Coal (650°C)

Compound	Fixed-Bed	Entrained-Flow
Indanes/Tetralins	4.31	0.75
Pyrenes	2.48	5.98
Dihydrobenzanthracenes	1.83	--
Hydroxybenzanthracenes	--	2.20
Hexacenes	--	0.40
Benzenes	5.32	--
Benzofurans	--	1.04
Phenylnaphthalenes	4.74	5.76
or Hydroxypyrenes		
Dihydroxy Benzanthracenes	--	2.54
Phenols	7.92	0.79
Anthracenes	3.60	5.87
Phenanthrenes		
Dihydroxytetralins		
Hydroxyphenyl	0.99	2.74
Naphthalenes		
Tetrahydropyrenes	1.87	--
Catechols	2.17	--
Acenaphthylenes	5.42	2.84
Phenanthrols	--	1.84
Dihydroxytetrahydro	--	3.74
Benzanthracenes		
Octahydrotetracenes	0.74	--
Pentacenes	--	0.28
Cyclohexanes	1.06	--
Acenaphthenes/Biphenyls	6.50	3.26
Benzopyrenes	1.01	5.09
Tetrahydronaphthyl	0.81	--
Phenyl Ether		
Hydroxypentacene	--	1.21
Naphthalenes	9.24	2.04
Hydroxytetrahydroanthracenes	--	1.32
Binaphthyls	1.81	3.69
Unknown	--	1.17
Tribenzopyrenes	0.17	1.39
Indenes	3.90	1.00
Octahydrophenanthracenes/	3.50	--
Dibenzofuran		
Dihydroxy	--	6.41
Tetrahydro		
Anthracenes		
Bianthryls	--	1.86
Dinaphtho	0.58	--
Thiophene		

FIGURE 1. Relative Composition of LC Fraction-1 of Fixed-Bed and Entrained-Flow Reactor Coal Liquids (Pittsburgh No. 8)

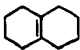
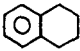

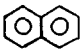

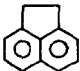
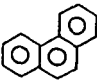
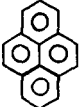
Compound/Structure		Fixed Bed		Entrained-Flow Reactor	
		Total Carbon	Naphthenic Carbon	Total Carbon	Naphthenic Carbon
Octahydronaphthalenes		165.1	101.6	0.0	0.0
Tetralins		65.0	20.0	13.0	4.0
Benzenes		36.9	0.0	8.1	0.0
Naphthalenes		124.8	0.0	107.9	0.0
Acenaphthylenes		141.0	0.0	106.5	0.0
Acenaphthenes		189.0	25.2	91.5	12.2
Phenanthrenes		0.0	0.0	163.2	0.0
Pyrenes		159.6	0.0	228.0	0.0

FIGURE 1. Relative Composition of LC Fraction-1 of Fixed-Bed and  
Entrained-Flow Reactor Coal Liquids (Pittsburgh No. 8)  
(Continued)

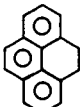
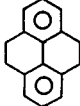
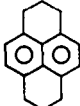
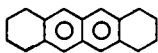
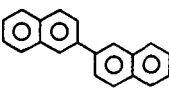
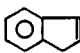
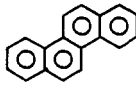
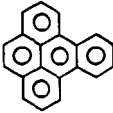

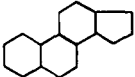
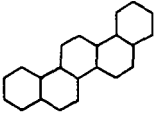
Compound/Structure		Fixed Bed		Entrained-Flow Reactor	
		Total Carbon	Naphthenic Carbon	Total Carbon	Naphthenic Carbon
Dihydropyrenes		176.7	18.6	140.6	14.8
Tetrahydropyrenes		30.4	6.4	106.4	22.4
Hexahydropyrenes		57.0	18.0	0.0	0.0
Octahydrobenzanthracenes		0.0	0.0	144.9	55.2
Binaphthyls		0.0	0.0	7.5	0.0
Indenes		56.4	4.7	21.6	1.8
Chrysenes		144.9	0.0	174.3	0.0

FIGURE 1. Relative Composition of LC Fraction-1 of Fixed-Bed and  
Entrained-Flow Reactor Coal Liquids (Pittsburgh No. 8)  
(Continued)

Compound/Structure	Fixed Bed		Entrained-Flow Reactor	
	Total Carbon	Naphthenic Carbon	Total Carbon	Naphthenic Carbon
Benzopyrenes 	0.0	0.0	213.9	0.0
Alkanes (n- and branched)	128.0	0.0	150.0	0.0
Monocyclic alkanes 	34.2	22.8	0.0	0.0
Tetracyclic alkanes 	14.0	11.9	84.0	71.4
Pentacyclic alkanes 	45.0	39.6	50.0	44.0
Total	1568	268.8	1811.4	225.8
% Naphthenic Carbon in LC Fraction-1		17.1		12.4
% Naphthenic Carbon in Total Liquid		7.3		4.1

## Oil Shale Pyrolysis by Triple Quadrupole Mass Spectrometry: Comparisons of Gas Evolution at 10°C/min Heating Rate.

John G. Reynolds, Richard W. Crawford, and Alan K. Burnham,  
University of California,  
Lawrence Livermore National Laboratory,  
Livermore, CA 94550.

### Abstract

Kimmeridge, Phosphoria, LaLuna, Teistberget, New Albany, Janus, Lias  $\epsilon$ , Maoming, Fushun, Woodford, and three Green River oil shales were subjected to programmed temperature pyrolysis at a heating rate of 10°C/min using Triple Quadrupole Mass Spectrometry (TQMS) as the detection method. Volatile compound evolution, including hydrocarbons, non-condensable gases, and heteroatomic compounds were monitored by on-line, real-time detection. As expected, the temperatures of maximum evolution depended on the oil shale and the species evolving. Generally, the  $T_{\max}$  values for total light volatile organic compound generation were between 430 to 500°C, with the New Albany giving the lowest values and Brotherson A from Green River giving the highest values. The heteroatomic species had  $T_{\max}$  values which were slightly lower than those for hydrocarbon evolution. Non-condensable gas formation was highly dependent upon the mineral matrix of the shale.

### Introduction

Locating oil in a formation, and predicting where generation will occur are relevant contemporary problems for geochemistry. We are studying the kinetics of oil generation through laboratory simulated pyrolysis of source rocks to better address these problems.<sup>1</sup> To extend our data base, we have selected several oil shales from various geographical locations, from both marine and lacustrine source types and subjected them to programmed temperature pyrolysis at various heating rates, from room temperature to 900°C using Triple Quadrupole Mass Spectrometry (TQMS) as the detection method. This technique has been utilized previously for several studies on pyrolysis of oil shale,<sup>2-5</sup> tar sands,<sup>6-8</sup> and coal.<sup>9</sup>

TQMS is particularly suited for this type of study because it provides on-line, real-time analysis. By these experiments, we follow the evolution as a function of temperature of various light hydrocarbons, N-, S-, and O-containing compounds, and non-condensable gases. The pyrolysis profiles obtained allow determination of evolution range and  $T_{\max}$ . Multiple heating rates allow determination of kinetic parameters for which the ultimate aim is extrapolation to geological conditions. This report is a preliminary account of the evolution behavior of several oil shales at the heating rate of 10°C/min. A full report will be issued later. In addition, the kinetics derived from multiple heating rates will be reported separately.

### Experimental

Instrumentation. The TQMS utilizes both MS and MS/MS detection coupled with computer controlled acquisition which allows for the detection of over 40 components in mat-

ters of seconds. Full details of this technique have been published elsewhere.<sup>10,11</sup> Compounds analyzed for are C<sub>1</sub>- through C<sub>7</sub>-hydrocarbons, C<sub>2</sub>- through C<sub>5</sub>- volatile sulfur compounds, the non-condensable gases, H<sub>2</sub>, CO, CO<sub>2</sub>, H<sub>2</sub>S, SO<sub>2</sub>, and COS, as well as H<sub>2</sub>O, CS<sub>2</sub>, and several nitrogen- and oxygen-containing compounds. In these experiments, the pyrolysis reactor was a 1/4 inch quartz tube holding approximately 0.5 grams of oil, and was heated at a rate of 10°C/min with a constant Ar sweep of 30 cc/min. The evolving components flowed into a trap kept at 140°C. This allowed for light volatile hydrocarbon and heteroatom (N,S,O) compounds up to C<sub>8</sub> to pass through to the mass spectrometer, while the heavy components were retained. In addition to qualitative detection, several of the volatile components were also quantitated. Total evolution data will be reported later. The width of the T<sub>max</sub> values indicate in all cases multiple activation energies. This will also be discussed in detail in the kinetics report.

Most of the samples were also characterized pyrolysis in a Pyromat (Lab Instruments) micropyrolysis instrument. 15 mg of sample is held in a quartz tube with a type K thermocouple inside. The sample is heated at a programmed heating rate, chosen to be 9.2°C/min in this case for comparison to the TQMS results. The total pyrolysate is monitored with an adjacent FID detector operated at 500°C.

Samples. Table 1 describes the shales examined in this study. Both marine and lacustrine samples from several locations throughout the world were examined. Pyrolysis experimental conditions and errors were determined by multiple runs on Woodford and NA-13 shales. Less abundant samples were examined generally 1 to 2 times.

Sources of several of the shales have been described previously.<sup>1</sup> In addition, NA-13 is from the New Albany formation; AP-24, Government 33-4, and Brotherson A are from the Green River formation; Wenzon comes from the Lias  $\epsilon$  formation. AP-24 comes from the Mahogany zone in Colorado. Government 33-4 and Brotherson A come from well cores in Utah. Government 33-4 contains 10% vitrinite and 5% exinite. (Numbers provided by DGSi company of The Woodlands, TX.) Brotherson A is just above the oil window. The Wenzon sample is from J. Rullkotter (KFA); LaLuna from S. Talukdar (INTEVEP); Janus and Teistberget from B. Dahl (Norsk Hydro).

Two samples each of Maoming and Fushun shales were also examined. These samples were from the same formation but obtained from different sources. The samples appended with I were obtained from R. C. Rex, Jr. (Hycrude Corporation) and those appended with II were obtained from Zhang Shi Ko of Sinopec International. Janus is a terrestrial shale with some marine mixed in. Full descriptions of the samples will be presented elsewhere.

## Results and Discussion

Hydrocarbon Evolution. Figure 1 shows the pyrolysis profiles for the evolution of C<sub>3</sub>H<sub>8</sub> for several of the shales listed in Table 1 (some were not presented for figure clarity). These profiles are typical of evolution seen for all the hydrocarbons, having an approximate Gaussian shaped prominent maximum with a temperature of maximum evolution (T<sub>max</sub>) around 450 to 500°C, depending upon the hydrocarbon species evolving and the particular shale. This maximum has been assigned as due to kerogen breakdown and bitumen cracking.<sup>2,12-14</sup> Little or no intensity is seen at temperatures below and above this

maximum, except in methane evolution and isolated cases for higher hydrocarbons (see below).

Table 2 shows the  $T_{\max}$  for the total light organics evolved, and compares this value to the  $T_{\max}$  for the  $C_4H_9^+$  ion and the  $T_{\max}$  measured by Pyromat. The total light organics evolution value comes from taking the total ion current of all the species evolving (which pass through the 140°C trap) at a specific temperature and subtracting the ion current contributions from non-hydrocarbon gases ( $SO_2$ ,  $CO_2$ ,  $H_2S$ ,  $HS$ ,  $O_2$ ,  $S$ ,  $H_2O$ ,  $NH_3$ ,  $H_2$ ) and the carrier and analysis gases (Ar, Kr). The  $C_4H_9^+$  ion is from monitoring  $m/z$  57 and is a result of contributions from most hydrocarbons of  $C_4H_{10}$  and higher. It is meant to be an indicator of these larger alkyl hydrocarbons as opposed to only butane. The Pyromat analysis was included to give a comparison measurement of total hydrocarbons which is not based on MS methods. Generally, for a given sample, the absolute values of the Pyromat technique are slightly lower than the total light organics from the TQMS, but the trends are the same.

Comparing  $T_{\max}$  for total volatile organics, two groupings are observed. The marine shales have temperature maxima between 447 and 471°C and the lacustrine shales between 471 and 484°C. This is normal behavior for these types of shales. The Maoming shales, however, are the exceptions. The  $T_{\max}$ , as well as other properties (see below), are much more like marine shale than lacustrine shale. The same grouping is observed for the  $C_4H_9^+$  ions, but with slightly different temperatures ranges.

Comparing corresponding  $T_{\max}$  values for total light organics and  $C_4H_9^+$  ions, in general, the values are similar. NA-13 has the lowest  $T_{\max}$  for both sets, while Brotherson A has the highest for both sets. The biggest differences between the two sets are for Wenzhen, where the  $T_{\max}$  for total light organics evolution is 8 °C higher than for the  $C_4H_9^+$  fragment. In some cases (Phosphoria, Wenzhen, Woodford, Government 33-4, Maoming II) the  $T_{\max}$  for total light organics generation is higher than the  $T_{\max}$  for  $C_4H_9^+$  ion, but in many cases it is the same or lower (NA-13, Janus, Maoming I, Kimmeridge, AP-24, Teistberget, Fushun I, Fushun II, Brotherson A, LaLuna).

The Pyromat derived  $T_{\max}$  values are generally lower than the corresponding  $T_{\max}$  values and exhibit a much smaller spread in values than for both total light organics and  $C_4H_9^+$  generation. However, the trends are roughly same. In this case, Phosphoria has the lowest  $T_{\max}$ , instead of NA-13. Brotherson A has the highest  $T_{\max}$ . Also, the lacustrine shales have a  $T_{\max}$  which is around 460°C, while the marine shales have a  $T_{\max}$  around 445°C. As in the case for total light organics generation, Maoming shale behaves more like a marine than lacustrine shale.

Table 3 shows the  $T_{\max}$  values for  $C_2H_4$ ,  $C_2H_6$ ,  $C_3H_8$ , and  $C_4H_{10}$  evolution. The value in parentheses in the  $T_{\max}$  column indicates another maximum is observed having a  $T_{\max}$  at the listed temperature in addition to the maximum assigned to hydrocarbon evolution. This low temperature maximum can be assigned to entrapped material in the mineral matrix which becomes labile when the bitumen in the shale begins to soften. This behavior is very prominent in tar sands where the bitumen content is much higher than in oil shale and has been assigned as such.<sup>6-8</sup>

For all cases, the  $C_2H_4$  evolution  $T_{max}$  values are higher than the  $T_{max}$  for total light organics evolution for the corresponding shale. For the lacustrine shales, Fushun I, Fushun II, Government 33-4, and Brotherson A show very little difference between the  $C_2H_4$   $T_{max}$  and the total light organics evolution  $T_{max}$  (2 to 6 °C) as shown in Table 2. For the marine shales, the difference between the  $T_{max}$  for  $C_2H_4$  evolution and the  $T_{max}$  for total light organics evolution is very large (15 to 35 °C). The two Maoming samples, however, behave like marine samples also which has been seen above for the total light organics,  $C_4H_9^+$  evolution, and Pyromat  $T_{max}$ .

Interestingly, the lacustrine samples tend to have  $T_{max}$  values for total light organics evolution which are *higher* than that for the marine shales, but in the case of  $C_2H_4$  evolution, the  $T_{max}$  values are *lower*. Fushun I and Fushun II have the lowest  $C_2H_4$  evolution  $T_{max}$  values for all the shales listed. Brotherson A which has the highest  $T_{max}$  for total light organics and  $C_4H_9^+$  ion evolution, and Pyromat  $T_{max}$ , is not even close for that value in Table 3.

Contrary to total light organics and  $C_2H_4$  evolution, the  $T_{max}$  values for  $C_2H_6$  evolution show no apparent grouping according to type. However, the differences in the  $T_{max}$  values for  $C_2H_6$  evolution compared to the  $T_{max}$  values for total light organics evolution are generally much larger for the marine shales than the lacustrine shales. Even the Maoming samples are consistent with this.

The difference in the  $T_{max}$  values for  $C_2H_4$  evolution and  $C_2H_6$  evolution are much larger for the marine shales than the lacustrine shales. (The ethane to ethene ratio are much closer to 1 for the marine shales). Once again, the Maoming samples are the exception as noted above. Brotherson A is also an exception. This shale is different than the other samples in that it is just above the oil generation window. As seen in Table 2, it has the highest  $T_{max}$  for total light organics and  $C_4H_9^+$  ion evolution. This is consistent with the lighter material being converted in the formation.

Our results are similar to earlier results for eastern Devonian shale,<sup>2,13</sup> Chinese shale,<sup>2</sup> and Green River shale.<sup>2,12</sup> Our  $T_{max}$  values are generally higher because our faster heating rate, but these appear to be minor differences from the earlier work<sup>12-14</sup> due to improvements in techniques.

The  $T_{max}$  values for  $C_3H_8$  evolution listed in Table 3 are lower than the  $T_{max}$  values for  $C_2H_4$  and  $C_2H_6$  evolution, and are similar to the  $T_{max}$  for total light organics evolution, for a given shale. This has been seen before NA-13 oil shale at 4°C/min<sup>13</sup> and for several tar sands.<sup>6-8</sup> Only Fushun II and Brotherson A counter this trend.

Of all the hydrocarbons listed in Table 3,  $C_4H_{10}$  had the lowest  $T_{max}$  for a given shale. These values are significantly lower than the  $T_{max}$  for total light organics evolution. The differences in  $T_{max}$  values of  $C_2H_4$  and  $C_4H_{10}$  for a given shale ranged from 54 °C to 10 °C. The lacustrine shales generally had smaller differential than the marine shales, which is expected. However, as seen before, the Maoming shales had behavior which was similar to marine shales. Brotherson A was another exception, which exhibited very little difference in the  $T_{max}$  values for all the hydrocarbons listed in Table 3. As stated above, Brotherson A is located above the oil generation window, which is probably responsible for its aberrant behavior. The  $T_{max}$  for  $C_4H_{10}$  generation for NA-13 is slightly lower (3°C)



than the value found at 4°C/min, but probably within experimental error.<sup>13</sup> The AP-24 value is higher as expected for the higher heating rate.<sup>12</sup>

**Methane.** Figure 2 shows the pyrolysis profiles for the evolution of methane as a function of pyrolysis temperature for selected shales. In contrast to the other hydrocarbon evolution profiles, the typical methane profile exhibits not only the prominent maximum at hydrocarbon evolution temperatures, but also a shoulder on the high temperature side of this maximum. The prominent maximum has a  $T_{\max}$  higher than for the corresponding other hydrocarbons, ranging from 2 to 146 °C above the  $T_{\max}$  for total light organics generation, depending upon the shale. This has also been assigned to kerogen breakdown and bitumen cracking reactions.<sup>12-14</sup>

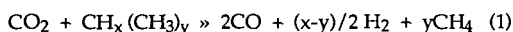
The evident shoulder on many of the profiles in Figure 2 has been assigned to evolution of methane by secondary charring reactions. As the kerogen is further pyrolyzing, and the non-volatile bitumen is laying down as precoke and coke on the mineral matrix, more methane is evolved. This behavior has been seen previously for oil shale<sup>12</sup> and tar sands.<sup>6-8</sup> However, for several shales (LaLuna, Phosphoria, Government 33-4) have shoulders in the methane profiles on the low temperature side of the prominent maximum. This behavior has been seen before for NA-13 shale.<sup>2</sup> This suggests the major peak is due to charring reactions instead of organic evolution. Because at the higher heating rates, the shoulders are poorly resolved, this aspect will be examined in more detail at the 1°C/min heating rate.

Table 4 lists the  $T_{\max}$  for methane evolution for all the shales studied. Kimmeridge exhibits the highest  $T_{\max}$  while AP-24 exhibits the lowest. The AP-24 value is 15°C higher than the  $T_{\max}$  reported earlier at a 4°C/min heating rate, which is consistent with the higher heating rate.<sup>12</sup> The  $T_{\max}$  for NA-13 also agrees with values for eastern shales heated at 4°C/min reported by Coburn<sup>13</sup> and Oh et al.<sup>2</sup> We also observe a shoulder on the low temperature side of the prominent maximum at about 470°C. This is in agreement with Oh et al. who see the shoulder at 450°C and assign it as probably due to CH<sub>4</sub> generation from kerogen pyrolysis. Oh et al. also reports the Maoming I and Fushun I shales having  $T_{\max}$  at 500°C. These values are reasonably close to those in Table 4 which would not be expected at the different heating rates. Because of the broad nature of the CH<sub>4</sub> peak,  $T_{\max}$  values are difficult to assign when the signal-to-noise is not optimal. In addition, they observed shoulders at temperature around 600°C, which is also consistent with Table 4.

Regardless of the  $T_{\max}$  for a particular shale, the shoulder appears at approximately 100°C higher. Although there is no shoulder temperature listed for Janus, examination of the profile in Figure 2 shows a very broad peak which defies resolution in the temperature range expected for the shoulder. This could be due to the noise in the profile, or the two methane forming reaction pathways being about equal in intensity. Experiments at different heating rates will help clarify this, and are in progress.

Evident in Figure 2 for Government, LaLuna, Teistberget, and AP-24 oil shales are small maxima in the 700 to 900°C evolution range. Because the data is from the unique MS/MS combination of 16/14, these are not artifacts of other species which produce m/z 16 ions.<sup>11</sup> Examination of the CO<sub>2</sub> profiles show that these maxima coincide with intense CO<sub>2</sub> evolu-

tion for the same shale. This suggests CO<sub>2</sub> gasification of organic char (from decomposing kerogen and bitumen) in the mineral matrix. Equation (1) describes this reaction:



**Carbon Oxide Evolution.** The CO<sub>2</sub> evolution profiles for the shales can be grouped into three types: 1) high carbonate shales (LaLuna, Wenzhen, Brotherson A, Government 33-4, Teistberget, and AP-24), 2) low CO<sub>2</sub> mineral shales (Phosphoria, Woodford, Kimmeridge, and Janus), and 3) high siderite shales (Maoming I, Maoming II, Fushun I, and Fushun II). The high carbonate type shales show a very small maximum around 400 to 450°C, and prominent evolution in the 650 to 900°C range. The former has been previously tentatively assigned in oil shales and tar sands to be due to the decomposition of oxygen-containing organic compounds, such as carboxylic acids and salts, and ketones.<sup>6-8,12,13,15,16</sup> The high temperature evolution is has been assigned to carbonate mineral decomposition dominating the CO<sub>2</sub> evolution. Table 1 lists Brotherson A, Wenzhen, LaLuna, and AP-24 having calcite and/or dolomite as the major mineral. Government and Teistberget are the only other shales that have any appreciable carbonate minerals. Independent acid carbonate determinations show this is the case for AP-24, Wenzhen, and LaLuna (Government and Teistberget are being determined). These results are in agreement with previously published results on AP-24 and NA-13 shales.<sup>2,12,13</sup>

The low mineral shales show CO<sub>2</sub> evolution behavior which is very complex. In most cases, CO<sub>2</sub> evolution correlates well with water and H<sub>2</sub>S evolution in the temperature range around 475 to 600°C. Some of this evolution can be described by: 1) the  $\alpha$  to  $\beta$  transition for quartz around 560°C (evolves not only water, but some CO<sub>2</sub>),<sup>17</sup> and 2) the reaction of H<sub>2</sub>S is also known to react with iron and mixed metal carbonates<sup>18</sup> at fairly moderate temperatures.

The high siderite shales (Chinese shales), minerals release CO<sub>2</sub> at relatively low temperatures (Shale, T<sub>max</sub>: Maoming I, 465°C; Maoming II, 462°C; Fushun I, 497°C; Fushun II, 487°C) most likely due to the decomposition of siderite. For the Maoming shales, CO<sub>2</sub> release is coincidental with H<sub>2</sub>S and hydrocarbon evolution, indicating reaction of H<sub>2</sub>S (probably generated from organo-sulfur compound decomposition) with minerals may be catalyzing the release in this temperature range.

No evolution of CO is seen below 300°C, after which evolution begins. In most of the profiles, a small maximum is evident around 440°C and falls in the range of hydrocarbon evolution due to kerogen breakdown and bitumen cracking reactions. The chemical species responsible for this evolution is not certain, but may be the decarbonylation of carboxylic acids and salts.<sup>19</sup>

The majority of the CO evolved occurs above 600°C, and is not directly related to hydrocarbon generation. This high temperature CO could have a variety of origins<sup>20</sup>: 1) the water-gas shift reaction, 2) the Boudouard reaction (similar to equation 1), and 3) char gasification by water from mineral breakdown.

**Hydrogen.** Figure 3 shows the H<sub>2</sub> evolution profiles as a function of temperature for several of the oil shales studied. Except for Wenzhen, the profiles show no hydrogen evolution before approximately 350°C. Several maxima are seen above this temperature, depending

upon the oil shale. For AP-24, Teistberget, Maoming I, Maoming II (not shown), Fushun I (not shown), Fushun II (not shown), the best defined maximum is around 475°C. This is also evident to a lesser extent for all the other shales. Table 5 lists the  $T_{\max}$  for this maximum, along with the % of total evolution (by integration) accounted for by this maximum, and the total evolution of hydrogen (cc/gr of TOC) for the entire profile. No correlation between shale type and  $T_{\max}$  was observed. This maximum occurs at the same temperature range as the maximum for total light organic evolution and is attributed to kerosene breakdown, aromatization, cracking, and dehydrogenation reactions of non-volatile bitumen. The differences between this  $T_{\max}$ , and the  $T_{\max}$  for total light organic evolution (see Table 2) depended upon the shale, varying from 0 (Wenzen) to 48°C (NA-13). This type maximum has been observed before in oil shale,<sup>2,12-14</sup> and tar sands<sup>6-8</sup> pyrolysis.

Figure 3 also shows the majority of the hydrogen is evolving above this maximum assigned to sources other than hydrocarbon generation, and can be attributed to several reactions, depending upon the temperature and the shale. The  $H_2$  evolving in the 500 to 650°C ranging has been assigned previously<sup>12</sup> to char pyrolysis reactions where the residual kerosene, and non-volatile bitumen are further decomposing yielding surface coke,  $H_2$ , and  $CH_4$  (see above discussion).  $H_2$  evolving above this can have additional contributions from a variety of secondary reactions including the water-gas shift equilibrium, char gasification, and the Boudouard reaction.

**Heteroatomic Compounds.** Several sulfur-, nitrogen-, and oxygen-containing compounds also evolved during the pyrolysis of the oil shales. Of all these compounds, methylthiophene generally produced the most intense signal due to concentration and response of the species. Figure 4 shows the methylthiophene evolution profiles as a function of pyrolysis temperature for most of the shales studied. The profile behavior is very similar to that of the hydrocarbons, where maximum evolution occurs at temperatures of oil generation. Also listed in Figure 4 are the  $T_{\max}$  for the methylthiophene. The values, in °C, for the shales not shown are: Maoming II, 454; Woodford, 437; Fushun II, 446; Brotherson A, 487; NA-13, 436; Janus did not evolve methylthiophene. In general, these values are lower than the corresponding  $T_{\max}$  for total light organics generation listed in Table 2 from 4 to 32°C. However, there appears no grouping according to shale type. Excluding Brotherson A, LaLuna exhibited the smallest difference (4°C), while Wenzen exhibited the largest (32°C). Brotherson A is the exception, where  $T_{\max}$  is 3°C higher than the  $T_{\max}$  for total evolution. No other shale has exhibited this behavior. However, this may be due to Brotherson A being above the oil generation window. This evolution behavior for methylthiophene and other heteroatomic species has been seen before for AP-24, NA-13,<sup>5</sup> Maoming,<sup>2</sup> Kimmeridge,<sup>1</sup> and Fushun,<sup>2</sup> oil shales, and tar sands.<sup>6-8</sup>

Figure 5 shows the acetic acid evolution profiles for several shales studied. The  $T_{\max}$  values are also listed. The  $T_{\max}$  values, in °C, for the shales not shown in the figure are: NA-13, 391; Wenzen, 431; Fushun II, 442; Maoming II, 400; Woodford, 389; Janus and Brotherson A did not evolve any acetic acid. In general, the profiles are similar to the methylthiophene and hydrocarbon profiles except the acetic acid profiles tend to be broader, and the  $T_{\max}$  values are even lower than the corresponding  $T_{\max}$  values for methylthiophene. The difference between  $T_{\max}$  for acetic acid evolution and  $T_{\max}$  for total light organics evolution was as much as 74°C (Woodford).

The  $T_{\max}$  for acetic acid suggests these compounds may not be bound in the kerogen the same way the hydrocarbons are. The most obvious choice would be binding through a carbon oxygen bond. This should have less bond strength, and therefore a lower  $T_{\max}$ . Another possibility is the acid is entrained in the matrix, but due to donor-acceptor interactions, evolves at much higher temperatures than entrapped hydrocarbons (see bimodal distribution shown in Table 3, for example). These, and other alternatives are under investigation in our laboratories.

### Conclusions

1) For all shales studied, the hydrocarbon evolution behaved approximately the same. Evolution did not begin until approximately 300°C, reaching a maximum for total light organics hydrocarbon evolution ranging from 447 to 484°C (depended upon the shale), and rapidly decreasing to completion about 550°C.

2) The  $T_{\max}$  values for total light organics evolution for lacustrine shales were generally higher than for marine shale. The Maoming samples were the exceptions, acting more like marine than lacustrine shales.

3) The  $T_{\max}$  values for  $C_4H_9^+$  ion evolution were quite similar to the  $T_{\max}$  from total light organics evolution, and exhibited similar trends with shale type.

4) The hydrocarbons,  $C_2H_4$ ,  $C_2H_6$ ,  $C_3H_8$ , and  $C_4H_{10}$ , all exhibited individualized behavior. The  $T_{\max}$  for  $C_2H_4$  and  $C_2H_6$  evolution is much higher than the  $T_{\max}$  for total light organics evolution. In addition, type behavior is opposite that for total light organics evolution: lacustrine shales have  $T_{\max}$  for  $C_2H_4$  which is lower than that for marine shales. The  $T_{\max}$  values for  $C_3H_8$  and  $C_4H_{10}$  hydrocarbons were progressively lower in temperature for a given shale.

5)  $CO_2$  generation divided the shales into three categories: 1) high carbonate shales, which the evolution was dominated by the high temperature decomposition due to calcite, and dolomite, 2) low carbonate mineral shales, where the  $CO_2$  evolution exhibited no distinctive source, and 3) siderite shale which exhibited prominent  $CO_2$  evolution in the 450 to 475°C evolution range.

6)  $CO$  evolution occurs in two regimes: 1) a minor amount in the temperature range around 400 to 450°C which corresponding to kerogen breakdown and bitumen cracking, and 2) the major amount at high temperature due to char gasification reactions and water-gas shift equilibrium.

7) Hydrogen evolution exhibited a sharp maximum concurrent with kerogen breakdown and bitumen cracking. The majority of the hydrogen evolution occurred above 500°C due to char pyrolysis and mineral decomposition induced gasification reactions.

8) Heteroatomic compound behavior was typified by methylthiophene and acetic acid evolution, where the  $T_{\max}$  values were generally lower than the corresponding  $T_{\max}$  for total light organics evolution by as much as 32°C for methylthiophene, and even lower for acetic acid. In addition, the profiles were much broader than those observed for hydrocarbon and other heteroatom compound evolution.

### Acknowledgments

We thank Jack Clarkson for the Pyromat measurements and Armando Alcaraz for experimental assistance. This work was performed under the auspices of the U. S. Department of Energy by the Lawrence Livermore National Laboratory under contract number W-7405-ENG-48.

## References

1. Burnham, A. K., Braun, R. L., Gregg, H. R., and Samoun, A. M. 1987. *Energy and Fuels*, 1, 452.
2. Oh, M. S., Coburn, T. T., Crawford, R. W., and Burnham, A. K. 1988. 21st Oil Shale symposium, Beijing, China, Ed.
3. Wong, C. M., Crawford, R. W., and Burnham, A. K. 1984. *Anal. Chem.*, 56, 390-395.
4. Oh, M. S., Taylor, R. W., Coburn, T. T., and Crawford, R. W. 1988. *Energy and Fuels*, 2(1), 100-106.
5. Coburn, T. T., Crawford, R. W., Gregg, H. R., and Oh, M. S. 1987. 1986 Eastern Oil Shale Symposium, KECL86-158, 291-299.
6. Reynolds, J. G., Crawford, R. W., and Coburn, T. T. 1988. 1987 Eastern Oil Shale Symposium, KECL87-175, 101-108.
7. Reynolds, J. G., and Crawford, R. W. 1989. *Fuel Sci. Tech. Int'l.* 7(5), XXX.
8. Reynolds, J. G. 1989. 1988 Eastern Oil Shale Symposium, KECL 88-YYY, XXX.
9. Burnham, A. K., Oh, M. S., Crawford, R. W., and Samoun, A. M. 1989. *Energy and Fuels*, 3, 42-55.
10. Wong, C. M., Crawford, R. W., Barton, V. C., Brand, H. R., Neufeld, K. W., and Bowman, J. E. 1983. *Rev. Sci. Instrum.*, 54(8), 996-1004.
11. Crawford, R. W., Brand, H. R., Wong, C. M., Gregg, H. R., Hoffman, P. A., and Enke, C. G. 1984. 56, 1121-1127.
12. Campbell, J. H., Koskinas, G. J., Gallegos, G., and Gregg, M. 1980. *Fuel*, 59, 718-725.
13. Coburn, T. T. 1983. *Energy Sources*, 7(2), 121.
14. Burnham, A. K., Huss, E. B., and Singleton, M. F. 1983. *Fuel*, 62, 1199-1204.
15. Huss, E. B., and Burnham, A.K. 1982. *Fuel*, 61, 1188.
16. Burnham, A. K., Clarkson, J. E., Singleton, M. F., Wong, C. M., and Crawford, R. W. *Geochim. Cosmochim., Acta*, 46, 1242 (1982).
17. Reynolds, J. G., and Crawford, R. W. unpublished results.
18. Taylor, R. W., Coburn, T. T., and Morris, C. J. 1989. 1988 Eastern Oil Shale Symposium, KECL88-XXX, YYY.
19. Reynolds, J. G., Crawford, R. W., and Alcaraz, A. 1988. ACS Div. Petrol. Chem., Preprint, Los Angeles.
20. Campbell, J. H., and Burnham, A. K. 1978. Proceedings of the 11th Shale Oil Symposium, Colorado School of Mines: 242-259.

Table 1. Oil Shale Descriptions

Shale	Country	Type	Minerals
Kimmeridge	North Sea	Marine	Quartz, Illite, Pyrite (m), Feldspar (tr), Dolomite (tr), Kaolinite (tr)
Phosphoria	Montana	Marine	Quartz, Illite (m), Siderite (tr), Pyrite (tr), Siderite (tr), Kaolinite (tr)
Teisberget	Norway	Marine	Quartz, Siderite (m), Calcite (m), Pyrite (m), Illite (m), Kaolinite (m)
NA-13	Kentucky	Marine	Quartz, Illite (m), Kaolinite (tr), Feldspar (tr), Pyrite (tr)
Janus	Norway	Terrestrial/Marine	Quartz, Illite (m), Kaolinite (tr), Pyrite (tr)
Woodford	Oklahoma	Marine	Quartz, Pyrite (tr), Kaolinite (tr), Illite (tr), Smectite (tr)
LaLuna	Venezuela	Marine	Calcite, Quartz, Kaolinite (tr)
Wenzen	West Germany	Marine	Calcite, Quartz, Kaolinite (m), Illite (tr), Pyrite (tr)
Maoming I	China	Lacustrine	Quartz, Kaolinite, Siderite (tr), Illite (tr)
Maoming II	China	Lacustrine	Quartz, Kaolinite, Siderite (m), Illite (tr)
Fushun I	China	Lacustrine	Quartz, Kaolinite, Siderite (m), (Halite), Illite (tr), Smectite (tr)
Fushun II	China	Lacustrine	Quartz, Kaolinite, Siderite (m), (Halite)
AP-24	Colorado	Lacustrine	Dolomite, Quartz, Calcite (m), Feldspar (m), Analcime (m), Pyrite (tr), Illite (tr)
Government 33-4	Utah	Lacustrine	Quartz, Dolomite (m), Calcite (m), Illite (m), Analcime (tr), Kaolinite (tr)
Brotherson A	Utah	Lacustrine	Dolomite, Quartz, Calcite, Feldspar (m), Smectite (m), Analcime (m), Illite (tr)

Minerals in {} are tentative

(m) = minor components

(tr) = trace components

Table 2

Temperatures of Maximum Evolution for Total Light Organics,  $C_4H_9^+$  Ions From Hydrocarbons, and Total Pyrolysate From Pyromat Micropyrolyzer

Shale	Total Light, °C Organics	$C_4H_9^+$ , °C	Pyromat, °C
Kimmeridge	454	454	442
Phosphoria	465	461	441
Teistberget	466	469	456
NA-13	447	447	443
Janus	471	471	463
Woodford	463	460	444
LaLuna	462	466	444
Wenzen	467	459	444
Maoming I	465	465	451
Maoming II	466	463	na
Fushun I	473	476	462
Fushun II	471	472	na
AP-24	452	456	459
Government 33-4	478	474	452
Brotherson A	484	487	467

na = not available

Table 3

Volatile Hydrocarbon Evolution for Selected Shales at 10°C/min Heating Rate

Shale	$C_2H_4$ $T_{max}$ , °C	$C_2H_6$ $T_{max}$ , °C	$C_3H_8$ $T_{max}$ , °C	$C_4H_{10}$ $T_{max}$ , °C
Kimmeridge	480	465 (187)	453	433
Phosphoria	500	477	463	454
Teistberget	491	474 (225)	465	462
NA 13	480 (176)	458	446	437
Janus	495	482 (192)	480	471
Woodford	495	467	458	441
LaLuna	482	474	464	455
Wenzen	482	467	459	448
Maoming I	499	472 (200)	468	451
Maoming II	487	469	459	447
Fushun I	476	473 (250)	471	462
Fushun II	473	469 (244)	471	459
AP-24	478	470	469	461
Government 33-4	484	478	473	474
Brotherson A	489	488	493	479

Table 4

CH<sub>4</sub> Evolution for Selected Shales at 10°C/min Heating Rate

Shale	T <sub>max</sub> °C	Shoulder °C	Evolution cc/gr of TOC <sup>a</sup>
Kimmeridge	500	600	30.12
Phosphoria	520	588	62.24
Teist	513	610	(3.24) <sup>b</sup>
NA 13	500	460	60.59
Janus	509	600	(0.78) <sup>b</sup>
Woodford	504	584	48.54
LaLuna	512	-	55.73
Wenzen	482	600	38.40
Maoming I	500	600	30.52
Maoming II	490	582	30.46
Fushun I	487	590	39.96
Fushun II	479	590	41.06
AP-24	454	540	34.44
Government 33-4	500	620	82.46
Brotherson A	492	595	27.05

a. TOC = total organic carbon

b. cc/gr of shale

Table 5

## Hydrogen Evolution Behavior for Selected Oil Shales at 10°C/Min

Shale	T <sub>max</sub> , °C <sup>a</sup>	% Total Evolution <sup>b</sup>	Total Evolution cc/gr of TOC <sup>c</sup>
Kimmeridge	472	26.4	100.8
Phosphoria	494	16.5	137.5
Testberget	469	22.2	(9.5) <sup>d</sup>
NA-13	495	23.4	92.0
Janus	482	31.8	(4.26) <sup>d</sup>
Woodford	471	23.5	113.5
LaLuna	466	23.8	96.0
Wenzen	467	32.4	75.2
Maoming I	472	23.1	155.2
Maoming II	473	35.2	137.2
Fushun I	508	37.6	244.9
Fushun II	500	36.2	191.5
AP-24	470	36.5	117.0
Government 33-4	500	37.2	170.3
Brotherson A	515	42.1	168.0

a. T<sub>max</sub> for maximum at hydrocarbon evolution

b. % of total hydrogen evolution due to primary peak at hydrocarbon evolution

c. TOC = total organic carbon

d. cc/gr of shale



### Figures

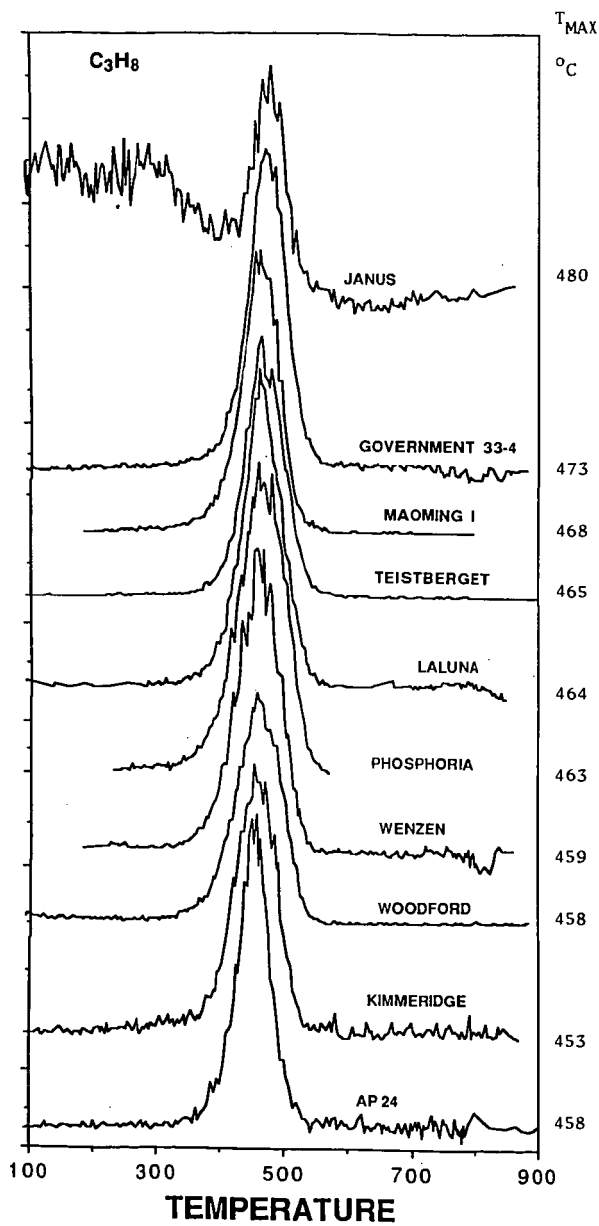
**Figure 1.**  $C_3H_8$  Evolution as a Function of Pyrolysis Temperature for Selected Oil Shales at the Heating Rate of  $10^\circ\text{C}/\text{min}$ .

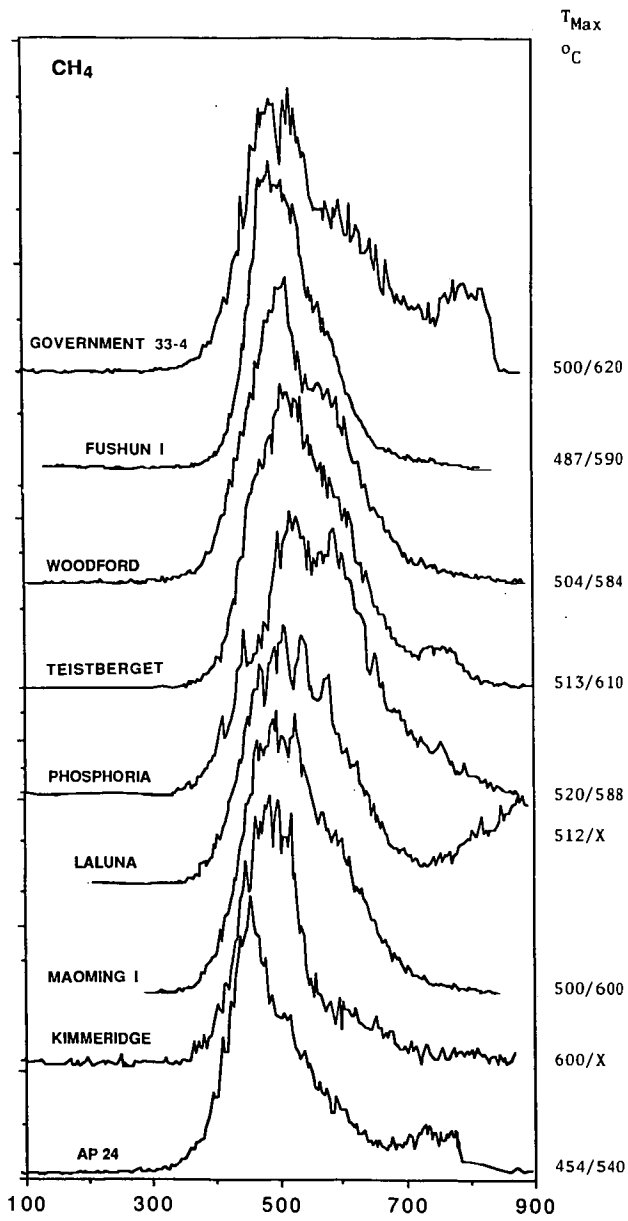
**Figure 2.** Methane Evolution as a Function of Pyrolysis Temperature for Selected Oil Shales at the Heating Rate of  $10^\circ\text{C}/\text{min}$ .

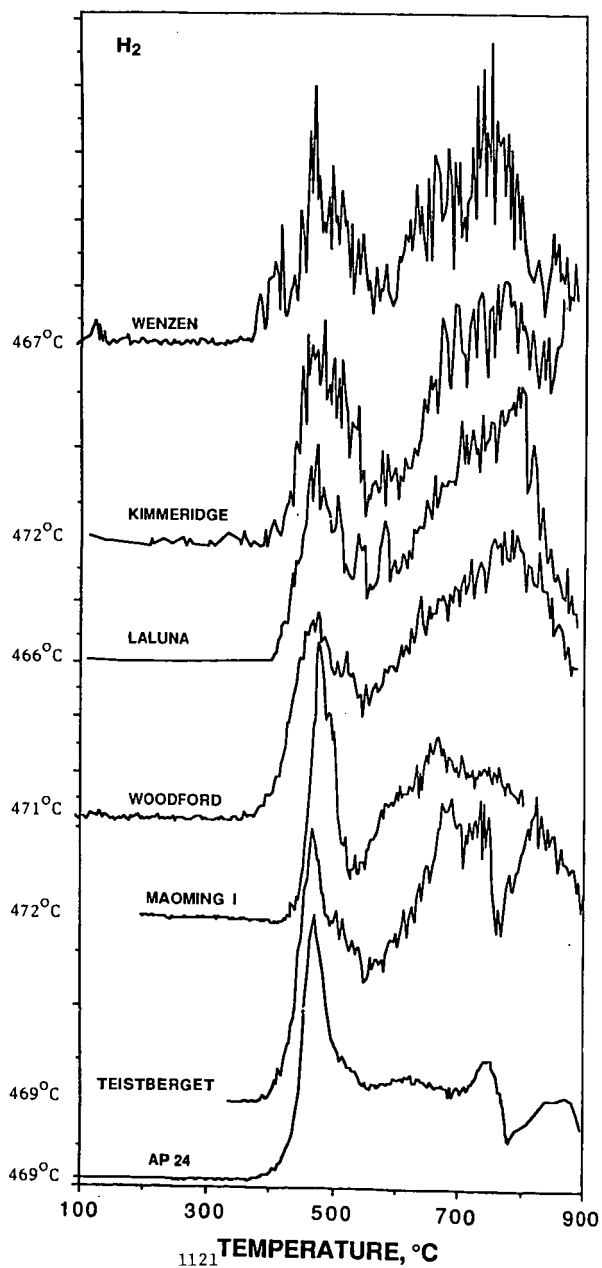
**Figure 3.** Hydrogen Evolution as a Function of Pyrolysis Temperature for Selected Oil Shales at the Heating Rate of  $10^\circ\text{C}/\text{min}$ .

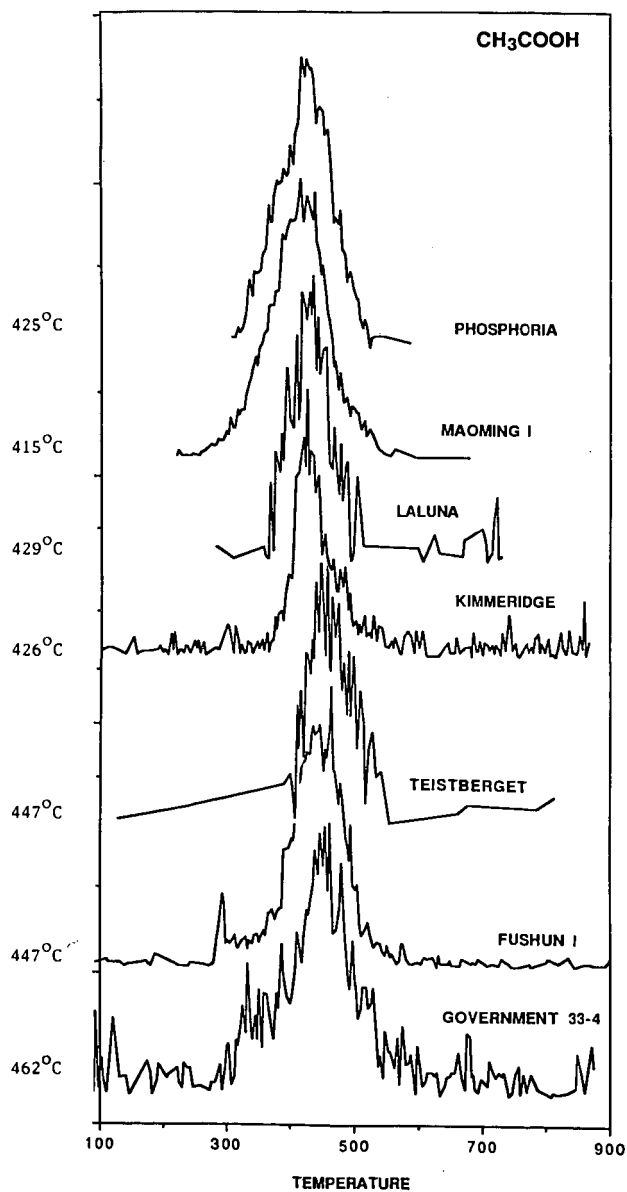
**Figure 4.** Methylthiophene Evolution as a Function of Pyrolysis Temperature for Selected Oil Shales at the Heating Rate of  $10^\circ\text{C}/\text{min}$ .

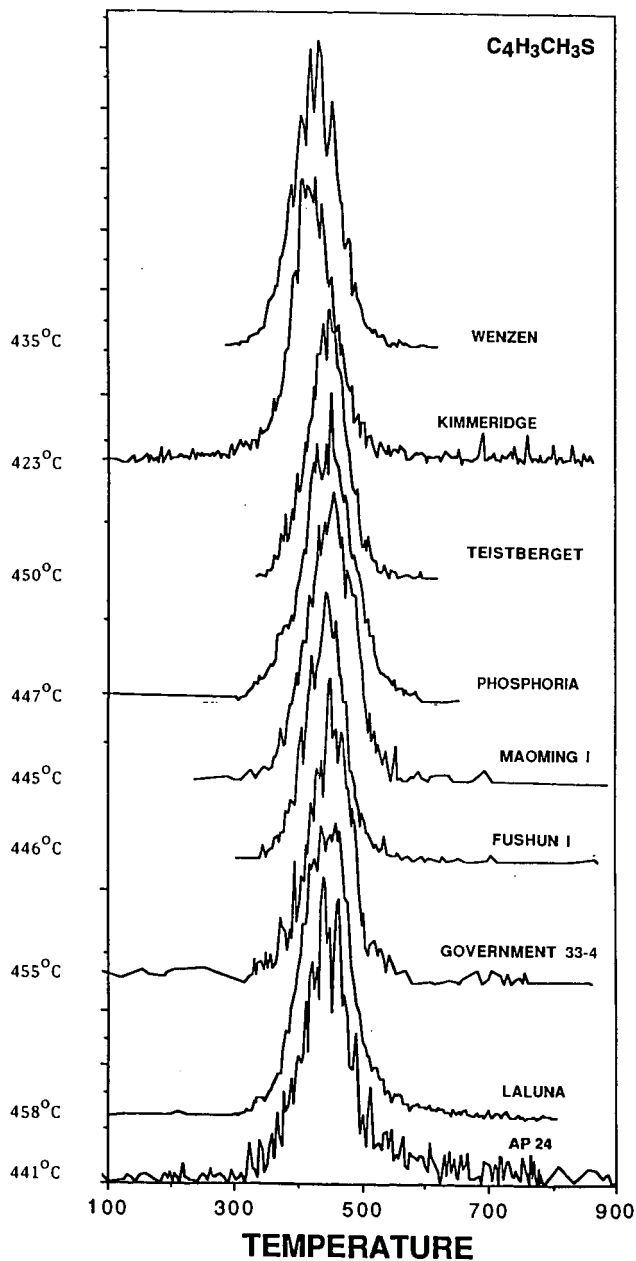
**Figure 5.** Acetic Acid Evolution as a Function of Pyrolysis Temperature for Selected Oil Shales at the Heating Rate of  $10^\circ\text{C}/\text{min}$ .











## THE EFFECTS OF CARBON DIOXIDE AND CATION CONTENT ON THE RAPID PYROLYSIS OF A LIGNITE

Robert B. Reuther  
U.S. Department of Energy  
Morgantown Energy Technology Center  
Morgantown, WV 26507-0880

Robert G. Jenkins  
College of Engineering  
University of Cincinnati  
Cincinnati, OH 45221-0018

### INTRODUCTION

With the development of newer, more advanced technologies, especially those operating at higher pressures and under rapid heating conditions, the significance of certain variables on the pyrolysis process has been raised. The potential for developing the large deposits of low rank coals in the central regions of the United States using these technologies is leading a drive to examine these variables under conditions which simulate or approximate the technologies, especially with regard to rapid heating. Two variables of potential consequence to the processing of these low rank coals are carbon dioxide atmosphere and inherent cation content.

Until recently, the effect that the cations which are associated with certain oxygen functionalities on low rank coals have on pyrolysis has been ignored. There has been considerable interest about their effects in catalytic gasification and on combustion, especially with regard to slagging and fouling. But, with the work of Schafer (1980), Tyler and Schafer (1980), Morgan (1983), and Franklin et al. (1983), information is coming to light that removal of these species has a potentially important consequence on the yield and distribution of the products of pyrolysis. Thus, this effect also has potential repercussions on conversion processes. Ignition phenomena may be affected, for instance. It may also be possible to take advantage of this effect to produce premium products such as high density liquid fuels through a commercial pyrolysis process. The pyrolysis of a lignite is carried out in both a raw and an acid-washed state in order to confirm these findings and extend them to higher pressures.

It is well known that  $\text{CO}_2$  reacts with coal via the Boudouard reaction. This reaction is considered unimportant on the time scale of rapid pyrolysis, however. On the other hand,  $\text{CO}_2$  is present as a gaseous product during gasification and combustion as well as during pyrolysis. When low rank coals are pyrolyzed, the production of  $\text{CO}_2$  can be significant through the destruction of large numbers of oxygen-containing moieties, especially carboxyl groups, present on such coals. It is hypothesized that the presence of  $\text{CO}_2$  in the pores of a devolatilizing coal may have an impact on pyrolysis through interactions with the primary pyrolysis products. The capability of the atmospheric pressure entrained-flow reactor (APR) at Penn State to provide primary and secondary flow streams of different gas composition coupled with the high pressure capabilities of the high pressure reactor (HPR), also at Penn State, allows a unique study of the effect of  $\text{CO}_2$  on rapid pyrolysis. This includes a focus on the interaction of  $\text{CO}_2$  on both raw and acid-washed coal samples.

## EXPERIMENTAL

### Coal Sample Selection and Preparation

The coal selected for this study is PSOC-412, a lignite from the Darco seam in eastern Texas. Samples of the coal were obtained from the Penn State Coal Sample Bank. The coal was ground, sieved and resieved in order to provide a narrow size distribution, and then stored in closed containers at ambient conditions. All solid particles pyrolyzed in the experiments were collected between U.S. Standard Sieve mesh sizes 140 and 200. The mean diameter of these particles as determined by the Rosin-Rammler technique is 79 microns. Portions of the sized coal sample were used to prepare acid-washed samples according to a method used by Morgan (1983). The acid-washing is performed to remove the cations which are associated with the carboxyl group functionality on low rank coals. Portions of the acid-washed samples were then used to prepare a small amount of calcium-exchanged samples, again according to a method used by Morgan (1983). This procedure replaces the hydrogen ions on the carboxyl groups with calcium ions.

### Pyrolysis Procedure

Pyrolysis experiments were conducted in the entrained-flow tube furnace systems at Penn State. The construction of these furnaces is based on a design by Badzioch and Hawksley (1970).

The APR was originally constructed by Scaroni (1979). Modifications to design and operating procedure subsequently evolved as documented by Maloney (1983) and Morgan (1983). Operation of the APR in this study follows the procedure described by Maloney (1983), except for one important difference. In these experiments, the hopper which held the solid sample prior to injection into the furnace was flushed continuously with the entraining gas. The reader is referred to Maloney (1983) for details of the operational procedure for the APR.

All the tests in the APR were conducted at atmospheric pressure and 900°C. Primary and secondary volumetric flowrates were held constant at approximately 1 and 35 standard liters per minute, respectively. Residence times were varied by placing a water-cooled collector probe coincident with the axis of the reactor at various distances from the injector tip. Residence times were determined using velocity models (see below). The solids flowrate was held constant at 1 gram per minute. The primary, or entraining, gas was He or CO<sub>2</sub>, and the secondary gas was either N<sub>2</sub> or CO<sub>2</sub>, depending on the test matrix. The Reynolds number for the total gas flow, calculated at 900°C, was in the neighborhood of 200 for N<sub>2</sub> and 350 for CO<sub>2</sub> (ignoring the small, primary gas flow of He when present).

The HPR was constructed to provide information about devolatilization studies under conditions more severe than those possible with the APR. It was designed to conduct pyrolysis at pressures to 1500 psig, temperatures to 1300°C, and in reducing atmospheres, including pure hydrogen. All experiments in the HPR were conducted at a nominal temperature of 900°C and at pressures of 200 psig. Due to the design of the HPR (and unlike the APR), the composition of the primary and secondary gas was necessarily the same for a given experiment. Pyrolysis was conducted in either He or in CO<sub>2</sub> atmospheres. The gas Reynolds number for the experiments in He ranged between 50 and 250. For CO<sub>2</sub> the gas Reynolds number varied between 500 and 2500. The solids flow rate was 1 gram per minute. As with the APR, residence times were determined using velocity models (see below). The reader is referred to Reuther (1988) for details of the pyrolysis procedure in the HPR.

### Residence Time Determination



The designs of the APR and the HPR make measurement of particle velocities and residence times extremely difficult. Instead, the distances over which the particles are entrained in the hot zones of the reactors (from injector tip to collector probe entrance) are transformed into residence times using a gas velocity model coupled with a particle velocity model. The approach used is similar to that used by Morgan (1983), Maloney (1983), and Tsai and Scaroni (1984) and was originally described by Morgan (1983) for the APR. The design of the reactors and the associated pyrolysis procedures cause the gases and entrained particles to enter the reaction zone under laminar plug flow conditions with development of a parabolic flow profile following immediately. The particles are injected with a cold entraining gas (primary stream) through nozzles which are inserted down the axes of the reactors. The much larger flow of hot secondary gas flows into the reactors through the annular region created by the nozzles.

The development of the parabolic profile, created by the drag of the gas along the wall, affects the gas velocity at every point in the reactor. Also, because the gas velocity is accelerating in the region in which the particles reside, the effect this has on particle velocities must subsequently be considered. The model used for the development of the parabolic flow profile was originally described by Campbell and Slattery (1963).

The equation governing particle velocity is derived by considering the forces acting on the entrained particle (Shu, 1978). This equation is numerically solved using the fourth-order Runge-Kutta computational technique. As a consequence of the solution, one can determine the distance the particles have fallen as a function of time, thus giving a residence time for the particles in the reactor.

#### Discussion of Particle Temperatures

The particles are assumed to be heated primarily by the hot, secondary gas stream. That is, radiation from the walls is believed to be an important mode of heat transport under the experimental design. Thus, the gas temperature is an important parameter in determining particle temperatures. For particle diameters less than 100 microns, the particle temperature closely follows the surrounding (primary) gas temperature, and the primary gas temperature is most sensitive to conductive heating by the secondary gas. These assumptions are in general agreement with previous studies on heat transfer in such systems (see e.g., Sass, 1972; Freihaut et al., 1977; Tsai and Scaroni, 1984; Suuberg, 1987; Hajaligol, 1987). Flaxman and Hallett (1987) have subsequently confirmed these results for an entrained-flow reactor which is based on the same design and operating principles as the APR at Penn State.

Thus, the most effective way to enhance particle heating rate is to use a low heat capacity, high thermal conductivity gas (i.e., a gas with a high thermal diffusivity) as the primary (cold) gas. This is equivalent to external heat transfer control for particle heating. It follows that particle temperatures and heating rates are higher when a gas with a high thermal diffusivity, such as He, is used as the primary gas than when a gas with a lower thermal diffusivity, such as N<sub>2</sub>, is substituted. It is argued, based on the above statements, that when a lower thermally diffusive gas is substituted for a higher in the primary stream, the particle temperature is the same or lower for a given residence time. Thus, if the weight loss is found to be higher, such increased weight loss must be due to something other than temperature. In this work, the controversy concerning the temperature of the particles during pyrolysis in a dilute-phase, entrained-flow environment is avoided as much as possible by accepting the preceding arguments and those which follow. When drawing conclusions from comparisons among pyrolysis experiments it is assumed that (1) any two experiments run under the same conditions of gas flow and composition but with different 'kinds' of solid particles (raw versus acid-washed, etc.) have equivalent particle heating rates and final temperatures and (2) when the gases are different but the particles are the same, it is pointed out which particles may have heated up faster and/or to

a final higher temperature. The overriding assumption is that particles which heat up faster and to a higher temperature lose weight more rapidly and that higher pyrolysis temperatures result in higher weight losses. It should be noted that it is not assumed that the particles pyrolyze isothermally.

#### Weight Loss Analysis

All char samples were subjected to a moisture analysis followed by a proximate ash analysis in order to determine weight lost during a pyrolysis run. The procedures used were slight modifications of those specified by the American Society for Testing Materials (ASTM) Test D3173-73, Moisture in the Analysis Sample of Coal and Coke, and Test D3174-73, Test for Ash in the Analysis Sample of Coal and Coke. The procedural modification in each case was to substitute approximately 0.5-gram samples for the suggested 1.0-gram sample amounts in order to conserve sample. All samples were done in duplicate. If any of the duplicate values differed significantly (i.e., outside of the recommended ASTM limits of 0.5%), further samples were ashed until the discrepancy was resolved. The amount of organic material that was devolatilized in each experiment, i.e., the weight lost, was calculated from the proximate ash values of the devolatilized sample and the undevolatilized sample using the "ash tracer" technique, as described by Scaroni (1979).

### RESULTS AND DISCUSSION

#### Weight Loss Results

Weight loss results are presented below as a function of the presence of cations and CO<sub>2</sub> atmosphere.

#### Effect of Cations

The effect of the presence of cations on rapid pyrolysis was studied in both the APR and the HPR. Pyrolysis was performed on raw, acid-washed, and, to some extent, calcium-exchanged coal samples. The results of these experiments in various atmospheres are plotted in Figures 1, 2, 3, 4, and 5.

Figures 1, 2, and 3 are from experiments at atmospheric pressure (i.e., in the APR). Figure 1 shows the results of pyrolysis on raw, acid-washed, and calcium-exchanged coals in He/N<sub>2</sub>. (This nomenclature (e.g., 'He/N<sub>2</sub>') is followed throughout this discussion. The first gas listed is the primary or entraining gas, and the second gas is the secondary flow gas.) Figure 2 presents weight loss results on the same three solid samples in He/CO<sub>2</sub>. Figure 3 displays the results of pyrolysis in CO<sub>2</sub>/CO<sub>2</sub> on the raw and the acid-washed samples, only. There is a dramatic drop in weight loss for the calcium-exchanged sample in both He/N<sub>2</sub> (Figure 1) and He/CO<sub>2</sub> (Figure 2) at longer residence times. There appears to be a small drop in weight loss for the raw sample compared to the acid-washed sample in He/N<sub>2</sub>, which is most significant at intermediate residence times. The results in He/CO<sub>2</sub> are similar to those in He/N<sub>2</sub>. In CO<sub>2</sub>/CO<sub>2</sub> (Figure 3), where only raw and acid-washed samples were compared, there is again a drop in weight loss in going from acid-washed to raw sample. In this case the difference appears to be more significant than in He/N<sub>2</sub> or He/CO<sub>2</sub>, however, and occurs throughout the range of residence times examined.

The preliminary conclusions to be drawn from these three figures are:

1. Removal of cations appears to have had a small impact on weight loss with this coal, being most significant at intermediate to longer residence times.

2. Replacement of hydrogen ions on the carboxyl groups by calcium ions to a saturation level had a dramatic effect on weight loss.
3. The presence of  $\text{CO}_2$  in the pores at the onset of pyrolysis has an added effect on weight loss from the acid-washed coal sample compared to the raw sample.

Figures 4 and 5 are the results of experiments in the HPR at 200 psig. Figure 4 presents the weight loss results of raw and acid-washed samples in He/He. Figure 5 shows the pyrolysis of these same two samples in  $\text{CO}_2/\text{CO}_2$ . The weight loss of the raw sample in He/He is again reduced compared to the acid-washed sample except for the longest residence time recorded, which occurs at what appears to be an asymptotic or ultimate rapid pyrolysis yield under these conditions. When these same two samples are pyrolyzed in  $\text{CO}_2/\text{CO}_2$ , however, only at the earlier residence times considered is there a noticeable reduction in weight loss for the raw sample compared to the acid-washed sample. At the longer residence times, as with Figure 4, weight losses are virtually identical.

Thus, as with the APR results, the presence of cations appears to reduce weight losses during the earlier periods of rapid pyrolysis in an inert atmosphere (He). The weight loss reduction is more significant at this higher pressure and may be an indication that the species which are contributing to reduced weight loss are themselves affected by mass transfer considerations. If, for example, the cations are retarding weight loss by attaching themselves to potential volatile species which, in turn, makes it more difficult for them to exit the particle under mass diffusion considerations (increased molecular weight and size), then additional constraints to mass transfer, such as increased pressure, could enhance this effect. Or, if the cations reduce weight loss via cracking reactions, then mechanisms which impede mass transfer, such as increased pressure, will allow more time for this process to occur. Both of these possible roles for cations as weight loss inhibitors are discussed by Morgan (1983) and others. What is also significant, however, is that ultimate weight loss is virtually the same in both Figures 4 and 5. This indicates that most (if not all) of the mass associated with the initially formed volatiles eventually exits the particle given enough time, although it may not have the same molecular structure as when first formed because of one or more secondary reactions. ("Initially formed volatiles" is taken to mean those species which are originally solid but which exist in the vapor state, however transiently, under the conditions of the experiment upon the initial breaking of a bond which had held it to the rest of the solid matrix.)

Finally, Figure 5 reinforces the impression that the presence of  $\text{CO}_2$  is having an effect on weight loss. To confirm this, the pyrolysis results were replotted to show the effect of atmosphere for each coal sample (raw and acid-washed) in each reactor (APR and HPR).

#### Effect of Atmosphere

Figure 6 shows the results of the pyrolysis of the raw coal in the APR in He/ $\text{N}_2$ , He/ $\text{CO}_2$ , and  $\text{CO}_2/\text{CO}_2$  atmospheres. The weight loss in He/ $\text{N}_2$  is less than in He/ $\text{CO}_2$  or in  $\text{CO}_2/\text{CO}_2$  over most of the residence time measured. The particle temperature in He/ $\text{N}_2$  and in He/ $\text{CO}_2$  should be very nearly the same from a thermodynamic standpoint. This is because the primary gas is the same in the two cases, and the heat content of the secondary gases are identical (the volumetric flowrates and volumetric heat capacities are the same). Thus, the increased weight loss in He/ $\text{CO}_2$  over He/ $\text{N}_2$  is clearly due to some interaction of  $\text{CO}_2$  with the devolatilizing sample. Also, heat transfer in  $\text{CO}_2/\text{CO}_2$  should be lower than in He/ $\text{CO}_2$  based on the thermal diffusion arguments. Thus, it might be expected that a higher weight loss would occur in  $\text{CO}_2/\text{CO}_2$  over He/ $\text{CO}_2$  on a temperature-adjusted basis at the earlier residence times.

Figure 7 shows the results of the pyrolysis of the acid-washed sample in He/ $\text{N}_2$ , He/ $\text{CO}_2$ , and  $\text{CO}_2/\text{CO}_2$  atmospheres. Again, there is a difference in weight loss between

He/N<sub>2</sub> and He/CO<sub>2</sub> which can only be due to the interaction of CO<sub>2</sub> and the devolatilizing sample. Weight loss in CO<sub>2</sub>/CO<sub>2</sub> exceeds even that in He/CO<sub>2</sub> at early residence times, but by the longest residence time measured the weight losses have converged. Weight lost from He/N<sub>2</sub> is still below that from the other two gas compositions for the longest residence time measured, however, which is in contrast to Figure 6.

Figures 8 and 9 show the results of experiments conducted in the HPR. Figure 8 shows pyrolysis of raw coal in He/He and CO<sub>2</sub>/CO<sub>2</sub>. Figure 9 shows pyrolysis of acid-washed coal in He/He and CO<sub>2</sub>/CO<sub>2</sub>. The pyrolysis of raw coal in He/He has significantly less weight loss than in CO<sub>2</sub>/CO<sub>2</sub> over the intermediate residence times. Again, heat transfer in CO<sub>2</sub>/CO<sub>2</sub> may be poorer than in He/He, thus reinforcing the weight loss differences. Again, at long residence times the weight losses converge.

Figure 9 shows a smaller difference in weight loss over intermediate times with ultimate weight losses again converging. Still, some effect of CO<sub>2</sub> over intermediate times even with the acid-washed sample is evident.

It is instructive to first go back to Figure 8 to explain the role of CO<sub>2</sub> in rapid pyrolysis. Even at the earliest recorded residence time (~76 milliseconds), weight lost in the CO<sub>2</sub> atmosphere exceeds weight lost in He by nearly a factor of two. By 135-140 milliseconds residence time, weight loss in CO<sub>2</sub> is more than twice that in He. Eventually, however, the weight losses converge at the longest residence times. Since it has been shown that the cations inhibit weight loss over this same time interval and at this pressure, the CO<sub>2</sub> must somehow be counteracting this effect. It is hypothesized that CO<sub>2</sub> could be tying up the calcium, perhaps converting CaO (calcium oxide, a known tar cracker) to CaCO<sub>3</sub> (calcium carbonate, inert to cracking reactions?). (The increase in char weight due to the carbonate formation is only on the order of 1% assuming all the calcium in the raw coal were carbonated. Thus, it should not significantly affect the weight loss analysis). Alternatively, the CO<sub>2</sub> could be enhancing weight loss by affecting active sites on the char directly. For example, active carbon sites on the pyrolysing char (created by initial bond breaking to form volatiles) could have CO<sub>2</sub> adsorb onto them. This would make the sites unavailable for reattachment or cracking of previously formed volatiles. Finally, CO<sub>2</sub> could be stabilizing reactive volatiles through the formation of carboxyl groups at the reactive sites in a Kolbe-type reaction (Morrison and Boyd, 1973, p. 804). This would allow the volatiles to more readily escape the devolatilizing char matrix. Again, it is instructive that the weight losses converge, strongly implying that all (or nearly all) of the potential volatiles exit the devolatilizing lignite given enough time, although not necessarily in the same molecular form. Also, the weight loss increase due to CO<sub>2</sub> is probably not due to the Boudouard reaction. More needs to be said about the second point. If the Boudouard reaction were important, it is likely that increased ultimate volatile matter would appear in CO<sub>2</sub> atmospheres. This is not evident. Also, most measures of the Boudouard reaction show it to be much slower than the weight loss rates considered here.

A further indication that the Boudouard reaction is not important is illustrated in Figure 9. The effect of CO<sub>2</sub> on acid-washed coal is not as strong as it is with raw coal. An increase in weight loss over intermediate times is apparent, however. If increased weight loss were due primarily to the Boudouard reaction, one would expect to see the differences in weight losses evident in Figure 8 as well as increased weight loss at the longest residence time. On the other hand, a comparison between Figures 8 and 9 does show that much of the effect of CO<sub>2</sub> in the HPR experiments is probably due to the direct effect of CO<sub>2</sub> on the cations.

The results of Figures 6 and 7 can thus be explained as follows. Figure 7 shows the effect of the presence of CO<sub>2</sub> in the absence of the complication from cations. Initial weight loss in He/CO<sub>2</sub> exceeds that in He/N<sub>2</sub> because of a stabilizing effect of CO<sub>2</sub> on developing active sites on the char and/or stabilization of volatiles. An additional increase in weight loss is seen in CO<sub>2</sub>/CO<sub>2</sub> because of the presence of CO<sub>2</sub> in the pores at the onset of pyrolysis.

Figure 6 also shows that  $\text{CO}_2$  has a strong stabilizing effect on initially formed volatiles. Additional weight loss due to the initial presence of  $\text{CO}_2$  in the pores is masked by the inhibitory effect of cations and by (again) the somewhat scattered nature of the  $\text{He}/\text{CO}_2$  data from the raw coal sample.

It has been hypothesized that  $\text{CO}_2$  may be blocking the effect of calcium to retard weight loss through formation of  $\text{CaCO}_3$ . In the HPR the partial pressure of  $\text{CO}_2$  is sufficient to tie up calcium as the carbonate. In the APR the equilibrium condition is not as well-defined because of the proximity of the operating condition to the calcination condition. In  $\text{He}/\text{CO}_2$  atmospheres there would not be enough concentration of  $\text{CO}_2$  in the pores initially to block the effect of the cations. The indication that a  $\text{CO}_2$  atmosphere does enhance weight loss under these conditions thus supports an argument that  $\text{CO}_2$  must diffuse to the surface of the coal particle rather quickly and then penetrate at least part way into the macropore space where it accelerates weight loss by blocking the effect of cations and/or by stabilizing tar/char. In the  $\text{CO}_2/\text{CO}_2$  experiments in the APR, there is probably a high enough pressure of  $\text{CO}_2$  in the pores initially to tie up the cations, thus accelerating weight loss. In addition, there is  $\text{CO}_2$  present for stabilization as the first bonds in the coal matrix break, thus leading to the even greater weight loss at early residence times in this atmosphere compared to  $\text{He}/\text{CO}_2$ , which is most clearly seen in Figure 7.

#### Gas Analyses

Most experiments in the HPR had gas analyses of the product gas performed using a dedicated gas chromatograph (Carle 158S Automated Gas Chromatograph). The only peaks to appear which were large enough to measure quantitatively were those associated with  $\text{CO}_2$ ,  $\text{CO}$ ,  $\text{CH}_4$ ,  $\text{C}_2\text{H}_6$ , and  $\text{C}_2\text{H}_4$ . It was somewhat surprising that little measurable hydrogen appeared. In addition, the  $\text{C}_2\text{H}_4$  peak was unresolvable during pyrolysis experiments in  $\text{CO}_2$  atmospheres due to its proximity to the  $\text{CO}_2$  peak.

The following items are noteworthy. First, the  $\text{C}_2\text{H}_4$  content of the product gas generally increased with increased weight loss or residence time during pyrolysis of both the raw and acid-washed samples in  $\text{He}$ . There was significantly more  $\text{C}_2\text{H}_4$  produced at similar weight losses from the raw sample than from the acid-washed sample. This is consistent with the observation that there appears to be more cracking-type reactions occurring in the presence of the cations, since  $\text{C}_2\text{H}_4$  is often a by-product of the cracking of larger species.

Second, both the  $\text{CO}$  and the  $\text{CO}_2$  content are higher for comparable weight losses when cations are present during pyrolysis in  $\text{He}$ . This is consistent with the observations of Schafer (1980) in again giving a role to the cations, primarily as calcium, in creating additional carbon oxides from reactions with oxygen-containing species other than carboxyl.

#### SUMMARY AND CONCLUSIONS

There are two likely roles that the cations could be playing to inhibit weight loss. First, they could be attaching themselves to potential volatile species, and thereby inhibiting their release by retarding mass diffusion. Second, potential volatile species could be cracked by the cations, thereby depositing at least some of the cracked material back onto the solid surface, at least temporarily. A third possibility, also suggested by Morgan (1983) in his study, is strongly discounted here. That is that the cations are inhibiting the release of volatiles by blocking pore exits. Although this could be a minor contribution, the indication that the presence of  $\text{CO}_2$  reverses the effect of the cations argues strongly against pore blockage being a major impediment to volatiles release. This same argument also applies, although somewhat more weakly, to the supposition that cations inhibit pyrolysis via mass diffusion. In addition, gas analyses were shown to substantiate

the hypothesis that the cations affect weight loss through cracking reactions. It was also hypothesized that flooding the pores of the devolatilizing coal with  $\text{CO}_2$  inhibited the cracking reactions by tying up the calcium ions in a nonreactive form.

It was also shown that the presence of  $\text{CO}_2$  enhances weight loss even in the absence of cations. This is most likely due to chemical interactions between  $\text{CO}_2$  and the developing char surface and/or between  $\text{CO}_2$  and reactive volatile species. The  $\text{CO}_2$  is hypothesized to stabilize reactive sites on the surface, which in turn prevents cracking of volatiles, and/or to cap reactive volatile species such as hydrogen is believed to do during hydropyrolysis.

#### REFERENCES

- Badzioch, S. and P. G. W. Hawksley (1970), "Kinetics of Thermal Decomposition of Pulverized Coal Particles", Ind. Eng. Chem. Process Des. Dev., 9, 521-530.
- Campbell, W. D. and J. C. Slattery (1963), "Flow in the Entrance of a Tube", J. Basic Eng., Trans. Am. Soc. Mech. Eng., 41-46 (March, 1963).
- Flaxman, R. J. and W. L. H. Hallett (1987), "Flow and Particle Heating in an Entrained Flow Reactor", Fuel, 66(5), 607-611.
- Franklin, H. D., R. G. Cosway, W. A. Peters and J. B. Howard (1983), "Effects of Cations on the Rapid Pyrolysis of a Wyodak Subbituminous Coal", Ind. Eng. Chem. Process Des. Dev., 22, 39-42.
- Freihaut, J. D., A. A. Leff and F. J. Vastola (1977), "The Combined Influence of Chemical and Physical Factors Upon Coal Particle Temperature Profiles During Rapid Heating Pyrolysis", Am. Chem. Soc., Div. Fuel Chem. Prepr., 22(1), 149-157.
- Hajaligol, M. R., W. A. Peters and J. B. Howard (1987), "Intraparticle Heat Transfer Effects in Coal Pyrolysis", Am. Chem. Soc., Div. Fuel Chem. Prepr., 32(3), 8-23.
- Maloney, D. J. (1983), "Effects of Preoxidation on Rapid Pyrolysis Behavior and Resultant Char Structure of Caking Coals", Ph.D. Thesis, Fuel Science, The Pennsylvania State University, University Park, PA.
- Morgan, M. E. (1983), "Role of Exchangeable Cations in the Pyrolysis of Lignites", Ph.D. Thesis, Fuel Science, The Pennsylvania State University, University Park, PA.
- Morrison, R. T. and R. N. Boyd (1973), "Organic Chemistry", 3rd Ed., Allyn and Bacon, Boston, MA.
- Reuther, R. B. (1988), "The Effects of Pressure, Carbon Dioxide, and Cation Content on the Rapid Pyrolysis of a Lignite", Ph.D. Thesis, Fuel Science, The Pennsylvania State University, University Park, PA.
- Sass, A. (1972), "The Garrett Research and Development Process for the Conversion of Coal into Liquid Fuels", paper presented at the 65th Annual AIChE Meeting, New York, NY.
- Scaroni, A. W. (1979), "Kinetics of Lignite Pyrolysis in Fixed-Bed and Entrained-Flow Reactors", M.S. Thesis, Fuel Science, The Pennsylvania State University, University Park, PA.

Schafer, H. N. S. (1980), "Pyrolysis of Brown Coals. 3. Effect of Cation Content on the Gaseous Products Containing Oxygen from Yallourn Coal", Fuel, 59, 295-301.

Shu, M.-T. (1978), "Concurrent Two-Phase Flow of Gas and Coal Particle Mixtures", M.S. Thesis, Drexel University, Philadelphia, PA.

Suuberg, E. M. (1987), "The Significance of Transport Effects in Determining Coal Pyrolysis Rates and Yields", Am. Chem. Soc., Div. Fuel Chem. Prepr., 32(3), 51-58.

Tsai, C. Y. and A. W. Scaroni (1984), "Pyrolysis During the Initial Stages of Pulverized Coal Combustion", Twentieth Symp. (Int.) on Combustion, The Combustion Institute, Pittsburgh, PA, 1455-1462.

Tyler, R. J. and H. N. Schafer (1980), "Flash Pyrolysis of Coals: Influence of Cations on the Devolatilization Behaviour of Brown Coals", Fuel, 59, 487-494.

#### ACKNOWLEDGMENTS

This work was funded in part by the U.S. Department of Energy under contract EX-76-C-01-2030.

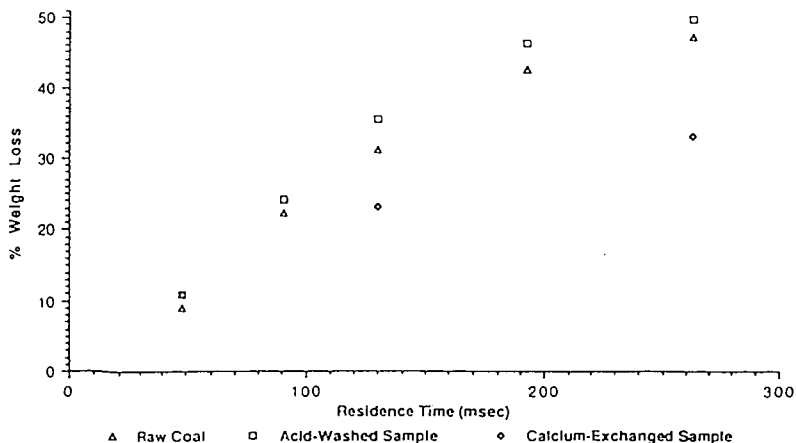


Figure 1 The Effect of Cations on Pyrolysis, P=0 psig, He/N<sub>2</sub> Atmosphere

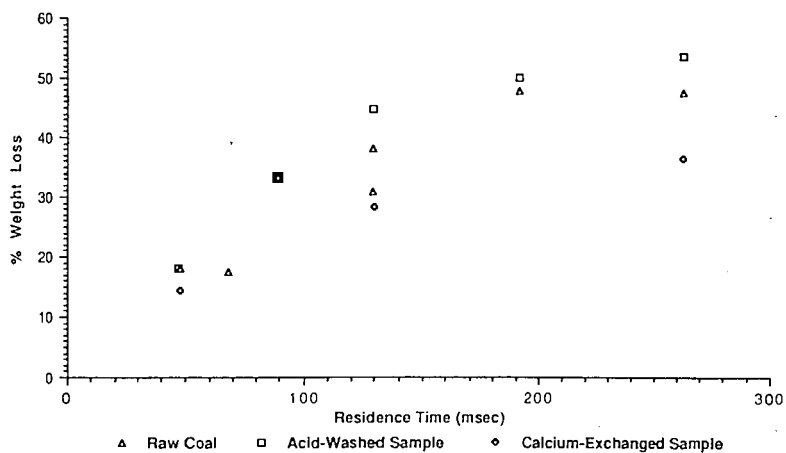


Figure 2 The Effect of Cations on Pyrolysis, P=0 psig, He/CO<sub>2</sub> Atmosphere

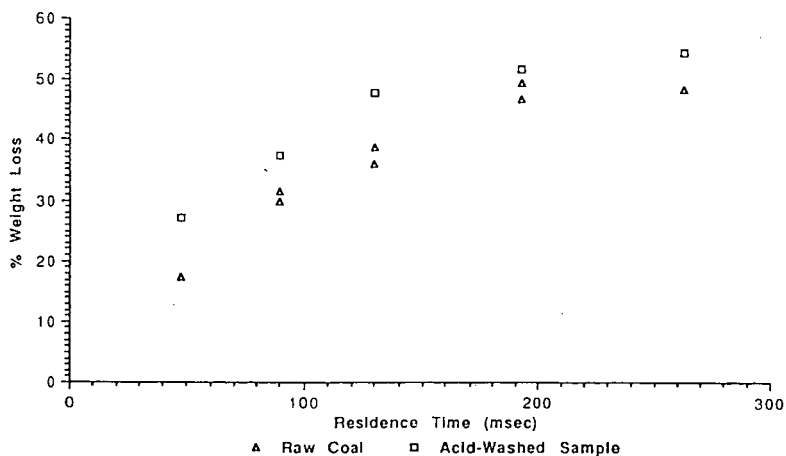


Figure 3 The Effect of Cations on Pyrolysis, P=0 psig, CO<sub>2</sub>/CO<sub>2</sub> Atmosphere



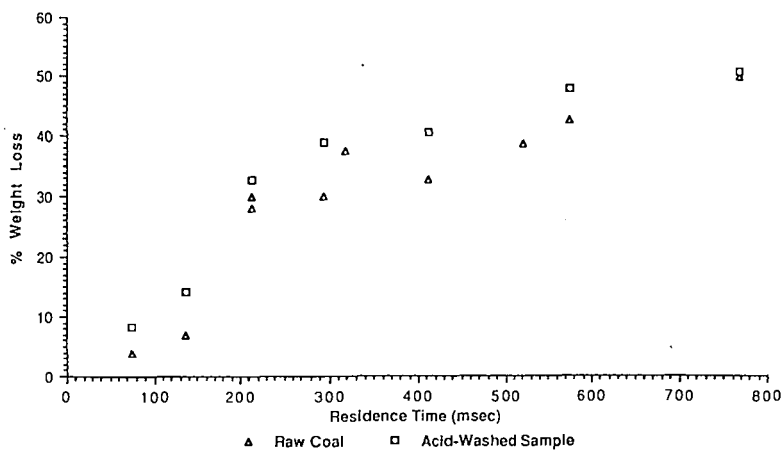


Figure 4 The Effect of Cations on Pyrolysis, P=200 psig, He/He Atmosphere

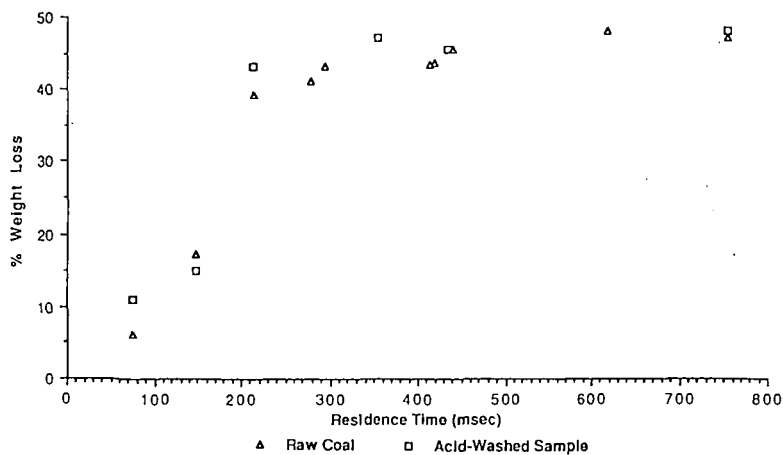


Figure 5 The Effect of Cations on Pyrolysis, P=200 psig, CO<sub>2</sub>/CO<sub>2</sub> Atmosphere

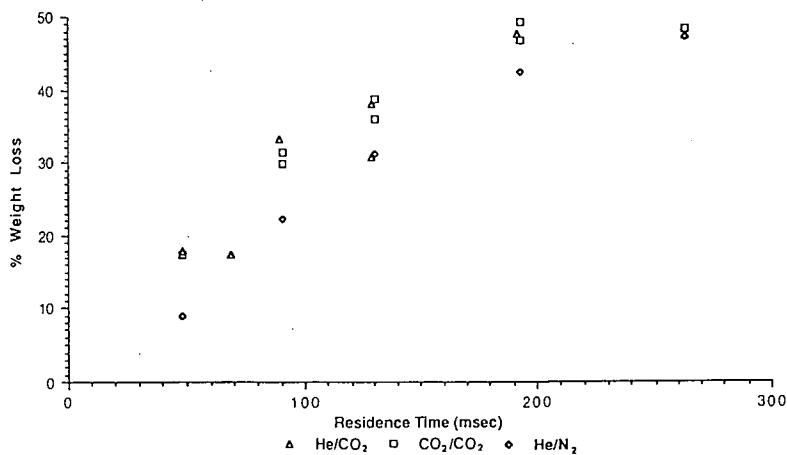


Figure 6 The Effect of Atmosphere on Pyrolysis, P=0 psig, Raw Coal

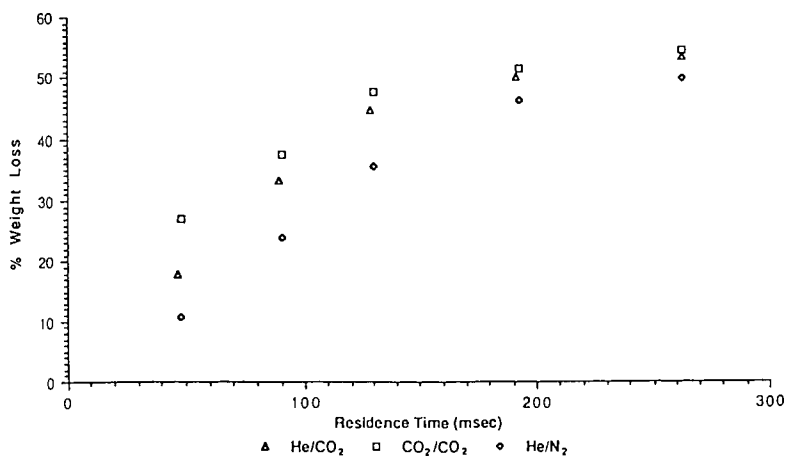


Figure 7 The Effect of Atmosphere on Pyrolysis, P=0 psig, Acid-Washed Sample

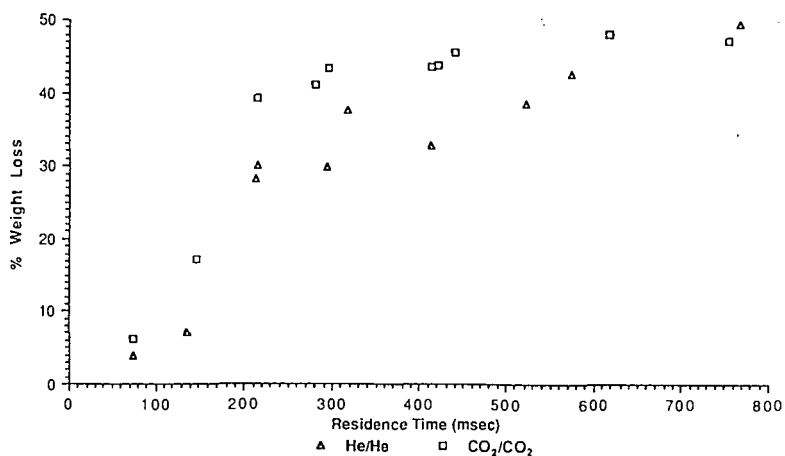


Figure 8 The Effect of Atmosphere on Pyrolysis, P=200 psig, Raw Coal

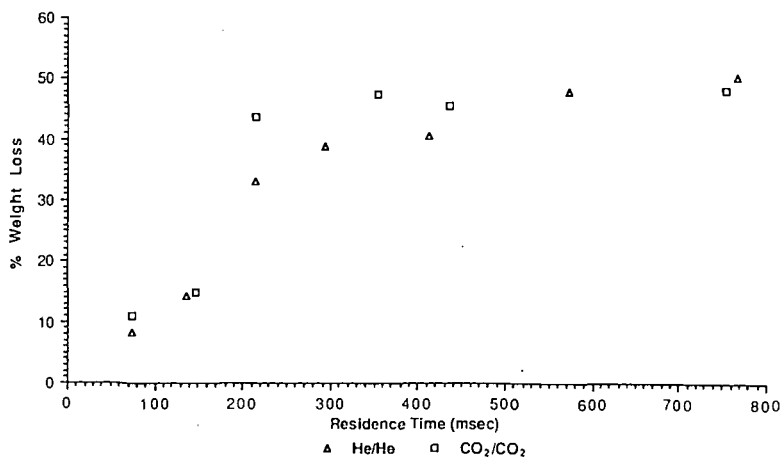


Figure 9 The Effect of Atmosphere on Pyrolysis, P=200 psig, Acid-Washed Sample

## A COMPARISON OF UINTA BASIN, UTAH CRUDE OIL AND BIODEGRADED PRODUCTS

H. J. Hatcher<sup>1</sup>, K. B. Barrett<sup>1</sup>, K. Taghizadeh<sup>2</sup>,  
D. R. Quigley<sup>1</sup>, H. L. C. Meuzelaar<sup>2</sup>

### INTRODUCTION

The Green River Formation of Wyoming, Colorado, and Utah contains a significant portion of the world's oil shale (1). In addition, the area contains large deposits of tar sands and bituminous rocks, particularly in the Uinta Basin of Utah. Commercialization of coal, oil and gas deposits are important in the economy of Utah.

The Green River Formation is considered to be rather unique in character because it has been spared extensive disruption from the forces of temperature, pressure, and fracture (2). It has probably been more thoroughly studied by organic geochemists than any other formation in the world. However, the microbiology of the formation and its relationship to hydrocarbon transformations has not been extensively investigated.

The importance of microbial activity to fossil fuel hydrocarbon transformations is widely recognized (3). The metabolic activities of the microflora over a period of time can contribute to changes in pH and redox potential which, in turn, can significantly alter the geological environment (3). These changes need not be directly involved with hydrocarbons. Sulfate-reducing anaerobic bacteria do not metabolize hydrocarbons but can, in the presence of oxygen-consuming aerobic bacteria, actively reduce sulfate to sulfide (4). A case in point is growth of anaerobic *Desulfovibrio* sp. under growth of aerobic *Beggiatoa* sp. Thiobacilli can also contribute significantly to acidification of the environment. As a consequence, sulfur and metal availability can be significantly altered thereby changing the course of subsequent hydrocarbon-generating events.

Most investigators have found that the first hydrocarbons removed from crude oil by bacteria are n-alkanes followed by alicyclics, aromatics, and acyclic isoprenoids (5). Disagreement exist regarding biodegradation of steranes and to a lesser extent hopanes. Nevertheless, it is agreed that biodegradation of a crude oil leads to another oil having a lower API gravity and greater chemical stability (6). Some evidence has been presented that suggests that paraffinic crude oils are precursors of heavy to medium-gravity naphthenic crude oils (7). Observations indicate that primary paraffinic crude oils are expelled from deep source beds. Before, during, or after a generally upward migration, the paraffinic crude is transformed microbiologically into a naphthenic crude oil. In another investigation (8) biodegradation decreased API gravities of a group of common-source crude oils and tar sands 8-fold, increased sulfur 3-fold, and metal content 6-fold. Hydrocarbon content was altered with n-alkanes, isoprenoids light aromatics, and light thiophenes completely removed (8). In

1. Idaho National Engineering Laboratory, Center for Bioprocessing Technology and Biotechnology Unit. P.O. Box 1625, Idaho Falls, ID 83415.
2. Center for Micro-Analysis and Reaction Chemistry, University of Utah, Salt Lake City, Utah.

in severely degraded samples steranes were partially removed while triaromatic steranes and diasteranes were resistant to biodegradation. In a long term study of the effects of a fuel spill on the microbiology of an agricultural soil, biodegradation of the fuel was achieved (9) after three years. Coryneform bacteria and certain fungi were responsible for hydrocarbon degradation. The most active fungi in hydrocarbon degradation were Aspergillus and Penicillium sp.

## EXPERIMENTAL

### Sample Sources and Procedures

Samples of oil shale were collected from Hell's Hole Canyon in Utah, the C-b Tract Mine in Colorado, and the Southman Canyon area in Utah. Tar sands were collected from Asphalt Ridge in Utah. Gilsonite was collected from the Bonanza area of Utah. Petroleum samples were collected from the Red Wash Oil Field and the Altamont-Bluebell Oil Field in Utah. Solid samples were placed in plastic bags and water samples in sterile plastic tubes. The samples were transported to the Idaho National Engineering Laboratory Research Center in Idaho Falls, Idaho for microbiological studies. Samples designated for pyrolysis gas chromatography/mass spectrometry studies were sent to the Center for Micro-Analysis and Reaction Chemistry, University of Utah, Salt Lake City, Utah.

### Microbial Isolation, Identification and Maintenance Procedures

Samples of solid materials were carefully cleaned and the inner surfaces exposed. The inner surfaces were scraped and the scrapings placed on trypticase-soy agar medium in petri dishes. Aqueous samples were streaked on the medium. The medium was incubated aerobically and anaerobically at about 25°C for seven to fourteen days. Colonies were examined for morphology and slides were prepared for microscopic examination. After culture purity was assured, cultures were maintained on trypticase-soy agar.

Identification of cultures was based on API Procedures (API Laboratory Products, 8114 Trans Canada Highway, Suite B, St. Laurent, Quebec H4S 1M5).

### Model Compound Utilization Procedures

A basal salts medium was added to screw-cap test tubes and sterilized by autoclaving at 121°C for 20 minutes. The compound to be investigated (Table 2) was added at 0.1% concentration after sterilization. The tubes were inoculated using a pure culture and incubated at room temperature as roller tubes at about 10-20 revolutions per minute. The tubes were examined daily for growth as shown by turbidity in the tubes. Response was graded as 1+ to 4+ (poor to best).

### Petroleum Utilization Studies

These were carried out much as the model compound investigation except that cultures were prepared in Erlenmeyer flasks and petroleum was added at 1% concentration. Cultures were incubated at 30°C on a rotary shaker operating at about 20 revolutions per minute.

### Pyrolysis Gas Chromatography/Mass Spectrometry (Py GC/MS)

Py GC/MS analyses were carried out at the University of Utah Center for Micro-Anlysis and Reaction Chemistry, University of Utah, Salt Lake City, Utah.

A basic Curie-point Py GC/MS technique was used with a Curie-point filament temperature of 610°C(10). The gas chromatography was conducted using a Hewlett-Packard 5890 instrument with a 15 meter DB-5 column heated at 40° to 320°C, 10°C/minute. An ion-trap detector was used and a Finnigan Mass Spectrometer.

## RESULTS AND DISCUSSION

### Microbiological Characterization

Genera of bacteria isolated from samples are listed in Table 1. Coryneform bacteria are not listed individually because the members of this group are difficult to classify. At present it is believed that four genera are represented: Arthrobacter, Corynebacterium, Nocardia, and Rhodococcus. However verification is still pending. Only coryneform bacteria could utilize hydrocarbons and heterocyclic compounds provided as carbon sources. All coryneforms were isolated from within bitumen-containing rock and none from water associated with the rock.

Cell counts of coryneforms were at the  $10^4$  to  $10^5$  cfu/gm level. Table 2 shows the performance of the six coryneform isolates which grew best on the model substrates. Not all coryneforms could utilize these materials. In some cases, growth of the isolate was difficult to maintain and some were lost, consequently, some tests could not be completed. It is noteworthy that t-butylcyclohexane was poorly utilized. Apparently, the branched alkyl substituent on the cyclohexane ring inhibited utilization. The result is in accord with experiences with such compounds as branched alkyl benzene sulfonates, notorious in the detergent industry for resistance to biodegradation. The position of the methyl group on the alkyl chain may be significant. Isoprenoid substituents on structures such as steranes are apparently degraded.

During the course of this work, it was observed that certain differences existed between microorganisms and their capability to grow on the model compounds. The wild strains of coryneform bacteria were generally more capable of growing on the unusual substrates provided than laboratory strains obtained from commercial culture collections. The point is significant for those who would study fossil fuel degradation by microorganisms. Figure 1a compares the growth of a laboratory Arthrobacter with oil shale isolate OS-2 on pristane. Figure 1b compares laboratory Nocardia sp. with oil shale-isolate OS-2 and gilsonite-isolate G2 on the heterocyclic compound ethyl nipecotate. Growth was measured by turbidity. In Figure 2a and 2b, a laboratory strain of Arthrobacter is compared with gilsonite-isolate G2 growing on pristane. Growth was measured by oxygen consumption. OS-2, the wild strain, in these and other growth experiments, required several days of adaption before rapid growth occurred. The response suggested that enzyme induction was necessary. In contrast, G-2, also a wild strain, consistently showed immediate growth on substrates provided suggesting constitutive enzyme formation.

### Petroleum Biodegradation

Figure 3a is a GC/MS chromatogram of a waxy crude oil (Bluebell Control), Figure 3b is a chromatogram of the petroleum residue of the oil after degradation by the oil shale-isolate OS-3. The residue primarily consists of isoprenoid components, with almost complete removal of n-alkanes. Figure 3c is a chromatogram of the petroleum residue after degradation by an isolate from oil shale kerogen. The residue consists of isoprenoid and triterpenoid components. Similar results for biodegradation are shown in GC/MS chromatograms for the waxy Red Wash petroleum in Figure 4a. The undegraded petroleum is primarily paraffinic in character. Degradation by the oil shale-isolate OS-3 (Figure 4b) and the gilsonite-isolate G-2 (Figure 4c) gave residue chromatograms showing primarily triterpenoid compounds remaining.

Figure 5a is a GC/MS chromatogram of an asphaltic petroleum. Degradation of the oil by the tar sand-isolate TS-8 (Figure 5b) and the oil shale-isolate OS-2 (Figure 5c) gave residues containing similar components. Pristane and phytane (shown in the 795 and 860 positions) were only partially degraded. The same is true for triterpenoids in the 1400-1600 position. The large peak in the 1760 region corresponds to perhydro- $\beta$ -carotene (2). This substance seems resistant to biodegradation.

### CONCLUSION

Coryneform bacteria can play a significant role in crude oil biodegradation. The capability of these bacteria for hydrocarbon degradation varies between individual bacteria and between the specific forms of hydrocarbon attacked. Tri- and tetraterpenoid compounds are resistant to degradation. Consequently, oil degraded in the laboratory tends to assume the mature character observed under natural conditions.

### ACKNOWLEDGMENT

This work was supported under Contract No. DE-AC07-76ID01570 from the U.S. Department of Energy to the Idaho National Engineering Laboratory/EG&G Idaho, Inc.

### REFERENCES

1. W. E. Reed. 1977. "Molecular Compositions of Weathered Petroleum and Comparison with Its Possible Source." Geochemica et Cosmochemica Acta 41:237-247.
2. M. T. Murphy, A. McCormic, G. Eglinton. 1967. "Perhydro- $\beta$ -Carotene in the Green River Shale." Science 157:1040-1042.
3. J. R. Hills, G. W. Smith, E. V. Whitehead. 1970. "Hydrocarbons from Fossil Fuels and Their Relationships with Living Organisms." Journal of the Institute of Petroleum 56(549):127-137.
4. A. M. Jobson, F. D. Cook, D. W. S. Westlak. 1979. "Interaction of Aerobic and Anaerobic Bacteria in Petroleum Biodegradation." Chemical Geology 24:355-365.

5. N. S. Goodwin, P. J. D. Park, A. P. Rawlinson. 1981. "Crude Oil Biodegradation under Simulated and Natural Conditions." Advances in Organic Geochemistry. John Wiley and Sons. pp. 650-658.
6. N. J. L. Bailey, A. M. Jobson, M. A. Rogers. 1973. "Bacterial Degradation of Crude Oil: Comparison of Field and Experimental Data." Chemical Geology 11:203-221.
7. G. T. Philippi. 1965. "On the Depth, Time, and Mechanism of Petroleum Generation." Geochemica Et Cosmochemica Acta 29:1021-1049.
8. D. E. Miiller, A. G. Holba, W. B. Hughes. 1984. "Effects of Biodegradation on Crude Oils." AAPG Studies in Geology #25. Research Conference. Santa Maria, CA. October 29-November 2, 1984, pp. 233-241.
9. J. Oudot, P. Fusey, D. E. Abdelouahid, S. Haloui, M. F. Roquebert. 1987. "Capacités Degratives de Bacteries et de Champignons Isolés Contamine par un Fuel." Can. J. Microbial. 33:232-243.
10. H. L. C. Meuzelaar, W. Windig, J. H. Futrell, A. M. Harper, S. R. Larter. 1982. "Pyrolysis Mass Spectrometry and Multivariate Analysis of Several Key World Oil Shale Kerogens and Some Recent Alginites." ASTM Special Technical Publication 902. T. Aczel, Ed. pp. 81-105.



TABLE 1. IDENTIFICATION OF BACTERIAL ISOLATES

<u>Source</u>	<u>Group or Genus</u>	<u>Number of Isolates</u>
Oil shale	Coryneform, <u>Aeromonas</u> <u>Flavobacterium</u> <u>Streptomyces</u>	7
Tar sands	Coryneform	6
Gilsonite	Coryneform	3
Oil shale-Mine water	<u>Pseudomonas</u> <u>Aeromonas</u> <u>Flavobacterium</u> <u>Desulfovibrio</u> <u>Beggiatoa</u>	6

TABLE 2. MODEL COMPOUND

Isolated Bacteria ( <i>Coryneform</i> )	Cyclohexanol	Ethyl Nipeotate	Ethyl-1 Methylnipeotate	Hexadecane	Pristane	Tert-butyl Cyclohexane
G-2	±	4+	3+	3+	2+	-
OS-2	3+	2+	2+	3+	3+	±
OS-3	3+	ND	ND	ND	3+	ND
TS-6	3+	-	-	1+	-	1+
TS-7	2+	ND	ND	3+	2+	±
TS-8	2+	ND	ND	ND	3+	ND

---

 ND = Culture not viable for test.

Figure 1 is a line graph showing the growth of *Arthrobacter* #15590 and *OS2* on different carbon sources over a period of 10 days. The y-axis represents Absorbance at 450 nm, ranging from -0.005 to 0.195. The x-axis represents Time in days, ranging from 0 to 10. The legend indicates three data series: Controls (solid circles), *Arthrobacter* #15590 (solid squares), and *OS2* (solid triangles). The carbon sources are labeled as  $(CH_3)_2CH(CH_2)_3CH(CH_3)_2$ ,  $(CH_2)_3CH(CH_3)$ , and  $(CH_2)_3CH(CH_3)_2$ .

Time (Day)	Controls (●)	<i>Arthrobacter</i> #15590 (■)	<i>OS2</i> (▲)
0	0.000	0.000	0.000
3	0.000	0.140	0.060
4	0.000	0.195	0.145
5	0.000	0.190	0.150
6	0.000	0.155	0.185
7	0.000	0.150	0.180

Figure 1 is a line graph showing the growth of *Nocardia* #21145 in the presence of various inhibitors. The y-axis represents Absorbance at 430 nm, ranging from -0.005 to 0.195. The x-axis represents Time in days, ranging from 0 to 9. Four data series are plotted: Controls (solid circles, dashed line), G2 (solid squares, solid line), *Nocardia* #21145 (solid triangles, solid line), and OS2 (solid inverted triangles, solid line). The Controls series remains relatively flat near 0.195. The G2 series shows a steady increase in absorbance over time. The *Nocardia* #21145 series shows a slight increase in absorbance over time. The OS2 series shows a significant increase in absorbance, peaking around day 6 and then slightly decreasing. A chemical structure of the inhibitor is shown in the top right corner.

Time (Day)	Controls (●)	G2 (■)	<i>Nocardia</i> #21145 (▲)	OS2 (▼)
0	0.195	0.000	0.000	0.000
3	0.195	0.060	0.015	0.045
4	0.195	0.095	0.025	0.135
5	0.195	0.105	0.030	0.145
6	0.195	0.115	0.025	0.155
7	0.195	0.110	0.025	0.145

# RESPIROMETER STUDIES

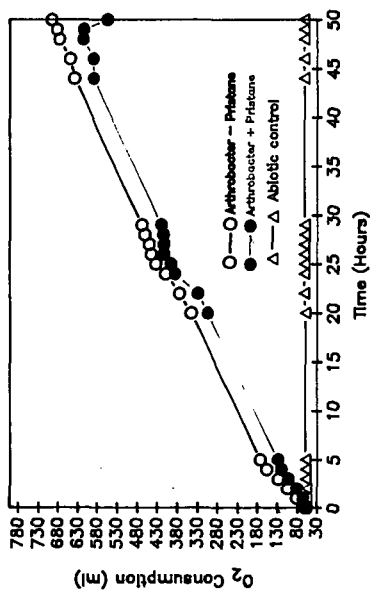


Figure 2a

# RESPIROMETER STUDIES

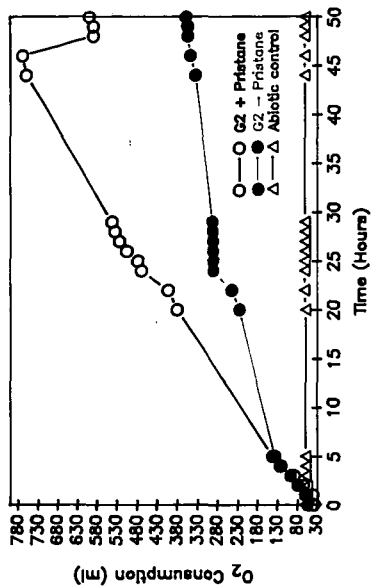


Figure 2b

FIGURE 3

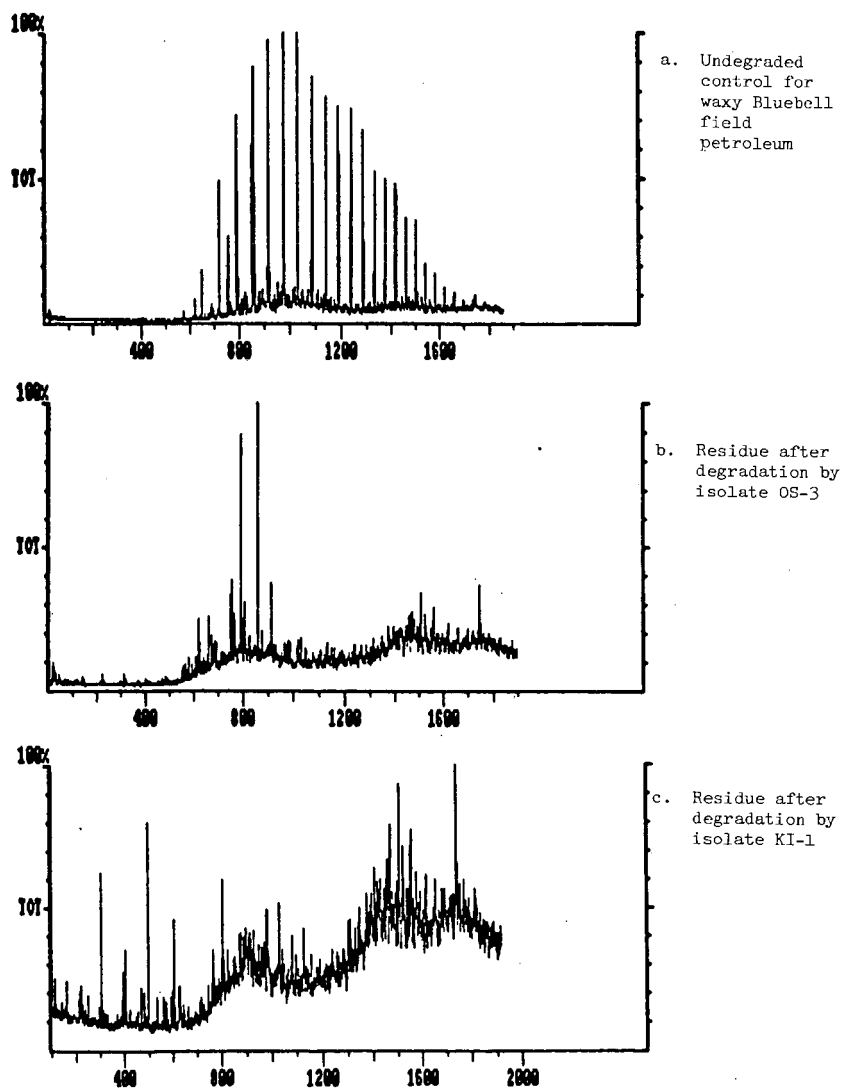


FIGURE 4

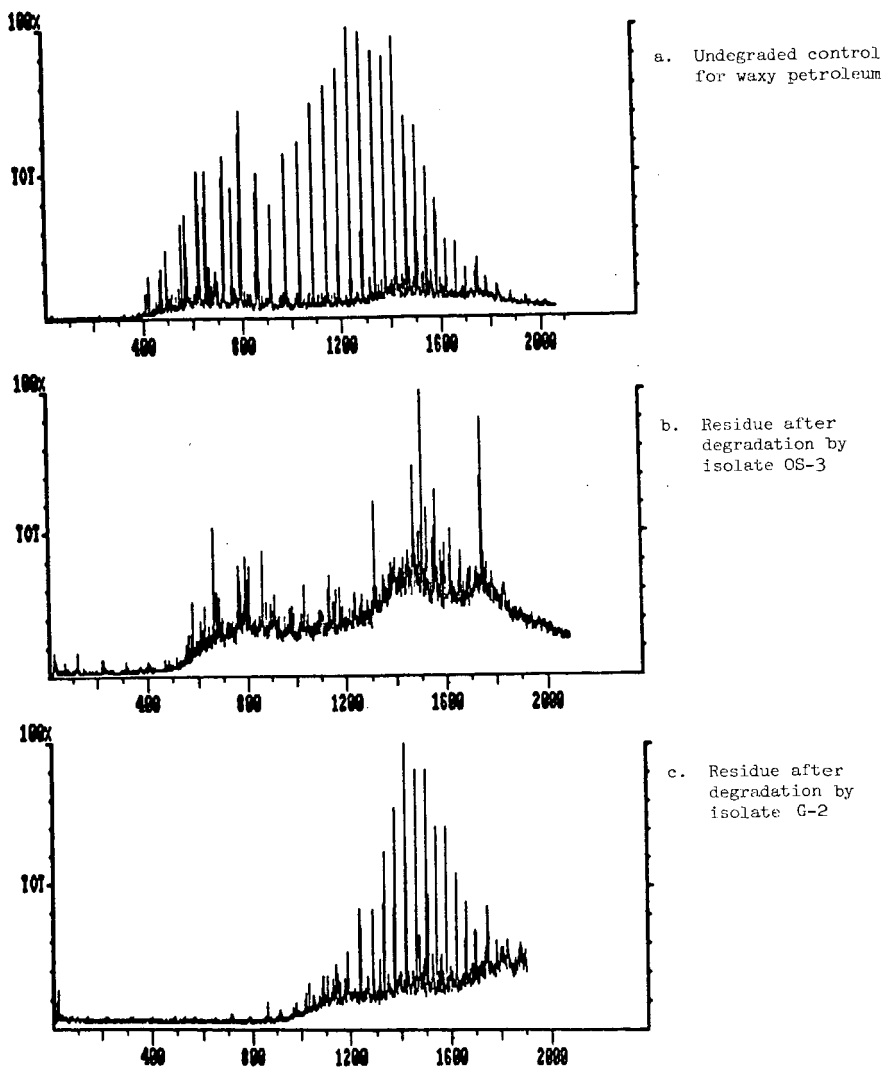
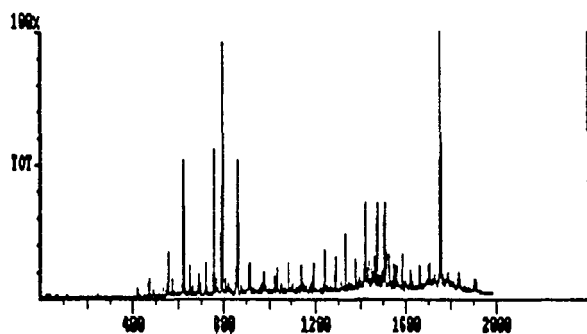
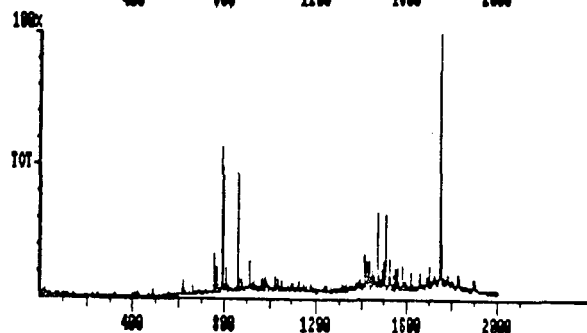


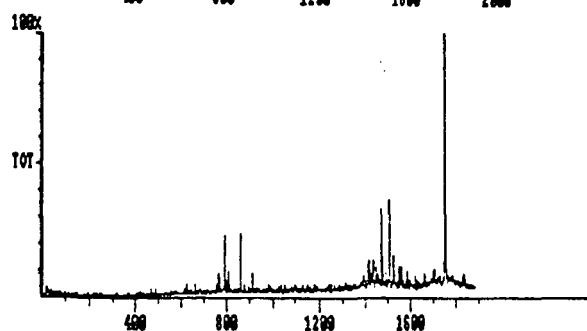
FIGURE 5



a. Undegraded control  
for asphaltic  
petroleum



b. Residue after  
degradation by  
isolate TS-8



c. Residue after  
degradation by  
isolate OS-2

ALL-SYNTHETIC DIESEL FUEL FROM ATHABASCA BITUMEN:  
PROPERTIES, TESTING AND OPERATING EXPERIENCE

by

W.W. Almdal, R.P. Kirchen, S.N. Lau, E.C. Sanford  
Syncrude Canada Limited  
Box 5790, Station L, Edmonton, Alberta, Canada, T6C 4G3

and

S.J. Hinkle  
Detroit Diesel Corporation  
13400 Outer Drive West  
Detroit, Michigan, 48239-4001

Syncrude Canada Ltd. operates an integrated oil sands plant in the Athabasca region in northern Alberta. Oil sand is extracted and the separated bitumen is upgraded by a combination of coking and hydrocracking processes. Distillates are hydrotreated to produce synthetic crude oil, which is shipped by pipeline to refineries for further processing and blending. Daily production of synthetic crude oil is approximately 23,850 m<sup>3</sup> or 150,000 bbl (1988 daily average production).

Throughout the plant, 125,000 liters/day of diesel fuel are being consumed. Heavy haulers (170 tons, 33 units) operating in the oil sands mine are major consumers, although an appreciable amount of fuel is also used to power a variety of other units. Historically, diesel fuel was purchased from commercial sources. An opportunity to reduce operating cost by substituting the purchased fuel (45 million liters/year) with a plant derived synthetic material was identified.

Typically, during the production and refining of diesel fuel, its chemical and physical properties are modified and adjusted by blending in order to meet specifications. The blending option was not available in this case where the direct use of an existing plant stream was proposed. Although several studies and tests were reported on synthetic materials of this type, more information was needed for assuring the economical and reliable operation of a large fleet under extreme temperature conditions.

Chemical, physical and ignition properties of the all-synthetic fuel were measured and compared to conventional fuels and to diesel fuel specifications. The fuel was also tested on heavy-duty diesel engine test rigs. Following this fuel evaluation study, the fuel was approved by Syncrude for use on its equipment at its oil sands plant. The switch to all-synthetic diesel fuel took place in the spring of 1988.

Properties, test results and operating experience with Athabasca bitumen derived diesel fuel will be discussed.

#### Results and Discussion

Athabasca bitumen is extracted from the sand matrix by the hot water process. It is then subjected to thermal cracking in fluid cokers (1). Distillate cuts are individually hydrotreated and the hydrotreated streams are blended to form synthetic crude oil (SCO) product. This is transported by pipeline to



refineries for further processing and blending. Properties of the bitumen feedstock and of the synthetic crude oil are shown in Table 1.

The stream identified for diesel fuel use is derived from a unit which prepares naphtha needed as a diluent in the extraction process. The diluent preparation unit uses a hydrotreated distillate as feed and separates the naphtha diluent. It is the bottoms stream of this distillation which was identified as a potential diesel fuel. Although a distillation residue, this stream is quite light and highly refined, due to its prior processing. It is typically blended back into the synthetic crude oil product. Hence, the proposed fuel is readily available as part of normal plant operation (Figure 1). Properties of this stream are shown in Table 2, together with those of typical commercial diesel fuels. The corresponding boiling curves are shown in Figure 2.

The boiling curve of the all-synthetic material (Figure 2) is similar to that of commercial winter diesel fuel, which is the lighter of the three seasonal fuel blends typically used in northern Alberta (Table 2). Because this stream is, in fact, a "by-product" of an existing operating unit (diluent preparation unit), it is not practical to seasonally adjust the boiling range.

Chemical and physical properties of this stream reflect its synthetic origin and its processing history. In this list, deviations from specifications or from typical values observed for conventional fuels are indicated: + indicates an advantage for the synthetic fuel. Specifically, the following properties reflect the origin: low cloud (+) and low pour points (+), low cetane number (-) and low aniline point (-). Conversely, the following properties reflect the hydrotreating severity: low values for ash, sulfur, corrosion, acidity, carbon residue and water/sediments, good color (all +) and low viscosity (+/-).

Of these properties, two are discussed in greater detail: cetane number and viscosity.

Current Canadian diesel fuel specifications (Table 3) and minimum engine manufacturer's requirements for cetane number is 40 (ASTM D613); the measured value for the all-synthetic fuel was 31-32. However, the cetane number of a fuel can be improved by doping with an ignition improver. Typically, an alkyl nitrate is used, although other compound classes were also studied (2). Response of the all-synthetic fuel to the addition of a commercial ignition improver is shown in Figure 3. A cetane number of 40 was reached by doping the synthetic fuel with approximately 0.3% ignition improver. This is in the same range as measured in an earlier study (3) with Athabasca derived diesel fuel. The proposed "1990 Canadian specifications" (4) are met by doping with only 0.15 wt% additive.

Viscosity of a fuel is often linked to its lubricating properties or lubricity. The fuel injection system of a diesel engine relies on the fuel it is pumping for lubrication.

Viscosity of the material under investigation was low and similar to that of commercial winter fuel. Low viscosity is usually equated with low lubricity. However, there are reports (5, 6) indicating that this proportionality might only hold for fuels of similar origin, composition and processing history.

Therefore, it was desirable to obtain a direct, viscosity-independent measure of the lubricating properties of this material. This was done by using the "Ball on Cylinder Lubricity Evaluator" (BOCLE) test method (7, 8). Lubricity of the synthetic material was similar to that of commercial winter diesel fuel. Response of the synthetic fuel to the addition of lubricity improver was also

investigated. Lubricity of intermediate season fuel was reached by doping with approximately 50 ppm of commercial lubricity improver.

In summary, many of the properties of the all-synthetic fuel are similar to those of commercial diesel fuels, and in particular to winter diesel. In fact, only properties related to cetane number and lubricity are at variance. And, as shown, the fuel also responds well to the addition of additives, if this is desired. However, is the addition of additives needed, and what are the benefits obtained by doing so?

By definition, fuel specifications represent a body of chemical and physical properties that has proven sufficient to qualify a fuel. These correlations between chemical/physical data and engine performance are based on a database obtained with conventional fuels. Is the same set of chemical/physical data also sufficient (or is the full set indeed needed) to qualify a material of 100% synthetic origin? The significance of this issue can probably best be appreciated by considering the fact that even the specifications are subject to occasional review (4).

In the absence of a database covering operating experience with synthetic fuels, and to address the issue of actual engine performance, the properties of this fuel were reviewed with engine manufacturers. Based on these discussions, an engine durability test was performed at Detroit Diesel Corporation's test facility. In addition, dynamometer tests combined with emission measurements were also carried out. For the durability test, one cylinder bank of a 149 series heavy-duty engine was operated on synthetic fuel, whereas the other bank was run on conventional fuel. The engine was fully performance instrumented and was operated at various power settings, including elevated power output for more than 500 hours. Also, to obtain data truly indicative of the all-synthetic fuel, it had been agreed to run this test without any additive.

As part of the durability test, the engine was disassembled and its components were inspected. Overall, test results were definitely in favor of the all-synthetic fuel, in terms of operating parameters, as well as component wear. As indicated above, this test was run with no additives.

Eleven mode steady state emission tests revealed a measurable reduction in  $\text{NO}_x$  and CO for the all-synthetic fuel as compared to #2 diesel fuel. Further emission testing with the all-synthetic fuel and #1 diesel fuel on the U.S. Federal Transient Emission Test showed a 10% reduction in brake specific particulates. However, for this transient cycle test with the lighter #1 diesel fuel, the measurable reduction in  $\text{NO}_x$  and CO was nullified; indeed, the trend reversed itself and a slight increase in CO and  $\text{NO}_x$  was measured.

Since the all-synthetic fuel has very little sulfur content (0.01 wt %), the  $\text{SO}_x$  emissions from engines burning the all-synthetic fuel were consistently lower and this was likely a contributor to the lower brake specific particulate measurement. Low sulfur content also has a beneficial impact on sulfur induced corrosion of engine components.

Brake specific fuel consumption (LB/BHP-HR) was moderately higher (2%) for the all-synthetic fuel relative to #1 diesel fuel. This is likely related to the fuel spray of the less viscous all-synthetic fuel. This hypothesis is supported by test runs on various internal injector components which yielded a greater sensitivity to these changes than did #1 diesel fuel or kerosene. However, addition of ignition improver additives may provide an offset for this slight performance loss.

In view of the extreme low temperatures ( $-40^{\circ}\text{C}$ ) measured at the plant site during winter, cold weather performance of any diesel fuel used at this location is of crucial significance. Two factors to be considered here are the fluidity and the ignition properties of the fuel at these temperatures. Good performance in both areas is typically associated with diverging trends in chemical composition. Indeed, n-alkanes which are thought to promote good ignition, tend to solidify and form wax particles at low temperatures.

As part of an earlier study, field tests at temperatures down to  $-28^{\circ}\text{C}$  had been carried out. A variety of engines with power ratings from 200 to 870 HP were used. For low temperature tests, ignition improver (0.3 vol %) had been added. At temperatures above freezing no ignition improver was added. No non-starts were observed (9).

As part of the present study, additional startability tests at even lower temperatures were carried out at Detroit Diesel Corporation's test facility. One engine was equipped with an electronic fuel injection system (Detroit Diesel Corporation - DDEC II) and glow plug heads. A second engine of similar design, with flow plug heads but mechanical injector system was also tested.

It was shown that, at  $-46^{\circ}\text{C}$ , the engine equipped with electronic injection started in 12 seconds when using the synthetic fuel with a small amount of ignition improver added to enhance the cetane number to 40 cetane. Without this ignition improver and at 32 cetane number, this all-synthetic fuel started at  $-43^{\circ}\text{C}$  in 23 seconds. However, the other engine equipped with the mechanical injection system and using the 32 cetane synthetic fuel was unable to start at  $-4^{\circ}\text{C}$  until small quantities of ether were injected. This engine was cranked in excess of 275 seconds with glow plug assist prior to the injection of the small amount of ether. Even with the ether injection, a considerable crank time (179 seconds) was required for the mechanical injection start.

These results can be interpreted as follows. Electronic fuel injection appears to play a significant role, at least under the conditions of this test. More work is still planned to investigate this observation. The nature of the synthetic fuel is definitely a strong contributing factor, considering that non-starts with conventional fuels are not unusual at these conditions. We feel that the unusually low pour point and cloud point ( $-66$  and  $-61^{\circ}\text{C}$  respectively), as well as the low viscosity of the all-synthetic fuel allow the fluidity and atomization into fine fuel droplets to be maintained even at these extreme temperatures, thereby ensuring fuel ignition. However, these fuel properties alone are not sufficient in some applications to provide ignition of the non additive added fuel (32 cetane), as shown by the tests with the engine equipped with a mechanical injection system.

In practical terms, the low temperature test results confirm that the synthetic fuel is an excellent blendstock, mainly because of its high fluidity at low temperature. Taken alone, without further blending or addition of ignition improvers, it is a good fuel at moderate temperatures for all the engines tested. However, its low temperature performance is affected by the type and design of the individual engines, particularly in the case of naturally aspirated low compression engines.

Almost all the engines at the Syncrude plant site have a mechanical injection system. Furthermore, the fleet includes low and high compression engines, as well as naturally aspirated and super/turbocharged engines.

On the basis of this fuel evaluation study, the all-synthetic fuel was approved by Syncrude for plant-wide use, on Syncrude owned equipment, at its oil sands

plant. The switch to synthetic fuel occurred in the spring of 1988. Throughout most of the year, the fuel is essentially used as it becomes available from the diluent preparation unit, without further processing.

Specifically, no ignition improver is added during this period. However, on the basis of the low temperature tests, the cetane number is raised during the winter months by the addition of cetane improver. Although this may not be required for all the engine types of the fleet, logistics are less complex when only one type of fuel is used at any time.

Government regulations require the addition of an approved dye. Furthermore, to prevent the build-up of static electricity, a conductivity additive is added. These materials are added together as a blend. Cost of these two additives is not a significant factor. Lubricity improver additive is not added.

### Conclusions

Physical, chemical and ignition properties of an all-synthetic material derived from Athabasca bitumen were measured with respect to its use as a diesel fuel. This stream is readily available as part of the production of synthetic crude oil, and as such is not specially blended or processed for diesel fuel use.

Many properties of the synthetic fuel are similar to conventional diesel fuel, particularly to winter diesel. Cloud point and pour point show a significant advantage over conventional fuels and exceed requirements set by fuel specifications. Cetane number and viscosity are lower than for conventional fuels and specifications.

Fuel specifications were developed on the basis of operating experience with conventional fuels, whereas this is an all-synthetic fuel. In the absence of a similar database specifically addressing operating experience with synthetic fuels, performance and durability tests on heavy-duty diesel engine test rigs were carried out.

The synthetic fuel is being used, on Syncrude owned equipment, plant-wide at Syncrude's integrated oil sands plant. Throughout most of the year, unmodified fuel is used. Only during the winter months is a higher cetane number required, particularly for naturally aspirated low compression engines. This can be achieved by addition of ignition improver.

Further studies are in progress to optimize the low temperature performance of the fuel.

### Acknowledgments

The authors would like to acknowledge the contributions of their co-workers and members of the investigating teams. We thank Syncrude Canada Ltd. and Detroit Diesel Corporation for granting permission to publish this paper.

### References and Notes

1. Since this study was carried out, a 40,000 bpd hydrocracker was integrated into the primary upgrading process. Fresh bitumen is fed to this hydrocracker. Distillates are routed to the hydrotreaters, whereas hydrocracker pitch is blended into the coker feed stream.

2. Bowden, J.N., Frame, E.A., "Effect of Organic Sulfur Compounds on Cetane Number", Ind. Eng. Chem. Prod. Res. Dev., v. 25, p. 156-159 (1986).
3. Cooley, J.M., Nowlan, V.J., Tan, F.O., unpublished data (1980).
4. Whyte, R.B., Gardner, L., "Update on Canadian Fuel Trends", SAE paper 841403, Fuels and Lubricants Meeting and Exposition, Baltimore, Maryland, Oct. 8-11, 1984.
5. Wei, D., Spikes, H.A. "Lubricity of Diesel Fuels", Wear, 111, p. 217 (1986).
6. Appeldorn, J.K., Dubek, W.G. "Lubricity of Jet Fuels", report SAE660712, 1966, Society of Automotive Engineers, Warrendale, Pennsylvania.
7. Coordinating Research Council, Inc. "Aviation Fuel Lubricity Evaluation" CRC report No. 560 (1988) Atlanta, Georgia, 30346.
8. The test was performed by Ethyl Petroleum Additives Ltd., Bracknell, U.K.
9. Houghton, R.E. "Utilization of Synthetic Duesel Fuel in Mobile Equipment: Syncrude Case History", American Society of Mechanical Engineers, Energy Resources Technical Conference, Houston, Texas, 1983, paper 83-DGP-5, 4 pp.

---

Bitumen	
d (g/mL)	1.02
API	7.7
C (wt %)	88.3
H (wt %)	10.4
N (ppm)	5000
S (wt %)	4.5 - 5.0
Ni (ppm)	70
V (ppm)	200
Asphaltenes (C5)	17
+524°C (vol %)	59

---

Synthetic Crude Oil	
API Gravity (API)	31.4
Total Sulfur (wt ppm)	1500
Total Nitrogen (wt ppm)	623
99% Point (°C)	516

Naphtha (C5 - 177°C)	
API Gravity	64.4
Total Sulfur (wt ppm)	5.0
Total Nitrogen (wt ppm)	0.9

Light Gas Oil (177 - 343°C)	
API Gravity	29.8
Total Sulfur (wt ppm)	428
Total Nitrogen (wt ppm)	126

Heavy Gas Oil (343°C+)	
API Gravity (API)	18.6
Total Sulfur (wt ppm)	3430
Total Nitrogen (wt ppm)	1470

---

Table 1: Typical Properties of Athabasca Bitumen and of Synthetic Crude Oil

	Synthetic Diesel	Summer Diesel	Fall/Spring Diesel	Winter Diesel
d (20°C):	0.837	0.860	0.845-0.850	0.816
API:	36.8-37.8	33	35-36	42
Visc Kinemat (40°C):	1.28	2.0-4.1	1.4-2.4	1.3-2.1
Saybolt SUS (100°F):				
S wppm:	75			
Dist (D-86), IBP:	162			
10%:	174	238	215	215
50%:	199			
90%:	243	360	324	315
FBP:	278	385	338	319
Flash Point (°C):	52	45	45	45
Cloud Point (°C):	-61	0	-35	-40
Pour Point (°C):	-66	-7	-40	-45
Cetane Index:		43	43	43
Cetane Number:	31.6	40 (up to 45)	40 (up to 45)	40 (up to 45)
Aniline Point (°C):	40.6	62	57	58
Water + Sedim. (vol %):	0.00			
C-Resid, 10% bott (wt %):	0.005			
Ash (wt %):	0.00			
Copper Corrosion:	1a	0.5-1.5	0.5-1.5	0.5-1.5
Acidity (mg KOH/g):	0.00			
Color:	+14			

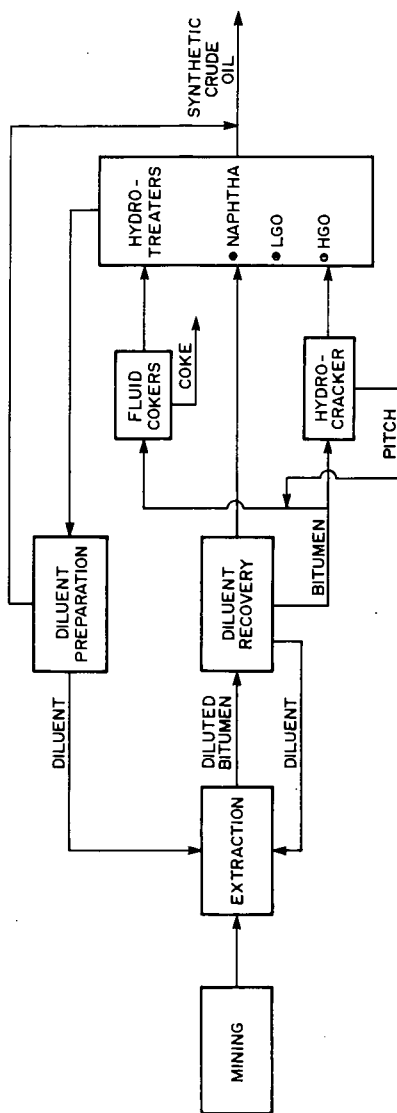
Table 2: Properties of Synthetic and of Commercial Diesel Fuels

Property	Fuel Type				
	Type AA	Type A	Type B	Type C	Type D
Flash point, min. °C	40	40	40	40	40
Cloud Point, max. °C	-48	-34	-23	-18	0
Pour Point, max. °C	-51	-39	-30	-24	-6
Kinematic Viscosity @ 40°C					
minimum, mm <sup>2</sup> s <sup>-1</sup>	1.2	1.3	1.4	1.4	1.4
maximum, mm <sup>2</sup> s <sup>-1</sup>	-	4.1	4.1	4.1	4.1
Distillation, 90% recovered max., °C	290	315	360	360	360
Water & Sediment, max. % vol.	0.05	0.05	0.05	0.05	0.05
Total Acid Number, max.	0.10	0.10	0.10	0.10	0.10
Sulfur, max. % mass	0.2	0.5	0.7	0.7	0.7
Copper Corrosion, 3 hrs at 100°C max.	#1	#1	#1	#1	#1
Carbon Residue (Ramsbottom) on 10% bottoms, max. % mass	0.15	0.15	0.20	0.20	0.20
Ash, max. % mass	0.01	0.01	0.01	0.01	0.01
Ignition Quality, Cetane No., min.	40	40	40	40	40

Table 3: Canadian Diesel Fuel Specifications (CAN 2-3.6-M81)



Figure 1. SIMPLIFIED DIAGRAM OF SYNCRUDE OIL SANDS PLANT



## DIESEL FUELS

### ASTM D-2887 Simulated Distillation

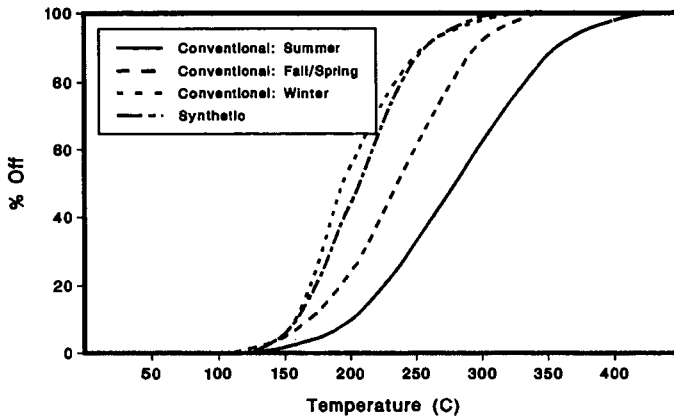


Figure 2. Boiling curves of synthetic and commercial diesel fuels.

### EFFECT OF IGNITION IMPROVER

on synthetic diesel fuel

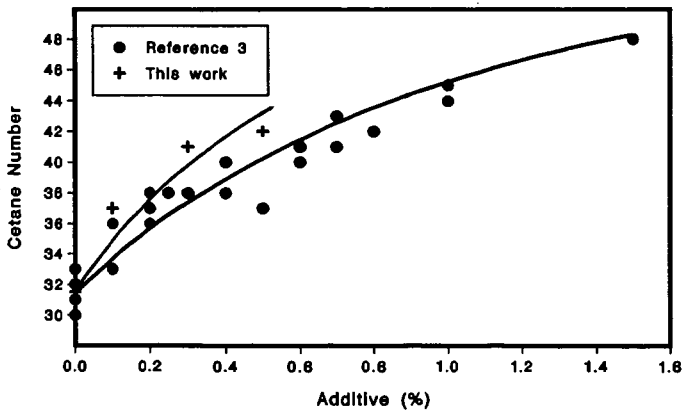


Figure 3. Effect of ignition improver on synthetic diesel fuel cetane number.

## LIQUID HYDROCARBON FUELS FROM BIOMASS

Douglas C. Elliott and Gary F. Schiefelbein  
Pacific Northwest Laboratory\*  
P. O. Box 999  
Richland, WA 99352

### INTRODUCTION

Renewable resources can provide a substantial energy resource for the United States. The direct production of liquid fuels from renewable resources, however, is limited to the use of biofuels. Liquids are preferred for use as transportation fuels because of their high energy density and handling ease and safety. Both biomass and municipal waste are being studied as the feedstock for production of liquid fuels [1]. Liquid fuel production from these feedstocks can be accomplished by several processes including hydrolysis and fermentation of the carbohydrates to alcohol fuels, thermal gasification and synthesis of alcohol or hydrocarbon fuels, direct extraction of biologically produced hydrocarbons such as seed oils or algae lipids, or direct thermochemical conversion of the biomass or municipal waste to liquids and catalytic upgrading to hydrocarbon fuels. This paper discusses direct thermochemical conversion to achieve biomass liquefaction.

### BIOMASS LIQUEFACTION

Direct liquefaction of biomass by thermochemical means has been studied as a process for fuel production for the last twenty years. Modern development of the process can be traced to the early work at the Bureau of Mines as an extension of coal liquefaction research [2,3] and to the work on municipal waste at the Worcester Polytechnical Institute [4]. Ongoing work at universities and national laboratories in the U.S., Canada, and Scandinavia has resulted in much progress since the mid-1970's [5 and references therein]. Currently the research has focused on two general processing configurations, high-pressure liquefaction and atmospheric flash pyrolysis.

High-pressure liquefaction of biomass, shown conceptually in Figure 1, has been studied at a number of sites around the world and includes a number of process variations. The processing temperature is generally in the range of 350°C with operating pressures in excess of 1000 psig. The feedstock is generally fed as a slurry, with the nature of the slurry vehicle being a major variable in the studies. Engineering of the high-pressure feeding system is a major difficulty in the development of this type of process. The presence of added reducing gas or catalyst is another important variable. Most studies show that the operation in the presence of alkali facilitates the formation of liquids with lower oxygen contents. Product recovery is also a major issue and is highly dependent on the slurry vehicle. Various systems of centrifugation, distillation, and solvent fractionation have been tested.

The atmospheric flash pyrolysis concept, shown in Figure 2, can be traced to the ancient process of charcoal manufacture. Modern engineering methods have optimized the yield of liquid product through control of feedstock particle

\*Operated for the U. S. Department of Energy by Battelle Memorial Institute under Contract DE-AC06-76RLO 1830

size, residence time, and processing temperature. Current process development utilizes short residence time, <1 second, in isothermal, fluidized- or entrained-bed reactors. The feedstock is carried by an inert gas carrier into the reactor where it thermally decomposes to tar vapors, water vapor, gases, and char solids. Recovery of the vapors as liquid product is a major difficulty for this process. Various systems for vapor quench and recovery have used complicated condensing and coalescing systems including electrostatic precipitators, cyclones, filters, and/or spray towers.

The products from the high-pressure liquefaction and atmospheric flash pyrolysis processes are vastly different from each other. The properties of the two products are summarized in Table 1. The high-pressure product is a viscous, phenolic oil. Its physical properties of high viscosity, high boiling point, and limited water solubility are readily understood as resulting from the oxygenated and aromatic character of the product components. The flash pyrolyzate is much more oxygenated and is more water soluble. As a result of the high level of dissolved water in the product, the flash pyrolyzate is much less viscous. The more oxygenated components in the product, acids and aldehydes/ethers, cause it to be more corrosive and more thermally unstable, respectively.

#### UPGRADING BIOMASS-DERIVED LIQUIDS

Because of the chemical differences in the two products described above, different upgrading schemes have been derived for converting the products into usable hydrocarbon fuels. Catalytic hydroprocessing is an obvious choice based on the existing knowledge of sulfur removal from petroleum products. Catalytic hydrodeoxygenation of the products has been studied in several laboratories [6,7,8]. Developments in further product refinement by catalytic cracking and hydrocracking have also been presented [9,10]. This type of processing is most directly applicable to the high-pressure liquefaction products; however, a process has been identified which allows the use of catalytic hydroprocessing of the thermally unstable pyrolyzate product [11]. Another alternative, which has been used successfully with the pyrolyzate products, is the catalytic cracking of the vapors over a zeolite catalyst without the intermediate quenching and recovery of the tars [12]. Further discussion of the products from this type of processing is not included in this paper.

Catalytic hydroprocessing of biomass-derived liquid products has been investigated at Pacific Northwest Laboratory (PNL) in a fixed-bed, continuous-feed, catalytic reactor system (shown schematically in Reference 6). Products from both high-pressure processes and flash pyrolysis processes have been upgraded [13,14]. The reactor system includes gas feed from a high-pressure (6000 psig) bottle, oil feed by positive displacement pump, a 1-liter reactor vessel containing 850 mL of alumina-supported metal sulfide catalyst (sulfided in place), pressure control by a back-pressure regulator, and product recovery in a cooled, atmospheric-pressure gas-liquid separator. Feed gas is measured by a mass flow meter; feed oil is measured in a volume flow meter; and off-gas is measured in a wet test meter. The off-gas is analyzed by gas chromatography using both a thermal conductivity detector for fixed gases and a flame ionization detector for hydrocarbon vapors up to C7.

## ANALYSIS OF PRODUCTS FROM HYDROPROCESSING BIOMASS-DERIVED OILS

A range of products has been produced in the PNL hydrotreater depending on the processing conditions and the feedstock. Several representative samples are presented in Table 2. In comparison with the biomass-derived oils shown in Table 1, the hydrotreated products are significantly upgraded. The oxygen content is greatly reduced and, coincidentally, so is the density of the products. The density difference has a significant impact because, although the mass yield of the hydrotreated products is in the range of 80%, the volume yield in many cases exceeds 100%. A primary concern throughout the research has been the maintenance of the aromatic character of the biomass oil in order to minimize hydrogen consumption and to produce a higher octane gasoline blending stock. As seen in Table 2, the hydrogen-to-carbon ratio in the products is highly variable depending on the processing conditions. The extent of saturation as shown by the H/C ratio is a useful indicator of the aromatic character of the product. Saturation of the aromatic components has a strongly deleterious effect on the octane of the product. A review of the literature shows that cyclic hydrocarbons have poor octanes similar to straight-chained hydrocarbons. Our analyses also show that although the crude hydrotreated products do contain minor amounts of oxygen, water solubility in the products remains low. In addition, although sulfided catalysts are used in the hydrotreating, little incorporation of sulfur into the nearly sulfur-free biomass oils is occurring.

## COMPONENT ANALYSIS IN GASOLINE-RANGE DISTILLATES

More detailed analysis of several gasoline-range distillates from the hydrotreated biomass-derived oils has been undertaken. These analyses provide additional detail on the makeup of the products and also further substantiate the relationships of the product composition to product properties. As seen in Table 3, elemental compositions can be compared with component fractionations and component analysis by instrumental methods. To fractionate the components of the distillates, we used the ASTM D 1319 method for determining hydrocarbon types by fluorescent indicator adsorption. By nuclear magnetic resonance (NMR) of carbon-13, similar component groups can be identified and quantified.

For most of the samples listed in Table 3, the D 1319 data compare quite favorably with the C-13 NMR results. The aromatic and aliphatic portions are nearly identical. The D 1319 consistently shows a small olefin fraction in the oil, while the NMR analysis detects essentially no olefinic carbon atoms. Further analysis of the fractions from the D 1319 separation was performed by gas chromatography with a mass selective detector (HP 5970). Individual components in each fraction were identified and semi-quantitatively determined by the intensity of the total ion current for each peak. Components in each of the fractions are listed in Table 4. With this analysis, the NMR results were confirmed, as the primary components of the olefin fraction were found to be bicyclic components. Some difficulty was encountered with this analysis because of the small fraction size and the contamination by the aliphatic fraction. However, no mass spectra of olefin components were confirmed, and the primary components in the fraction could be determined by comparison with the aliphatic fraction analysis.

## REFERENCES

1. Thermochemical Conversion Program Annual Meeting, June 21-22, 1988. SERI/CP-231-3355, Solar Energy Research Institute, Golden, CO. July 1988.
2. Appell, H. R., Y. C. Fu, S. Friedman, P. M. Yavorsky, and I. Wender. 1971. Converting Organic Wastes to Oil: A Replenishable Energy Source. Report of Investigations 7560, Pittsburgh Energy Research Center, Pittsburgh, PA.
3. Appell, H. R., Y. C. Fu, E. G. Illig, F. W. Steffgen, and R. D. Miller. 1975. Conversion of Cellulosic Wastes to Oil. Report of Investigations 8013, Pittsburgh Energy Research Center, Pittsburgh, PA.
4. Kaufman, J. A., and A. H. Weiss. 1975. Solid Waste Conversion: Cellulose Liquefaction. PB 239 509, National Technical Information Service, Springfield, VA.
5. Beckman, D., and D. C. Elliott. 1985. "Comparisons of the Yield and Properties of the Oil Products from Direct Thermochemical Biomass Liquefaction Processes." Can. Jour. Chem. Eng. 63(1):99-104.
6. Elliott, D. C., and E. G. Baker. 1986. Catalytic Hydrotreating of Biomass Liquefaction Products to Produce Hydrocarbon Fuels: Interim Report. PNL-5844, Pacific Northwest Laboratory, Richland, WA.
7. Gevert, S. B. 1987. Upgrading of Directly Liquefied Biomass to Transportation Fuels. Chalmers University of Technology, Göteborg, Sweden.
8. Soltes, E. J., and S-C. K. Lin. 1984. "Hydroprocessing of Biomass Tars for Liquid Engine Fuels." In: Progress in Biomass Conversion, Vol. 5, p. 1. D. A. Tillman and E. C. Jahn, eds., Academic Press, New York.
9. Elliott, D. C., and E. G. Baker. 1988. "Catalytic Hydrotreating Processes for Upgrading Biocrude Oils." In: Thermochemical Conversion Program Annual Meeting, pp. 45-56. SERI/CP-231-3355, Solar Energy Research Institute, Golden, CO.
10. Gevert, S. B., and J-E. Otterstedt. 1987. "Upgrading of Directly Liquefied Biomass to Transportation Fuels - Catalytic Cracking." Biomass 14:173-183.
11. Elliott, D. C., and E. G. Baker. 1989. "Process for Upgrading Biomass Pyrolyzates." U.S. Patent #4,795,841, issued January 3, 1989.
12. Scahill, J., J. P. Diebold, and A. Power. 1988. "Engineering Aspects of Upgrading Pyrolysis Oil Using Zeolites." In: Research in Thermochemical Biomass Conversion, pp. 927-940. eds. A. V. Bridgwater and J. L. Kuester, Elsevier Science Publishers, LTD., Barking, England.
13. Baker, E. G., and D. C. Elliott. 1988. "Catalytic Hydrotreating of Biomass-Derived Oils." In: Pyrolysis Oils from Biomass: Producing, Analyzing and Upgrading - ACS Symposium Series 376, pp. 228-240. E. J. Soltes and T. A. Milne, eds., American Chemical Society, Washington, DC.
14. Baker, E. G., and D. C. Elliott. 1988. "Catalytic Upgrading of Biomass Pyrolysis Oils." In: Research in Thermochemical Biomass Conversion, pp. 883-895. A. V. Bridgwater and J. L. Kuester, eds., Elsevier Science Publishers, LTD., Barking, England.

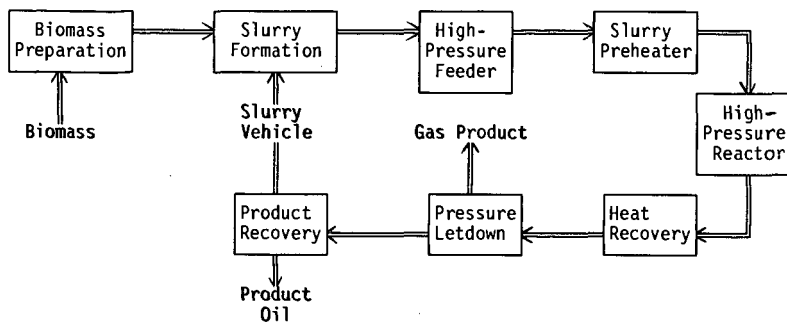


FIGURE 1. Conceptual High-Pressure Liquefaction Process

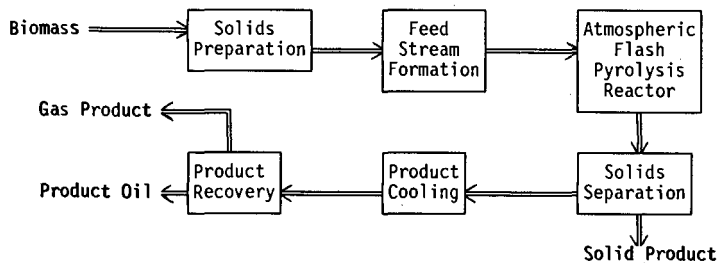


FIGURE 2. Conceptual Atmospheric-Pressure Flash Pyrolysis Process

TABLE 1. Properties of Direct Liquefaction Products from Biomass

	High-Pressure Liquefaction	Flash Pyrolysis
Elemental Analysis		
Carbon, wt%	72.6	43.5
Hydrogen, wt%	8.0	7.3
Oxygen, wt%	16.3	49.2
Sulfur, ppm	<45	29
H/C atom ratio (dry)	1.21	1.23
Density, g/mL	1.15	1.23
Moisture, wt%	5.1	24.8
HHV, Btu/lb	15,340	9,710
Viscosity, cps	15,000 @ 61°C	59 @ 40°C
Distillation Range		
IBP-225°C	8%	44%
225°C-350°C	32%	coked
350°C-EP(°C)	7%	

TABLE 2. Range of Properties of Hydrotreated Biomass Liquefaction Products

Elemental Analyses	
Carbon, wt%	85.3 - 89.2
Hydrogen, wt%	10.5 - 14.1
Oxygen, wt%	0.0 - 0.7
Sulfur, ppm	50
H/C atom ratio	1.40 - 1.97
Density, g/mL	0.796 - 0.926
Moisture, ppm	10 - 80
HHV, Btu/lb	18200 - 19500
Viscosity, cps	1.0 - 4.6 @ 23°C
Aromatic/ Aliphatic Carbon	38/62 - 22/78
Distillation Range	
IBP-225°C	>97% - 36%
225°C-350°C	0% - 41%
EP(°C)	188°C - 348°C



TABLE 3. Distillate Products from Hydrotreatment

ELEMENTAL ANALYSES, %		Density		HHV		gasoline BP range		C-13 NMR		Octane Numbers	
Carbon	Hydrogen	(H/C ratio)	Oxygen	g/mL	Btu/lb	IBP-225C	arom/alpha	actual arom	arom/alk/olef D1319	MON	RON
86.6	12.1	1.66	1.3	0.844		100% 23-225C	28/72	43%	44.1/55.1/0.8	72.0	77.0
85.4	12.5	1.74	2.2	0.791		100% 68-176C	29/71	25.4%	39.5/53.6/6.9		
87.1	12.0	1.64	0.9	0.859		100% 23-225C	30/70	29.0%	47.4/48.3/4.3		
86.2	13.1	1.81	0.6	0.823	18990	100% 23-225C	24/76	32%	33.9/63.3/2.8	72.8	78.1
				0.81		100% 23-165C	20/80	28%	28.3/69.9/1.8		
86.0	12.7	1.75	1.3	0.803		100% 72-157C	22/78	29%	33.7/59.1/7.2		
84.3	13.7	1.93	1.5	0.782		100% 57-183C	12.4/8	18%	18.1/77.1/4.8		
85.6	13.3	1.84	1.2	0.802		100% 63-149C	16/84	20%	28.3/68.6/3.1		

TABLE 4. Components of D 1319 Chromatography Fractions  
(within each fraction, from highest total ion current)Saturated Hydrocarbons

ethylcyclohexane  
 propylcyclohexane  
 methylcyclohexane  
 methylcyclohexane  
 methylpropylcyclohexane  
 methylcyclohexane  
 methylpropylcyclopentane  
 ethylpropylcyclohexane  
 dimethylcyclohexane  
 methylcyclopentane

Aromatic Hydrocarbons

ethylmethylbenzene  
 methylpropylbenzene  
 propylbenzene  
 C4-alkyl-benzene  
 C2-alkyl-tetralin  
 methyltetralin  
 tetralin  
 methylindan  
 C5-alkyl-benzene  
 methylpropylbenzene

Olefinic Hydrocarbons

octahydroindene  
 octahydropentalene  
 methyloctahydropentalene

Alcohol Soluble Components

dimethylphenol  
 naphthalene  
 ethylphenol  
 cresol  
 ethylmethylphenol  
 cresol  
 methyl naphthalene  
 ethylmethylphenol  
 dimethylphenol  
 ethyl phenol

MILD GASIFICATION OF COAL AND HEAVY OIL MIXTURES  
TO ENHANCE LIQUID YIELD/QUALITY+

M. Rashid Khan  
Texaco Research Center,  
Texaco Inc, P.O. Box 509, Beacon, NY 12508

F. Y. Hsieh  
Oak Ridge Associated University  
Morgantown Energy Technology Center  
Morgantown, WV 26505

Larry Headley  
U.S. Department of Energy  
Morgantown Energy Technology Center  
Morgantown, WV 26505

INTRODUCTION AND BACKGROUND

Our previous studies demonstrated that relatively high quality (high H/C) liquid fuels from coal can be produced by low-temperature devolatilization (1). However, the liquids produced by low-temperature pyrolysis are typically of low yield. Therefore, there is an interest to identify ways to increase the yield of the liquids produced during pyrolysis.

Coprocessing of coal and heavy petroleum residue at relatively mild conditions may provide an avenue to enhance yield. Some important advantages of coprocessing can be the following: (a) upgrading of a petroleum residue in a reaction with coal; (b) conversion of coal to synthetic crudes which can be further upgraded into premium liquid fuels. In coprocessing, the petroleum residues may serve as the "liquefaction solvent" or hydrogen donor and the aromatics present in coal liquid may serve as hydrogen "shuttlers" by efficiently transferring hydrogen to moieties where it is most deficient. Coal also can enhance the conversion of petroleum residues to lighter liquid products through the catalytic effects of the mineral matters present in the coal. Liquefaction of coal and petroleum residues are typically performed at temperatures in the range of 400° to 500°C under pressurized hydrogen atmosphere. Catalysts are generally also added for the hydroconversion of coal and petroleum residues.

Coprocessing of the coal with petroleum, heavy crudes, and petroleum residues through catalytic hydrogenation (2-7) or solvent extraction (8-10) has been extensively studied. However, relatively little has been reported in the literature regarding the coprocessing of coal with petroleum residues by simple pyrolysis (i.e., without the complicating influences of pressurized hydrogen or hydrogenation catalysts).

+This work was performed at Morgantown Energy Technology Center

Sekrieru, et al. (11), investigated copyrolysis of brown coal and petroleum products. Vikhorev, et al. (12), also investigated copyrolysis of brown coal and coal tar or petroleum residue. Both of these studies apparently noted increases in liquid yield during copyrolysis. It was suggested that the additives (coal tar and petroleum residue) can swell or weaken the coal structure leading ultimately to a higher liquid yield. Huttering and Sperling (13) studied flash hydrocopyrolysis of coals doped with aromatics, hydroaromatics (2 percent of loading) and observed that coprocessing of coal with additives resulted in an increase in the tar yield (by 5 to 10 percent) at the expense of char yield. In contrast, Malhotra, et al. (14), pyrolyzed coal with 10 percent of coal tar and prehydrogenated coal tar at various heating rates. Their limited results show that the addition of coal tar and prehydrogenated coal tar (containing 10 to 20 percent of hydroaromatics) to coal had no beneficial effect on pyrolysis yield. However, extensive characterization data on any of the studies were not reported.

Khan, et al. (16), studied the pyrolysis of raw coal, pyridine extract and extracted coal residue by a thermogravimetric analyzer (TGA) and found that the combined weight loss of extract and extracted coal residue at 600°C is considerably lower than the weight loss obtained for the raw coal alone. Therefore, it was suggested that the presence of hydrogen-rich portions of the coal (i.e., extract) in the coal structure increases the overall weight loss for coal during pyrolysis. The extractable portion of coal may serve as the source of internal hydrogen during pyrolysis by supplying hydrogen to hydrogen deficient moieties that would otherwise undergo coking reaction (forming solid residue) rather than desirable volatiles. In other words, the extractable portion of coal, being more hydroaromatic, can serve as hydrogen-donors in partially hydrogenating the insoluble portion of coal during pyrolysis, thereby increasing the yield of volatile matter from the residue.

It is generally believed in coal liquefaction, that hydrogen-donor solvent can donate hydrogen and "cap-off" the thermally generated free radicals to form stable volatiles. The rate of coal liquefaction process apparently depends on the rate at which hydrogen can be donated from the solvent. McMillen, et al. (17), suggested a mechanism for the formation of liquid products during pyrolysis in which strong linkages (such as diarylmethane, alkylaromatic, and dialylether) are cleaved at 400°C as a result of hydrogen transfer from solvent-derived cyclohexadienyl radicals in a direct bimolecular step. Existing literature data suggest that petroleum residue may serve as an external hydrogen source by enhancing the bond-scission reactions via formation of cyclohexadienyl radicals (18) during coprocessing. It is our hypothesis in this study that copyrolysis of coal with petroleum residue at a relatively low temperature (500°C) can increase the tar yield while improving the quality of the tar perhaps by hydrogen transfer and hydrogen-transfer-promoted, bond-scission reactions. To fully test our hypothesis and to extend the data available in the literature, a copyrolysis study was initiated. The copyrolysis products were extensively characterized. Relatively little has been reported in the literature regarding the characteristics of the liquids generated by copyrolysis of coal and heavy residue (in the absence of a catalyst or high-pressure hydrogen).

## EXPERIMENTAL

**Feedstocks Origin and Pyrolysis Procedure:** The experimental procedures for the production of pyrolysis liquids from solid fuels including reactor system, experimental procedures, and reproducibility of results have been described by Khan (1a). A fixed-bed reactor known as slow heating rate organic devolatilization reactor (SHRODR) was used to generate the pyrolysis liquids at 500°C. In addition, a thermogravimetric analysis (TGA) reactor was used for our studies. The Pittsburgh No. 8 coal (high volatile bituminous) and the Wyodak subbituminous coals were used in this study. All sample preparation and handling procedures were performed in inert atmospheres. The Kern River heavy residue was provided by the Stanford Research Institute. Additional details on the origin of these samples can be found elsewhere (1b).

## RESULTS AND DISCUSSION

The proximate and ultimate analyses of Pittsburgh No. 8 coal, Wyodak coal (PSOC 1520) and Kern River heavy residue are shown in Table 1. The pyrolysis weight loss in a TGA during heat-treatment to 500°C at 20°C/min (Table 2) for the Pittsburgh No. 8 coal was 25.7 weight percent (daf) and that for the heavy residue was 80.0 weight percent (daf). The weight loss of 50/50 mixture was 62.9 weight percent (daf), which is 9.0 weight percent higher than that for the projected value (53.9 weight percent) based on the yields of the individual components. These results suggest that the presence of heavy residue increases the overall weight loss during pyrolysis of Pittsburgh No. 8 coal. The heavy residue (hydrogen-rich) may serve as hydrogen-donor providing some of the labile hydrogen to the coal (hydrogen-poor) moieties and thereby suppressing the regressive reactions during pyrolysis. Figure 1 shows the pyrolysis (derivative thermogravimetric analysis) DTG curves of Pittsburgh No. 8 coal, heavy residue, and their 50/50 mixture. There is only one major peak shown in the DTG curve for coal. Two major peaks were shown in the DTG curves of heavy residue and 50/50 mixture. The first peak in the DTG curves of heavy residue and 50/50 mixture is related to the decomposition and devolatilization of light molecules (or components), and the second peak is presumably related to the decomposition and devolatilization of original and newly formed heavy molecules (or components). As shown in Figure 1, copyrolysis of coal with heavy residue slightly shifts the first peak to a lower temperature while simultaneously lowering the second peak by 40°C as compared to the pyrolysis of heavy residue alone. These findings provide credence to the concept of synergistic effects during copyrolysis of coal and heavy residue.

Figure 2 presents the yield of gas, tar, and char products from pyrolysis of Wyodak coal, heavy residue, and the 50/50 mixture at 500°C in the fixed-bed reactor. The tar yield from pyrolysis of 50/50 mixture is 52.2 weight percent (daf), which is 5.1 weight percent higher than the predicted value (47.1 weight percent [daf]). This observation is consistent with the TGA copyrolysis data.

Table 3 shows the ultimate analyses and heating values of tars from pyrolysis of Wyodak coal (PSOC 1520), heavy residue, and their 50/50 mixture at 500°C in the fixed-bed reactor (SHRODR). It appears that the elemental composition of tar from 50/50 mixture is similar to that for the tar from heavy residue. The tar from 50/50 mixture has higher H/C ratio, lower O/C ratio, and higher

heating value than those for the tar from coal. This confirms that copyrolysis of coal with heavy residue produces a better quality tar as compared to the pyrolysis of coal alone. Table 4 shows the elemental analyses of chars from pyrolysis of Wyodak coal, heavy residue, and the mixture. It is expected that the elemental composition of char from the mixture is similar to that for the char from Wyodak coal. The char from pyrolysis of 50/50 mixture has slightly higher heating value than that for the char from pyrolysis of coal. These results indicate that copyrolysis of coal with heavy residue upgrades the tar quality without necessarily degrading the char quality.

Figure 3 compares the composition of evolved gases from pyrolysis of Wyodak coal, heavy residue, and the mixture. It is obvious that pyrolysis of Wyodak coal resulted in a relatively high yield of CO and CO<sub>2</sub>, which is due to the decomposition of oxygenated functional groups in Wyodak coal. Pyrolysis of heavy residue produced a relatively high yield of CH<sub>4</sub> and C<sub>2</sub>H<sub>4</sub>. This is probably due to the higher concentration of long-chain aliphatic components present in the heavy residue. Heavy residue has lower content of sulfur as compared to Wyodak coal. However, pyrolysis of heavy residue alone produces a higher yield of H<sub>2</sub>S. This implies that the sulfur-containing compounds in heavy residue (e.g., thiol and disulfide) is more volatile than those present (e.g., thiophene, thiopyrone) in the Wyodak coal. Pyrolysis of 50/50 mixture produced lower yield of H<sub>2</sub>S (18 percent lower) than that for the projected value. Therefore, the carbonate minerals in the Wyodak coal may also act as scavengers of hydrogen sulfide during copyrolysis of coal with heavy residue. In general, the yield of various gases for pyrolysis of the mixture ranked in the region between pyrolysis of Wyodak coal and heavy residue.

The tars from pyrolysis of coals (Wyodak coal and Pittsburgh No. 8 coal), heavy residue, and the mixture were separated by sequential elution solvent chromatography (data not shown). In general, the tars from pyrolysis of the mixture contain higher content of alkane/alkene neutral aromatics, lower content of monophenols, polyphenols, and other oxygen-containing compounds as compared to the tars from pyrolysis of coal alone. This implies that copyrolysis of coal and heavy residue upgrades the quality of coal tars.

The average structure parameters of tars from pyrolysis of Wyodak coal, heavy residue, and the mixture have been characterized by using proton NMR analysis (data not shown). The carbon aromaticity of tar from the mixture is similar to that for the tar from pyrolysis of heavy residue and much lower than that for the tar from pyrolysis of coal. The tar from the mixture contains lower content of mono-aromatics and higher content of di- and tri-aromatics than that for the tar from coal. It is interesting to note that the tar from the mixture contains higher content of naphthenic carbon and naphthenic rings/molecule than those for the tar from coal. This finding suggests that the tar from the mixture can be much easily upgraded to match the specifications of high-density jet fuel.

#### SUMMARY AND CONCLUSIONS

Our previous results demonstrated that relatively high-quality liquid fuel can be produced from coal by low-temperature devolatilization. Ongoing studies are aimed at producing a high-quality liquid while achieving a high yield of liquids. To better understand whether copyrolysis is a viable option to enhanced liquid yield, a coal and a heavy residue sample were copyrolyzed in a

fixed-bed reactor at a relatively low temperature and the products were characterized. Results demonstrated that there is a synergism during copyrolysis of coal and heavy residue. This synergism enhances both the yield and quality of the liquid products during copyrolysis.

In general, the tars from pyrolysis of the mixture contain higher content of alkane/alkene neutral aromatics, lower content of monophenols, polyphenols, and other oxygen-containing compounds as compared to the tars from pyrolysis of coal alone. The tars from the mixture also contain lower content of mono-aromatics and higher content of di- and tri-aromatics than that for the tar from coal. Therefore, they can be much easily upgraded to match the specifications of high-density jet fuel.

#### ACKNOWLEDGEMENTS

Funding for this study was provided by the U.S. Department of Energy, Assistant Secretary for Fossil Energy, Office of Coal Utilization, Advanced Conversion and Gasification. FYH acknowledges support received from U.S. DOE through the Oak Ridge Associated Universities (ORAU) Program.

#### REFERENCES

- 1a. Khan, M. R., Fuel Science and Technology International, 1987, 5(2), 185.
- 1b. Khan, M. R., Seshadri, K. and Kowalski, T. accepted for publication in Energy and Fuels, 1989.
2. Lenz, U, and J. Wavzinek; Am. Chem. Soc. Div. Fuel Chem. Prepr., 1988, 33(1), 27.
- 3a. Curtis, C. W., J. A. Guin, M. C. Pass, and K. J. Tsai; Fuel Science and Technology International, 1987, 5(3), 245.
- 3b. Curtis, C. W., K. J. Tsai, and J. A. Guin; Ind. Eng. Chem. Process Des. Dev., 1985, 24, 1259.
4. Aulich, T. R., P. L. Holm, C. L. Knudson, and J. R. Ridut; Am. Chem. Soc. Div. Fuel Chem. Prepr., 1988, 33(1), 103.
5. Schwartz, M. M., and A. L. Hensley; Am. Chem. Soc. Div. Fuel Chem. Prepr., 1988, 33(1), 163.
6. Fouda, S. A., J. F. Kelly, and P. M. Rahimi; Am. Chem. Soc. Div. Fuel Chem. Prepr., 1988, 33(1), 179.
7. Oelert, H. H., R. Bloss, and P. F. Zhang; Am. Chem. Soc. Div. Fuel Chem. Prepr., 1988, 33(1), 185.
8. Mochida, I., Y. Moriguchi, Y. Korai, H. Fujitsu, and K. Takeshita; Fuel, 1981, 60, 746.
9. Moschopedis, S. E., R. W. Hawkins, J. F. Fryer, and J. G. Speight; Fuel, 1980, 59, 647.
10. Yan, T. Y., and W. F. Espenscheid; Fuel Processing Technology; 1983, 7, 121.
11. Sekriera, V. I., Z. S. Smutkina, and T. A. Titova; Solid Fuel Chemistry, 1978, 12(5), 45.
12. Vikhoven, A. A., A. M. Syroezhko, V. A. Proskuryakov, and N. A. Akhmedov; Solid Fuel Chemistry, 1987, 21(2), 78.
13. Huttlinger, K. J., and R. E. Sperling in proceedings of the 1987 International Conference on Coal Science, J. A. Moulijn, K. A. Nator, and H. A. G. Chermin, Editors; Elsevier Science Publishers B. V., Amsterdam, 1987, p. 699.

14. Malhotra, R., G. St. John, D. S. Tse, and D. F. McMillen; Am. Chem. Soc. Div. Fuel Chem. Prepr., 1988, 30(2), 257.
15. Brown, H. R., and P. L. Waters; Fuel, 1966, 45, 17.
16. Khan, M. R., R. Usman, E. Newton, S. Beer, and W. Chisholm; Fuel, 1988, 67, 1668.
17. McMillen, D. F., R. Malhotra, G. P. Hum, and S.-J. Chang; Energy and Fuel, 1987, 1, 193.
18. McMillen, D. F., R. Malhotra, D. S. Tse, and S. E. Nigenda; Am. Chem. Soc. Div. Fuel Chem. Prepr., 1988, 33(1), 58.
19. Seshadri, K. S., and D. C. Cronauer; Fuel, 1983, 62, 1436.

TABLE 1

PROXIMATE AND ULTIMATE ANALYSES OF PITTSBURGH NO. 8 COAL,  
WYODAK COAL (PSOC 1520), AND KERN RIVER HEAVY RESIDUE

	Pittsburgh No. 8 Coal	Wyodak Coal	Kern River Heavy Residue
% C, daf	83.74	73.78	85.43
% H, daf	5.46	4.62	11.15
% N, daf	1.56	1.11	0.86
% S, daf	2.15	1.38	0.97
% O, daf (by difference)	7.09	19.11	1.59
% Ash (as-received basis)	7.27	9.08	< 0.01
% Moisture	0.57	26.69	0
H/C Atomic (daf)	0.78	0.75	1.57
O/C Atomic (daf)	0.064	0.19	0.014

TABLE 2

TGA PYROLYSIS OF PITTSBURGH NO. 8 COAL, KERN RIVER  
HEAVY RESIDUE, AND 50/50 PITTSBURGH NO. 8 COAL/  
KERN RIVER HEAVY RESIDUE MIXTURE

Samples	Weight Loss (daf) at 500°C
Pittsburgh No. 8 Coal	25.7
Kern River Heavy Residue	80.0
50/50 Coal/Heavy Residue Mixture	62.9
Projected Weight-Loss for Mixture	53.9 <sup>a</sup>

<sup>a</sup> Predicted weight loss (daf) of 50/50 mixture, assuming no synergism.

TABLE 3

ULTIMATE ANALYSES AND HEATING VALUES OF TARS FROM PYROLYSIS OF WYODAK COAL (PSOC 1520), KERN RIVER HEAVY RESIDUE AND 50/50 WYODAK COAL/KERN HEAVY RESIDUE MIXTURE AT 500°C

	Tar from Coal	Tar from Heavy Residue	Tar from 50/50 Mixture	Projected*
% C, daf	78.44	86.17	84.30	85.05
% H, daf	10.59	12.28	11.96	12.03
% N, daf	0.52	0.69	0.70	0.67
% S, daf	0.55	0.17	1.14	0.22
% O, daf	9.9	0.69	1.90	2.03
(by difference)				
H/C Atomic (daf)	1.62	1.71	1.70	1.70
O/C Atomic (daf)	0.09	0.006	0.017	0.018
Heating Value, Btu/lb	15,615	18,662	18,470	

\* Projected values are calculated based on (a) the composition of individual components, and (b) their respective yield during pyrolysis. Assumes no synergism.

TABLE 4

ULTIMATE ANALYSIS AND HEATING VALUES OF CHARS FROM PYROLYSIS OF WYODAK COAL (PSOC 1520), KERN RIVER HEAVY RESIDUE, AND 50/50 WYODAK COAL/KERN RIVER HEAVY RESIDUE MIXTURE AT 500°C

	Char from Coal	Char from Heavy Residue	Char from 50/50 Mixture	Projected*
% C, daf	85.92	89.69	85.76	86.32
% H, daf	3.26	3.26	3.43	3.26
% N, daf	1.49	3.04	1.17	1.65
% S, daf	1.30	0.95	1.59	1.27
% O, daf	8.03	3.06	8.05	7.50
(by difference)				
H/C Atomic (daf)	0.46	0.44	0.48	0.45
O/C Atomic (daf)	0.07	0.026	0.07	0.065
Heating Value, Btu/lb	11,806	14,755	12,104	

\* See definition of projected values on Table 3.



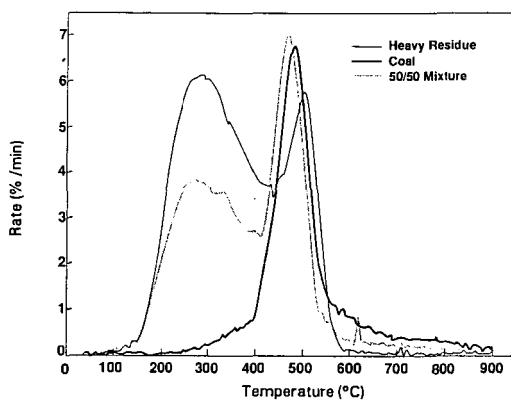


FIGURE 1 EFFECT OF CO-PROCESSING ON PYROLYSIS RATE PROFILES

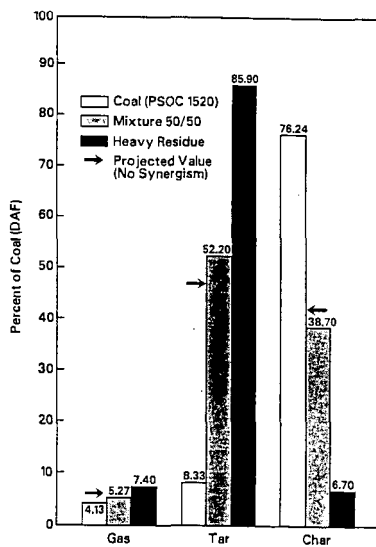


FIGURE 2 CO-PROCESSING OF COAL AND HEAVY RESIDUE

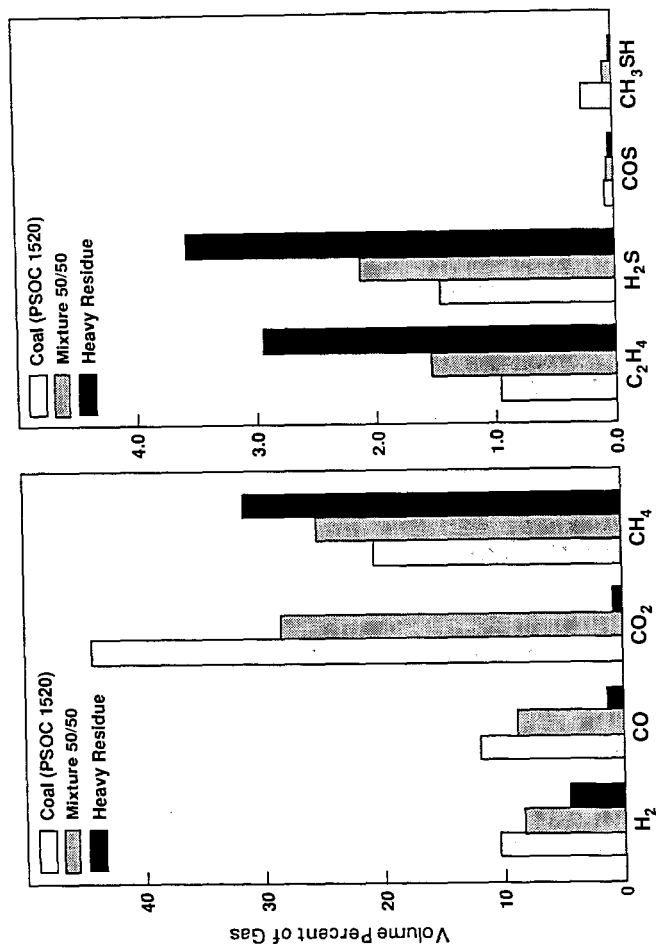


FIGURE 3 INFLUENCE OF CO-PROCESSING ON PRODUCT YIELD/COMPOSITION

# FLASH PYROLYSIS OF COAL IN THE ATMOSPHERE CONTAINING SOLVENT VAPORS

Kouichi Miura, Kazuhiro Mae, Akihiro Murata  
and Kenji Hashimoto\*

\*Research Laboratory of Carbonaceous Resources  
Conversion Technology,  
Department of Chemical Engineering, Kyoto University  
Kyoto 606, Japan

## INTRODUCTION

We have recently presented a new coal pyrolysis method<sup>1)</sup>, in which coal particles swollen by hydrogen donor solvents at around 250 °C were pyrolyzed in a Curie-point pyrolyzer. Both the conversion and the tar yield drastically increased by this pyrolysis method. The increases were brought about by the pore enlargement caused by swelling and the effective hydrogen transfer from/via the solvent to the fragments of the primary coal decomposition. This method is, however, a little complicated to be scaled up to a commercial process.

In this paper, we propose a much simpler flash pyrolysis method, in which coal particles are pyrolyzed continuously in the gas stream containing hydrogen donor solvents. It is shown that this pyrolysis method successfully increases the tar yield, and presents a possibility of an in situ control of the product distribution.

## EXPERIMENTAL

The coal used was Morwell brown coal. It was ground and screened to -125 +74  $\mu\text{m}$ . The properties of the coal are given in Table 1. Figure 1 shows the diagram of the entrained bed type of pyrolyzer used in this study. Reactor is a coil of stainless steel tube of 1/4 inch in outer diameter. Three different length of reactors, 0.89, 2.65 and 4.64 m, were used to change the residence time of the coal. The dried coal was fed to the reactor by a tablefeeder with nitrogen gas at the feed rate of 4 to 20 g/h. The flow rate of nitrogen was 4.0 l/min (STP). Vapor of tetralin and decalin was added to the flow of coal-nitrogen mixture at the top of reactor as shown in Figure 1. The feeding ratio of the solvent to coal was 0.12 to 0.15 by weight. Experiments without the solvent were also performed for comparison. The coal was pyrolyzed while passing the reactor, and gas, tar and char produced were led to cyclone connected to the exit of the reactor to separate the gas and tar from char. The tar and the gas were led to the condensers, where the tar was trapped. A part of the gas was collected in a gas bag.

The char and the tar yields were calculated from the changes in weight of the char collector and the tar trap, respectively. The composition of the gas was analyzed by a gaschromatograph (Shimazu GC 9A) equipped with both TCD and FID. The water in the tar was analyzed using the Karl Fischer titration (Kyoto Electronics Co., Ltd.). The tar component was also analyzed by a gaschromatograph with OV-101 column and FID. The material balance of this experiment was obtained

within 95 to 105 %. To estimate the effect of solvents on the pyrolysis of coal properly, the pyrolysis yields in the solvent vapors must be represented excluding the yields coming from solvents. So, the pyrolysis of each solvent was performed under same experimental conditions without feeding coal, and each yield in the solvent vapors,  $Y_i$ , was calculated by following equation:

$$Y_i = (\text{Yield in the solvent vapor}) - w(\text{Yield from solvent}) \quad (1)$$

where  $w$  is the feeding ratio of solvent vapor to coal.

## RESULTS AND DISCUSSION

### Pyrolysis in an Inert Atmosphere

To examine how we can control the product distribution of the pyrolysis of in inert atmosphere, the effects of residence time of coal and the pyrolysis temperature were examined.

#### Effect of Residence Time

Figure 2 shows the change of conversion, tar and gas yields with the increase of residence time ( $t_R$ ) at the pyrolysis temperature of 650 °C. The conversion increased with the increase of residence time, and reached a constant value over  $t_R=2$  s. The gas yield increased monotonously with the residence time. The tar yield reached a maximum at  $t_R=2$  s, then decreased with increasing  $t_R$ . It indicates that the decomposition reaction of tar vapor to gas becomes significant with the increase of residence time. Figure 3 shows the similar results at the pyrolysis temperature of 800 °C. The trends of the conversion and the char yield were similar as those at 650 °C, although the final conversion level was larger than that at 650 °C. The residence time which maximizes the tar yield shifted to smaller residence time. This means that the cracking reaction rate of tar vapor at 800 °C is much faster than that at 650 °C. Figures 2 and 3 show that the primary decomposition of coal is almost completed in  $t_R=2$  s.

#### Effect of temperature

Figure 4 shows the change of the product distribution with the pyrolysis temperature ( $T_p$ ). The char yield decreased with temperature. On the contrary, the gas yield increased with temperature. The tar yield reached a maximum, 13.1 wt%, at 650 °C. These trends coincided with those of several researches<sup>2,5</sup> using the continuous equipments. The broken lines show the yields of the flash pyrolysis performed using a Curie point pyrolyzer (CPP), in which the gas phase reaction is suppressed because only the coal is heated and the products are cooled immediately by the He flow of room temperature in CPP. The char yields of both experiments were nearly equal, indicating that the coal conversion is determined solely by the pyrolysis temperature. The gas yield of the pyrolysis in the entrained bed was larger than that of the pyrolysis in the CPP. On the other hand, the tar yield in the entrained bed was smaller than in the CPP. This indicates that the decomposition of tar is occurring in the entrained bed pyrolyzer, in which the gas stream is

also heated. Figure 5 shows the product distribution of gas component with the temperature. The yield of  $C_4-C_6$  gas reached a maximum at 700 °C, which was 50 °C higher than the temperature for the maximum tar yield. On the other hand, the yields of  $H_2$  and  $C_1-C_3$  gases increased drastically with the temperature. These results also show that the gas phase reaction which decomposes tar becomes significant with the increase of temperature, and the tar yield decreased. Thus, the maximum tar yield obtained in the entrained bed pyrolyzer was 13.1 wt.% daf at  $T_p=650$  °C and  $t_R=2$  s. This value is 17 wt.% daf lower than that obtained in the CPP<sup>R</sup>. The maximum tar yield attained in the entrained bed pyrolyzer will not exceed that obtained in the CPP.

#### Flash pyrolysis in the Vapor of solvents

Above discussion indicates that there is a limitation to increase the tar yield by controlling the temperature and the residence time as far as the pyrolysis is performed in an inert atmosphere. Then, we intended to increase the tar yield by pyrolyzing the coal in the atmosphere containing the solvent vapor. The residence time of coal was fixed as 2 s, because the primary decomposition of coal was completed in  $t_R=2$  s as stated earlier.

#### Effect of the Kind of Solvents

Figure 6 shows the changes of tar yields of the pyrolysis in  $N_2$ , in tetralin vapor and in decalin vapor with increasing  $T_p$ . The yields were calculated excluding the yield from solvent vapor<sup>R</sup> by Eq. 1. The tar yield in tetralin vapor reached up to 25.2 wt.% at  $T_p=750$  °C. This is twice larger than that in an inert atmosphere. Thus, the proposed pyrolysis method is found to be successful at least to increase the tar yield drastically. The effect of decalin vapor was only 2 to 3 wt.% larger than that in  $N_2$  atmosphere at  $T_p=700$  to 800 °C.

#### The Mechanism of Pyrolysis in Tetralin Vapor

Since the pyrolysis of coal in tetralin vapor was found to be effective to increase the tar yield, the mechanism of the pyrolysis was examined by comparing the yields obtained from the pyrolysis of tetralin, the pyrolysis of coal in  $N_2$  atmosphere and the pyrolysis in tetralin vapor. The yields were all represented based on the unit weight of daf coal.

Figures 7 to 10 show the yields of char, tar, total gas, and hydrocarbon gasses, respectively. The broken line in each figure is the sum of the yield from the pyrolysis of coal in  $N_2$  and that from the pyrolysis of tetralin. The yield in tetralin vapor coincides with the broken line if tetralin has no effect on the pyrolysis of coal.

The char yield in tetralin vapor almost coincided with the broken line as shown in Fig. 7, although it seemed to deviate at  $T_p=800$  °C. This suggests that tetralin is not effective to increase the conversion. In other word, tetralin does not affect the primary

decomposition of coal. The tar yield in tetralin vapor exceeded broken line at  $T_P=700$  to  $800^\circ\text{C}$ , and it reached more than twice at  $T_P=750^\circ\text{C}$  as shown in Fig. 8. On the contrary, the yields of total gas and hydrocarbon gases in Figs. 9 and 10 lay far below the broken lines to compensate the increase of tar yield.

Above discussion shows that tetralin vapor contributed to the rearrangement of the product distribution of the primary decomposition of coal. The reactive radicals produced by the pyrolysis of tetralin reached mainly with light hydrocarbon gases to convert them into liquid products. The analysis of tar components, now being performed, will help us to clarify the mechanism.

#### CONCLUSION

A new and simple method was developed for increasing the tar yield of coal, in which coal particles were pyrolyzed in the gas stream containing the solvent vapor. The feeding rate of solvent is only around 10 wt.% of that of coal by weight. The tar yield was successfully increased up to 25 wt.% daf in the atmosphere containing the tetralin vapor from 13 wt.% daf in an inert atmosphere. This method is expected to be easily realized in a commercial scale because of its effectiveness and simplicity.

#### ACKNOWLEDGMENT

This work was performed in the framework of the "Priority-Area Research" and "Japan-Canada Joint Academic Research Program" which was sponsored by the Ministry of Education, Culture and Science of Japan.

#### REFERENCES

1. Miura, K., Mae, K., Yoshimura, T. and Hashimoto K., Proc. Div. Fuel Chem., Am. Chem. Soc. is submitted. (Miami) Sep. (1989)
2. Teo, K.C. and Watkinson, A.P., Fuel, 65, 949 (1986)
3. Tyler, R.J., Fuel, 58, 680 (1979)
4. Scaroni, A.W., Walker, P.L. and Essenhight R.H., Fuel 60, 71 (1981)
5. Scott, D.S. and Pickorz J., Fuel Processing Technology, 13, 157 (1986)
6. Miura, K., Mae, K., Asaoka, S., Uchiyama, M. and Hashimoto, K., Proc. Int. Conf. on Coal Science is submitted. (Tokyo) Oct. (1989)

Table 1 Properties of Coal

Proximate Analysis (wt%)			Ultimate Analysis (wt% daf)				
FC	VM	ASH	C	H	N	S	O
48.2	50.3	1.5	67.1	4.9	0.6	0.3	27.1

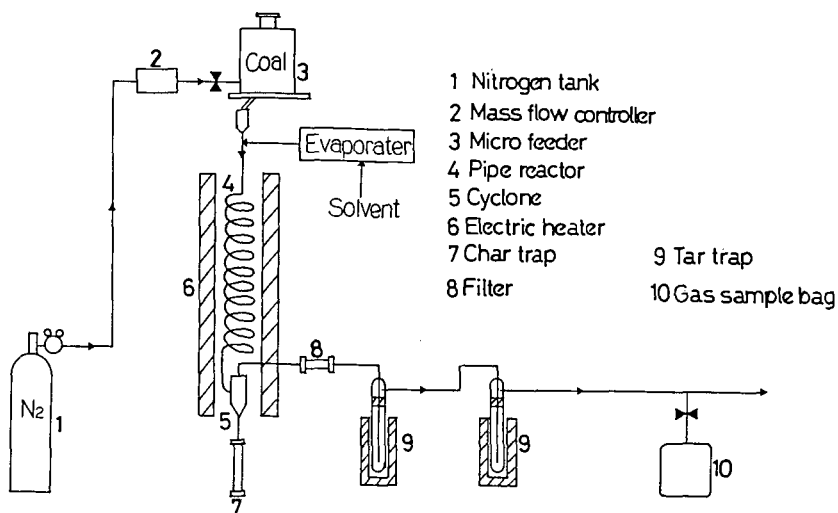


Fig.1 Schematic flow of continuous entrained bed type equipment for the pyrolysis of the coal

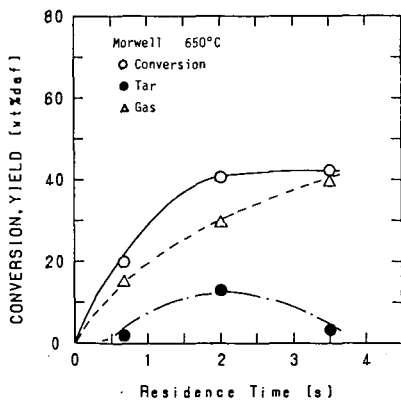


Fig.2 Effect of the residence time of coal on the product distribution ( $T_p=650^\circ\text{C}$ )

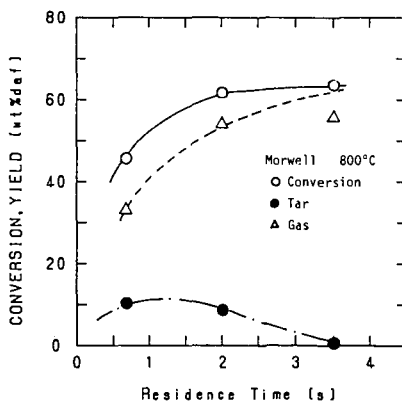


Fig.3 Effect of the residence time of coal on the product distribution ( $T_p=800^\circ\text{C}$ )

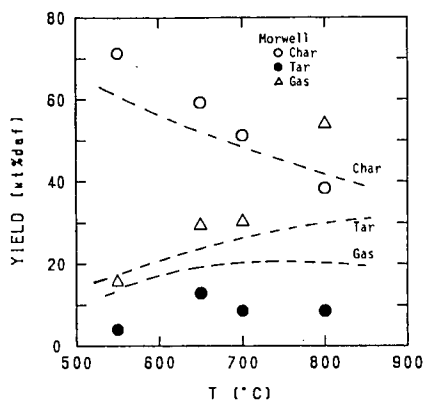


Fig.4 Effect of the pyrolysis temperature on the product distribution ( $t_p=2$  s) (broken lines: results obtained from the pyrolysis using a Curie-point pyrolyzer)

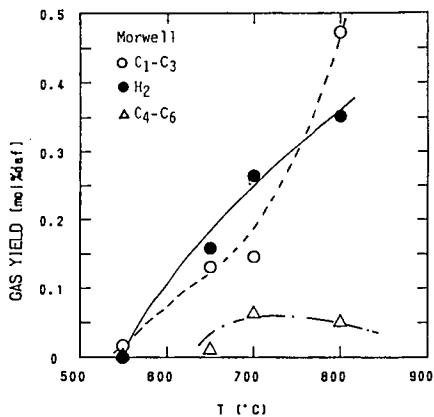


Fig.5 Effect of the pyrolysis temperature on the gas yield

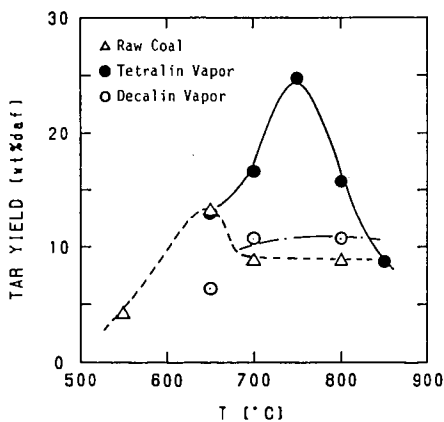


Fig.6 Effect of the atmosphere containing solvent vapor on tar yield during the pyrolysis



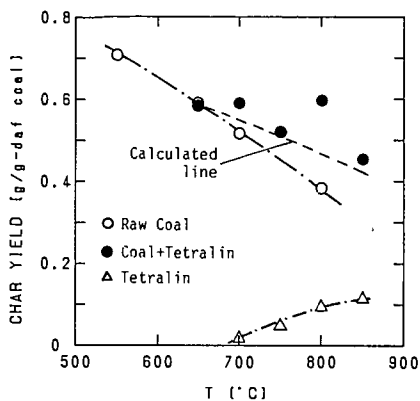


Fig.7 Effect of the atmosphere containing tetralin vapor on char yield during the pyrolysis

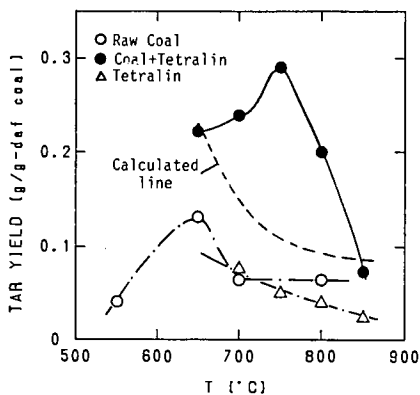


Fig.8 Effect of the atmosphere containing tetralin vapor on tar yield during the pyrolysis

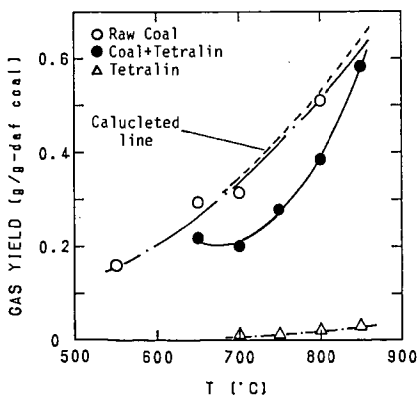


Fig.9 Effect of the atmosphere containing tetralin vapor on gas yield during the pyrolysis

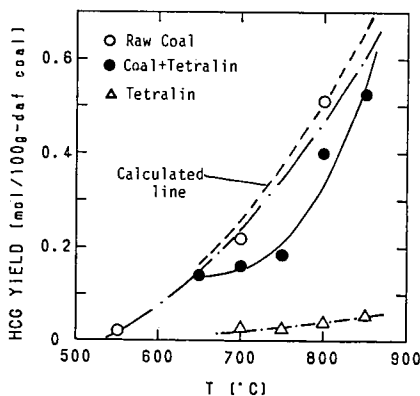


Fig.10 Effect of the atmosphere containing tetralin vapor on HCG yield during the pyrolysis

PREDICTION OF HYDROGEN CONSUMPTION FOR  
UPGRADING OF PYROLYSIS LIQUIDS<sup>1</sup>

Clint Williford  
University of Mississippi,  
University, MS 38677

M. Rashid Khan<sup>2</sup>  
Texaco Research Center  
Texaco Inc, P.O. Box 509, Beacon, NY 12508

H. F. Bauer  
U.S. Department of Energy  
Morgantown Energy Technology Center  
Morgantown, WV 26505

INTRODUCTION AND BACKGROUND

High performance aircraft require fuels with maximum heat of combustion per unit volume to achieve their maximum performance. A special class of hydrocarbon liquids can offer a relatively high energy density, fuel stability, high boiling point, and low viscosity. These fuels include bicyclic compounds composed of five- and six-ring structures such as decalin and biphenyl. Their heats of combustion range from 8800 to 9600 cal/ml versus 8000 cal/ml for JP-6 (Letort, 1962). On a volume basis such fuels would thus increase an aircraft's traveling range by 10-20%. Production of such fuels from petroleum (much of which is imported) derivatives appears to be relatively expensive. In contrast, coal liquids produced from low temperature pyrolysis or "mild gasification" may provide a rich source of aromatic bicyclics. These occur predominantly in the naphthalene or "heart-cut" of about 220-350°C boiling range (Hawk et al., 1965; Letort, 1962). Use of coal liquids however does require substantial upgrading to meet product specifications. Full boiling range liquids contain on the order of 60-75% aromatics, 1.6-10% oxygen, 0.5-3.0% sulfur, and 0.3-2.0% nitrogen (Gray et al., 1983; Hawk et al., 1965; Khan, 1986, 1987). Resulting jet fuels should meet specifications approximating those shown in Table 1.

Recent investigation at Naval Propulsion Center indicated that hydrogen content can serve as the decisive specification for aviation fuel quality (Moses et al., 1984; Masters et al., 1987). Investigators concentrated on combustion

---

<sup>1</sup> A portion of the work was done at Morgantown Energy Technology Center.

<sup>2</sup> Adjunct Professor of Chemical Engineering, University of Mississippi, University, MS 38677.

properties such as burning with minimal soot formation. They found that engines could operate satisfactorily on fuels with a hydrogen content below a reference of 13.8 wt%. Most engines could operate without adverse effects with fuels having a hydrogen content down to 13.3 wt%; and some, to 12.8 wt% of hydrogen. Likewise, Sullivan (1987) reported that fuels hydrotreated to meet combustion specifications should meet other specifications such as viscosity or freezing point.

A typical strategy for upgrading would include distillation of a heart-cut about 220-350°C. Severe hydroprocessing can be applied e.g., about 400°C and 2500 psig with a suitable nickel-containing catalyst. In some cases, it may be preferable to desulfurize first with a Co/Mo catalyst to improve the efficiency of the hydrogenation stage (Hawk et al., 1965). In addition it would be beneficial to hydrocrack 3-ring structures, phenanthrene, to 2-ring structure while limiting cracking of bicyclics.

Certain general observations can be made for the hydrogenation of a naphthalene heart-cut to low aromatics. First, the severe conditions noted above will essentially remove heterocyclic compounds from the products well before the <20 LV% aromatics specification is met. Therefore, there is no need to calculate incremental hydrogen consumption, but only a total consumption for given heteroatom content (Hawk et al., 1965; Eisen and Tice, 1977). Second, saturated and partially saturated bicyclics will dominate product composition. The degree of hydrogenation thus represents the extent of aromatic rings within a fairly stable, predictable molecular environment.

The objective of this study was to predict hydrogen consumption for conversion of a defined coal derived liquid to usable high density fuels. Literature on hydrogen consumption for upgrading coal derived liquids is extremely sparse. Many investigators do not determine hydrogen consumption in their studies. An excellent article published by Letort (1962) gave a clear picture of feed and product compositions and material balanced yields. The paper also reported hydrogen consumption for production of a high density jet fuel meeting JP-5 specification. Sullivan (1983) performed an extensive hydrotreating studies on upgrading a variety of coal derived liquids and determined the hydrogen consumption and jet fuel properties. Our analysis and subsequent predictions of hydrogen consumption are based on Letort's results with appropriate supporting data from Sullivan and others. This approach should be quite realistic for potential upgrading of bicyclic-rich coal derived heart-cuts.

## EXPERIMENTAL

The analysis presented in this study is based almost entirely on literature data, primarily reported by Letort. Letort (1962) performed a series of hydrogenation experiments on 230-310°C coal liquid distillate cut. The liquids were generated presumably in a commercial coal carbonization process. Hydrogenation experiments were performed in lab-pilot plant and commercial scale equipment. Calculations on hydrogen requirement were also performed based on the in-house data generated using a fixed-bed reactor. Detailed description of the reactor unit has been previously presented (Khan, 1987).

## RESULTS AND DISCUSSION

Upgrading mild gasification liquids into high quality fuels (e.g., high energy liquids) requires that the liquids be further treated to remove sulfur and nitrogen and to increase hydrogen content. This can be done by reacting the liquids with hydrogen gas. Ideally, the hydrogen required would be a product of the mild gasification process. While the amount of hydrogen required (approximately 2,000 SCF/bbl of liquids) is relatively low for the mild gasification process liquids, it is greater than the 10-20 volume percent (hydrogen) normally present in the mild gasification product gas. Typically, any additional required hydrogen is produced by gasifying the product char which adds process complexity; however, a preliminary experiment indicates that a calcium oxide bed can produce sufficient hydrogen by cracking methane and other hydrocarbon in the pyrolysis off-gas. In this experiment the gas products from coal pyrolyzed at 500°C were cracked over a bed of calcium oxide at 800°C. The product gas from the calcium oxide bed contained 50 percent hydrogen, which could be sufficient to totally upgrade the mild gasification liquids. Additionally, the hydrogen sulfide in the off-gas was greatly reduced by reaction with the calcium oxide. As an alternative, carbon monoxide and methane present in the product gas can be shifted and reformed to provide additional hydrogen.

Two approaches were used for hydrogen consumption calculation: (1) a simple approach using the H/C ratio of the feed and product streams; and (2) a more complex approach using molecular types in the feed.

In the simplified approach, hydrogen requirements for converting tars from different coals into usable liquids with H/C of 2. Table 2 presents the yields and analyses of tars from various coals from the fixed-bed reactor. Hydrogen consumption for upgrading the tars from fixed-bed reactor is compared to those from fluidized-bed reactor (Tyler, 1980; and Yeboah, 1980), from heated-grid reactor (Suuberg, 1979). Results on the hydrogen requirements (in gm of hydrogen needed to upgrade 100 g of raw pyrolysis liquids to a product with H/C of 2.0) from this comparison are plotted against the H/C in tars and coals as shown in Figure 1. It is noted from Figure 1 that an increase in hydrogen consumption occur with the decrease of H/C ratio of the raw tars. Figure 1 data also demonstrates that the liquids from the high heating rate processes such as fluidized bed and heated grid, have a smaller H/C ratio than those from a fixed bed reactor, which is a slow heating process.

Hydrogen consumption was also determined for a 180-280°C coal tar cut (Hawk et al., 1965) using this simplified approach. By material balance on the hydrogen content in the feed, product gas and product streams, hydrogen consumption of 5.16 SCF/100 lb of feed is estimated. This is in general consistent with the reported values.

In the second approach, the molecular structure and content for a 230-310°C coal tar distillate cut drawn from Letort's data were shown in Table 3. In this analysis the composition reported in Table 3 were taken as representative of the aromatic portion of a feedstock. For simplicity we are using this 100% aromatic-heteroatomic blend. In effect we are assuming that the saturated materials are carried through any given process as a diluent. Therefore one would use the methods presented here to calculate hydrogen consumption of the aromatic-heteroatomic portion and adjust results to reflect overall hydrogen

consumption on a "total barrel" basis. Table 4 shows expected reactions for hydrogenation and cracking of feedstock components. Note that phenanthrene is effectively converted to decalin.

In our analysis we have used the given feed, product compositions, yields, and reaction types outlined in Tables 3 and 4 to construct Tables 5a and 5b. This gives the distribution of products from each feed component upon upgrading. A number of modest assumptions were made regarding the material balancing of various ring structures. Table 6 summarizes hydrogen consumption calculations for the original base case from Letort (1962) leading to 19.82 LV% aromatic in the jet fuel cut.

In our analysis we have combined several pieces of information from Letort (1962). Letort hydrogenated a feed of the Table 3 composition to 10.2 LV% aromatics. He also reported a product component distribution. Using this product distribution as a guide we have estimated product distribution for a case of about 20 LV% product aromatics. (This aromatic content would be more in line with jet fuel specifications.) Essentially we assumed that the ring structure and degree of cracking between the two cases would be very similar with the main difference lying in a quantitative difference in the content of aromatic molecules. Working directly from the product distribution reported by Letort we doubled the content of aromatic products and accordingly decreased the amount of saturated product components. We then performed a lb mole balance analysis for the conversion of feed components to product components. This appears in Table 5a. We then determined the lb moles of  $H_2$  consumption to convert each lb mole of feed component to the respective product components. We present the hydrogen consumption for each product component in Table 5b.

In more detail, Table 5a presents an estimated product distribution for the hydrogenation of 100 lb of an aromatic feed described in Table 3 (Letort, 1962). Along each row are product components resulting from the hydrogenation of each feed component, listed on the left. For example, 0.328 lb moles of naphthalenes and alkyl naphthalenes enter as feed, of which 0.214 lb moles are converted to decalins; 0.0168 lb moles, to alkylindanes; and so forth. The total product components in each row equals the lb moles of feed, except where the feed molecule cracks into two molecules as noted by "x2" below the product amount.

From the product distribution estimates in Table 5a we calculated hydrogen consumption as presented in Table 5b. Values shown are estimated lb moles  $H_2$  consumed to convert feed components listed in the left hand column to the product components listed along each row.  $H_2$  consumption was estimated by multiplying the lb moles for each product component in Table 5a by the lb moles  $H_2$  required to convert the feed component (left hand column) to the product component in the same row. For example 0.328 lb moles naphthalenes/alkyl naphthalenes enter as feed and 0.214 lb moles are converted to decalins with 5 lb moles  $H_2$  required for each lb mole converted. Multiplying  $0.214 \times 5 = 1.07$  lb moles  $H_2$  consumed, listed under the column labeled "Decalins."

We also applied this estimation technique to Letort's data. We estimated a hydrogen consumption of 16.19 SCF/lb feed at 10.2 LV% product aromatics and a

product density (based on component densities) of 0.8696 g/cc. Letort (1962) reported 15.8 SCF/lb feed and 0.886 g/cc.

In order to estimate incremental hydrogen consumption we started with the initial case of 19.82 LV% aromatic in the product. The hydrogen consumption was then calculated for a case of 10.2 LV% product aromatics and the difference was calculated. Dividing by the change in aromatics gave an average incremental hydrogen consumption per LV% aromatics in the range of interest.

The average incremental hydrogen consumption, calculated is about 32 SCF/LV% aromatics/bbl in the 10-20 LV% range. This is comparable to the "rule of thumb" value (25 SCF/LV%aromatic/bbl) applied to petroleum distillate fractions. Note that once the fuel has been hydrogenated to about 20 LV% aromatics the hydrogen consumption for heteroatom removal approaches zero. Also note that in the original case much of the biphenyl cracks to a light cut (B.pt.<150°C) or gas. This is undesirable due to hydrogen consumption and destruction of a fuel component. The saturated dicyclohexyl has a heating value/ml about 12% higher than that for JP-6 (Letort, 1962).

It is very likely that satisfactory hydrogenation can be achieved with much less cracking. Hawk et al. (1965) hydrogenated comparable liquids with only 1.7 wt% loss to gases versus about 10% by Letort (1962). Sullivan (1983) reported losses to C<sub>4</sub> of less than 0.5%. Thus an optimum process should promote cracking of 3- to 2-ring species but suppress as much as possible the cracking of biphenyl. The benefits are threefold: (1) hydrogen consumption is lower than the other cases, (2) aromatics are lower, at 16.8 LV%, and (3) fuel cut yield is higher, at about 100 lb versus 85.5 lb for the two previous cases that exhibited the relatively large extent of cracking consistent with Letort's observation. Hydrogen consumption for three cases was considered by Letort, representing hydrogen consumption for a 100% aromatics feed to low product aromatics concentration of 10-20 LV%. On a barrel basis this would amount to about 5,000 SCF/bbl, a very high value. Sullivan (1983) gave more representative values, i.e. from 700-2,550 SCF/bbl, for a number of coal liquids hydrogenated to 20 LV% aromatics.

One should recognize that hydrogenation to about 20 LV% aromatics and consequently about 0 LV% heteroatoms is literally a given requirement. Further hydrogenation would be used to meet the remaining specifications, e.g., smoke point. Excessive hydrogenation must be minimized to conserve hydrogen and because hydrogenation generally reduces density.

The relationship between aromatic saturation and liquid properties is an interesting topic. Letort (1962) reported that his fuels ranged from 0-11 wt% aromatics and met freezing point and viscosity specifications for JP-5. Results from Eisen and Tice (1977) who used syncrudes from Utah and west Kentucky coals reveal the impact of percent aromatics on properties such as freezing, flash, and smoke points.

Comparing the data for each coal in the two aromatics ranges shows little change in physical properties below 25 LV% aromatics. Only smoke point and density change modestly. What this shows is that hydrogenation alone can be used to meet aromatics LV% and smoke point specifications. However, once aromatics have been reduced to about 20 LV%, properties such as flash or

freezing point will depend on more subtle characteristics of the mixture of molecular structures.

#### SUMMARY AND CONCLUSIONS

Based on a review of literature it appears that specific information on hydrogen consumption appears to be limited for upgrading of pyrolysis liquids. The appropriate tar fraction for upgrading to jet fuel is the 220-350°C cut which is composed of mainly aromatics with 2-ring structures with a minor amount of phenanthrene.

To achieve about 20 LV% product aromatics results in almost total heteroatom removal during the hydrogenation of aromatics.

For a 100% aromatic feed stream hydrogen consumption will be approximately 15.33/lb feed to yield 20 LV% product aromatics. However, typical values for actual coal liquids will range from 70-2,500 SCF/bbl. Suppression of cracking, perhaps through catalyst choice, could potentially reduce hydrogen consumption by 10-20% and improve product yields.

Incremental hydrogen consumption is about 30-32 SCF/bbl/LV% aromatics in the 10-20 LV% product aromatics range.

Additional aromatic saturation in the 10-20 LV% product aromatic range affects transport properties little, but does modestly affect smoke point and density.

Excessive hydrogenation must be avoided through choice of process conditions and catalysts because it wastes hydrogen and decreases density. Hydrogen content (12.8-13.3 wt%) may serve as the decisive specification for jet fuel quality.

It is important to crack phenanthrene to meet product specifications, e.g., viscosity, but biphenyl cracking should be suppressed. This conserves hydrogen and increases product yields with the saturated bicyclohexyl form, a high density fuel component.

**ACKNOWLEDGEMENT:** A portion of this study was performed at the US Department of Energy, Morgantown Energy Technology Center (by MRK, see ref 5).

#### REFERENCES

1. Antoine, A. C., and J. P. Gallagher. 1977. "Jet Fuels from Synthetic Crudes," Coal Processing Technology, vol. 3, P.107-114.
2. Arnold, M. St. J., and P. F. M. Paul. 1980. "Aviation Fuels from Coal," Journal of the Institute of Energy, June:55-62.
3. Eisen, F. S., and J. D. Tice. 1977. "Gas Turbine Engine Fuel from Synthetic Crude," Coal Processing Technology, vol. 3, P.115-121.
4. Hawk, C. O., and others. 1965. Hydrorefining Coal-Oils to Fuel for Supersonic Aircraft. U.S. Bureau of Mines, Rep. Invest. No. 6655.
5. Khan, M. R., March 1986. Production of a High-Quality Liquid Fuel from Coal by Mild Pyrolysis of Coal-Lime Mixtures. 13 pp. DOE/METC/86-4060. NTIS/DE86006603. Also, Khan, M. R., 1987, Fuel Science and Technology International, 5(2).

6. Letort, M. 1962. "Now-Make Jet Fuels from Coal," Hydrocarbon Processing and Petroleum Refiner 41(7):83-88.
7. Masters, A. I. and others. March 1987. Additional Development of the Alternate Test Procedure for Navy Aircraft Fuels, Final Report for Naval Air Propulsion Center, Trenton, N.J., NAPC-PE 160C.
8. Moses, C. A. and others. August 1984. An Alternate Test Procedure to Qualify Fuels for Navy Aircraft. Phase II, Final Report for Naval Air Propulsion Center, Trenton, N.J. NAPC-PE-145.
9. Stein, T. R., S. E. Voltz, and R. B. Callen. 1977. "Upgrading Coal Liquids to Gas Turbine Fuels. 3. Exploratory Process Studies," Industrial and Engineering Chemistry Product Research and Development 16(1):61-68.
10. Suuberg, E. M. W. Peters, and J. Howard. 1979. Combustion Symposium (International), The Combustion Institute, p.117.
11. Sullivan, R. F. November 16-17, 1983. "Refining of Syncrude from Direct Coal Liquefaction Processes," Paper Presented at DOE Direct Liquefaction Contractors Project Review Conference, Pittsburgh, PA.
12. Sullivan, R. F. April 5-10, 1987. "High-Density Jet Fuels from Coal Syncrudes," Paper Presented at Symposium on Structure of Future Jet Fuels, ACS Meeting, Division of Petroleum Chemistry, Denver, CO.
13. Tyler, R. 1980. Fuel, 59, 218.
14. Tamas, J. 1986. "Determining Physical Properties for Multicomponent Hydrocarbon Mixtures," Chemical Engineering September:103-108.
15. Yeboah, Y. D. and others. 1980. Industrial and Engineering Chemistry Process Design and Development, 19(4), pp. 646-653.

Table 1  
JP-5 Specifications  
(Risen and Tice, 1977)

Distillation, °F:		
10%.....	400	max
E.P.....	550	max
Gravity, °API.....	36-48	
Freezing Point, °F.....	-51	max
Aromatics, Vol.%.....	25	
Smoke Point, mm.....	19.0	min
Flash Point, °F.....	140	min
Viscosity, cSt -30°F.....	16.5	max



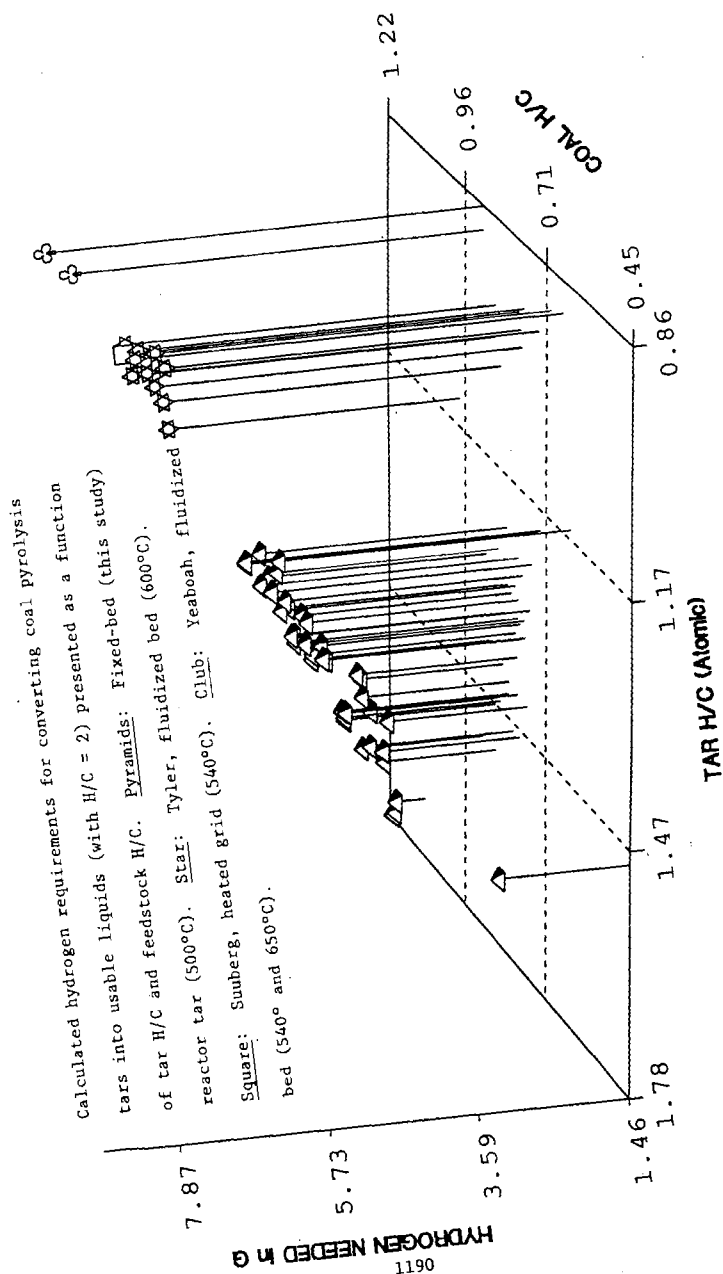


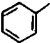
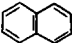
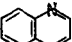
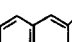
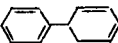
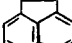



FIGURE 1

TABLE 2  
Yield and Analyses of Liquids Generated from Various Coal  
in the Fixed-Bed Reactor

OBS	Sample	Rank	Tar*	Gas (L)	Char*	Tar H	Tar C	H/C
1	PSOC 123	hvAb	14.8	6.04	75.2	10.19	84.89	1.44
2	PSOC 181	Sub A	13.8	7.90	81.9	9.36	83.01	1.35
3	PSOC 267	hvA	14.3	7.02	75.4	8.90	85.09	1.26
4	PSOC 275	hvAb	12.6	5.58	73.6	9.58	82.38	1.40
5	PSOC 296	hvAb	15.4	6.34	76.7	9.38	83.89	1.34
6	PSOC 306	hvAb	10.3	5.88	78.1	8.66	80.32	1.29
7	PSOC 355	hvAb	12.2	7.78	75.8	8.81	81.12	1.30
8	PSOC 375	hvAb	15.2	7.04	75.3	8.66	79.37	1.31
9	PSOC 1109	hvCb	25.0	9.29	56.6	11.66	78.70	1.78
10	PSOC 1313	mvb	5.5	6.02	84.7	8.59	85.91	1.20
11	PSOC 1323	hvBb	14.9	9.30	71.5	8.59	73.10	1.41
12	PSOC 1443	Sub C	10.5	9.80	66.6	10.33	80.93	1.53
13	PSOC 1445	hvC	14.1	9.80	69.5	10.78	84.51	1.53
14	PSOC 1448	hvAb	15.7	7.10	76.5	10.41	84.93	1.47
15	PSOC 1449	hvAb	23.6	7.12	62.3	11.06	78.04	1.70
16	PSOC 1451	hvA	14.1	3.10	80.5	8.70	82.01	1.27
17	PSOC 1469	hvAb	8.4	6.48	83.0	9.07	84.01	1.30
18	PSOC 1470	hvAb	9.2	3.82	76.8	8.22	80.08	1.23
19	PSOC 1471	hvAb	16.1	7.00	74.7	8.69	79.66	1.31
20	PSOC 1472	hvAb	14.8	8.06	76.2	9.37	86.03	1.31
21	PSOC 1473	hvAb	18.8	5.78	70.4	9.52	85.75	1.33
22	PSOC 1475	hvAb	15.8	7.84	75.1	10.08	84.58	1.43
23	PSOC 1481	hvAb	15.3	6.54	73.1	8.91	74.68	1.43
24	PSOC 1492	hvCb	13.7	7.90	70.5	8.60	74.67	1.38
25	PSOC 1499	hvAb	15.4	8.34	69.6	10.32	83.56	1.48
26	PSOC 1502	hvCb	12.7	8.40	69.9	10.01	81.07	1.48
27	PSOC 1504	hvAb	14.9	7.68	72.4	10.33	84.82	1.46
28	PSOC 1508	lv	3.2	5.50	91.0	--	--	--
29	PSOC 1516	lv	6.9	5.50	95.2	7.74	80.53	1.15
30	PSOC 1517	hvAb	14.2	8.60	75.3	8.88	79.73	1.34
31	PSOC 1520	Sub C	7.9	8.42	53.8	9.75	78.57	1.49
32	PSOC 1523	hvAb	12.7	6.30	80.5	9.25	83.66	1.33
33	PSOC 1524	hvAb	11.9	7.20	78.1	9.17	81.75	1.35
34	Pitts No. 8	hvAb	17.7	7.00	75.3	9.10	80.70	1.35
35	Ill. No. 6	hvCb	14.0	7.60	76.7	9.05	76.22	1.42
36	Ohio No. 6	hvCb	12.9	5.60	71.7	8.32	78.52	1.27
37	Wellmore No. 8	hvAb	14.2	7.00	75.6	8.76	84.30	1.25
38	AMAX	hvAb	14.1	7.70	77.1	8.53	85.86	1.19
39	N.D. Lignite	lig	4.0	11.40	64.1	9.14	75.04	1.46
40	Miss. Lignite	lig	21.3	13.00	54.2	11.40	77.80	1.76

\* Tar and char yield in weight percent (dry-basis)

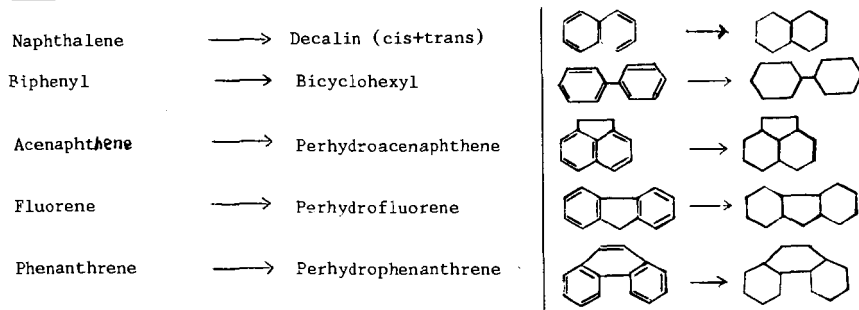
TABLE 3  
REPRESENTATIVE FEED COMPOSITION FOR COAL LIQUID AROMATICS

Formulas	Constituents	Weight %
	Light Constituents	1.1
	Naphthalene	10.3
	Quinolines	1.8 (0.2% Nitrogen)
	Alkyl Naphthalenes	38.7
	Biphenyl	5.4
	Acenaphthene	14.6
	Dibenzofuran	16.7 (1.6% Oxygen)
	Fluorene	6.9
	Phenanthrene	11
	Various Alkyl-biphenyls Alkyl-fluorenes	3.4
		<hr/> 100.0

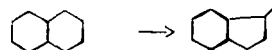
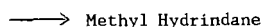
Tar fraction boiling between 230 and 310°C contains ring compounds in the quantities shown. Letort (1962).

TABLE 4  
TYPICAL REACTIONS FOR COAL LIQUID UPGRADING TO JET FUEL

RING SATURATION

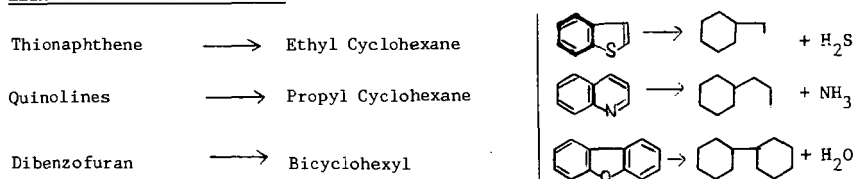


Isomerization  
Decalin



Ring saturation and isomerization reactions take these forms.

ELIMINATION OF HETERO ATOMS



CRACKING

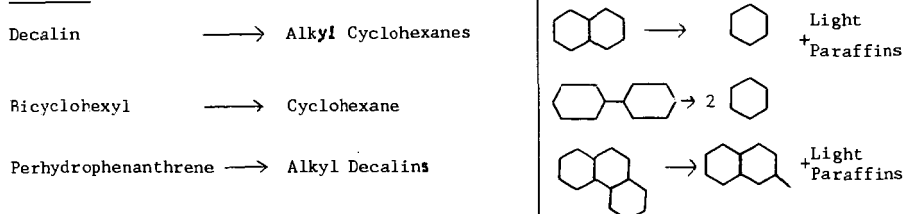


TABLE 5a

**ESTIMATED PRODUCT DISTRIBUTION FROM  
HYDROGENATION/CRACKING OF COAL TAR**

(values are feed, product lb moles on a 100 lb liquid feed basis)

19.8 LV% Product

Aromatics

Product Components

Feed Components

Feed	Alkyl-cyclohexanes	Decalins	Dicyclohexyl	Perhydro- acenaphthene	Perhydro- fluorene	Alkylbenzene	Alkylindanes	Tetralins	Cyclohexyl- benzene	Tetrahydro- acenaphthene	Hydrindanes	Phenanthrene
Light Constituents	.012	.008				.004						
Naphthalenes and Alkyl-naphthalenes	.328	.214					.0168	.048			.05	
Quinolines	.014	.008				.006						
Biphenyl, Alkylbiphenyl, and Dibenzofuran	.144	.0005 x2	.026			.013 x2			.01			
Acenaphthene	.095	.041	.039				.0012	.0068		.003	.004	
Fluorene and Alkylfluorene	.051	.0033 x2			.0066		.003	.0032			.007	
Phenanthrene	.062	.0375					.003	.008			.009	.004
Product Totals		.3008	.026	.039	.0066	.036	.024	.066	.01	.003	.07	.004

presented here is an estimated product distribution for the hydrogenation of 100 lb of an aromatic feed described in Table 3 (Letort, 1962). Along each row, are product components resulting from the hydrogenation of the feed. The total product amount is 139 lb moles of naphthalenes and alkyl-naphthalenes enters as feed, of which 0.214 lb moles are converted to decalins; 0.0168 lb moles, to alkylindanes; and so forth. The total product components in each row equals the lb moles of feed, except where the feed molecule cracks into two molecules as noted by "x2" below the product amount.

We derived the product distribution shown here for about 20 LV% aromatics from Letort's work in which he hydrogenated the given feed to 10.2 LV% product aromatics. For the estimate we doubled the product aromatics to 20 LV% product aromatics. The amount of saturated products so as to material balance with the feed component in each row. We assumed that the extent of ring opening and other cracking reactions would remain little changed between the two cases.

TABLE 5b

**ESTIMATED HYDROGEN CONSUMPTION FOR PRODUCTION  
OF PRODUCT DISTRIBUTION IN TABLE 5a**

(Values are lb moles H<sub>2</sub> consumed on a 100 lb feed basis)

19.8 LV% product

Aromatics

Product Components →

Feed Components ↓

	HDS, HDN, HDO	Alkyl- cyclohexanes	Decalins	Dicyclohexyl	Perhydro- acenaphthene	Perhydro- fluorene	Alkylbenzene	Alkylindanes	Tetralins	Cyclohexyl- benzene	Tetrahydro- acenaphthene	Hydrindanes	Perhydro- phenanthrene
Light Constituents		.024					0						
Naphthalene and Alkyl naphthalenes			1.07					.0326	.096			.35	
Quinolines	.042	.032					.006						
Biphenyl and Alkylbiphenyl Dibenzofuran	.2	.0035		.1296			.026			.03			
Acenaphthene			.082		.156			.0048	.0272		.006	.028	
Fluorene and Alkylfluorene		.184	.0664			.0396		.015	.016			.056	
Phenanthrene			.3375					.018	.048			.081	.028

Values shown are estimated lb moles H<sub>2</sub> consumed to convert feed aromatics to the product components listed along each row. Product components are listed in Table 5a. H<sub>2</sub> consumption was estimated by multiplying the lb moles of each product component in Table 5a by the lb moles H<sub>2</sub> required to convert the feed component (left hand column) to the product component in the same row.

For example 0.328 lb moles naphthalenes/alkyl naphthalenes enter as feed and 0.214 lb moles are converted to decalines. The difference of 0.114 lb moles H<sub>2</sub> required for each lb mole of feed naphthalenes/alkyl naphthalenes is listed under the column labeled "decalines".

TABLE 6  
SUMMARY OF HYDROGEN CONSUMPTION TO PRODUCE  
PRODUCT WITH 20 LV% AROMATICS  
(From feed described in Table 3)

Description of Hydrogen Consumption	H <sub>2</sub> Consumed
Aromatics Saturation	2.894 lb moles
Heteroatom Removal	0.242 lb moles
Production of Light Cut (<150°C)	0.365 lb moles
Production of Gases	<u>0.770 lb moles</u>
TOTAL:	4.271 lb moles H <sub>2</sub> /100 lb feed
	or 15.33 SCF/lb feed

**HIGH ENERGY DENSITY MILITARY FUELS  
BY HYDROPROCESSING OF COAL PYROLYZATES**

Marvin Greene, Steven Huang, Vincent Strangio, James Reilly  
LUMMUS CREST INC  
Bloomfield, NJ 07003

**INTRODUCTION**

Lummus Crest Inc. (LCI), a subsidiary of Combustion Engineering Inc., successfully responded to a DOE-Morgantown Energy Technology Center (METC) solicitation for development of high energy density fuels from mild gasification coal liquids and other selected synfuels and is currently carrying out a multi-year test program at its Engineering Development Center. With Amoco Oil Company as a major subcontractor, LCI's program is directed towards the determination of the minimum processing requirements to produce high energy density distillate fuels for use in military aircraft and/or diesel-powered vehicles.

The specific objectives of the program are:

- o Conduct a technical and economic assessment of promising processing and upgrading methods to convert raw liquid products from mild coal gasification and other selected synfuel processes into advanced high volumetric energy density test fuels;
- o Conduct screening tests of alternative processing methods; and
- o Generate test quantities, ca., 100 gallons each, of two advanced fuels from mild coal gasification liquids and from Colorado shale oils provided by DOE contractors for a Phase I program and from two additional synfuels to be specified for an optional Phase II program.

**BACKGROUND AND STATEMENT OF PROBLEM**

METC has recently been reassessing the technologies for best utilizing our domestic coal resources to provide for the future demand for transportation fuels and generation of clean power. Much of the technological strategies has been unidimensional, i.e., development and marketing of coal utilization technologies that produce a main product such as liquid boiler fuel, refinery syncrude, desulfurized clean coal, etc.

As part of its assessment, METC has concluded that there is a technology type, referred to as Mild Coal Gasification (MCG), which has the potential to simultaneously satisfy the transportation and power generation fuel needs in a most cost-effective manner. MCG is based on low temperature pyrolysis, a technique known to the coal conversion community for over a century. Most past pyrolysis developments were aimed at maximizing the liquids yield which results in a low quality tarry product requiring significant and capital intensive upgrading.

By properly tailoring the pyrolysis severity to control the liquid yield-liquid quality relationship, it has been found that a higher quality distillate-boiling liquid can be readily "skimmed" from the coal. The resultant liquids have a much higher H/C ratio than conventional pyrolytic tars and therefore can be



hydroprocessed at lower cost. These liquids are also extremely enriched in 1-, 2-, and 3-ring aromatics. The co-product char material can be used in place of coal as a pulverized fuel (pf) for power generation in a coal combustor. In this situation where the original coal has a high sulfur content, the MCG process can be practiced with a coal-lime mixture and the calcium values retained on the char can tie up the unconverted coal sulfur upon pf combustion of the char. Lime has also been shown to improve the yield and quality of the MCG liquids.

Aviation turbine fuels represent less than 10 percent of the refinery production in the U.S. The growing scarcity of light sweet petroleum crude could impact the future availability of a minor refinery product such as jet fuel. Thus, alternate feedstocks such as coal liquids, shale oils and tar sands bitumen, may eventually be utilized as feedstocks for distillate fuels.

Future aircraft, military as well as commercial, may need to meet certain performance criteria such as extended flying range or need to fly at supersonic or hypersonic speeds. Similarly, future military land vehicles may need to have extended ranges between fuel reloading. With the exception of selected relatively low volume refinery streams (e.g., rerun reformates, pyrolysis gas oils), the bulk of petroleum-derived turbine fuels contains a significant concentration of aliphatic materials. These paraffinic compounds do not possess the desirable specific gravity-calorific value or the endothermic (dehydrogenation ability) characteristics of those of cyclic compounds. These latter cyclic or naphthenic materials, whose precursors can be single or multi-ring aromatics, are the only known and practical hydrocarbons that meet the high energy volumetric density and/or endothermic properties required for the advanced High Energy Density Fuels, hereinafter referred to collectively as HEDF.

Thus, there is a beneficial synergism between the distillable aromatics-rich liquids produced by mild gasification and the production of advanced HEDF.

While the MCG liquids are enriched in the HEDF precursors, namely, 1-, 2-, and 3-ring aromatics, they must be processed in such a manner as to generate a product meeting all environmental and technical specifications for HEDF aviation turbine and diesel fuels. LCI, as a process technology firm, has developed a whole family of hydrogenation processes for hydroprocessing various refinery and petrochemical streams from C<sub>4</sub>'s all the way to vacuum residua, utilizing both fixed-bed and expanded-bed hydroprocessing reaction systems. The latter system is of special importance for feedstocks contaminated with trash metals and/or for reactions requiring critical heat removal due to the severe exothermicity of the hydroprocessing reactions. LCI's general approach consists of a combination of mid-distillate hydrotreatment; atmospheric resid or VGO hydrocracking; delayed coking of the atmospheric resid portion of the synfuel liquids. Selection of the optimal processing routes will be identified by use of Amoco's refinery linear programming models.

The MCG liquids contain significant heteroatom content in the form of phenols, aromatic sulfur compounds, pyridines and other organic nitrogen compounds. These materials have to be processed in such a way as to remove the heteroatoms without dearomatizing the ring structure and at conditions that will minimize hydrogen consumption. Although it may be possible to utilize one catalyst having all the required functionalities, i.e., HDN, HDS, HDO and ring saturation, and charged in a single reaction system, an overall loss in selectivity and activity will probably result. It may therefore be more cost effective to segregate the process

functions into separate stages thereby allowing the utilization of more selective and active catalysts for the heteroatom removal and the aromatic ring saturation steps.

The proposed technical approach for the distillate hydrotreating step is to identify the optimal reaction conditions for each step of the two-step process (heteroatom removal followed by ring saturation). The identification of the preferred catalysts in each stage is a key component of the program. Focus will be placed on determining the minimum processing steps including necessary separation or recycle systems to produce the advanced HEDF.

### HIGH ENERGY DENSITY FUELS

Three advanced HEDF types have been defined for the program by the DOE:

#### Category I - Aviation Turbine Fuel

This advanced fuel is defined as one having a Lower Heating Value (LHV) in excess of 130,000 Btu/gal and having high thermal stability. For comparison, conventional JP-4 turbine fuel has an LHV of only 119,400 Btu/gal and typical kerosene has a value of about 123,000. Decalin, an unsubstituted 2-ring cycloparaffin, has an LHV of 135,400 Btu/gal and an alkylated decalin has an LHV of 134,950 Btu/gal. This Category I advanced fuel must conform to the operational requirements reflected in the DOD fuel specifications for JP-4 and JP-8 but with necessary chemical composition variations required to achieve the desired higher volumetric energy densities and/or to reduce the required processing severity.

#### Category II - Endothermic Turbine Fuel

This advanced fuel must have a high energy density value but also must have those properties to make it a satisfactory fuel for use in advanced hypersonic aircraft. At hypersonic speeds, significant thermal problems arise due to the effect of stagnation temperature, the latter being the resultant temperature due to the resistance of the air molecules impeding the motion of the vehicle. Heat can be removed by either a mechanical refrigeration system; a non-combustible coolant; or by the fuel itself, the latter being the most preferred. Three types of endothermic processes can be used depending upon fuel type: a) catalytic dehydrogenation of naphthenes; b) thermal cracking of various hydrocarbons; and c) depolymerization of polymers. All of these systems have varying heat sink limits and the prior R&D reported in the literature (1) has pinpointed the naphtha dehydrogenation route as a preferred endothermic mechanism. Typical compounds having good heat sinks include methylcyclohexane(MCH), methycyclopentane(MCP), decalin, dicyclohexyl, etc. Compounds of these types or their unsaturated precursors might exist in the Mild Coal Gasification liquids at some appreciable concentrations to result in the production of a reasonable yield of the Category II advanced fuel.

#### Category III - High Energy Diesel Fuel

This advanced fuel must meet DOD's diesel spec VV-F-800D and have an energy density comparable to that of the Category I turbine fuel thus allowing extended driving range for military vehicles such as tanks. This spec has no volumetric energy density limitation per se, but the Cetane No. spec can be affected by hydrocarbon type, in particular, aromatics, and the latter will affect the

resultant energy density of the fuel. The three grades of VV-F-800D diesel fuel, namely, DF-A, DF-1 and DF-2, have varying operability characteristics pursuant to the climactic specification. Grade DF-A, Arctic grade, has the lowest viscosity requirement and distillation end point limit. Back-end diesel cut blending to achieve the desired high volumetric energy density will have to be balanced against front-end blending to insure that the Distillation End Point, Viscosity and Carbon Residue specifications are not violated.

#### PROGRAM METHODOLOGY

Eight contract work tasks were defined with the bulk of the experimental testing consolidated into Tasks 3 and 5. Task 3 consists of a screening program to collect process operating data for each of the candidate processes over a relatively wide range of conditions. These data will be used as the input to the Task 4 modeling studies being performed by Amoco for the purpose of identifying the near optimal commercial processing sequences. Based on the latter, the Task 5 pilot plant program will be carried out to produce 100-gal each of two types of advanced HEDF fuel for each candidate synfuel feedstock. Resultant samples as well as liter quantities of test samples produced during the screening task will be delivered to DOE contractors for further evaluation.

Two feedstocks have been identified for the Phase I program: a mild coal gasification liquid and a Colorado shale oil. These liquids were required in 1000-gal quantities and therefore they had to be obtained from relatively large scale pilot or commercial plants. Since MCG technology is currently being scaled up from the laboratory or bench scales, DOE elected to provide a commercially available material having properties comparable to those anticipated for the MCG process. The resultant MCG liquid provided to LCI was derived from the British COALITE Process. The latter is a low temperature carbonization process developed in the early 1900's (2) based on the use of a vertical retort. A COALITE plant built in 1936 at the Bolsover Works of Coalite and Chemical Products Ltd. is still in operation and the 1000-gal sample was procured and delivered to LCI by United Coal Company Research Corporation under a separate DOE-METC contract. Table 1 is a summary of the properties of the whole range COALITE and the nominal 300-650F mid-distillate fraction which served as the feedstock for fixed-bed hydrotreating. The COALITE was produced from a medium coking British coal and is expected to have properties similar to those of U.S. Eastern bituminous coals. The balance of this paper will review the process variables scan testing of the fixed-bed hydrotreatment of the 350-650F COALITE mid-distillates.

The fixed-bed hydrotreating unit consists of a two-stage, close-coupled, fixed-bed reactor system equipped with high pressure liquid and gaseous (hydrogen) feed systems and a product recovery system. Each reactor contains about 100-150 cc of catalyst and both reactors can be operated in series or the second reactor can be bypassed with only the first reactor in use. To date, three catalyst types are being evaluated: a nickel tungsten; a promoted nickel tungsten; and a nickel moly.

The major technical challenge to achieving the minimum energy density specification is the addition of hydrogen to the mid-distillates in such a way that the rate of decrease in specific gravity upon hydrogenation does not exceed the rate of increase of gravimetric heat content. Otherwise, the net volumetric energy density will deviate from the target. Catalysis and operating severity must be controlled to minimize ring opening as well as to minimize hydrogen-consuming gas forming reactions.

In evaluating the process screening data, we found good correlations between the Refractive Index (R.I.) and the other HEDF fuel properties of interest, namely, volumetric energy content, API gravity, hydrogen content, Smoke Point, Cetane Index, Luminometer No., aromatics content, etc. Figure 1 maps the interaction of the API gravity-R.I. relationship vs. the predicted volumetric energy density expressed as lower heating value (LHV). Upon interchanging the API and the R.I. axes (Figure 2), we can see the extent of the hydrogenation on the whole distillate LHV for a series of hydrotreating tests made with the nickel tungsten catalyst. The slope of the regressed data is slightly skewed to the lines of constant LHV. It would appear that at hydrogenation severities resulting in whole distillate product R.I.'s below about 1.49, continued hydrogenation to reduce heteroatoms and smoke-forming aromatics results in excursions away from the LHV target of 130,000 Btu/gal.

However, it is important to appreciate that other jet and diesel properties besides energy density need to be met, such as for example, flash point and freeze (or pour) point, if the HEDF fuel is to be successfully implemented. The original test distillate feedstock was arbitrarily defined as a nominal 350-650F fraction. During hydrotreatment, the heteroatoms, in particular, phenolics and cresylics, are hydrogenated to their cyclic hydrocarbon counterparts and these materials (e.g., cyclohexane, methylcyclohexane). These have boiling points below those in the 350-650F starting material and adversely affect the flash point properties. Furthermore, the selected end point of 650F was apparently too high because it resulted in high freeze points for the whole distillate product. Accordingly, a post-hydrotreating fractionation operation is required to top and tail the material in order to meet the volatility and freeze point properties of HEDF fuels.

Table 2 shows the properties of distillate products recovered from the topping and tailing of the hydrotreated 350-650F COALITE distillates. Even though the whole hydrotreated distillate products from these runs had energy densities some 2.2 to 2.8% below the target, the removal of portions of the front-end and back-end by distillation resulted in a net increase in the LHV to within 0.7 to 1.3% of the 130,000 Btu/gal target. While the removal of the lighter front-end for flash point adjustment increases the LHV to above the target, the simultaneous removal of the heavier back-end for freeze point adjustment reduces the specific gravity with a resultant net LHV fractionally below the target. In tailing the two products shown in Table 2, we apparently removed too much of the back-end causing freeze points (-54 to -57F) better than the -40F spec. Easing off on the tailing operation should increase the LHV to within less than 0.5% of the target. We also are investigating other hydrotreating catalysts that have the potential for further improvements in selectivity towards the desirable 2-ring cyclics in order to meet and/or exceed the 130,000 Btu/gal LHV target.

#### ON-GOING AND FUTURE WORK

Nominal 350-650F distillates derived from the expanded-bed hydrocracking via LC-Fining<sup>sm</sup> of the 650F+ residual fraction of the COALITE were produced and subjected to fixed-bed hydrotreatment. Noticeable differences in severities to achieve HEDF specs were observed for the LC-Finates in comparison to the raw

(sm) LC-Fining is a service mark of LCI for engineering, marketing and technical services relating to hydrocracking and hydrodesulfurization processes for reduced crudes and residual oils.

hydrotreated distillates, with the LC-Finates being more reactive. Similar testing was carried out with coker distillates derived from delayed coking of the 650F+ COALITE. The process scanning program is also being carried out for the Colorado shale oil sample supplied to LCI by Western Research Institute. The Colorado shale oil is not as aromatic as the MCG liquids and therefore the degree of hydrogen addition is not as severe as for the case of the COALITE. However, tailoring the catalyst functionality to produce the proper mix of cyclics and aliphatics in the hydrotreated shale oil distillates is a technical challenge and is being addressed in this program.

#### ACKNOWLEDGEMENTS

This work is being supported by the Department of Energy under DOE Contract No. DE-AC21-88MC25020. LCI would like to acknowledge the technical and management support of Charles Byrer and Jim Burchfield of METC. We would also like to acknowledge the efforts of Lou Senario, LCI's pilot plant supervisor, and Sam Mikhail, LCI's analytical services supervisor. Supporting technical consulting by Joe Masin and Dave Soderberg of Amoco has also been beneficial to the program.

#### REFERENCES

- (1) Lander, H. and Nixon, A.C., "Endothermic Fuels for Hypersonic Vehicles", 15th Annual AIAA Meeting, Philadelphia (October 21-24, 1968).
- (2) G.S. Pound, "The Production of Chemicals From Low Temperature Tar", J.Inst. Fuels, Coke & Gas, (October 1952).

Table 1. Summary of Properties of Whole Range and 350-650F COALITE Distillate

	<u>WHOLE DEWATERED COALITE</u>	<u>350-650F DISTILLATE</u>
<u>Elementals, wt%</u>		
Carbon	83.56	84.00
Hydrogen	8.55	9.26
Nitrogen	1.10	0.81
Sulfur	0.85	0.73
Oxygen	5.94	5.20
H/C Atomic Ratio	1.23	1.32
Specific Gravity @ 60F	1.039	0.9923
R.I. @ 20C	-	1.5469
VLHV, Btu/gal	133,100(est.)	132,741
Con Carbon Residue, %	3.52	<0.1
<u>TYPE ANALYSIS, 1vol%</u>		
Saturates	-	24.3
Olefins	-	14.6
Aromatics	-	61.1
<u>Distillation, F</u>	<u>D-1160</u>	<u>D-86</u>
10% distilled	415	422
30% distilled	543	460
50% distilled	655	504
70% distilled	771	552
90% distilled	-	616
End Point	958 (87%)	652

Table 2. Summary of Analytical Inspections of Finished COALITE-derived HEDF<sup>(1)</sup>

<u>Source</u>	<u>Test FB-47</u>	<u>Test FB-48</u>
LHV, Btu/gal	129,095 <sup>(2)</sup>	128,295 <sup>(3)</sup>
Aromatics, %	4.3	17.1
Specific Gravity @ 60F	0.8388	0.8504
Refractive Index @ 20C	1.4570	1.4640
Viscosity @ -4F, cs	7.5	7.0
Freeze Point, F	-54	-57
Flash Point, F	115	115
Aniline Point, F	136	116
Diesel Index	50.6	40.5
Smoke Point, mm	30	20
Luminometer No.	82	66
Existent Gum, mg/100 ml	4	10
Accelerated Stability, mg/100 ml	<0.1	2.0
<u>D-86 Distillation, F</u>		
IBP	311	315
10% distilled	347	352
30% distilled	390	393
50% distilled	412	415
70% distilled	448	449
90% distilled	486	486
EP	540	534

- (1) Promoters such as oxidation inhibitors, corrosion inhibitors and deicing agents are not reflected in the analyses of these samples.
- (2) Increases to an estimated 129,775 Btu/gal if Freeze Pt. is relaxed to the equivalent of a -40F max. spec.
- (3) Increases to an estimated 129,275 Btu/gal if Freeze Pt. is relaxed to the equivalent of a -40F max. spec.

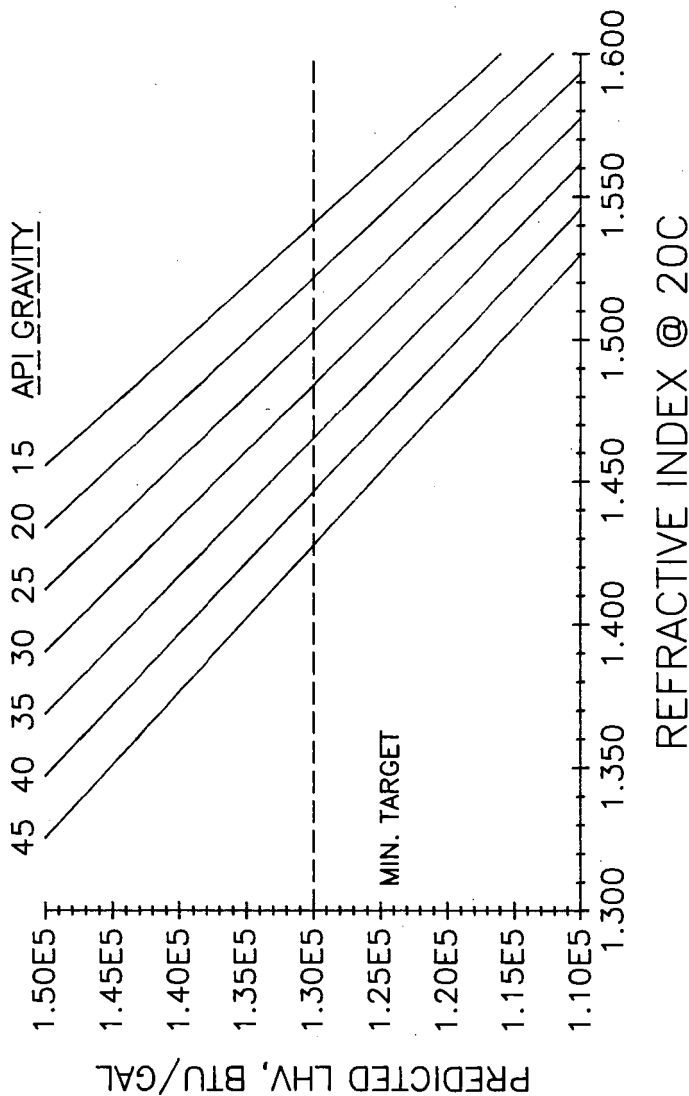


Figure 1. Predicted LHV of Hydrotreated 350–650F COALITE Distillates

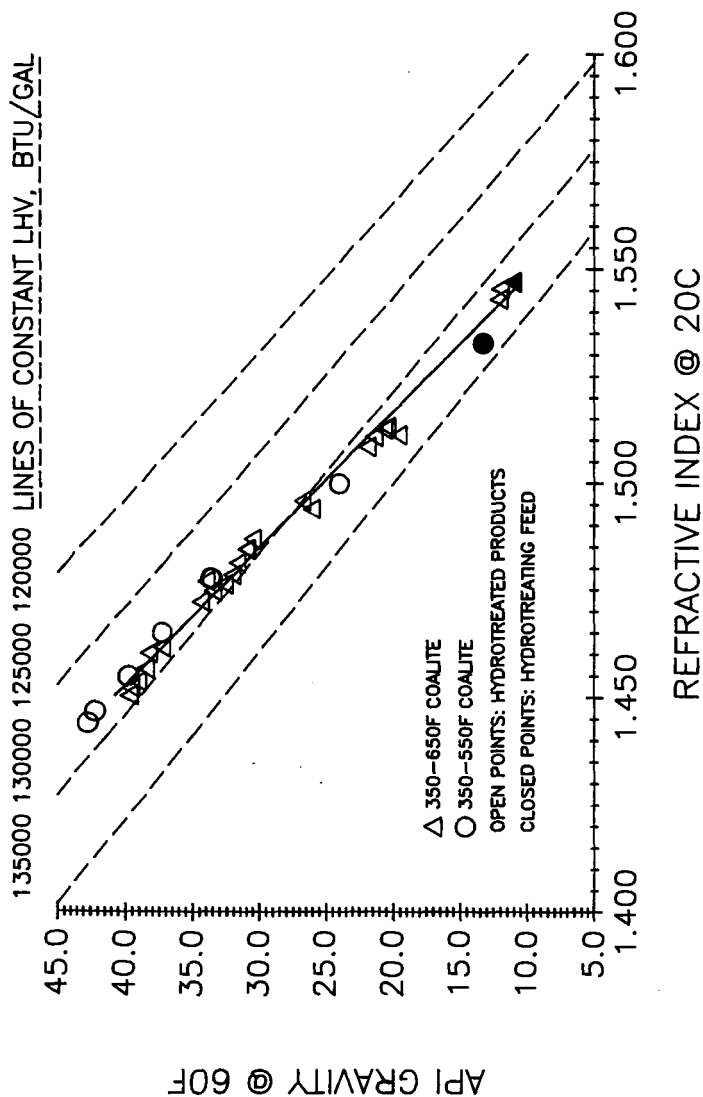


Figure 2. LHV-R.I.-API Relationships For Whole Hydrotreated COALITE Distillates



SYMPOSIUM ON PYROLYSIS PRODUCTS DERIVED FROM COAL,  
OIL SHALE, TAR SANDS, BIOMASS, AND HEAVY OIL

Presented Before the  
Fuel Chemistry Division  
American Chemical Society  
Miami Beach, Florida

September 10-15, 1989

STATUS OF THE CHARACTERIZATION OF JET  
FUELS FROM COAL LIQUIDS

by

M.B. Perry, G.W. Pukanic, and J.A. Ruether  
U.S. Department of Energy  
Pittsburgh Energy Technology Center  
P.O. Box 10940  
Pittsburgh, Pennsylvania 15236

INTRODUCTION

In the future, jet fuels will need higher densities and higher heat contents. These fuels will increase the range of aircraft and/or permit heavier payloads to be transported. Furthermore, these fuels will also be required to function as heat exchange fluids to remove heat from leading edges and vital engine parts. Very stringent specifications are placed on the composition, physical and chemical properties, thermal stability, and stability upon storage of fuels for commercial and military jet engines. Of the three basic hydrocarbon types -- paraffins, naphthenes (cycloparaffins), and aromatics -- naphthenes have the most desirable properties for jet fuels. One potential source of such a fuel is coal. Many of the compounds in coal are aromatic, and coal liquefaction products are likewise highly aromatic. Coal liquids can be further hydrotreated to produce naphthenes.

Many studies have involved the production of conventional and high-density jet fuels from coal liquids [1-21]. Sullivan et al., at Chevron Research Company, Richmond, California, conducted a number of studies for the Department of Energy to assess the feasibility of refining synthetic coal liquid feedstocks to distillate fuels, such as high-density jet fuels [5-14,22-24]. The upgrading of products from single-stage processes, such as SRC-II [5,8], H-Coal [6,8,14], and EDS [7-8], and from two-stage coal liquefaction processes, such as the Lummus Crest Integrated Two-Stage Liquefaction Process (ITSL) [9-11,13-14] and the HRI Catalytic Two-Stage Liquefaction Process (CTSL) [12-14], has been carried out. "Key factors that determine how easy or difficult a particular syncrude is to refine are EP [endpoint], boiling range, hydrogen content, and heteroatom content [14]."

In September 1986, the Fuels Branch of the Aero Propulsion Laboratory at Wright-Patterson Air Force Base, Ohio, began an investigation of the potential for production of jet fuel from the liquid by-product streams produced by the gasification of lignite at the Great Plains Gasification Plant located in Beulah, North Dakota. Funding was provided to the Department of Energy (DOE) from the Air

Force to administer the experimental portion of the effort. The Morgantown Energy Technology Center administered the effort (DOE Contract Number DE-FC21-86MC11076) at Western Research Institute, which studied the potential of the liquid by-product streams for the production of jet fuels [25]. The Pittsburgh Energy Technology Center (PETC) administered the effort (DOE Contract Number DE-AC22-87PC90016) at the University of North Dakota Energy and Mineral Research Center, which characterized these liquid by-product streams [26]. The PETC also administered the effort (DOE Contract Number DE-AC22-87PC90015) of Amoco Oil Company and Lummus Crest, which conducted a preliminary analysis of upgrading alternatives for the production of aviation turbine fuels from the Great Plains liquid product streams [27]. A small research effort was also conducted in-house at PETC.

The in-house research effort at PETC sought to further characterize jet fuels produced at Chevron and the coal-derived syncrudes from which they were prepared. While some of the characterization data may replicate the work of Sullivan et al. [9,10,12,22-24], the nuclear magnetic resonance data (NMR), the low-voltage high-resolution mass spectrometric (LVHRMS) data, and the test of "fit" to correlations previously developed at PETC for narrow-boiling range coal distillates are supplemental to and amplify the characterizations performed at Chevron. Furthermore, in-house characterization of the properties of the Great Plains tar oil was carried out, including NMR and LVHRMS analyses. The tar oil was distilled and the bottoms were hydrotreated. The overhead and bottoms (before and after hydro-treatment) were similarly characterized.

Interest in the properties of these materials and of similar materials derived from tar sands and oil shale culminated in a symposium on the structure of future jet fuels presented before the Division of Petroleum Chemistry at the American Chemical Society Meeting in Denver, April 5-10, 1987. At that symposium, Sullivan gave a summary report on this investigation related to high-density fuels from coal [24]. It was also at that meeting that Knudson et al. presented results of their evaluation of jet fuels from tar oil obtained from the Great Plains Gasification Plant (GPGP) at Beulah, North Dakota [28].

The present report will compare results of analyses and correlations of properties carried out on samples of high-density fuels from the ITSL process. These samples were produced at Chevron. We will also describe in part those investigations carried out on GPGP tar oil.

## EXPERIMENTAL

Samples that have been characterized at the PETC from the ITSL process include three wide-boiling-range coal-derived syncrudes and four jet-boiling-range products produced at Chevron. The syncrudes include an Illinois No. 6 coal-derived oil, and a light and heavy oil derived from Wyodak. The jet-boiling-range products include hydrotreated Wyodak light and heavy oils, and hydrotreated and hydrocracked Illinois No. 6 oils. Procedures used for upgrading the syncrudes have been reported [9-10]. Other samples that have been characterized include the GPGP tar oil stream, as well as the overhead and bottoms from distillation of the tar oil and the hydrotreated distillation bottoms of the tar oil; the North Dakota lignite used to produce the tar was also characterized.

Chemical and physical property measurements were carried out at PETC and at Huffman Laboratories (Wheatridge, Colorado); and numerous property measurements were reported by Sullivan [9-10,12,22-24]. Characterizations include simulated

distillation by gas chromatography (ASTM D2887) for boiling-point-range determination [29], CHONS elemental analysis [30-32], Karl Fischer determination of water [33], molecular weight [32], refractive index [34], specific gravity [32], viscosity [35], Carbon-13 and proton NMR [36], IR [37], low-resolution mass spectrometry with an ionizing voltage of 70 eV (ASTM D2789 type analysis was used to calculate the compound classes), and LVHRMS [38-39]. Detailed results of these analyses are the subject of an in-house report in preparation [40]. The data relevant to this report are summarized in Tables 1 through 6. Additionally, correlations developed at PETC for narrow-boiling-range coal liquid distillates [41] were applied to these samples.

The Great Plains Gasification Plant operated by the ANG Coal Gasification Company for the Department of Energy produces 150 million scf of substitute natural gas per day [26]. Three by-product hydrocarbon liquid streams -- tar oils, crude phenols, and naphtha -- are also produced. Of the three liquid streams, the tar oil stream (produced at the rate of 2900 bbl/day [27]) is thought the most appropriate for conversion to jet fuel [26]. The tar oil from the GPGP had a boiling range of 107°C to 524°C. About 20 liters of the tar oil were vacuum distilled to an atmospheric equivalent cut point of 350°C at the University of Pittsburgh Applied Research Center. About 66% of the tar oil was found in the overhead, and 34% in the vacuum bottoms. A 300-g portion of the 350°C+ bottoms was hydrotreated in a 1-liter batch autoclave at 350°C under 13.6 MPa H<sub>2</sub> (3 scf/hr) using a presulfided Shell 324 catalyst for one hour. Five runs were made and a total of 1500 g of product hydrotreated.

## RESULTS AND DISCUSSION

Coal liquids derived from two-stage processes were lower in oxygen and nitrogen, and for a given boiling range, Sullivan found these liquids easier to upgrade than products from single-stage processes [14]. The properties of jet-fuel products, consisting mostly of cyclic hydrocarbons, were virtually the same from both the single-stage and two-stage processes. For all processes evaluated at Chevron, the jet-fuel products had high densities and high volumetric energy contents. The Wyodak CTSI light oil [12] was easier to upgrade than the other syncrudes, apparently because of its low-boiling-point end point, higher hydrogen content, and lower heteroatom content [14]. For syncrudes with a high-boiling-point end point, a successful upgrading procedure was developed that consisted of a two-step process: (1) hydrotreatment for heteroatom removal and (2) low-temperature hydrogenation for aromatic saturation [9,13,14].

The hydrotreatment process that produces the jet-boiling-range products from the coal-derived syncrudes removes heteroatoms, breaks down heavy paraffins into lighter paraffins, and hydrogenates aromatic rings, creating cyclic aliphatic functionalities. This is observed in the characterization data. The hydrogen contents of the hydrotreated products are greater than those of the syncrudes; and proton NMR, as well as carbon-13 NMR, confirms the predominance of aliphatics over aromatics in the hydrotreated product versus the predominance of aromatics in the syncrude. Results from LVHRMS and low-resolution mass spectrometry indicate a larger amount of the desirable lighter cyclic hydrocarbons in the jet-boiling-range products than in the corresponding syncrudes.

Table 3 compares properties of the four jet-fuel products prepared and characterized by Sullivan [9,10,12], and further characterized and studied here, to those of a Jet A specification fuel [13] and a high-density fuel [42]. The coal-derived jet-fuel products meet most of the Jet A and high-density fuel speci-

cations. The Illinois ITSL hydrocracked product exceeds the minimum for flash point, and the distribution of hydrocarbon types does not quite meet the specifications, although a high concentration of naphthenes is desirable. The four jet-fuel products do exceed the API gravity specifications, that is, they have higher densities than the specification fuels. This specification, however, is probably not necessary for aircraft with modern fuel-flow controllers [14]. There were previously no jet-fuel products with an API gravity below 37 that have met the other specifications [13]. The higher densities would probably be an advantage, since the fuel would have a higher volumetric energy content. These four products otherwise meet most of the jet-fuel specifications and have the desirable high naphthenic content and thus have potential for serious consideration as aviation jet fuels.

Franck et al. [43] recently concluded that two- or three-ring cycloparaffins with molecular weights in the range of 120 to 200 give the best performance in describing the different properties of jet fuels. Of the compound types that they studied, these cycloparaffins were the only ones to show simultaneously the following properties [13]:

- o high heating value by volume
- o satisfactory heating value by weight
- o excellent thermal stability
- o very low freezing point
- o low volatility, high flash point
- o acceptable low-temperature viscosity
- o acceptable flame characteristics (smoke point, etc.)

"No other hydrocarbons in the jet-boiling-range have all of these properties [13]." Analyses of the four ITSL jet-boiling-range products at PETC (Table 4) confirm that the predominant compounds classes are indeed 1-, 2-, and 3-ring cycloparaffins, and the molecular weights (Table 1) are slightly below 200. Analysis of the Wyodak Light ITSL Syncrude by LVHRMS required 31 compound types in the range  $C_5$ - $C_{21}$  to account for the sample, while the same analysis of the Wyodak light ITSL hydrotreated product required only 13 compound types in the range  $C_6$  to  $C_{16}$  to account for the sample [41]. Thus, hydrotreating this syncrude resulted in a less complex sample. Part of this loss in diversity can be accounted for by the fact that a certain distillate range was selected for the product, but in part, the diversity is lower because of heteroatom removal. Conceivably, a processing mode could be developed that would result in a product consisting of only a few compounds. The GPGP tar oil and overhead both fall in the molecular weight range of jet products, but only the overhead has the right boiling range. The GPGP overhead, however, has a high heteroatom content (37.81%  $C_6$ - $C_{12}$  hydroxybenzenes), as measured by LVHRMS (Table 5). The phenolic oxygen in the tar bottoms is less than half of that in the overhead (Table 2).

The GPGP tar oil, as well as the 350°C overhead and 350°C+ bottoms, is clearly very different (see Tables 1 and 2) from the coal liquefaction syncrudes evaluated by Sullivan. The twelve predominant compound types (from LVHRMS) found in the tar, the distillate overheads, and the bottoms are given in Table 5. The tar oil contains 33% of  $C_6$ - $C_{12}$  hydroxybenzenes, and the overheads contain almost 38%. The bottoms contain no large quantities of any compound types. The differences are most obvious in the NMR data (Table 2). Aromatic hydrogen and aromatic carbon are significantly higher in the GPGP tar oil samples. The weight percent oxygen as phenols (Table 2) is also higher in the GPGP samples. Surprisingly, the hydrotreated GPGP 350°C+ bottoms have properties very similar to the

Wyodak heavy ITSL syncrude. Presumably, this material could be further processed to produce a jet-fuel fraction that would have properties similar to the jet fraction produced by hydrotreating the Wyodak heavy ITSL syncrude. Similarly, the overheads could be hydrotreated to produce a jet-fuel-like distillate product. However, the oxygen content of the overhead fraction would require efficient heteroatom removal because oxygen functionalities have been implicated in problems with stability upon storage.

Correlations developed for narrow-boiling-range coal liquids [41] were successfully applied to the GPGP tar oil products as well as to the syncrudes and jet-boiling-range products. The results are reported in Table 6. The Illinois ITSL hydrocracked product gave the largest error when correlations were used to estimate molecular weight (15.93%) and refractive index (4.26%). An error of 7.8% resulted from estimation of the molecular weight of the tar oil, and an error of 1.32% resulted from estimation of the refractive index of the Wyodak heavy ITSL hydrotreated product. It is unclear why the hydrocracked product properties are difficult to estimate, but if this product is eliminated from the set, the average error in the estimated molecular weight is 2.37%, and the average error in the estimated refractive index is 0.49%. Khan recently reported successful applications of correlations based on refractive index to other liquids produced by coal pyrolysis [44].

Finally, bench-scale experiments conducted by Amoco have provided the basis for a process plan, established pilot-plant conditions, and produced small amounts of JP-8, JP-8X, and JP-4 jet fuels from GPGP tar oil [27]. With clay treatment and antioxidant additives, the JP-4 product was expected to meet all specifications except heating value, and the JP-8 and JP-8X were expected to meet all specifications except flash point. Two barrels of JP-8 jet fuel were jointly produced by Amoco and Lummus for evaluation by the Air Force.

## CONCLUSIONS

Jet fuels can be prepared from a wide range of coal liquids produced in single-stage and two-stage liquefaction processes, as well as from by-product streams of gasification processes. The high aromaticity of coal, the very property that makes it an excellent candidate as a feedstock for high-density fuels, exacts a heavy penalty, however, in hydrogen consumption. The high heteroatom content not only consumes large amounts of hydrogen to produce mostly  $\text{NH}_3$ ,  $\text{H}_2\text{S}$ , and  $\text{H}_2\text{O}$ , but the remaining nitrogen tends to poison catalysts, and the nitrogen in jet fuel is blamed for gum formation. Oxygen compounds have been implicated in oxidative coupling reactions resulting in degradation of fuels upon storage.

In the future, with the decline in production of high-quality crudes, refiners will be pressed to process lower quality petroleum crudes. At some point then, production of jet fuels from coal will become an attractive and viable alternative. In the near term, there is still time to perform the requisite research yet remaining.

## ACKNOWLEDGMENTS

The authors are grateful to Karl Waldner for assistance in the laboratory throughout this work. We gratefully acknowledge Chuck Schmidt for performing the mass spectrometry experiments; Dick Lett, Richard Sprecher, Marjorie Hough, and Paula Flenory for the nuclear magnetic resonance analyses; Adam Vayda for the distillation of the Great Plains gasifier tar oils; and Richard Hlasnik for con-

ducting the high-pressure hydrotreatment runs. We are also grateful to Gary Stiegel for copies of the contractor reports on investigations of Great Plains gasifier tar oils and for the trip to Wright Patterson Air Force Base, where we met in a planning session with the principal investigators at WRI, UNDERMC, and the Air Force.

#### DISCLAIMER

Reference in this paper to any specific commercial product, process, or service is to facilitate understanding and does not necessarily imply its endorsement or favoring by the United States Department of Energy.

#### BIBLIOGRAPHY

1. Fraser, Malcolm D., Proceedings of Third Annual Pittsburgh Coal Conference, September 1986.
2. Hibbard, R.R., and W.T. Olson, Proceedings of Conference on Fuels and New Propellants, 1964.
3. Refining Synthetic Liquids from Coal and Shale, National Academy Press, Final Report of the Panel on R&D Needs in Refining of Coal and Shale Liquids, Washington, D.C., 1980.
4. Kalfadelis, C.D., H. Shaw, and W.F. Taylor, A Preliminary Engineering Assessment of Jet Fuel Production from Domestic Coal and Shale Derived Oils, Government Research Laboratories, Exxon Research and Engineering Company, 11th IECEC.
5. Sullivan, R.F., and H.A. Frumkin, Third Interim Report, Processing of SRC-II Syncrude, March 1980, FE-2315-47.
6. Sullivan, R.F., D.J. O'Rear, and H.A. Frumkin, Fifth Interim Report, Processing of H-Coal Syncrude, September 1981, FE-2315-61.
7. Sullivan, R.F., D.J. O'Rear, and H.A. Frumkin, Ninth Interim Report, Processing of Texas-Lignite EDS Syncrude, June 1984, DOE/ET/10532-T19.
8. Frumkin, H.A., Tenth Interim Report, Revised Stock Balances and Updated Cost Estimates, May 1985, DOE/ET/10532-T23, FE-2315-115.
9. Sullivan, R.F., Eleventh Interim Report, Processing of Illinois ITSL Oil: Experimental Studies, May 1985, DOE/ET/10532-T25.
10. Sullivan, R.F., Twelfth Interim Report, Processing of Wyodak and Illinois ITSL Oil: Experimental Studies, November 1985, DOE/ET/10532-T28.
11. Frumkin, H.A., Thirteenth Interim Report, Processing of 750°F End Point Illinois ITSL Oil: Engineering Design Studies and Estimated Processing Costs, August 1986, DOE/ET/10532-T31.
12. Sullivan, R.F., Fourteenth Interim Report, Processing of Wyodak CTSL Oil and Related Experimental Studies, DOE/ET/10532-T32, August 1986.

13. Sullivan, R.F., American Chemical Society, Division of Petroleum Chemistry, Chicago Meeting, September 8-13, Preprints, Vol. 30, No. 3, pp. 503-512, 1985.
14. Sullivan, R.F., Transportation Fuels from Two-Stage Liquefaction Products, Chevron Research Company, Richmond, California; American Chemical Society, Division of Fuel Chemistry, Anaheim, Sept. 7-12, Vol. 31, No. 4, pp. 280-293, 1986.
15. Nowack, C.J., J. Solash, and R.J. Delfosse, Coal Processing Technology, Vol. 3, 1977.
16. Eisen, F.S., and J.D. Tice, Coal Processing Technology, Vol. 3, 1977.
17. Gallagher, J.P., and A.C. Antoine, Coal Processing Technology, Vol. 3, 1977.
18. Arnold, M. St. J., and P.F.M. Paul, Journal of the Institute of Energy, June 1980.
19. Hawk, C.O., M.D. Schlesinger, P. Dobransky, and R.W. Hiteshue, ROI-6655, 1964.
20. Schlesinger, M.D., and R.W. Hiteshue, ROI-5902, 1961.
21. Providing R&D Test Fuels from Alternate Energy Sources, An Assessment of Options, National Academy Press, Washington, D.C., 1983.
22. Sullivan, R.F., and H.A. Frumkin, American Chemical Society, Division of Fuel Chemistry Preprints, April 13-18, New York, 31(2), 325-339, 1986.
23. Sullivan, R.F., U.S. DOE Direct Liquefaction Contractors' Review Meeting, October 20-22, 1986, Abstracts, p. 5, Marriott Monroeville, Pittsburgh, Pennsylvania.
24. Sullivan, R.F., American Chemical Society, Division of Petroleum Chemistry Preprints, April 5-10, Denver, 32(2), 584-590, 1987.
25. Smith, E.B., F.D. Guffey, and L.G. Nickerson, AFWAL-TR-87-2042, Vol. III, May 1988.
26. Knudson, C.L., AFWAL-TR-87-2042, Vol. II, May 1988.
27. Furlong, M.W., Draft Final Report: Tasks 2 and 3 Results of Bench-Scale and Pilot-Plant Testing, Mail Station H-4, Naperville, IL 60566.
28. Knudson, C.L., W.G. Wilson, D.J. Miller, R.O. Ness, Jr., and A. Ruud, American Chemical Society, Division of Petroleum Chemistry Preprints, April 5-10, Denver, 32(2), 591-594, 1987.
29. ASTM Method D-2887-73 (1978), Standard Method of Test for Boiling Range Distribution of Petroleum Fractions by Gas Chromatography, Annual Book of ASTM Standards, Volume 05.02 (1982).
30. Houde, M., J. Champy, and R. Furminieux, J. Micro Chem., 24, 300-309 (1979).

31. Merz, W., Fresenius Z. Anal. Chem., 237, 272-279 (1968).
32. Schmidt, C.E., M.B. Perry, C.M. White, G.A. Gibbon, and H.L. Retcofsky, DOE/PETC/TR-87/4 (DE87002513), October 1986.
33. Mitchell, J., Jr., and D.M. Smith, Aquametry, 2nd Ed. Part III, 5, 107-136 (1980).
34. ASTM Method D-1218-61 (1977), Test for Refractive Index and Refractive Dispersion of Hydrocarbon Liquids, Annual Book of ASTM Standards, Volume 05.02, 10.03 (1984).
35. ASTM Method D-2170, Standard Method of Test for Kinematic Viscosity of Asphalts, Annual Book of ASTM Standards, Volume 04.03 (1984).
36. Brown, J.K., and W.R. Ladner, Fuel 39, 87 (1960).
37. Lett, R.G., C.E. Schmidt, D.H. Finseth, and H.L. Retcofsky, Appendix 2. Qualitative Determination of N-H and O-H Functional Groups in Coal-Derived Asphaltenes via Near-Infrared Spectroscopy. DOE/PETC/TR-82/13, July 1982.
38. Johnson, B.H., and T. Aczel, Anal. Chem., 39, 682 (1967).
39. Schmidt, C.E., R.F. Sprecher, and B.D. Batts, Anal. Chem., 39, 2027 (1987).
40. Pukanic, G.W., M.B. Perry, and J.A. Ruether, Technical Report in Preparation.
41. White, C.M., M.B. Perry, C.E. Schmidt, and L.J. Douglas, Energy and Fuels, 1, 99-105 (1987).
42. Production of Jet Fuel from Coal-Derived Liquids, Request for Proposal Number DE-RP22-87PC90015, September 1986.
43. Franck, J.P., J.F. LePage, G. de Gaudemaris, and P. Bonnifay, Hydrocarbon Processing, 56(13), 287-289 (1977).
44. Khan, M. Rashid, Energy and Fuels, 2, 834 (1988).



Table 1. Inspection Properties of Coal-Derived Jet-Boiling-Range Products, Syncrudes, and GPCP Tar Oil, Overhead, and Bottoms.

Sample	Boiling Range OF, 5-95%	T <sub>b</sub> mid, OF	MM	RI	Specific Gravity	Density
Illinois ITSL Hydrotreated	302-561	462	185	1.4741	0.8750	0.8742
Illinois ITSL Hydrocracked	261-545	403	192	1.4600	0.8504	0.8497
Wyodak Heavy ITSL Hydrotreated	302-566	454	187	1.4679	0.8596	0.8589
Wyodak Light ITSL Hydrotreated	359-567	484	188	1.4772	0.8840	0.8832
Illinois ITSL Syncrude	212-731	546	201	1.5314	0.9513	0.9505
Wyodak Heavy ITSL Syncrude	347-850	652	229	1.5733	1.0074	1.0065
Wyodak Light ITSL Syncrude	331-713	575	205	1.5360	0.9596	0.9588
Great Plains Tar Oil	287-873	545	187	1.5700	ND	1.0193
GPCP Tar Overhead	274-665	472	155	1.5471	ND	0.9674
GPCP Tar Bottoms	652-967	776	355	ND	ND	1.0990
GPCP Tar Bottoms Hydrotreated	517-956	738	ND	ND	ND	ND

ND means not determined.

Table 2. NMR and IR Characterization of Coal-Derived Product

Sample	H-Aromatic Fraction	H <sub>a</sub>	H <sub>g</sub>	H <sub>y</sub>	C Aromatic	wt% Oxygen as Phenols
Illinois ITSL Hydrotreated	0.02	0.03	0.69	0.26	0.04	ND
Illinois ITSL Hydrocracked	0.01	0.02	0.61	0.36	0.00	ND
Wyodak Heavy ITSL Hydrotreated	0.01	0.01	0.69	0.29	0.03	ND
Wyodak Light ITSL Hydrotreated	0.01	0.01	0.70	0.28	0.02	ND
Illinois ITSL Syncrude	0.14	0.16	0.53	0.17	0.38	0.1
Wyodak Heavy ITSL Syncrude	0.19	0.21	0.47	0.13	0.49	0.1
Wyodak Light ITSL Syncrude	0.14	0.15	0.53	0.18	0.35	0.1
Great Plains Tar Oil	0.24	0.32	0.35	0.09	0.69	2.4
GPCP Tar Overhead	0.26	0.36	0.30	0.08	0.64	3.2
GPCP Tar Bottoms	0.22	0.22	0.45	0.11	0.66	1.5
GPCP Tar Bottoms Hydrotreated	0.15	0.23	0.48	0.14	0.49	ND

ND means not determined.

Table 3. Properties of Jet Fuel Products

Sample	Illinois ITSL	Hydrocracked <sup>a</sup>	Illinois ITSL	Wyodak Heavy ITSL	Wyodak Light ITSL	Hydrocracked <sup>c</sup>	Jet A <sup>d</sup>	High-Density <sup>e</sup> Fuel
Gravity, API	29	34	34	32	28	37 Min.	35 Min.	
Smoke Point, mm	19	21	21	21	17	20 Max.		
Freeze Point, °F	<-94	<-94	<-94	<-94	<-94	-40 Max.		
Flash Point, °F	128	107	107			100 Min.		
Paraffins, LV %	1	2	7	82	5			
Naphthenes, LV %	91	96	96	86	86			
Aromatics, LV %	8	2	11	9	9			
Viscosity	10.2	6.2				20 Max.		
at -40°F, cSt						8 Max.		

<sup>a</sup>Reference 9; <sup>b</sup>Reference 12; <sup>c</sup>Reference 10; <sup>d</sup>Reference 13; and <sup>e</sup>Reference 42.

Table 4. Analysis of Jet-Boiling-Range Products by Mass Spectrometry

Compound Classes, Percent	Illinois ITSL Hydrocracked	Illinois ITSL Hydrocracked	Wyodak Heavy ITSL Hydrocracked	Wyodak Light ITSL Hydrocracked
Paraffins	4.16	2.59	8.26	5.95
Monocycloparaffins	20.54	53.29	39.44	35.88
Dicycloparaffins	53.23	27.64	30.45	33.83
Tricycloparaffins	12.92	11.88	13.27	15.80
Benzenes	6.45	4.33	3.99	5.21
Naphthalenes	0.31	0.14	0.23	2.76
Indans	2.39	0.13	4.37	0.53

NOTE: These analyses were obtained at low resolution with an ionizing voltage of 70 eV. The ASTM D2789 type analysis was used to calculate the compound classes.

Table 5. Analysis of Great Plains Tar Oil, 350°C Overheads, and 350°C+ Bottoms by LVHRMS  
(Twelve Major Constituents)

Tar Oil	Overheads <350°C	Bottoms >350°C
33.00% C <sub>6</sub> -C <sub>12</sub> hydroxybenzenes	37.81% C <sub>6</sub> -C <sub>12</sub> hydroxybenzenes	7.05% C <sub>5</sub> -C <sub>9</sub> diolefins/cycloalkenes
11.71% C <sub>10</sub> -C <sub>18</sub> naphthalenes	14.72% C <sub>10</sub> -C <sub>16</sub> naphthalenes	6.98% C <sub>16</sub> -C <sub>22</sub> pyrenes
8.81% C <sub>6</sub> -C <sub>15</sub> benzenes	10.15% C <sub>6</sub> -C <sub>15</sub> benzenes	5.74% C <sub>14</sub> -C <sub>21</sub> phenanthrenes
4.78% C <sub>8</sub> -C <sub>15</sub> indans/tetralins	4.00% C <sub>5</sub> -C <sub>10</sub> pyridines	5.68% C <sub>5</sub> -C <sub>9</sub> olefins/cycloalkanes
3.70% C <sub>5</sub> -C <sub>10</sub> pyridines	3.98% C <sub>9</sub> -C <sub>14</sub> indans/tetralins	4.83% C <sub>13</sub> -C <sub>20</sub> hydroxyace- naphthalenes/hydroxyfluorenes
3.41% C <sub>8</sub> -C <sub>14</sub> hydroxyindenes	3.69% C <sub>8</sub> -C <sub>14</sub> hydroxyindenes	4.56% C <sub>14</sub> -C <sub>20</sub> hydroxyphenanthrenes
3.33% C <sub>10</sub> -C <sub>17</sub> hydroxynaphthalenes	3.03% C <sub>10</sub> -C <sub>15</sub> hydroxynaphthalenes	4.31% C <sub>16</sub> -C <sub>22</sub> hydroxypyrenes
3.32% C <sub>9</sub> -C <sub>14</sub> indenes	3.53% C <sub>9</sub> -C <sub>14</sub> indenes	4.40% C <sub>6</sub> -C <sub>11</sub> benzenes
2.68% C <sub>14</sub> -C <sub>20</sub> phenanthrenes	2.10% C <sub>5</sub> -C <sub>9</sub> diolefins/cycloalkenes	3.50% C <sub>12</sub> -C <sub>18</sub> hydroxybenzofurans/ dihydroxyfluorenes
2.33% C <sub>6</sub> -C <sub>10</sub> diolefins/cycloalkanes	1.80% C <sub>12</sub> -C <sub>17</sub> acenaphthylenes/ fluorenes	2.97% C <sub>10</sub> -C <sub>15</sub> naphthalenes
2.32% C <sub>5</sub> -C <sub>9</sub> olefins/cycloalkenes	1.64% C <sub>8</sub> -C <sub>12</sub> hydroxyindans/ hydroxytetralins	2.97% C <sub>18</sub> -C <sub>24</sub> chrysenes
2.20% C <sub>12</sub> -C <sub>18</sub> acenaphthylenes/ fluorenes	1.61% C <sub>14</sub> -C <sub>18</sub> phenanthrenes	2.85% C <sub>15</sub> -C <sub>22</sub> cyclopenta[def] phenanthrene/dihydropyrene

LVHRMS data taken from reference 40.

Table 6. Test of Fit to Existing Correlations Between Refractive Index, Molecular Weight, and Density

Sample	Refractive Index, $n_D$			Molecular Weight, MW <sub>b</sub>		
	Experimental	Calculated	% Error	Experimental	Calculated	% Error
Illinois ITSL Hydrotreated	1.4741	1.4625	0.79	185	182	1.80
Illinois ITSL Hydrocracked	1.4600	1.3978	4.26	192	161	15.93
Wyodak Heavy ITSL Hydrotreated	1.4679	1.4486	1.32	187	184	1.36
Wyodak Light ITSL Hydrotreated	1.4772	1.4784	0.08	188	189	0.51
Illinois ITSL Syncrude	1.5314	1.5168	0.96	201	198	1.61
Wyodak Heavy ITSL Syncrude	1.5733	1.5814	0.52	229	234	2.00
Wyodak Light ITSL Syncrude	1.5360	1.5381	0.14	205	210	2.21
Great Plains Tar Oil Feed	1.5700	1.5676	0.15	187	172	7.79
Great Plains Overhead	1.5471	1.5466	0.03	155	158	1.67

<sup>a</sup>Calculated using Equations 1 and 2 of reference 41.

<sup>b</sup>Calculated using Equation 5 of reference 41.

## **Towards a deeper understanding of coal-tar pitch structure and its relation to thermally induced pitch reactivity**

M. Zander

Rütgerswerke AG, D-4620 Castrop-Rauxel, FRG

Coal-tar pitch is the residue of the technical distillation of high-temperature coal-tar; it is obtained in 50 % yield, relative to crude coal-tar. Pitch serves predominantly as an important raw material for the manufacture of electrodes for electrochemical and electrothermal metallurgy (1). Moreover, it can be used for manufacturing pitch-based carbon fibres (2).

Since the appearance of the fundamental work of Brooks and Taylor (3) in 1965 of an intermediate mesophase state in the carbonization of pitches interest in pitch research has grown tremendously. It became also increasingly evident that a deeper understanding of the structure and the thermally induced (carbonization) chemistry of coal-tar pitch is of high interest from both the industrial and scientific point of view.

### **1. The toluene-soluble fraction of coal-tar pitch / molecular weight range and chemical structure principles**

The toluene-soluble fraction ("TS-fraction") of pitch typically amounts to ca. 75 % per weight, relative to the entire pitch.

As follows from gas chromatography/mass spectrometry examination the smallest molecules present in the TS-fraction (in very low concentrations) have molecular weights of about 200 Dalton. Typical examples are: fluorene, phenanthrene, anthracene, carbazole, pyrene and fluoranthene. However, molecular mass of TS-fraction constituents cover a wide range; for example, TS-subfractions with mean molecular masses up to approximately 2200 Dalton have been isolated by a chemical method (Charge-Transfer Fractionation, see below). <sup>1</sup>H nmr spectroscopy revealed that these fractions are highly aromatic in nature. This leads to an important and interesting question: Are the higher-molecular TS-fraction constituents large monomeric polycyclic systems or rather oligomeric systems where medium-sized aromatic units are connected by e.g. C-C single bonds (oligo-aryl type), -CH<sub>2</sub>-groups, ether bridges, etc.? The two possible structure models of the higher molecular TS-fraction constituents are schematically depicted in Fig.1. The circles symbolize aromatic units of different size, the lines C-C single bonds between aromatic units and -X- denotes bridging functions.

Experimental findings obtained with the higher-molecular weight TS-subfractions indicate that the oligomeric structure model is much more likely:

- Solubility in organic solvents: In spite of their high molecular weights, the materials are surprisingly readily soluble in organic solvents. The non-planar (twisted) arrangement of the aryl/heteroaryl units, due to steric hindrance, explains in known fashion the relatively good solubility of the oligomeric systems.
- Clathration ability with respect to smaller aromatic molecules: It has been observed that the higher-molecular TS-subfractions contain smaller molecules e.g., fluoranthene, pyrene, benzopyrenes, and others which in spite of their good solubility in organic solvents cannot easily be removed by extraction with e.g., toluene at boiling temperature (4). It must therefore be concluded that these smaller "guest" molecules are relatively strongly bonded to the higher-molecular

components which act as "host" molecules. Again an oligomeric structure model of the host molecules provides a much more obvious explanation of their clathration ability than a monomeric structure model can do. For an oligomeric structure it can be assumed that it contains three-dimensional "cages" which can act as traps captivating the smaller guest molecules.

- nmr spectroscopy: As discussed elsewhere (5, 6)  $^1\text{H}$  and  $^{13}\text{C}$  nmr spectra also support strongly the oligomeric structure model.

## 2. The basic character of the higher-molecular portion of the TS-fraction

Assuming a statistical distribution of nitrogen among pitch constituents it has to be concluded that the probability for finding a nitrogen containing molecule in a pitch fraction increases with increasing molecular mass of the fraction. On this assumption and in spite of the rather low nitrogen content (typically 1 %) of the TS-fraction, the higher-molecular portion of the TS-fraction may be expected to contain a relatively large amount of nitrogen-containing compounds. By treatment of a toluene solution of coal-tar pitch with gaseous HCl (at room or boiling temperature) a precipitate of hydrochlorides of organic bases is obtained in 27 % yield, relative to TS-fraction (26 % calc. for the Cl-free fraction). It has been shown by model experiments that under the experimental conditions used only basic nitrogen-containing compounds form insoluble hydrochlorides while polycyclic aromatic hydrocarbons, carbazoles, and oxygen containing compounds do not (4). As found by GC/MS approximately 90 % of the basic TS-subfraction consists of molecules with molecular weight > 300 Dalton. The higher-molecular mass portion of the basic TS-subfraction shows the properties of an oligomeric system as described in section 1. With regard to a further specification of our model of the higher-molecular portion of the TS-fraction we can now conclude that most of the oligomeric molecules contain at least 1 basic nitrogen atom. Besides that other N functions (carbazole structures) as well as O and S containing functions are present as follows from elemental analyses.

The basic TS-subfraction can be further separated by a chemical method that has been termed "Charge-Transfer Fractionation" (CTF) (4,5,6). The first step in the CTF of pitches or pitch fractions is to prepare a solution in a suitable solvent; the solvents most widely used in CTF are toluene and chloroform. An electron acceptor species (picric acid or elementary iodine) is then added to the solution at room temperature. Immediately after the acceptor has been added a mixture of charge-transfer complexes of pitch constituents precipitates from the solution and is isolated by filtration. It has been shown that the nitrogen-containing basic pitch constituents are the compounds that predominantly form CT complexes (4). Decomposition of the CT complexes allows the recovery of the uncomplexed (electron donor) pitch molecules. The most important experimental parameter in the CTF of pitches is R, the ratio per weight of electron acceptor to pitch (or pitch fraction) dissolved (7). With decreasing R the yield of CT complexes obtained decreases. The same applies to the amount of electron acceptor present in the complexes. The nitrogen content of the uncomplexed donor material (obtained after decomposition of the complexes) also decreases with decreasing R while the mean molecular mass of the material increases. Clearly CTF fractionates the basic TS-constituents according to molecular mass. An example of the relation between R and the mean molecular mass of basic TS-subfractions obtained by CTF (electron acceptor: picric acid) is given in Fig.2a. Similarly Fig.2b shows the relation between R and the nitrogen content of the fractions obtained, while Fig.2c gives the relation between mean molecular mass and nitrogen content of these fractions.

### 3. Do pitches contain very large monomeric polycyclic aromatics ?

The idea that the higher-molecular portion of the TS-fraction consists predominantly of oligomeric systems where medium-sized aromatic/heteroaromatic units are connected by C-C single bonds and bridging functions, does, of course, not exclude the possibility that pitches also contain very large monomeric polycyclic aromatic systems.

The presence of such systems may be particularly suspected in those pitch fractions that are only sparingly soluble in organic solvents. This applies to e.g., the toluene and the chloroform insoluble fractions. Electrical measurements, in fact, indicate that these fractions rather consist of very large monomeric aromatics than of oligomeric systems.

It is well established that polycyclic aromatic hydrocarbons, after addition of small amounts of iodine, are electrical semiconductors. Fig.3a shows the exponential dependence of the electrical resistance on molecular size for the polyacenes (after addition of 1 % iodine). Electrical resistance decreases with increasing molecular size. For theoretical reasons this must apply to all topologies. In Fig.3b the yield of chloroform-insoluble material of various coal-tar pitches is plotted against the logarithm of the electrical resistance (measured after addition of 1 % iodine) of the chloroform-insoluble fractions. An exponential decrease of electrical resistance with increasing yield of chloroform-insoluble material is observed (8). The preliminary though most likely interpretation of this result includes the assumptions that (i) the yield of the chloroform-insoluble fraction increases with increasing mean molecular weight of the fraction and (ii) (by analogy with the result obtained for the acenes) the size of the fully-conjugated aromatic systems present increases regularly with molecular weight. To fit the latter assumption with the oligomeric structure model additional assumptions on the structure of the systems would be necessary.

### 4. Carbonization chemistry of medium-sized polycyclic aromatic pitch constituents

The reaction types characteristic of the thermal chemistry of medium-sized pitch constituents were examined taking by way of example perylene (I) (Fig.4) as the model substance (9). The thermolysis experiments were carried out in isothermal conditions at 450°C in an argon atmosphere. After a reaction time of 20 h perylene conversion amounted to 42 %. The compounds identified from the liquid phase thermolysis of perylene are shown in Fig.4. The yield of products formed by condensation through loss of hydrogen ("aromatic growth"), i.e., biaryls IV, V, and VI, higher-molecular peri-condensed systems II and III and semicoke-like material was found to amount to 85 % in total, related to converted starting material. In addition fragmentation products (compounds VII - X) were formed in approximately 5 % yield. Formation of fragmentation products occurs by hydrogen transfer to intact perylene molecules and subsequent splitting of C-C single bonds initially formed. Due to fragmentation reactions methyl and ethyl hydrocarbon radicals are also formed that lead to alkylated products (compounds XI - XV) of the parent hydrocarbon.

Whereas in terms of quality the thermal chemistry of polycyclic aromatic hydrocarbons and structurally related heterocyclic systems is extensively independent of the structure of the reactants, in terms of quantity a heavy reactant depend-

ence is evident, i.e., in thermolytic reactions the conversion rate of hydrocarbons and heterocycles varies greatly with their size and topology. Carbonization rates of the polycyclic aromatic hydrocarbons listed in Fig.5 have been measured (10). Highly purified samples of each hydrocarbon were isothermally treated in sealed glass tubes at 430°C, i.e., above the melting points of the compounds, for 4 h. The conversion rates were determined by uv/vis spectroscopy and high-pressure liquid chromatography. Dependent on size and topology of the systems conversion rates range from 9 to 99 %, related to starting material. A linear free energy relation between the logarithms of conversion rates and a reactivity index (lowest Dewar localization energy) derived from MO theory has also been observed (10).

#### 5. Carbonization chemistry of coal-tar pitch fractions/role of mean molecular weight, structure and nitrogen content

Carbonization experiments in liquid phase (430°C) clearly revealed that the higher-molecular basic TS-subfraction obtained with gaseous HCl (see section 2) is much more reactive than the corresponding lower-molecular non-basic material obtained from the mother liquor of HCl treatment. Similarly TS-subfractions obtained by CTF (section 2) are more reactive than the TS-fraction itself or the entire pitch. This follows unambiguously from formation rates of toluene-insoluble material (TI), relative rates of mesophase formation as well as from activation energies of TI and QI formation (QI = quinoline insoluble material). For example, activation energy of QI formation from the entire pitch amounts to 36 kcal/mol but to 17 kcal/mol from a CT fraction obtained with picric acid as the electron acceptor ( $R = 0.05$ , see section 2) (6, 11).

The thermally more reactive materials are distinguished from the less reactive ones by: (1) higher mean molecular weight, (2) probably an oligomeric structure (as opposed to the assumed monomeric structure of the less reactive material) and (3) by slightly higher nitrogen contents.

For all topologies of polycyclic aromatic systems reactivity increases with molecular size. Therefore an increase of thermal reactivity of pitch fractions with mean molecular weight is not unexpected. An oligomeric structure of the reacting material is particularly suited for intramolecular cyclization reactions. The drastic reduction in solubility following thermal treatment of the reactive pitch fractions can be easily explained with the formation of large planar aromatic systems. As is known from numerous examples planar aromatic compounds are much less soluble in organic solvents compared to non-planar ones with the same molecular size. There is some experimental evidence (7, 12) that nitrogen containing constituents enhance the thermal reactivity of pitch fractions. The effect, however, has been shown to be rather small (13). It cannot quantitatively explain the pronounced thermal reactivity of pitch fractions obtained by e.g., CTF (14).

In summary, the higher thermal reactivity of pitch fractions obtained by CTF or by treatment of the TS-fraction with gaseous HCl compared to that of the entire TS-material can be explained with the higher molecular weights of these fractions and particularly with their proposed oligomeric structure.



## 6. Role of free radicals and their precursor molecules in pitch carbonization

Although it is controversial whether free radicals play a dominant role in the **primary** step of the thermally induced polymerization of polycyclic aromatic hydrocarbons (15, 16), the importance of free radical formation in pitch carbonization has been unambiguously proven (17). Because of their much longer lifetimes  $\pi$ -radicals are more relevant than  $\sigma$ -radicals (15). The most important  $\pi$ -radical precursor molecules present in pitch are dihydro aromatics of the 9,10-dihydro-anthracene type, amines, and phenols. The  $\pi$ -radicals are formed by thermally induced cleavage of the CH, OH, and NH bonds, respectively. Thermally abstractable hydrogen from CH<sub>2</sub>, OH and NH groups amounts in total to approximately  $6 \cdot 10^{-2}$  % H, relative to the entire pitch (6).

## References

1. Stadelhofer, J.W.; Marrett, R.; Gemmeke, W. *Fuel* **1981**, 60 877.
2. Singer, L.S. *Fuel* **1981**, 60, 839.
3. Brooks, J.D.; Taylor, G.H. in *Chemistry and Physics of Carbon*, vol.4, p.243, Walker, P.L.; Thrower, P.A., Eds.; Marcel Dekker: New York 1968.
4. Zander, M. *Erdöl Kohle Erdgas Petrochem.*, in press (1989).
5. Blümer, G.-P.; Zander, M. *DGMK-Compendium 77/78* (Suppl. to *Erdöl Kohle Erdgas Petrochem.*) pp.235-251.
6. Zander, M. *Fuel* **1987**, 66, 1459.
7. Zander, M. Abstract of Papers, International Conference on Carbon (Carbon '88), Newcastle upon Tyne, UK, 1988, pp. 55-57.
8. Zander, M.; Palm, J. *Erdöl Kohle Erdgas Petrochem.* **1985**, 38, 162.
9. Zander, M.; Haase, J.; Dreeskamp, H. *Erdöl Kohle Erdgas Petrochem.* **1982**, 35, 65.
10. Zander, M. *Fuel* **1986**, 65, 1019.
11. Zander, M. *Erdöl Kohle Erdgas Petrochem.* **1985**, 38, 496.
12. Sato, M.; Matsui, Y.; Fujimoto, K. Abstract of Papers. 17th Biennial Conference on Carbon, Lexington, Kentucky, 1985, pp.326-327.
13. Cerny, J. *Fuel* **1989**, 68, 402.
14. Zander, M.; Palm, J. *Erdöl Kohle Erdgas Petrochem.* **1987**, 40, 408.
15. Stein, S.E. *Carbon* **1981**, 19, 421.
16. Stein, S.E.; Griffith, L.L.; Billmers, R.; Chen, R.H. *J.Org.Chem.* **1987**, 52, 1582.
17. Lewis, I.C.; Singer, L.S. in *Polynuclear Aromatic Compounds*, Advances in Chemistry Series 217, p.269, American Chemical Society, Washington, DC 1988.

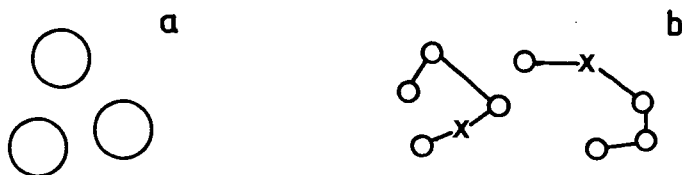


Fig.1. Structure models of higher-molecular TS-fraction constituents: a) "monomeric", b) "oligomeric" model.

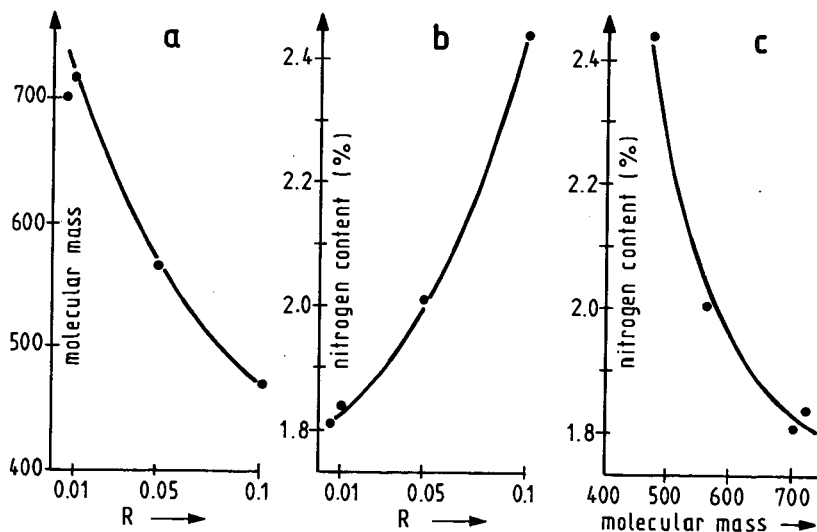


Fig.2. Charge-Transfer-Fractionation. - Relation between ratio R (per weight) of picric acid: pitch dissolved and molecular mass (a) or nitrogen content (b) of CT fractions obtained; (c) relation between molecular mass and nitrogen content of CT fractions.

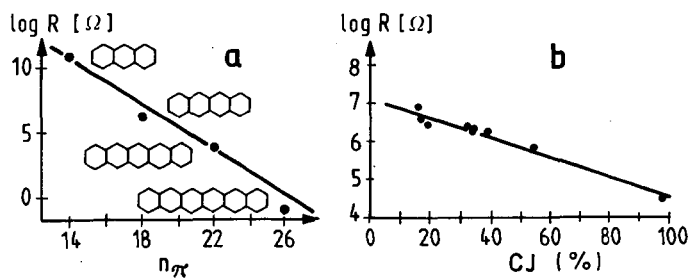


Fig. 3. (a) Relation between electrical resistance R (after addition of 1 % iodine) and number of  $\pi$ -electrons of the polyacenes; (b) relation between R and yield of the chloroform-insoluble fraction of 9 coal-tar pitches.

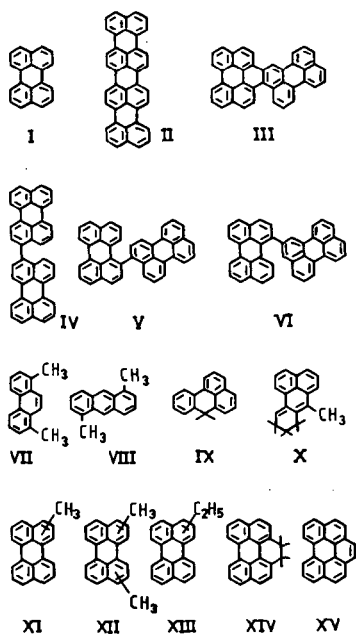


Fig. 4. Identified compounds from the thermolysis (450°C) of perylene.

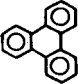
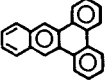
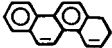
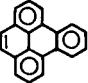
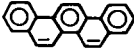
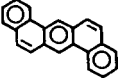
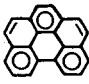
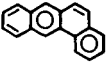
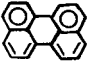
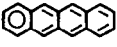
Hydrocarbon	Conversion rate (%)	Hydrocarbon	Conversion rate (%)
	9		36
	20		40
	24		50
	27		53
	30		99

Fig.5. Carbonization rates (430°C, 4 h) of polycyclic aromatic hydrocarbons

CHARACTERIZATION AND UPGRADING OF COAL LIQUIDS  
DERIVED FROM MILD GASIFICATION PROCESSES

John E. Mrochek, Radha P. Krishnan, and Ronald L. Graves

Oak Ridge National Laboratory\*  
Oak Ridge, Tennessee 37831

ABSTRACT

Mild gasification processes produce coal liquids that have the potential to be upgraded for use as transportation fuels. The quality and yield of these liquids vary widely depending upon the severity of the gasification process. Chemical upgrading of coal liquids may offer a viable and potentially economical alternative to conventional hydrotreating processes. Coal liquids from the United Coal Company Research Corporation, the KILnGAS, the SGI International, and Coalite (United Kingdom) processes have been characterized. These liquids and some of their distillates were subjected to solvent extraction upgrading with formic, acetic, and phosphoric acids to remove the basic nitrogenous fraction. Nitrogen removal ranged from about 50 to as high as 98%, with a recovery factor of about 75%. The most cost-effective reagent appears to be 25 vol % phosphoric acid.

INTRODUCTION

Mild gasification of coal has been shown to be capable of producing relatively light liquids, possibly suitable as an engine fuel, and char that may be suitable for boiler fuel or other purposes. Process conditions greatly influence the product quality; in particular, liquid product quality suffers with increasing yield (Graves et al., 1984). Some liquid upgrading (or blending) will be required even under mild gasification conditions before these liquids can be successfully utilized as transportation fuels. However, the severity and cost of upgrading are predicted to be less compared with conventional hydrotreating. The economics of upgrading mild gasification liquids varies with the raw liquid quality (Graves and Fox, 1984).

Complete and consistent data for mild gasification liquids are sparse in the literature. Often times, the data are of limited use since they have not been obtained by standard methods. Complete chemical and physical analyses of the liquids are essential to (1) determine the feasibility and degree of upgrading needed to produce marketable products from these liquids, (2) evaluate

---

\*Operated by Martin Marietta Energy Systems, Inc., for the U.S. Department of Energy under contract DE-AC05-84OR21400.

the performance of these liquids as transportation fuels, and (3) optimize the mild gasification processes with respect to product yield and product quality.

In this paper, recent results pertaining to the characterization and chemical upgrading of coal liquids from typical mild gasification processes are presented. The studies were conducted at the Oak Ridge National Laboratory (ORNL) for the Morgantown Energy Technology Center (METC), Department of Energy (DOE). The liquid characterization and upgrading are being conducted in conjunction with the char characterization.

#### LIQUID CHARACTERIZATION

Coal liquid samples from four mild gasification processes were examined in this study. The liquids examined came from the United Coal Company Research Corporation's mild gasification process development unit (UCCRC MGU) in Bristol, Virginia; from the KILnGAS commercial module being operated by the Allis-Chalmers Coal Gas Corporation in East Alton, Illinois; from the low-temperature pyrolysis process being tested by SGI International at the Salem Furnace Company in Pittsburgh, Pennsylvania; and from the Coalite low-temperature carbonization commercial plant in the United Kingdom. The latter product was supplied by UCCRC. Information on the processes is limited since it is deemed proprietary by the process developers.

#### PROCESS DESCRIPTION

UCC MGU. The UCC system is a batch process capable of processing up to 68 kg (150 lb) of coal per batch, over a 5-h duration, at temperatures of up to 816°C (1500°F) under atmospheric pressure to mild vacuum. Two 0.2-m- (8-in.-) diam. stainless steel tubes, each connected to 0.2 x 2.4 m (0.7 x 8 ft) tall sweep gas heaters located adjacent to the individual reactor tubes comprise the reactor system. Coal is fed to the reactor at the top, and the resulting char is withdrawn at the bottom. The liquids are condensed from the reactor effluent gas. Noncondensable gas is either recycled as sweep gas or flared (Chu, 1988).

Tests have been conducted on 38 mm x 0 (1.5 in. x 0) and 3 mm x 0 (1/8 in. x 0) Kentucky HK bituminous coal containing 33.8 wt % volatile matter, 59.4% fixed carbon, 5.0% ash, and 1.8% moisture. Ultimate analysis of the coal is C - 78.18%, H - 5.24%, N - 1.46%, S - 0.98%, Cl - 0.13%, and O - 9.01%. The optimum reactor temperature is considered to be 538°C (1000°F) for the best liquid quality. A small amount of sweep gas is maintained through the reactors to enhance the heatup rate (1.4 -18°C/min) and to reduce the residence time of the product gas in the reactor. Liquid yield on "as-received" coal is 12 to 15%, of which 4% is water.

KILnGAS Commercial Module (KCM). This is a 600-ton/d coal gasification demonstration plant which uses a ported, pressurized, rotary kiln gasifier. Coal entering the feed end of the gasifier is progressively dried and heated by hot producer gas as it moves toward the discharge end. The hot coal is devolatilized and then reacted with air and steam. Gasification occurs about midway through the gasifier and continues to the discharge end. Agglomerated ash is removed at the discharge end. Gasification occurs at 1037°C (1900°F) at 3.1 bar (45 psi) pressure. Devolatilization occurs around 537°C (1000°F).

The gasifier, which measures 3.2 x 41 m (10 x 136 ft), is divided into five zones with multiple air/steam ports in each zone.

The KILnGAS process can gasify a wide variety of coals without requiring pretreatment. Most of the tests, however, have been done on high-sulfur Illinois No. 6 coal. Condensable hydrocarbons and tars are separated from the reactor effluent gas. The tar is recycled to the gasifier, and the condensates are processed in the wastewater pretreatment plant where the oils are recovered (Parekh, 1982).

SGI Pilot Plant. The SGI system is a small, batch-fed atmospheric pyrolyzer with a nominal operating temperature of 537°C (1000°F) and a residence time of 20 min, and is capable of feeding 22.7 kg (50 lb) of coal per batch. The coal tested is a Montana Rosebud subbituminous coal containing 39.0 weight % volatile matter, 51.8% fixed carbon, 19.8% moisture, and 5.0% ash. Ultimate analysis of this coal is C - 54.8%, H - 3.7%, N - 0.8%, S - 0.6%, and Cl - 0.02%. Liquid yield (naphtha and distillates) is 11 to 13% on a moisture-ash-free coal basis (Esztergar, 1987).

Coalite Commercial Plant. This is a commercial, low-temperature carbonization plant operating in the UK. Bituminous coal with a volatile content of 35% is carbonized in metal retorts at about 600°C (1112°F). The volatile products are condensed in water-cooled take-off pipes. The remaining noncondensable gases pass through electrostatic precipitators and are further condensed before they are recycled and used for heating the retorts. Liquid yield on an "as-received" coal basis is about 9% (W. A. Bristow, 1947).

#### CHARACTERIZATION METHODS AND RESULTS

The coal liquids were characterized by standard ASTM procedures in most cases; however, other well-accepted procedures were used for some parameters. The following properties were included in the characterization:

##### Elemental analysis (Leco analyzer)

Carbon

Hydrogen

Nitrogen  $\geq$  1.0 wt %; (for N <1.0%, use modified Method 351.2, EPA

Methods for Chemical Analysis of Water and Waste)

Sulfur

Oxygen (by neutron activation)

- Water content (ASTM 96-73)
- Specific gravity (ASTM D 287-67)
- Viscosity (ASTM D 88)
- Heating value (ASTM D-2015-85)
- Simulated distillation curve by gas chromatography (ASTM D-2887)
- Aliphatics/Aromatics (Proton NMR)

Two liquid samples were provided by UCCRC and were designated as UCC-1 (parametric run) and UCC-2 (production run).

A summary of the data obtained on the four coal liquids is presented in Table 1. For illustration, the simulated distillation curve for the UCC-1 liquid is shown in Fig. 1.

The following trends can be observed in Table 1:

1. H/C ratios of the coal liquids are less than the corresponding ratio for diesel fuel. Some degree of upgrading and/or blending will be required to enhance the H/C ratio if these liquids are to be substituted for diesel fuel.
2. Except for the SGI liquid, the H/C ratios are slightly lower than those found for liquids produced in a batch reactor in a previous study (Graves and Fox, 1984) where the carbonization temperature was below 500°C.
3. The viscosity of coal liquid is much higher than that of diesel fuel.
4. Aromatic carbon contents for the coalite and UCCRC liquids are similar but much higher than the aromaticity of the diesel fuel. Increase in aromaticity with a concomitant decrease in H/C ratio is indicative of increasing aromatic ring condensation. A priori, increased hydrogen content leads to decreased aromaticity (White et al., 1987).
5. Aromaticity of the KILnGAS liquid is the highest of all the liquids, which is attributable to process conditions. Process conditions in the KILnGAS gasifier are much more severe compared with Coalite, UCCRC, and SGI. The higher pressure, temperature, and longer residence time in the reactor could cause thermal cracking for this product, indicative of greater aromatic ring condensation (product contained elevated amounts of naphthalene).
6. The SGI liquid measured the lowest aromatic carbon, even less than that of diesel fuel. The sample from Test 1003, is a second-stage liquid, which is perhaps a much lighter fraction compared with the raw liquid. The high hydrogen and low oxygen contents of this liquid are puzzling.

#### UPGRADING STUDIES

Hydrotreating is the conventional technology used in the petroleum industry for heteroatom removal and product upgrading. It has also been used for upgrading liquids derived from several different coal liquefaction and shale oil processes. In a previous DOE-sponsored program designed to study the upgrading of coal- and oil shale-derived liquids, fixed-bed hydrotreating at three different severity levels was used to produce gasoline, jet, and diesel fuels from SRC II, Exxon Donor Solvent, and H-coal liquids. Satisfactory fuels were obtained, although high hydrogen consumption was observed [1000 to 3000 SCF/bbl, depending on the severity level and the coal liquid (Guerin, 1986)]. It was found that the hydrotreating operation was very sensitive to asphaltene-like impurities in the feed liquid. In addition to reducing their detrimental effect on catalyst performance, the removal of these impurities enabled significant reduction (factors of 1.5- to 3-fold) in the size of the hydrotreater reactor for jet fuel production (Sullivan, 1981).

Hydrotreating, requiring high-pressure equipment, catalysts, and hydrogen, is expensive and difficult because of the nature of the coal liquids. Chemical means of upgrading have the potential to be more cost effective. Primary emphasis, in the upgrading studies reported in this work, was on the removal of the basic nitrogen fraction from these coal condensibles by solvent extraction with acidic reagents. Principal reagents tested included formic, acetic, and



phosphoric acids in concentrations ranging from 25 to 90 vol %. The effect of acid strength was briefly examined on an early UCCRC condensible using acetic (pKa = 4.75), monochloroacetic (pKa = 2.85), and trichloroacetic (pKa = 0.70) acids at 50 vol % concentrations.

#### Extraction Studies on UCCRC Liquids

Illustrated in Table 2 is a comparison of formic and acetic acid extractions at 50, 75, and 90 vol % (formic only) concentrations using one of the early samples of UCCRC coal condensibles. Early samples from the UCCRC MGU were obtained under nonoptimum operating conditions and at a higher operating temperature of about 1300°F (optimum temperature is now considered to be about 1000°F). This, of course, resulted in a somewhat more viscous and more highly aromatic liquid product having an H/C ratio of 0.88. Extraction data in Table 2 indicate better extraction by acetic acid, with 50.9% of the nitrogen removed by 75 vol % acetic acid. Oxygen assays show little tendency for the organic phase to retain water for extraction with either of these two acids. Qualitatively, acetic acid also showed better extraction of the basic nitrogenous fraction than either monochloroacetic or trichloroacetic acids, suggesting that increased acid strength did not improve nitrogen removal.

Phosphoric acid was tested as a nitrogen extractant during the course of this work, based on similar experiments on shale oil (Johnson, 1981). Acid concentrations of 25, 50, and 75 vol % were tested, utilizing the same UCCRC condensible liquid and contacting procedure employed with acetic and formic acids. Unextracted nitrogen assays were 0.46, 0.44, and 0.37 wt %, respectively, with the highest acid concentration providing the greatest removal (66%). A third phase, which made clean separations difficult to achieve, was formed for the higher concentrations (50 and 75 vol %) in these experiments. Note, however, that even at 25 vol % phosphoric acid concentration, the nitrogen removal was 57.4%, which is still better than that obtained with 75 vol % acetic acid extraction (50.9%).

A more representative sample of the UCCRC coal condensible liquid is UCC-1 in Table 1. Extractions of the nitrogen content of this product were attempted with both acetic and phosphoric acids. However, extraction with 75 vol % acetic acid proved impossible because, at this concentration, the two liquids were completely miscible. This suggests that the UCC-1 liquid is different from the previous liquids tested. The acetic acid concentration was reduced to 50 vol %, and nitrogen removal was compared to that obtained with 25 vol % phosphoric acid. Nitrogen content was reduced to 0.36 and 0.34 wt %, respectively, or 36% removal with acetic acid and 39% removal with phosphoric acid. Nitrogen removal was less complete for this liquid compared with the previous UCCRC samples, suggesting that the liquid generated at the lower gasifier temperature had a lower basic nitrogen content.

#### Extraction Studies on a KILnGAS Condensible

A relatively large sample (about 5 gal) of a KILnGAS condensible, described as a "high-naphthalene-content" product, was received through the courtesy of the Allis-Chalmers Coal Gas Corporation. Its elevated aromatic content was verified by the NMR analysis shown in Table 1. A vacuum distillation of this product was performed, and the fraction boiling under 650°F was collected. The nitrogen content was reduced by about 53% (to 0.31 wt %), and the H/C ratio was increased to 0.83. Little change was noted for the other heteroatoms. Extractions were performed on both the raw liquid and the distillate with varying concentrations of acetic acid. The results, shown in Table 3, indicate 67% reduction in nitrogen content for extraction of the raw product with 75 vol % acetic acid and 58% reduction for the distillate.

#### Extraction Studies on an SGI Liquid

The condensible product from SGI International was described as a second-stage product using coal from the Rosebud Mine in Montana. Few details are known about this particular sample; however, its appearance and analysis (see Table 1) suggested that, at the very least, it was some sort of distillate. Its analytical properties, with the exception of the nitrogen assay, were better than the typical commercial diesel fuel shown in Table 1. The aromatic content, as measured by NMR, and the oxygen and sulfur assays were unusually low for a coal condensible liquid.

Solvent extraction studies with both acetic and formic acids showed nearly complete removal of nitrogen (98 to 99%) at all concentrations tested (see Table 4). Clean separations were observed with this extremely light organic liquid, as indicated by the oxygen assays of the organic phase. The nitrogen removal demonstrated for this product, coupled with the already low oxygen, sulfur, and aromatic assays, is probably sufficient to enable it to be used directly as a fuel in some diesel engines; however, its actual relationship to a working mild gasification process remains to be verified.

#### CONCLUSIONS

The characterizations of the condensible products from various coal gasification projects give an indication of the need for upgrading in order to produce a fuel suitable for transportation uses. It is evident that lower temperatures (<1000°F) in the gasifier are desirable in order to reduce aromatic content and subsequently increase the H/C ratios.

Solvent extraction studies on limited amounts of three condensible liquids must be deemed tentative. However, based only on raw material prices (acetic acid -- \$0.27/lb; formic acid -- \$0.365/lb; and phosphoric acid, 85% -- \$0.255/lb), the most economical process would utilize 25 vol % phosphoric acid as an extractant. Extraction experiments performed with several condensible samples showed that 75% recovery of the nitrogen-depleted organic phase was achievable with careful attention to experimental procedure. However, it should be pointed out that the aqueous raffinate from any solvent extraction process of this nature may generate an environmental disposal problem that has not been addressed during the course of this work.

#### REFERENCES

- W. A. Bristow, "The Development of Liquid Products from Low-Temperature Carbonization," *J. Inst. Fuel*, Vol. XX, No. 113 (1947).
- C. I. C. Chu, Development of Mild Gasification Process, Project Report UCC R&D C-17-20 to Morgantown Energy Technology Center (Sept. 1988).
- E. E. Esztegar, personal communication to R. L. Graves, Oak Ridge National Laboratory (May 1987).
- C. A. Johnson, C. Ward, H. F. Moore, and R. Hettinger, "Combination Process for Upgrading Oil Products of Coal, Shale Oil, and Crude Oil to Produce Jet Fuels, Diesel Fuels, and Gasoline," U.S. Patent 4,409,092 (1983).
- R. L. Graves, S. S. Lestz, S. S. Trevitz, and M. D. Gurney, "Screening Tests of Coal Pyrolysis Liquids as Diesel Fuel Extenders," SAE Technical Paper Series, Paper No. 841002, San Diego (Aug. 1984).
- R. L. Graves and E. C. Fox, "Diesel Fuels from Minimally Processed Coal Pyrolysis Liquids -- Exploratory Investigations," presented at the 19th IECEC Meeting, San Francisco (Aug. 1984).
- M. R. Guerin, W. H. Griest, C-H. Ho, L. H. Smith, and H. P. Witschi, *Integrated Report on the Toxicological Mitigation of Coal Liquids by Hydrotreatment and Other Processes*, ORNL/TM-10070 (1986).
- R. D. Parekh, "Handbook of Gasifiers and Gas Treatment Systems," DOE/ET/10159-T24 (DE 83004846) (1982).
- R. F. Sullivan and D. J. O'Rear, *Refining and Upgrading of Synfuels from Coal and Oil Shales by Advanced Processes*, FE-2315-60 (1981).
- C. M. White, M. B. Berry, C. E. Schmidt, and L. J. Douglas, "Relationship Between Refractive Indices and Other Properties of Coal Hydrogenation Distillates," *Energy & Fuels*, Vol. 1, 99 (1987).

Table 1. Summary of coal liquids characterization data

Properties	Coalite	UCC-1 (parametric run)	UCC-2 (production run)	Kilm- GAS	SGI	Typical commercial diesel fuel
Elemental analysis (wt %)						
C	80.83	84.24	83.69	88.45	87.34	86.5
H	8.57	9.42	9.34	5.58	12.96	12.8
S	0.72	0.42	0.39	4.6	0.07	0.3
N	1.02	0.56	0.68	0.66	0.40	0.01
O (by neutron activation)	7.74	4.89	5.11	1.6	0.171	
H/C	1.27	1.34	1.34	0.76	1.77	1.78
Water content, %	1.80	0.790	0.900	0.14	0.004	nil
Specific gravity (at 25°C)	1.03	0.972	0.989	1.133	0.872	0.85
Viscosity (at 25°C), CP	290.0 <sup>a</sup>	12.06 <sup>b</sup>	25.55 <sup>b</sup>	34.0 <sup>b</sup>	18.0 <sup>b</sup>	3.0 <sup>b</sup>
Heating value, Btu/lb	16,300	17,100	17,000	16,500	19,400	18,150
Aromatic hydrogen content, wt %	30.4	30.2	26.9	86.1	8.7	14-16
Aromatic carbon content, wt %	57.7	55.9	52.4	94.8	20.0	34-37
Aliphatic hydrogen content, wt %	61.8	59.2	68.1	13.9	91.3	84.0
Simulated distillation data						
Initial BP, °C	147	48	58	58	142	
Final BP, °C	437	397	425	431	433	
Average BP, °C	234	214	211	218	273	
Percentage of oil distilled at 246°C	56	67	75	66	34	

<sup>a</sup>Measured by a Brookfield viscometer.<sup>b</sup>Measured by a Canon-Fenske viscometer.

ASTM average temperature corresponding to the 50% boiling point for diesel fuel.

Table 2. Extraction studies on a UCCRC liquid with aqueous formic and acetic acids

Element	Raw liquid	Organic-phase concentration, wt %					
		Formic acid			Acetic acid		
		50 <sup>a</sup>	75 <sup>a</sup>	90 <sup>a</sup>	50 <sup>a</sup>	75 <sup>a</sup>	90 <sup>a</sup>
Nitrogen	1.08	0.85	0.74	0.59	0.56	0.53	b
Oxygen	5.24	4.70	4.64	7.96	4.54	4.79	b

<sup>a</sup>Vol %.

<sup>b</sup>Insufficient sample for analysis.

Table 3. Extraction of nitrogen from raw and distilled KILnGAS products using acetic acid

Acetic acid (vol %)	Remaining nitrogen, wt %	
	Raw KILnGAS <sup>a</sup>	<650°F distillate <sup>b</sup>
25	0.31	0.22
50	0.32	0.17
75	0.22	0.13
90	0.21	NA <sup>c</sup>

<sup>a</sup>Original N content, 0.66 wt %.

<sup>b</sup>Original N content, 0.31 wt %.

<sup>c</sup>Not analyzed.

Table 4. Extraction studies on an SGI liquid with aqueous formic and acetic acids

Element	Raw SGI	Organic-phase concentration, wt %							
		Formic acid				Acetic acid			
		25 <sup>a</sup>	50 <sup>a</sup>	75 <sup>a</sup>	90 <sup>a</sup>	25 <sup>a</sup>	50 <sup>a</sup>	75 <sup>a</sup>	90 <sup>a</sup>
Nitrogen	0.40	<0.01	<0.01	0.01	<0.01	<0.01	<0.01	0.02	<0.01
Oxygen	0.16	0.12	0.13	0.11	0.10	0.14	0.11	0.10	0.08

<sup>a</sup>Vol %.

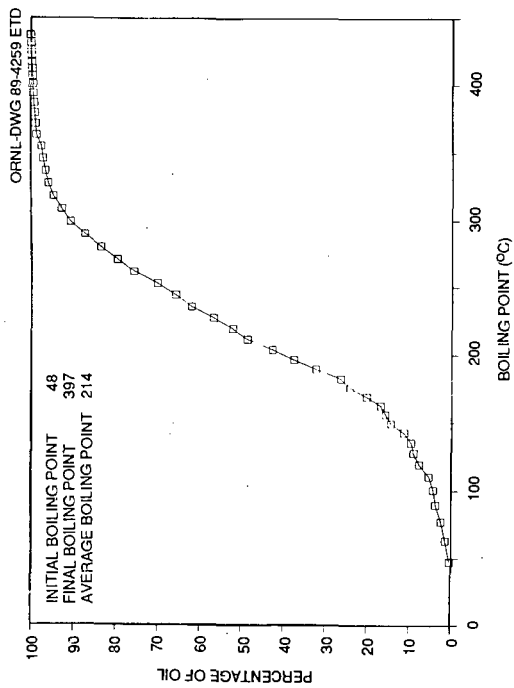


Fig. 1. Simulated distillation curve for UCC-1 coal liquid.

Catalytic Cracking of a Gas Oil  
Derived from Eastern Canadian Oil Shale

S. H. Ng

Synthetic Fuels Research Laboratory, CANMET  
Energy, Mines and Resources Canada  
Ottawa, Ontario, Canada K1A 0G1

Introduction

Large oil shale deposits have been discovered in Central and Eastern Canada.<sup>1</sup> In the past few years, considerable research was conducted on Eastern oil shales.<sup>2-5</sup> Primary liquid products from retorting of oil shales are superior to Canadian heavy oil and tar sand bitumen.<sup>5</sup> In a continuing effort to evaluate the processability of the shale oil produced, a catalytic cracking study on its gas oil fraction was recently undertaken at CANMET. This paper reports the primary results.

Experimental Section

The raw shale oil was produced by retorting a New Brunswick oil shale from Albert Mines near Moncton, New Brunswick. The retort system in the pilot plant has been reported previously.<sup>5</sup> The shale oil was distilled under vacuum to give the gas oil fraction which constituted 80 wt % of the feed. For comparison, a conventional gas oil was obtained from a refinery which processes the Alberta crudes transported to Eastern Canada through the Interprovincial Pipe Line (IPPL). The two gas oils were analyzed using ASTM or other accepted methods. The results are shown in Tables I and II.

Three equilibrium catalysts DA-440, Nova D and GX-30 obtained from Davison of W. R. Grace were used in this study. Prior to their characterization and testing, the catalysts were decoked at 590 °C for 3 h. Surface characteristics were determined by both N<sub>2</sub> adsorption-desorption technique and by mercury porosimetry. Zeolite surface areas and zeolite contents were estimated based on a method reported in the literature.<sup>6</sup> Their physical and chemical properties are given in Table III.

Catalytic cracking of the gas oils was performed in a microactivity test (MAT) unit which was modified from the ASTM D3907 version. It consists of a fixed bed quartz reactor packed with 4.2 g of catalyst heated at 470-530 °C in a three-zone furnace. Feeds were delivered using a syringe pump with catalyst/oil ratio varying from 2-6 while keeping the hourly weight space velocity (WHSV) constant at 20 h<sup>-1</sup>. A flow of nitrogen purge gas at 20 mL/min was maintained throughout the 20-min test period. Liquid products were collected in a glass receiver cooled in an ice-water bath whereas the gaseous products were trapped using water displacement. After the test, both products were quantitatively measured before analysis. The amount of coke formed on the spent catalyst was also determined. Conversion was calculated based on the fraction of liquid product having a boiling point above 216 °C.

Denitrogenation of the shale vacuum gas oil (VGO) was done by both extraction in which dimethylsulfoxide (DMSO) containing 6 wt % 2N sulphuric acid was used as solvent, and adsorption in which an Attapulugus clay was used as adsorbent.

## Results and Discussion

Table I shows that the quality of the shale VGO is better than or equivalent to that of the IPPL gas oil except its nitrogen contents are much higher. The basic nitrogen is undesirable in FCC feedstocks as it can neutralize the acid sites of the cracking catalysts resulting in a rapid loss of activity.<sup>7-9</sup> The high nitrogen level is also reflected by the polars in the hydrocarbon type analysis (Table II). Polars in the shale oil may also include oxygen compounds. If these polars are considered crackable, the conversion constraints based on the compositional analysis can be estimated at 80.6 and 81.1 wt % for IPPL and shale VGO respectively, assuming that the diaromatics and the more highly condensed structures including aromatic sulphurs cannot be converted to light products with boiling points less than 216 °C due to the stability of the benzene rings.

Figure 1 shows the effects of temperature and catalyst/oil ratio (C/O) on conversion. Significant differences can be seen between the two feedstocks. For IPPL gas oil, the conversion tends to level off and approaches its limit at high severity. Furthermore, it is less sensitive to the temperature change. On the other hand, for shale VGO, the conversion increases sharply and linearly with C/O ratio and is far below its expected limit even at much higher severity. The conversion is obviously very temperature-dependent. This suggests that the catalysts were seriously poisoned during cracking by the basic nitrogen of shale VGO as this type of poisoning is mainly a surface adsorption phenomenon and high temperature tends to promote desorption. Between the two catalysts, Nova D is apparently more active in cracking IPPL conventional gas oil due to its higher zeolite content. This agrees with Davison's microactivity results (Table III). However, this trend is reversed for shale VGO, with DA-440 being more active. This suggests that the shale oil contains larger molecules which do not have access to the small pores of the zeolite but can be cracked by the matrix of DA-440 which has a larger pore diameter (Table III). A similar phenomenon was also observed in a separate cracking study which deals with other nonconventional gas oils including those derived from resids, tar sand bitumens and heavy oils.<sup>10</sup>

For IPPL gas oil, favourable and optimum gasoline yield (54 wt %) is obtained at about 73% conversion beyond which overcracking seems to take place. The gasoline yield decreases slightly with increased temperature at constant conversion. Between the two catalysts, DA-440 is slightly more selective for gasoline production. This does not necessarily mean that it produces a better gasoline, in terms of higher octane number, as DA-440 is not an octane-enhancing catalyst but Nova D is. It is known that the dealuminated ultra-stable Y-zeolite catalysts (USY) yield higher octane gasoline by producing more olefinic compounds,<sup>11</sup> compared with the rare earth exchanged Y zeolite catalysts (REY). For shale VGO, the gasoline yield increases linearly and monotonously with conversion without obvious effects of temperature and catalyst. The experimental maximum gasoline yield is less than 30 wt % which is unacceptably low.

The coke yields of the two gas oils increase exponentially (IPPL) or linearly (shale oil) with conversion. At constant conversion, higher temperature



for the same catalyst tends to lower the coke yield because C/O ratio can be reduced to achieve the same conversion. Contrary to the literature,<sup>11</sup> Nova D (USY) yields more coke than its counterpart DA-440 (REY) in cracking shale VGO whereas for IPPL gas oil, Nova D shows slightly better or equivalent coke selectivity than DA-440. A similar phenomenon was also observed in a separate cracking study involving other nonconventional feedstocks.<sup>10</sup> It is thus believed that the superiority of USY catalysts over REY catalysts with respect to coke selectivity depends also on the nature of the feedstock.

It has been observed that a linear correlation exists between the second-order conversion (conversion/[100 - conversion]) and the coke yield. The linear relationship is expected based on the equations proposed by Wollaston et al.<sup>12</sup> For IPPL gas oil, the straight lines at different temperatures pass through the origin indicating that all the coke formed results from catalytic cracking and is therefore "catalytic" coke.<sup>13</sup> However, for shale VGO, the straight lines intersect the x-axis at different coke values. These values obtained at 0% conversion represent neither "catalytic" coke nor "contaminant" coke since the nickel and vanadium contents of the catalysts are rather low (Table III). This suggests that they belong to the "additive" coke resulting from the basic nitrogen of the shale gas oil which contains little Conradson carbon - another possible precursor for the "additive" coke.<sup>13</sup> The "additive" coke found is independent of the catalyst type and is estimated at 1.47, 1.25, 1.09 and 0.97 wt % at 470 °C, 490 °C, 510 °C and 530 °C, respectively.

Product distribution for the two feedstocks at 50% conversion is shown in Table IV. It can be seen that the shale VGO produces more gases, less gasoline and much more coke compared with IPPL gas oil. The high decant oil yield (39 wt %) for IPPL VGO may be misleading as the majority of its precursor is crackable at higher severity. At 73% conversion, this value drops to 8 wt % raising the gasoline yield from 35 to 54 wt %.

Three methods have been used to achieve higher conversion of the shale oil. The first is to crack with GX-30, a very active catalyst because of its higher zeolite content. The other methods involve upgrading of gas oils by removing some of the nitrogen compounds using either DMSO/acid extraction or Attapulgus clay adsorption. One disadvantage of the rejection methods is the accompanying loss of the hydrocarbon value. Table V shows the weight recovery and the nitrogen contents of the upgraded feedstocks. It is evident that the clay method is superior to the extraction technique since it removes almost 50% more basic nitrogen for the same recovery. Table VI shows a comparison of cracking yields of raw and treated feedstocks cracked at various conditions while keeping catalyst/oil ratio constant at 6. For the untreated shale oil, although the use of GX-30 results in some improvement over DA-440 in conversion and gasoline yield, the coke yield is unacceptably high. Evidently, DMSO raffinate shows better performance than the raw shale oil whereas the clay treated shale oil is the best due to its lowest basic nitrogen content.

Let us consider two approaches in further evaluation of the data: one involves cracking of the raw shale oil as a whole whereas the other involves the separation of the shale oil into two fractions prior to individual cracking under the same conditions. In the latter case, the recovered fraction contains less nitrogen and is therefore better in quality whereas the rejected fraction is assumed, for simplicity, to be unconvertible either because of its high nitrogen level or a refractory nature. One can calculate their cracking yields on a

"total oil" basis by multiplying the yields, based on the recovered portion, with the weight fraction of recovery. The results are illustrated in Fig. 2. Here, the increases in conversion and gasoline yields of the treated shale oils over those of the untreated ones reflect the net poisoning effect on the catalyst by the basic nitrogen.

Based on the data obtained from nitrogen rejection methods (extraction or adsorption), linear correlation can be established between the cracking results, in terms of conversion and gasoline yield, and the basic nitrogen content (1750-4600 ppm) of MAT feeds. A cracking study was also made on the blends prepared from IPPL and raw shale oil. The data points obtained from this dilution method appear to coincide with those from rejection methods over the same basic nitrogen range. This suggests that the rejected portion of the raw shale oil would have been cracked if the catalyst had not been poisoned by the basic nitrogen in the first place. Also, the basic nitrogen content of the shale oil, rather than its compositional differences from the IPPL gas oil, is the determining factor for the cracking yields. Following the trends created by the dilution method, the shale oil produces a cracking result similar to that of IPPL at the same basic nitrogen level, i.e., 72 vs 73.5 wt % in conversion and 51 vs 53 wt % in gasoline yield at 510 °C and a catalyst/oil ratio of 4.

#### Acknowledgement

The authors would like to thank Dr. T. de Bruijn and Dr. J. Kriz of CANMET for many valuable discussions and suggestions.

#### REFERENCES

- (1) Duncan, D. C. Oil Shale (Eds. Yen, T. F.; Chilingarian, G. V.), 1976, p.19, Elsevier, New York.
- (2) Furimsky, E.; Synnott, J.; Boorman, R. S.; Salter, R. S. Fuel Process. Technology, 1984, 8, 293-306.
- (3) Boorman, R. S.; Salib, P. F.; Gilders, R.; Gemmell, D. E. Can. Inst. Min., Proc. 3rd Meeting, Fredericton, N. B. 1982.
- (4) Karman, D.; Kresta, S. PREPRINTS, Div. of Petrol. Chem., ACS, 1987, 32(1), 94-96.
- (5) Salib, P. F.; Barua, S. K.; Furimsky, E. Can. J. Chem. Eng. 1986, 64(6), 1001-1007.
- (6) Johnson, M. F. J. Catal. 1978, 52, 425-431.
- (7) Fu, C. M.; Schaffer, A. M. Ind. Eng. Chem. Prod. Res. Dev. 1985, 24(1), 68.
- (8) Scherzer, J.; McArthur, D. P. Oil Gas J. Oct. 27, 1986, pp 76.
- (9) Scherzer, J.; McArthur, D. P. Ind. Eng. Chem. Res. 1988, 27(9), 1571-1576.
- (10) Ng, S. H. Unpublished results.
- (11) Ritter, R. E.; Creighton, J. E.; Chin, D. S.; Roberie, T. G; Wear, C. C. Catalagran, Davison, 1986, 74, 5.
- (12) Wollaston, E. G.; Haflin, W. J.; Ford, W. D; D'Souza, G. J. Hydrocarbon Process. 1975, 54(19), 93.
- (13) Cimbalo, R. N.; Foster, R. L.; Wachtel, S. J. Oil Gas J. 1972, 70(20), 112.

Table I. Feedstock Inspection Data

Properties	IPPL	Shale
*API	24.2	25.0
Aniline point, °C	93.7	80.0
Conradson carbon, wt %	0.43	0.18
Total nitrogen, ppm	1150	7150
Basic nitrogen, ppm	310	4570
Total sulphur, wt %	0.66	0.52
Viscosity at 40 °C, cSt	65.0	17.3
Simulated distillation, °C		
IBP	305	209
10%	369	290
50%	444	394
90%	538	489
FBP	594	536

Table II. Feedstock Compositional Analysis (wt %)

Hydrocarbon type	IPPL	Shale
Paraffins	23.8	21.8
Monocycloparaffins	14.3	13.5
Condensed cycloparaffins	24.2	13.1
Monoaromatics	13.2	16.9
Diaromatics	9.3	11.4
Polynuclear aromatics	7.9	6.1
Polars	4.3	15.4
Aromatic sulphur	2.2	1.4

Table III. Properties of Cracking Catalysts

Properties	DA-440	Nova D	GX-30
Type	REY	USY	REY
BET surface area, m <sup>2</sup> /g	75.0	95.5	107.5
Zeolite surface area, m <sup>2</sup> /g	43.7	48.4	66.8
Relative zeolite content, wt %	7.3	8.1	10.8
Pore volume, mL/g	0.245	0.266	0.257
Avg. pore diameter, Å	280	208	355
V, ppm	141	351	538
Ni, ppm	374	114	400
Al <sub>2</sub> O <sub>3</sub> , wt %	42.1	45.3	33.1
Unit cell dimension, Å	24.42	24.28	24.39
Microactivity (Davison), wt %	70	72	78

Table IV. Comparison of Product Yields at 50% Conversion\*

Gas oil Catalyst Reactor temperature, °C	IPPL DA-440 470	Shale DA-440 530
Total dry gas, wt %	1.0	3.5
C <sub>3</sub> + C <sub>4</sub> , wt %	8.5	13.0
C <sub>5</sub> + gasoline, wt %	35.0	30.0
Light cycle oil, wt %	14.0	27.0
Decant oil, wt %	39.0	20.5
Coke, wt %	2.6	6.6

\* Extrapolated data

Table V. Weight Recovery and Nitrogen Contents of Upgraded Shale Oils

Shale oil	Untreated	DMSO	Clay
Recovery, wt %	100	85.3	86.1
Total nitrogen, ppm	7150	5618	3496
Basic nitrogen, ppm	4570	3007	1745

Table VI. Cracking Yields (wt %) at C/O = 6

Shale oil	Temp. °C	Catalyst	Conver- sion	C <sub>5</sub> + Gasoline	Coke
Raw	510	DA-440	45.0	25.2	6.5
DMSO treated	510	DA-440	53.2	31.7	6.4
Clay treated	510	DA-440	65.3	40.0	6.4
Raw	530	DA-440	47.9	26.5	6.6
Raw	530	GX-30	59.8	31.7	9.1
Clay treated	530	DA-440	70.0	42.5	6.4

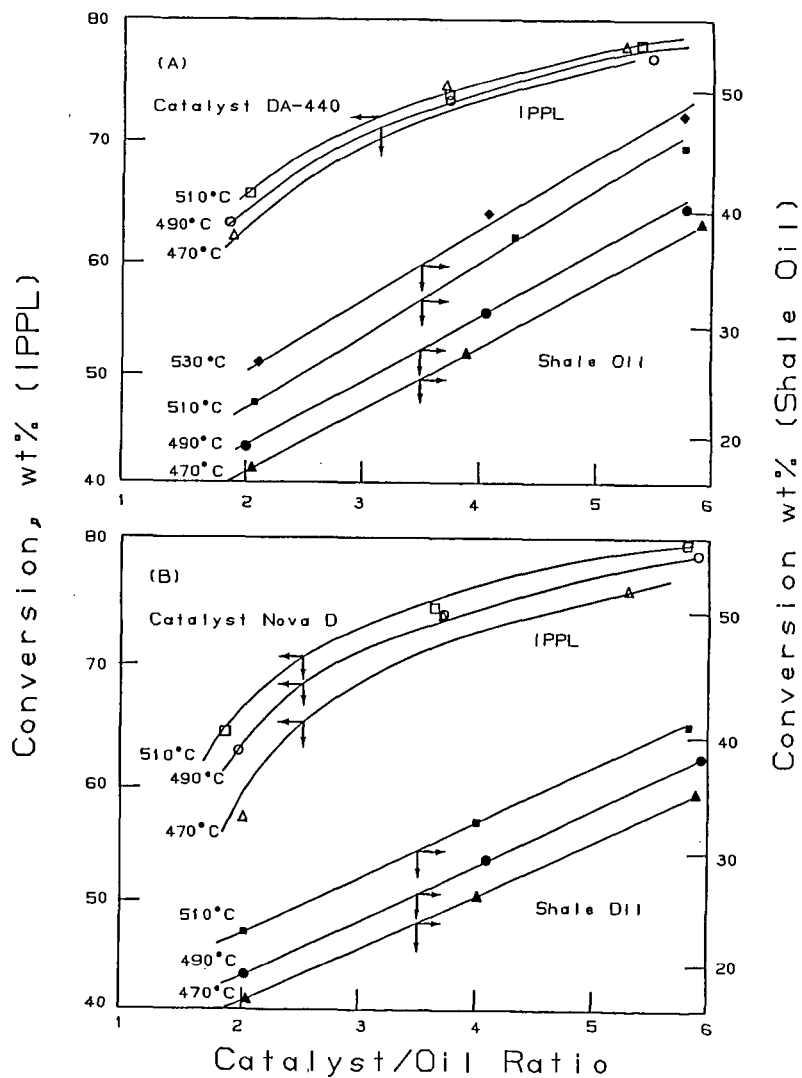


Figure 1. Effects of temperature and catalyst/oil ratio on conversion.

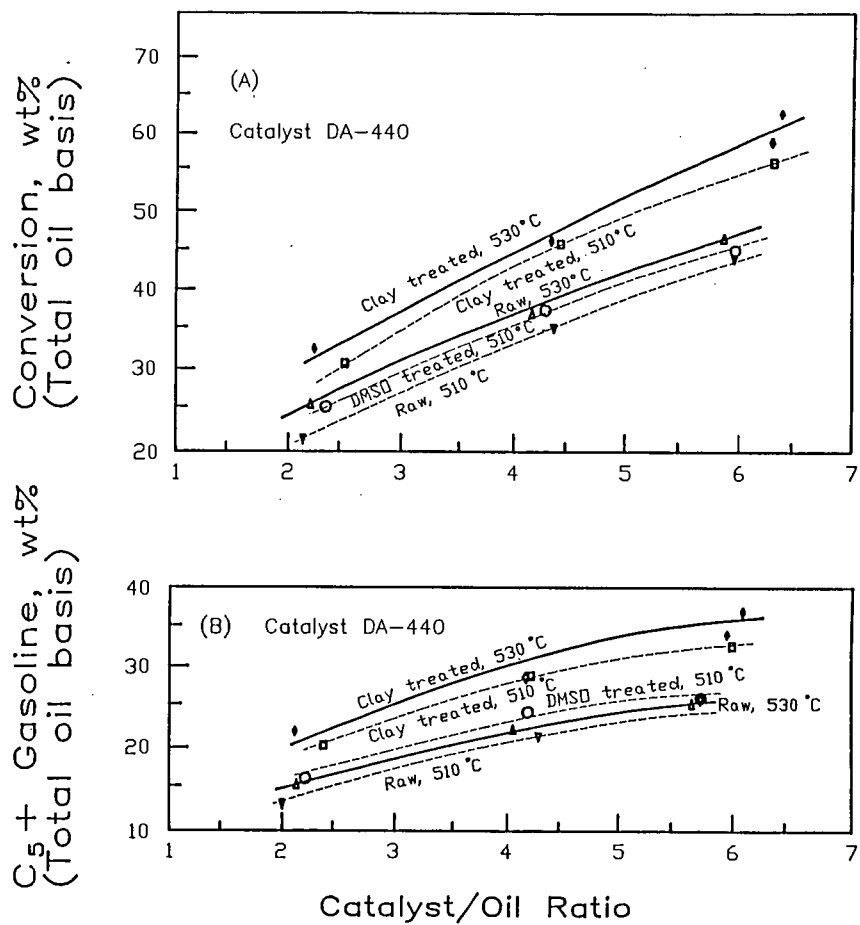


Figure 2. Conversions and gasoline yields of raw and treated shale gas oils calculated on total oil basis.

INFLUENCE OF STEAM ON COAL DEVOLATILIZATION AND ON  
THE REACTIVITY OF THE RESULTING CHAR<sup>1</sup>

M. Rashid Khan  
Texaco Research Center, Texaco Inc  
P.O. Box 509, Beacon NY 12508

F. Y. Hsieh<sup>2</sup>  
Morgantown Energy Technology Center  
Morgantown, West Virginia

ABSTRACT

Improved reactivity of the mild gasification char is highly desirable for the economic viability of a mild gasification process aimed at producing liquid fuel from coal by pyrolysis. In this study, it is demonstrated that devolatilization of coal in the presence of steam atmosphere increases pyrolysis volatile (and liquid) yield and produces a more reactive char. Devolatilization of coal was effected either in a thermogravimetric analyzer or in a slow heating rate organic devolatilization reactor (SHRODR). The chars prepared in steam have a lower oxygen chemisorption capacity than the chars prepared in helium. Fourier transform infra-red (FTIR) spectroscopic studies indicate that the steam char has a higher concentration of hydroxyl groups than the char prepared in He. This implies that pyrolysis of coal in steam may introduce some hydroxyl functional groups which may have a favorable influence during subsequent char gasification/combustion.

INTRODUCTION AND BACKGROUND

It is well known that gasification reactivity of coal char is a strong function of rank of parent coal and pyrolysis conditions used to generate the char (e.g., maximum heat-treatment-temperature, heating rate, and soak time at peak temperature). Numerous studies have been addressed on the influence of thermal history of pyrolysis and the role of the minerals and cations on the reactivity of the resulting char (1-12). However, relatively little attention has been received on the influence of gas atmosphere used during pyrolysis on the reactivity of the resulting char.

Sharma and coworkers (13) studied the low temperature (up to 650°C) pyrolysis of coal in argon, steam, and hydrogen under 1 to 66 atmosphere. Based on very limited studies, it was concluded that pyrolysis gas atmosphere or pressure had no influence on the reactivities of the resulting chars. Christosora and coworkers (14) studied the effect of pyrolysis atmosphere (argon, steam, and hydrogen) on the reactivity (in steam) of produced chars (900°C char) and observed that the

---

<sup>1</sup> Work performed at Morgantown Energy Technology Center.

<sup>2</sup> Post-doctoral trainee through the Oak Ridge Associated Universities

presence of reactive gases (steam and hydrogen) did not affect the rates of reaction of product chars. It was suggested that the pressure of reactive gases (1 bar) during pyrolysis was too low to effect deeper penetration of the reactive gases into the char structure thus causing changes in the chemical and physical properties of chars that would otherwise affect the reactivity of char.

The purpose of this study is to investigate by means of systematic experiments the effect of steam on the pyrolysis weight loss of coals and on the reactivities of resulting chars. The hypothesis of this study is that pyrolysis of coal under steam atmosphere may introduce oxygen containing functional groups to the coal/char structures which may have positive contribution to the reactivity of char.

## EXPERIMENTAL

The coals were devolatilized in a thermogravimetric analysis system (Dupont 1090 thermal analyzer) and in a slow heating rate organic devolatilization reactor (SHRODR) either in He or in steam/He mixture. For the devolatilization in the TGA system, steam was introduced to the TGA system by bubbling He through a filtered dish of a sealed saturator. The temperature of saturator was maintained at a constant temperature of 25°C. The saturation pressure of steam at room temperature is 3 kPa. For the devolatilization in the SHRODR, steam was introduced to the reactor by pumping water to the reactor at the rate of 0.2 cc/min. The analyses of coals used in this study are presented in Table 1. Wyodak coal was acid-washed with 0.1 N HCl solution according to the procedures described by Morgan, et al. (15) to remove exchangeable cations in the coal. The extract solution was analyzed by atomic absorption spectrometry. The exchangeable cation content of Wyodak coal were determined and given in Table 2.

Chemisorption was carried out at 155°C and 0.1 MPa O<sub>2</sub> for 15 h using the TGA. The oxygen chemisorption capacity (OCC) or the active surface area of chars (ASA) were calculated from the amount of oxygen chemisorbed on the chars. Isothermal char reactivities were determined using TGA at 400°C in 0.1 MPa O<sub>2</sub>.

The reproducibilities of coal pyrolysis (devolatilization) and char reactivities determination in the TGA system can be seen in Figures 1a and 1b, respectively. It is obvious that the reproducibility of our experiments was very good.

## RESULTS AND DISCUSSION

### Effect of Steam on Pyrolysis Weight Loss of Coals

Tables 3 and 4 summarized the pyrolysis weight loss of Wyodak coal and Pittsburgh No. 8 coal during pyrolysis in He and steam (3 kPa) up to 650° and 950°C. Weight loss (both for temperature up to 650° to 950°C) is a function of coal rank. The weight loss of Wyodak coal (subbituminous coal) is higher than that for the Pittsburgh No. 8 coal (high volatile bituminous coal). The steam gasification process is thermodynamically favorable when the temperature is higher than 500°C. Table 3 shows that pyrolysis of coals in steam up to 650°C increases weight loss by 3.5 percent for Wyodak coal and 7.0 percent for Pittsburgh No. 8 coal. Wyodak coal contains relatively high concentration of exchangeable cations (Table 2) which are excellent catalysts for steam gasification. As shown in Table 4, pyrolysis of Wyodak coal up to 950°C in steam increases weight loss by 28.8 per-



cent. However, weight loss for Pittsburgh No. 8 coal is increased by only 6.0 percent. These results suggest that steam has small but significant effect on the weight loss of coals at lower pyrolysis temperature (Ca 650°C). However, steam appears to have a significant influence on the weight loss of Wyodak (sub-bituminous) coal at higher pyrolysis temperature (950°C). Tables 3 and 4 also indicate that steam has very little effect on the pyrolysis weight loss of acid-washed Wyodak coal both in the high (950°C) and low (650°C) temperature pyrolysis. This demonstrates that the effect of steam on the pyrolysis weight loss of Wyodak coal is mostly due to the catalytic effect of the exchangeable cations present in this low-rank coal.

Table 5 shows the effect of steam and heating rate on the pyrolysis weight loss of Pittsburgh No. 8 coal up to 900°C. The results suggest that heating rate has relatively small influence on devolatilization of coal in He. In contrast, the overall weight loss during pyrolysis of coal in steam is a strong function of heating rate. The weight loss during devolatilization in steam is 37 percent at 50°C/min which increases to 50 percent when a heating rate of 5°C/min was utilized. This increase in weight loss is attributable to gasification of coal/char by steam which is facilitated by longer residence time at slow heating rates.

#### Influence of Steam Atmosphere on the Reactivities of the Resulting Chars

Table 6 shows the effect of steam on the reactivities of chars prepared at low (650°C) and high (950°C) temperatures. There are several ways to express the reactivity of chars. As continuations of a previous study (5), we are reporting the reactivity data using maximum gasification rate ( $R_m$ ) and the time for 10 percent char conversion ( $T_{0.1}$ ). It can be seen that the 650° steam-prepared chars have higher  $R_m$  and shorter  $T_{0.1}$  than those for the 650° helium-prepared chars. The 950° steam-prepared chars also have higher  $R_m$  (except for acid-washed Wyodak coal char) than those for the 950° helium-prepared chars. However, the  $T_{0.1}$  of 950° steam-prepared chars are longer than  $T_{0.1}$  of 950° helium-prepared chars. By viewing the total gasification profiles of 950° chars, it is evident that the 950° steam-prepared chars are less reactive than 950° helium-prepared chars. It appears that  $R_m$  does not serve as a good parameter for describing char reactivity in some cases. This is not surprising keeping in mind that char reactivity is a function of char conversion. In order to express the char reactivity properly, we suggest that it is appropriate to report both the maximum gasification rate and the time needed for certain levels of char conversion (e.g.,  $T_{0.1}$ ).

Table 7 compares the reactivities and oxygen chemisorption capacity (OCC) for various chars prepared at 650°C. It can be seen that steam-prepared chars have lower OCC and higher reactivity than helium-prepared chars. Long and Sykes (18,19) studied the mechanism of steam-carbon reaction and suggested that steam can dissociate to form an absorbed hydrogen atom and a hydroxyl group which is absorbed on a neighboring carbon atom of the char. They also suggested that the absorbed hydroxyl groups can undergo further reaction to form carbonyl groups and finally desorb as carbon monoxide. Hence, a probable explanation for the lower OCC of steam-prepared chars is that the "newly formed hydroxyl groups" could occupy some of the active sites for oxygen chemisorption and, therefore, lower the OCC of chars. These hydroxyl groups of chars could undergo gasification reaction to form monoxide and, thereby, enhance the reactivity of chars. The FTIR spectra demonstrate that steam-prepared char has slightly higher concentration of hydroxyl groups than those for the helium-prepared char. This implies that the "absorbed

hydroxyl groups" (or part of them) serve as surface complexes on the char surface which could have positive contribution to char reactivity. The data shown in Table 7 indicate that the enhanced effect of steam on the char reactivity ( $R_m$ ) is dominant for the bituminous coal (Pittsburgh No. 8 coal) than for the subbituminous coal (Wyodak coal). This is perhaps due to the higher concentration of cations in Wyodak coal which catalytically promote char gasification. After acid-washing, the catalytic effect became less significant and the effect of steam on char reactivity became more dominant.

Because steam gasification reaction is highly favorable at 950°C, the lower reactivity of 950° steam-prepared chars as compared with 950° helium-prepared chars can be attributed to the relatively severe conditions which was utilized for coal pyrolysis.

Table 8 presents the effect of steam on the pyrolysis tar yields of Pittsburgh No. 8 coal in a fixed-bed reactor (SHRODR) and isothermal reactivity of produced char at 400°C. It can be seen that pyrolysis of coal in the presence of steam enhances the tar yield and reactivity of produced chars. Sharma and his coworkers (13) observed that pyrolysis of coal in steam increases the weight loss. However, there was no report regarding the effect of steam on the pyrolysis tar yield. We propose that steam can dissociately sorb on the char surface. This could reduce the recombination reactions and thereby suppress the char formation and increase the tar yield. In order to further confirm the enhanced effect of steam on char reactivity, a non-isothermal reactivity test has also been performed.

Steam-prepared and helium-prepared chars were heated in a TGA unit under 0.1 MPa oxygen at 10°C/min from 400°C to 900°C. Figure 2 shows the non-isothermal gasification profiles of these two chars. It is clear that the steam-prepared char is more reactive than helium-prepared char. Figure 3 shows the non-isothermal gasification rates DTG curves for the two chars. The maximum gasification rate of steam-prepared char is 25 percent higher than that for the helium-prepared char. The temperature for the maximum gasification rate of steam-prepared char is 8°C lower than that for the helium-prepared char. These results again confirm that pyrolysis of coal in the presence of steam at relatively lower temperature (650°C) enhances both the tar yield and reactivity of the resulting chars.

#### SUMMARY AND CONCLUSIONS

The above results demonstrate that pyrolysis of coal in the presence of steam at relatively lower temperature ( $\leq 650^\circ\text{C}$ ) not only increases the weight loss and tar yield but also enhances the reactivity of the resulting char. Steam can dissociatively absorb on the char surface and thereby inhibit the recombination reactions between tar-free radicals and char-free radicals and, thereby, suppress the retrogressive reactions and increasing tar yield. The newly formed "hydroxyl surface complexes" can undergo further reaction to form carbon monoxide during gasification. Devolatilization of coal in the presence of steam at relatively higher

temperature (950°C) enhances the pyrolysis weight loss, primarily due to the steam gasification of coal char. However, the char prepared at elevated temperatures in steam is less reactive perhaps due to loss of volatiles in the presence of steam during the pyrolysis step.

**ACKNOWLEDGEMENT:** Funding for this work was provided by the US Dept of Energy, Morgantown Energy Technology Center.

#### REFERENCES

1. Bradbury, A. G. W., and F. Shafizadel, "Chemisorption of Oxygen on Cellulose Char," Carbon, 1980, 18, 109.
2. Furimsky, E., "Effect of H/C Ratio on Coal Ignition," Fuel Processing Technology, 1988, 19, 203.
3. Van Heek, K. H., and H.-J. Mühlen, "Effect of Coal and Char Properties on Gasification," Fuel Processing Technology, 1987, 15, 113.
4. Rybak, W., "Reactivity of Heat-Treated Coals," Fuel Processing Technology, 1988, 19, 107.
5. Khan, M. R., "Significance of Char Active Surface Area for Appraising the Reactivity of Low- and High-Temperature Chars," Fuel, 1987, 66, 1626.
6. Radovic, L. R., K. Steczko, P. L. Walker, Jr., and R. G. Jenkins, "Combined Effects of Inorganic Constituents and Pyrolysis Conditions on the Gasification Reactivity of Coal Chars," Fuel Processing Technology, 1988, 10, 311.
7. Patel, M. M., D. T. Grow, and B. C. Young, "Combustion Rates of Lignite Char by TGA," Fuel, 1988, 67, 165.
8. Solomon, P. R., M. A. Serio, and S. G. Herringer, "Variations in Char Reactivity with Coal Type and Pyrolysis Conditions," ACS Division of Fuel Chemistry Preprints, Vol. 31, No. 3, pp. 186.
9. Floess, J. K., J. P. Longwell, and A. F. Sarofim, "Intrinsic Reaction Kinetics of Microporous Carbons," Energy and Fuel, 1988, 2(6), 756.
10. Smith, L. W., "The Intrinsic Reactivity of Carbons to Oxygen," Fuel, 1978, 57, 409.
11. Hsieh, F. Y., and G. N. Richards, "Factors Influencing Chemisorption and Ignition of Wood Chars," Combustion and Flame, in Press.
12. Tsai, C. Y., and A. W. Scaroni, "Reactivity of Bituminous Coal Chars During the Initial Stage of Pulverized-Coal Combustion," Fuel, 1987, 66, 1400.
13. Sharma, D. K., A. Sulimma, and K. H. Van Heek, "Comparative Studies of Pyrolysis of Coal in Inert Gas, Steam, and Hydrogen Under Pressure," Erdoel Kohle, Erdgas, Petrochem, 1986, 39(4), 173.
14. Christosora, C. T., H.-J. Mühlen, K. H. Van Heek, and H. Jüntgen, "The Influence of Pyrolysis Conditions on the Reactivity of Char in H<sub>2</sub>O," Fuel Processing Technology, 1987, 15, 17.
15. Ternan, M., and M. V. C. Sekhar, "The Catalytic Steam Gasification of Chars from Various Sources by K<sub>2</sub>CO<sub>3</sub>," Fuel Processing Technology, 1985, 10, 77.
16. Morgan, M. E., and R. G. Jenkins, "Pyrolysis of a Lignite in an Entrained-Flow Reactor. Effect of Cations on Total Weight Loss," Fuel, 1986, 65, 757.
17. Garcia, X., and L. R. Radovic, "Gasification Reactivity of Chilean Coals," Fuel, 1986, 65, 292.
18. Long, F. J., and K. W. Sykes, "The Mechanism of the Steam-Carbon Reaction," Proc. Roy. Soc. A., 1948, 183, 377.
19. Long, F. J., and K. W. Sykes, "The Effect of Specific Catalysts on the Reaction of the Steam Carbon System," Proc. Roy. Soc. A., 1952, 215, 100.

TABLE 1  
Proximate and Ultimate Analysis of  
Pittsburgh No. 8 Coal, Wyodak Coal  
(PSOC 1520)

	Pittsburgh No. 8 Coal	Wyodak Coal
% C, daf	83.74	73.78
% H, daf	5.46	4.62
% N, daf	1.56	1.11
% S, daf	2.15	1.38
% O, daf (by difference)	7.09	19.11
<hr/>		
% Ash (as-received basis)	7.27	9.08
% Moisture	0.57	26.69
H/C Atomic (daf)	0.78	0.75
O/C Atomic (daf)	0.064	0.19

TABLE 2  
Exchangeable Cation Content  
of Wyodak Coal

Cation	% of Dry Coal
Ca	1.30
Mg	0.275
K	0.005
Na	0.020
Fe	0.275

TABLE 3

Effect of Steam<sup>a</sup> on the Pyrolysis Weight Loss of  
Coals Up To 650°C (Heating Rate = 20°C/min)

Sample/Pyrolysis Atmosphere	Weight Loss During Pyrolysis Up To 650°C, % of Coal (Dry Base)
Wyodak Coal/He	39.7
Wyodak Coal/Steam	43.2
Acid-Washed Wyodak Coal/He	38.2
Acid-Washed Wyodak Coal/Steam	38.2
Pittsburgh No. 8 Coal/He	30.2
Pittsburgh No. 8 Coal/Steam	37.2

<sup>a</sup> Pressure of Steam: 3 kPa

TABLE 4

Effect of Steam<sup>a</sup> on the Pyrolysis Weight Loss of  
Coals Up To 950°C (Heating Rate = 20°C/min)

Sample/Pyrolysis Atmosphere	Weight Loss During Pyrolysis Up To 950°C, % of Coal (Dry Base)
Wyodak/He	57.6
Wyodak/Steam	86.4
Acid-Washed Wyodak Coal/He	49.5
Acid-Washed Wyodak Coal/Steam	50.8
Pittsburgh No. 8 Coal/He	41.5
Pittsburgh No. 8 Coal/Steam	47.5

<sup>a</sup> Pressure of Steam: 3 kPa

TABLE 5  
Effect of Steam and Heating Rate on the  
Pyrolysis Weight Loss of Pittsburgh  
No. 8 Coal Up To 900°C

Heating Rate (°C/min)	Weight Loss During Pyrolysis Up To 900°C	
	He	Steam
5	38.0	50.0
10	37.0	44.5
20	37.0	40.5
50	37.0	37.0

TABLE 6  
Effect of Steam on the Reactivities of Chars Prepared  
at Low (650°C) and High (950°C) Temperature

Sample/Pyrolysis Temperature and Atmosphere	Maximum Gasification Rate at 400°C, %/min (daf)	Time for 10% Conversion (To.1), min
Wyodak/TGA 650/He	10.14	10.0
Wyodak/TGA 650/Steam	10.84	9.0
Wyodak/TGA 950/He	1.58	40.0
Wyodak/TGA 950/Steam	2.81	42.5
Acid-Washed Wyodak/TGA 650/He	3.56	13.0
Acid-Washed Wyodak/TGA 650/Steam	4.06	13.0
Acid-Washed Wyodak/TGA 950/He	1.16	36.7
Acid-Washed Wyodak/TGA 950/Steam	1.05	42.5
Pittsburgh No. 8/TGA 650/He	1.06	30.5
Pittsburgh No. 8/TGA 650/Steam	1.31	28.0
Pittsburgh No. 8/TGA 950/He	0.45	64.5
Pittsburgh No. 8/TGA 950/Steam	0.58	81.0

TABLE 7

Comparison of Reactivities and Active Surface Areas for Various Chars<sup>a</sup>

Sample/Pyrolysis Temperature and Atmosphere	$g^b$ , (% of Char, daf)	$Rm^c$ (400°C) (g g <sup>-1</sup> h <sup>-1</sup> , daf)	ASA <sup>d</sup> , (g/m <sup>2</sup> )	$k^e \times 10^3$ (g m <sup>-2</sup> h <sup>-1</sup> )
Pittsburgh No. 8/TGA 650/He	5.73	0.64	172	3.72
Pittsburgh No. 8/TGA 650/Steam	4.93	0.79	148	5.34
Wyodak/TGA 650/He	8.51	6.08	255	23.84
Wyodak/TGA 650/Steam	6.91	6.50	207	31.40
Acid-Washed Wyodak/TGA 650/He	5.62	2.14	169	12.66
Acid-Washed Wyodak/TGA 650/Steam	5.35	2.44	161	15.16

<sup>a</sup> Pyrolysis was performed at 20°C/min.<sup>b</sup> Chemisorption capacity. Chemisorption was performed at 155°C in oxygen for 15 h.<sup>c</sup> Maximum gasification rate at 400°C in oxygen.<sup>d</sup> Active surface area or oxygen chemisorption capacity (OCC).<sup>e</sup> Reactivity per unit active surface area.

TABLE 8

Influence of Steam on the Pyrolysis Tar Yield for Pittsburgh  
No. 8 Coal and the Reactivity of the Resulting Chars<sup>a</sup>

Pyrolysis Atmosphere	Tar Yield, % of Coal (daf)	Maximum Gasification Rate at 400°C, %/min (daf)	Time for 10% Conversion, min
He	14.5	1.11	31.6
Steam	16.3	1.36	23.1

<sup>a</sup> Pyrolysis was performed in SHRODR at 500°C, 20 min.

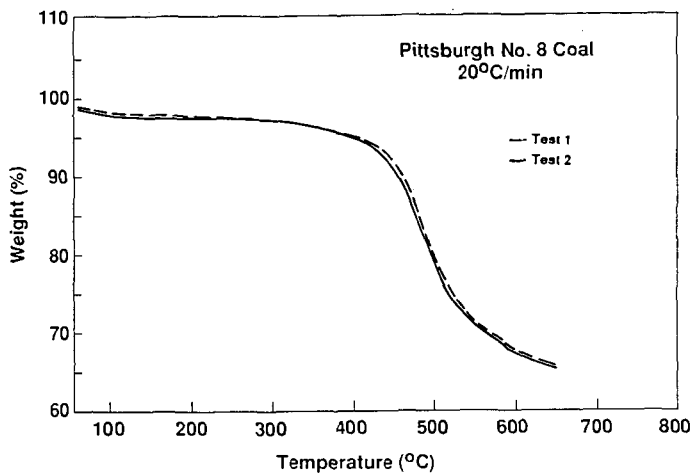


FIGURE 1a. Reproducibility of TGA Devolatilization Runs

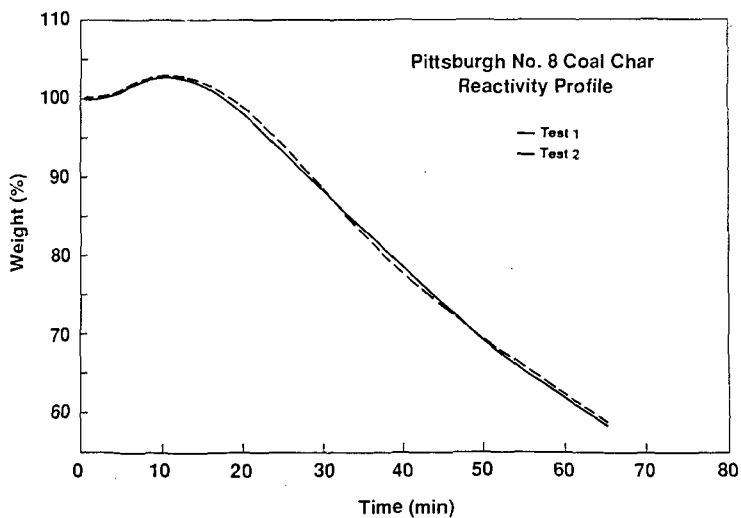


FIGURE 1b. Reproducibility of TGA Reactivity Profiles



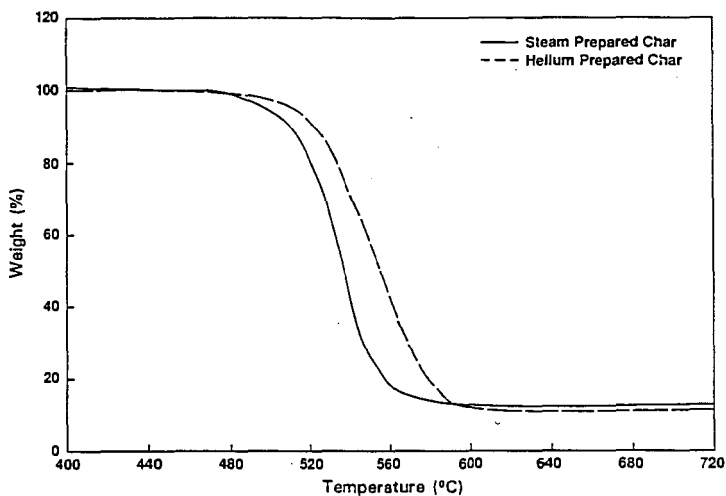


FIGURE 2. Comparison of Non-isothermal Gasification Profiles of Chars Prepared Under Helium and Steam

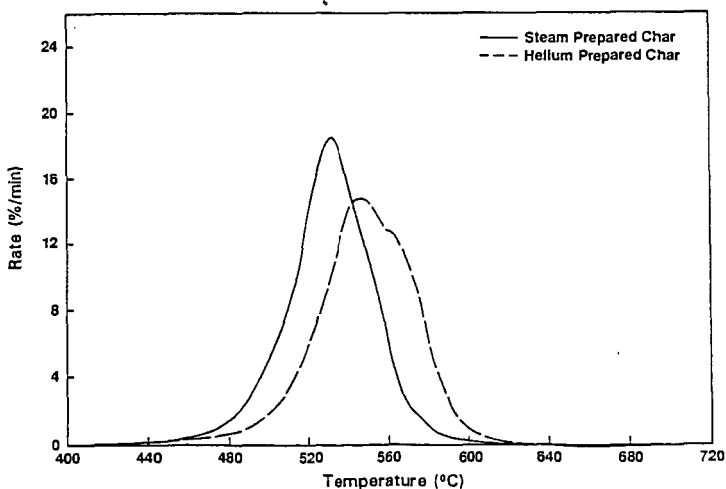


FIGURE 3. Comparison of Non-isothermal Gasification Rates of Chars Prepared Under Helium and Steam

## COMBUSTION CHARACTERISTICS OF MILD-GASIFICATION CHARS

C. Stuart Daw  
Oak Ridge National Laboratory\*  
Bldg. 9108, P. O. Box 2009, Oak Ridge, TN 37831

### INTRODUCTION

The commercial success of mild coal gasification (MG) depends on economical utilization of the byproduct char. While various utilization options are being considered (e.g., coke manufacture, activated carbon production, and further gasification), the boiler fuel market is likely to be the largest potential consumer. A key concern is the combustion performance of MG chars relative to more conventional boiler fuels. This paper summarizes recent results of MG char characterizations conducted by Oak Ridge National Laboratory (ORNL) for Morgantown Energy Technology Center (METC) of the Department of Energy (DOE). The char characterizations are being conducted in conjunction with MG liquid characterizations.

### EXPERIMENTAL METHODS AND MATERIALS

#### Char and Reference Fuel Samples

Char samples were obtained from two MG processes, one developed by the United Coal Company (UCC) and the other by SGI International (SGI). A single UCC char sample was obtained from a typical test on the UCC MG test unit [test run P1/12; United Coal Company (1988)]. In this case, the parent coal was Kentucky Williamson No. 2 seam, a high-volatile, bituminous coal. Three SGI char samples were obtained, each representing successively higher devolatilizations of Montana Rosebud subbituminous coal. These samples were produced in cooperative tests between SGI and Peabody Coal Company [Estergar(October 1988)]. Four widely-used reference fuels were also included to extend the applicability of the results: Texas lignite; Kentucky No. 9 high-volatile, bituminous; delayed petroleum coke, and anthracite.

Table 1 summarizes proximate, ultimate, and BET analyses of the char samples, typical analyses of the parent coals, and reference fuel analyses. It is clear that all the SGI chars have more volatiles and much greater surface area than the UCC char. Such differences are believed to be due both to the parent coals and to higher temperature and residence time in the UCC process.

#### Thermogravimetric Tests

Low-temperature combustion tests were conducted for each char and reference fuel using a Netsch model STA 429 thermogravimetric (TG) analyzer. Previous studies [e.g., Jenkins et al (1973),

\* This work was conducted at Oak Ridge National Laboratory operated by Martin Marietta Energy Systems, Inc. for the U.S. Department of Energy under contract DE-AC05-84OR21400. By acceptance of this article, the publisher acknowledges the U. S. Government's right to retain a nonexclusive, royalty-free license in and to any copyright.

Ceely and Daman (1981), Khan (1987)] have demonstrated the usefulness of TG comparisons of coals and chars. Standard operating procedure involved heating approximately 20 mg of 105-125  $\mu\text{m}$  particles from ambient up to 1273 K. Heating rate was 10 K/min, and gas flow was 190 cc/min. Dry air (21% oxygen) was injected directly into the sample crucible. Sample weight, rate of weight change, and temperature were continuously monitored.

The limiting external oxygen mass-transfer rates for similar conditions have been determined previously [Daw and Mitchell (1986)]. These limits were reevaluated during the current tests based on the observed burning rates for previously tested reference fuels and on the asymptotic high-temperature burning rates of the chars [see Mulcahy and Smith (1969)]. Measured burning rates were corrected to true intraparticle rates by the relationship of Young and Smith (1981):

$$RI = R/[1 - (R/RMT)]^n \quad (1)$$

where RI is the internally-limited burning rate (i.e., the rate limited solely by intraparticle processes), RMT is the maximum rate possible due to external mass transfer of oxygen, R is the observed burning rate, and n is the effective reaction order in oxygen. In most cases such corrections were small.

#### Fixed-Bed Reactor Tests

Higher-temperature combustion tests were conducted using the fixed-bed reactor at Babcock and Wilcox's (B&W) Alliance Research Center. This reactor was constructed for the Atmospheric Fluidized Bed Combustion Fuels Characterization Program sponsored by the Electric Power Research Institute (EPRI). B&W has used this reactor to characterize a range of coals, refuse derived fuels, and coal-cleaning refuse for EPRI and Consolidated Edison Company of New York [Chandran et al (1988, 1989)]. Described in detail elsewhere [Chandran et al (1987)], the reactor is a 5.1-cm diameter quartz vessel containing a bed of spent fluidized bed combustor sorbent. The bed is heated electrically, and preheated nitrogen/oxygen mixtures enter the top, flowing down through the bed. Fuel particles are injected batchwise via a solenoid valve, and they land on top of the bed where they devolatilize and burn. The reactor is designed for gas velocities, temperatures, gas compositions, and particle sizes similar to those expected for AFBC. The operating ranges for each of the fuels in this study were: 1045-1215 K gas temperature, 3-10 volume % oxygen, 1.5-1.6 atm total pressure, and 1.3-1.5 m/s superficial gas velocity.

Fuel particles were prescreened into two narrow fractions: 1) 105-125  $\mu\text{m}$  (115  $\mu\text{m}$  mean) and 2) 500-595  $\mu\text{m}$  (547  $\mu\text{m}$  mean). The fuel batch weight was chosen such that the reactor oxygen concentration decreased by less than 10% at the maximum combustion rate. Devolatilization and combustion were monitored by continuous analysis of the reactor exit gas for carbon dioxide, carbon monoxide, and hydro-carbons. Net carbon loss-vs.-time was determined by integrating total gas carbon concentration. Particle temperatures were estimated by heat balances accounting for conduction, convection, radiation, and heat of combustion.

## EXPERIMENTAL RESULTS AND DISCUSSION

### Thermogravimetric Results

Figures 1 and 2 illustrate the observed variation in the rate-vs-temperature profiles for the reference fuels. From these plots it is clear that the UCC char ignites and burns more slowly than all three SGI chars at the conditions tested. Many different ignitability/reactivity measures can be derived from TG profiles. Table 2 lists some example measures to illustrate comparisons of the fuels tested here. While minor variations occur depending on the measure used, the general trends are readily apparent: 1) Texas lignite<sup>o</sup> is by far the most ignitable and reactive; 2) the SGI chars and Kentucky 9 bituminous are similar and slightly less ignitable and reactive than lignite; 3) the UCC char and petroleum coke are similar and significantly less ignitable and reactive than the SGI chars and Kentucky 9; and 4) anthracite is by far the most difficult to burn.

### Fixed-Bed Reactor Results

Figure 3 compares the fixed-bed profiles for 115  $\mu$ m particles of each fuel exposed to 3% oxygen at 1100-1120 K. As with the TG results, the fixed-bed profiles clearly distinguish among the fuels. Texas lignite burns by far the most rapidly, followed closely by Kentucky No. 9 bituminous and the SGI chars. Petroleum coke, UCC char, and anthracite are again much slower. Quantitative comparisons can be made using various profile measurements such as: 1) burning rate at char ignition, 2) degree of fixed carbon conversion after a fixed elapsed time, and 3) time to achieve a given fixed-carbon conversion. For the fuels tested the basic profile shapes following char ignition are similar, and thus all three of the above measures give identical rankings. Measurement 1 above, the burning rate at char ignition, is selected as the key index for further discussion.

Table 3 compares the estimated initial char burning rates for the profiles in Figure 3. The fuel ranking resulting from these burning rates is virtually identical with the rankings developed from burning rates evaluated at other fixed-bed conditions. An important point emerging from these comparisons is that the relative fuel reactivities are consistent over the range of fixed-bed and TG conditions tested.

### Combined Burning-Rate Expressions

Estimates of the true intra-particle combustion rate at char ignition,  $RI$ , were made for each fuel and test condition (both TG and fixed-bed) using Eqn. 1. As expected, the corrected rates were found to follow the standard Arrhenius rate expression:

$$RI = A \exp(-E/R_g T_p) PO_2^n = k_w PO_2^n \quad (2)$$

where  $A$  is the pre-exponential rate coefficient,  $E$  is the effective activation energy,  $R_g$  is the ideal gas constant,  $T_p$  is particle temperature,  $PO_2$  is bulk-gas-oxygen partial pressure, and

kw, was determined assuming  $n$  to be 0.5. Within the scope of this study it is not possible to select with certainty any value of  $n$  between 0.5 and 1. Essenhigh(1981) has shown that Zone 2 combustion (combustion in which pore diffusion is a significant controlling factor) should exhibit an effective reaction order of 0.5. As discussed below, the Arrhenius fits of the present data suggest Zone 2 burning. Selection of  $n=0.5$  is also consistent with earlier fixed-bed data [Daw (1988)] and conforms more closely to the comprehensive study by Suuberg et al (1988).

Figure 4 depicts the combined Arrhenius fits for the chars and reference fuels (note: the horizontal axis is the reciprocal of estimated particle temperature not gas temperature). Comparing slopes, the activation energies for all four chars do not seem to differ greatly. Table 4 summarizes the Arrhenius parameters quantitatively. Within experimental uncertainty, all the activation energies fall within the 4.8 to 9.6 kJ/mole (20 to 40 kcal/mole) expected for Zone 2 burning [Essenhigh (1981)]. Thus the assumption of 0.5 oxygen reaction order is reasonable.

#### CONCLUSION

The above results suggest that the bituminous char tested is more suitable for firing in non-sensitive applications, such as fluidized beds, stokers, or U-flame boilers. The subbituminous chars evaluated may be sufficiently reactive for pulverized firing in bituminous boilers with little or no supplemental fuel.

#### REFERENCES

- Coely, F. J. and Daman, E. L., "Combustion Process Technology," in Chemistry of Coal Utilization, M. A. Elliot, editor, John Wiley and Sons, pp 1313-1387, 1981.
- Chandran, R. R., Duqum, J. N., Jafari, M. C., Rowley, D. R., and Perna, M. A., "Fuels Characterization Project- Interim Report," Report by Babcock and Wilcox to EPRI, RDO:88:4753-06-55:D1, 1987.
- Chandran, R. R., Duqum, J. N., Perna, M. A., Rowley, D. R., Daw, C. S., Petrill, E. W., and McGowin, C. R., "AFBC Fuels Characterization Program Results For Different Coals, Refuse-Derived Fuel (RDF), and Coal-Cleaning Refuse," EPRI Seminar on Fluidized-Bed Combustion Technology for Utility Applications, vol 1, Palo Alto, California, May 1988.
- Chandran, R. R., Duqum, J. N., Perna, M. A., Sutherland, D. D., Rowley, D. R., Pirkey, J., and Petrill, E. W., "Ranking Fuels and Sorbents for Utility Scale AFBC Application," Tenth International Conference of Fluidized Bed Combustion, San Francisco, May 1989.
- Daw, C.S., "Second Interim Report to the Tennessee Valley Authority on the Analysis of the Kentucky Fixed-Bed Reactor Data from the Babcock and Wilcox Alliance Research Center," April 1988.
- Daw, C. S. and Mitchell, R. E., "Char Combustion Kinetics for Kentucky No. 9 Coal," Proceedings of the AFB Technology for Utility Applications Seminar sponsored by the Electric Power Research Institute, Palo Alto, California, April 1986.
- Essenhigh, R. H., "Fundamentals of Coal Combustion," in Chemistry of Coal Utilization, M. A. Elliot, editor, John Wiley and Sons, pp 1153-1312, 1981.
- Esterger, E. P., SGI International, La Jolla, California, personal communication, October 1988.

Jenkins, R. G., Satyendra, P. N., and Walker, P. L., Jr., Fuel, vol 52, pp 288-293, October 1973.

Mulcahy, M. F. R. and Smith, I. W., Rev. Pure and Appl. Chem., 19, pp 81-108, 1969.

Saueberg, E. M., Wojtowicz, M., and Calo, J. M., "Reaction Order for Low Temperature Oxidation of Carbons," Proceedings of the Twenty-Second International Symposium on Combustion, The Combustion Institute, Pittsburgh, Pennsylvania, p 1988.

Young, B. C. and Smith, I. W., Proceedings of the Eighteenth International Symposium on Combustion, The Combustion Institute, Pittsburgh, Pennsylvania, p 1245, 1981.

United Coal Company, Project Status Report, UCC R&D C17-20, Contract No. DE-AC21-87MC23289, September 16, 1988.

Table 1. Ultimate and proximate analyses of the test chars, parent coals, and reference fuels.

Chars:	Ultimate*				Tot. S	Pyr. S	Sul. S	Org. S
	C	H	N	Cl				
UCC	83.88	3.18	1.46	0.077	0.70	0.036	0.0061	0.66
SGI 4	63.40	3.07	1.00	0.0037	0.78	0.055	0.053	0.67
SGI 20	68.31	2.34	1.13	0.0009	0.99	0.016	0.0094	0.96
SGI 48	66.50	3.27	1.12	0.0022	0.64	0.16	0.021	0.46
Parent Coals:								
KY WIL. 2 (UCC)	78.18	5.24	1.46	0.13	0.98	-	-	-
MT ROS. (SGI)	54.82	3.72	0.79	0.02	0.63	0.33	0.040	0.42
Ref. Fuels:								
TX LIG.	33.27	3.28	0.77	-	0.75	-	-	-
KY 9	65.82	4.72	1.40	-	3.48	-	-	-
PET. CK.	85.75	3.87	1.46	-	5.18	-	-	-
ANTH.	79.80	1.79	0.78	-	0.53	-	-	-

Chars:	Proximate*				BET <sup>+</sup>
	WATER	ASH	VM	FC	
UCC	2.32	5.86	11.49	80.33	0.197
SGI 4	10.82	15.27	18.34	55.57	22.6
SGI 20	6.84	15.63	13.99	63.54	30.5
SGI 48	8.61	11.52	23.72	56.15	11.2
Parent Coals:					
KY WIL. 2	1.80	5.00	33.80	59.40	-
MT ROS.	19.84	9.16	39.02	51.82	-
Ref. Fuels:					
TX LIG.	33.27	7.25	30.58	28.90	-
KY 9	6.78	10.81	37.75	44.66	-
PET. CK.	1.10	2.14	13.86	82.90	0.230
ANTH.	4.23	10.85	5.74	79.18	-

\* All analyses as weight percent on an as-received basis (i.e., moisture and ash included).

+ BET surface area by N<sub>2</sub> adsorption (m<sup>2</sup>/g).

Table 2. Example measures of TG reactivity for the fuels tested.

<u>Fuel</u>	<u>Tign</u>	<u>Rign</u>	<u>Tmax</u>	<u>FCCL</u>	<u>FCCh</u>	<u>T50</u>
UCC	753	$7.2 \times 10^{-4}$	847	0.10	0.50	823
SGI 4	723	$9.6 \times 10^{-4}$	753	0.39	0.71	785
SGI 20	703	$5.9 \times 10^{-4}$	801	0.33	0.71	793
SGI 48	713	$1.3 \times 10^{-3}$	778	0.45	0.84	781
TX LIG.	668	$2.6 \times 10^{-3}$	681	0.84	0.91	703
KY 9	748	$1.9 \times 10^{-3}$	798	0.28	0.59	798
PET. COKE	761	$7.8 \times 10^{-4}$	823	0.0	0.36	838
ANTHRACITE	793	$2.7 \times 10^{-4}$	918	0.0	0.05	883

Tign = char ignition temperature (K) ; Rign = rate at char ignition (g/g s) or (1/s); Tmax = maximum burning rate temperature (K); FCCL = fractional fixed carbon conversion at 773 K; FCCh = fractional fixed carbon conversion at 823 K; T50 = temperature at which fixed carbon conversion reaches 0.5 (K)

Table 3. Typical fixed-bed combustion results for 115 micron particles in 3% oxygen at 1100-1120 K.

<u>Fuel</u>	<u>Tg</u>	<u>Vo</u>	<u>Tp</u>	<u>Rign</u>
UCC	1120	1.51	1127	0.059
SGI 4	1120	1.48	1174	0.30
SGI 20	1114	1.69	1164	0.36
SGI 48	1120	1.45	1183	0.47
TX LIGNITE	1101	1.60	1189	1.5
KY 9	1103	1.59	1141	0.59
PET. COKE	1116	1.67	1132	0.090
ANTHRACITE	1114	1.46	1117	0.024

Tg = gas temperature (K) ; Vo = superficial gas velocity (m/s) ; Tp = estimated particle temperature (K); Rign = burning rate (1/s)

Table 4. Arrhenius char combustion parameters derived from the combined combustion data.

<u>Fuel</u>	<u>A*</u>	<u>E<sup>+</sup></u>	<u>r<sup>2</sup></u>
UCC	$1.7 \times 10^4$	$5.71 \pm 0.57$	0.990
SGI 4	$7.2 \times 10^5$	$6.70 \pm 0.57$	0.997
SGI 20	$3.0 \times 10^4$	$7.00 \pm 0.88$	0.994
SGI 48	$4.9 \times 10^4$	$5.61 \pm 0.53$	0.997
TX LIGNITE	$1.8 \times 10^6$	$5.38 \pm 0.31$	0.999
KENTUCKY 9	$1.6 \times 10^6$	$7.05 \pm 0.91$	0.996
PET. COKE	$2.0 \times 10^4$	$5.73 \pm 0.55$	0.990
ANTHRACITE	$2.8 \times 10^4$	$6.47 \pm 1.15$	0.974

A = Arrhenius pre-exponential factor ( $s^{-1} atm^{-0.5}$ );  
E<sub>2</sub> = activation energy (kJ/mole) and 95% confidence interval;  
r<sup>2</sup> = coefficient of determination for regression

(X 1E-4)

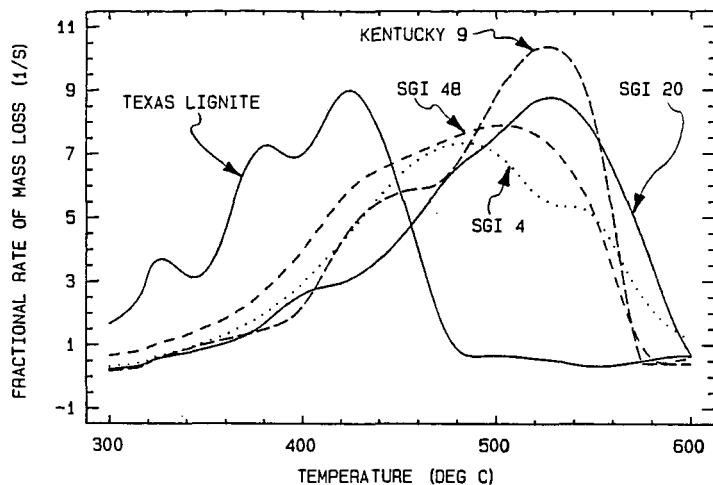


Figure 1. TG rate profiles for the more reactive fuels.

(X 1E-4)

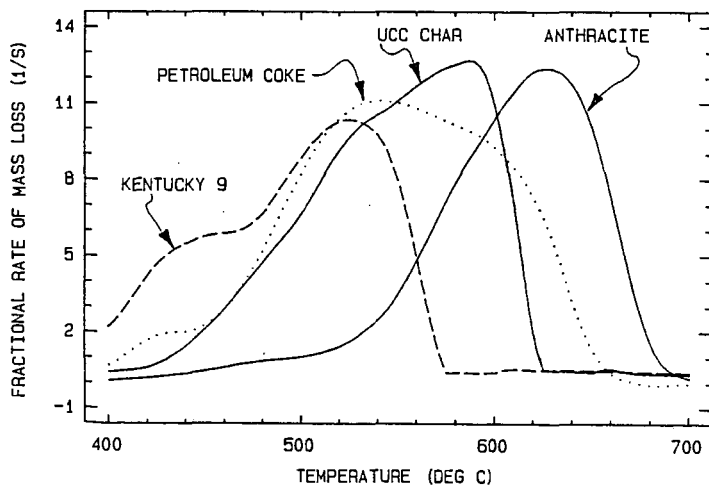


Figure 2. TG rate profiles for the less reactive fuels.



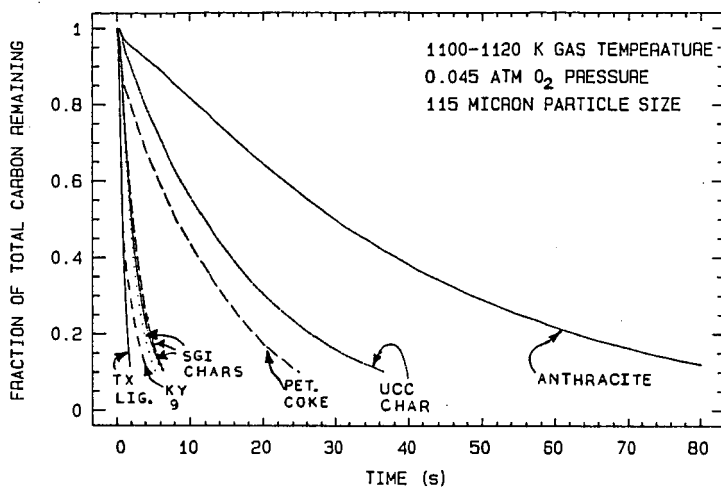


Figure 3. Comparison of the fixed-bed profiles for all the fuels at one test condition.

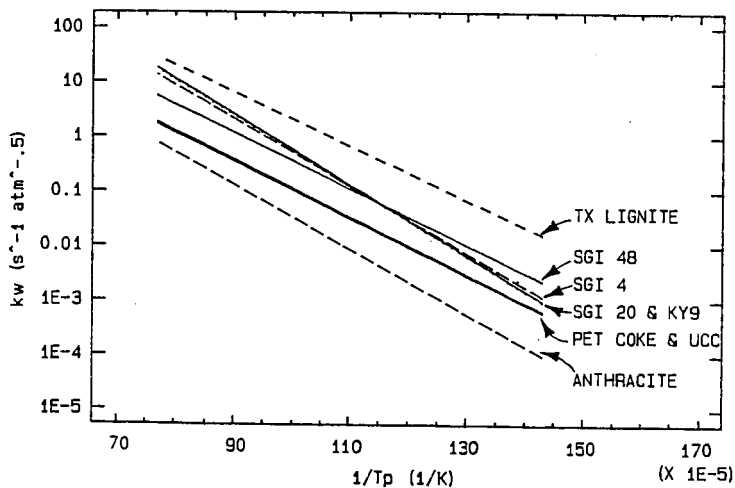


Figure 4. Comparison of Arrhenius plots for all the fuels tested.

## REACTIVITY OF MILD GASIFICATION CHARS DERIVED FROM AN ILLINOIS COAL

M. Rostam-Abadi<sup>1</sup>, J. A. DeBarr<sup>1</sup>, W.T. Chen<sup>1</sup>, D. P. McCollor<sup>2</sup>, and S. A. Benson<sup>2</sup>

<sup>1</sup> Illinois State Geological Survey, 615 E. Peabody Drive, Champaign, IL 61820

<sup>2</sup> University of North Dakota, Energy and Minerals Research Center, Grandfork, North Dakota 58202

### INTRODUCTION

In recent years, some emphasis has been given to producing premium liquids by mild gasification of coal<sup>1-3</sup>. The principle product from the mild gasification process is a partially devolatilized coal that must be effectively utilized (burned or gasified) to help the overall economics of the process. The loss of volatile matter indicates loss of hydrocarbon materials from the coal that can influence reactivity and combustion characteristics such as ignition, flame stability and carbon burn-out.

A large number of studies have been conducted on the oxidation reactivity and combustion properties of coal chars<sup>4-6</sup>. However, the majority of these studies have focused on chars prepared in laboratory reactors under rapid heating rates (10<sup>4</sup>°C/sec). A few studies have dealt with the ignition<sup>7</sup> and reactivity of industrial process chars<sup>8</sup>. Reactivities of chars prepared under mild pyrolysis conditions have been recently reported<sup>9</sup>. Fuels prepared in laboratory reactors by heating coals at 12.5 to 20°C/min to 500°C were more reactive than either the parent coals or chars produced at higher pyrolysis temperatures. The present authors reported the reactivities of chars prepared from an Illinois coal under various pyrolysis conditions<sup>10</sup>. The results suggested that lower pyrolysis temperatures, higher heating rates, and shorter soak times increased reactivity.

In this paper, the reactivities and ignition temperatures of chars derived from an Illinois coal in a pilot scale reactor under mild gasification conditions are reported. The paper focuses on the influence of volatile matter and particle size on char reactivity.

### EXPERIMENTAL

#### Char Preparation

Chars, also referred to as partially devolatilized (PD) coals, were produced in the Mild Gasification Unit at United Coal Company Research Corporation in Bristol, Virginia in October 1986. The coal was from the Illinois Basin Coal Sample Program, Sample IBC-103. The details of PD coal production have been reported elsewhere<sup>11</sup>. In brief, the PD coals were prepared by heating the coal under a slight vacuum in a fixed bed reactor (8-inch diameter, and 8-foot long) which was located inside a natural gas fired furnace. The furnace temperature was kept at 760°C during the production runs. Three PD coals designated as PD-1, PD-2, and PD-3 were prepared at residence times of 1.70, 2.90 and 3.17 hours.

Five size fractions of coals and PD coals were prepared by grinding the -8 mesh fuels in a rod mill. The crushed samples were dry sieved to obtain 65x100, 100x150, 150x200, 200x270, and 270x400 mesh fractions. The samples were stored under nitrogen to prevent oxidation.

### Ignitability Tests

An ignitability test apparatus, shown in figure 1, was used to determine ignition temperatures of fuels. It consisted of an oxygen reservoir, a sample holder tube, a quartz reactor tube and an electric furnace. Fuel particles were injected into the reactor by oxygen gas through a built-in orifice. Six thin wire (0.0076 cm) type K thermocouples spaced at 2 cm apart measured axial temperature variations inside the reactor. The thermocouples were interfaced with a computer for automatic data collection. Typical data acquisition rates were six simultaneous measurements at 50 millisecond intervals.

In a typical ignition test, 20 mg of sample was injected into the preheated (between 390 and 500°C) reactor. The volume of oxygen carrier gas used to inject the sample was 10 cc at 5 to 7 psig. The relatively low pressure and volume of the carrier gas ensured that the fuel particles traveled with velocities approaching their free fall velocities inside the reactor.

Criteria for positive ignition were a brilliant flash and an abrupt increase in temperature inside the reactor during the test. If a negative test was noted, the reactor temperature was increased in 5°C increments and the test procedure was repeated.

### Thermogravimetric Tests

An Omnitherm thermogravimetric analyzer (TGA) which was interfaced with a computer was used to obtain burning profiles (non-isothermal TGA) and isothermal reactivity data. Burning profiles were obtained by heating a sample mass of < 5 mg at a constant rate of 20°C/min in air to 850°C. A gas flow rate of 200 cc/min (STP) was used.

In isothermal reactivity tests, a sample mass of 2 to 4 mg was heated at 50°C/min under nitrogen flow to 550°C. The sample was then cooled to between 400 and 525°C and the nitrogen flow was replaced with dry air flowing at 200 cc/min. The weight of the char remaining, the rate of weight loss, and temperature were monitored by the computer at 5 to 40 second intervals depending on the reaction temperature. A modified TGA quartz furnace tube was used to obtain reliable rate data in the initial stage of oxidation<sup>12</sup>. The objective was to achieve the desired oxygen concentration in the furnace tube as quickly as possible.

### Drop Tube Furnace Tests

These tests were conducted using the University of North Dakota Energy and Minerals Research Center drop tube furnace (DTF). The details of the furnace assembly, are given elsewhere<sup>12</sup>.

Combustion tests were performed on the 65x100 and 270x400 mesh size fractions of the coal and three PD coals. The furnace temperatures selected were 900°C and 1300°C. The gas in the tube furnace (6.5 cm i.d.) contained 3% oxygen - 97% nitrogen and flowed at a nominal rate of 5 l/min. The flow rate was chosen to keep the residence times within a single furnace segment for nearly all the tests. The flow rate was adjusted to give residence times of 0.1 and 0.8 seconds. Carbon conversion efficiencies were calculated using the ash tracer method.

## RESULTS AND DISCUSSION

### Characterization of Fuels

The analyses of the coal and PD coals are summarized in tables 1 and 2. The volatile matter content, hydrogen and fixed carbon were nearly identical for the five size fractions of coal. However, for PD coals, volatile matter and hydrogen contents increased while carbon contents decreased with decreasing particle size range. The amount of volatiles increased from 24.8% to 29.2% for PD-1, from 15.7% to 21.3% for PD-2, and from 11.5% to 15.7% for PD-3 as particle size range decreased from 65x100 mesh to 270x400 mesh. Hydrogen content remained unchanged for PD-1 samples but increased by 21% for PD-2 and by 41% for PD-3 samples.

Comparison of the devolatilization profile (non-isothermal TGA under nitrogen atmosphere) of the fuels indicated that a major decomposition stage for the coal and PD coals occurred between 380 and 530°C<sup>12</sup>. The average weight losses were 25.6, 14.0, 7.4, and 4.8% for coal, PD-1, PD-2, and PD-3 respectively. These results confirmed the presence of varying amounts of coal-like materials in the PD-coals. This was attributed to the manner in which PD coals were prepared. Because the reactor was externally heated, the temperature at the wall of the reactor was much higher than at the center. Therefore, the coal particles near the wall were highly devolatilized whereas those at the center were not. The devolatilization profiles suggest that a fraction of coal was never devolatilized during processing.

### Burning Profiles

Burning profiles obtained for the 65x100 mesh coal, PD-1, PD-2, and PD-3 coals are shown in figure 2. The profiles are offset to avoid overlap. The onset of burning was about 375°C for all the samples. However, there are clear differences among the burning profiles. Raw coal exhibited a single-burn profile, while double-burn profiles were observed for PD-1, PD-2 and PD-3. The second burn appeared as a shoulder peak for PD-1 and became more pronounced for PD-2 and PD-3. The double-burn behavior observed for the PD coals suggested the presence of at least two types of combustibles in the fuels. The two portions of combustibles burned in two distinct stages with peak burn rates at approximately 500°C and 550°C. The higher reactivity constituents (low temperature burn) had burning properties similar to coal and was present in larger concentrations in PD-1 followed by PD-2 and PD-3<sup>12</sup>. Fuels with higher volatile matter content burned more rapidly. For example at 500°C, the amount of combustible materials burned (not shown) was 70% for the raw coal, 55% for PD-1, 40% for PD-2, and 20% for PD-3. Differences in volatile matter had the greatest impact on burn-out temperatures which were 580, 630, 660 and 690°C for the coal, PD-1, PD-2 and PD-3. The results indicate that under the conditions used, raw coal was the most readily combusted fuel, followed by PD-1, PD-2 and finally PD-3.

### Ignition Temperatures

The effect of volatile matter on ignition temperatures is presented in figure 3. Ignition temperatures varied between 406 and 494°C and were independent of volatile matter (except for 270x400 mesh fuels) in the range of 28 to 41% (daf). Below 28%, the volatile matter effect on ignition temperature appears to be significant among all the different particle size fractions tested (ignition temperature increased between 40 and 70°C). However, it has been shown in the literature that the role of volatile matter on the ignition temperature is little or none<sup>7</sup> (heterogeneous ignition

theory). Therefore, the differences in ignition temperatures observed could be attributed to inherent reactivity differences among the fuels tested.

The influence of particle size on ignition temperature is illustrated in figure 4. The particle size dependence of ignition temperature appeared to be rather mild with a spread of 30°C separating the studied size fractions. With the exception of the 65x100 mesh fraction (180µm average particle size), the ignition temperatures for the coal and PD coals increased with decreasing particle size. Ignition curves exhibited a minimum at 100x150 mesh size range (130µm).

The presence of a minimum on the ignition curves and the observed narrow temperature difference among different size fractions could be attributed to contributions of particle and cloud ignition. According to the Semenov thermal explosion theory<sup>13</sup>, which is commonly used to model single coal particle ignition, large particles ignite at lower temperatures. However, it has been shown that under dust cloud conditions, ignition temperatures of fine particles are lower than those of large particles<sup>14</sup>. In this work, regardless of particle size range, a constant sample mass of 20 mg was used. Therefore, samples containing finer particles had higher solid mass density (mass/unit reactive volume) than those containing coarser particles, and the ignition approximated cloud ignition rather than particle ignition. As a result, there was a shift from dust cloud ignition to single particle ignition as particle size range increased. Because the opposite nature of these two mechanisms offset the other, a minimum and a narrow temperature difference were observed for ignition curves of the fuels:

#### Isothermal Reactivity Studies

Initial reactivity tests were conducted at 475°C. The data were used to calculate apparent rate, R,

$$R = \frac{-1}{f} \frac{df}{dt} \quad (1)$$

and

$$f = (M - M_a) / (M_o - M_a) \quad (2)$$

where f = fraction combustible remaining at time t, M = mass of sample at time t, M<sub>o</sub> = initial sample mass, M<sub>a</sub> = mass of sample at complete conversion, i.e. ash. At 475°C, the rates were the same for all particle sizes, indicating the data were obtained under diffusion-free conditions. The apparent rates at 50% conversion were 0.013, 0.025 and 0.062 g/g/min for PD-1, PD-2 and PD-3, respectively. The rate for a char (18% volatile matter) that was prepared in the TGA at 500°C under nitrogen atmosphere was 0.2 g/g/min.

Additional tests were performed at temperatures between 400 to 525°C to evaluate activation energies for the oxidation of 200x270 mesh fuels. In figure 5, the values of ln(-df/dt/f) evaluated at 50% burn-off are plotted against 1/T. The activation energies obtained from the slopes of the plots were 146, 137, 134, and 125 kJ/mole for the 500°C char, PD-1, PD-2 and PD-3. The observed activation energies are comparable with previously reported values for various types of coal chars<sup>8,9</sup>. The data shown in figure 5 indicate that the 500°C char is 2.5, 6.2, and 9.5 times more reactive than PD-1, PD-2, and PD-3.

### Drop Tube Furnace Tests

Figure 6 shows carbon conversion at 900°C for 0.1 and 0.8 second residence times for 65x100 mesh and 270x400 mesh size fractions of coal and PD coals. Carbon conversions ranged from 10 to 28% at 0.1 second residence time and from 10 to 75% at 0.8 seconds residence time as volatile matter content increased from 12 to 40% (daf basis). These data indicate that 1) the fraction of carbon burned increased with increasing volatile matter, with a larger increase noted at 0.8 seconds, and 2) the effect of residence time on carbon loss was more pronounced for fuels with higher volatile matter content. The particle size effect on carbon conversion was small, although it was more pronounced at longer residence times.

Carbon conversion data at 1300°C are shown in figure 7. Carbon conversion increased with increasing volatile matter and increasing residence time. The data indicate that the effects of volatile matter and residence time on carbon conversion were more pronounced at the higher furnace temperatures. The percent of carbon combusted at 1300°C and 0.8 second residence time varied between 62 and 90 for the 65x100 mesh size fractions and between 72 and 99 for the 270x400 size fractions as volatile content of fuels increased from 10.5 to 40% (daf basis). Data also revealed that carbon conversion curves at 1300°C and 0.1-second were almost identical to those at 900°C and 0.8 second. This observation indicates that temperature and residence time are interrelated.

The DTF data suggest that variables which had significant influence on the combustion efficiency were temperature and residence time, followed by fuel type (volatile matter) and particle size. Statistical analyses of the test data indicated that: 1) there was no interaction between volatile matter and any other variable, and 2) external particle surface area was a contributing factor. This indicates that at high combustion temperatures, burning rates were partially controlled by the external mass transfer rate. Finally, DTF data revealed similar trends in reactivity as that obtained with the TGA method.

### **CONCLUSIONS**

Fuels used in this study consisted of a mixture of highly devolatilized coal and relatively unheated coal with the proportion of each depending on the overall volatile matter content. Burn-out temperature and ignition temperatures increased significantly with decreasing volatile matter below 28%. High-temperature drop tube furnace tests revealed that temperature and residence time affected combustion efficiencies most, followed by fuel volatile matter content and particle size.

### **ACKNOWLEDGEMENTS**

This work was funded in part by grants from the Illinois Coal Development Board through the Center for Research on Sulfur in Coal.

### **REFERENCES**

1. Khan, M. R., 1987, Fuel Science and Technology International, 5(2), p. 185-291.
2. Chu, C. I. C., C. J., Im, B. L. Gillespie, 1989, DOE Report, DE-AC-2187MC23289.
3. Williams, A. D., M. D. Stephenson, C. W. Kruse, and M. Rostam-Abadi, 1988, Final Technical Report, Center for Research on Sulfur in Coal, Champaign, IL, August.
4. Nsakala, N. Y., R. L. Patel, and T. C. Lao, 1982, Final Report, EPRI AP-2601.

5. Solomon, P. E., M. A. Serio and S. G. Heninger, 1986, ACS preprints, 31(3) p. 200-205.
6. Tsai, C.-Y. and A. W. Scaroni. 1987, Fuel, 66(10) p. 1400-1406.
7. Chen, M. R., L. S. Fan and F. H. Essenhigh. 1984. Twentieth Symposium (Int.) on Combustion, p. 1513-1521.
8. Wells, W. F., S. K. Kramer, L. D. Smoot, A. U. Blackham, 1984, Twentieth Symposium (International) on Combustion, p. 1539-1546.
9. Khan, M. R. 1987. ACS preprint, 32(1), p. 298-309.
10. Rostam-Abadi, M., J. A. DeBarr, 1988, ACS preprint, 33(4), p. 864-874.
11. Rostam-Abadi, M., J. A. DeBarr, R. D. Harvey, R. R. Frost and C. W. Kruse, 1987. Final Report, Center for Research on Sulfur in Coal, Champaign, Illinois, August.
12. Rostam-Abadi, M., J. A. DeBarr, W.-T. Chen, S. A. Benson and D. P. McCollor, 1988. Final Report, Center for Research on Sulfur in Coal, Champaign, IL, August.
13. Semenov, N. N., 1935, Oxford, Clarendon Press.
14. Cassel, H. M., and I. Liebman, 1969, Combustion and Flame, 37, p. 207-10.

Table 1. Analyses of coal\*, wt% (dry basis)

Volatile Matter	39.2	Hydrogen	4.9
Fixed Carbon	52.4	Carbon	73.8
H-T Ash	8.4	Nitrogen	1.7
BTU/lb	13437	Oxygen	8.7
Moisture	5.4	Sulfur	2.3
		Chlorine	.2

\*Illinois hvBb coal. Predominantly Springfield (No. 5), 20% Herrin (No. 6) blended at washing plant.

Table 2. Characterization data for chars

Particle size, mesh	65x100	100x150	150x200	200x270	270x400
<u>PD-1</u>					
volatile matter	24.8	24.6	25.7	27.8	29.2
fixed carbon	75.2	75.3	74.3	72.2	70.8
hydrogen	3.9	3.9	3.9	4.0	4.0
<u>PD-2</u>					
volatile matter					
carbon	15.7	15.9	17.3	19.5	21.3
hydrogen	84.2	83.8	82.7	79.9	78.7
	2.5	2.7	2.8	2.9	3.1
<u>PD-3</u>					
volatile matter	11.5	11.7	12.4	13.7	15.7
carbon	88.5	88.3	87.5	85.5	84.2
hydrogen	1.8	1.9	2.0	2.2	2.5

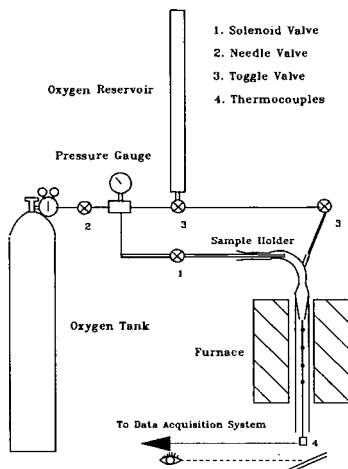


Figure 1. Ignitability test apparatus

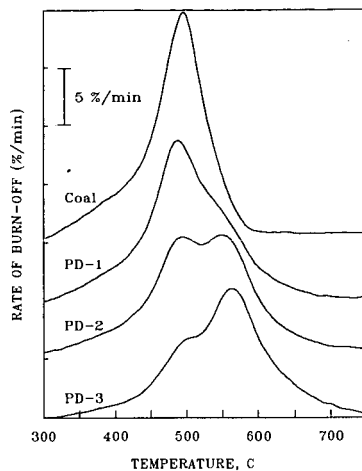


Figure 2. Burning profiles for coal and PD coals

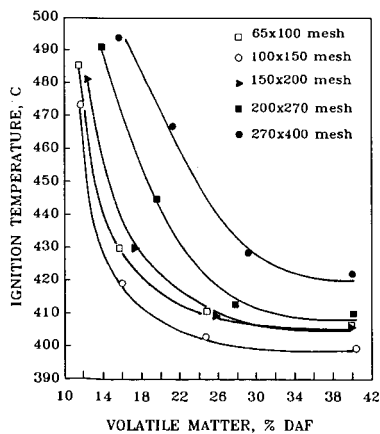


Figure 3. Effect of volatile matter on ignition temperature.

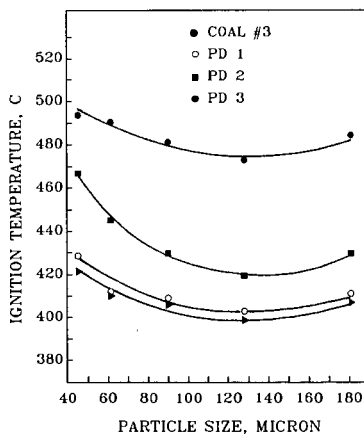


Figure 4. Effect of particle size on ignition temperature.



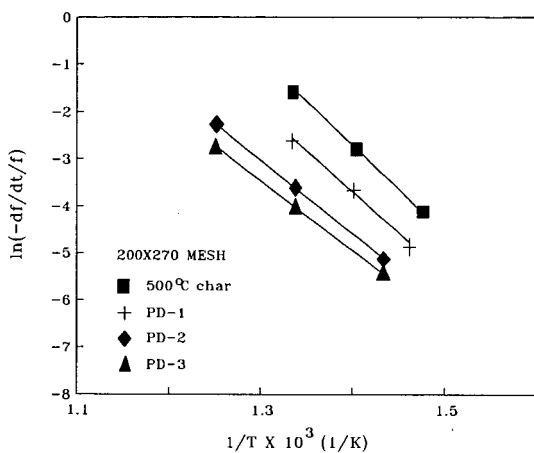


Figure 5. Arrhenius plot from isothermal TG data for 200x270 mesh fuels.

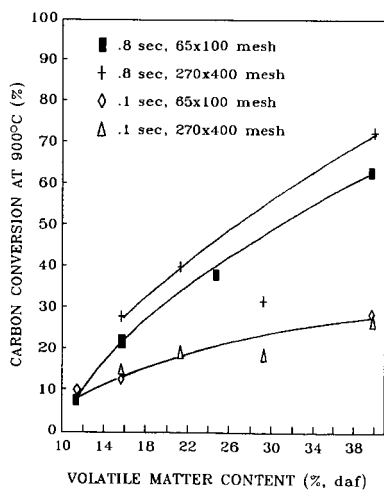


Figure 6. Effect of volatile matter content on carbon conversion in the drop tube furnace at 900°C.

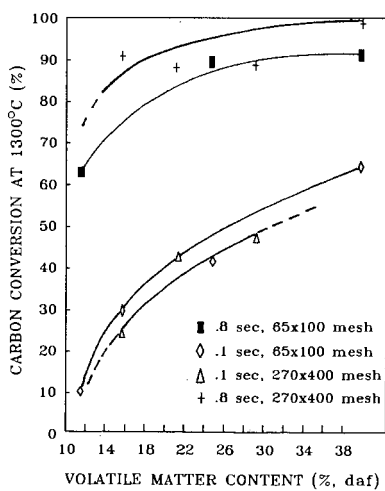


Figure 7. Effect of volatile matter content on carbon conversion in the drop tube furnace at 1300°C.

## **A Chemical Percolation Model for Devolatilization: Temperature and Heating Rate Effects\***

Thomas H. Fletcher and Alan R. Kerstein  
Combustion Research Facility  
Sandia National Laboratories  
Livermore, California 94551-0969

Ronald J. Pugmire and David M. Grant  
Department of Chemistry  
University of Utah  
Salt Lake City, Utah 84112

### **INTRODUCTION**

It is well known that the yield of volatile matter obtained from a pulverized coal is dependent upon the temperature history of the particle. However, the effect of heating rate on volatiles yield is difficult to study independently of final temperature. For example, the volatile yields obtained in an entrained flow reactor study by Kobayashi, et al. [1] increase with both temperature and heating rate, but the independent contribution of heating rate could not be assessed. Heated screen experiments were developed to study devolatilization behavior at different heating rates independently from the final particle temperature. The data of Anthony and Howard [2] show little increase in volatiles yield when particles are heated to the same final temperature on a heated screen at different heating rates. In a more recent study, Gibbins-Matham and Kandiyoti [3] show evidence for small increases in the volatiles yield from a Pittsburgh #8 coal as the heating rate is increased from 1 K/s to 1000 K/s on a heated screen. Coal samples were heated at 5 different heating rates to a final temperature of 700°C and held for 30 s. Experiments were repeated several times in order to ensure accuracy of the data. The total volatiles yield increases from 41.5% at 1 K/s to 46.8% at 1000 K/s, a relative increase in yield of 13%. This increase in yield with increase in heating rate is small, but is larger than associated experimental errors.

The chemical percolation devolatilization (CPD) model [4] was developed as a means to describe coal devolatilization behavior based upon the chemical structure of the parent coal. Some of the input parameters for this model are obtained from NMR characterizations of the parent coal. Percolation statistics are used to describe the probability of generating finite tar fragments from the infinite coal matrix. Pyrolysis yields of tar, gas, and char for three different types of coal are described using a single set of kinetic parameters; only chemical structure parameters are changed for the different coals. The initial description of the CPD model [4] allowed for a temperature dependence of the competition between side chain formation and char formation. However, this option was not exercised in the initial study in order to demonstrate general utility of the model for one set of devolatilization data on three coals collected over a narrow range of temperatures and heating rates. In the present work, the Gibbins-Matham and Kandiyoti data are used to determine additional coefficients for the CPD model that accurately predict the changes in char and tar yield as a function of heating rate.

---

\* Work supported by the U. S. Department of Energy's Pittsburgh Energy Technology Center's Direct Utilization AR&TD Program and by the National Science Foundation through the Advanced Combustion Engineering Research Center (ACERC) at Brigham Young University and the University of Utah.

## THEORY

### The Chemical Percolation Devolatilization Model

Coal is treated in the CPD model as a macromolecular array of clusters representing the interconnections of aromatic ring structures of various sizes and types. These clusters are connected by a variety of chemical bridges of different bond strengths. Percolation statistics applicable to a Bethe lattice (a loopless tree structure) allow a mathematical description of the bridge-breaking process in closed form, providing an efficient alternative to Monte-Carlo techniques. Tar is formed as finite aromatic clusters separate from the infinite coal lattice. Labile bridges  $L$  decompose into a reactive intermediate  $L^*$ , as follows:



The reactive intermediate is unstable, and reacts quickly in a competitive reaction sequence. In one reaction pathway, the reactive intermediate may recombine to form a stable char bridge  $c$  with the associated release of light gas  $g_2$ :



In a competing reaction pathway, the reactive intermediate is stabilized and forms side chains  $\delta$  (rather than recombining to form char):



The cleavage of the reactive intermediate in this step constitutes the bridge-breaking step, and is tied to the generation of tar fragments through percolation statistics. The side chains eventually react to form light gas  $g_1$ :



The competition for  $L^*$  is governed by the ratio of the rate of side chain formation to the rate of char formation, and it is convenient to define a composite rate constant  $p$ :

$$p = \frac{k_\delta}{k_c} = \frac{A_\delta}{A_c} \exp\left[\frac{-(E_\delta - E_c)}{RT}\right] = A_p \exp\left[\frac{-E_p}{RT}\right] \quad (5)$$

The dynamic variables of the theory are the bridge population parameters,  $L$  and  $c$ , and the chain fragment parameter  $\delta$ . A steady-state approximation is invoked for the reactive intermediate  $L^*$  (i.e.,  $dL^*/dt = 0$ ), yielding differential expressions for the reaction rates of  $L$ ,  $c$ , and  $\delta$  [4].

### Modifications to the CPD Model

In the initial formulation of the CPD model [4], the temperature dependence of  $p$  was neglected by setting  $E_p$  to zero and adjusting  $A_p$  to match the experimental data. This approach was sufficient to allow determination of an effective rate coefficient  $p$  that explained the pyrolysis behavior of a limited set of data with a well-characterized temperature history obtained for three different coals

at one heating rate [5]. Measurements of the devolatilization rate performed recently at Sandia [6] include single particle temperature measurements, and show general agreement with the rates obtained by Serio, et al. [5]. In a subsequent study, the sensitivity of the CPD model to nonzero values of  $E_p$  was explored, and it was shown that the total yield predicted by the model changes as a function of heating rate, as expected. However, sensitivity studies show that regardless of the value of  $E_p$ , the model cannot accurately predict tar yields over a wide range of heating rates. Physical mechanisms that limit the production of tar were therefore considered that would allow more realistic predictions using the CPD model.

The ratio of the tar yield to the char yield is affected by the amount of hydrogen in the coal. For example, in the limiting case, anthracites contain little hydrogen, and hence release little volatile matter. All of the hydrogen in the coal, however, is not available to support the release of tar during devolatilization. In some coals, a considerable amount of hydrogen is contained in aliphatic groups, such as methyl ( $-CH_3$ ) groups, which are released in the form of light gases rather than combining with larger reactive molecules to produce volatile tars. The amount of available hydrogen for tar stabilization is therefore not directly related to the total amount of hydrogen present in the coal. The amount of available hydrogen for tar formation has been used in several recent coal devolatilization models [7,8]. At present, quantitative experimental methods for measuring the amount of hydrogen available for stabilization of reactive intermediates that lead to tar are not available.

In the CPD model, production of tar can be limited by introduction of a variable to represent the amount of hydrogen available for stabilization of the reactive intermediate  $L^*$ . To include the available hydrogen  $h$  explicitly in the reaction sequence, Eq. 3 is modified as follows:



Here  $h$  is normalized by the total possible number of bridges in the lattice (the same basis as  $L$ ). As  $h$  is depleted, the reactive intermediate is no longer able to form side chains, causing preferential formation of char. This equation becomes a bimolecular reaction, rather than a unimolecular decomposition reaction (Eq. 3), with an overall reaction order of two rather than one. The reaction rate for  $L$  is unchanged, but the reaction rates for  $c$  and  $\delta$  include the term  $ph$  instead of  $p$ . In addition, the reaction rate of  $h$  is formulated as follows:

$$\frac{dh}{dt} = -k_\delta L^* h = -\frac{k_\delta k_p L h}{k_c + k_\delta h} = -\frac{k_b \rho h L}{1 + \rho h} \quad (7)$$

where  $\rho$  is defined in Eq. 5. The variable  $h$  is highly coupled to the composite rate constant  $\rho$ , evidenced by the fact that  $\rho$  and  $h$  appear together in all of the equations except in the derivative term  $dh/dt$  in Eq. 7. As discussed later, this high degree of coupling restricts independent evaluation of  $\rho$  and the initial amount of available hydrogen  $h_0$  using experimentally measured release rates of tar and total volatiles. The method of relating the production of finite clusters to the number of intact bridges remains unchanged by the introduction of the variable  $h$ ; the mass fractions of tar, gas, and char are therefore calculated as a function of the dynamic variables  $L$ ,  $c$ , and  $\delta$  [4].

## DISCUSSION

Coal specific parameters for the CPD model are ideally obtained from independent chemical analyses, such as NMR characterizations [9]. In practice, the NMR data can only guide the

selection of coal specific parameters such as the coordination number ( $\sigma+1$ ), the initial fraction of intact bridges  $p_0$ , the initial fraction of char bridges  $c_0$ , and the ultimate gas yield  $f_\infty$ . Refinements of these structural parameters are obtained from least squares fits of experimentally measured rates and yields of tar and total volatiles. The kinetic parameters used by the model are assumed to be coal independent, and these parameters were previously obtained [4] by comparison with data [5].

#### Determination of Structural Parameters for Pittsburgh #8 Coal

The coal investigated by Gibbins-Matham and Kandiyoti [3] was a Pittsburgh #8 hva bituminous coal. The results of Serio, et al. [5] for three different coals (Illinois #6 hvb bituminous, Montana Rosebud, and North Dakota Beulah Zap lignite) were previously used to set parameters for the original development of the CPD model [4], but data were unavailable for Pittsburgh #8 coal. A Pittsburgh #8 coal (PSOC-1451D) was investigated by Fletcher [6] and by Freihaut [10]. Based on the devolatilization rates obtained by Fletcher [6] which include single particle temperature measurements, the heated screen experiments performed by Gibbins-Matham and Kandiyoti and by Freihaut appear to have reasonable estimates of particle temperature during devolatilization. The tar and total volatiles yield data of Freihaut are therefore used to determine chemical structure parameters for the CPD model for the Pittsburgh #8 coal using the kinetic parameters from the previous study [4]. The parameters required by the CPD model that represent the chemical structure of the parent coal are the coordination number ( $\sigma+1$ ), the initial concentration of labile bridges  $L_0$ , the initial concentration of char (or refractory) bridges  $c_0$ , and the ultimate gas yield  $f_\infty$ . The coordination number ( $\sigma+1$ ) used in this study is 5.8, as determined for Pittsburgh #8 hva bituminous coal by  $^{13}\text{C}$  NMR spectroscopy and carbon-counting techniques [9].

Values for  $L_0$ ,  $c_0$ , and  $f_\infty$  are obtained from least squares fits to Freihaut's heated screen data (tar and char yields) at 1000 K/s with zero hold time at the maximum temperature. In these simulations,  $E_p$  was set to zero, and the coal was assumed to cool at 1000 K/s after the desired temperature was achieved. Results of this least squares fit are  $L_0 = 0.311$ ,  $c_0 = 0.138$ ,  $f_\infty = 0.305$ . The comparison with Freihaut's data is shown in Figure 1. The model predicts both the yield and temperature dependence of the char formation and tar release data. The fact that the predicted initial tar yield is non-zero is indicative of finite lattice clusters existing in the parent coal. A study of vaporization mechanisms of this tar precursor material is in progress.

#### Determination of $A_p$ and $E_p$

The values of  $A_p$  and  $E_p$  in this model control the temperature dependence of the competition between char formation and gas formation, which is assumed to be relatively independent of coal type. It is anticipated that  $h_0$  will be determined in the future from some type of chemical analysis of the parent coal structure, but for the present, existing methods are insufficient to determine this parameter. The experimental data on Pittsburgh #8 coal can be modeled equally well with different values of  $h_0$ , as long as  $h_0$  is large enough to permit adequate tar yields. Predicted tar yields decrease when values of  $h_0$  of 0.2 or lower are used for the Pittsburgh #8 and Illinois #6 coals, since the available hydrogen is completely consumed and side chain formation is no longer possible. For values of  $h_0$  greater than 0.25, finite concentrations of h exist after depletion of the labile bridges L, and the tar yield is not decreased. Successful CPD model predictions of the devolatilization behavior of both the Illinois #6 and Pittsburgh #8 coals can be made using values of  $h_0$  ranging from 0.25 to 0.4. Studies to determine the appropriate value of  $h_0$  as a function of coal type will be conducted in the future. For each value of  $h_0$  used, a different set of values for  $A_p$  and  $E_p$  is required to fit the Serio, et al. [5] Illinois #6 data. Since these data were obtained at

only one heating rate, there is insufficient resolution to determine both  $A_p$  and  $E_p$ . A correlation for  $A_p$  was therefore determined for different input values of  $E_p$  that best fit the Serio, et al. data. Figure 2 shows the least squares fits to the data with  $h_0 = 0.3$  and  $E_p = 3.0$  kcal/mole. The reaction histories of the dynamic variables used in this calculation are shown in Figure 3. The available hydrogen,  $h$ , is consumed rapidly as the tar is released, but a modest residual value remains when the population of labile bridges goes to zero. The reaction histories of the dynamic variables other than  $h$  ( $L$ ,  $c$ ,  $g_1$ ,  $g_2$ , and  $\delta$ ) are similar to those predicted by the original CPD model [4], and are seemingly unaffected by  $h$  except when the value selected for  $h_0$  is low enough to restrict side chain formation (and hence affect tar and gas yields).

A fitting routine was used to determine a suitable value for  $E_p$  from the data of Gibbins-Matham and Kandiyoti. The total volatiles yield measured by Gibbins-Matham and Kandiyoti differs from the yield measured by Freihaut, which is not surprising, since all Pittsburgh #8 hva bituminous coals are not identical. Therefore, only the difference in measured yields as a function of heating rate were used in the determination of  $E_p$ , thereby avoiding problems in fitting the absolute yields at each heating rate. In this numerical simulation of the experiment, particles are heated to 700°C at the specified heating rate and held at that temperature for 30 s. The fitting procedure determines the changes in total yield using the chemical structure coefficients obtained from NMR analysis [9] and least squares fit to Freihaut's data [10] ( $\sigma+1 = 5.8$ ,  $L_0 = 0.311$ ,  $c_0 = 0.138$ , and  $f_{\infty} = 0.305$ ). The only fitting parameter used to correlate the change in yield versus heating rate is  $E_p$ ;  $A_p$  is calculated from the correlation based on  $E_p$  developed from the Serio, et al. data. Results of this least squares fit are shown in Table 1 for  $h_0 = 0.3$ ,  $E_p = 3.0$  kcal/mole, and  $A_p = 26.8$  s<sup>-1</sup>. The  $\Delta V$  columns represent the difference in total volatile yield from the 1 K/s condition. The modest value determined for  $E_p$  of 3 kcal/mole is not surprising since  $E_p$  is a difference of two activation energies ( $E_\delta - E_c$ ). In contrast, the activation energy associated with labile bridge scission  $E_b$  is 55 kcal/mole [4]. Thus, the temperature dependence of side chain formation with rate  $k_\delta$  is only slightly more favorable than the temperature dependence of the rate of char formation  $k_c$  under these conditions.

**Table 1**  
**Predicted and Measured Changes in Total Volatiles Yield**  
**as a Function of Heating Rate for Pittsburgh #8 Hva Bituminous Coal**

Heating Rate (K/s)	Measured by [3] $\Delta V$ (%)	CPD Model $h_0 = 0.30$ $\Delta V$ (%)
1	0.0	0.0
3	- 0.7	0.6
10	2.2	1.4
100	3.0	3.3
1000	5.3	5.3

#### Extension to Other Heating Rates and Temperatures

The CPD model can be used to predict the effects of heating rate over a broader range of temperatures and heating rates using the coefficients obtained from the least squares fits to the above-mentioned data sets. Figures 4-5 show the heating rate dependence of the model for the devolatilization of Illinois #6 coal. In these calculations, the coal is heated to 1500 K at rates from 1 K/s to 10<sup>5</sup> K/s. The effect is two-fold: (a) the temperature at which the reactions occur

increases as the heating rate increases, and (b) the total volatiles yield (gas + tar) increases as the heating rate increases. The predicted change in yield with heating rate is only a function of  $E_p$ . When  $E_p = 0$ , there is no predicted difference in volatiles yield as a function of heating rate. The shift in reaction temperature with heating rate is a result of competition between the devolatilization rate and the heating rate. The competition between chemical reactions and heat transfer governs changes in reaction temperatures with heating rate. The decrease in overall tar yield at higher temperatures is due to gas phase thermal cracking, resulting in the production of light gas.

The temperature dependence of the model can be explored further by comparison with devolatilization data obtained at high heating rates and long hold times at different temperatures. Freihaut [10] performed devolatilization experiments on Pittsburgh #8 hva bituminous coal at 1000 K/s, and varied the hold time from 0 to 100 s at different temperatures. The tar yield measured at the 100 s hold time condition is much greater than the zero hold condition at any given temperature between 700 and 900 K. He postulates that additional low-temperature coking reactions are needed to model this phenomena. Using the chemical structure coefficients described above, and the values of  $E_p$  and  $A_p$  corresponding to the best fits to the Gibbins-Matham and Kandiyoti data with  $h_0 = 0.3$ , predictions of the Freihaut 100 s and 50 s hold-time data were performed using the modified CPD model (see Figure 6). The model successfully predicts both the temperature dependence of tar evolution and the increase in yield at the 100 s hold time condition. The comparison with the limited 50 s hold condition is not quite as good. It is interesting that the CPD model is able to explain these experimental data without additional low temperature reactions. In addition, the CPD model allows the tar to continue to crack and release light gas as if it were at the same temperature as the coal particle. This results in the predicted decrease in tar yield at 800 K for the 100 s hold time condition and at 1000 K for the immediate quench (zero hold time) condition.

#### SUMMARY

The chemical percolation devolatilization (CPD) model was modified to account for differences in total volatiles yield attained at different heating rates. Modifications include the addition of a new dynamic variable to account for the hydrogen available to stabilize side chains formed from reactive intermediates of labile bridge scission. The temperature dependence of the competition between side chain formation and char formation was explored in some detail and found to give rise to changing tar yields with variations in heating rate. Coefficients were developed for the resulting model based on (a) NMR data for Pittsburgh #8 hva bituminous coal [9], (b) tar and char yield data for Pittsburgh #8 coal [10], (c) kinetic rate data from an Illinois #6 hvb bituminous coal [5], and (d) volatiles yield data as a function of heating rate for a Pittsburgh #8 coal [3]. Simulations were performed to show the predicted effects of heating rate and final temperature. Successful predictions of the devolatilization behavior of the Pittsburgh #8 coal and the Illinois #6 coal were performed using values for the initial amount of available hydrogen  $h_0$  ranging from 0.25 to 0.4. Future studies will explore methods to determine a suitable value for this parameter by comparison with additional experimental data on other coals at various heating rates.

#### ACKNOWLEDGEMENTS

The authors would like to thank Dr. James Freihaut, Dr. Jon Gibbins-Matham, and Dr. Peter Solomon for discussions regarding experimental data and regarding meaningful tests of model assumptions and capabilities.

## REFERENCES

- [1] Kobayashi, H., Howard, J. B., and Sarofim, A. F., *Sixteenth Symp. (Int.) on Comb.*, The Comb. Inst., 411 (1976).
- [2] Anthony, D. B., Howard, J. B., Hottel, H. C., and Meissner, M. P., *Fifteenth Symp. (Int.) on Comb.*, The Comb. Inst., 1303 (1974).
- [3] Gibbins-Matham, J. and Kandiyoti, R., "The Effect of Heating Rate and Hold Time on Primary Coal Pyrolysis Product Distribution," *ACS Div. of Fuel Chem. Prepr.*, **32**:4, 318 (Sept., 1987).
- [4] Grant, D. M., Pugmire, R. J., Fletcher, T. H., and Kerstein, A. R., *Energy and Fuels*, **3**, 175, (1989).
- [5] Serio, M. A., Hamblen, D. G., Markham, J. R., and Solomon, P. R., *Energy and Fuels*, **1**, 138 (1987).
- [6] Fletcher, T. H., "Time-Resolved Particle Temperature and Mass Loss Measurements of a Bituminous Coal During Devolatilization," accepted for publication *Comb. and Flame* (1989).
- [7] Ko, G. H., Sanchez, D. M., Peters, W. A., and Howard, J. A., "Correlations for Effects of Coal Type and Pressure on Tar Yields from Rapid Devolatilization," presented at the *Twenty-Second Symp. (Int.) on Comb.*, Seattle, Washington (August, 1988).
- [8] Solomon, P. R., Hamblen, D. G., Carangelo, R. M., Serio, M. A., and Deshpande, G. V., *Energy and Fuels*, **2**, 405 (1988).
- [9] Solum, M., Pugmire, R. J., and Grant, D. M., "<sup>13</sup>C NMR Structural Determination of the Coals in the Premium Coal Sample Bank," accepted for publication in *Energy and Fuels*, see also ACS Division of Fuel Chem. Prepr., **32**:4, 273 (Sept., 1987).
- [10] Freihaut, J. D., "Kinetics of Coal Pyrolysis and Devolatilization," Technical Progress Report for DOE Contract DE-AC22-84PC70768 by United Technologies Research Center, East Hartford, Connecticut (for the period Nov. 1, 1987 - Jan. 31, 1988).

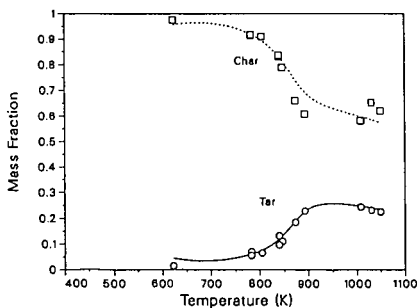


Figure 1. Results of least squares fit to Freihaut PSOC-1451D hva bituminous coal pyrolysis data [10] (points) using the CPD model (continuous lines). In Freihaut's experiment, coal particles are heated at 1000 K/s to the designated final temperature, and then cooled immediately to room temperature (zero hold time). Coefficients determined from this fit to the data are  $L_0 = 0.311$ ,  $c_0 = 0.138$ , and  $f_{\infty} = 0.305$ .

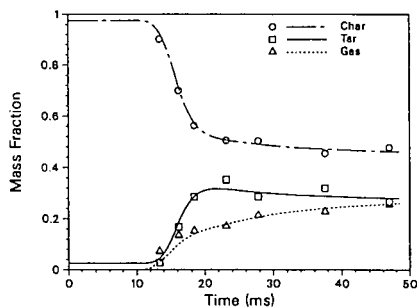


Figure 2. Results of least squares fit to Serio, et al. [5] devolatilization data (points) using the CPD model (continuous lines). In this experiment, Illinois #6 hvb bituminous coal particles are heated in an entrained flow reactor to 1040 K. The model calculations were made using  $h_0 = 0.3$  and  $E_p = 3,000$  cal/mole.



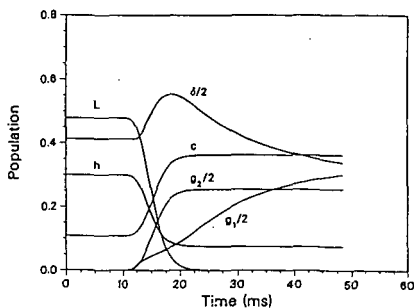


Figure 3. Predictions of dynamic variables used in the CPD model for the Illinois #6 coal,  $h_0 = 0.3$ ,  $E_p = 3000$  cal/mole. Variables  $\delta$ ,  $g_1$  and  $g_2$  are scaled by a factor of 2.

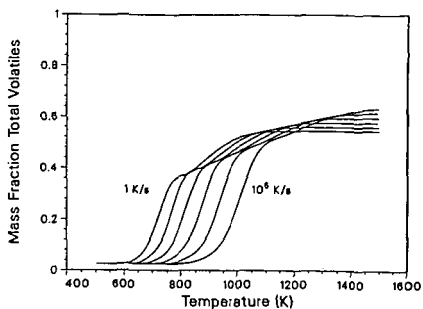


Figure 4. Predicted effect of heating rate on total volatiles yield from Illinois #6 hvb bituminous coal. Numerical experiments performed by heating at the designated rate to 1500 K (zero hold time).

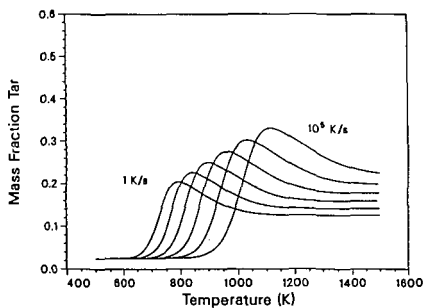


Figure 5. Predicted effect of heating rate on tar yield from Illinois #6 hvb bituminous coal. Numerical experiments performed by heating at the designated rate to 1500 K (zero hold time).

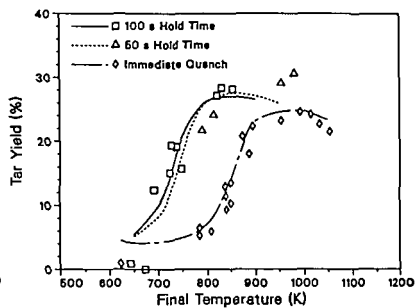


Figure 6. Comparison of CPD model calculations (curves) with Freihaut Pittsburgh #8 coal devolatilization data [10] at different hold times. Experiments were conducted by heating the coal at 1000 K/s to the final temperature and holding for 0, 50, and 100 s before quenching.

## NETWORK MODELS OF COAL THERMAL DECOMPOSITION

P.R. Solomon, D.G. Hamblen, and Z.Z. Yu  
Advanced Fuel Research, Inc., 87 Church Street, East Hartford, CT 06108

### INTRODUCTION

Many recent studies have proposed that coal can be thought of as having a macromolecular network structure to which concepts of crosslinked polymers can be applied (1-10). These concepts have been employed to understand and model such properties of coal as: i) the insolubility; ii) the equilibrium swelling and penetration of solvents; iii) the viscoelastic properties; iv) similarities between the parent coal and products of hydrogenolysis, or mild oxidation; v) crosslinking during char formation (11,12); and vi) the formation of coal tar in pyrolysis (13-17). With the success of these concepts in describing coal properties, it appears logical to extend macromolecular network concepts to completely describe coal thermal decomposition behavior. This has been done by applying statistical methods to predict how the network behaves when subjected to thermally induced bond breaking, crosslinking, and mass transport processes (17-30).

In applying network models to coal thermal decomposition, one considers the coal to consist of aromatic ring clusters linked together by bridges in some geometry designated by the coordination number ( $1 + \sigma$ ) which is the total number of allowable bridges per cluster. When the coal is heated, the bridges can break and new bridges can form. Various statistical methods can be employed to predict the concentration of single aromatic ring clusters (monomers) and linked clusters (oligomers of  $n$  clusters, "n-mers") up to a totally linked network. By assigning an average or distribution of molecular weights to the monomers, the amounts of tar, extractables, liquids or char can then be defined from the distribution of oligomer sizes. The models vary in the assumed chemistry of bond breaking and crosslinking, in the definition of tar, extracts, liquids, and char and in the statistical methods used.

Gavalas et al. employed statistical methods to predict the release of monomers from a randomly connected network (20). The model of Niksa and Kerstein employed percolation theory in a model called DISARAY (28) which extended their previous model built on chain statistics (24,25). Grant et al. employed percolation theory in a model called Chemical Percolation Devolatilization (CPD) (30). Solomon et al. employed Monte Carlo methods in a network model called the Depolymerization, Vaporization, and Crosslinking (DVC) model (21-23,27). This was an extension of their previous model for linear polymers (17,20). The DVC model was recently combined with their Functional Group (FG) model (27,29) to produce the general FG-DVC pyrolysis model. This model is currently being applied to predict the fluidity of coals (31). Other statistical methods for network behavior have been employed in the polymer literature (32-37).

In view of the importance of macromolecular network models to the accurate predictions of coal processing behavior, this paper assesses the assumptions and limitations of the proposed models. It appears that the way one performs the statistics (Monte Carlo, percolation theory, or other statistical methods) makes little difference. For example, we have substituted percolation theory methods for Monte Carlo calculations in the FG-DVC model and obtained comparable predictions for appropriately restricted cases. The important differences among models are in the assumptions for: 1) the network geometry; 2) the chemistry of bond breaking; 3) the chemistry of crosslink formation; 4) hydrogen utilization; and 5) mass transport. The paper compares the models and considers how the assumed network properties relate to behavior observed for coal.

### MACROMOLECULAR NETWORKS

**GENERAL PROPERTIES OF NETWORK** - Figures 1 and 2 present the networks employed in the FG-DVC Monte Carlo calculations and percolation theory, respectively. For the FG-DVC Monte Carlo calculation, oligomers of  $\epsilon$  clusters of a molecular weight distribution defined by  $M_{wg}$  and deviation (shown as the horizontal chains of clusters) are linked by  $m_c$  crosslinks per monomer (shown as the vertical double lines) (26,29). The crosslinks are the branch points in the network where more than two bridges connect a cluster. During thermal decomposition, bridges break, crosslinks are added and the molecular weight of the oligomers is calculated by randomly distributing these changes.

For the percolation theory, a Bethe lattice is employed (28,30,39). Lattices are characterized by the coordination number ( $\sigma + 1$ ), which is the number of possible bridges per cluster. Figure 2 shows lattices for  $\sigma + 1 = 2.2$  and  $\sigma + 1 = 4$ . The Bethe lattice has no loops, but it has been demonstrated that this lattice is a good approximation to a lattice of equivalent coordination number containing loops (39).

The loop free geometry of the Bethe lattice allows for the number of free oligomers to be analytically expressed as a function of  $\sigma$  and the probability  $p$  of bonds being unbroken. This is the feature which makes the percolation theory so attractive from the stand point of computer efficiency and for understanding the behavior of networks under conditions of varying bridge populations. In Fig. 3 we present calculations using percolation theory for three values of  $\sigma + 1$  for the monomer, the sum of oligomers up to 3, up to 10, and the sum of all free oligomers as a function of the number of unbroken bonds per ring cluster  $\alpha$ , where  $\alpha = 1/2 p (\sigma + 1)$ . If  $\sigma$  remains constant during pyrolysis, the molecular weight distribution is a single valued function of  $\alpha$ . For ring clusters of molecular weight 300 amu, the sum of 1 to 3 oligomers corresponds roughly to the potential tar fraction (up to 900 amu), the sum of 1-10 corresponds to the extractable fraction (up to 3000 amu), and the sum of all oligomers corresponds to the liquids fraction (all free oligomers). It can be seen that with increasing  $\sigma$ , more broken bonds are required to achieve equivalent fractions of free oligomers. Also the relative amounts of tar, extracts, and liquids vary with  $\sigma$ .

**NETWORK GEOMETRIES REPRESENTATIVE OF COAL** - The three important parameters of the network are the average ring cluster size  $M_{avg}$ , the coordination number ( $\sigma + 1$ ), and the starting probability,  $p_0$ . For comparing networks of different coordination numbers, it is convenient to use  $\alpha$  rather than  $p$ .

**Ring Cluster Size** - Ring cluster sizes have been estimated from NMR alone (40), NMR and FT-IR (41), mild degradation (42), and molecular weight distribution of tar (15,16,29). Based on these results, the average ring cluster size for coals with less than 90% carbon is expected to be between 2 and 3 aromatic rings or a total molecular weight per cluster including peripheral groups of 200-400 amu.

DISARAY assumes a value of 1400 amu for the monomer which can split into two 700 amu tar fragments. CPD does not specify the monomer molecular weight. For coals with less than 90% carbon, FG-DVC employs a distribution of monomers with an average  $M_{avg}$  of 256 amu.

**Coordination Number** - Information on the coordination number comes from estimates from solvent swelling measurements of the average molecular weight between crosslinks,  $M_c$  (2-9) and recent estimates made using NMR of the number of non-peripheral group attachments to the cluster (40). The  $M_c$  determinations suggest that there are between 4 and 8 repeating units between crosslinks (or branch points). This indicates a value for  $\sigma + 1$  between 2.13 and 2.25. The NMR data suggest that there are between 2 and 3 bridge or loop attachments per cluster (see Fig. 8 of Ref. 40). This suggests  $\sigma + 1$  is between 2 and 3. Based on these two above measurements, the coordination number for the starting coal for describing the break up of the network by bridge cleavage should be less than 3, and probably between 2.2 and 2.5. A different value of  $\sigma + 1$  might be appropriate for describing crosslinking as discussed later.

To model a high volatile bituminous coal, the different models used networks with ( $\sigma + 1$ ) = 3.25 (DISARAY), 4.6 (CPD), and  $\approx 2.1$  (FG-DVC).

**Initial Bond Population** - The starting macromolecular network for FG-DVC is chosen to match the measured extract yield and molecular weight between crosslinks by picking two parameters: i) the length of the oligomer chain,  $\epsilon$ , ii) the number of initial crosslinks per monomer,  $m_0$ . First  $m_0$  is picked such that  $m_0 = M_{avg}/M_c$  where  $M_{avg}$  is the average monomer molecular weight and  $M_c$  is the molecular weight between crosslinks determined from solvent swelling (2-9). Then  $\epsilon$  is chosen so that when the molecule is randomly constructed, the weight percent of oligomers less than 3000 amu matches the measured extract yield. There is the implicit assumption that the extract yield is due to the unpolymerized fraction of a homogeneous network. Exinites and polymethylenes should really be treated as separate components but are not. The initial value of  $\alpha$  is approximately  $((\epsilon - 1)/\epsilon + m_0)$  which for the Pittsburgh Seam coal modeled in Ref. (29) is  $\alpha_0 \approx 0.95$ . This initial

value is indicated in Fig. 3a.

In DISARAY,  $\sigma + 1$  is set equal to 3.25 and  $p_o$  is set equal to 1 ( $\alpha_o = 1.63$ ). This is illustrated in Fig. 3b.

The starting macromolecular network in the CPD model is chosen by picking two parameters: i) the coordination number  $\sigma + 1$ , picked to match the average number of attachments (**bridges and peripheral groups**) per ring determined by NMR (30,40); and ii)  $p_o$  the starting probability of unbroken bonds. For the high volatile bituminous coal simulated in Ref. (30)  $\sigma + 1 = 4.6$ ,  $\alpha_o = 1/2 p_o (\sigma + 1) = 1.36$ . This initial value is indicated in Fig.3c.

### PROCESSES CONTROLLING THE NETWORK DECOMPOSITION

**BOND BREAKING AND HYDROGEN UTILIZATION** - Both the FG-DVC and CPD models assume similar (within a factor of 3) bond breaking rates,  $0.86 \times 10^{15} \exp^{-(55,400/RT)} \text{ sec}^{-1}$  for FG-DVC<sup>†</sup> and  $2.6 \times 10^{15} \exp^{-(55,400/RT)} \text{ sec}^{-1}$  for CPD. Both models employ rank independent kinetics. The FG-DVC model rate was determined in experiments in which particle temperatures were directly measured (43). The rate was recently confirmed within a factor of 2 by Fletcher et al. in a second experiment which directly measures particle temperatures (44).

There are some minor differences in FG-DVC and CPD assumptions for bond breaking. The FG-DVC model includes three kinds of bonds: labile bridges, unbreakable bridges, and crosslinks. For each broken labile bridge, FG-DVC requires that hydrogen be available to stabilize the free radicals. It is assumed that all the donatable hydrogen (aliphatic plus hydroaromatic) is located in the labile bridges, so that only half the labile bridges can break with the other half becoming unbreakable with the donation of their hydrogen (i.e., there is a 1:1 ratio between bond breaking and the formation of additional unbreakable bridges). The weight fraction of the initial bridges in the chain of length  $\epsilon$  which are labile is given by the parameter  $W_b$ ; the rest are assumed to be unbreakable bonds.  $W_b$  is a fitting parameter chosen to make the model fit the pyrolysis data.

In a similar manner, in CPD, there are both unbreakable bridges with probability  $c_o$  and labile breakable bridges with probability  $\alpha_o$  ( $\alpha_o + c_o = p_o$ ). As pyrolysis proceeds, the labile bridges can break and react by two possible routes to form unbreakable "char" bridges or broken bridges. CPD assume a 0.9:1.0 ratio for the ratio of bond breaking to char bridge formation. That assumption is almost identical to the FG-DVC 1:1 ratio required for hydrogen availability.

The DISARAY model assumes a bridge disassociation rate of  $6 \times 10^8 \exp^{-(30,000/RT)} \text{ sec}^{-1}$  <sup>†</sup> which can produce monomers. The monomers subsequently decompose at  $1.4 \times 10^7 \exp^{-(31,000/RT)} \text{ sec}^{-1}$  to form tar. These rates have activation energies which appear to be too low to describe chemical processes.

**CROSSLINKING** - CPD does not assume any crosslinking processes. The char forming processes are only those occurring as one possible end of the bridge breaking reaction.

DISARAY assumes char formation occurs at a rate  $2 \times 10^8 \exp^{-(24,600/RT)}$ . Char formation is assumed to occur by monomers attaching to the original lattice or to each other.

FG-DVC assumes two independent crosslinking reactions, in addition to the unbreakable bond formation accompanying hydrogen donation. One occurs at low temperature (below that for bond breaking) for low rank coals and is associated with oxygen functional groups (COOH or OH) and probably  $\text{CO}_2$  evolution (11,12,45). Crosslinking also occurs at moderate temperatures, slightly higher than bond breaking and appears to be associated with the evolution of  $\text{CH}_4$  or other peripheral groups (e.g., ethyl, propyl).

**MASS TRANSPORT** - A combination of chemistry and mass transport controls the production of the tar in pyrolysis. The motivation for including mass transport processes in tar formation is the observation that tar yields are strongly influenced by external pressure (29,46,47).

<sup>†</sup> both FG-DVC and DISARAY employ distributed activation energy expressions. The rates quoted above are for the center of the distribution

In FG-DVC, the Monte Carlo calculation is employed to determine the molecular weight distribution in the decomposing char. Then a mass transport equation is applied to determine the probability of the light n-mers evolving as tar. The transport equation assumed that a molecular weight dependent vapor pressure controls the appearance of these molecules in the gas phase and that they escape the coal particles by convective transport of the gas (29). Tar is thus the light end of the molecular weight spectrum, i.e., those with sufficiently high vapor pressures. This produces tar with number average molecular weights of 300-400 amu and maximum weights of 800-1000 amu. Thus in FG-DVC, tar is approximately the sum 1-3 in Fig. 3a. Extractable material is defined as all molecules up 3000 amu (sum 1-10) and liquids are defined as all molecules not attached to the starting molecule.

In DISARAY, tar is defined as half the monomer, and the monomer is taken as 1400 amu. So the tar would be defined as some fraction of the monomer curve in Fig. 3b.

No transport equations were employed in CPD. Tar was defined as all molecules not attached to the infinite lattice. Thus tar is represented by the highest line in Fig. 3c.

One advantage of the Monte Carlo method over the percolation theory is that when tar is produced, molecules can be removed from the network. In percolation theory, there is no mechanism for removing molecules from the network. If there are crosslinking events, as in FG-DVC, all the small molecules can reconnect to the network. CPD avoids this problem by excluding any independent crosslinking which would reconnect oligomers. This presents the limitation that independent crosslinking and mass transport cannot be treated with the exact percolation theory expressions.

## EXAMPLES OF MODEL CALCULATIONS

**FORMATION OF PYROLYSIS PRODUCTS** - The evolution of the macromolecular network in the CPD model is illustrated in Fig. 4. Figure 4a shows the percolation theory predictions for the total of unattached oligomers (defined to be the tar) as a function of  $\alpha$ . The coal is represented at  $\alpha_0 = 1/2 p_0 (\sigma + 1) = 1.36$ . During pyrolysis the labile bridges form either broken bridges or unbreakable char bridges in the ratio 0.9 to 1.0. Figure 4b shows how  $\alpha$  changes during pyrolysis. Pyrolysis proceeds until  $\alpha_{\min}$  is reached where  $\alpha_{\min} = 1/2 (\sigma + 1) (c_0 + (1.0/1.9)\bar{L}_c) = 0.83$ . Thus the change in  $\alpha$  during pyrolysis was 0.53.

The evolution of the macromolecular network for FG-DVC computed using the Monte Carlo method for a bituminous coal is illustrated in Fig. 5. Figure 5a shows the calculated extract yield as a function of  $\alpha$ . The initial probability of unbroken bridges,  $\alpha_0$  starts out at close to 1.0 to produce the measured extract yield (30%). Figure 5b shows the computed value of  $\alpha$  with its contributions from the initial crosslinks  $m_0$ , the conversion of labile bridges to broken bonds and unbreakable bonds and the added crosslinks. For the bituminous coal, the added crosslinks are almost all due to  $\text{CH}_4$  related processes. Note that  $\alpha$  goes back up in the FG-DVC model to resolidify the lattice. This is necessary to model fluidity effects (31).

Results of the FG-DVC model applied to a lignite are presented in Fig. 6. The formation of  $\text{CO}_2$  crosslinks prevents  $\alpha$  from being reduced and no additional extract is produced.

**UTILIZATION OF DONATABLE HYDROGEN** - As discussed above,  $W_0$ , the initial fraction of labile bridges is a parameter of the FG-DVC model. This parameter is related to the fraction of donatable hydrogen by  $H(d) = 2/28 W_0$ ; i.e., there are two donatable hydrogens per labile bridge. This parameter has a strong affect on  $\alpha_{\min}$  and hence the yield of tar, extracts, and liquids.

There are two ways to estimate the amount of hydrogen donated. During pyrolysis, the donation of hydrogen converts two aliphatic or hydroaromatic hydrogens into a donated aliphatic hydrogen plus a newly formed aromatic hydrogen. We can measure both the increase in aromatic hydrogen in the pyrolysis products and the increase in aliphatic hydrogen in the tar using quantitative FT-IR analysis (48,49). The results for a Pittsburgh Seam coal are summarized in Fig. 7. They show that the aromatic hydrogen in the total pyrolysis products increased from 2.1 to 2.4% or an increase of 0.3% on a starting coal basis. This increased aromatic content is all in the char. The aromatic content in the tar remains about the same. The tar, which is approximately 30% of the starting coal increases

its aliphatic hydrogen content by about 1% or 0.3% on the starting coal basis. The two numbers are thus consistent; 0.6% donatable hydrogens in the coal are converted to 0.3% new aromatics plus 0.3% donated aliphatics. If it is assumed that a monomer has a molecular weight of 300 amu, then one breakable bridge per monomer with four aliphatic carbons is 1.33% donatable hydrogen. Half the bridges can break (0.67%) and the other half can donate hydrogen (0.67%) in reasonable agreement with the experimentally estimated value of 0.6% hydrogens actually donated. The value assumed in FG-DVC for H(d) for the Pittsburgh Seam coal is 0.67% (29).

The value of H(d) has implications for the CPD model, if  $\Delta\alpha$  is limited to 0.33 rather than 0.53, then the value of  $\sigma + 1$  would have to be reduced to match the data. Also, the average molecular weight for the unattached molecules is too high to be identified as tar. If a more reasonable definition of tar is used (e.g., the sum of oligomers up to 3) then  $\sigma + 1$  would have to be reduced still further.

**COMPARISON OF MONTE CARLO CALCULATION WITH PERCOLATION THEORY** - To further illustrate some of the differences between the FG-DVC Monte Carlo model and percolation theory calculations, the extract yield calculated for a case similar to that in Fig. 5a, but with tar evolution not permitted is plotted in Fig. 8 along with the predictions of percolation theory for several values of  $\alpha$ . The FG-DVC Monte Carlo predictions are not a single valued function of  $\alpha$ . As pyrolysis proceeds, the increase in extract yield follows  $\sigma + 1 \approx 2.2$  while the decrease in extract yield follows  $\sigma + 1 \approx 4$ .

It is important to know whether this result is an artifact of the Monte Carlo calculation or a real feature of pyrolysis. Based on what is happening in pyrolysis, the result does make sense. For a bituminous coal, the initial process occurring in pyrolysis is bond breaking. This occurs by breaking bridges in the network described by  $\sigma + 1$  between 2.1 and 2.5. No crosslinking is occurring initially as the solvent swelling ratio is observed to increase during this period (45). Eventually crosslinks start forming, resulting in an increase in the coordination number and in  $\alpha$ . The network thus cannot adequately be described by a single coordination number. There is a coordination number for labile bridges and a separate coordination for crosslinks. This observation motivated the development of a more general percolation network with two coordination numbers discussed below.

#### LATTICE MODEL WITH TWO BOND TYPES

**Two- $\sigma$  Model** - In order to deal with a structure with a time dependent coordination number, we consider a Bethe lattice with two types of bonds, with coordination numbers and probabilities of occupation given by  $\sigma_1 + 1$ , p and  $\sigma_2 + 1$ , q for the two types, respectively. Such a lattice for  $\sigma_1 = \sigma_2 = 1$  is illustrated in Fig. 9. The analysis can be carried through using the same procedures as Fisher and Essam (39) or Ref. 30, but with extensions to deal with the extra variables. The probability  $F_{s,u}(p,q)$ , that a site is a member of a cluster of n sites with s type 1 bridges and u type 2 bridges is given by

$$F_{s,u}(p,q) = a_{s,u} p^s (1-p)^\tau q^u (1-q)^\nu \quad (1)$$

where

$$\begin{aligned} n &= u + s + 1 \\ \tau &= (\sigma_1 + 1) n - 2s \\ \nu &= (\sigma_2 + 1) n - 2u \end{aligned} \quad (2)$$

and  $\tau$ ,  $\nu$  are the number of broken bridges of type 1 and 2, respectively, on the perimeter of the cluster, and  $a_{s,u}$  is the number of different ways to form such a cluster. Following the same procedure used by Fisher and Essam, we can derive an expression for the configuration coefficient

$$a_{s,u} = \left( \frac{(\sigma_1 + 1)(\sigma_2 + 1)}{(s + \tau)(u + \nu)} \right) \binom{s + \tau}{s} \binom{u + \nu}{u} (u + s + 1) \quad (3)$$

Note that for  $u = 0$  (no type 2 bonds), this reduces to the quantity  $nb_n$  in Ref. (30). To determine the probability,  $F_n(p,q)$  that a given site is a member of a cluster of n sites, i.e., the fraction of n-mers, we must sum Eq. 1 over all possible values of s and u that give an n-site cluster:

$$F_n(p, q) = \sum_{s=0}^{n-1} a_{s,u} p^s (1-p)^r q^u (1-q)^v; \quad u = n - s - 1 \quad (4)$$

The total fraction of sites,  $F(p, q)$  in finite clusters is the sum over all  $s$  and  $u$

$$F(p, q) = \sum_{s=0}^{\infty} \sum_{u=0}^{\infty} F_{s,u}(p, q) = \left( \frac{1-p}{1-p^*} \right)^{\sigma_1+1} \left( \frac{1-q}{1-q^*} \right)^{\sigma_2+1} \quad (5)$$

where  $p^*$  and  $q^*$  are obtained by finding the least roots of

$$\begin{aligned} p^* (1-p^*)^{\sigma_1+1} (1-q^*)^{\sigma_2+1} - p(1-p)^{\sigma_1+1} (1-q)^{\sigma_2+1} &= 0 \\ q^* (1-q^*)^{\sigma_2+1} (1-p^*)^{\sigma_1+1} - q(1-q)^{\sigma_2+1} (1-p)^{\sigma_1+1} &= 0 \end{aligned} \quad (6)$$

The critical point, where an infinite lattice begins to form (i.e.,  $F(p, q)$  begins to decrease) becomes a critical curve which divides the  $p$ - $q$  plane into two regions. Note that for  $q = 0$ , the equations all reduce to the single  $\sigma$  case given in Ref. 30.

**Application of Two- $\sigma$  Model** - Figure 10 presents a comparison of the prediction for pyrolysis assuming the FG-DVC chemistry using: a) the Monte Carlo calculation, b) the two- $\sigma$  percolation calculations ( $\sigma_1 = 1, \sigma_2 = 1$ ) and c and d) two cases of the one- $\sigma$  percolation calculation ( $\sigma = 2.2$  and  $\sigma = 3.2$ ). The calculations are made under the assumption that no tar is evolved. The tar values in Fig. 10 are the sum of 1-3 n-mers remaining in the char. The Monte Carlo calculation in Fig. 10a is matched best by the two- $\sigma$  model if liquids are assumed to be the sum of the first 100 n-mers (i.e., up to 300,000 amu). The two- $\sigma$  model has a reasonable value for the initial extract yield but predicts slightly more initial tar. Neither of the one- $\sigma$  cases is a good match. Use of  $\sigma = 2.2$  is good at low temperature but over predicts the maximum values of extracts and liquids. Use of  $\sigma = 3.2$  does a much better job on predicting the maximum values but the initial ratio of tar to extract is not consistent with what is observed for coal and the rate of increase of n-mers is too slow. It thus appears that the two- $\sigma$  model can be used instead of the Monte Carlo calculations when no tar is evolved, while one- $\sigma$  calculations are less accurate.

The real test, however, is how well the models fit the data for coal. A comparison of tar yield is not a sufficient test since  $\alpha_o$  and  $\Delta\alpha$  can always be selected in conjunction with the network geometry to fit the data. A critical test requires a careful comparison of how  $\alpha_o$  and  $\alpha(t)$  match with measurement of functional group changes in the char (e.g., the transformation of hydrogen functional groups and bridges), solvent swelling behavior (i.e., crosslink density), and the complete molecular weight distribution as reflected in the amounts of tar, extracts, and fluidity.

## COMPARISON OF NETWORK MODELS

A summary of the processes predicted by the three recent network models, CPD, DISARAY and FG-DVC is presented in Table I. All the models predict their primary objective, the variations in tar and gas yield with time and temperature. All three are capable of predicting variations of tar yield with heating rate, but CPD has not yet done this. All three models are capable of predicting the complete molecular weight distributions of fragments, but only FG-DVC uses this information to predict the extract yield, the tar yield and the tar molecular weight distribution. DISARAY uses only the prediction for monomers (defined as tar precursor) and CPD uses only the prediction for all oligomers (defined as tar). In a paper presented at this conference, the total oligomer population computed by the FG-DVC model is used to predict coal fluidity behavior (31). Only FG-DVC employs a mass transport equation which is necessary to predict tar molecular weights and the variations of yield and molecular weights with pressure. Only FG-DVC predicts the solvent swelling ratio.

## CONCLUSIONS

- 1) The extension of macromolecular network concepts to describe coal thermal decomposition

appears to be very successful and versatile in allowing the prediction of tar, extract yield, and total liquids.

- 2) A complete model requires a description of: i) labile bridge breaking with hydrogen utilization; ii) rank dependent crosslinking processes; and iii) mass transport.
- 3) Monte Carlo methods for computing the network statistics are the most versatile but are computationally demanding.
- 4) The use of percolation theory is computationally efficient and helps provide insight into network behavior, but the use of a fixed coordination number may be inadequate to accurately describe coal thermal decomposition. The network appears to require a coordination number between 2.2 and 2.5 for labile bridge breaking and greater than 3 for crosslinking.
- 5) An expanded percolation theory for a network with two coordination numbers was developed.
- 6) When the two- $\sigma$  percolation model is applied using the FG-DVC chemistry to cases in which tar is not removed, it gives results which are comparable to the Monte Carlo calculation. Applying percolation theory to cases where tar is removed requires additional approximations.
- 7) Of the three models which were compared (CPD, DISARAY, and FG-DVC), FG-DVC is the most complete in treating the molecular weight of network fragments and vaporization and mass transport to define tar, tar molecular weight distribution and extract yield.
- 8) Of the three models, FG-DVC is the most closely related with the previous concepts of coal as a macromolecular network by requiring that the network predict the coal and, char solvent swelling ratios and measured extract yields. The assumption which define the parameters of the starting network are open to question and must be explored.
- 9) Future effort should focus on identifying the chemistry for the processes of bond breaking, low temperature crosslinking, moderate temperature crosslinking, and hydrogen utilization.

#### ACKNOWLEDGEMENT

The authors gratefully acknowledge the support for the work provided by the Morgantown Energy Technology Center of the Department of Energy under Contract No. DE-AC21 86MC23075.

#### REFERENCES

1. Van Krevelen, D.W., Coal, Elsevier, Amsterdam, (1961).
2. Green, T.K., Kovac, J., and Larsen, J.W., *Fuel*, **63**, 935 (1984).
3. Green, T.K., Kovac, J., and Larsen, J.W., in "Coal Structure," R.A. Meyers, Ed., Academic Press, NY (1982).
4. Lucht, L.M. and Peppas, N.A., *Fuel*, **66**, 803, (1987).
5. Lucht, L.M., Larsen, J.M., and Peppas, N.A., *Energy & Fuels*, **1**, 56, (1987).
6. Larsen, J.W., *ACS Fuel Chem. Div. Preprints*, **30**, (4), 444, (1985).
7. Green, T., Kovac, J., Brenner, D., and Larsen, J., Coal Structure, (R.A. Meyers, Ed.), Academic, NY, p 199, (1982).
8. Hall, P.J., Marsh, H., and Thomas, K.M., *Fuel*, **67**, 863, (1988).
9. Sanada, Y. and Honda, H., *Fuel*, **45**, 295, (1966).
10. Suuberg, E.M., Yoshi, O., and Deevo, S., *ACS Div. of Fuel Chem. Preprints*, **33**, (1), 387, (1988).
11. Suuberg, E.M., Lee, D., and Larsen, J.W., *Fuel*, **64**, 1668, (1985).
12. Suuberg, E.M., Unger, P.E., and Larsen, J.W., *Energy & Fuels*, **1**, 305, (1987).
13. Brown, J.K., Dryden, I.G.C., Dunevein, D.H., Joy, W.K., and Pankhurst, K.S., *J. Inst. Fuel*, **31**, 259, (1958).
14. Orning, A.A. and Greifer, B., *Fuel*, **35**, 318, (1956).
15. Solomon, P.R. and Hamblen, D.G., Chemistry in Coal Conversion, (R.H. Schlosberg, Ed.),



- Plenum, New York, p. 121, Chapter 5, (1985).
16. Solomon, P.R., New Approaches in Coal Chemistry, ACS Symposium Series 169, ACS, Washington, DC p. 61, (1981).
17. Solomon, P.R., and King, H.H., *Fuel*, **63**, 1302, (1984).
18. Gavallas, G.R., Coal Pyrolysis, Elsevier, NY, p. 51, (1982).
19. Gavallas, G.R., Cheong, P.H., and Jain, R., *Ind. Eng. Chem. Fundam.*, **20**, 122, (1981).
20. Squire, K.R., Solomon, P.R., Carangelo, R.M., and DiTaranto, M.B., *Fuel*, **65**, 833, (1986).
21. Squire, K.R., Solomon, P.R., DiTaranto, M.B., and Carangelo, R.M., *ACS Div. of Fuel Chem. Preprints*, **30**, (1), 386, (1985).
22. Solomon, P.R., Squire, K.R., and Carangelo, R.M., *Proceedings of the Int. Conf. on Coal Science*, Pergamon: Sydney, Australia, p. 945, (1985).
23. Solomon, P.R., and Squire, K.R., *ACS Div. of Fuel Chem. Preprints*, **30**, (4), 347, (1985).
24. Niksa, S., and Kerstein, A.R., *Combustion and Flame*, **66**, 95, (1986).
25. Niksa, S., *Combustion and Flame*, **66**, 111, (1986).
26. Solomon, P.R., Hamblen, D.G., Deshpande, G.V. and Serio, M.A., A General Model of Coal Devolatilization, International Coal Science Conference, The Netherlands, October 1987.
27. Solomon, P.R., Hamblen, D.G., Carangelo, R.M., Serio, M.A., and Deshpande, G.V., *Combustion and Flame*, **71**, 137, (1988).
28. Niksa, S. and Kerstein, A.R., *Fuel*, **66**, 1389, (1987).
29. Solomon, P.R., Hamblen, D.G., Carangelo, R.M., Serio, M.A. and Deshpande, G.V., *Energy and Fuels*, **2**, 405, (1988).
30. Grant, D.M., Pugmire, R.J., Fletcher, T.H., and Kerstein, A.R., *Energy & Fuels*, **3**, 175, (1989).
31. Solomon, P.R., Best, P.E., Yu, Z.Z., and Deshpande, G.V., "A Macromolecular Network Model for Coal Fluidity", *ACS Div. of Fuel Chem. Preprints*, **34**, paper presented at this meeting, (1989).
32. Nielsen, L.E., Mechanical Properties of Polymers and Composites, Vol. 2, Marcel Dekker, Inc. NY, (1974).
33. Bartels, C.R., Crist, B., Felters, L.J., and Graessley, W.W., *Macromolecules*, **19**, 785, (1986).
34. Nazem, F.F., *Fuel*, **59**, 851, (1980).
35. Macosko, C.W., *Brit. Polymer Journ.*, **17**, 239, (1985), and references therein.
36. Flory, P.J., *J. Am. Chem. Soc.*, **63**, 3083, 3097, (1941); see also Principles of Polymer Chemistry, Cornell University Press, Ithaca, NY, Chapter 9, (1953).
37. Stockmayer, W.H., *J. Chem. Phys.*, **11**, 45, (1943); also **12**, 125, (1944).
38. Serio, M.A., Solomon, P.R., Yu, Z.Z., Deshpande, G.V., and Hamblen, D.G., *ACS Div. of Fuel Chem. Preprints*, **33**, (3), 91, (1988).
39. Fisher, M.E., and Essam, J.W., *J. Math. Phys.*, **2**, 609, (1961).
40. Solum, M., Pugmire, R.J., and Grant, D.M., *Energy & Fuels*, **3**, 40, (1989).
41. Gerstein, B.C., Murphy, D.P., and Ryan, L.M., Coal Structure, (R.A. Meyers, Ed.), Academic Press, NY, p. 87, Chapter 4, (1982).
42. Hooker, D.T., II, Lucht, L.M., and Peppas, N.A., *Ind. Eng. Chem. Fundam.*, **25**, 103, (1986).
43. Solomon, P.R., Serio, M.A., Carangelo, R.M., and Markham, J.R., *Fuel*, **65**, 182, (1986).
44. Fletcher, T.H., "Time Resolved Temperature Measurements of Individual Coal Particles During Devolatilization", Submitted to *Combustion Science and Technology*.
45. Deshpande, G.V., Solomon, P.R., and Serio, M.A., *ACS Div. of Fuel Chem. Preprints*, **33**, (2), 310, (1988).
46. Unger, P.E. and Suuberg, E.M., 18th Symposium (Int) on Combustion, The Combustion Institute, Pittsburgh, PA, p. 1203, (1981).
47. Suuberg, E.M., Unger, P.E., and Lilly, W.D., *Fuel*, **64**, 956, (1985).
48. Solomon, P.R. and Carangelo, R.M., *Fuel*, **61**, 663, (1982).
49. Solomon, P.R. and Carangelo, R.M., *Fuel*, **67**, 949, (1988).

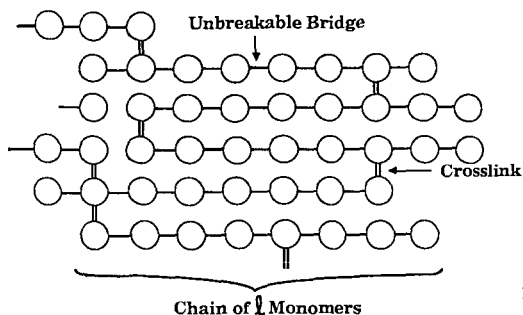


Figure 1. Macromolecular Network Used in Monte Carlo Simulation.

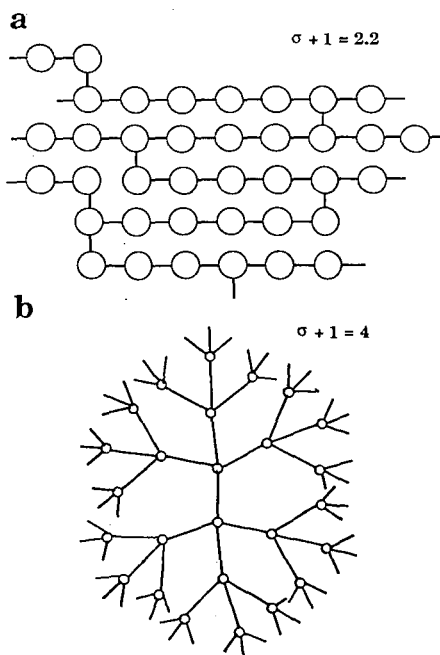


Figure 2. Bethe Lattice for a) Coordination Number 2.2 and b) Coordination Number 4.

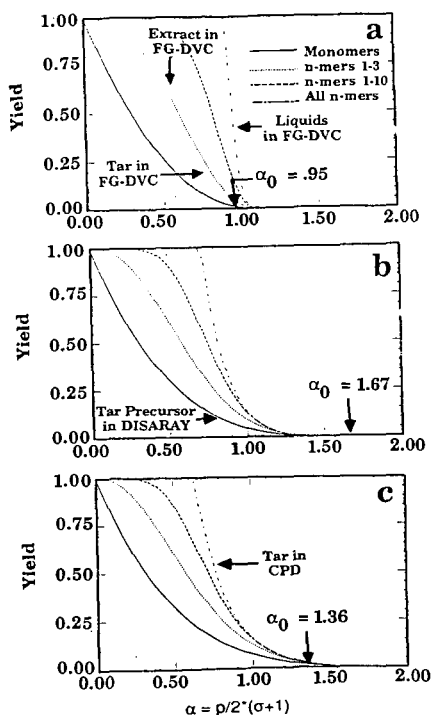


Figure 3. Percolation Theory Predictions for Pyrolysis Products (monomers, tar, extracts and total liquids) for Three Values of the Coordination Number ( $\sigma + 1$ ). a)  $\sigma + 1 = 2.2$ , b)  $\sigma + 1 = 3.25$  and c)  $\sigma + 1 = 4.6$ .

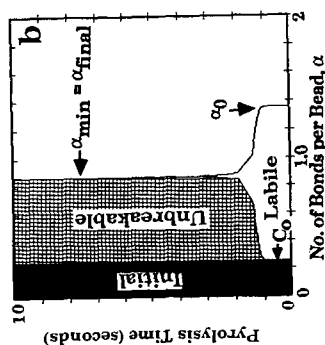
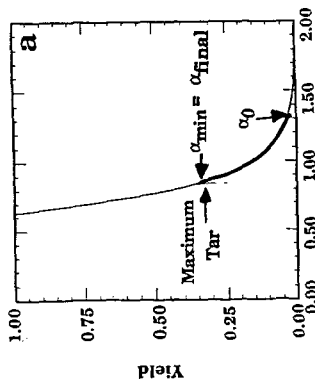


Figure 4. Tar Yield for a Bituminous Coal by the CPD Model. a) Tar Yield vs.  $\alpha$ , b) Variation in  $\alpha$  with Time Heating at 450°C/min to 936K.

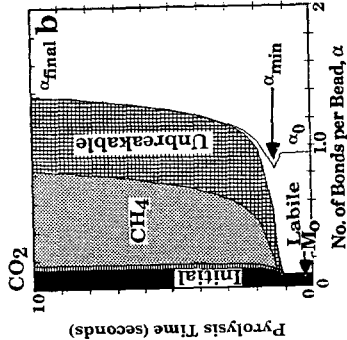
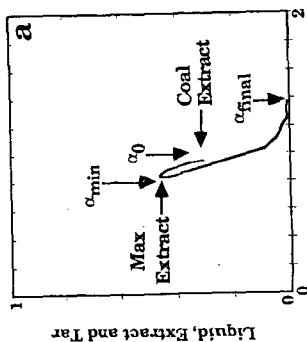


Figure 5. Extract Yield for a Bituminous Coal Predicted by the FG-DVC Model. a) Extract Yield vs.  $\alpha$  and b) Variation in  $\alpha$  with Time Heating at 450°C/min to 936K.

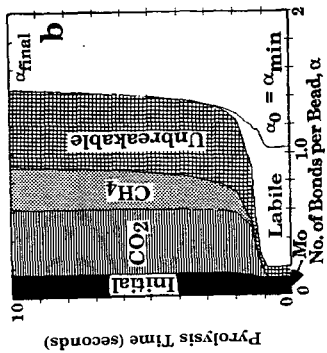
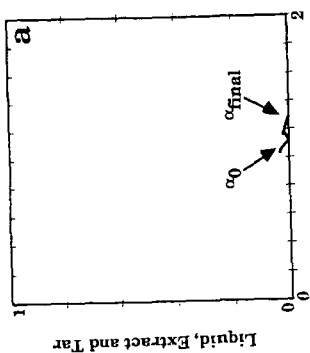


Figure 6. Extract Yield for a Lignite Predicted by the FG-DVC Model. a) Extract Yield vs.  $\alpha$  and b) Variation in  $\alpha$  with Time Heating at 450°C/min to 936K.

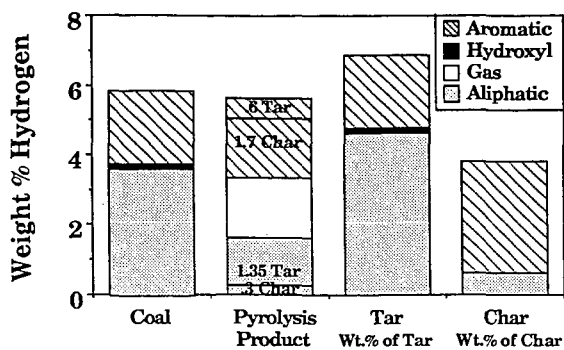


Figure 7. Distribution of Hydrogen in Coal and Pyrolysis Products. Pyrolysis Produced Approximately 53% Char, 30% Tar and 21% Gas.

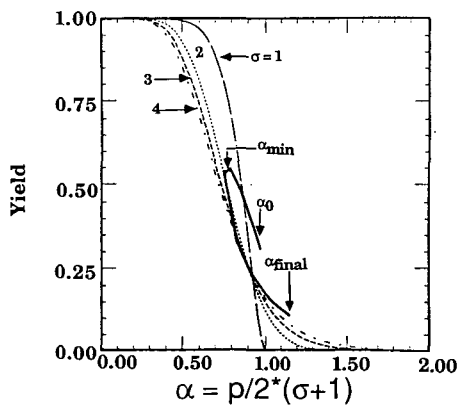
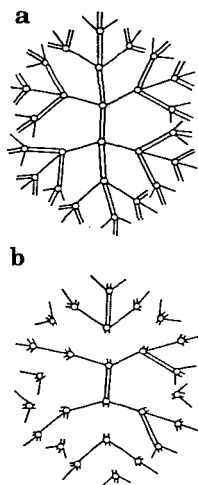
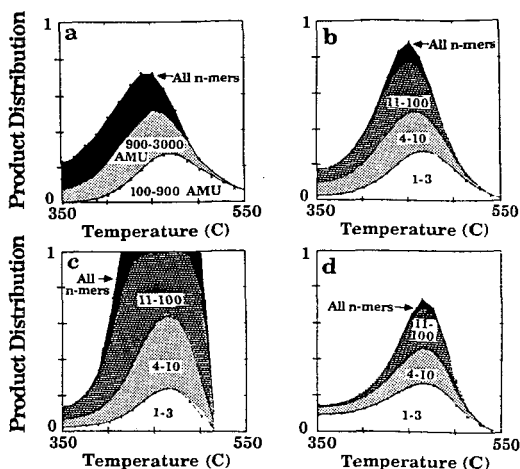


Figure 8. Comparison of Extract Yield in FG-DVC Model with Percolation Theory for  $\sigma = 1, 2, 3$  and  $4$ . FG-DVC is for Pittsburgh Seam Coal Heated at  $450^\circ\text{C/sec}$  to  $936\text{K}$  with No Tar Evolved.



**Figure 9.** Bethe Lattice for Two- $\sigma$  Model with  $\sigma_1 = 1$  (shown as single bonds) and  $\sigma_2 = 1$  (shown as double bonds). a) Fully Linked Case ( $p = q = 1$ ) is Like One- $\sigma$  Model with  $\sigma = 3$ . b) With Most Double Bonds Representing the Crosslinks Not Yet Formed to Represent the Starting Coal. The Lattice is Like a One- $\sigma$  Model with  $\sigma = 1$ , Linear Chains.



**Figure 10.** Comparison of Distribution of n-mers for Pyrolysis at 450°C/sec to 936K. a) Monte Carlo Calculation, b) Two- $\sigma$  Model ( $\sigma_1 = 1$ ,  $\sigma_2 = 1$ ), c) One- $\sigma$  Model ( $\sigma = 1.2$ ) and d) One- $\sigma$  Model,  $\sigma = 2.2$ .

**Table 1 - Comparison of Network Models.**

	CPD	DISARAY	FG-DVC Monte-Carlo or 2 $\sigma$	Relevant Model Process
Tar Yield vs Time	Yes	Yes	Yes	Bond breaking
Extract Yield vs Time	No <sup>a</sup>	No	Yes	Bond breaking
Gas Yield vs Time	Yes	Yes	Yes	From peripheral groups
Tar Yield vs Heating Rate	Not Yet	Yes	Yes	Relative rates of bond breaking and crosslinking
Variation of Tar Molecular Weight with Heating Rate	No	No	Yes	Relative rates of bond breaking and crosslinking
Molecular Weight of Tar	No	No	Yes	Mass transport Limitation
Tar Yields vs Pressure	No	No	Yes	Mass transport Limitation
Molecular Weight vs Pressure	No	No	Yes	Mass transport Limitation
Solvent Swelling of Char	No	No	Yes	Crosslinking

<sup>a</sup> All oligomers are defined as tar

## INTERPRETING COAL DEVOLATILIZATION AS A FLASH DISTILLATION DRIVEN BY COMPETITIVE KINETICS FOR DEPOLYMERIZATION AND REATTACHMENT

Stephen Niksa  
Mechanical Engineering Department  
Stanford University  
Stanford, CA 94305

Alan R. Kerstein  
Combustion Research Facility  
Sandia National Laboratories  
Livermore, CA 94550

### Introduction

According to the most recent theories<sup>1-4</sup>, the evolution rates, distribution, and molecular characteristics of the volatile products of coal devolatilization express the independent influences of chemical reaction rates and macromolecular configuration. Generally speaking, these approaches firm up the connections between the modeling species associated with the reactant and coal's structural features and functional groups inferred from chemical analyses. Obviously such connections are essential to systematic interpretations of the behavior of various coals. But chemical kinetics and configurational probabilities alone cannot account for the reduced tar yields and smaller tar fragments from devolatilization at elevated pressures. Reduced tar yields have long been attributed to redeposition of tar from the gas phase on the time scale for transport of volatiles through the particle surface, although an alternate scheme<sup>5</sup> based on flash distillation correlates yields as well as tar molecular weight distributions (MWDs) without invoking any finite-rate, mass transport mechanism.

The theory introduced in this paper extends the development of models based on chemical kinetics, macromolecular configuration, and flash distillation, and is called FLASHCHAIN. Like DISCHAIN<sup>1</sup> and DISARAY<sup>2</sup>, it comprises simplified kinetic mechanisms and analytical expressions to account for configurational effects, and to describe their evolution in time. However, the complete size distributions of all fragments are now determined. And like FLASHTWO<sup>3</sup>, this theory invokes a phase equilibrium among intermediates in the condensed phase and tar components in the vapor to rationalize the pressure dependence. Whereas the fragment distribution in FLASHTWO is assumed a priori, it is now computed from the configurational model.

In the sections which follow, the main features of the theory are outlined briefly, largely to explain the various modeling parameters. Then model correlations are presented for the devolatilization of high volatile bituminous coals, including the proportions of tar and noncondensable gases, and tar molecular weights for broad ranges of temperature, heating rate, reaction time, and pressure.

### Overview of the Theory

Coal is modeled a distribution of linear chains composed of refractory aromatic nuclei interconnected pairwise by two types of linkages, labile bridges and refractory char links. The initial coal constitution is specified by the proportions of labile and broken bridges and char links, and the probability that peripheral groups appear on the ends of fragments. Initially and throughout pyrolysis, the condensed phase species are subdivided into reactant, intermediate, and metaplast lumps, in order of decreasing size.

Although the cutoff sizes are arbitrary, their proportions are described by analytical expressions for the complete size distribution as a function of the instantaneous numbers of bridges, char links, and ends. Consequently, for the initial coal reactant species, the sizes in the fragment distribution shift toward smaller values as the initial fraction of broken bridges is increased, and more of the coal appears as a lighter mobile phase which is taken to be the initial amount of metaplast.

Labile bridges either dissociate during pyrolysis or spontaneously decompose into char links. Consequently, bridge dissociation initiates two distinct reaction pathways, either to generate smaller fragments with new peripheral groups on the newly-created fragment ends, or to form a new char link and noncondensable gases. These pathways are designated as bridge scission and spontaneous condensation, respectively. Bridge scissions increase the amount of metaplast, at the expense of the reactant and intermediate, but spontaneous char formation tends to retain more of the coal mass in the heavier lumps, by lowering the number of sites available for fragmentation. Both reaction rates are based on the same Gaussian distribution of activation energies, and a stoichiometric coefficient specifies the selectivity between these two pathways.

Additional char links and noncondensable gases may also form by bimolecular recombination, but only within a restricted range of fragment sizes. Neither the reactant nor the intermediate species participate in bimolecular recombination, but nevertheless accumulate char links by spontaneous condensation. Recombinations among the ends of metaplast fragments produce additional char links, and also additional gases if peripheral groups are present on the ends which participate.

Tar formation is also developed from the metaplast only, using the flash distillation analogy; i. e., a phase equilibrium relates the instantaneous mole fractions of like fragments in the tar vapor and metaplast. Representing the equilibrium with Raoult's law for continuous mixtures characterizes the impact of fragment size on the phase change. While no finite mass transport rates appear, all volatile species are presumed to escape by a convective flow process, so that the evolution rate of tar is proportional to that of noncondensables when weighted by the ratio of their respective mole fractions.

Tar quality is expressed in terms of its molecular weight distribution, and the proportions of peripheral groups, labile and refractory links, as a coarse scale for aromaticity. Tar quality varies throughout the process, due in part to the greater impact of bimolecular recombination during the later stages.

#### **Guidelines for the Data Correlations and Model Parameters**

Taken together, the four laboratory studies<sup>6-9</sup> selected for the model evaluation depict the behavior for wide ranges of the relevant operating conditions, and all coal samples were Pittsburgh Seam HVA bituminous coals; ultimate and proximate analyses appear in the primary references. Among the results reported by Oh, only those which include tar yields and close the mass balance to within 5 wt% are included here. Wire-grid heaters in which the sample was dispersed in a layer which is only a few particles deep were used in all cases. Process temperatures were determined with fine-wire thermocouples and are regarded as the actual reaction temperature. One study featured forced rapid quenching, although decomposition during cooling is included in all simulations using the reported cooling rates.

All simulations in this study are based on the parameters in Table 1. The molecular weight of aromatic nuclei, and the MW ratios for bridges and peripheral groups were assigned from <sup>13</sup>C NMR analyses of HVA bituminous coals<sup>10</sup>, to match the carbon

aromaticities and measured average molecular weights of noncondensibles (25g/g-mole). At the tabulated initial probability for all links, there is 9.4 wt % of metaplast in the reactant, which is similar to the amounts of THF extracts from such coals. All other values and the rate parameters were assigned to match the transient product distributions and tar molecular weights for atmospheric pyrolysis at  $10^3$  K/s. Once assigned, only the operating conditions of pressure, temperature, heating rate, and/or time were varied to match those in all other experiments. While the pressure is usually assigned as the ambient pressure, simulations of vacuum pyrolysis are based on a pressure of 0.025 MPa.

A simulation of each thermal history requires about 2 minutes on a 386 personal computer operating at 20 MHz, with an 8-Bit Fortran compiler.

### Data Correlations

The predicted distribution of all reaction species for atmospheric pyrolysis is compared with measured weight loss and tar yields in Fig. 1. The thermal histories consist of uniform heating at  $10^3$  K/s to the stated temperatures immediately followed by cooling at  $10^4$  K/s. The correlations of both weight loss and tar yields are within the experimental uncertainty throughout. Note that the proportions of tar to gas decrease continuously, and that tar formation is completed by about 900K, but gas evolution persists through higher temperatures.

The largest fragments in the coal, the reactant lump, are rapidly converted into intermediates up to about 950K. Note that, due to spontaneous char formation, not all of the reactant fragments dissociate into either of the smaller lumps. The intermediate accumulates continuously, initially by fragmentation of the reactant and ultimately by bimolecular recombination of metaplast. The predicted amount of metaplast is maximized at 800K, then falls during the most rapid stage of tar evolution; its disappearance coincides with the end of tar formation.

The predicted number-average molecular weight of tar for vacuum and atmospheric pressure are compared with Oh's measurements in Fig. 2. The predicted values for vacuum are within the experimental uncertainty, but seem low by several percent for the atmospheric tars. Notwithstanding, the theory captures the observations that (1) the first tar fragments are somewhat lighter than the bulk of the tar fraction; and (2) increasing the pressure shifts the tar to substantially lower molecular weights. Both of these features are tied to the flash distillation mechanism. Although predicted distributions are omitted here, they all are of the form of Gamma-distributions.

Variations in the thermal history for nearly-atmospheric pyrolysis are examined in Fig. 3. These three cases depict the influence of extended reaction times at constant temperature following uniform heating, and variations in heating rate of three orders of magnitude. For the case of heating at  $10^3$  K/s with immediate quenching, the predictions are within the experimental uncertainty, except at the highest temperatures. The predicted impact of a 30 s reaction period at each temperature is qualitatively correct, in that most of the weight loss is observed at temperatures between 650 and 900K. But the predicted ultimate yields above 900 K are consistently lower than the data by about 6 wt %. As these investigators acknowledge, their ultimate yields are higher than the bulk of reported values for atmospheric pyrolysis, which are represented by the data in Fig. 1.

Similarly, the predicted variation due to lowering the heating rate from  $10^3$  K/s to 1K/s is qualitatively accurate, and also within the experimental uncertainty for temperatures up to 800K. But at higher temperatures the predicted weight loss is about 12% lower than the data. We have not yet determined that raising the predicted yields at



10<sup>3</sup>K/s would bring the predictions for 1K/s into quantitative agreement, although it would certainly improve the correlation.

This theory omits both gas-phase tar deposition and mass transport limitations which have long been regarded as the mechanistic basis for the pressure effect; instead, it relies on the phase equilibrium between metaplast and tar to retain more light fragments in the condensed phases as the pressure increases. This mechanism strongly influences the tar yields, especially at pressures up to several atmospheres. In Fig. 4, predicted tar yields at three pressures are validated by the available data.

An evaluation over a much wider pressure range, in Fig. 5, involves weight loss for extended reaction periods following heatup at 10<sup>3</sup>K/s to 1025K. The quantitative discrepancies for pressures less than 5 atm are generally within 5 wt % of the data. Perhaps more importantly, the predicted approach to a near-asymptotic weight loss at pressures above 10 atm is clearly consistent with the data. The predicted tar yields (not shown) decrease with increasing pressure, but remain substantial at the highest pressures; e. g., at 10 atm, the predicted tar yield is 16 wt%. Predicted gas yields increase with increasing pressure, in accord with an established trend.

## Discussion

Qualitatively, this theory captures the influences of all of the important operating conditions on the devolatilization behavior of high volatile bituminous coals, and in most cases the quantitative agreement is within the experimental uncertainties. But its greatest potential lies in the formalism to rationalize the behavior of different coals. In this study, only the connection to the structural parameters from <sup>13</sup>C NMR analyses has been demonstrated, and the general reliability of the predictions is encouraging. Future reports will evaluate the predicted behavior for variations in the parameters which describe the initial constitution of the coal.

## Acknowledgement

We are happy to acknowledge the U. S. Department of Energy for financial support. Partial support for S. Niksa and the computational facilities were provided by the Advanced Research and Technology Development Program administered by the Pittsburgh Energy Technology Center. Partial support for A. R. Kerstein was provided by the Office of Basic Energy Sciences.

## References

1. Niksa, S. and Kerstein, A. R., *Combust. Flame* 66:95 (1986).
2. Niksa, S. and Kerstein, A. R., *Fuel* 66:1389 (1987).
3. Solomon, P. R. et al., *Energy Fuels* 2:405 (1988).
4. Grant, D. M. et al., *Energy Fuels* 3:175 (1989).
5. Niksa, S., *AIChE J.* 34:790 (1988).
6. Oh, M. S., "Softening Coal Pyrolysis", Sc. D. thesis, Department of Chemical Engineering, MIT, 1985.
7. Gibbins-Maltham, J. and Kandiyoti, R., *Energy Fuels* 2:505 (1988).
8. Suuberg, E. M., Unger, P. E., and Lilly, W. D., *Fuel* 64:966 (1985).
9. Bautista, J. R., Russel, W. B., and Saville, D. A., *Ind. Eng. Chem. Fundam.* 25:536 (1986).
10. Solum, M. S., Pugmire, R. J., and Grant, D. M., *Energy Fuels* 3:187 (1989).

TABLE 1. MODEL PARAMETERS

Coal Characteristics		
MW of Aromatic Nuclei	186 g/g-mole	
MW Ratio, Bridges to Nuclei	0.785	
MW Ratio, Char Links to Nuclei	0.300	
MW Ratio, Peripheral Groups to Nuclei	0.134	
Initial Fraction of Total Links	0.912	
Initial Fraction of Labile Bridges	0.600	
Rate Parameters		
Reaction	A-Factor, s <sup>-1</sup>	Ea, kJ/mole
Bridge Dissociation	$3 \times 10^{11}$	176 ( $\sigma = 25$ )
Recombination	$4 \times 10^{14}$	209
Per. Group Elim.	$1 \times 10^{15}$	230
Selectivity Coefficient for Bridge Scission 0.35		
$P_{\text{metaplast}}^{\text{SAT}}(T, \text{MW}) = 1.5 \times 10^3 \exp(-165 \text{ MW}^{0.6}/T)$ , MPa		

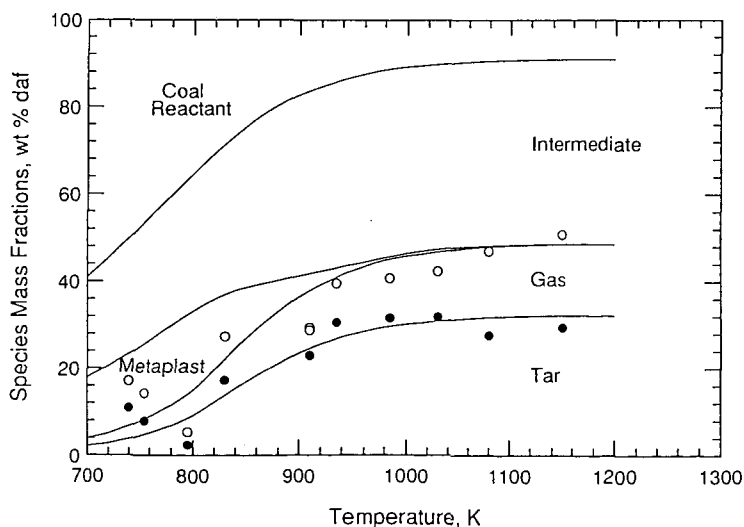


Fig. 1. The predicted distribution of reaction species for atmospheric pyrolysis for heating at  $10^3$  K/s followed by immediate cooling at 100K/s, compared to Oh's<sup>8</sup> measurements of weight loss and tar yields.

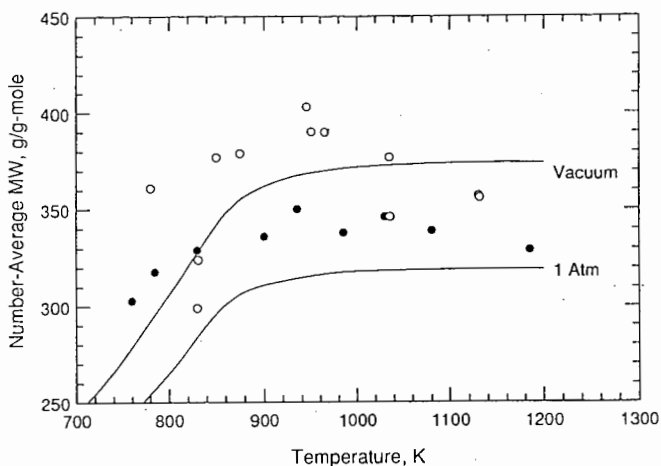


Fig. 2. An evaluation of the predicted number average molecular weights of tar for vacuum and atmospheric pyrolysis against Oh's<sup>9</sup> GPC determinations. Thermal histories are the same as in Fig. 1.

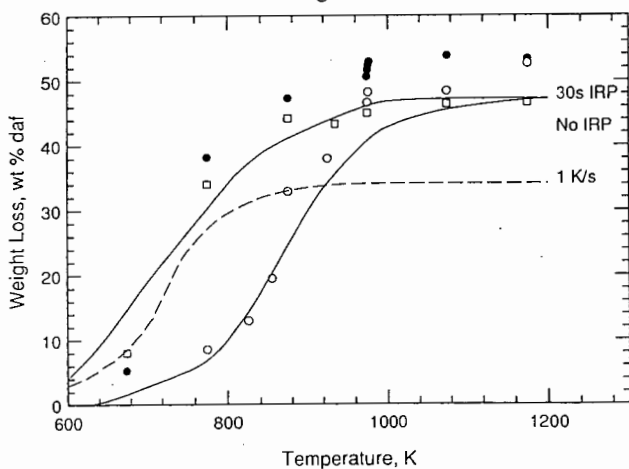


Fig. 3. An evaluation of the predicted weight loss for various thermal histories against the data recorded at 0.12 MPa<sup>7</sup>. Both solid curves are for a heating rate of 10<sup>3</sup> K/s, with different reaction times at constant temperature of 30s (upper curve and filled circles) and 0s (open circles). The dashed curve and open squares depict the behavior at 1 K/s.

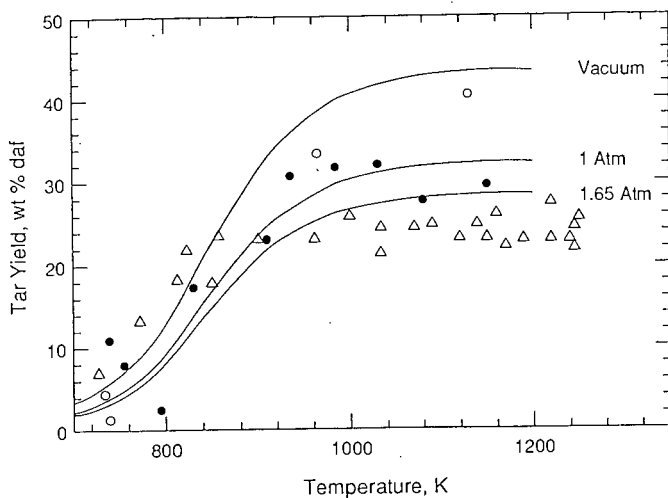


Fig. 4. An evaluation of the predicted tar yields for vacuum and atmospheric pyrolysis, with data from Oh<sup>6</sup>, and for pyrolysis at 0.165MPa, with data from Suuberg et al.<sup>8</sup> The thermal histories are the same as in Fig. 1.

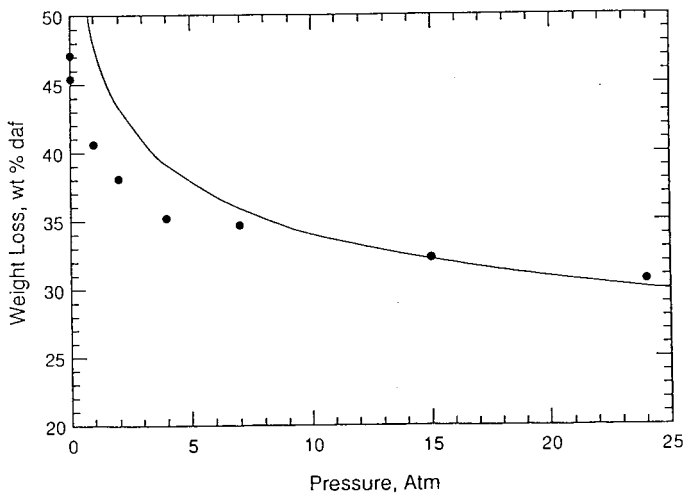


Fig. 5. An evaluation of the predicted weight loss at various pressures for heatup at  $10^3$  K/s to 1025K with 10s reaction times. The data are from Bautista et al.<sup>9</sup>

## Approximating Rapid Pyrolysis of Coal Particles with Shrinking Core Model

Mohammad R. Hajaligol and Sung C. Yi  
Philip Morris U.S.A.  
Research Center, P.O.Box 26583  
Richmond, Va 23112

### INTRODUCTION

Coal pyrolysis is a complex phenomenon and when it is accompanied with rapid heating conditions, it becomes even more complex. A robust but mathematically simple approach is needed when such complexities are encountered. Literature on coal pyrolysis modeling are extensive. Part of this literature describes empirical approaches (1-2), while others include phenomenological and/or physico-chemical approaches (3-6) toward modelling this complex system. Due to these complexities the outcomes of the models appear to be more of a mathematical correlation than mechanistic relations. Accurate knowledge of pyrolysis temperature is one of the essentials in these studies. This becomes more dominant when heating rates approach extremely high values. According to Hajaligol et al. (7,8) and others (2,9,15), at lower heating rates, pyrolysis occurs volumetrically and there exist conditions where pyrolysis is controlled by chemical kinetics. With higher heating rates pyrolysis becomes controlled by heat transfer to the particle that eventually enters an ablation regime (9). On the other hand there are indications that pyrolysis kinetics is influenced by heating rate (11). Since pyrolysis occurs at higher temperatures for higher heating rates, the mechanism of reaction might have been altered. These complexities have led some investigators to believe that pyrolysis has to be explained with a scheme different than chemical reactions (12).

The focus of this study is to show that for high heating rates ( $> 10^5$  K/s), pyrolysis in a particle occurs according to a shrinking core model rather than a volumetric model in which temperature gradient is the driving force. Quite simply it is shown that temperature at pyrolysis front is different than that of particle surface temperature under this extreme heating condition. This temperature is uniquely dependent upon the pyrolysis kinetics, but not on the external heating conditions nor on the thermal properties of the particle. This study provides information on the primary pyrolysis kinetics of coal which can be estimated under these heating conditions.

### MATHEMATICAL ANALYSIS

Pyrolysis is modelled for a single spherical coal particle which is pyrolyzed via a single first-order reaction with Arrhenius kinetics

$$\frac{dv}{dt} = (V^* - V)k_0 \exp(-E/RT) \quad (1)$$

Thermophysical properties of the particle can be constant or variable and depend on the temperature. Heat is transmitted into the particle by conduction. Other modes of heat transfer are shown to be less significant under these heating conditions. A standard heat balance on

the particle leads to the following governing partial differential equations

$$\rho C_p \frac{\partial T}{\partial t} = \frac{1}{r^2} \frac{\partial}{\partial r} (r^2 \lambda \frac{\partial T}{\partial r}) - \rho u C_p \frac{\partial T}{\partial r} + (-\Delta H) \rho (V^* - V) k_o \text{EXP}(-E/RT) \quad (2)$$

$$\frac{\partial p}{\partial t} = - \frac{1}{r^2} \frac{\partial}{\partial r} (r^2 \rho u) + \rho (V^* - V) k_o \text{EXP}(-E/RT) \quad (2a)$$

Equation (2) is solved numerically for the particle temperature field with following initial and boundary conditions. The initial condition is a uniform temperature,  $T_o$ , throughout the particle

$$T = T_o \text{ for } t \leq 0 \text{ and all } r \quad (3a)$$

The first boundary condition is the mathematical expression for center-line symmetry of the particle temperature field

$$\frac{\partial T}{\partial r} = 0 \text{ at } r = 0 \text{ for all } t \quad (3b)$$

Second boundary condition can be chosen as a heating rate condition greater than  $10^5$  K/s or a heat flux density greater than 100 watt at the surface to a desired final temperature as follows:

case a)

$$\begin{aligned} T &= T_o + mt & \text{at } r = R_p, t \leq t_1 \\ T &= T_s & \text{at } r = R_p, t > t_1 \end{aligned} \quad (3c)$$

case b)

$$\begin{aligned} -\lambda \frac{\partial T}{\partial r} &= q & \text{at } r = R_p, t \leq t_1 \\ T &= T_s & \text{at } r = R_p, t > t_1 \end{aligned} \quad (3d)$$

The solution to Equation (2) is prediction of the temperature field throughout the particle. This information is then used to compute the instantaneous conversion at any given point to monitor, (i) the pyrolysis front within the particle (points of > 98% conversion) (ii) the temperature where 98 % of conversion has been reached at that point, and (iii) the particle fractional conversion and the total pyrolysis time for the conversion.

## RESULTS AND DISCUSSION

Either boundary condition prescribed by a heat flux density (3d) or a surface heating rate (3c) to provide a surface heating time of 1 ms. is used in the above analysis to predict pyrolysis behavior under these thermal conditions. Unless stated, the following numerical values were used for the analysis:  $\rho=1.3\text{g/cm}^3$ ,  $\lambda=0.0006 \text{ cal/cm-s-K}$ ,  $C_p=0.4\text{cal/g-K}$ ,  $\Delta H=1000\text{cal/g}$ ,  $k_o=10^{13} \text{ sec}^{-1}$ , and  $E=50\text{Kcal/mole}$ .

Figure 1 shows the effects of pyrolysis time on the radial position, and the shape of the pyrolysis front for a 100  $\mu\text{m}$  diameter particle. It clearly demonstrates that under these heating conditions the region

where 98 % conversion has occurred is confined in a thin layer which moves inward with a velocity that depends on the thermo-chemical properties of the particle and external heating loads imposed on the particle. Figure 2 presents the effects of different surface temperatures for a given pyrolysis time on the shape and position of the pyrolysis front. As expected, the higher the surface temperature, the larger the driving force ( $\Delta T$ ), thus the higher the velocity of a pyrolysis front and the shorter the pyrolysis time. Figure 2 also shows that the shape of the pyrolysis front (region with 98 % conversion) does not change with the surface temperature. This is true unless the surface temperature drops below a threshold value.

Results from Figures 1, 2 as well as results for other particle diameters (up to 2 mm) show that regardless of the position of pyrolysis front, particle diameter and surface temperature, the temperature of the pyrolysis front is constant. As will be discussed further, when thermal properties of the particle were changed ( $\lambda$ ,  $\Delta H$ , etc.) or variable thermal properties were assumed or other heating rates ( $10^5$  K/s) were applied, the temperature at the pyrolysis front (where 98 % conversion is reached) did not change. Analysis shows that this temperature ( $T_1$ ) is a unique function of pyrolysis kinetics, i.e., if  $k_0$  or  $E$  were to change, the temperature would change accordingly. This is what we called threshold value for temperature.

All the above observations indicate that the pyrolysis under these circumstances could be approximated by a shrinking unreacted core model. Following Szekly et al. (13), but exchanging heat for mass diffusion in their description leads to

$$t = \left[ k_0 e^{-\frac{E}{RT_1}} \right]^{-1} p(x) + \frac{R_p^2 \rho \left[ C_p (T_1 - T_0) + \Delta H \right]}{\lambda (T_s - T_1)} g(x) \quad (4)$$

where  $p(x)$  and  $g(x)$  are given elsewhere (13). It can be shown that under rapid heating conditions, the first term on the right hand side (which describes the kinetic effects) is insignificant and thus pyrolysis is controlled by diffusional resistance (second term). In order to observe the validity of this hypothesis, a parametric study was conducted using Equation (2). The pyrolysis time for complete conversion was compared with that of Equation (4). Given  $T_s$ ,  $E$ ,  $k_0$ , and  $\Delta H$ , when  $\lambda$  or  $R_p$  is varied, pyrolysis time will scale with  $\lambda$  and increase with the square of  $R_p$  (Figure 3). As can be seen this matches well with Equation (4). When  $\Delta H$  or  $T_s$  varied, the results from Equation (2) did not match well with what predicted from Equation (4), although they did show the same trend (Figure 4).  $\Delta H$  in the range of 0 to 1000 cal/g does not have a significant effect on Equation (2). This is due to the fact that under these heating conditions the ratio of heat transmitted into the particle to the heat consumed by the pyrolysis at the front is high. When higher values of  $\Delta H$  ( $>10000$  cal/g) were examined (a hypothetical case) the pyrolysis time and  $\Delta H$  correlation would come out the same from both Equations (2) and (4). Part of the heat which is transmitted into the particle will also be used to heat up that part of the particle through which the pyrolysis front will pass, this effect becomes less noticeable with increasing  $T_s$  as predicted by Equation (4). Again for the very large  $T_s$  or  $(T_s - T_1)$  where the portion

of total heat which is needed for sensible heat of particle is very small in comparison to the total heat transmitted into the particle, prediction of Equations (2) and (4) are exactly the same.

As presented above when any combination of  $E$  and  $k_0$  according to Nsakala et al. (14) were chosen, regardless of  $T_s$ ,  $\lambda$ ,  $\Delta H$ ,  $R_p$ , the temperature at the pyrolysis front ( $T_i$ ) showed a dependency only on  $k_0$  and  $E$ . Results can be seen in Figure 5 where  $k_0$  is constant and  $T_i$  increases as  $E$  increases. When dimensionless time ( $t = at/R_p^2$ ) was plotted against the pyrolysis rate constant ( $k_0 e^{-E/RT_i}$ ), the results fall on a single line for any given  $T_s$  (Figure 6). This indicates a unique correlation between pyrolysis kinetics and the total pyrolysis time. This is due to the strong functionality of pyrolysis time with  $\lambda$  and  $R_p$  (embedded in dimensionless time) and pyrolysis kinetics as discussed above. Furthermore, the results of pyrolysis time for total conversion are consistent with Essenhigh (10,14) and others. Effects of  $T_s$  can be calculated from Figure 4 and presented with families of curves in Figure 6 using  $T_s$  as a parameter.

Effects of variable thermal properties were also studied. For instance, if a variable  $\lambda(t) = 1.226 \times 10^{-5} [1.3 + 0.96x(V/V')] ]^{3.5T^{1/2}}$  was assumed instead of  $\lambda = 0.006$  cal/cm-s-k the total pyrolysis time would have changed only by 10%. This is because the effective thermal conductivity is controlled by the char thermal conductivity (outer layer of pyrolysis front) and that is relatively constant for the temperature range studied (1200 - 1500 K). This effect is even less significant for heat of pyrolysis, as discussed above where  $\Delta H$  was varied from 0 to 1000 cal/g.

The practical implication of these results is that by measuring pyrolysis time for a given particle diameter and surface temperature, one could use Figure 6 to estimate  $T_i$  and  $k$ . This  $T_i$  and  $k$  can be used along with Figure 5 to estimate the kinetic parameters for primary pyrolysis of coal under severe thermal conditions.

#### CONCLUSIONS

1. For the rapid heating rates ( $>10^5$  K/s), pyrolysis is confined to a thin layer and reaction occurs according to the shrinking core model rather than a volumetric reaction model.
2. Under these heating conditions pyrolysis occurs totally under diffusional limitations (in the ablation regime).
3. Activation energy ( $E$ ) and thermal conductivity ( $\lambda$ ) are the most stringent parameters on pyrolysis followed by heat of reaction and the surface temperature.
4. Temperature at the pyrolysis front is different from the surface temperature and is uniquely correlated to the pyrolysis kinetics.
5. Intrinsic pyrolysis kinetics under these heating conditions can be estimated using results of existing analysis.

#### ACKNOWLEDGEMENTS

Authors gratefully acknowledge Dr. Bruce Losee and Dr. Sarajini A. Deevi of Philip Morris U.S.A. for their helpful comments.



# NOMENCLATURES

C <sub>p</sub>	heat capacity, [Cal/g-K]
E	activation energy, [Cal/gmole]
k <sub>o</sub>	frequency factor, [1/s]
m	heating rate, [K/s]
g(x), p(x)	conversion functions [-]
q	heat flux density, [Cal/cm <sup>2</sup> -s]
r	radius, [cm]
R <sub>c</sub>	pyrolysis front, [cm]
R <sub>p</sub>	particle radius, [cm]
T	temperature [K]
T <sub>o</sub>	initial temperature [K]
T <sub>i</sub>	temperature at pyrolysis front [K]
T <sub>s</sub>	surface temperature [K]
t	time [s]
u	volatiles velocity [cm/sec]
V	percent weight loss
V*	ultimate weight loss
ΔH	heat of pyrolysis [Cal/g]
λ	thermal conductivity [Cal/cm-s-K]
ρ	density [g/cm <sup>3</sup> ]
τ	dimensionless time [-]

# REFERENCES

- 1 Howard, J.B., Chemistry of Coal utilization, 2nd supplementary volume, chapter 12, Elliot M.A., Ed., Wiley-Interscience, NY 1981.
- 2 Galvalas, G.R., Coal pyrolysis, Elsevier Scientific, NY 1982.
- 3 Solomon, P.R., Hamblen, D.G., Carangelo, R.M., Serio, M.A., and Deshpande G.V., ACS., Div. Fuel Chem. prep., 32(3), 83, 1987.
- 4 Niksa, S., Combustion and Flame, 66, 111, 1986.
- 5 Niksa, S., AIChE J., 34, 5, 790, 1988.
- 6 Suberg, E.M., in Chemistry of Coal Conversion, R. Schlosberg, Ed., 67 Plenum, 1985.
- 7 Hajjaligol, M.R., Peters, W.A. and Howard, J.P., Energy and Fuels, 2, 430, 1988.
- 8 Hajjaligol, M.R., Peters, W.A. and Howard, J.P., to be submitted to AIChE, 1989.
- 9 Villiermaux, J., Antoine B., Lede J., and Soullignac, F., ACS Div. Fuel Chem. prep., 28(5), 390, 1983.
- 10 Misra M.K., and Essenhigh, R.H., ACS Div. Fuel Chem. prep., 32(2), 59, 1982.
- 11 Ko, C.H., Sanchez, D.M., Peters, W.A. and Howard, J.P., ACS, Div. Fuel Chem. prep., 33(2), 112, 1988.
- 12 Hertzberg, M., Zlochower I.A., Conti, R.S. and Cashdollar K.L., ACS Div. Fuel Chem. prep., 32(3), 24, 1987.
- 13 Szekeley, J., Evans, J.W., and Sohn, H.Y., Gas-Solid Reactions, Academic Press, N.Y., 1976.
- 14 Nsakala N., Essenhigh, R.H., and Walker, P.L., Combustion Sci. Tech., 16, 153, 1977.
- 15 Wanzl, W., Kabler P., Van Heck K.H., and Junten H., ACS Div. Fuel Chem. prep., 32(3), 125, 1987.

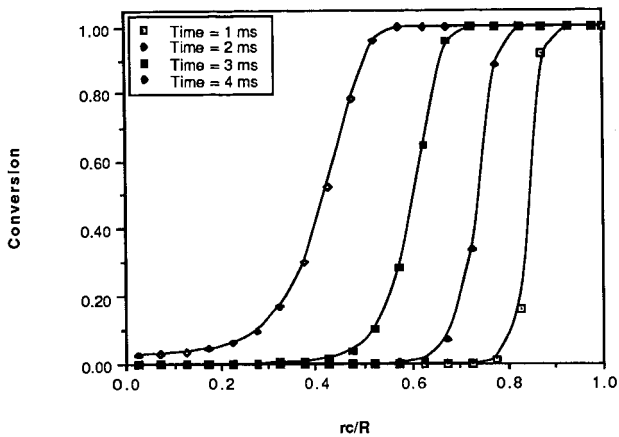


Figure 1. Effect of pyrolysis time on the position and shape of pyrolysis front ( $T_s=1500$  K,  $R_p=50\mu\text{m}$ )

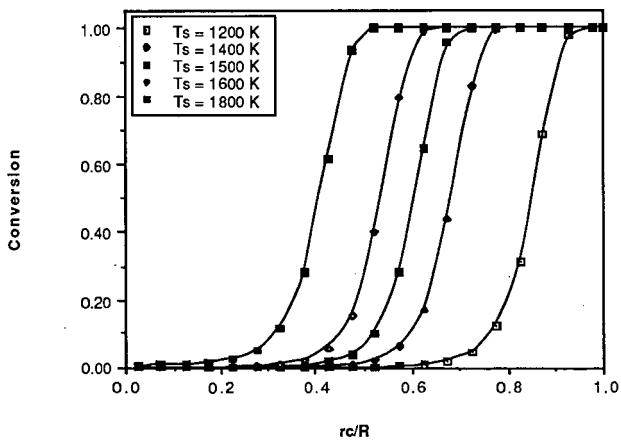


Figure 2. Effect of surface temperature on the position and shape of pyrolysis front ( $R_p=50\mu\text{m}$ , 5ms)

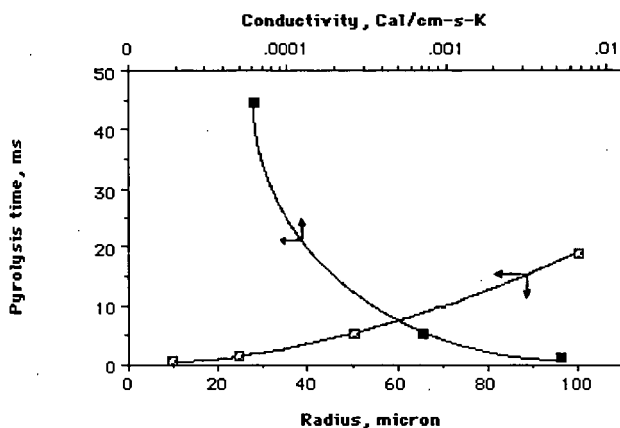


Figure 3. Effect of thermal conductivity and radius on the total pyrolysis time ( $T_s=1500$  K,  $R_p=50\mu\text{m}$ )

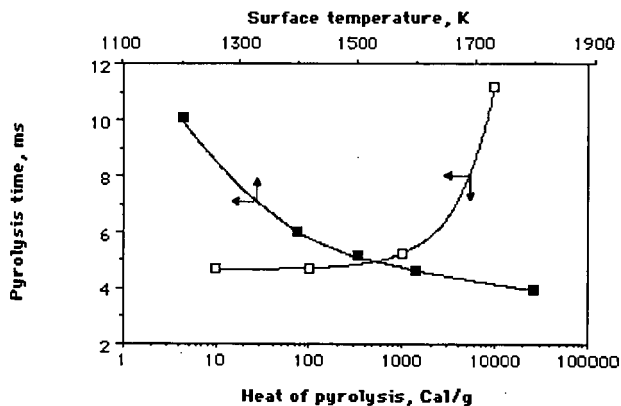


Figure 4. Effect of heat of pyrolysis and surface temperature on the total pyrolysis time ( $T_s=1500$  K,  $R_p=50\mu\text{m}$ )

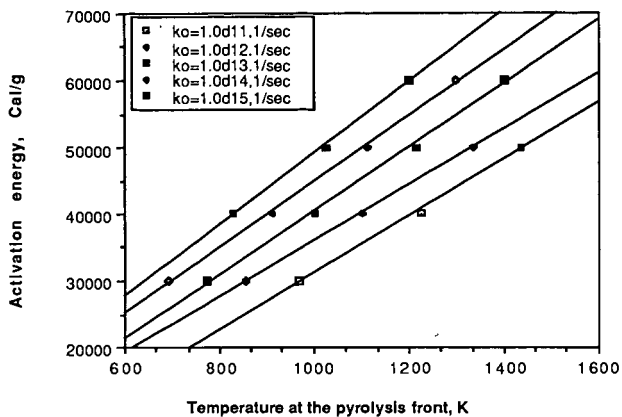


Figure 5. Correlation between activation energy ( $E$ ), frequency factor ( $k_o$ ) and the temperature at the pyrolysis front ( $T_i$ )

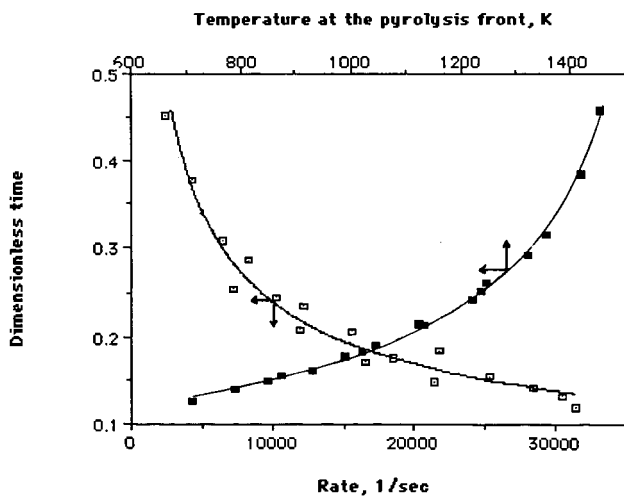


Figure 6. Effect of pyrolysis kinetic and temperature on the pyrolysis dimensionless time

ESTIMATION OF COAL DEVOLATILIZATION MODELING PARAMETERS FROM THERMOGRAVIMETRIC  
AND TIME-RESOLVED SOFT IONIZATION MASS SPECTROMETRIC DATA

Yongseung Yun, Wallace Maswadeh, Henk L.C. Meuzelaar, Norbert Simmleit\*  
and Hans-Rolf Schulten\*\*

Center for Micro Analysis & Reaction Chemistry, University of Utah  
Salt Lake City, Utah 84112

\*Institut Fresenius, Chemical and Biological Laboratories  
D-6204 Taunusstein-Neuhof, F.R.G.

\*\* Fachhochschule Fresenius, Dept. Trace Analysis  
D-6200 Wiesbaden, F.R.G.

#### INTRODUCTION

Nowadays it is widely recognized that the initial pyrolysis step in coal conversion processes has a profound effect on the yield and distribution of end products such as coal-derived liquids, gases, coke, or pollutant emissions. Two general approaches for modeling coal pyrolysis reactions can be distinguished, namely: (a) phenomenological modeling and (b) chemical modeling [1]. The phenomenological modeling approach is useful in conversion processes such as high temperature gasification where detailed chemical information may be advantageous but is probably not indispensable. Other conversion processes, however, e.g., liquefaction and hydropyrolysis, may require more detailed chemical information to predict the distribution of final products [2]. Whether pyrolysis ("devolatilization") models for pulverized coal combustion processes require detailed information on coal structure and reactivity or can be based primarily on a phenomenological approach is still a matter of considerable debate [3].

Heated screen pyrolysis techniques have been widely used to provide modeling parameters for phenomenological models based on the thermal behavior of light gas components detected by gas chromatography, mass spectrometry (MS) and other spectroscopic techniques [4]. Due to limitations of the analytical techniques used, tar components are generally lumped into a single component.

Since time-resolved mass spectrometry (TR-MS) data can be used to analyze single mass profiles or mass spectra as a function of temperature, TR-MS results from thermogravimetry/low-voltage electron impact mass spectrometry (TG/EIMS) [5] and pyrolysis-field ionization mass spectrometry (Py-FIMS) [6] can provide detailed chemical information on gas and tar products [5].

The aim of this study is to present several possibilities for estimating kinetic parameters to model coal pyrolysis phenomena from TR-MS data. Our estimations will be based on the chemical assignment of tar components observed in soft ionization mass spectra in combination with kinetic evaluation or temperature-resolved intensity profiles of single mass peaks and measured or simulated thermogravimetric weight loss curves.

#### EXPERIMENTAL

Three -100 mesh Argonne Premium coal samples of different rank (Pocahontas #3, 1vb; Pittsburgh #8, hvAb; and Beulah-Zap, lignite) were analyzed by vacuum TG/EIMS and Py-FIMS. Conventional characterization data on the coal samples can be found elsewhere [7].

The TG/EIMS system consists of a Mettler TA1 Thermoanalyzer directly interfaced to a Finnigan MAT 3200 quadrupole mass spectrometer. Devolatilization was performed directly in front of the ion source in order to avoid

recombination reactions and/or secondary decomposition of reactive compounds as well as to reduce the loss of polar compounds through adsorption and condensation. Sample aliquots of 4-5 mg were heated under vacuum ( $3-6 \times 10^{-7}$  torr) as the sample temperature was increased from 60 C to 730 C at 25 C/min. MS conditions were as follows: electron energy 14 eV (set value), mass range scanned  $m/z$  33-200, total number of scans 80, and total scanning time 27 minutes.

For temperature-programmed pyrolysis in combination with TR-FIMS, about 100  $\mu$ g samples were transferred into a commercially available quartz crucible and introduced into the high vacuum ( $10^{-7}$  torr) of the ion source (200 C). The instrumental setup using a Finnigan MAT 731 double-focussing mass spectrometer, a combined EI/FI/FD/FAB ion source and a AMD Intectra direct introduction system has been previously described in detail [6]. The samples were heated linearly from 50 C to 750 C at a rate of 100 C/min. The crucible temperature was measured with a thermocouple at the bottom of the oven. In general, 34 FI mass spectra were recorded in the  $m/z$  50-900 mass range. The mass signals and the total ion intensities (TII) of the mass spectral series were used to calculate tar weight loss curves [8].

A three parameter kinetic fitting procedure, based on Marquardt's algorithm [9], was employed after scaling the activation energy, pre-exponential factor, and reaction order to similar orders of magnitude. The distributed activation energy kinetic model used was based on Gaussian distributed activation energies with a fixed pre-exponential factor and a reaction order of 1 [10].

## RESULTS AND DISCUSSION

From the vacuum TG observations, char yields at 25 C/min and maximum temperature of 730 C were found to be 71, 48, and 58 wt% (based on as received samples) for Pocahontas #3, Pittsburgh #8, and Beulah-Zap coals respectively. Consequently, the (gas+tar) yield of the three coals under vacuum TG conditions can be put at 29, 52 and 42 wt %, respectively.

Figure 1 shows temperature profiles of low molecular weight (MW) tar products recorded by means of vacuum TG/EIMS. Since the data plotted in the figure show the rate profile versus temperature, kinetic parameters can be calculated for each mass signal. Although each of the mass profiles shown at  $m/z$  56, 108 and 124 can be expected to originate from several different sources the most abundant ion species at these  $m/z$  values in coal pyrolyzates are thought to represent butenes ( $C_4H_8^+$ ;  $m/z$  56), cresols ( $C_7H_8O$ ;  $m/z$  108) and methyl-dihydroxybenzenes ( $C_7H_8O_2$ ;  $m/z$  124) [11].

The results of the kinetic estimates are also presented in Figure 1. First the normalized raw data (total weight loss fraction due to single mass signal  $\approx 1$ ) have been fitted to a 1st order Arrhenius model ( $n=1$ ) yielding apparent activation energies  $E$ , pre-exponential factors  $A$  and in general a good fit of the ascending part of the temperature/nominal mass signal profile (Figure 2). In a second step, maintaining  $E$  and  $A$  constant, the fit of the descending part of the curve was improved by varying the reaction order  $n$ . Similar combinations of reaction orders, activation energies and pre-exponential factors could also be obtained in a single step by nonlinear regression based on Marquardt's algorithm. In most cases studied this led to a satisfying result (Figure 2a). In other cases, however, no satisfying fit could be achieved with any of the methods applied (Figure 2b). This is probably due to the presence of two or more overlapping processes [5]. In an independent third step the normalized raw data were fitted to a distributed activation model (DAE,  $n=1$ ) yielding a frequency factor  $A$ , the mean activation energy  $E_0$  and the standard deviation of the activation energy  $\sigma_E$ . For the EI mass signal  $m/z$  124 evolved from Pocahontas coal it was not possible to apply the DAE model due to a poor signal-to-noise ratio.

With the exception of mass signal  $m/z$  124 of the Beulah Zap coal apparent activation energies estimated by 1st order Arrhenius model are not in the range of the corresponding activation energies  $E_0 + 36E$  estimated by the DAE model. The kinetic parameters  $E_0$  and  $A$  derived from the DAE model are higher and in particular  $A$  is several orders of magnitude higher when estimated by the DAE model. The mean activation energy  $E_0$  is higher due to the effect of distribution functionality. Accordingly,  $A$  has to be much higher due to the compensating effect between  $E$  and  $A$ . The data in Figure 1 show that most of the reactions studied are not of reaction order  $n=1$ . With exception of the mass signal  $m/z$  56 of Beulah Zap coal the reaction order ranges between 1.3 and 1.8 apparently indicating the occurrence of intermolecular reactions, e.g., char formation, at higher temperatures. In general, apparent and distributed activation energies, and consequently the pre-exponential factors, increase with coal rank, i.e., with higher degree of condensation. During pyrolysis of Pittsburgh and Pocahontas coals the activation energies decrease with increasing polarity of the thermal degradation products. The opposite effect is observed for the lignite coal (Beulah Zap). Presumably, this indicates an effect of amount and availability of thermal degradation products formed during pyrolysis of the three coals of different rank.

Figures 3-5 show Py-FIMS results of the three ANL coals of different rank. The upper left corner figures (3a-5a) are thermograms which illustrate with increasing temperature the total ion intensity of each spectrum scanned. The upper right corner figures (3b-5b) are the time-integrated mass spectra obtained by summing all spectra scanned on each coal indicating that much higher MW compounds are released during coal pyrolysis than detected under the conditions of the TG/EIMS experiment. The bottom left hand side figures (3c-5c) show calculated weight loss curves for selected mass ranges. Due to the absence of significant mass spectrometric fragmentation and relatively uniform response factors for aromatic and hydroaromatic compounds, FIMS provides reliable information on the (MW) distribution of most types of tar products detected. The product of an  $m/z$ -value and its corresponding FI signal intensity equals the calculated weight loss of thermal degradation products with  $MW=m/z$  evolving from the sample in a specific temperature interval. The total weight loss was calculated for mass ranges of 100 Dalton and plotted in a cumulative way. Thus, the bottom line in the simulated TG curve represents the total relative weight loss of tar components with temperature. The bottom right hand figures (3d-5d) show the integrated Py-FI mass spectra of the low temperature pyrolysis products. The integrated temperature interval is hatched in the upper left hand figures (3a-5a).

There are two distinct maxima in the TII profiles. The early peak is most dominant in low volatile bituminous (lvb) Pocahontas #3 coal (Figure 5a) whereas high volatile bituminous (hvb) Pittsburgh #8 coal shows a least pronounced peak in the same temperature interval (Figure 4a). The absolute weight loss of the Pittsburgh coal in the low temperature region, however, may be higher since the TII recorded represents only the tar components in the mass range  $m/z$  50-900 excluding the gas components  $m/z$  <50. Three spectra around the maximum of the early peaks were summed and shown in Figures 3d-5d.

In Beulah-Zap coal (Figure 3d), there is little if any contribution of naphthalenes as may be expected in lignite coals. Instead, it shows a distinct homologous series of FI signals at  $m/z$  368, 396, 424, 452, 480 which may be due to n-fatty acids or monomeric esters ( $C_{24}$ - $C_{32}$ ) and an abundant FI signal at  $m/z$  544, which could indicate the presence of an aromatic diester. The described signals are known from Py-FIMS analyses of soil organic matter in temperature ranges below 300 C and may be due to stable degradation products of plant lipids or aliphatic biopolymers such as cutin or suberin [12].

The lignite (Beulah Zap) releases most of its thermal degradation products at higher temperatures around 440 C (Figure 3a). These products are known to be mainly derived from fossil lignin-like components [13] and, hence, the most prominent FI signals in integrated Py-FI mass spectrum over the whole temperature range (Figure 3b) can be seen at  $m/z$  94, 110, 124, 138 and 152 indicating phenol and alkyl-substituted dihydroxy-benzenes, respectively. Besides the high MW aliphatic compounds released mainly in the lower temperature range, the Py-FI mass spectrum in Figure 3b also shows FI signals of short-chain alkenes at  $m/z$  56, 70 and 84. Obviously, no condensed high-molecular weight pyrolysis products  $MW > 400$  are formed during the high temperature pyrolysis of the lignite sample.

The Pittsburgh coal behaves in a similar manner by releasing most of its thermal degradation products detected in the higher temperature range (Figure 4a). Hence, the integrated Py-FI mass spectrum (Figure 4b) is very different from the corresponding low-temperature spectrum (Figure 4d) showing primarily FI signals of pyrolysis products which have been evolved at temperatures above 400 C. The most prominent signals in Figure 4b at  $m/z$  94, 108, 122, 136 and 150 are due to alkyl-substituted phenols. Furthermore, the signal at  $m/z$  64 ( $SO_2^+$ ) indicates the presence of oxidized sulfur forms.

In the low temperature region Pittsburgh #8 coal releases noticeable amounts of alkyl-substituted naphthalenes which form molecular FI ion signals at  $m/z$  142, 156, 170, 184, 198 and 212 (Figure 4d). The most abundant species are the  $C_2$ - and  $C_3$ -alkyl substituted naphthalenes at  $m/z$  156 and 170. A homologous series of alkyl-substituted FI signals of acenaphthene species can be seen at  $m/z$  168, 182, 196, 210, 224 and 238 with the  $C_3$ - and  $C_4$ -alkyl substituted species being most abundant. Recent high resolution Py-FIMS analyses of Polish coals showed that the homologous series of FI signals at  $m/z$  204, 218, 232, 246, 260 and 274 may be primarily due to alkyl-substituted cyclopentaphenanthrenes [13]. According to the Py-FI mass spectrum, the  $C_4$ - and  $C_5$ -alkyl substituted species would be dominant in the low temperature release step of Pittsburgh #8 coal. At present detailed interpretation of higher mass signals is not possible, however it should be noted that two  $(CH_2)_2$ -homologous series of FI signals at  $m/z$  308, 336, 364, 392, 420 and at  $m/z$  296, 324, 352, 380, 408, 436 dominate the mass range  $m/z > 300$ .

As most of the thermal degradation products are already released from Pocahontas coal in the low-temperature range 300-400 C (Figure 5a), the corresponding spectrum (Figure 5d) looks very similar to the integrated spectrum in (Figure 5b). Major differences are due to high temperature pyrolysis products in the mass range  $m/z > 500$  and in the mass range  $m/z < 200$ . The latter products account for alkyl-substituted benzenes at  $m/z$  78, 92, 106, 120, naphthalenes at  $m/z$  142, 156, 170 and phenanthrenes at  $m/z$  178, 192, 206, 220.

Pocahontas #3 coal shows insignificant contributions of naphthalenes in the early devolatilization step (Figure 5d). Thus, in contrast to the Pittsburgh coal, the most abundant Py-FI mass signals have been recorded in the mass range  $m/z > 210$ . The mass range  $m/z < 325$  is dominated by pyrene species as the homologous series of alkyl-substituted pyrenes at  $m/z$  216, 230, 244, 258, 272, 286 and the homologous series of alkyl-substituted benzopyrenes at  $m/z$  252, 266, 280, 294, 308, 322 show. For both components the most abundant species are the  $C_3$ -alkyl species at  $m/z$  244 and at  $m/z$  294. Again it is difficult to interpret the higher mass signals, but other  $CH_2$ -homologous series at  $m/z$  316, 330, 344, 358, 373, 386, 400 and  $m/z$  326, 340, 354, 368, 382, 396, 410, 424 dominate the mass range  $m/z > 300$  of the Pocahontas coal when compared with the Pittsburgh coal.



## CONCLUSIONS

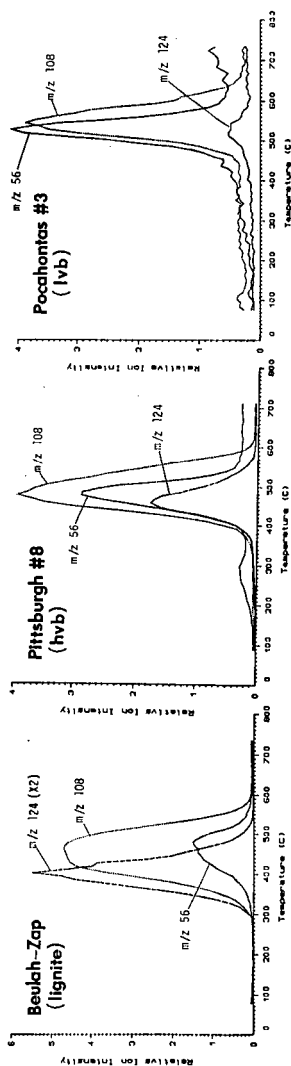
There are dramatic effects of rank (and probably depositional environment) on the devolatilization behavior of each coal. Although the main focus of coal pyrolysis modeling is on bituminous coals due to their higher yield in coal conversion processes, preferably the chemical pyrolysis model should have the ability to predict tar MW distributions as a function of temperature as well as to predict the chemical nature of tar molecules produced by different rank coals. Time-resolved soft ionization mass spectrometric techniques provide detailed information on the thermal evolution of distinct pyrolysis products. In particular FIMS is suited to obtain molecular weight distributions of tar components. Using single mass profiles, it is feasible to estimate kinetic parameters for pyrolysis products. The estimated kinetic parameters of thermal degradation products reflect the coal rank, the polarity of the pyrolysis products and the fitting technique employed. First order Arrhenius parameters enable a satisfactory fit to the temperature resolved mass profiles at  $T < T_{\max}$  whereas for  $T > T_{\max}$  higher reaction orders ( $1 < n < 2$ ) markedly improve the goodness of fit. By contrast, the use of distributed activation energies, although improving the overall fit, tends to lead to unexpectedly high values for mean activation energies and pre-exponential factors.

## ACKNOWLEDGEMENTS

This work was sponsored by the Advanced Combustion Engineering Research Center. Funds for this center are received from the National Science Foundation, the State of Utah, and 23 industrial participants. FIMS work was supported in part by the Deutsche Forschungsgemeinschaft, Bonn-Bad Godesberg (F.R.G.). The authors wish to thank R. Muller, Taunusstein for technical assistance.

## REFERENCES

1. Gavalas, G.R., Coal Pyrolysis, Elsevier, Amsterdam, 1982.
2. Chakravarty, T., Meuzelaar, H.L.C., Khan, R.H., "Modeling and Prediction of Pyrolysis Liquid Composition Based on Pyrolysis Mass Spectra of the Parent Fuels using Canonical Correlation Technique", submitted to Ind. Eng. Res., 1989.
3. Grant, D.M., Pugmire, R.J., ACS Preprints (Div. of Fuel Chem.), 33(2), 1988, 322-332.
4. Suuberg, E.M., Peters, W.A., Howard, J.B., I&EC Process Des. Dev., 17(1), 1978, 37-46.
5. Yun, Y., Meuzelaar, H.L.C., ACS Preprints (Div. of Fuel Chem.), 33(3), 1988, 75-84.
6. Schulten, H.-R., Simmleit, N., Muller, R., Anal. Chem., 59 (1987) 2903-2908.
7. Vorres, K.S., Janikowski, S.K., ACS Preprints (Div. of Fuel Chem.), 32(1), 1987, 492-499.6.
8. Schulten, H.-R., J. Anal. Appl. Pyrol. 12 (1987), 149-186.
9. Marquardt, D.W., J. Soc. Ind. Appl. Math., 11(2), 1963, 431-441.
10. Howard, J.B., Chemistry of Coal Utilization, Chap. 12, Elliott, M.A., ed., Wiley, New York, 1981.
11. Nip, M., de Leeuw, J.W., Schenck, P.A., Meuzelaar, H.L.C., Stout, S.A., Given, P.H., Boon J.J., J. Anal. Appl. Pyrol. 8 (1985), 221-239.
12. Hempfling, R., Zech, W., Schulten, H.-R., Soil Science, 146 (1988), 262-276.
13. Schulten, H.-R., Marzec, A., Simmleit, N., Dylan, P., Muller, R., Energy & Fuels (1989) in press.



m/z	coal	Beulah-Zap		Pittsburgh #8		Pocahontas #3	
		1st order	nth order	1st order	nth order	1st order	nth order
m/z 56	$E_0$	25.6	25.6	47.5	47.5	51.0	51.0
	$\phi E$	0	0	0	0	0	0
	A	$3.9 \times 10^5$	$3.9 \times 10^5$	$7.8 \times 10^{11}$	$7.8 \times 10^{11}$	$1.1 \times 10^{12}$	$1.1 \times 10^{12}$
m/z 108	$E_0$	27.9	27.9	40.0	40.0	51.2	51.2
	$\phi E$	0	0	0	0	0	0
	A	$2.4 \times 10^6$	$2.4 \times 10^6$	$5.9 \times 10^9$	$5.9 \times 10^9$	$7.2 \times 10^{11}$	$7.2 \times 10^{11}$
m/z 124	$E_0$	35.8	35.8	39.1	39.1	37.9	37.9
	$\phi E$	0	0	0	0	0	0
	A	$4.9 \times 10^9$	$4.9 \times 10^9$	$1.2 \times 10^{10}$	$1.2 \times 10^{10}$	$2.4 \times 10^8$	$2.4 \times 10^8$
		n	n	n	n	n	n

( $E_0, \phi E$  in Kcal/mol, A is  $s^{-1}$ )

Figure 1. Kinetic parameters estimated for selected nominal mass signal profiles recorded during TG/EIMS analysis of three coals. Parameters have been calculated by fitting the normalized raw data to 1st order, nth order and distributed activation energy (DAE) models.

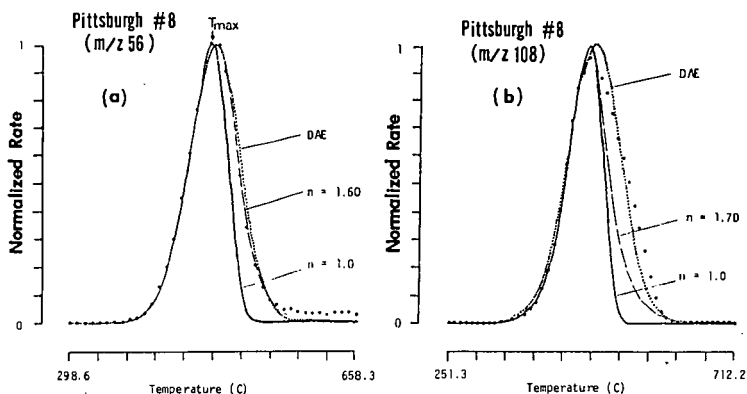


Figure 2. Selected examples of recorded temperature/EI mass signal profiles (•) and simulated mass signal profiles using kinetic parameters estimated by 1st and nth order model and DAE model. Principally, it was aimed to fit the rising part and the baseline of the profile. (a) shows a good fit of the whole profile, whereas (b) shows a bad fit of the declining part of the profile.

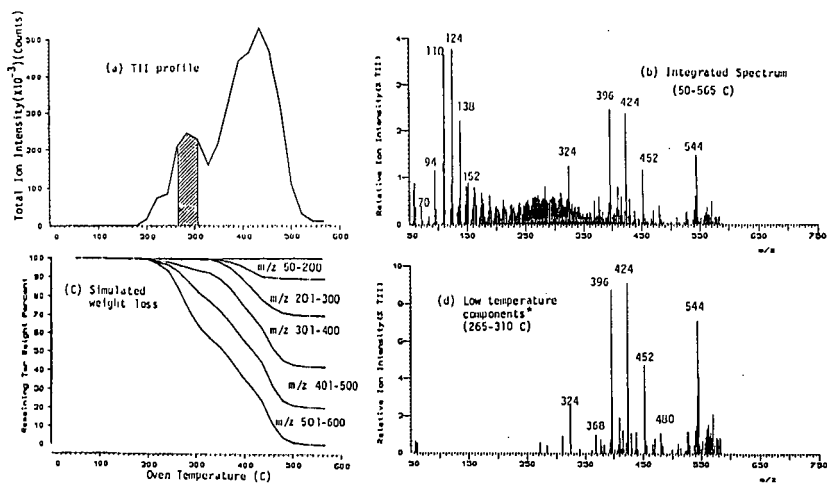


Figure 3. Py-FIMS results from Beulah Zap (lignite) coal. Simulated weight loss curves are cumulative for each mass range, thus the lowest curve shows the total weight loss of all components. \*Integrated spectrum of hatched area in (a).

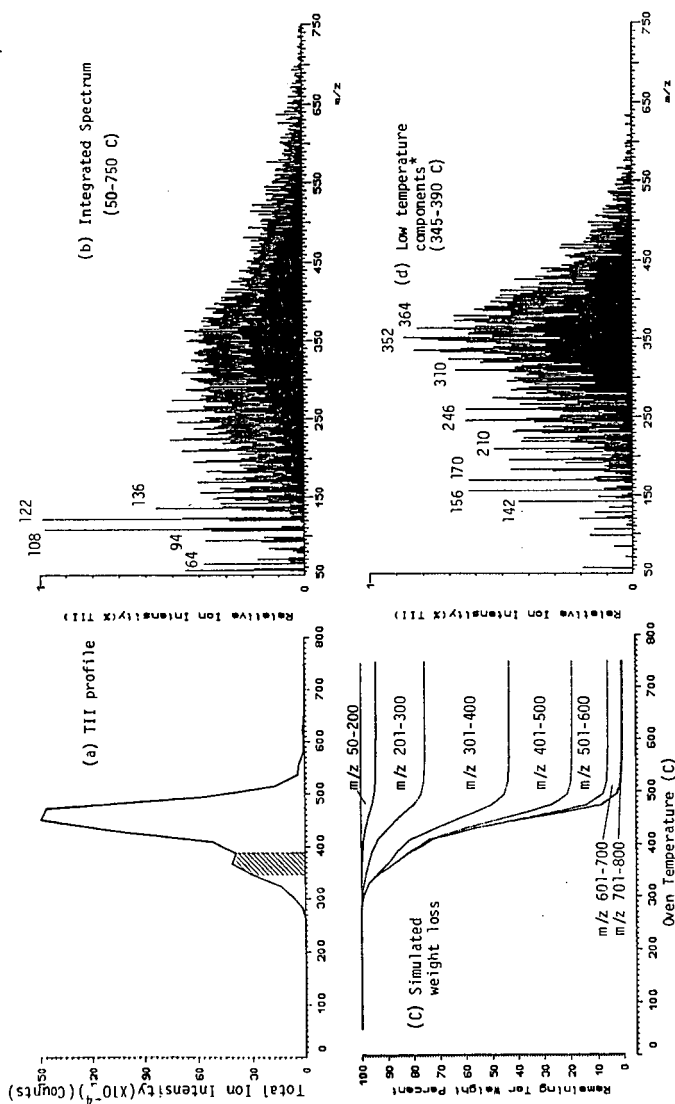


Figure 4. Py-FIMS results from Pittsburgh #8 (hvb) coal. Simulated weight loss curves are cumulative for each mass range, thus the lowest curve shows the total weight loss of tar components. \*Integrated spectrum of hatched area in (a).

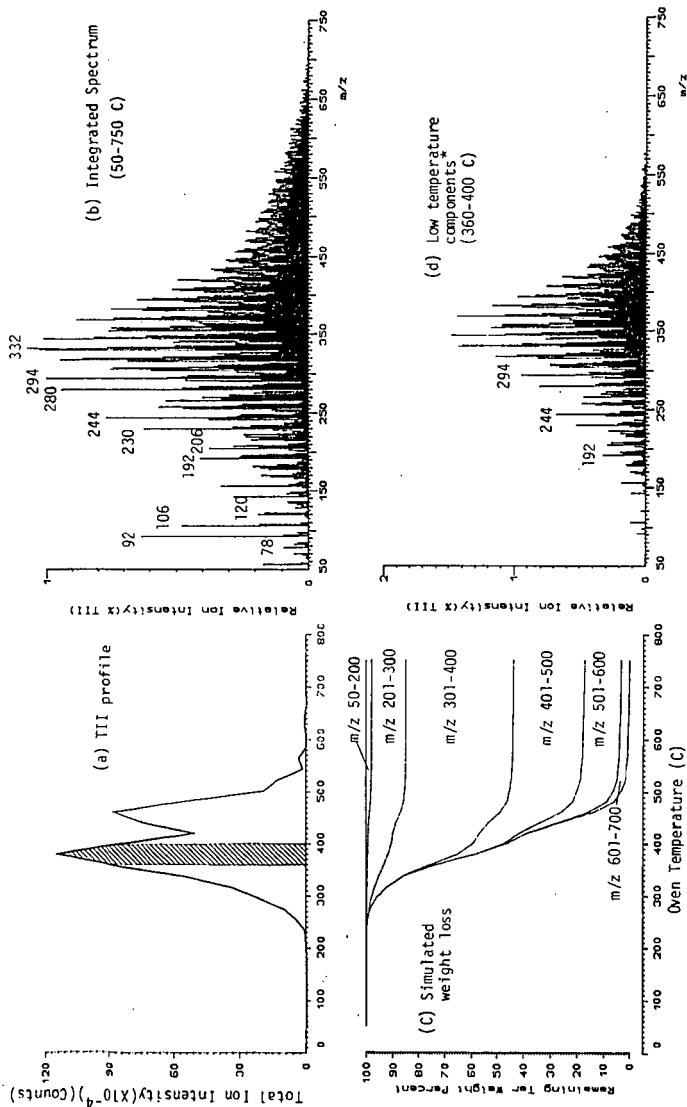


Figure 5. Py-FIMS results from Pocahontas #3 (lvb) coal. Simulated weight loss curves are cumulative for each mass range, thus the lowest curve shows the total weight loss of tar components. \*Integrated spectrum of hatched area in (a).

# COAL THERMOLYSIS MODELING. THE EFFECTS OF RESTRICTED DIFFUSION ON THERMAL REACTION PATHWAYS

A. C. Buchanan, III, P. F. Britt, and C. A. Biggs

Chemistry Division  
Oak Ridge National Laboratory  
P. O. Box 2008  
Oak Ridge, Tennessee 37831-6197

## INTRODUCTION

The technique of model compound immobilization by covalent surface attachment is being employed to investigate the potential impact of restricted diffusional mobility on the thermal reactivity of coal. This restricted mobility may be imposed in coal as a consequence of its cross-linked, macromolecular structure.<sup>1</sup> Thermolysis studies at 350-400 °C of model coal structures covalently attached to a silica surface have shown that significant perturbations in free-radical reaction mechanisms can occur, and result in altered reaction rates and product distributions compared with corresponding fluid phase behavior.<sup>2-4</sup> A detailed study of the thermolysis of surface-immobilized bibenzyl ( $\equiv\text{SiOPhCH}_2\text{CH}_2\text{Ph}$ , represented as  $\sim\text{PhCH}_2\text{CH}_2\text{Ph}$ ) showed that the rate of unimolecular C-C homolysis is similar to that in fluid phases.<sup>2</sup> However, restricted radical and substrate mobility led to the onset of complex free-radical chain pathways on the surface, which produced substantial isomerization, cyclization-dehydrogenation, and hydrodealkylation of bibenzyl moieties. Recent studies have focused on the thermally induced, free radical chain decomposition reactions for surface-immobilized 1,3-diphenylpropane ( $\sim\text{Ph}(\text{CH}_2)_3\text{Ph}$ ,  $\sim\text{DPP}$ )<sup>3</sup> and 1,4-diphenylbutane ( $\sim\text{Ph}(\text{CH}_2)_4\text{Ph}$ ,  $\sim\text{DPB}$ ).<sup>4</sup> For  $\sim\text{DPP}$ , we find that both the reaction rate and product composition are strongly dependent on surface coverage and, hence, the proximity of  $\sim\text{DPP}$  molecules and hydrogen abstracting radicals on the surface. The rates and selectivities of these key bimolecular reaction steps on the surface might also be affected by the structure of neighboring molecules. In the current study, we are beginning to probe this feature by examining the influence of the structure of co-attached aromatic molecules such as biphenyl ( $\sim\text{PhPh}$ ) and diphenylmethane ( $\sim\text{PhCH}_2\text{Ph}$ ) on the reaction rate and regioselectivity in the thermolysis of  $\sim\text{DPP}$ .

## EXPERIMENTAL

Procedures for the synthesis of surface-attached 1,3-diphenylpropane ( $\sim\text{DPP}$ ) by the condensation reaction of  $p\text{-HOPh}(\text{CH}_2)_3\text{Ph}$  (HODPP) with the surface hydroxyls of a high surface area, fumed silica have been fully described elsewhere.<sup>3</sup>  $p\text{-Phenylphenol}$  ( $p\text{-HOPhPh}$ ) was purified by multiple recrystallizations from benzene/hexanes to give a product with GC purity of >99.9%.  $p\text{-Benzylphenol}$  ( $p\text{-HOPhCH}_2\text{Ph}$ ) was first eluted from a silica column with benzene, and then recrystallized two times from benzene/hexanes to give a product with GC purity of >99.9%.

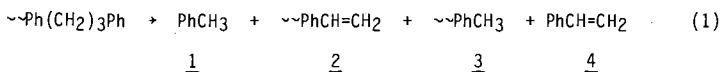
The two-component surfaces were prepared in a manner analogous to that used for preparation of  $\sim\text{DPP}$  with both phenolic components adsorbed onto the surface in a single step prior to the surface attachment reaction. In one case for comparison, a batch of  $\sim\text{DPP}/\sim\text{BP}$  was synthesized in two separate steps. A

saturation coverage batch of  $\sim\sim$ BP was prepared and then reacted with HODPP in a second step to chemically exchange some  $\sim\sim$ DPP molecules with  $\sim\sim$ BP molecules. All surface coverages were analyzed by GC with internal standards following a base hydrolysis procedure that liberates the attached organics as phenols.<sup>3</sup>

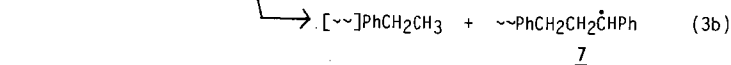
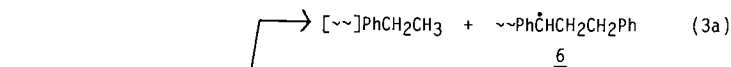
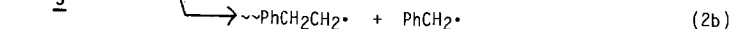
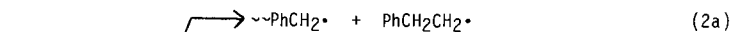
Thermolyses were conducted in sealed, evacuated ( $2 \times 10^{-6}$  torr) T-shaped tubes as described previously.<sup>2,3</sup> Volatile products were collected in a cold trap and analyzed by GC and GC-MS with the use of internal standards. Surface-bound products were removed from the silica by base hydrolysis, and the resulting phenols (or the corresponding trimethylsilyl ether derivatives) were analyzed as above.

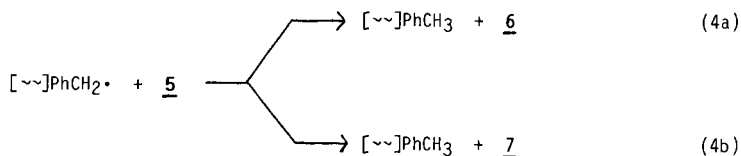
## RESULTS AND DISCUSSION

Thermolysis of  $\sim\sim$ DPP at 345–400 °C and low conversions produces the four major products shown in Eq. 1 analogous to the cracking reaction observed previously for fluid phase DPP.<sup>5–7</sup> The formation of these products was explained by a



free-radical chain decomposition pathway shown in Eqs. 2–7 with the propagation steps being Eqs. 4–6.<sup>3a</sup> The bracket notation used in Eqs. 3 and 4 indicates that two equations may be written in each case, one with a surface-immobilized species and one with a vapor-phase species.





Regioselectivity in the reaction is determined by the relative rates of formation of radicals 6 and 7 by hydrogen abstraction, since the unimolecular  $\beta$ -scission steps (Eqs. 5 and 6) occur very efficiently. We found an increasing selectivity for formation of the product pair 3 and 4 (cycling through radical 7) with increasing  $\sim\sim$ DPP conversion and decreasing initial surface coverage. The surface coverage effect is illustrated at low  $\sim\sim$ DPP conversions in Table 1, which contains new data obtained at a coverage of 0.102 mmol/g. We again use the styrene/toluene yield ratio as the experimental measure of selectivity. Our interpretation is that, at lower coverages, geometrical constraints induced by restricted radical and substrate mobility increasingly favor hydrogen abstraction at the benzylic methylene site farthest from the surface (to favor formation of radical 7) as  $\sim\sim$ DPP molecules become increasingly distant from hydrogen abstracting radicals on the surface. This concept is illustrated in Figure 1.

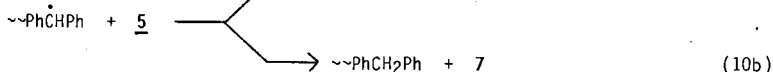
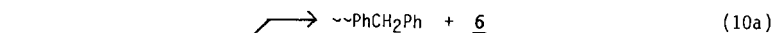
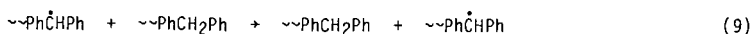
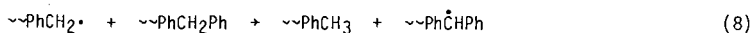
We also note that the rate of thermolysis of  $\sim\sim$ DPP is more sensitive to changes in surface coverage than fluid phase DPP is to changes in concentration.<sup>5,6</sup> A four-fold decrease in surface coverage resulted in a rate depression by a factor of 17-23.<sup>3a</sup> This result again appears to reflect a substantial sensitivity of bimolecular reaction rates on the surface, such as in Eqs. 3 and 4, to the proximity of  $\sim\sim$ DPP molecules and hydrogen abstracting radicals.

Initial results on the influence of co-attached aromatics on the thermolysis of  $\sim\sim$ DPP are shown in Table 2. Surprisingly, the presence of co-attached biphenyl molecules does not have a major effect on the  $\sim\sim$ DPP thermolysis rate or selectivity compared with corresponding coverages of  $\sim\sim$ DPP alone. This does not appear to be the result of the sample preparation procedure since a  $\sim\sim$ DPP (0.126 mmol/g)/ $\sim\sim$ BP (0.509 mmol/g) batch prepared by a two-step chemical exchange process (see experimental) gave results comparable to those from surfaces prepared by the conventional one-step procedure. The reason for the apparent 2-fold rate acceleration for the  $\sim\sim$ DPP surface in the presence of  $\sim\sim$ BP is under further investigation.

These preliminary data also show that the presence of diphenylmethane molecules has a dramatic effect on the thermolysis of  $\sim\sim$ DPP. Independent control



experiments show that  $\sim\sim\text{DPM}$  alone is thermally stable under the reaction conditions employed (as is  $\sim\sim\text{BP}$ ).<sup>2</sup> In the presence of  $\sim\sim\text{DPM}$ , the rate of  $\sim\sim\text{DPP}$  thermolysis is substantially accelerated (ca. 8-fold increase in conversion) compared with  $\sim\sim\text{DPP}$  alone at comparable coverages, while the product regioselectivity (which is normally  $>1.0$  and increases with larger  $\sim\sim\text{DPP}$  conversions) is essentially eliminated. Our hypothesis at this stage is that bimolecular hydrogen transfer reactions on the surface involving  $\sim\sim\text{DPM}$  are providing a chemical means for "mobilizing" radical centers in an immobilized environment. This radical exchange concept is illustrated in Eqs. 8-10.



This hypothesis of rapid bimolecular hydrogen exchange reactions occurring on the surface is supported by our recent findings that surface-immobilized 1,4-diphenylbutane ( $\sim\sim\text{Ph}(\text{CH}_2)_4\text{Ph}$ ) at high coverages thermally cracks at 400 °C through both benzylic and nonbenzylic radical sites with little selectivity as a consequence of such hydrogen exchange reactions.<sup>4</sup> In the present case, hydrogen transfer steps 8 and 9 could effectively decrease the distance between a radical center and a  $\sim\sim\text{DPP}$  molecule on the surface. This would remove the conformational restrictions leading to the regiospecificity in the reactions that favor formation of 7 over 6, which occur at equivalent  $\sim\sim\text{DPP}$  coverages without  $\sim\sim\text{DPM}$ . By similar arguments, the enhanced  $\sim\sim\text{DPP}$  thermolysis rate could result from an enhanced rate of production of 6 and 7. Research is in progress to further elucidate this interesting reaction chemistry for mixed component surfaces.

#### SUMMARY

Two-component surfaces of surface-attached  $\text{Ph}(\text{CH}_2)_3\text{Ph}$  ( $\sim\sim\text{DPP}$ ) with either  $\text{PhPh}$  ( $\sim\sim\text{BP}$ ) or  $\text{PhCH}_2\text{Ph}$  ( $\sim\sim\text{DPM}$ ) have been prepared, and their thermolysis behavior compared with that of  $\sim\sim\text{DPP}$  alone at comparable surface coverages. In the case of  $\sim\sim\text{DPP}/\sim\sim\text{BP}$  surfaces, no major effects on the  $\sim\sim\text{DPP}$  thermolysis rate or product selectivity were observed. On the other hand, the presence of  $\sim\sim\text{DPM}$  molecules led to a significant acceleration (ca. 8-fold increase in conversion) in the  $\sim\sim\text{DPP}$  thermolysis rate while eliminating the regioselectivity in product formation that was observed previously for  $\sim\sim\text{DPP}$  alone. Our current hypothesis based on this preliminary data is that facile bimolecular hydrogen exchange reactions on the surface involving  $\sim\sim\text{DPM}$  are eliminating conformational restraints on hydrogen abstraction reactions from  $\sim\sim\text{DPP}$  by effectively placing

radicals more proximate to ~DPP molecules on the surface. These results have significant implications for the efficiency with which similar structural features will thermally decay in coal at low temperatures (350-400 °C) by radical chain processes under conditions of restricted diffusion.

#### ACKNOWLEDGMENT

Research was sponsored by the Division of Chemical Sciences, Office of Basic Energy Sciences, U.S. Department of Energy under contract DE-AC05-84OR21400 with Martin Marietta Energy Systems, Inc.

#### REFERENCES

1. (a) Green, T. K.; Kovac, J.; Brenner, D.; Larsen, J. W., In Coal Structure; Meyers, R. A., Ed.; Academic Press: New York, 1982; Chapter 6. (b) Larsen, J. W.; Green, T. K.; Kovac, J., J. Org. Chem. 1985, 50, 4729. (c) Brenner, D., Fuel 1985, 64, 167. (d) Lucht, L. M.; Peppas, N. A., Fuel 1987, 66, 803.
2. Buchanan, III, A. C.; Dunstan, T. D. J.; Douglas, E. C.; Poutsma, M. L., J. Am. Chem. Soc. 1986, 108, 7703.
3. (a) Buchanan, III, A. C.; Biggs, C. A., J. Org. Chem. 1989, 54, 517. (b) Buchanan, III, A. C.; Biggs, C. A., Prepr. Pap. - Am. Chem. Soc., Div. Fuel Chem. 1987, 32(3), 175.
4. Britt, P. F.; Buchanan, III, A. C.; Biggs, C. A., Prepr. Pap. - Am. Chem. Soc., Div. Fuel Chem., 1989, 34(2), 567.
5. Poutsma, M. L.; Dyer, C. W., J. Org. Chem. 1982, 47, 4903.
6. Gilbert, K. E.; Gajewski, J. J., J. Org. Chem. 1982, 47, 4899.
7. King, H.-H.; Stock, L. M., Fuel 1984, 63, 810.

Table 1. Effect of Surface Coverage on the Selectivity for Thermolysis of  $\sim\sim\text{Ph}(\text{CH}_2)_3\text{Ph}$  at 375 °C.

$\sim\sim\text{DPP}$ Coverage (mmol/g)	$\sim\sim\text{DPP}$ Conversion Range (%)	Selectivity <sup>a</sup>
0.566, 0.586 <sup>b</sup>	2.2 - 4.8	1.00 - 1.03
0.142 <sup>b</sup>	1.5 - 3.1	1.11 - 1.17
0.102	1.0 - 2.8	1.24 - 1.30

<sup>a</sup>Defined as  $\text{PhCH}=\text{CH}_2/\text{PhCH}_3$  yield ratio over the  $\sim\sim\text{DPP}$  conversion range given.

<sup>b</sup>Data from reference 3a.

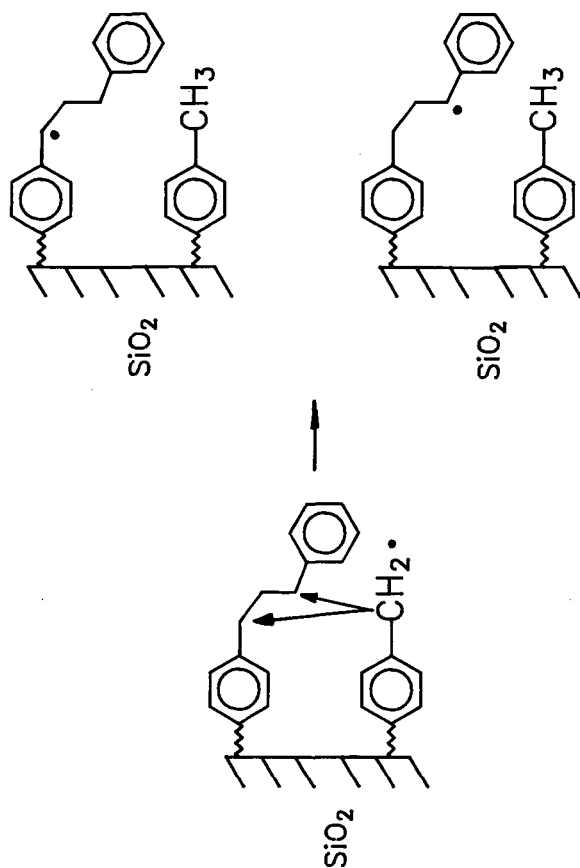
Table 2. Effect of Co-Attached Aromatics on the Thermolysis of  $\sim\sim\text{Ph}(\text{CH}_2)_3\text{Ph}$ .<sup>a</sup>

Coverage (mmol/g)			$\sim\sim\text{DPP}$ Conversion (%)	Selectivity <sup>c</sup>
$\sim\sim\text{DPP}$	$\sim\sim\text{BP}^b$	$\sim\sim\text{DPM}^b$		
0.142 <sup>d</sup>	-	-	2.2	1.17
0.142 <sup>d</sup>	-	-	2.2	1.16
0.132 <sup>d</sup>	-	-	2.6	1.17
0.150	0.462	-	4.5	1.15
0.145	0.505	-	5.5	1.11
0.126 <sup>e</sup>	0.509	-	4.6	1.12
0.133	-	0.368	17	0.99
0.133	-	0.368	16	0.99
0.168	-	0.398	19	0.96

<sup>a</sup>Thermolyses were performed at 375 °C for 150 min. <sup>b</sup> $\sim\sim\text{BP}$  and  $\sim\sim\text{DPM}$  are surface-attached biphenyl ( $\sim\sim\text{PhPh}$ ) and diphenylmethane ( $\sim\sim\text{PhCH}_2\text{Ph}$ ), respectively.

<sup>c</sup>Defined as  $\text{PhCH}=\text{CH}_2/\text{PhCH}_3$  yield ratio. <sup>d</sup>Data from reference 3a. <sup>e</sup>Material prepared by a two-step exchange procedure; see text.

Figure 1· Regiospecific Hydrogen Abstraction



## THE EFFECT OF RANK ON COAL PYROLYSIS KINETICS

M.A. Serio, P.R. Solomon, Z.Z. Yu, R. Bassilakis,  
J.R. Markham, and J.G. Klapheke

Advanced Fuel Research, Inc., 87 Church Street, East Hartford, CT 06108 USA

### INTRODUCTION

The rank dependence of coal pyrolysis kinetics has been a subject of controversy for several years (1,2). Some have claimed that the rank variations are responsible for much of the several orders of magnitude variation in reported rates. Others have found that in experiments where the rank was the only experimental parameter, these differences were not very profound when compared to the large variations in reported rates. We subscribe to the latter view, but acknowledge that there are circumstances where relatively small rank variations may be important. One such case is the prediction of coal fluidity (3). The maximum fluidity observed experimentally depends strongly on rank and the time temperature history (heating rate, final temperature). When modeling fluidity, it was found that relatively small differences in the methane evolution rate (which is related in our model to moderate temperature crosslinking) and in the tar evolution rate (which is related to the bridge breaking rates) adversely affected the fluidity predictions (3).

This paper examines the variation in kinetic rate at both low and high heating rate. The rate for methane and for tar evolution from the Argonne premium coals were determined from a series of experiments which were done with these coals over a range of low heating rates. These will be compared with kinetic parameters determined by Burnham et al. (4) for the same coals. In addition, we report weight loss data obtained at high heating rates in a transparent wall reactor (TWR) on samples of Pittsburgh Seam and Zap Lignite coals, which provide further information on the rank variations of kinetic rates.

### EXPERIMENTAL

**Coal Properties** - Elemental data are given for the Argonne coals in Ref. 5. The analyses of the Zap Lignite and Pittsburgh Seam bituminous coals used in the TWR experiments are given in Ref. 6.

**Reactors** - Pyrolysis experiments were done with the Argonne premium coals at heating rates 3, 30, 50, and 100°C/min up to 900°C in a TGA with FT-IR analysis of evolved products (TG-FTIR). The TG-FTIR is the TG/Plus from Bomem, Inc. The TG/Plus couples a DuPont 951 TGA with a Bomem Michelson 100 FT-IR spectrometer (7,8).

High heating rate measurements were made in a transparent wall reactor (TWR) which has been previously described (9). Nitrogen is passed through a heat exchanger and enters a reaction section at approximately 850°C. Coal entrained in cold nitrogen carrier gas is injected through a co-axial 7 mm diameter tube into the preheated stream. An octagonal glass enclosure shields the pyrolyzing stream from room air currents. This reactor allows particle temperature measurements to be made. One difficulty in making pyrolysis kinetic measurements at high temperatures is that the measurement of particle temperatures from the particle's emitted radiation is difficult if the pyrolysis reactor has hot walls. In this case, wall radiation scattered by the particles interferes with the emitted radiation. To overcome this problem, the reactor section has relatively cold walls. The glass enclosure has movable KBr windows to allow access to the flame for radiation measurements. Particle velocities were measured using a video camera under slightly oxidizing conditions which allowed a small

percentage of the particle to ignite.

**Temperature Measurements** - To measure the temperature of pyrolyzing coal particles, several other problems had to be overcome. Because pyrolysis in this reactor occurs at relatively low temperatures (600-800°C), the measurements are made in the mid-infrared where sufficient energy is emitted. In addition, coal is not a gray-body and its emissivity changes during pyrolysis. To overcome this problem, the temperature has been measured using the amplitude of the radiated energy in a frequency range where the emissivity is close to one and independent of the extent of pyrolysis. The transmission is used to determine the emitting surface area of the particles. Finally, soot radiation can make the particle temperature appear much higher than it really is. Measurements have been made with a gas temperature of 850°C so soot formation did not occur.

## RESULTS AND DISCUSSION

**Low Heating Rate Studies** - A recent paper reported the development of a network model for coal fluidity based on the FG-DVC model and its application to predict fluidity data for a wide range of coals (3). In order to fit both the fluidity data and species evolution data, the bridge breaking and methane kinetic rates were adjusted from those used in the original model which were rank independent (5,6,10). An independent investigation was made of the rank dependence of the pyrolysis kinetics by doing experiments in a TG-FTIR reactor over a series of heating rates (3, 30, 50, 100°C/min) with three coals (Pocahontas, Pittsburgh, No. 8, and Zap lignite) which are at the extremes and midpoint of the rank range for the Argonne set. A comparison of the rank dependence of the rate constants for bridge breaking, tar evolution and CH<sub>4</sub> evolution at 450°C determined from analyzing the TG-FTIR data at several heating rates and from fitting the FG-DVC model to fluidity, weight loss and methane evolution data at a single heating rate (3°C/min) is shown in Fig. 1.

The rates for tar evolution are lower than those used in the FG-DVC model for bridge breaking. This makes sense since the latter does not include transport. The rates for tar evolution or bridge breaking vary by about a factor of 10 if the Pocahontas coal is excluded, which is consistent with previous results for coals from the same range of ranks. If the Pocahontas is included, the rank variation for the tar evolution or bridge breaking rates is about a factor of 50. The rates for tar evolution are consistent with those obtained by Burnham et al. for total hydrocarbon evolution from Rock Eval analysis of the same coals (6). This data is also shown in Fig. 1.

The kinetic parameters determined by either method for methane (loose) evolution are similar and show a much lower rank dependence. Finally, the rank independent parameters used in the original FG model are shown as horizontal dashed lines. These are in better agreement with results from the lower rank coals, which was expected since the set of coals used to obtain those parameters did not include the higher rank coals (5,6,10).

**Experiments in the TWR** - Particle temperatures were determined by matching the theoretical curves to the radiance at 1600 cm<sup>-1</sup>, where the emissivity is approximately 1.0 (11,12). Measurements were obtained for both coals at positions between 5 and 40 cm. In addition, char samples were captured at a number of locations. The results for the Zap lignite are summarized in Fig. 2. Figure 2a shows the temperature measurements in the reactor made using a thermocouple and the FT-IR E/T technique to determine both particle and CO<sub>2</sub> temperatures (9,11-13). The CO<sub>2</sub> and particle temperatures agree to within 100°C. The thermocouple temperature measurements averaged across the estimated width of the particle stream are also in reasonable agreement except early in the reaction when the particle are heating and late when the gas is cooling. The particle's heating rate is about

5000°C/sec.

Figure 2b shows the weight loss determined by ash tracer analysis. These are compared to predictions of the FG-DVC model (10). The kinetic rates for bridge breaking used in the FG-DVC model is  $k_b = 8.6 \times 10^{14} \exp(-228,500/RT) \text{ sec}^{-1}$ . The predictions using 10 and 0.1 times this rate are also shown. The agreement for the Zap lignite is best with the highest of the three rates.

The results for the Pittsburgh Seam coal are presented in Fig. 3. These results also agree best for  $k_b \times 10$ . Consequently, the high heating rate data do not show much of a rank variation. However, these measurements are not as sensitive to factors of 10 difference in rate.

## CONCLUSIONS

- The rank dependence of the chemical kinetic rates is important in the prediction of fluidity data. It can also be important in predicting tar evolution rates for very high rank coals (>90% carbon). It is less important in the case of methane.
- Both the low and high heating rate experiments support the previous conclusion that the rank variations for kinetic rates are usually less than a factor of 10, except for the case of tar evolution from very high rank coals.

## ACKNOWLEDGMENTS

This work was supported under DOE Contract DE-AC21086MC23075. Richard Johnson is the Project Manager.

## REFERENCES

1. Solomon, P.R. and Hamblen, D.G., Finding Order in Coal Pyrolysis Kinetics, Topical Report Submitted to the U.S. Department of Energy, under Contract No. DE-AC21-FE05122, (1983), also Progress in Energy and Combustion Science, 9, 323, (1983).
2. Solomon, P.R. and Serio, M.A., "Evaluation of Coal Pyrolysis Kinetics", in Fundamentals of the Physical-Chemistry of Pulverized Coal Combustion, (J. Lahaye and G. prado, Eds.), 126, Marinus Nijhoff Publishers, (1987).
3. Solomon, P.R., Best, P.E., Yu, Z.Z. and Deshpande, G.V., A Macromolecular Network Model for Coal Fluidity, to be presented at ACS Fuel Chem. Div. Meeting, Miami, FL, (9/89).
4. Burnham, A.K., Oh, M.S., Crawford, R.W. and Samoun, A.M., Energy and Fuel, 3, 42, (1989).
5. Serio, M.A., Solomon, P.R., Yu, Z.Z., Deshpande, G.V. and Hamblen, D.G., ACS Fuel Chem. Preprints, 33, (3), 91 (1988).
6. Serio, M.A., Hamblen, D.G., Markham, J.R., Solomon, P.R., Energy and Fuel, 1, 138, (1987).
7. Carangelo, R.M., Solomon, P.R. and Gerson, D.J., Fuel, 66, 960, (1987).
8. Whelan, J.K., Solomon, P.R., Deshpande, G.V., and Carangelo, R.M., Energy and Fuel, 2, 65, (1988).
9. Solomon, P.R., Chien, P.L., Carangelo, R.M., Best, P.E., and Markham, J.R., "Application of FT-IR Emission/Transmission (E/T) Spectroscopy to Study Coal Combustion Phenomena", 22nd Symp. (Int) on Combustion, The Combustion Institute, Pittsburgh, PA (in press).

10. Solomon, P.R., Hamblen, D.G., Carangelo, R.M., Serio, M.A. and Deshpande, G.V., *Energy and Fuel*, **2**, 405, (1988).
11. Best, P.E., Carangelo, R.M., Markham, J.R., and Solomon, P.R., *Combustion & Flame*, **66**, 47, (1986).
12. Solomon, P.R., Carangelo, R.M., Best, P.E., Markham, J.R., and Hamblen, D.G., 21st Symp. (Int) on Combustion, The Combustion Institute, Pittsburgh, PA p. 437, (1986).
13. Solomon, P.R., Carangelo, R.M., Best, P.E., Markham, J.R., and Hamblen, D.G., *Fuel*, **66**, 897, (1987).



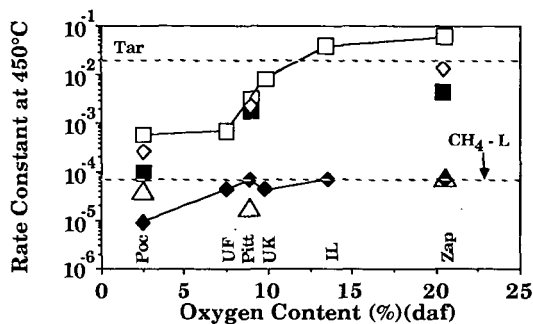


Figure 1. Comparison of Kinetic Rates at 450°C for Bridge Breaking (BB), Tar Formation, and Methane-Loose ( $\text{CH}_4$ -L) Formation. (■) BB, (△)  $\text{CH}_4$ -L from FG-DVC Model Fits; (□) Tar, (●)  $\text{CH}_4$ -L from TG-FTIR Data; (◇) Tar from Burnham et al. (4). Dashed Lines are Rank Independent Parameters.

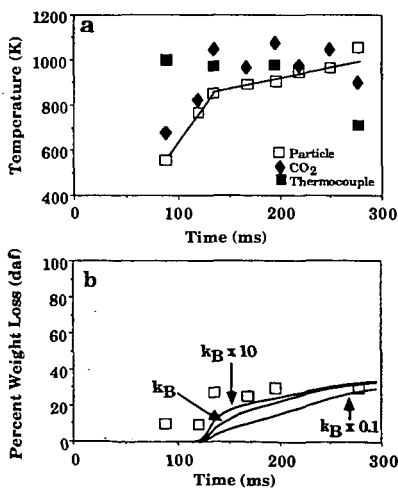


Figure 2. Pyrolysis Results for Zap North Dakota Lignite. a) Temperatures and b) Weight Loss.

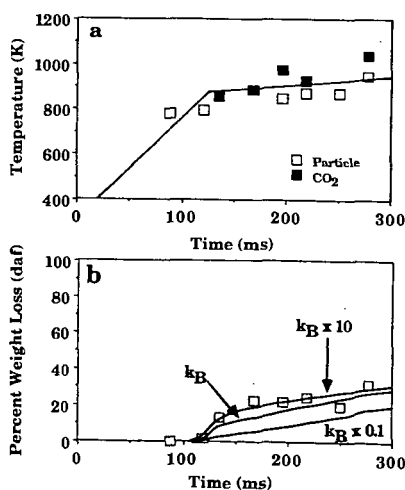


Figure 3. Pyrolysis Results for Pittsburgh Seam Bituminous. a) Temperatures and b) Weight Loss.

## Development of Char Structure During Pyrolysis of a hvB Bituminous Coal

Guangwei Huang and Alan W. Scaroni  
The Combustion Laboratory  
The Pennsylvania State University  
404 Academic Activities Bldg  
University Park, PA 16802

### Introduction

When coal particles are heated rapidly they undergo radical changes in chemical and physical properties. The sequence of events in the pyrolysis of caking coals includes heatup of the coal particles, plasticity development in part of, or the whole coal particle, swelling, and resolidification. The occurrence and the nature of these events depend on the rank of the coal and its thermal history. The rate of evolution of gaseous products of pyrolysis is affected by mass transfer inside the pores. There has been much work published on the thermoplastic behavior of coals and the development of char structure during pyrolysis of pulverized coal (1-7). However, very little work has been published recently on the behavior of millimeter-sized coal particles, even though this size is widely used in fluidized-bed combustors. The objective of this work was to study the morphological and compositional changes in the chars produced during pyrolysis of single particles of a hvB bituminous coal using scanning electron microscopy (SEM) and elemental analysis (CHN). The mechanism for the transport of volatiles out of the pyrolyzing coal particle is also discussed.

### Experimental

Pyrolysis experiments on single coal particles 1.0 to 1.5 mm in diameter were performed in an electrically heated reactor, details of which have been provided elsewhere (8,9). A hvB bituminous coal (volatile matter 48.3%, fixed carbon 47.1%, ash 4.6%) was used in this study. For each run, a coal particle was injected into the preheated reactor which was maintained at a temperature of 973 K under an atmosphere of nitrogen. The temperature gradients in the gas surrounding the particle were measured using a thermocouple array and the particle surface temperature history was obtained by extrapolation of the measured gas temperature gradients (10). Before particle injection, the gas flow was stopped so that the experiments were carried out essentially in a stagnant system.

Char particles were collected and weighed after the required residence time by quickly withdrawing them from the reaction zone into an extension of the quartz reactor and cooling them to ambient temperature using a high flow rate of nitrogen. A calculation considering the heat lost by convection and radiation from the particles estimated that cooling to below 400 °C occurred in about 0.5 s.

### Results and Discussion

The elemental analyses of the coal and the chars were performed using a Leco CHN-600 Determinator and are given in Table 1. Weight Loss was calculated by averaging the weight of the chars from 10 runs conducted at the same residence time. The weight loss ( $\Delta W$ ) and the average rate of weight loss ( $\Delta W/\Delta t$ ) between successive

residence times are also listed in Table 1. The rate of weight loss reached its maximum between 3.0 to 4.5 s, representing a 21% loss in weight in 1.5 s (weight loss from 15 to 36 %), and then decreased sharply. Little weight loss was observed after 6 s. The overall H/C ratio for the volatiles evolved was 1.48. The atomic H/C ratio for the volatiles released between successive residence times (H/C (VM)) was determined from a mass balance using the weight loss and ultimate analysis data. The H/C ratio for the volatiles released before 763 K was slightly greater than one, probably due to the carbon oxides released during decarboxylation. The H/C ratio for the volatiles released during the maximum rate of weight loss was one, which is almost the same as the value for the starting coal (0.94). These numbers indicate that a) the relatively weakly held volatiles such as those physically adsorbed in micropores or weakly bonded to the coal matrix are released early and possess intermediate H/C values (1 to 2); b) the major fraction of the volatiles escaping the coal particles by evaporation or diffusion during the peak devolatilization rate has the lowest H/C value, (~1); and c) the volatiles released last, produced by cracking or repolymerization reactions, have the highest H/C value (~4).

A scanning electron microscope was used to examine the changes in morphology of the coal particles at different extents of reaction. Figure 1 shows the surface of a raw coal particle. At 1000 $\times$  magnification the surface appears smooth with some scattered mineral clusters. An obvious morphological change (Figure 2) is observed for the char after 1.5 s corresponding to about 10 % weight loss. The coal particle appears to have become partially molten and some open holes and bubbles have appeared. Further pyrolysis (Figure 3) yields a char having a molten surface with fewer bubbles than observed at shorter residence time. The fact that some bubbles adjacent to open holes have deflated instead of bursting suggests the development of internal pores which allowed the decomposed gaseous products trapped in the bubbles to escape through new tunnels into neighboring open holes. The char morphology shown in Figure 4 clearly indicates a surface structure resulting from resolidification of the fluid phase. A lower magnification of 500 $\times$  was used for Figure 4 to show a larger region of the char surface. It is noteworthy to see a strong viscous fluid pattern for a hvB bituminous coal classified as a poor coking coal. The viscous coal melt has flown over the particle surface and sealed some open holes. The exiting gases have had to escape from a very viscous melt to create vortex-like structures (as seen in the concentric patterns in Figure 4). A similar behavior for a lignite was reported by Solomon et al (11), suggesting that the melting, bubbling, and swelling phenomena may be due to the high heating rate, which mitigates the crosslinking reactions responsible for decreasing fluidity.

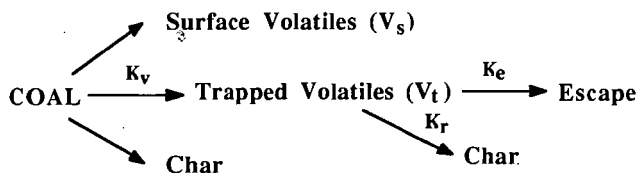
The open holes mentioned above are defined as those found on the particle surface throughout the pyrolysis (from beginning to end). An open hole is distinguished from a blowhole by its smooth rim and larger size (5~30  $\mu\text{m}$  in diameter). The cause of early open holes on the coal surface may be the expansion of existing micropores or the localized acceleration of devolatilization due to catalytic pyrolysis by the dispersed mineral clusters.

In order to examine internal structural changes, a char particle collected at a residence time of 5 s at about 40% weight loss was cut in half and the electronmicrograph of its cross section is shown in Figure 5. The very porous internal structure shown in Figure 5 consists of interconnected pores formed by coalescence of bubbles of various size, with a few large pores (up to 400  $\mu\text{m}$ ) in the center and many smaller ones near the surface. The surface, however, is a relatively dense crust with a thickness of about 30  $\mu\text{m}$ . Figure 6 shows the pore structure beneath the dense crust, revealed by peeling off the surface layer of the char, indicating a more developed structure consisting of many macro-

and meso-pores. The internal surface area provided by these pores, nevertheless, would generally be inaccessible for char gasification and/or combustion unless the reactants could pass through the dense crust.

A major morphological change in the chars during the maximum rate of evolution of volatiles can be seen from Figure 3 (residence time of 3 s and 15% weight loss) and Figure 4 (residence time of 5 s and 40% weight loss). Before the peak rate of volatiles evolution (Figures 2 and 3), the coal particle undergoes melting, bubbling, and release of volatiles through the open pores and from the external surface. Blowholes generated from bursting of bubbles were not observed before 15% weight loss. Most bubbles caused by the buildup of pressure of the gaseous products in the coal melt either flattened (Figure 3), or later burst (Figure 4) during the period of the maximum rate of volatiles evolution.

Suuberg et al (12) suggested a competitive kinetic scheme for metaplast evaporation and repolymerization. In order to explain the increased rate of evolution of volatiles with higher heating rate Niksa et al (13) classified the products of primary devolatilization into two categories, namely the light, stable volatiles from the elimination of peripheral groups and the reactive intermediates from bridge cleavage. A similar scheme with more emphasis on volatiles transfer out of coal particles is proposed below:



Here, surface volatiles ( $V_s$ ) represent the easily released volatiles, generated by decomposition reactions on the external surface or on the internal surface of the open holes, leaving the particle as soon as they are formed. The resistance to volatiles liberation from the coal particle is negligible. Trapped volatiles ( $V_t$ ) are those produced within the tortuous micropores or trapped in the bubbles, and are not registered as weight loss even though they are decomposed from the coal matrix. Trapped volatiles can either: (1) leave the particle by bursting the bubbles or penetrating to the particle surface or neighboring open holes, or (2) redeposit onto the solid residue (R) by repolymerization. The total yield of volatiles is given by the sum of  $V_s$  and  $V_t$ . The  $K_v$ ,  $K_r$ , and  $K_e$ , represent the rate constants for the formation and repolymerization of the trapped volatiles, and the overall mass transfer coefficient for the liberation of trapped volatiles, respectively. Both the trapped volatiles formation and the repolymerization processes have been modeled as first order reactions (14). It is suggested that  $K_e$  should be proportional to an ordinary bulk diffusion coefficient, which in turn varies inversely with pressure. Therefore, the total yield of volatiles should also be pressure sensitive.

Unlike the cenospheres found with smaller particles, large caking coal particles were observed to form porous, but not hollow, char structures with dense external crusts under the experimental conditions of this study. The volatiles were formed mainly in the internal micropores (due to the larger surface area) as trapped volatiles rather than on the external surface or in open holes as surface volatiles. This implies a dependence of the total yield of volatiles on pressure and heating rate. High pressure is detrimental to high yields

because the coal melt is more viscous and less penetrable. On the other hand, a high heating rate is beneficial due to an increased internal pressure and increased fluid range of the coal melt.

## Conclusions

Two kinds of holes were found on the surface of the chars produced from the hvB bituminous coal particles under the experimental conditions studied. The open holes played the predominant role during volatiles release, whereas the blowholes made a contribution to the weight loss only near the maximum rate of devolatilization. The average H/C ratio of the released volatiles was about 1.5. The volatiles released at higher conversion had H/C ratios as high as 4. Micrographs of the cross sections of the char particles indicated a well developed internal pore structure covered by a dense crust at the particle surface.

## References

- 1 Solomon, P. R., Ch 4 in 'Chemistry of Coal Conversion' (Ed. R.H. Schlosberg), Plenum Press, New York, 1985
- 2 Tsai, C. Y. and Scaroni, A. W., *Fuel* 1987, 66, 220
- 3 Khan, M. R., Lee, C. W., and Jenkins, R. G., *Fuel Processing Technol.*, 17, 1987, 63-71
- 4 Lowenthal, G., Wanzl, W., and Heek, K. H. V., *Fuel*, 1986, 65, 346
- 5 Shibaoka, M., *J. Inst. Fuel* 1969, 59, 42
- 6 Khan, M. R., and Jenkins, R. G., *Fuel* 1986, 65, 725
- 7 Gray, V. R., *Fuel* 1988, 67, 1298
- 8 Huang, G., Vastola, F. J., and Scaroni, A. W., *Prepr. Am. Chem. Soc., Div. Fuel Chem.*, 1987, 32 (3), 1
- 9 Huang, G., Vastola, F. J., and Scaroni, A. W., *Energy & Fuels*, 1988, 2, 385
- 10 Huang, G., Vastola, F. J., and Scaroni, A.W., *Prepr. Am. Chem. Soc., Div. Fuel Chem.*, 1988, 33 (1), 283
- 11 Solomon, P. R., Serio, M. A., Carangelo, R. M., and Markham, J. R., *Fuel*, 1986, 65, 182
- 12 Suuberg, E. M., Peters, W. A., and Howard, D. B., 17th Symp. (International) on Combustion, The Combustion Institute, Pittsburgh, 1979, 117
- 13 Niksa, S., Heyd, L. E., Russel, W. B., and Saville, D. A., 20th Symp. (International) on Combustion, The Combustion Institute, Pittsburgh, 1984, 1445
- 14 Anthony D. A., Howard, J. B., Hottel, H. C., and Meissner, H. P., 15th Symp. (International) on Combustion, The Combustion Institute, Pittsburgh, 1974, 1303

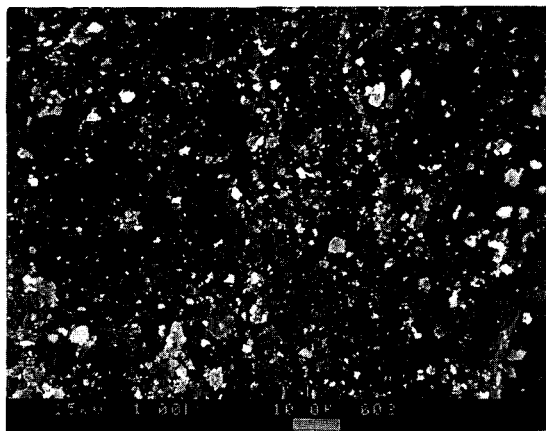
Table 1. Characterization of the Coal, Chars, and Volatiles

Time (s)	0	1.5	3.0	4.5	6.0	9.0
Weight Loss* (g/goal×100)	0	9.1	14.8	35.8	41.0	43.2
ΔW (g/goal×100)	9.1	5.7	21.0	5.2	2.2	
ΔW/Δt (g/goal/s×100)	6.1	3.8	14.0	3.4	0.7	
Ultimate Analysis**						
C	75.9	77.7	77.3	77.6	78.7	80.9
H	5.9	5.7	5.3	4.7	3.3	3.2
N	1.5	1.4	1.5	1.5	1.6	1.6
S+O	13.1	11.3	11.7	10.7	10.4	8.1
Ash	3.6	3.9	4.2	5.5	6.0	6.2
H/C (char)	0.94	0.88	0.82	0.73	0.51	0.48
H/C (VM)***	1.13	2.27	1.01	3.77	3.82	

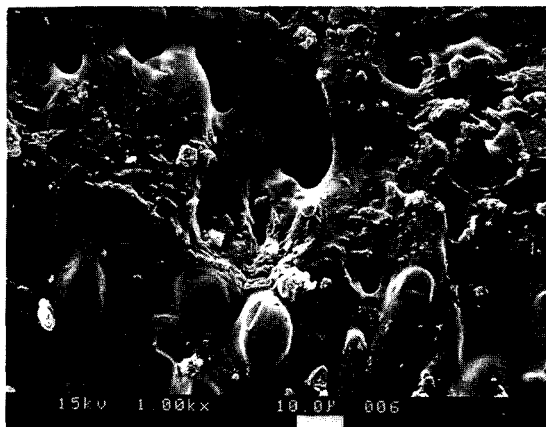
\* Weight loss is the average for 10 runs

\*\* Dry basis

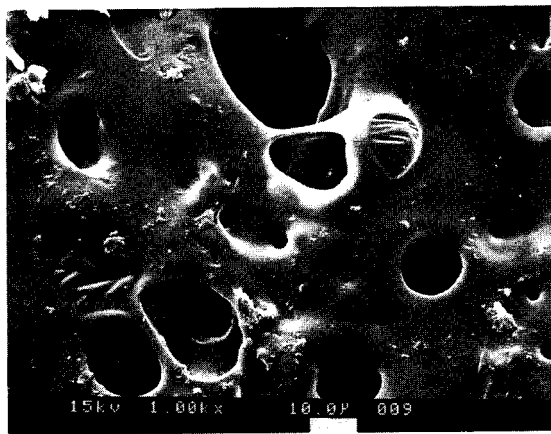
\*\*\* Overall H/C for released volatiles is 1.48



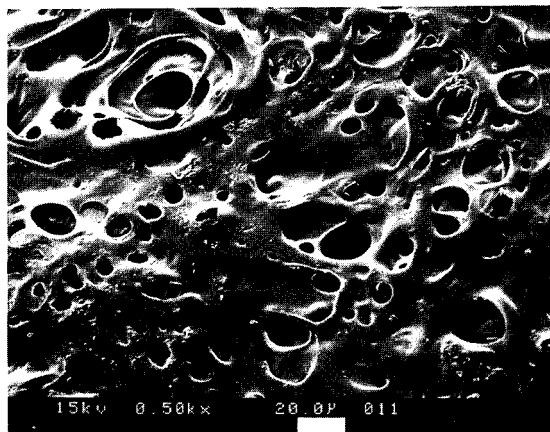
**Figure 1 SEM micrograph of a PSOC 435 coal particle**



**Figure 2 SEM micrograph of a char particle from pyrolysis of PSOC 435 at 973 K, 1.5 s**

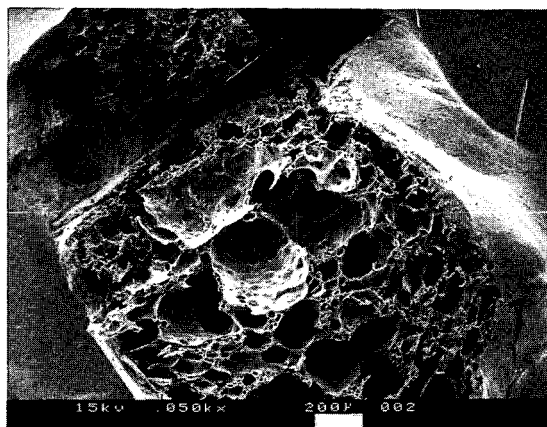


**Figure 3** SEM micrograph of a char particle from pyrolysis of PSOC 435 at 973 K, 3.0 s

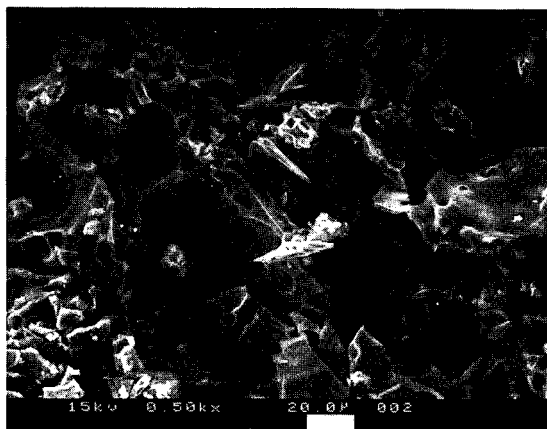


**Figure 4** SEM micrograph of a char particle from pyrolysis of PSOC 435 at 973 K, 5.0 s





**Figure 5** SEM micrograph of the cross section of a char particle from pyrolysis of PSOC 435 at 973 K, 5.0 s



**Figure 6** SEM micrograph of the pore structure beneath the particle surface of a char particle from pyrolysis of PSOC 435 at 973 K, 5.0 s

## Solid State $^{13}\text{C}$ NMR Studies of Coal Char Structure Evolution

M.S. Solum, R.J. Pugmire, D.M. Grant, T.H. Fletcher, and P. Solomon

University of Utah  
Salt Lake City, Utah 84112

Combustion Research Facility  
Sandia Livermore National Laboratory  
Livermore, California 94550

and  
Advanced Fuel Research  
Hartford, Connecticut 06108

### ABSTRACT

Solid state  $^{13}\text{C}$  NMR techniques have been used to study the evolution of char structure during pyrolysis processes. The effects of residence time, heating rate, and final char temperature are observed. The NMR data demonstrates that extensive loss of aromatic ring bridge material precedes significant change in aromatic cluster size.

### I. Introduction

All coal conversion processes are controlled by thermal decomposition in which the coal is transformed into volatiles and char. To study this process, investigators have focused on how various parameters change with the extent of decomposition (such as weight loss, volatile evolution, functional group composition, reactivity, solvent swelling ratio, tar molecular weight distribution, extract yields, etc.) In this study a series of chars for which weight loss and volatile evolution data has been previously obtained has been subjected to a variety of measurements to characterize the coal to char transformation. This report focuses on  $^{13}\text{C}$  solid state NMR spectroscopy to obtain functional group composition and other structure data. A subsequent paper will present characteristics of the same chars obtained by  $^{13}\text{C}$  NMR, FT-IR, solvent swelling, and oxygen reactivity<sup>1</sup>. The identification of the chemistry of the coal to char transformation is particularly important to the development of network models for coal thermal decomposition (1,2).

In the past decade  $^{13}\text{C}$  solid state NMR spectroscopy, because of its nondestructive nature and unique capabilities, has been used in the structural analysis of solid fossil fuel samples.<sup>3,4</sup> Using cross-polarization<sup>5-9</sup> (CP), magic angle spinning<sup>7,10-12</sup> (MAS), and dipolar decoupling techniques<sup>12,13</sup> a direct measurement of the relative number of aromatic and non-aromatic carbons is possible.<sup>14</sup> The aromaticity,  $f_a'$ , has been reported for whole coals, macerals, soil and other fossil fuel related materials.<sup>14-19</sup> Other researchers have also used dipolar dephasing (DD) techniques<sup>20-22</sup> along with normal CP/MAS integrations over selected chemical shift ranges to subdivide  $f_a'$  values into the amount of protonated and nonprotonated carbon<sup>23-27</sup>. These techniques have recently been used to estimate the average aromatic cluster size of the eight coals in the Argonne Premium Coal Sample Bank (APCSB).<sup>28</sup> In more sophisticated experiments, the analysis of chemical shielding tensor

components has been used to estimate the cluster size of anthracite coals and a fusinite coal maceral.<sup>29</sup>

We have recently turned our attention to the study of coal chars in order to assess the changes in the carbon skeletal structure of the char as compared to the parent coal. The char cluster size has been of particular interest as part of our long range goal of understanding the relationship between char structure and reactivity. We have recently begun a study of a series of chars produced from different coals at different heating rates and final temperatures.

## II. Experimental

### A. NMR Experiments

The data on coals and chars were obtained according to the method described by Solum.<sup>28</sup> Relaxation parameters were determined on the parent coal and each char as well as the carbon structural distribution.

### B. Char Preparation

Chars for this study were prepared at AFR (Zap and Pitt. #8 coals) by pyrolysis in an inert atmosphere in one of three reactors as discussed in Reference 30. The chars from the Illinois No. 6 coal were prepared in an entrained flow reactor at the Combustion Research Facility at Sandia National Laboratories as described in Reference 31.

## III. Results and Discussion

### A. Cluster Size Determination

The carbon skeletal structure of the parent coals and related chars are presented in Tables 1-4. The definition of these carbon structural distribution parameters is given by Solum, et. al.<sup>28</sup> As pointed out in the analysis of the APCSB coals, the amount of bridgehead carbon  $f_a^B$  present is an important structural parameter. The mole fraction of aromatic bridgehead carbons,  $\chi_b$ , is defined as  $\chi_b = f_a^B / f_a'$  where  $f_a'$  is the fraction of aromatic carbons present in the sample. This parameter is important as it can be used to estimate the aromatic cluster size (see reference 28).

### B. Char Structure Analysis

The data in Tables 1-4 represent a variety of experimental conditions on different coals. The data on the Zap coals were obtained by both rapid and slow heating techniques on two different coal samples. For the slow heating case, the chars were produced by heating an APCSB Zap coal at 0.5 deg/sec with a 3 minute hold at the final temperature. The rapid heating Zap, Illinois #6, and Pittsburgh #8 data were taken at heating rates of  $\sim 10^4$  deg/sec at various temperatures and residence times. The Illinois #6 data was obtained from a set of char samples produced from a 106-125  $\mu$  coal. The reactor residence times were 50 ms and 105 ms with sample temperatures measured at 850 and 1100°K, respectively for the two samples.

At this stage of the work, it appears that four structural parameters are informative. In Figure 1, the relationship between aromaticity and cluster size is apparent for the Pitt. #8 coal and related chars. Only char data from Table 3 for similar residence times are included in the plot. It is apparent from the remainder of the data on Pitt. #8 (and the Illinois #6 data) that

residence time at a given temperature is an important consideration. However, sufficient data is not available at the present time to permit a detailed assessment of this effect although the general trend is obvious from the data. While the aromaticity changes with temperature, it is clear that the cluster size has not changed at 973°K. At 1073°K, one observes the onset of cluster growth (but not at the shorter residence time, i.e., 1073°K/12" in Table 1) by a factor of 25% while at 1373°K the cluster size has doubled. In Figure 2 the percent of aliphatic carbon is compared to the aromatic attachment sites/100 carbons. As the pyrolysis temperature increases a significant reduction is noted in the aliphatic carbon content. However, the number of attachment sites (alkyl and alkoxy functional groups) on aromatic carbons exhibits essentially no change. Similar effects are noted in Figures 3 and 4 for the rapid and slow heating conditions for Zap lignite.

The data on PSOC-1493 represents only two samples from the pyrolysis series. While the aromaticity has started to increase at 1100°K (105 ms residence time) the aromatic cluster size has not changed (Figure 5). However, the decrease in aliphatic carbon content together with little or no change in the number of aromatic attachment sites per 100 carbon atoms is similar to the other char data.

The four sets of char data demonstrate a consistent pattern. As the temperature and/or residence time for pyrolysis increases, one observes an increase in aromaticity of the char (relative to the parent coal) and a concomitant decrease in the amount of aliphatic carbon remaining in the char. The average aromatic cluster size does not change in the 850-1100°K temperature range for the two high volatile bituminous coals studied and only increases significantly above ~ 1100°K. In the case of the Zap coals, the slow heating data displays a monotonic relationship between cluster size and final temperature. In the rapid heating case, the effects of residence time on cluster size is clearly evident. Whether this effect is due to the fact that the temperatures are in excess of 1000°K (1073 and 1873) or to the nature of the coal is not clear from this limited data set.

The other significant phenomena are the decrease in aliphatic carbon content with essentially no variation in the number of aromatic bridge and side chain attachment sites. These data are consistent with models<sup>1,2</sup> for coal devolatilization wherein tar production is accompanied by expulsion of bridge material and stabilization of dangling free radicals by hydrogen transfer reactions or expulsion as light gases. Hence, the data suggest that the evolution of char structure is a function of heating rate, final temperature, and residence time. During pyrolysis, aliphatic rich material is preferentially expelled as tar and light gases. In the initial stages of pyrolysis, it appears that there is no onset of aromatic cluster size growth until the temperature approaches 1100°K in the fast heating regime, i.e.,  $\sim 10^4$ /sec. The loss of aliphatic carbon appears to be through expulsion of bridge material which leaves a host of short side chains and bridges still intact. The details of this mechanism are being evaluated and we will supplement these preliminary char studies with a more extensive set of data<sup>30</sup> and a set of carefully prepared char/tar pairs.

#### Acknowledgements

This work was supported by the National Science Foundation under Cooperative Agreement No. CDR 8522618. Also participating in the funding of this effort in alphabetical order, were a consortium of organizations that include: Advanced Fuel Research Inc.; Allison Division (General Motors Corp.); Babcock and Wilcox; Chevron Research Co.; Combustion Engineering, Inc.; Conoco, Inc.; Convex Computer Corp.; Corning Glass Works; Dow Chemical USA; Electric Power Research Institute; Empire State Electric Energy Research Corp.; Foster Wheeler Development Corp.; Gas Research Institute; General Electric Co.; Los Alamos National Laboratory; Morgantown Energy Technology Center (U.S. Dept. of

Energy); Pittsburgh Energy Technology Center (U.S. Dept. of Energy); Pyropower Corp.; Questar Development Corp.; Shell Development Co.; Southern California Edison; the State of Utah; Tennessee Valley Authority; and Utah Power and Light Co. Brigham Young University and the University of Utah financial support is also acknowledged. Additional support (for Advanced Fuels Research) was provided by the DOE through the Morgantown Energy Technology Center (for AFR, Contract DEAC21-86MC23075) and the Pittsburgh Energy Technology Center (for CRF and through the Consortium for Fossil Fuel Liquefaction Science for the University of Utah).

### References

1. Solomon, P.R.; Hamblen, D.G.; Carongelo, R.M.; Serio, M.A.; and Desphande, G.V. *Energy & Fuels*, 1988 2, 405.
2. Grant, D.M.; Pugmire, R.J.; Fletcher, T.H.; and Kerstein, A.R. *Energy & Fuels*, 1989, 8, (in press).
3. Axelsson, D.E. *Solid State Nuclear Magnetic Resonance of Fossil Fuels*; Multi Science: Canada, 1985.
4. Davidson, R.M. *Nuclear Magnetic Resonance Studies of Coal*; IEA Coal Research: London, 1986.
5. Hartmann, S.R.; Hahn, E.L. *Phys. Rev.*, 1962, 128, 2042.
6. Pines, A.; Gibby, M.G.; Waugh, J.S. *J. Chem. Phys.*, 1972, 56, 1776.
7. Mehring, M. In *High Resolution NMR Spectroscopy in Solids*; Diehl, P.; Fluck, E.; Kosfeld, R., Eds.; *NMR-Basic Principles and Progress*; Springer Verlag: New York 1976; Vol 11.
8. Alemany, L.B.; Grant, D.M.; Pugmire, R.J.; Alger, T.D.; Zilm, K.W. *J. Am. Chem. Soc.*, 1983, 105, 2133.
9. Alemany, L.B.; Grant, D.M.; Pugmire, R.J.; Alger, T.D.; Zilm, K.W. *J. Am. Chem. Soc.*, 1983, 105, 2142.
10. Andrew, E.R.; Bradbury, A.; Eades, R.G. *Nature*, 1959, 183, 1802.
11. Lowe, I.J. *Phys. Rev. Lett.*, 1959, 2, 285.
12. Schaefer, J.; Stejskal, E.O.; Buchdahl, R. *Macromolecules*, 1975, 8, 291.
13. Pines, A.; Gibby, M.G.; Waugh, J.S. *J. Chem. Phys.*, 1973, 59, 569.
14. VanderHart, D.L.; Retcofsky, H.L. *Fuel*, 1976, 55, 202.
15. Botto, R.E.; Wilson, R.; Winans, R.E. *Energy & Fuel*, 1987, 1, 173.
16. Sullivan, J.J.; Maciel, G.E. *Anal. Chem.*, 1982, 54, 1615.
17. Vassallo, A.M.; Wilson, M.A.; Collin, P.; Oades, J.M.; Waters, A.G.; Malcolm, R.L. *anal. Chem.*, 1987, 59, 558.

18. Hagaman, E.W.; Chambers, R.R.; Woody, M.C. *Anal. Chem.*, 1986, 58, 387.
19. Vassallo, A.M.; Wilson, M.A.; Edwards, J.H. *Fuel*, 1987, 66, 622.
20. Alla, M.; Lippmaa, E. *Chem. Phys. Lett.*, 1976, 37, 260.
21. Opella, S.J.; Frey, M.H. *J. Am. Chem. Soc.*, 1979, 101, 5854.
22. Alemany, L.B.; Grant, D.M.; Alger, T.D.; Pugmire, R.J. *J. Am. chem. Soc.*, 1983, 105, 6697.
23. Alemany, L.B.; Grant, D.M.; Pugmire, R.J.; Stock, L.M. *Fuel*, 1984, 63, 513.
24. Wilson, M.A.; Collin, P.J.; Pugmire, R.J.; Grant, D.M. *Fuel*, 1982, 61, 959.
25. Wilson, M.A.; Pugmire, R.J.; Karas, J.; alemany, L.B.; Woolfenden, W.R.; Grant, D.M.; Given, P.H. *Anal. Chem.*, 1984, 56, 933.
26. Soderquist, A.; Burton, D.J.; Pugmire, R.J.; Beeler, A.J.; Grant, D.M.; Durand, B.; Huk, A.Y. *Energy & Fuels*, 1987, 1, 50.
27. Derenne, S.; Largeau, C.; Casadervall, E.; Laupretre, F. *Fuel*, 1987, 66, 1086.
28. Solum, M.S.; Pugmire, R.J.; and Grant, D.M. *Energy & Fuels*, 1989, 3, in press.
29. Sethi, N.K.; Pugmire, R.J.; and Grant, D.M. *Anal. Chem.*, 1988, 60, 1574.
30. Solum, M.S.; Pugmire, R.J.; Grant, D.M.; Fletcher, T.H.; and Solomon, P.R. solid State  $^{13}\text{C}$  NMR Studies of Coal Char Structure Evolution: I. Submitted.
31. Fletcher, T.H. Time-Resolved Temperature Measurements of Individual Coal Particles During Devolatilization Sandia Report , SAND88-8635, September, 1988.

TABLE 1. Carbon Structural Parameters for Chars Produced from A Zap Coal Under Rapid Heating ( $10^4$  deg/sec) Conditions

MATERIAL	$f_a$	$f_{a'}$	$f_a^C$	$f_H^H$	$f_a^N$	$f_a^P$	$f_a^S$	$f_a^B$	$f_{a1}$	$f_{a1}^H$	$f_{a1}^*$	$f_{a1}^O$
AFR ZAP	.74	.61	.13	.23	.38	.10	.19	.09	.26	.15	.11	.07
CHAR 800°C (0.5 m)	.75	.63	.12	.21	.42	.10	.17	.15	.25	.12	.13	.07
CHAR 800°C (2.4 m)	.87	.83	.04	.35	.48	.06	.19	.23	.13	---	---	.07
CHAR 1600°C (60 ms)	.83	.77	.06	.38	.39	.06	.18	.15	.17	---	---	.10
CHAR 1600°C (160 ms)	.88	.84	.04	.26	.58	.06	.22	.30	.12	---	---	.07

MATERIAL	$X_b$	CARBONS PER CLUSTER
AFR ZAP	0.148	8.5
CHAR 800°C 0.5 m	0.238	11.4
CHAR 800°C 2.4 m	0.277	13.3
CHAR 1600°C 0"	0.195	9.8
CHAR 1600°C 4"	0.357	17.8

TABLE 2. Carbon Structural Parameters for Chars Produced from Argonne PCSB Zap Coal. Hold Time at Final Temperature was 3 Minutes.

MATERIAL	$f_a$	$f_{a'}$	$f_a^C$	$f_H^H$	$f_a^N$	$f_a^P$	$f_a^S$	$f_a^B$	$f_{a1}$	$f_{a1}^H$	$f_{a1}^*$	$f_{a1}^O$
ZAP COAL	.61	.54	.07	.26	.28	.06	.13	.09	.39	.25	.14	.12
CHAR 200°C (3 min)	.72	.62	.10	.24	.38	.08	.17	.13	.28	.21	.07	.08
CHAR 300°C (3 min)	.77	.69	.08	.28	.41	.08	.18	.15	.23	---	---	.06
CHAR 400°C (3 min)	.79	.72	.07	.27	.45	.08	.19	.18	.21	---	---	.07
CHAR 500°C (3 min)	.86	.79	.07	.29	.50	.10	.17	.23	.14	---	---	.06

MATERIAL	$X_b$	CARBONS PER CLUSTER
ZAP COAL	0.167	9.0
CHAR 200°C (3 min)	0.210	10.4
CHAR 300°C (3 min)	0.217	10.6
CHAR 400°C (3 min)	0.250	12.0
CHAR 500°C (3 min)	0.291	14.1

TABLE 3. Carbon Structural Parameters for Pittsburgh #8 Coal and Chars Produced at Different Temperatures and Residence Times

MATERIAL	$f_a$	$f_{a'}$	$f_a^C$	$f_a^H$	$f_a^N$	$f_a^P$	$f_a^S$	$f_a^B$	$f_{a1}$	$f_{a1}^H$	$f_{a1}^*$	$f_{a1}^O$
PITTSBURGH #8	.71	.67	.04	.28	.39	.09	.16	.14	.29	.17	.12	.07
CHAR 700°C 24"	.80	.75	.05	.34	.41	.08	.19	.14	.20	.10	.10	.08
CHAR 800°C 12"	.76	.71	.05	.29	.42	.08	.20	.14	.24	.12	.12	.08
CHAR 800°C 24"	.80	.77	.03	.35	.42	.06	.16	.20	.20	.10	.10	.08
CHAR 1100°C 20"	.88	.85	.03	.33	.52	.04	.16	.32	.12	---	---	.06
CHAR 1100°C 24"	.89	.85	.04	.27	.58	.04	.21	.33	.11	---	---	.06
MATERIAL	$x_b$		CARBONS PER CLUSTER									
PITTSBURGH #8	0.209		10.3									
CHAR 700°C 24"	0.187		9.6									
CHAR 800°C 12"	0.197		9.9									
CHAR 800°C 24"	0.260		12.5									
CHAR 1100°C 20"	0.376		18.6									
CHAR 1100°C 24"	0.388		19.2									

TABLE 4. Carbon Structural Parameters for Chars Produced from an Illinois No. 6 Coal

MATERIAL	$f_a$	$f_{a'}$	$f_a^C$	$f_a^H$	$f_a^N$	$f_a^P$	$f_a^S$	$f_a^B$	$f_{a1}$	$f_{a1}^H$	$f_{a1}^*$	$f_{a1}^O$
PSOC-1493 COAL	.71	.67	.04	.27	.40	.08	.17	.15	.29	.15	.14	.07
CHAR 1250 K 40 mm	.72	.67	.05	.29	.38	.09	.19	.10	.28	.18	.10	.07
CHAR 1250 K 100 mm	.79	.74	.05	.34	.40	.07	.19	.14	.21	---	---	.08
MATERIAL	$x_b$		C		$\sigma + 1$							
PSOC-1493	0.224		10.8		4.0							
CHAR 1250 K 40 mm	0.149		9.6		4.0							
CHAR 1250 K 100 mm	0.189		9.7		3.4							



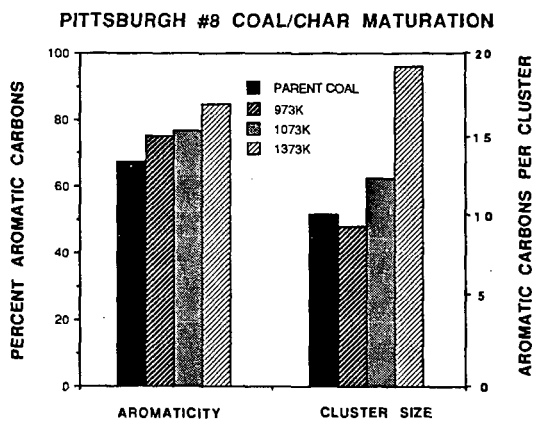


Figure 1. Relationship between aromaticity and cluster size for a Pitt. #8 coal and related chars.

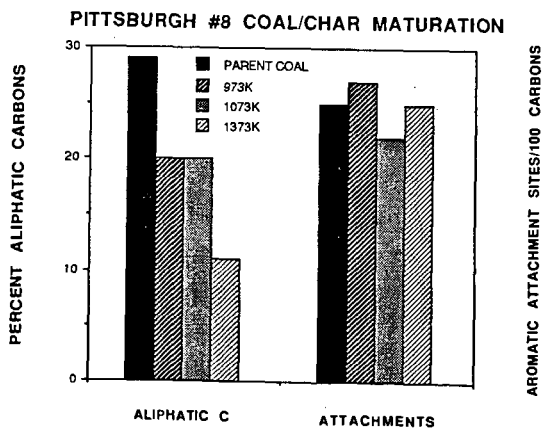


Figure 2. Relationship between aliphatic carbon content and number of aromatic attachment sites 1100 carbons for a Pitt. #8 coal and related chars.

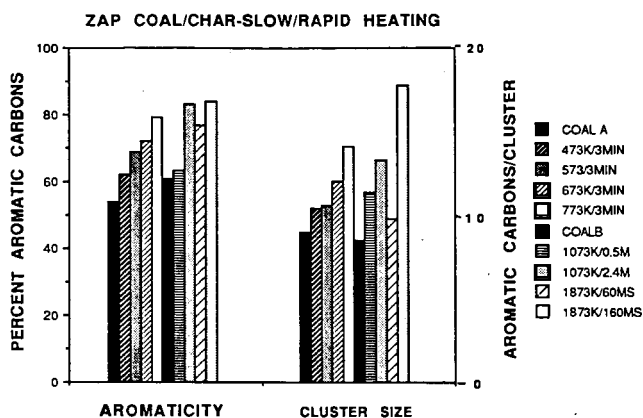


Figure 3. Relationship between aromaticity and cluster size for Zap coals and related chars heated under rapid heating conditions and APCSB Zap coal heated at 0.5 deg/sec with a hold time of 3 minutes.

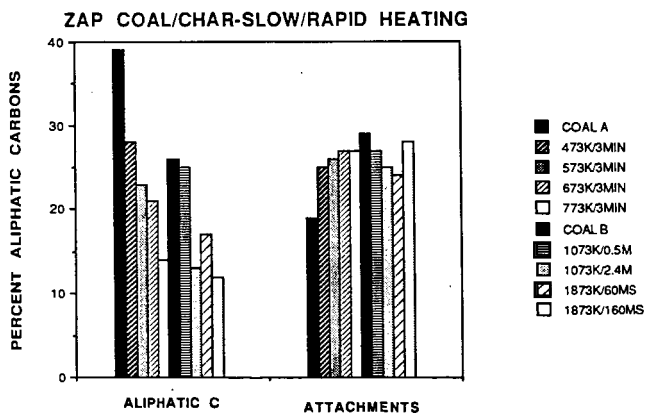


Figure 4. Relationship between aliphatic carbon content and number of aromatic attachment sites/100 carbons for the coals described in Figure 5.

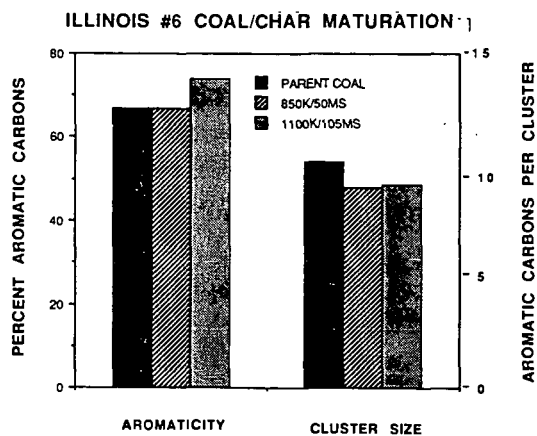


Figure 5. Relationship between the aromaticity and cluster size for an Illinois #6 coal (PSOC-1493) and related chars.

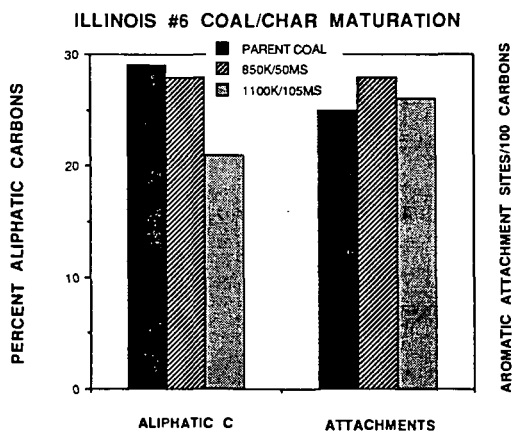


Figure 6. Relationship between aliphatic carbon content and number of aromatic attachment sites/100 carbons for the Illinois #6 coal and associated chars.

## RAPID COAL DEVOLATILIZATION IN A RADIANT COAL FLOW REACTOR

John Chen, Y. Cleo Chang, and Stephen Niksa  
High Temperature Gasdynamics Laboratory  
Mechanical Engineering Department  
Stanford University  
Stanford, CA 94305

### INTRODUCTION

Determinations of the product distributions from coal devolatilization under simulated pulverized fuel (p.f.) firing will enable better descriptions of the heat release, pollutant formation, sooting, and the evolution of polycyclic aromatic compounds (PAC). While these connections are widely recognized, only a handful of product distributions from very rapid coal devolatilization have been reported. Moreover, most of the available data was taken in entrained flow reactors, in which the time-temperature histories are obscured by mixing between preheated gases and the cold coal suspension at the injector as, for example, in Nenniger's study.<sup>1</sup> Also, since entrained process streams are very hot, the product distributions from primary devolatilization are significantly altered by secondary homogeneous chemistry.<sup>2</sup>

In this study, we introduce a novel radiant coal flow reactor which eliminates mixing and minimizes the extent of secondary chemistry. This system relies upon radiant heating of a thin coal suspension entrained into a stable, one-dimensional flow field. This furnace configuration is supported by rapid quenching to resolve reaction times on a scale of several milliseconds, aerodynamic segregation of particulate, aerosol, and gaseous products, and a battery of chemical analyses. Transient weight loss, tar yields, elemental compositions of the condensed products, and tar molecular weight distributions (MWDs) are reported for an Illinois #6, HVA bituminous coal. These results depict the devolatilization behavior at atmospheric pressure for particle residence times to 130 msec., furnace temperatures from 1000 to 1850K, heating rates exceeding  $10^4$  K/s, and suspension loadings to 2400 particles/cm<sup>3</sup>.

### EXPERIMENTAL

#### Overview and Performance Characteristics

A schematic of the radiant coal flow devolatilization experiment appears in Fig. 1. At the top of the system, a feeder delivers fuel particles into an argon entrainment stream, forming an optically-thin suspension which flows downward into a radiant furnace section. The radiant section consists of a quartz tube situated on the axis of an inductively-heated graphite cylinder. Near-blackbody thermal emission from the graphite rapidly heats the particles as they traverse the furnace. Note that since the suspension is optically thin, the radiant heat flux is uniform, and that no mixing with a preheated gas stream is involved. Also, since the argon is transparent to the radiation, the gas remains relatively cool, thereby minimizing secondary reactions among the volatiles. Even though suspension loadings up to several thousand particles per cubic centimeter are maintained, the behavior in this system can be interpreted in terms of single-particle phenomena because the interparticle separation is at least ten particle diameters.

A schematic of the induction furnace section appears in Fig. 2. It consists of a 10 cm I. D., 5 cm long graphite cylinder encased in zirconium-oxide insulation which is wrapped by four turns of a water-cooled, copper induction coil. This assembly is mounted within water-cooled copper plates and a quartz housing. The overall height of the furnace is 9.5 cm. The graphite is heated inductively by a 10 kW, 450 kHz power supply. Wall temperatures are monitored with a disappearing filament pyrometer sighted onto the graphite through a small hole in the insulation to an uncertainty of 20K. In characterization studies with two-color pyrometry, axial temperature profiles within the graphite enclosure are uniform to within 98% of the mean temperature, except for the outermost 5 mm at both ends, over which the temperature falls to about 75% of the mean value.

The coal suspension enters the 22 mm O. D. quartz tube located on the axis of the furnace from a 10 mm tube, and is stabilized by a co-flowing, argon sheath flow. The relative flowrates of

the entrainment and sheath flows are set to minimize the extent of particle dispersion over the length of the furnace. They are not matched; rather, the conditions which yielded a uniform, pencil-like flow of coal over the furnace length at each gas velocity in cold-flow visualization studies are implemented in the experiments. Also, the suspension loadings reported here are based on the cross section of the entrainment stream only, the calculated slip velocity of the particles, and the calibrated coal feedrate.

Time resolution is achieved by varying the gas transit time from the furnace inlet to an argon quench nozzle mounted near the outlet of the radiant section. The reported residence times are based on direct measurements under experimental conditions. Residence times are assigned as the time interval between the interruption of two HeNe laser beams by the leading edge of a long pulse of fuel suspension. The two beams are separated by 11 cm, and placed as close to the inlet and outlet of the furnace as possible; nevertheless, this configuration does not necessarily contain the entire length of the active radiant zone.

The pyrolysis products are segregated into char particles, tar aerosol, and noncondensable gases using virtual impaction in an aerodynamic classifier, which is sketched in Fig. 3. All of the condensed phase products (char and tar) are recovered, and the coal feedrate is stable and reproducible, so that their respective yields can be assigned gravimetrically. At the inlet, the cooled process stream contains char particles, tar aerosol, and noncondensable gases at low levels in an argon stream. Following Nenninger's<sup>4</sup> design guidelines, the inlet jet is turbulent ( $Re_j = 7000$ ), and the jet diameters and spacings are set at prescribed ratios. Most of the inlet gas stream is diverted radially outward into the annulus while a small portion passes through the central nozzle. This split is maintained by valves downstream of the impactor. Particles with sufficient inertia, viz. char particles, pass through this virtual impaction surface and into a wire mesh basket. Nominal sizes for the tar aerosol are only a few microns, while the char particles are at least 50 microns, so the separation efficiency is very high. For 50 micron coal particles, the separation efficiency into the mesh basket exceeded 97% in characterization studies, so that carry-over of char into the annulus is negligible.

A small portion of the inlet gas stream, typically 5%, passes through the lower nozzle, while the remainder of the flow convects the aerosol products into the annulus, where they deposit onto a four-stage assembly of glass fiber filters. Even though no tars could penetrate a single filter element, multiple stages are needed to manage the increasing pressure drop as the tars accumulate. The top three stages are punctured to decrease their flow resistance; nevertheless, most of the tar deposits onto these stages. The final stage scavenges the stream at the size threshold of the filters at 0.3 microns. Small amounts of aerosol also deposit onto the impactor wall, so this surface is isolated with a polypropylene liner, and such deposits are included in the reported aerosol yields.

Pure tar samples for subsequent chemical analyses are prepared by extraction with tetrahydrofuran (THF) in an ultrasonic bath, and filtration through a 0.5 micron Teflon membrane; any residue is weighed and denoted as the soot yield. The tar solution is concentrated before the remaining solvent is evaporated, following a procedure developed by Lafleur et al.<sup>5</sup>

Elemental compositions of the char and tar are measured with a Control Equipment 240X analyzer. Tar MWDs are based on gel-permeation chromatography in a Hewlett-Packard HP-1090 HPLC using three  $\mu$ Styragel columns (500Å and two 100Å) in series and broadband diode-array detection (212 to 400 nm). We adapted the calibration introduced by Rogers et al.<sup>8</sup> to diode-array detection using model compounds with molecular weights from 128 to 950; H/C ratios from 0.5 to 1.09; and proton aromaticities from 0.25 to 1. The calibration equation is:

$$\ln (MW \cdot (H/C)^{-0.0189}) = 10.7339 - 0.7611 \cdot \ln H_a + (-0.2202 - 0.0726 \cdot (\ln H/C)) \cdot V$$

where MW = Molecular weight

H/C = Hydrogen to carbon atomic ratio

$H_a$  = Proton aromaticity, aromatic/(aromatic+aliphatic protons)

$V$  = Retention volume, retention time\*flow rate

Proton distributions are determined by <sup>1</sup>H NMR with a Varian XL-400 spectrometer operating at 400 MHz and are interpreted with tabulated chemical shifts.<sup>9</sup>

## Coal Characteristics

The coal in these experiments is an Illinois #6, HVA bituminous coal (PSOC 1493D) obtained from the Pittsburgh Energy Technology Center (PETC). The ultimate and proximate analyses as reported by PETC are listed in Table I. The measured weight loss is converted to the dry, ash-free (daf) basis using the high-temperature ash value provided by PETC. These samples are aerodynamically classified, and two nominal size fractions are examined: 45-63 and 75-106 microns. All coal samples are dried at 60°C under vacuum for at least 12 hours and stored under argon.

## RESULTS

### Transient Devolatilization Behavior

The results in this section depict the influences of residence time and furnace wall temperature on the devolatilization behavior of the 75-106 micron sample. All of the results which follow are recorded at a reactor pressure a few inches of water above atmospheric, and a suspension loading of 400 particles/cm<sup>3</sup>. The volatiles yields as a function of the reactor wall temperature at average inlet gas velocities of 0.25, 0.67, and 2.0 m/s appear in Fig. 4. For a fixed inlet gas velocity, residence times at different wall temperatures will vary because the acceleration due to the changing gas density is significant.

As expected, the onset of devolatilization shifts to higher wall temperatures as the gas velocity is increased, going from 1450K at 0.25 m/s to 1800K at 2.0 m/s. For velocities greater than 0.67 m/s, the available residence times are insufficient to achieve complete devolatilization at even the highest wall temperature, indicating that the particle temperature at the furnace outlet is substantially lower than the wall temperature. But at 0.25 m/s, the ultimate yield of 56 wt% is observed at a wall temperature of 1840K. This value is significantly greater than the proximate volatile matter, as expected for these conditions of rapid heating. Also at 0.25 m/s, devolatilization commences at a wall temperature of 1500K and the product evolution rates increase rapidly for higher wall temperatures. Note that replicate runs in the study are generally reproducible to within 2 wt%.

The aerosol yields at a gas velocity of 0.25 m/s is shown with the corresponding total weight loss in Fig. 5. The aerosol yield becomes significant at 1600K and increases monotonically with temperature up to the maximum yield at 1840K, which constitutes 42% of the total volatiles yield. While the ultimate proportion of tar is consistent with expectations for atmospheric pyrolysis of HVA bituminous coals, the relatively small amount of tar at lower temperatures is surprising. For HVA Pittsburgh seam bituminous coals, the initial proportions of tar to noncondensable gases are typically 10:1 (but in studies at lower heating rates<sup>6,7</sup>), while these proportions are inverted for this Illinois #6 coal. The tar samples from these conditions were analyzed for soot, but negligible amounts were observed in all cases. This observation strongly corroborates the absence of secondary homogeneous chemistry in this system, since pyrolysis tars rapidly convert to soot at temperatures above 1450K.<sup>2</sup>

The next study examines variations in residence time, which are measured at selected wall temperatures to characterize the kinetics of mass loss and tar evolution; results appear in Fig. 6 for wall temperatures of 1570, 1680, and 1840K. Although the wall temperatures are fixed in these studies, particle temperatures are increasing exponentially with increasing residence times, and probably never achieve the wall temperature in the available furnace length.

The onset of devolatilization shifts to shorter residence times as the wall temperature is increased, as expected. The complete transient evolution is evident only at 1840K, and shows two distinct stages of product evolution which are delineated by a distinct surge in the evolution rate between 72 and 77 msec. As seen above in Fig. 5, the proportions of tar to noncondensibles are surprisingly low during the initial stages of product formation. The transient data at 1840K also show that tar evolution ceases long before the ultimate yield is achieved, as seen in the behavior of HVA bituminous coals at slower heating rates. The fraction of soot in the aerosols is again found to be negligible for all conditions. Although they do not cover the entire approach to ultimate yields, the transient yields at 1680 and 1570K reliably convey the onset of devolatilization, and the relatively small amount of tar formed during the initial stages.

The proportions of carbon, hydrogen, and nitrogen (CHN) in the char and tar for various residence times at 1840K appear in Fig. 7. Note that all values are normalized by the distributions in the parent coal as reported by PETC, and that the error bars represent the range of measured values for replicate cases. Carbon and nitrogen contents of the chars (Fig. 7a) remain the same throughout devolatilization, but the hydrogen content falls monotonically during product evolution. The corresponding elemental distributions for the tar aerosols in Fig. 7b are markedly insensitive to residence time and, hence, the extent of devolatilization. The carbon content of the aerosols closely resembles the parent coal's, but the tars are deficient in nitrogen, especially for tar collected during the earliest stages of devolatilization. As expected from the decreasing hydrogen content of the chars, the tars are uniformly enriched in hydrogen by about 40%.

Molecular weight distributions of tar generated at 66 msec. and 1840K (Fig. 6) are shown in Fig. 8. These distributions are partially integrated to depict the mass or mole fractions within 100 g/g-mole of the values on the abscissa. All tar samples have similar shapes with respect to the shoulders in the distributions. They do differ with extent of devolatilization, however, in both average molecular weights and proton aromaticity as shown in Table II for the tars generated at 1840K. With increasing residence time, hence, extent of devolatilization, the average molecular weight and proton aromaticities increase monotonically.

#### The Influence of Particle Size

In the next study, the nominal particle size was reduced to 50 microns, while the suspension loading was increased by a factor of six to 2400 particles/cm<sup>3</sup>. The temperature dependence of weight loss and tar yields at constant inlet gas velocity (1.0 and 0.25 m/s) appear in Fig. 9. Note the similarities to the features in Figs. 4 and 5 for the larger sizes at lower loading, especially at a gas velocity of 0.25 m/s. The data are virtually identical for these two cases, for both weight loss and aerosol yields. This agreement may seem counterintuitive in that these studies involve stages of transient heating and the heating rates, being inversely proportional to size, should be higher for the smaller sizes. So higher yields at lower temperatures could have been expected for the smaller sizes, but are not observed.

In conventional entrained flow systems, increasing the suspension loading decreases the aggregate convective heat flux because of poorer mixing and the higher thermal capacitance of the suspension, so thermal transients extend over longer times; i. e., heating rates are lower for denser suspensions, all else the same. But the radiant furnace behaves differently. Since the suspensions remain optically thin at even the highest loadings of interest, the radiant flux is independent of loading. But the convective losses from the suspension increase with increasing surface area, and, consequently, with increasing loadings. Consequently, higher loadings increase the heating rate of the gases, so that the gas temperature more closely tracks the increasing temperature of the suspension. In summary, in this experiment the heating rates of the suspension and of the entrainment gas increase as the loading is increased.

This argument explains the agreement among the data in Figs. 5 and 9, in so far as the higher loading would tend to increase the gas temperature, while the smaller size would tend to decrease the suspension temperature. Apparently, these two factors are compensating, although temperature measurements are needed to demonstrate this. Note that arguments which invoke interparticle interactions seem implausible because the minimum interparticle spacing is at least 12 diameters for the cases in Fig. 9.

#### Discussion

In the radiant coal flow experiment, the thermal history of the fuel particles is not complicated by mixing between hot gases and cold suspensions, which will enable more reliable determinations of the fuel's time-temperature history. Since secondary chemistry among the volatiles is minimized in this system, detailed characterizations of the product distributions from pyrolysis at very rapid heating rates are also feasible.

Weight loss and tar aerosol yields from an Illinois #6 HVA bituminous coal were recorded for furnace temperatures to 1850K and residence times to 130 msec. for two different size-cuts of coal. Qualitatively, the transient data and elemental compositions of the condensed products exhibit

several interesting features, particularly (1) a distinct surge in the devolatilization rate midway through the process; (2) surprisingly low proportions of tar (for an HVA bituminous coal) during the first stage of product evolution; and (3) a shift to higher average molecular weight and proton aromaticity with increasing weight loss.

While these data reliably convey the experimental uncertainties and operating domain of this experiment, they are not yet suitable for rate determinations or model validation studies. The fuel's thermal histories are particularly uncertain, and both models and diagnostics are now being developed to assign the particle and gas temperatures. Also, the impact on the devolatilization behavior of the short unheated length of flow tube from the furnace outlet to the quench point and the effectiveness of the argon quench have not been assessed.

#### Acknowledgement

We are happy to acknowledge funding for this work from the Exploratory Research Program of the Electric Power Research Institute and, for John Chen, a fellowship from the Link Foundation for partial financial support.

#### References

1. Nenniger, R.D., Howard, J.B., and Sarofim, A.F.: Proceedings from the 1983 International Conference on Coal Science, IEA, Pittsburgh, 1983, pp.521-524.
2. Wornat, M.J.: *Pyrolysis-Induced Changes in the Composition of Polycyclic Aromatic Compounds from a Bituminous Coal*, Sc.D. thesis, Department of Chemical Engineering, MIT, 1988.
3. Ballantyne, A., Chou, H., Neoh, K., Orozco, N., and Stickler, D.: Final Report prepared for the U. S. DOE, Pittsburgh Energy Technology Center, Contract No. DE-AC22-84PC30291, October 1983.
4. Nenniger, R.D.: *Aerosols Produced from Coal Pyrolysis*, Sc.D. thesis, Department of Chemical Engineering, MIT, 1986.
5. Lafleur, A.L., Monchamp, P.A., Plummer, and E.F., Kruzel, E.L.: *Analytical Letters* **19** (21 & 22), 2103 (1986).
6. Oh, M.S.: *Softening Coal Pyrolysis*, Sc.D. thesis, Department of Chemical Engineering, MIT, 1985.
7. Bautista, J.R., Russel, W.B., and Saville, D.A.: *Ind. Engr. Chem. Fundam.* **25**, 536, 1986.
8. Rogers, P.A., Creagh, A.L., Prange, M.M., and Prausnitz, J.M.: *Ind. Engr. Chem. Res.* **26**, 2312-2318, 1987.
9. Collin, P.J., Tyler, R.J., and Wilson, M.A.: *Fuel* **59**, 479-486, 1980.

Size (Microns)	Volatile Matter	Moisture Free Weight Percent					
		Ash	C	H	N	O	S
75 - 106	37.5	13.5	68.3	4.6	1.3	7.4	4.9
45 - 63	38.9	14.6	66.0	4.6	1.3	7.6	6.0

Table I: Proximate and Ultimate Analyses for Illinois #6, PSOC 1493D

Residence Time (ms)	Wt. Avg. $M_w$	No. Avg. $M_n$	Aromaticity $H_a$
66	706	501	0.28
72	807	557	0.28
77	813	556	0.29
87	834	568	0.33

Table II: Molecular Weight and Aromaticity of Tars Produced at 1840K



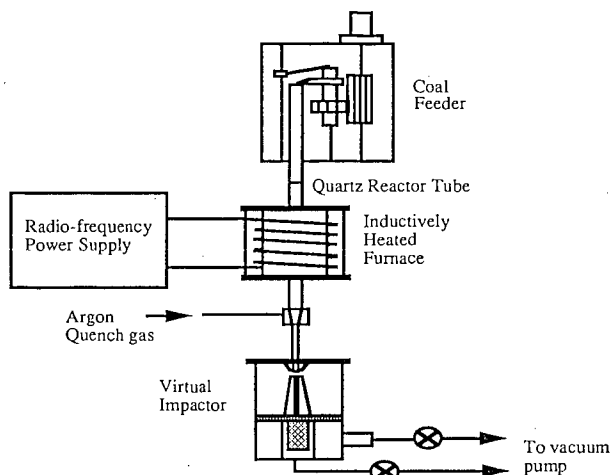


Fig. 1: The Radiant Coal Flow Reactor

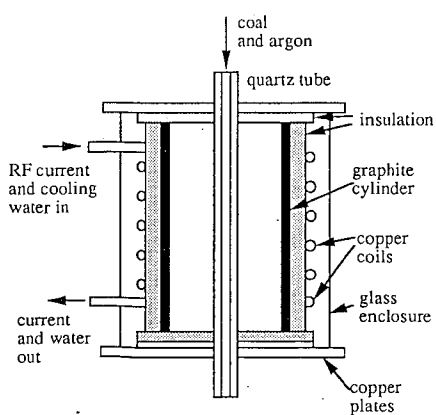


Fig. 2: The Inductively-Heated Furnace

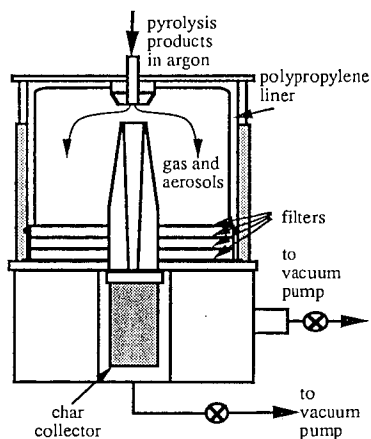


Figure 3: Schematic of the Virtual Impactor.

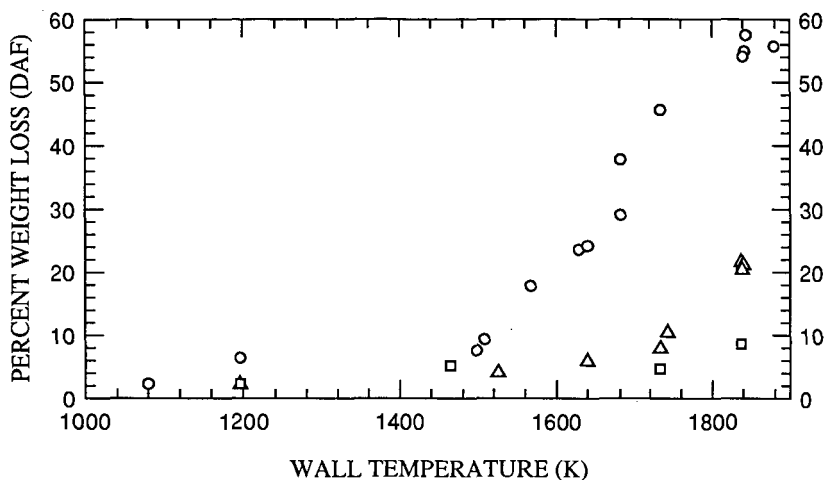


Fig. 4: Dry, ash-free weight loss for Illinois #6 coal, 75-106  $\mu\text{m}$ , ○ 0.25 m/s, △ 0.67 m/s, □ 2.0 m/s inlet gas velocity, 400 particles/cc.

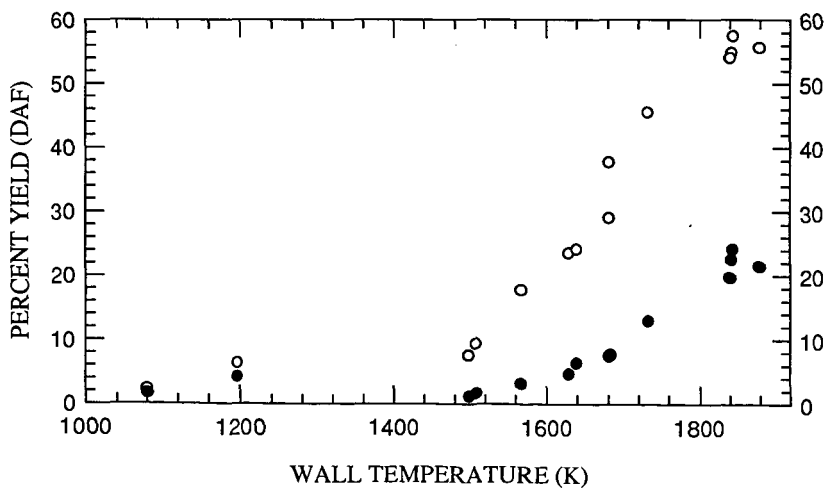


Fig. 5: Weight loss (OPEN symbols) and aerosol yield (FILLED symbols) for Illinois #6 coal, 75-106  $\mu\text{m}$  particles, 0.25 m/s inlet gas velocity, 400 particles/cc.

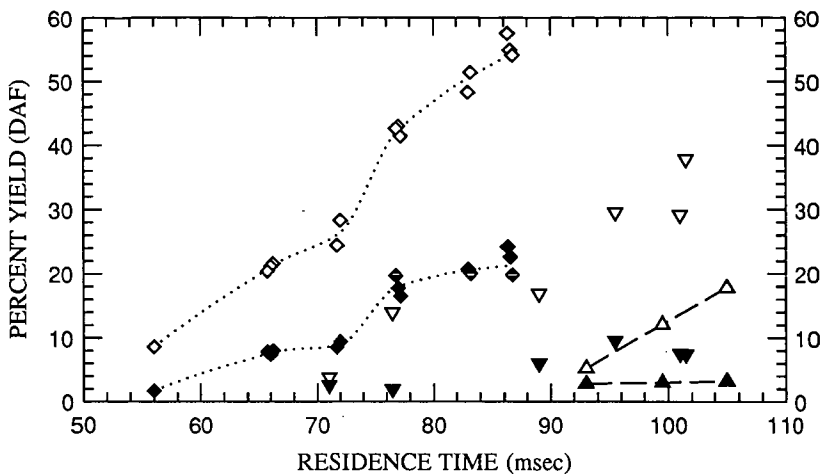


Fig. 6: Total (OPEN symbols) and aerosol yield (FILLED symbols) for Illinois #6 coal, 75-106  $\mu\text{m}$ ,  $\diamond$  1840,  $\nabla$  1680,  $\triangle$  1570 K wall temperature, 400 particles/cc.

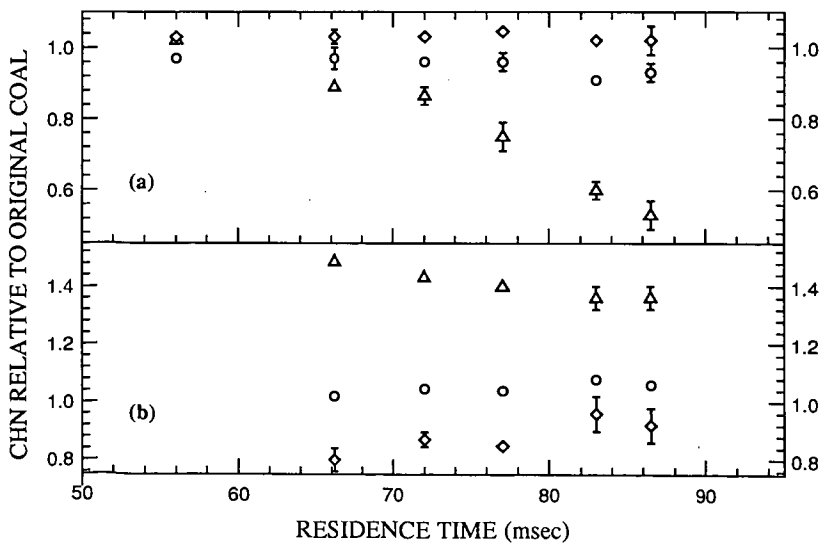


Fig. 7: Elemental composition of chars(a) and tars(b) for Illinois #6 coal, 75-106  $\mu\text{m}$ ,  $\circ$  carbon,  $\triangle$  hydrogen,  $\diamond$  nitrogen,  $T_w=1840$  K, 400 particles/cc.

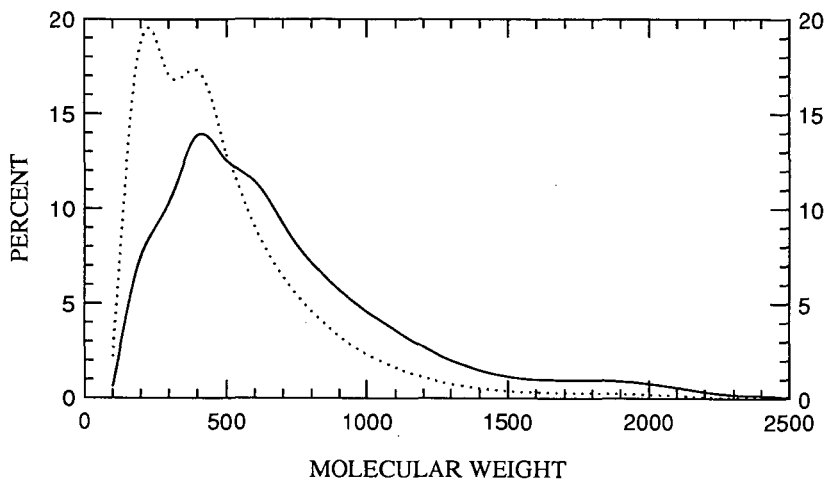


Figure 8: Molecular weight distributions of tar from Fig. 6 at 66 msec. and 1840K.  
 — weight-average distribution, ..... number-average distribution.

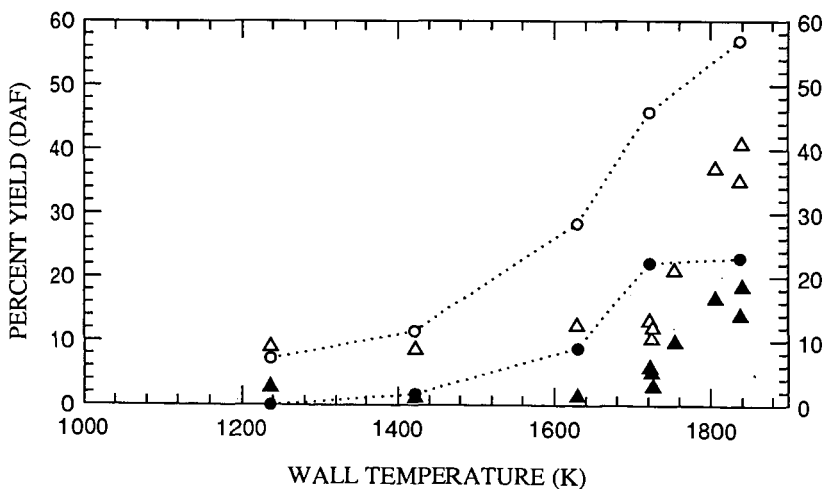


Fig. 9: Total (OPEN symbols) and aerosol yield (FILLED symbols) for 45-63  $\mu\text{m}$  particles  $\circ$  0.25 m/s,  $\Delta$  1.0 m/s inlet gas velocity, 2400 particles/cc.

## MODELING OF A COAL CARBONIZER

Amir Rehmat and Anil Goyal  
Institute of Gas Technology  
3424 S. State Street  
Chicago, IL 60616

James Van Hook and Archie Robertson  
Foster Wheeler Development Corporation  
12 Peach Tree Hill Road  
Livingston, NJ 07039

### ABSTRACT

A computer model has been developed, using data currently available in the literature, to simulate air-blown pyrolysis of coal in a carbonizer. A sorbent (limestone or dolomite) can also be added to the carbonizer to capture in-situ sulfur released into the gas. The sorbent, besides reacting with sulfur, also influences the product yields by cracking some tar to gases and soot, and hence like temperature and pressure, forms an independent parameter of the system. The char, soot, tar, spent sorbent, sulfur capture, air feed, and product gas flow rates and their compositions are determined by the computer model. This model has been used to predict carbonizer performance for Pittsburgh No. 8 bituminous coal at different operating conditions.

### INTRODUCTION

A team of companies, led by Foster Wheeler Development Corporation and consisting of Gilbert/Commonwealth, Institute of Gas Technology (IGT), Combustion Turbine Operations Division of Westinghouse Electric Corporation, and Research and Development Division of Westinghouse Electric Corporation, has embarked upon a three-phase 5-year program with the Department of Energy (DOE) to develop an advanced second-generation Pressurized Fluidized Bed (PFB) Combustion system. The targeted goals of this second-generation PFB combustion plant are a 45% efficiency and a cost of electricity that is at least 20% lower than conventional pulverized-coal-fired plants with stack gas scrubbers. In addition, the plant emissions should be within New Source Performance Standards and it should have high availability, be able to process different ranks of coal, and incorporate modular construction technologies. These goals are achieved by shifting power generation to the more efficient gas turbine cycle and away from the steam cycle while maintaining sulfur capture by the sorbent, and by providing significantly higher gas turbine inlet temperatures without increasing the bed temperature through the incorporation of a topping combustor in the system. In this arrangement, a carbonizer generates a coal-derived low-Btu fuel gas at approximately 1500°F which is mixed with flue gases from a PFB combustor operating at 1500° to 1600°F and is burned in a topping combustor to increase the gas turbine inlet temperature to approximately 2100° to 2200°F. The combustion air to the topping combustor is provided by high excess air present in the flue gas from the PFB combustor. The carbonizer thus, is an essential element of this system. The coal is primarily fed to the carbonizer. The coal char residue from the carbonizer is burned in the PFB combustor along with the balance of the plant coal, if there is any left. Calcium-based sorbent is injected into the carbonizer and PFB combustor to minimize carbonizer tar yield and

desulfurize the gases from both units. The targeted efficiency is dependent upon the performance of the carbonizer.

The coal carbonizer, depending upon the coal properties, can be designed as a bubbling or a fast fluidized-bed reactor, each having its own characteristics with respect to the coal and air injection and product recovery. These constraints associated with the carbonizer design were recognized and therefore a highly generalized model was developed to accommodate various coal carbonizer configurations. The model can simulate a bubbling or a fast fluidized-bed reactor with or without fines recycle in which the coal and sorbent can be introduced into the fluidized-bed region and/or into the freeboard region of the carbonizer. Later, the model was tailored specifically for the three most practical configurations of the carbonizer.

#### LITERATURE SEARCH AND DATA CORRELATIONS

An extensive literature search was conducted and correlations were developed for yields of various species as a function of coal properties and carbonizer operating parameters. Out of numerous data available on the subject of pyrolysis, only a handful of data were applicable for the type of coal processing used here. Much of the data for coal pyrolysis were obtained in a heated grid reactor where the coal is subjected to the desired temperature from a fraction of a second to about 2 seconds yielding only a fraction of the pyrolysis product. On the other hand, in a fluidized-bed reactor, coal is subjected to a sufficiently long residence time (a gas residence time of over 5 seconds and a solids residence time of several minutes) so that the maximum yield is typically obtained. The data available in this category were used to develop the correlations for the coal carbonization product yields and their compositions. These correlations have been developed for bituminous coals as well as for lignites to cover a wide range of feedstock properties.

The details of the literature findings and correlations development are beyond the scope of this paper. However, as an example, the effects of various parameters on the tar yield from bituminous coals are given below.

In Figure 1, the tar yield at 1 atm of inert pressure expressed as a fraction of feed carbon is plotted against temperature. The tar yield increases up to about 1250°F after which it decreases because of the increased activity of the secondary reactions of tar cracking. With respect to the effect of pressure, Suuberg *et al.* (1978) and Arendt and van Heek (1981) conducted experiments with bituminous coals and reported a considerable reduction in the carbon conversion to tar with an increase in pressure from 1 atm to 100 atm, as shown in Figure 2. The data indicate that the tar yield decreases logarithmically with pressure. A similar effect on the tar yield has been shown by Eklund and Wanzl (1981) with a subbituminous coal at 1472°F. Regarding the effect of limestone or dolomite addition, Yeboah *et al.* (1980) and Longwell *et al.* (1985) have reported an appreciable decrease in the tar yield when limestone or dolomite was added during the pyrolysis of coal (Figure 3). Simultaneously, an increase in the hydrocarbon gases, along with some soot formation on the surface of the limestone, was noticed. The effect of CaO on the char yield and other gases was very little. These observations led to a conclusion that the addition of limestone or dolomite during coal pyrolysis causes some of the evolved tar to crack into hydrocarbon gases and

soot. The effect of oxygen feed on tar yield is shown in Figure 4. The oxygen reacts with tar as well as char [Howard and Essenhig (1967), Boley and Fegley (1977), and Saito *et al.* (1987)] yielding primarily CO and CO<sub>2</sub>. However, the yields of methane, ethylene, and ethane are also higher in the presence of oxygen than those in the absence of oxygen. The increased yields are attributed to tar cracking. It should be recognized that the amount of tar and char reacting with the oxygen will depend on the amount of oxygen fed to the carbonizer, which is dictated by the reactor energy balance.

#### MODEL DESCRIPTION

The primary function of the model developed in this program is to make an estimate, for a given coal, of the product yields from a coal carbonizer operating at a specified temperature and pressure. In addition, sorbent (limestone or dolomite) may be added to capture *in-situ* sulfur released into the gas. The sorbent, besides reacting with sulfur, also influences the product yields from the coal carbonization and hence like temperature and pressure, forms distinctly an independent parameter of the system. The coal carbonizer, depending upon the coal properties, can take many forms from a bubbling fluidized bed to an entrained-flow reactor, each having its own peculiarities associated with the coal and air introduction and product recovery. These constraints were recognized and as a result a highly generalized model has been developed to accommodate different features that may be found in a coal carbonizer. Later, the model was tailored specifically to consider three practical configurations of the carbonizer.

#### General Description

For modeling purposes, and to accommodate various carbonizer configurations, the reactor has been divided into two sections, namely, the upper zone and the lower zone. The various streams leaving and entering these zones are shown in Figure 5.

The coal (stream S1) and sorbent (stream S2) are fed into the upper zone along with the transport gas (stream G4). The transport gas could be an inert gas, recycled gas, and/or air. Two additional gas streams (secondary gas streams G2 and G3) can also enter this zone, if needed. The product gas stream from the lower zone (stream G9) also enters this upper zone. Basically, the coal devolatilization takes place in the upper zone. If the air is fed to this zone (stream G1 or G4), then the oxygen present in the air will also react in this zone. The combustion in the upper zone and the sensible heat of the solids/gas from the lower zone provide the heat required for the coal devolatilization. The sulfur in the gas is captured by the sorbent present in this zone. The solids elutriated from this zone (stream S8) are captured by a cyclone and returned to the solids splitter (stream S7). The gas leaving this zone (stream G8) is the gas yield from the carbonizer. The carbonizer product gas also contains some char/sorbent fines (stream S4) and evolved tars (stream T1). The coal devolatilization temperature could be specified differently from the exit product gas temperature. Furthermore, the tar cracking occurs when sorbent is added to the system, producing soot and hydrocarbon gases. The soot formed in the carbonizer leaves the upper zone (stream S13) and enters the cyclone. The soot produced in the carbonizer may deposit on the char and the sorbent particles and thus leave the gasification system along with various solids

discharge streams (such as streams S4, S5, S6, and S12). However, for modeling purposes, this stream is assumed to be withdrawn from the cyclone (stream S14) along with the cyclone fines. The composition and flow rate of streams S13 and S14 are identical; however, they may differ in temperature.

The combustion air (stream G5) enters the lower zone along with the recycled char and reacted sorbent (stream S9) from the upper zone. The primary reaction in the lower zone is the char combustion reaction. If the temperature of this zone is high enough, then some slow rate gasification reactions will also take place. However, at present no such gasification reactions have been considered in the model. The solids stream containing char and spent sorbent (stream S5) can leave the carbonizer system from this zone. Alternatively, a part of the solids stream captured by the cyclone which contains char and spent sorbent (stream S7), may be removed from the system (stream S6). The sorbent (stream S3) can also be fed into this lower zone along with the transport gas (stream G7). For modeling purposes, it is assumed that the sorbent fed to the lower zone is calcined, if thermodynamically permitted, in this zone and transferred into the upper zone (stream S11). An additional gas stream (secondary gas stream G6) may also enter this zone, if needed. The gas produced in this lower zone enters the upper zone (stream G9).

The sorbent can be fed into the upper zone or the lower zone or into both the zones simultaneously. This will depend upon its sulfur capture capability and the system energy balance requirements for each zone. Furthermore, the temperature in each zone is assumed to be uniform, but not necessarily the same as the gas leaving the zone.

As shown in Figure 5, there are:

- Fourteen solids streams, 10 of which are unknown. Each solids stream can contain up to 15 species (C, H, O, N, S, Cl, Ash, Moisture,  $\text{CaCO}_3$ ,  $\text{MgCO}_3$ ,  $\text{CaO}$ ,  $\text{MgO}$ ,  $\text{CaS}$ ,  $\text{CaSO}_4$ , Inert).
- Nine gas streams, four of which are unknown. Each gas stream can contain up to 22 species ( $\text{CO}$ ,  $\text{CO}_2$ ,  $\text{H}_2$ ,  $\text{H}_2\text{O}$ ,  $\text{CH}_4$ ,  $\text{C}_2\text{H}_6$ ,  $\text{O}_2$ ,  $\text{N}_2$ ,  $\text{H}_2\text{S}$ ,  $\text{COS}$ ,  $\text{NH}_3$ ,  $\text{HCN}$ ,  $\text{HCl}$ ,  $\text{C}_2\text{H}_4$ ,  $\text{C}_2\text{H}_2$ ,  $\text{C}_3\text{H}_8$ ,  $\text{C}_3\text{H}_6$ ,  $\text{C}_4\text{H}_{10}$ ,  $\text{C}_6\text{H}_6$ ,  $\text{C}_7\text{H}_8$ ,  $\text{C}_{10}\text{H}_8$ ,  $\text{C}_6\text{H}_5\text{OH}$ ).
- One tar stream which is unknown (this stream is actually part of the product gas; however, for modeling purposes, it has been represented separately).

The above two zone model is an appropriate description of a fluidized-bed reactor or a fast fluidized-bed reactor in which the coal is fed into the reactor above the bed, that is, in the freeboard region. The model would also accommodate a carbonizer in which coal, sorbent, and air are fed in a single zone.

#### Yield Determination

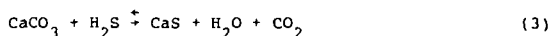
The method employed for the determination of the product yields in the carbonizer is illustrated in Figure 6. Basically, complete information is available for the coal pyrolysis as a function of temperature at 1-atm pressure in inert atmosphere. The individual effects of pressure, sorbent



(limestone or dolomite), and oxygen on these product yields are also available. However, the literature lacks information about the combined effects of these factors on the product yields. The model has been constructed by superimposing effects of these factors (Figure 6) to yield information about the products of coal pyrolysis as a function of temperature, pressure, sorbent, and oxygen.

As illustrated in Figure 6, the product yields are determined in four steps. In the first step, a complete product slate is determined for coal carbonization at 1-atm pressure in an inert atmosphere and at specified carbonizer temperature. In the second step, the yields are adjusted for pressure. In the third step, using the information derived for the effect of oxygen on pyrolysis yield at 1-atm pressure, and assuming the same effect to hold at pressure, the yields obtained in the second step are adjusted for the effect of oxygen feed. Finally in the fourth step, the effect of sorbent is integrated into the above third step. When doing so, it is again assumed that the relationships derived at 1-atm pressure between products of pyrolysis with and without the addition of sorbent in the inert atmosphere are also valid at elevated pressure in the presence of oxygen. The yields and compositions obtained in the fourth step are thus considered to have accounted for all the process parameters namely, temperature, pressure, sorbent, and oxygen.

Depending upon the partial pressure of  $\text{CO}_2$  in the carbonizer, the  $\text{CaCO}_3$  in the sorbent will either exist as  $\text{CaCO}_3$  or get calcined to  $\text{CaO}$ . This will also determine whether the  $\text{H}_2\text{S}$  will react with  $\text{CaCO}_3$  or  $\text{CaO}$ . The extent of the sulfur capture by sorbent will be determined by its approach to the appropriate reaction equilibrium. The following reactions show the calcination of  $\text{CaCO}_3$ , the reaction of  $\text{H}_2\text{S}$  with  $\text{CaO}$ , and the reaction of  $\text{H}_2\text{S}$  with  $\text{CaCO}_3$ , respectively.



Determining equilibrium decomposition pressures of calcite (Equation 1) has proved a durable problem, and dubious values have appeared in the literature. The following correlation (Squires, 1967) has been used here:

$$\log_{10} (P_{\text{CO}_2}) = -8799.7/\text{TK} + 7.521 \quad (4)$$

where --

$P_{\text{CO}_2}$  = equilibrium decomposition partial pressure of  $\text{CO}_2$  in gas, atm

TK = temperature, °K

The equilibrium for the above reactions 2 and 3 are given by the following equations (Squires *et al.*, 1971):

$$\log_{10} \{(\text{H}_2\text{O})/(\text{H}_2\text{S})\} = 3519.2/\text{TK} - 0.268 \quad (5)$$

$$\log_{10} [(H_2O)(CO_2)(P)/(H_2S)] = 7.253 - 5280.5/TK \quad (6)$$

where --

P = total system pressure, atm  
 (H<sub>2</sub>O) = mole fraction of H<sub>2</sub>O in gas  
 (CO<sub>2</sub>) = mole fraction of CO<sub>2</sub> in gas  
 (H<sub>2</sub>S) = mole fraction of H<sub>2</sub>S in gas  
 TK = temperature, °K

The product gas is also considered to be at water-gas shift equilibrium at the carbonizer exit temperature.

#### MODEL PREDICTIONS

##### Carbonizer Configuration

The computer model has been kept as general as possible to accommodate various possible carbonizer configurations. However, for the current study the simple configuration for the carbonizer shown in Figure 7 is considered. Here, coal and dolomite (sor bent) are fed into the fluidized bed, and the fines captured by the cyclone are not recycled to the reactor, instead they are directed to the combustor. The bed is fluidized primarily using air. A model representation for this case is also given in this figure. The carbonizer is essentially represented by a single stage (upper zone) configuration. The solids stream S7 is equal to the solids stream S6, while the solids streams S3, S5, S9, S10, and S11 are zero. Furthermore, the gas stream G9 is also equal to zero.

##### Model Predicted Carbonizer Performance at 14-atm Pressure

The model predicted carbonizer performance at 14-atm pressure for several cases is given here. Besides the base case at 14-atm pressure and 1500°F temperature for the Pittsburgh No. 8 bituminous coal containing 2.5% moisture, the other cases have accounted for the effect of using as-received coal without drying (6% moisture), operating the carbonizer at 1600°F, and using coal/water slurry instead of dried feed. The operating conditions and the results of the model predictions are summarized in Table 1. This table is based on a 1000 pounds of moisture-free coal feed to the carbonizer. The results on the moisture-free coal feed basis provide a better comparison of yields at different operating conditions. A detailed material balance for the base case at 14-atm pressure and 1500°F temperature is given in Figure 8.

The char, soot, spent dolomite, tar, air feed, and product gas flow rates and their compositions are determined by the computer model. The air feed requirement is based on the energy balance around the carbonizer. The heat losses from the carbonizer are assumed to be negligible. The relative humidity of the air is 50% at 70°F, which is equivalent to 1.235 mole percent moisture in the air. The H<sub>2</sub>S in the product gas is based on 92% approach to the equilibrium concentration, that is, the ratio of calculated equilibrium H<sub>2</sub>S

content in the product gas (using Equation 5 or 6) to the actual  $H_2S$  content in the product gas is 0.92. The dolomite feed rate to the carbonizer is based on feed Ca/S molar ratio of 1.75. It is also assumed that  $CaSO_4$  formation does not take place in the carbonizer. The product gas is in water-gas shift at the carbonizer exit gas temperature. The fines leaving the carbonizer have been included in the discharged solids stream. The computer model allows the formation of acetylene ( $C_2H_2$ ), naphthalene ( $C_{10}H_8$ ), and hydrogen cyanide (HCN). However, due to the lack of literature information, amounts of these species have been assumed to be zero in all the balances.

#### Model Predicted Carbonizer Performance at 10-atm Pressure

To determine the effect of pressure on the carbonizer performance, four balances were prepared under conditions similar to those of 14-atm pressure cases given above, except the pressure was reduced to 10 atm. These balances include carbonizer operation at 1500°F with the Pittsburgh No. 8 bituminous coal containing 2.5% moisture, and the effect of using as-received coal without drying (6% moisture), operating the carbonizer at 1600°F, and using coal/water slurry instead of dry feed. The operating conditions and the results of the model predictions are summarized in Table 2. The basis of these balances are the same as used for 14-atm cases.

#### CONCLUSIONS

The mathematical model has been used to predict carbonizer performance for Pittsburgh No. 8 bituminous coal at different operating conditions. The following conclusions are derived from this study.

- An increase in pressure results in a decrease in the amount of tar and soot, but somewhat reduced sulfur capture at a specified temperature.
- An increase in temperature results in a reduction in the amount of tar and soot as well as an improvement in the sulfur capture at a specified pressure.
- An increase in feedstock moisture or the use of slurry requires additional air, which in turn results in reduced amounts of tar and soot and lower quality product gas. Also, the sulfur capture is reduced due to higher steam partial pressure in the product gas.

#### ACKNOWLEDGMENT

The authors thank the Department of Energy, Morgantown Energy Technology Center, for their support of this work under Contract No. DE-AC21-86MC21023.

#### REFERENCES

- Arendt, P. and van Heek, K. H., "Comparative Investigations of Coal Pyrolysis Under Inert Gas and  $H_2$  at Low and High Heating Rates and Pressures Up to 10 MPa," Fuel **60**, 779 (1981).
- Boley, C. C. and Fegley, M. M., "Design and Operation of Two Refractory-Lined, Internally Heated, Entrained-Bed Carbonizers," Grand Forks Energy Research Center Report, Grand Forks, North Dakota, GFERC/R1/77/1 (1977).

Eklund, H. and Wanzl, W., "Pyrolysis and Hydropyrolysis of Solid Fuels at High Heating Rates ( $10^4$  K/s) Using Curie-Point Technique," Proceedings of the International Conference on Coal Science, Dusseldorf, Germany, D18, 701 (1981).

Floess, J. K., Plawsky, J., Longwell, J. P. and Peters, W. A., "Effects of Calcined Dolomite on the Fluidized-Bed Pyrolysis of a Colorado Oil Shale and a Texas Lignite," Ind. Eng. Chem. Process Des. Dev. 24, No. 3, 730 (1985).

Freihaut, J. D. and Seery, D. J., "An Investigation of Yields and Characteristics of Tars Released During the Thermal Decomposition of Coal," Preprints ACS Div. Fuel Chem. Prep. 26, No. 2, 133 (1981) March 29-April 3.

Graff, R. A., Zhou, P. and Brandes, S. D., "Conditioning Techniques for Mild Gasification to Produce Coproducts," Proceedings of Sixth Annual Gasification Contractors Meeting, 144 (1986) June.

Howard, J. B. and Essenhigh, R. H., "Pyrolysis of Coal Particles in Pulverized Fuel Flames," Ind. Eng. Chem. Process Des. Dev. 6, No. 1, 74 (1967).

Landers, W. S., Wagner, E. O., Gomez, M., Boley, C. C. and Goodman, J. B., "Entrained-Bed Carbonization of Bituminous Coal," U.S. Bureau of Mines, RI6608 (1965).

Longwell, J. P., Chang, C. S. and Peters, W. A., "Coal Gasification and Tar Conversion Reactions Over Calcium Oxide," Final Technical Report for the Period August 7, 1981-August 6, 1984, DOE/MC/16026-1839 (DE85011734), MIT, Cambridge, MA, May (1985).

Saito, M., Sadakata, M., Sato, M. and Sakai, T., "Devolatilization Characteristics of Single Coal Particles for Combustion in Air and Pyrolysis in Nitrogen," Fuel 66, 717 (1987).

Squires, A. M., "Cyclic Use of Calcined Dolomite to Desulfurize Fuels Undergoing Gasification," Advances in Chemistry Series: Fuel Gasification 69. Washington, D.C.: American Chemical Society, 1967.

Squires, A. M., Graff, R. A. and Pell, M., "Desulfurization of Fuels With Calcined Dolomite. Part 1. Introduction and First Kinetic Results," Chemical Engineering Progress Symposium Series: Important Chemical Reactions in Air Pollution Control 67, No. 115, 23. New York: American Institute of Chemical Engineers, 1971.

Suuberg, E. M., Peters, W. A. and Howard, J. B., "Product Composition and Formation Kinetics in Rapid Pyrolysis of Pulverized Coal -- Implication for Combustion," Proceedings of 17th Symposium (International) on Combustion, Leeds, England, 117 August 20-25 (1978).

Tyler, R. J., "Flash Pyrolysis of Coals. Devolatilization of Bituminous Coals in a Small Fluidized-Bed Reactor," Fuel 59, 218 (1980).

Xu, W. and Tomita, A., "Effect of Coal Type on the Flash Pyrolysis of Various Coals," Fuel 66, 629 (1987).

Yeboah, Y. D., "The Fluidized-Bed Pyrolysis of Coal in Both the Presence and the Absence of Dolomite Compounds," DSC Thesis, MIT (1979).

Yeboah, Y. D., Longwell, J. P., Howard, J. B., and Peters, W. A., "Effect of Calcined Dolomite on the Fluidized-Bed Pyrolysis of Coal," Ind. Eng. Chem. Process Des. Dev. **19**, No. 4, 646 (1980).

Yeboah, Y. D., Longwell, J. P., Howard, J. B. and Peters, W. A., "Pyrolytic Desulfurization of Coal in Fluidized-Beds of Calcined Dolomite," Ind. Eng. Chem. Process Des. Dev. **21**, No. 2, 324 (1982).

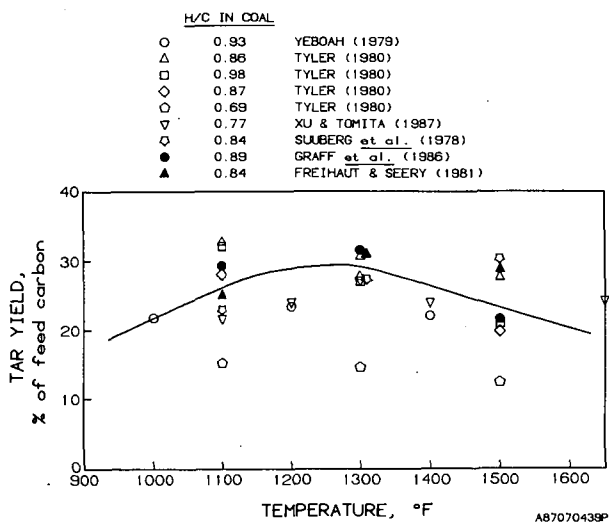


Figure 1. TAR YIELD AS A FUNCTION OF TEMPERATURE FOR BITUMINOUS COALS (Inert Atmosphere, 1 atm Pressure)

32WP/PAP/agpaper

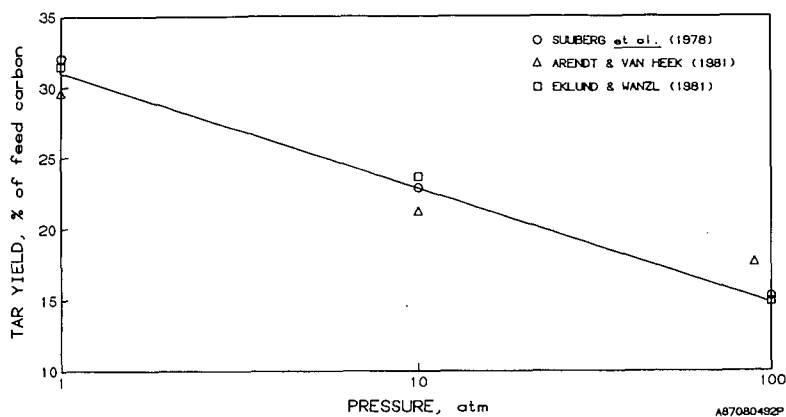


Figure 2. EFFECT OF PRESSURE ON TAR YIELD  
DURING PYROLYSIS OF BITUMINOUS COALS  
(Inert Atmosphere)

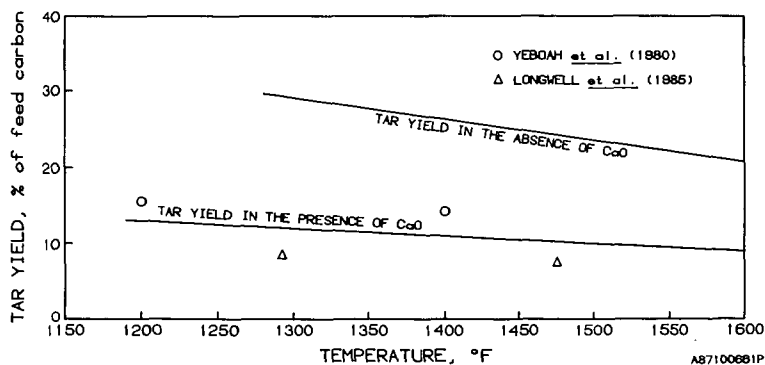


Figure 3. EFFECT OF LIME ADDITION ON  
TAR YIELD FOR BITUMINOUS COALS  
(Inert Atmosphere, 1 atm Pressure)

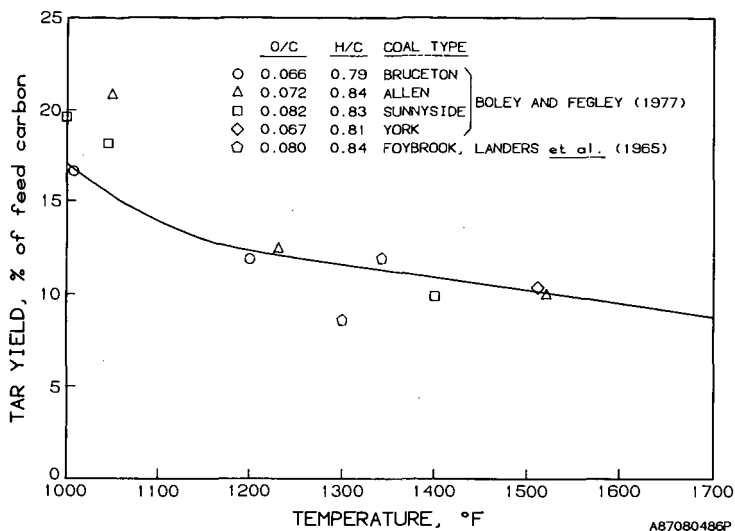


Figure 4. TAR YIELD BITUMINOUS COALS PYROLYSIS IN THE PRESENCE OF OXYGEN (1 atm Pressure)

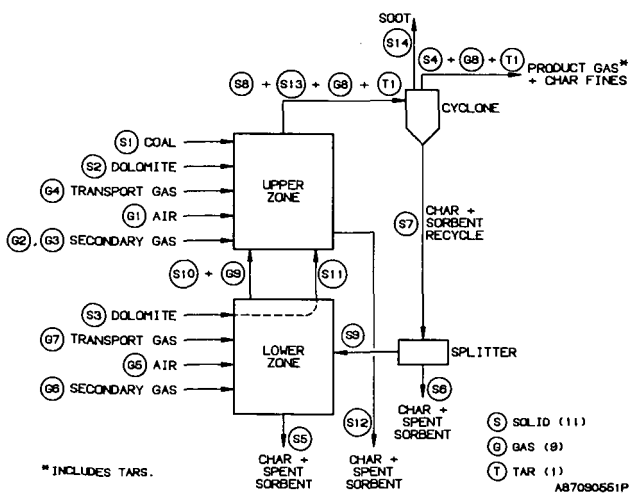


Figure 5. SCHEMATIC OF CARBONIZER MODEL

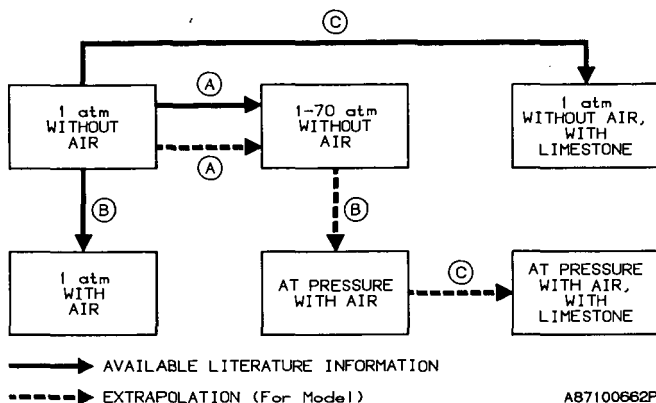


Figure 6. METHODOLOGY FOR CARBONIZER PRODUCT YIELD DETERMINATION

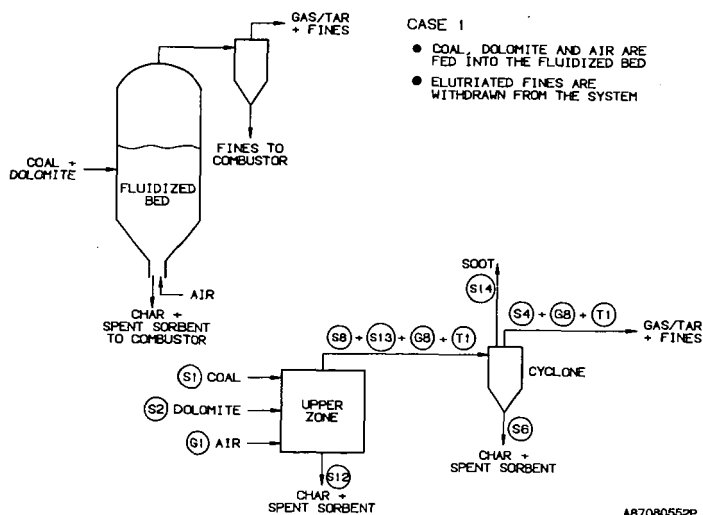
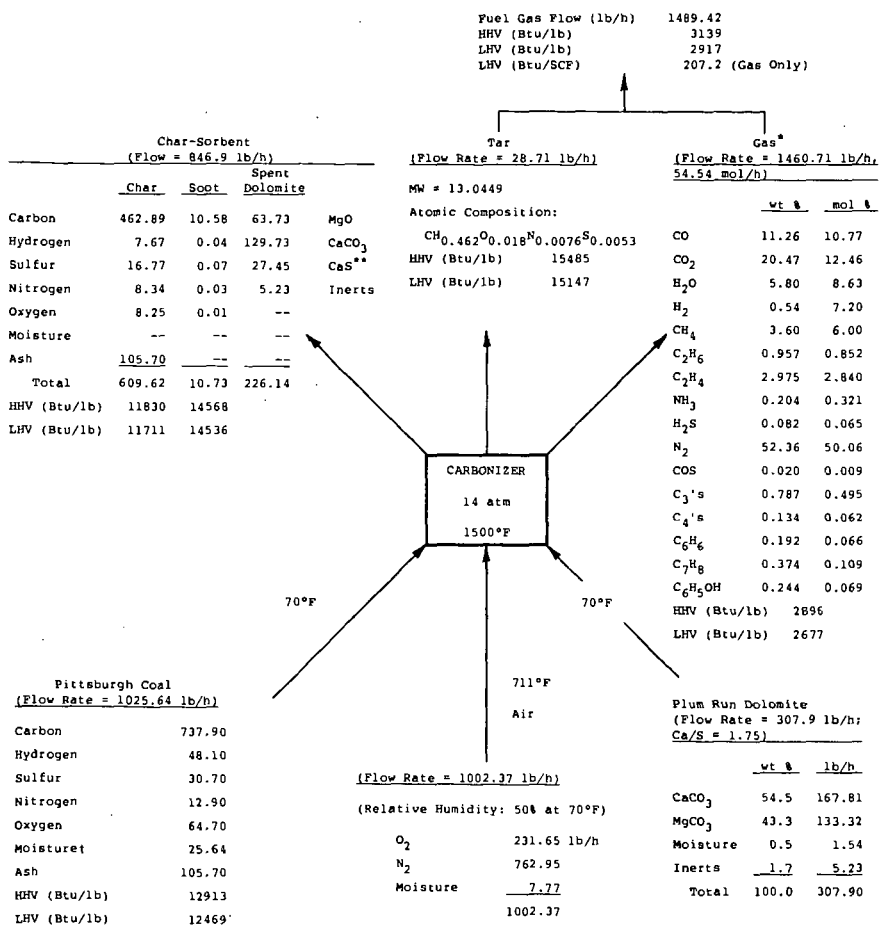


Figure 7. CARBONIZER CONFIGURATION FOR MODEL PREDICTIONS





\*Excludes Tar.

\*\*92% Approach to H<sub>2</sub>S/Sorbent Reaction Equilibrium.

†After Drying.

Figure 8. CARBONIZER BALANCE FOR PITTSBURGH COAL AT 14 atm, 1500°F, and 2.5% MOISTURE (Base Case)

Table 1. SUMMARY OF CARBONIZER MATERIAL BALANCES AT 14-atm PRESSURE  
(Basis: 1000 lb Moisture-Free Coal Feed)

Case Description	Base Case	6% Moisture	1500°F	30% Slurry
Carbonizer Temperature, °F	1500	1500	1600	1500
Coal Feed (moisture-free), lb	1000	1000	1000	1000
Moisture in Coal Feed, %	2.5	6.0	2.5	30.73*
Coal Feed (as-fed), lb	1025.6	1063.8	1025.6	1443.6
Sorbent (Dolomite) Feed, lb	307.9	307.9	307.9	307.9
Air Feed, lb	1002.4	1069.5	1102.0	1765.8
Char in Solids Discharged From Carbonizer, lb	609.6	605.1	598.5	558.4
Spent Sorbent in Solids Discharged From Carbonizer, lb	226.1	226.4	225.0	228.9
Soot Leaving Carbonizer System, lb	10.7	10.0	0.0	2.8
Product Gas (tar-free) Leaving Carbonizer, lb	1460.7	1572.8	1592.7	2719.6
Tars Leaving Carbonizer, lb	28.7	26.9	19.3	7.6
Product Gas (tar-free) HHV, Btu/lb	2896	2709	2917	1685
Tars HHV, Btu/lb	15485	15485	15462	15485
Feedstock HHV, Btu/lb (MF)	13244	13244	13244	13244
Total (product gas + tars) HHV/Feedstock HHV, %	35.3	35.3	37.3	35.5
Total (product gas + tars) LHV/Feedstock LHV, %	34.0	33.9	35.9	33.6
Product Gas (tar-free) HHV, Btu/SCF	224.2	212.8	227.5	146.7
Feedstock Carbon Conversion to Gas, %	32.25	33.14	35.93	42.31
Feedstock Carbon Conversion to Gas + Tars, %	35.84	36.49	38.33	43.26
MAF Coal Conversion to Gas, %	39.24	40.03	42.74	48.21
MAF Coal Conversion to Gas + Tars, %	42.45	43.03	44.89	49.06
Ca/S Feed Molar Ratio	1.75	1.75	1.75	1.75
Approach to H <sub>2</sub> S/Sorbent Reaction Equilibrium, %	92.0	92.0	92.0	92.0
Sulfur Captured by Sorbent, % of Coal Sulfur	39.73	38.85	43.82	29.51
Sulfur Appearing in Product Gas + Tars, % of Coal Sulfur	5.40	6.79	3.42	21.34

\* Includes slurry water.

Table 2. SUMMARY OF CARBONIZER MATERIAL BALANCES AT 10-atm PRESSURE  
(Basis: 1000 lb Moisture-Free Coal Feed)

Case Description	2.5% Moisture	6% Moisture	1600°F	30% Slurry
Carbonizer Temperature, °F	1500	1500	1600	1500
Coal Feed (moisture-free), lb	1000	1000	1000	1000
Moisture in Coal Feed, %	2.5	6.0	2.5	30.73*
Coal Feed (as-fed), lb	1025.6	1063.8	1025.6	1443.6
Sorbent (Dolomite) Feed, lb	307.9	307.9	307.9	307.9
Air Feed, lb	1000.8	1068.2	1100.3	1767.9
Char in Solids Discharged From Carbonizer, lb	606.4	602.1	596.5	557.4
Spent Sorbent in Solids Discharged From Carbonizer, lb	225.9	226.0	224.9	227.4
Soot Leaving Carbonizer System, lb	11.3	10.5	0.0	2.9
Product Gas (tar-free) Leaving Carbonizer, lb	1460.7	1573.2	1592.2	2724.2
Tars Leaving Carbonizer, lb	30.1	28.2	20.2	7.7
Product Gas (tar-free) HHV, Btu/lb	2907	2718	2927	1682
Tars HHV, Btu/lb	15485	15485	15462	15485
Feedstock HHV, Btu/lb (MF)	13244	13244	13244	13244
Total (product gas + tars) HHV/Feedstock HHV, %	35.6	35.6	37.6	35.5
Total (product gas + tars) LHV/Feedstock LHV, %	34.3	34.2	36.2	33.6
Product Gas (tar-free) HHV, Btu/SCF	225.4	213.8	228.6	146.6
Feedstock Carbon Conversion to Gas, %	32.42	33.30	36.08	42.44
Feedstock Carbon Conversion to Gas + Tars, %	36.18	36.81	38.59	43.40
MAF Coal Conversion to Gas, %	39.38	40.17	42.86	48.32
MAF Coal Conversion to Gas + Tars, %	42.76	43.32	45.12	49.17
Ca/S Feed Molar Ratio	1.75	1.75	1.75	1.75
Approach to H <sub>2</sub> S/Sorbent Reaction Equilibrium, %	92.0	92.0	92.0	92.0
Sulfur Captured by Sorbent, % of Coal Sulfur	40.70	40.22	44.31	35.07
Sulfur Appearing in Product Gas + Tars, % of Coal Sulfur	4.42	5.39	2.84	15.58

\* Includes slurry water.

## SELECTIVITY CONTROL UTILIZING ACTIVATION ENERGY DIFFERENCES HYDROGENATION OF CO

N. A. Bhore, K. B. Bischoff, W. H. Manogue, and G. A. Mills  
Center for Catalytic Science and Technology  
Department of Chemical Engineering  
University of Delaware  
Newark, DE 19716

### INTRODUCTION

Multifunctional catalysts offer important opportunities for scientific advances and industrial applications since they are able to activate different molecular species simultaneously. Of critical interest is the molecular structures of the catalyst responsible for such multiple activations, how the activated species interact, and how the reaction dynamics control activity and selectivity.

Hydrogenation of carbon monoxide is a widely studied reaction with many practical applications. The catalytic performances of supported Rh catalysts for CO hydrogenation are very dependent on the support and added modifiers (1-11). Of particular interest is the novel Rh-Mo/Al<sub>2</sub>O<sub>3</sub> catalyst system which displays exceptionally high activity for CO hydrogenation and high selectivity for formation of oxygenates.

Kinetic and characterization tests were carried out using catalysts consisting of Rh on Al<sub>2</sub>O<sub>3</sub> and on TiO<sub>2</sub> with various amounts of added molybdena. The results are discussed in terms of selectivity enhancement by utilizing differences in activation energies for selective and non-selective reactions. Reaction mechanisms are discussed in terms of a dual-site functionality with implications for design of improved catalysts.

### EXPERIMENTAL

Catalysts of composition shown in Table 1 were prepared by impregnation. All contain a nominal 3% Rh from rhodium nitrate solution. The alumina was Catapal and the titania Degussa P-25. Those containing molybdena were prepared in stages. The support was first impregnated with ammonium molybdate, pH 1, followed by drying and air calcination. Then rhodium was deposited. For the 15% Mo catalysts, a dual impregnation was used to overcome solubility limitation. Before testing, catalysts were reduced in flowing H<sub>2</sub> at 500° [All temperatures are °C]. Performance testing was in a flow reactor system. Data were obtained at 3 MPa, H<sub>2</sub>/CO = 2, at 3000 to 36,000 GHSV, 200° to 250°. Steady state product analysis was by on-line GC. To make comparisons, space rates were varied at constant temperature to obtain equal conversions (limited to 6%), then conversions were "normalized" to 3000 GHSV by multiplying by the factor : actual GHSV/3000. The reaction has been shown not to be mass or heat transfer limited (8). CO and irreversible H<sub>2</sub> chemisorption were measured at room temperature, the former using a pulse injection system and a thermal conductivity detector, and the latter using a static system. Previous to measurements, catalysts were reduced under the same schedule as for reactor runs.

### RESULTS AND DISCUSSION

Catalyst composition — effect on performance. The activity of supported Rh catalysts for CO hydrogenation at 250° was found to be TiO<sub>2</sub>-500 > TiO<sub>2</sub>-300 > Al<sub>2</sub>O<sub>3</sub> > SiO<sub>2</sub>. For TiO<sub>2</sub>, 500 and 300 refers to the reduction temperature used before testing. Detailed data for Rh/TiO<sub>2</sub> and Rh/Al<sub>2</sub>O<sub>3</sub> are found in Table 1. The effect of modifiers was also studied, particularly for selectivity enhancement. In this paper, selectivity refers to the conversion of CO to oxygenates relative to hydrocarbons. The results of some of the various modifiers on the selectivity of Rh/Al<sub>2</sub>O<sub>3</sub> and of Rh/TiO<sub>2</sub> are shown in Fig. 1. The line which is drawn for Rh/Al<sub>2</sub>O<sub>3</sub>, shows that selectivity decreases moderately with increasing conversion. The Mo-modified catalysts are unique in their high activities and increased selectivities (4,6,7,8,9). For instance the activity was increased 12-fold by addition of 7.5% Mo. A 4% conversion was obtained at 225° at 18,000 GHSV, and selectivity was 73%. When measured at 250°C, the % selectivity increased progressively with added % Mo : 29-0; 58-2.8; 65-7.5; 69-15, Table 1.

Molybdena added to Rh/TiO<sub>2</sub> was also effective in increasing activity and selectivity, Table 1.

In addition, molybdena brought a high capability for the shift-conversion reaction with as much as 25% of the converted CO going to CO<sub>2</sub>. The amount of CO<sub>2</sub> observed is consistent with the reaction  $\text{CO} + \text{H}_2\text{O} \longrightarrow \text{CO}_2 + \text{H}_2$  utilizing the amount of water produced from formation of hydrocarbons and higher alcohols.

**Temperature — effect on catalyst performance.** The rates of formation of some of the products as a function of temperature have been published previously (6) and additional data are shown in Fig. 2. The calculated values of apparent  $E_{\text{act}}$  given in Table 2 for overall CO conversion is the same for Rh/Al<sub>2</sub>O<sub>3</sub> and Rh/MO/Al<sub>2</sub>O<sub>3</sub>. Hence higher reaction rates with the latter catalyst is not due to a lower  $E_{\text{act}}$ . It should also be noted that for the Rh-Mo/Al<sub>2</sub>O<sub>3</sub> catalysts  $E_{\text{act}}$  for oxygenates as a group is 18.6 Kcal/mole, much lower than the 31.2 volume for hydrocarbons. Individual products show smaller but significant differences from these values, for example 32.4 for CH<sub>4</sub> and 27 for C<sub>2</sub>H<sub>6</sub>. The consequence is that there is a double penalty for operation at higher temperatures. Not only are hydrocarbons increased relative to oxygenates, but also the hydrocarbons consist of larger amounts of less valuable CH<sub>4</sub>. It is also significant that  $E_{\text{act, C}_2+\text{oxy.}} > E_{\text{act, C}_{1\text{oxy.}}}$ . This is believed due to the circumstance that CO dissociation is required for hydrocarbons and higher alcohols but not C<sub>1</sub> oxygenates.

**Utilizing activation energy differences for selectivity control.** The wide differences in  $E_{\text{act}}$  between formation of oxygenates and hydrocarbons results in a more rapid decrease in the rate of formation of hydrocarbon relative to oxygenates as temperature is decreased. Selectivity is increased. The relative rates for selective,  $r_o$ , and non-selective,  $r_h$ , reactions are expressed by the relationship

$$\frac{r_o}{r_h} = \frac{\text{selectivity to oxygenates}}{\text{selectivity to hydrocarbons}} = D \cdot e^{\frac{-(E_o - E_h)}{RT}}$$

D is a constant whose value,  $\log D = -5.60$ , was established from experimental selectivities for Rh/7.5Mo/Al<sub>2</sub>O<sub>3</sub>. The following selectivities to oxygenates represent those calculated and found and those predicted for various temperatures.

Temp.°	273	250	225	200	180	160	140
Calculated %	50	61	75	85	91	95	98
Found %		65	73	86			

One application of this calculation is to provide a prediction of the selectivities which may be obtained with catalysts of sufficient activity to be used at lower temperatures.

The use of lower temperatures to increase selectivity has a penalty — namely loss of conversion rate. The decrease in rate can also be calculated for selective and nonselective reactions as a function of temperatures:

$$\frac{\text{rate } T_1}{\text{rate } T_2} = e^{\frac{-E(T_1 - T_2)}{RT_1 T_2}}$$

This is illustrated by the following:

	oxygenates	hydrocarbon
$E_{\text{act}}$ cal/mole	18,600	31,200
50° decrease, 250° – 200°	7 fold	rate loss 24 fold
90° decrease, 250° – 160°	42 fold	524 fold

The above calculations can provide the initial basis for optimizing process design in which advantages of increased selectivity — improved product value, lower plant and operations costs for separation, and possible longer catalyst life — are calculated and related to disadvantages of lower rates of conversion — larger catalyst inventory and increased reactor investment. Thus an increase of selectivity from 65 to 86% for Rh/7.5%Mo/Al<sub>2</sub>O<sub>3</sub> in going from 250° to 200° may more than compensate for the requirements imposed by a 7-fold increase in catalyst inventory to reach the same conversion level.

Rate comparisons with other catalysts. It is of interest to compare the space-time-yield for Rh/Mo/Al<sub>2</sub>O<sub>3</sub> catalyst and industrial Cu/ZnO/Al<sub>2</sub>O<sub>3</sub> catalysts. The STY for Rh/7.5%Mo/Al<sub>2</sub>O<sub>3</sub> at 250° at 36,000 GHSV in g/hr/ml catalyst corresponds to 1.0 for all products, 0.76 for oxygenates and hydrocarbons, or 0.4 for oxygenate liquids (0.51 ml/hr/g). Commercial catalysts are said to produce 0.5 ml methanol/hr/ml cat. Thus the Rh/Mo/Al<sub>2</sub>O<sub>3</sub> catalyst is as active as commercial catalyst. They are by far the most active of supported Rh catalysts identified in a wide survey (11).

Kinetics. The coefficients of the kinetic power-law rate expression for CO hydrogenation

$$\text{Rate}_{\text{species}} = A \cdot p_{\text{H}_2}^x \cdot p_{\text{CO}}^y$$

were determined for Rh/Al<sub>2</sub>O<sub>3</sub> and Rh/Mo/Al<sub>2</sub>O<sub>3</sub>, Table 3 (3,6,8). A negative value for the exponent of pCO for the Rh/Al<sub>2</sub>O<sub>3</sub> catalysts is interpreted to indicate that there is an inhibition of the reaction by preferential adsorption of CO relative to H<sub>2</sub> on the Rh. However, for the Mo-modified catalyst the exponent of pCO is zero for the overall conversion of CO, for MeOH and for CO<sub>2</sub> formation. While CO<sub>2</sub> is mechanistically a secondary product, it follows the power-law because product water is immediately converted to CO<sub>2</sub>. Significantly, the exponent of pCO remains negative for the formation of methane and higher alcohols. This is interpreted to mean that formation of CH<sub>4</sub> and higher alcohols is occurring at Rh sites, and that dissociation of CO is involved which is subject to inhibition by CO. Formation of methanol does not involve CO dissociation and is not inhibited by CO.

H<sub>2</sub> and CO chemisorption and turnover frequency. The dispersion of Rh in the Rh/Al<sub>2</sub>O<sub>3</sub> catalyst was determined to be 39%, based on H<sub>2</sub> chemisorption and assuming 1H/1Rh. However, for Mo catalysts, H<sub>2</sub> cannot be used for this purpose because of the formation of non-stoichiometric Mo bronzes. Therefore, CO was used to measure Rh dispersion for Mo catalysts. H<sub>2</sub> adsorption on Rh/Al<sub>2</sub>O<sub>3</sub> provided an initial calibration point. It was determined that CO does not adsorb appreciably on partially reduced molybdena under the above-mentioned conditions. While CO can adsorb in different forms, as determined by infrared measurements, it is assumed that the stoichiometry of CO chemisorption on Rh does not change with increased Mo and can be used as a measure of Rh dispersion. The amount of CO chemisorbed decreased progressively and substantially with addition of molybdena, Table 4. Also shown is the overall rate of CO conversion, labelled the turn-over-frequency, for each Rh atom in the sample. The TOF shows an increase as increasing amounts of Mo are added. Thus, even though the number of CO adsorption sites decreases, the rate of CO conversion increases. Furthermore, more impressive increases are observed if the comparison is done on the TOF based on each CO adsorption site. Thus at 15% Mo, the overall activity per CO site increased by 150 fold!

## CONCLUSIONS AND COMMENTS

The exponential form of the reaction rate dependence on activation energy and temperature makes rates very sensitive to activation energies and temperatures. As a consequence, differences in activation energies between selective and non-selective reactions can provide for significantly increased selectivities at lower temperatures. Decreasing reaction temperatures from 250° to 200°, for Rh-MoAl<sub>2</sub>O<sub>3</sub> for example, increases selectivity to oxygenates (E<sub>act</sub> 18.6 Kcal/mole) from 65% to 85% relative to hydrocarbons (E<sub>act</sub> 31.2 Kcal/mole). Reaction rates are decreased 7-fold. The selectivity is predicted to increase to 98% at 160°. Changes in the distribution of individual hydrocarbons and oxygenates with reaction temperature are also predicted. Such considerations provide a preliminary basis for process optimization through temperature selection.

The greatly enhanced activity and selectivity imparted by Mo addition to Rh/Al<sub>2</sub>O<sub>3</sub> is not explained by activation energy differences alone. Gilhooley, Jackson and Rigby (5) found wide variations in the apparent activation energies and pre-exponential factors for Rh on various supports. They concluded that the compensation effect, which involves the pre-exponential factor, made conclusions on mechanism ambiguous.

Examination of the power-law exponents presented here show that the rate of hydrogenation of CO to hydrocarbons and oxygenate is inhibited by CO over Rh/Al<sub>2</sub>O<sub>3</sub> but not for methanol formation over Rh-Mo/Al<sub>2</sub>O<sub>3</sub>. Interestingly, the inhibition for CH<sub>4</sub> formation remains. The implication is that the mechanism of the rate determining step for methanol differs from methane and that the latter is dependent on the Rh.

Based on these results and other characterization tests (8), it is proposed that Rh-Mo/Al<sub>2</sub>O<sub>3</sub> catalysts operates by a dual site mechanism in which CO is activated by Rh and hydrogen is activated by MoO<sub>(3-x)</sub> with migration of activated hydrogen to the activated CO. A major point is that while Rh is capable of activating H<sub>2</sub>, its activation is inhibited by CO during CO hydrogenation. In contrast, H<sub>2</sub> activation by MoO<sub>3-x</sub> is not inhibited by CO. As a consequence of increasing the hydrogenation capability, which is rate-limiting, the overall catalytic activity for CO conversion is greatly accelerated. The increase in oxygenates is also due to increased hydrogenation ability which shows up particularly in methanol formation. The formation of hydrocarbons and higher alcohols involve CO dissociation believed to occur on Rh. As the power-law data show, their formation even over Rh-Mo/Al<sub>2</sub>O<sub>3</sub> is inhibited by CO which is visualized as strongly occupying the Rh sites.

For the practical purpose of achieving higher selectivities at lower temperatures, say 160°, catalysts of increased activity are required. The results discussed here are believed to provide a guide for design of improved dual-site catalysts. The search should be for a structure which provides a H<sub>2</sub> activation site not inhibited by CO. It is speculated that to fulfill this role requires a non-metallic, non-stoichiometric structure such as a partially reduced oxide. For Mo catalysts there is the potential for improvements by use of unusual oxide structures, or of reduction to a MoO<sub>3-x</sub> of more optimum level, or possibly by use of sulfides instead of oxides. A better knowledge of the interface of Rh and partially reduced molybdena is of great interest as well as the mobility of activated hydrogen to or from the Rh (4,8). The extremely high increase in activity, namely 150-fold, of Rh sites identified by CO chemisorption on the 15% Mo/Rh/Al<sub>2</sub>O<sub>3</sub> catalyst, illustrates the possibility of catalysts with greatly increased activity. These could be used with great advantage at lower temperatures than present industrial catalyst.

## ACKNOWLEDGEMENTS

Early experimental and conceptual contributions by Dr. C. Sudhakar are recognized. This work was supported by the Department of Energy Grant DE-FG22-84PC70780.

## REFERENCES

1. Wilson, T.P., Kasai, P.M., Ellgen, P.C. *J. Catal.* **69**, 193-201 (1981).
2. van den Berg, F.G.A., Glezer, J.H.E., Sachtler, W.M.H. *J. Catal.* **93**, 340-352 (1985).
3. Underwood, R.P., Bell, A.T. *Applied Catal.* **21**, 157 (1986).
4. Jackson, S.D., Braneth, B. J., Winstanley, D. *Applied Catal.* **27**, 325-333 (1986).
5. Gilhooley, K., Jackson, S.D., Rigby, S. *Applied Catal.* **21**, 349 (1986).
6. Sudhakar, C., Bhore, N.A., Bischoff, K.B., Manogue, W.H., Mills, G.A. in *Catalysis 1987*, Ward J.W., Ed., Elsevier Sc. Pub. Amsterdam, 115-124 (1988).
7. Bhore, N.A., Sudakar, C., Bischoff, K.B., Manogue, W.H., Mills, G.A. in *Catalysis: Theory to Practice*, Phillips, M. J., Tiernan, M., Eds., Chem. Inst. Canada, Ottawa v. 2 594-601 (1988) v5 (1989).
8. Bhore, N.A. *Modifiers in Rhodium Catalysts for Carbon Monoxide Hydrogenation: Structure - Activity Relationships*. Ph.D. Thesis, University of Delaware, 1989.
9. Kip, J. B., Hermans, E.G.F., Van Wolput, J.M.H.C., Hermans, N.M.A., van Grondelle, J., Prins, R. *Applied Catal.* **35**, 109-139 (1987).

10. Arakawa, H., Hamaoka, T., Takeuchi, K., Matsuzaki, T., Sugi, Y. ref. 6, v 2, 602-609 (1988).
11. Klier, K. in *Coal Liquefaction — A Research & Development Needs Assessment*. DOE Contract DE-AC01-87ER30110 (1989).

Table 1. CO Hydrogenation by Catalysts of Various Compositions,  $H_2/CO=2$ ; 3MPa.  
All contain 3% Rh.

	0% MoAl <sub>2</sub> O <sub>3</sub>		2.8% Mo Al <sub>2</sub> O <sub>3</sub>	7.5% Mo Al <sub>2</sub> O <sub>3</sub>				15% MoAl <sub>2</sub> O <sub>3</sub>		6% Mo TiO <sub>2</sub>	
Temp.	250	275	225	200	225	235	250	200	225	225	250
GHSV	3000	3000	3000	3000	18000	18000	36000	3000	3000	4700	11230
% Conversion of CO, includes CO <sub>2</sub>											
Conv. to CO <sub>2</sub>	5.7	12.5	9.0	7.3	4.0	6.0	5.3	6.0	27	11.2	12.3
	1	1	21.5	23.9	23.0	25.6	24.5	25	37	35	38
% of CO Converted, excludes CO <sub>2</sub>											
CH <sub>4</sub>	60	69	34.8	9.4	18.4	23.8	26.8	7.2	10.6	27.4	35
C <sub>2</sub> H <sub>6</sub>	4	4.1	4.5	3.1	5.8	4.7	5.9	2.4	4.4	11.6	15.3
C <sub>3</sub> H <sub>8</sub>	5	5.0	1.5	1.1	2.3	1.9	2.3	0.9	1.6	4.7	5.5
C <sub>4</sub> H <sub>10</sub>	2	1.4	0.4	0.3	0.6	0.5	0.6	0	0.5	1.6	2
C <sub>5</sub> H <sub>12</sub>		2.0		0	0	0	0			0	0
Total HCs	71	81.5	41.7	13.9	27.1	30.2	35.6	10.5	17.1		
MeOH	2	0.8	13.4	37.6	21.7	17.7	15.7	24.0	10.9	38.9	26
MeOMe	1	0.2	15.9	30.0	28.3	26.9	26.5	39.5	56.5	3.1	4.5
MeCHO	2	2.3	0	0	0	0	0	0	0	0	0
EtOH	11	5.2	12.3	5.8	7.4	7.4	6.7	18.0	1?	7.5	6.4
MeOAc	3	2.6	2.4	1.1	1.1	0.7	0.7	0.2	0.7	2.1	1.7
HOAc	0	0	0	0	0	0	0	0	0	0	0
EtCHO	0.4	0	0	0	0	0	0	0	0	0	0
C <sub>3</sub> H <sub>7</sub> OH	2.7	2.5	2.4	1.9	0.9	2.2	0.7	2.4	2.7	1.4	1.2
MeOEt	3	21.	12.6	9.9	14.0	14.5	14.5	7.0	11.2	3.0	2.5
EtOAc	3	3.6	0	0	0	0	0	0	0	0	0
C <sub>4</sub> H <sub>9</sub> OH	0	0.6	0	0	0	0	0	0	0.4	0	0
Total Oxy.	28.9	18.9	58.7	86.3	73.3	69.2	64.8	90	83	56	39
C <sub>1oxy.</sub>	5.1	2.6	34.3	71.4	55.0	49.6	47.3	65.9	71.3	43.6	30.8
C <sub>2oxy.</sub>	20.7	14.2	22.2	13.0	17.4	17.4	16.8	22.8	8.9	10.9	8.6
C <sub>3oxy.</sub>	3.0	2.5	2.4	1.9	0.9	2.2	0.7	2.4	2.6	1.4	1.2
C <sub>2+oxy.</sub>											
% of oxy.	82.4	86.2	41.6	17.2	21.7	28.1	26.7	27.7	14.0	19	21



Table 2. Apparent Activation Energies, CO Hydrogenation

	Product	Kcal/g mol
3% Rh/Al <sub>2</sub> O <sub>3</sub> 3% Rh/7.5% Mo/Al <sub>2</sub> O <sub>3</sub>	-CO	21.3 ± 0.3
	-CO	21.6 ± 0.9
	C <sub>1oxy</sub>	17.2 ± 0.7
	C <sub>2oxy</sub>	24.3 ± 2.4
	<u>C<sub>total oxy</sub></u>	<u>18.6 ± 0.9</u>
	CH <sub>4</sub>	32.3 ± 2.6
	C <sub>2</sub> H <sub>6</sub>	27.5 ± 3.6
	C <sub>3</sub> H <sub>8</sub>	28.6 ± 4.1
	C <sub>4</sub> H <sub>10</sub>	26.3 ± 2.9
	<u>C<sub>total HC</sub></u>	<u>31.2 ± 2.5</u>
	CO <sub>2</sub>	21.9 ± 0.7

Table 3. Power Law Coefficients for CO Hydrogenation Rate<sub>species</sub> = A · P<sub>H<sub>2</sub></sub><sup>x</sup> · P<sub>CO</sub><sup>y</sup>

Catalyst	Species	x	y
3%Rh/Al <sub>2</sub> O <sub>3</sub> 3%Rh-15%Mo/Al <sub>2</sub> O <sub>3</sub>	-CO	0.8	-0.3
	-CO	0.72 ± 0.05	-0.03 ± 0.09
	+CH <sub>4</sub>	1.02 ± 0.08	-0.32 ± 0.09
	+CH <sub>3</sub> OH	1.53 ± 0.01	-0.01 ± 0.11
	+C <sub>2</sub> +oxy.	0.91 ± 0.23	-0.47 ± 0.23
	+CO <sub>2</sub>	0.38 ± 0.05	-0.04 ± 0.06

Table 4. CO Chemisorption and Site Reactivity (TOF) as Function of Mo in 3%Rh,x%Mo/Al<sub>2</sub>O<sub>3</sub>.

Wt% Mo	CO Chemisorption μ moles/g	% Dispersion of Rh	#CO Reacted/site-sec.**	
			per atom Rh	per site Rh***
0	112	39*	0.4	1
2.8	74	26	4.0	15
7.5	46	16	8.0	50
15.0	28	10	15.0	150

\* Determined by H<sub>2</sub> chemisorption.

\*\* CO Hydrogenation at 225°.

\*\*\* Per CO site.

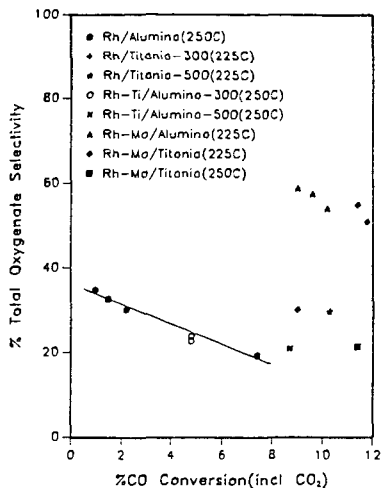


Figure 1. Effect of Catalyst Composition and Conversion Level on Selectivity to Oxygenates. 3%Rh on  $\text{Al}_2\text{O}_3$  or on  $\text{TiO}_2$  Modified by 1 Atom Mo or Ti per Atom Rh. CO Hydrogenation 3MPa,  $\text{H}_2/\text{CO}=1$ , Various Space Rates (Run Temp.  $^{\circ}\text{C}$ ).

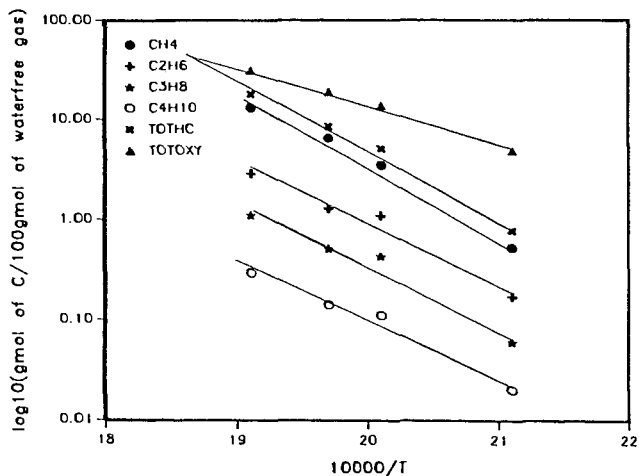


Figure 2. Rates of Formation of Hydrocarbons and Total Oxygenates Over 3%Rh/7.5%Mo/ $\text{Al}_2\text{O}_3$ . 3MPa  $\text{H}_2/\text{CO}=1$ . Rates Normalized to 3000 GHSV. See Table 2 for  $E_{\text{act}}$ .

## DEHYDROCOUPLING OF METHANE BY SUPPORTED ORGANOMETALLIC COMPLEXES

Robert B. Wilson Jr., Yee-Wai Chan, and Barry M. Posin

Inorganic and Organometallic Chemistry Program

SRI International, Menlo Park, CA, 94025

### INTRODUCTION

Two possibilities exist for dehydrocoupling of methane to higher hydrocarbons: The first is oxidative coupling to ethane/ethylene and water that is the subject of intense current research interest. As Labinger<sup>1</sup> and others have recently pointed out, oxidative coupling has an apparent upper limit on yield of C<sub>2</sub> hydrocarbons of around 30% at atmospheric pressure. Non-oxidative coupling to higher hydrocarbons and hydrogen is endothermic, but in the absence of coke formation the thermodynamic yield of hydrocarbons varies between 25% at 827 °C and 65% at 1100 °C and atmospheric pressure.<sup>2</sup> Additionally, after separation the unreacted methane can be recycled unlike oxidative coupling. These numbers are very attractive and a number of recent reports have appeared that prove this concept.<sup>3-9</sup> Yamaguchi's results are particularly interesting because he reported ~ 50% conversion of methane and ~ 85% selectivity to "aromatic oil" at 1300 °C. These values are very close to the thermodynamic equilibrium values.

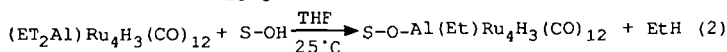
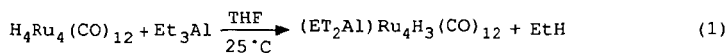
### RESULTS AND DISCUSSION

Research on the technique of surface confinement to produce novel catalysts for a wide variety of processes is continuing in many laboratories.<sup>10-13</sup> We have been working on the development of novel surface confined catalysts to dehydrocouple methane. The catalysts are prepared by reacting organometallic complexes of transition metals with inorganic oxide supports to produce surface-confined metal complexes.<sup>14</sup> The increased activity of highly dispersed catalysts is desirable for activating the relatively inert methane and additionally highly dispersed catalysts are resistant to coking. The use of zeolitic supports will provide further stabilization of the highly dispersed catalysts which are confined inside the zeolite pores. The variables we are studying include cluster size, supporting materials, and reaction conditions.

Synthesis of catalysts- The synthesis of these catalysts involves three steps. The first step is to synthesize the ruthenium cluster precursors. The second step is a novel approach developed in our laboratory involving the reaction of the organometallic clusters with alkyl aluminum. The final step is to anchor these catalysts on supports by a chemical reaction between the hydroxy group of the support and the alkyl groups of the organometallic cluster to give a covalent chemical bond.

The organometallic complexes include: a mono-ruthenium complex, Ru(allyl)<sub>2</sub>(CO)<sub>2</sub>; a tetrameric ruthenium cluster, H<sub>4</sub>Ru<sub>4</sub>(CO)<sub>12</sub>; a hexameric ruthenium cluster, H<sub>2</sub>Ru<sub>6</sub>(CO)<sub>18</sub>; and a mixed metal cluster, H<sub>2</sub>FeRu<sub>3</sub>(CO)<sub>13</sub>. All of these complexes are prepared according to literature procedures.<sup>15,16</sup> The hydrido clusters reacted with triethyl aluminum at room temperature (eq. 1). The reaction stoichiometries

are determined by measuring the quantity of ethane produced.<sup>14</sup> These alkyl aluminum carbonyl ruthenium clusters react with acidic supports:  $\gamma$ -alumina, 5A molecular sieves, and LZ-Y 52 zeolite. The reaction stoichiometries are again determined by measuring the quantity of ethane produced (eq. 2).



The monomeric ruthenium complex reacts directly with the acidic support to release one equivalent of propylene. The tetraruthenium and the mixed iron-ruthenium clusters have also been supported on magnesium oxide by the reaction of the acidic hydride and the basic groups on the MgO surface. All supporting materials are in powder form except for the 5A molecular sieves which was 60-80 mesh.

The ruthenium catalysts were tested at 750°C under 150 psig pressure. The results are summarized in Table 1. We used a commercial ruthenium catalyst which is supported on alumina (obtained from Engelhard) for comparison. The metal loadings were based on elemental analyses (Galbraith Laboratory). The flow-rate of input gases (20% methane in helium) were varied due to the detection limit of our GC. Effect of flow-rate will be discussed later.

**Effects of cluster size** - The commercial ruthenium catalyst gives a very high conversion of methane (71.2%) but no hydrocarbon product. Methane conversion on the mono-ruthenium catalysts are considerably lower than the ruthenium clusters ( $\text{Ru}_4$  and  $\text{Ru}_6$ ). In general, methane conversions depend on the type of support and decrease in the order alumina, 5A molecular sieve, and zeolite. These results suggested that the methane conversion is related to the amount of surface bonded metal. On alumina, the metals are located on the surface while on 5A molecular sieves and on zeolite, increasing amounts of metal are located inside the zeolite pore. The  $\text{Ru}_4$  catalysts demonstrated the greatest dependence on the support, the conversion decreased from 10.1 to 4.9 and to 1.7% on alumina, 5A molecular sieve, and Y-zeolite, respectively.

Our intention in using different supports is to confine the ruthenium cluster at different location on or within the support. Hence, the  $\text{Ru}_4$  and  $\text{Ru}_6$  clusters are dispersed on the alumina surface but are confined inside the pores of the zeolite supports. The pore size of the 5A molecular sieve is too small for the  $\text{Ru}_6$  cluster but should be large enough for the  $\text{Ru}_4$  cluster. Since the Y-zeolite has the largest pore ( $\sim 17\text{\AA}$ ), most of the  $\text{Ru}_4$  or  $\text{Ru}_6$  clusters are located inside the zeolite pore.

**Product selectivity** - All the ruthenium catalysts produced  $\text{C}_2$  hydrocarbons which included ethane and ethylene. The selectivity of  $\text{C}_2$  hydrocarbon observed with  $\text{Ru}_4$  cluster catalysts increased as the percent conversion of methane decreased. These results also suggest the advantage of having the metal cluster confined inside the zeolite cage. The  $\text{Ru}_6\text{AL}$  has the highest total hydrocarbon yield which is probably due to the higher metal loading. The total hydrocarbon yield for  $\text{Ru}_6\text{MS}$  and  $\text{Ru}_6\text{ZL}$  are about the same, but the  $\text{Ru}_6\text{ZL}$  has a higher selectivity for  $\text{C}_2$  product. Confining the metal cluster inside the zeolite cage may also limited the propagation of methane polymerization. The ruthenium

monomers gave relatively low hydrocarbon yields indicating that polymerization of methane required more than one metal atom.

**Coking** - The results listed in Table 1 show that more than one equivalent of hydrogen was produced per methane reacted, which suggests coke formation. The elemental analyses listed in Table 2 show that the Ru<sub>4</sub>AL, Ru<sub>4</sub>MS, Ru<sub>6</sub>AL and Ru<sub>6</sub>MS catalysts contained more carbon after reaction with methane. In contrast, the carbon content of Ru<sub>4</sub>ZL decreased after reaction. This phenomena indicates that those catalysts that have metal dispersed on the support surface promote coke formation while the metals confined inside the zeolite cages do not. For Ru<sub>4</sub>MS, the carbon content only increased slightly to 4.38% as compared with more than 20% for the Ru<sub>4</sub>ZL which suggests that a portion of the metal clusters are located inside the cages of the support. The decrease of carbon content on Ru<sub>4</sub>ZL was due to the decomposition of the ruthenium complexes, i.e. release of carbon monoxide.

**Effect of reaction conditions** - The effect of reaction temperature is similar for every catalyst. Higher methane conversion and product yield are obtained at higher temperatures. Increasing the reaction pressure has a similar effect on the methane conversion. However, the product selectivities for hydrogen and C<sub>2</sub> hydrocarbons decrease but increases for C<sub>6</sub>+ hydrocarbons (Table 3). Highest selectivity is observed at 150 psig. As expected, increasing the space velocity lowers the methane conversion but increases the selectivity for hydrocarbon products.

**Basic support and mixed metal cluster** - Methane conversion over the magnesia supported ruthenium monomer and the FeRu<sub>3</sub> cluster are much higher than the zeolite supported analogs (Table 4). However, the product selectivities to hydrocarbons are lower.

For the mixed iron-ruthenium catalysts, magnesia support also increases the methane conversion. At 600°C, the methane conversion was 8.87% for FeRu<sub>3</sub>MgO and was 3.07% for FeRu<sub>3</sub>ZL. At 750°C, methane conversion increased to 41.5% and 23.05% for FeRu<sub>3</sub>MgO and FeRu<sub>3</sub>ZL, respectively. These catalysts behave similarly to the ruthenium monomers that the hydrocarbon yields were lower on the magnesia supported catalyst.

**In-Situ FTIR** - In-Situ diffuse reflectance FTIR is being used to study these catalysts. Our diffuse reflectance FTIR (DRIFTS) technique is very similar to the ones recently reported by Vannice<sup>17</sup> and Moser.<sup>18</sup> We have been able to collect data using this system up to 600 °C.

Figure 1 demonstrates the kind of data that can be collected using this FTIR technique. In Figure 1 we have compared the thermal behavior of two of the clusters (FeRu<sub>3</sub> and Ru<sub>4</sub>) supported on MgO under N<sub>2</sub>. The carbonyl stretching region of the spectra is shown starting in the upper left at 25 °C. The two spectra are different as would be expected for the different clusters. The Ru<sub>4</sub> spectra is very similar to that observed by Gates<sup>19</sup> for H<sub>4</sub>Ru<sub>4</sub>(CO)<sub>12</sub> adsorbed on magnesia and treated at 100 °C under He and very similar to the spectra observed by Guglielminotti for Ru<sub>3</sub>(CO)<sub>12</sub> on magnesia.<sup>20</sup> The spectra of FeRu<sub>3</sub> is similar to that observed by Basset and Shore on reacting H<sub>2</sub>FeRu(CO)<sub>12</sub> with hydrated magnesia.<sup>21</sup> However, more dramatic is the difference in thermal behavior. The FeRu<sub>3</sub> cluster has drastically changed by 200 °C and has completely disappeared by 300 °C. The Ru<sub>4</sub> cluster is considerably more robust maintaining most of its features to 300 °C.

We then started with fresh samples and studied their IR behavior in flowing 5% methane in argon to simulate the conditions that we use in our dehydrocoupling experiments. The results were quite dramatic and are shown in Figure 2. The spectra are shown starting at 25 °C on the bottom left. Here clearly the  $\text{FeRu}_3$  cluster begins to interact with the methane even at room temperature, while the  $\text{Ru}_4$  has the identical spectra to that observed under nitrogen. Notice the increased intensity of the absorption, here over 6 units while under nitrogen the spectra of  $\text{FeRu}_3$  had an intensity of less than 0.2 units, and also the loss of features (compare to upper left spectra of Figure 1). This broad absorption band is similar to a feature observed by Guzzi<sup>22</sup> that was attributed to mobile subcarbonyls which arise from decomposition of the cluster. However, by 400 °C the two spectra have become identical (bottom right of Figure 2), a broad featureless absorption. This contrast to the spectra under nitrogen where by 400 °C both clusters and completely lost their absorption. We interpret these results as segregation of the metals. We hope next to study the C-H stretching region of the spectra to learn more about hydrocarbon fragments on the catalysts.

#### REFERENCES

1. J. A. Labinger, *Catalysis Letters* 1988, 1, 371.
2. D. J. H. Smith, *Chimie-Raffinage* 1985, 10.
3. O. V. Bragin, T. V. Vasina, Ya. I. Isakov, B. K. Nefedov, A. V. Praobrazhenskii, N. V. Palishkina, and Kh. M. Minacher, *Izv. Akad. Nauk. SSSR, Ser. Khim.* 1982, (4), 954. CA Abstract 97:23370n.
4. S. S. Shepelev and K. G. Ione, *Kinet. Katal.* 1984, 25(2), 347. CA Abstract 101:110432d.
5. T. Yamaguchi, A. Kadota, and C. Saito, *Chem Letters* 1988, 681.
6. A. H. P. Hall and J. J. McCarroll, U.S. Patent 1987, No. 4,695,663.
7. O. M. Gondouin, U.S. Patent 1987, No. 4,705,908.
8. H.L. Mitchell, III and R.H. Waghorne, U.S. Patent 1980, No. 4,239,658.
9. L. Devries and P. R. Ryason, U.S. Patent 1985, No. 4,507,517.
10. M.E. Dry and J.C. Hoogendoorn, *Catal. Rev.* 1981, 23, 265.
11. D.L. King, J.A. Cusumano, and R.L. Garten, *Catal. Rev.* 1981, 23, 203.
12. H.C. Foley, S.J. D-Cani, K.D. T Au, K.J. Chao, J.H. Onuferko, C. Dybowski, and B.C. Gates, *J. Am. Chem. Soc.* 1983, 105, 3074.
13. J.P. Candlin and H. Thomas, "Supported Organometallic Catalysis", in *Homogeneous Catalysis II*, D. Forster and J.F. Roth, eds., *Adv. Chem. Series* 1974, 132, 212-239.

14. Y.I. Yermakov, B.N. Kuznetsov, and V.A. Zakharov, "Catalysis by Supported Complexes," Vol.8, Studies in Surface Science and Catalysis, Elsevier, Amsterdam, (1981).
15. A.A. Bhattacharyya, C.L. Nagel, and S.G. Shore, *Organometallics* 1983, 2, 1187.
16. G.L. Geoffroy and W.L. Gladfelter, *J. Am. Chem. Soc.* 1977, 99, 7565.
17. J.J. Venter and M.A. Vannice, *Applied Spectroscopy* 1988, 42, 1096.
18. W. R. Moser, C.-C. Chiang, and R. W. Thompson, *J. Catalysis* 1989, 115, 532.
19. S. Uchiyama and B. C. Gates, *J. Catalysis* 1987, 110, 388.
20. E. Guglielminotti, *Langmuir* 1986, 2, 812.
21. A. Choplin, L. Huang, J.-M. Basset, R. Mathieu, U. Siriwardane, and S. G. Shore, *Organometallics* 1986, 5, 1547.
22. S. Dobos, I. Boxzormenyi, J. Mink, and L. Gucci, *Inorg. Chim. Acta* 1986, 120, 135 and 145.

Table 1

ACTIVITY OF RUTHENIUM CATALYSTS FOR METHANE DEHYDROGENATION<sup>a</sup>

Catalyst <sup>b</sup>	Ru (wt%)	Flow rate (mL/min)	Methane Conver (%)	% Selectivity <sup>c</sup> to		
				H <sub>2</sub>	C <sub>2</sub>	C <sub>6</sub> <sup>±</sup>
Ru-com	0.50	50	71.2	151.0	-- <sup>d</sup>	--
RuAL	0.35	10	3.0	139.9	2.8	--
RuMS	0.31	10	2.3	147.5	1.2	--
RuZL	0.37	10	1.7	177.5	2.6	--
Ru <sub>4</sub> AL	0.61	100	10.1	78.6	1.62	--
Ru <sub>4</sub> MS	0.49	100	4.9	146.6	3.52	--
Ru <sub>4</sub> ZL	0.61	50	1.7	25.3	6.9	28.9
Ru <sub>6</sub> AL	1.26	50	6.1	113.4	6.9	41.4
Ru <sub>6</sub> MS	0.19	50	5.6	192.8	1.0	14.8
Ru <sub>6</sub> ZL	0.20	50	3.6	161.9	3.6	10.0

<sup>a</sup>Reaction condition: temperature=750°C, pressure=150 psig

<sup>b</sup>Abbreviation: Ru-com=commercial ruthenium catalyst from Engelhard; Ru<sub>4</sub>=(C<sub>2</sub>H<sub>5</sub>)<sub>2</sub>AlRu<sub>4</sub>H<sub>3</sub>(CO)<sub>12</sub>; Ru<sub>6</sub>=(C<sub>2</sub>H<sub>5</sub>)<sub>2</sub>AlRu<sub>6</sub>H(CO)<sub>18</sub>; Ru=Ru (Allyl) (CO)<sub>2</sub>; AL=B- $\gamma$ -alumina; MS=5A molecular sieve; ZL=LZ-Y zeolite.

<sup>c</sup>Selectivities were calculated on converted methane.  
Selectivity to hydrocarbons are based on carbon number.

<sup>d</sup>Not detected.

Table 2  
ELEMENTAL ANALYSES OF RUTHENIUM CATALYSIS FOR METHANE  
REFORMING<sup>a</sup>

Catalyst	Before reaction			After reaction		
	%C	%H	%Ru	%C	%H	%Ru
Ru <sub>4</sub> AL	5.09	1.04	0.61	26.50	0.40	0.57
Ru <sub>4</sub> MS	1.46	1.13	0.49	4.38	0.46	0.64
Ru <sub>4</sub> ZL	5.25	1.53	0.61	0.58	0.22	1.26
Ru <sub>6</sub> AL	9.77	1.84	1.26	23.24	0.67	0.55
Ru <sub>6</sub> MS	0.95	1.68	0.19	22.29	0.19	0.32

<sup>a</sup>Reaction with methane at 750°C for 15 h.

Table 3  
EFFECT OF REACTION PRESURE AND SPACE VELOCITY TO  
THE ACTIVITY OF Ru<sub>6</sub>ZL<sup>a</sup> AT 750°C

Pressure (psig)	Flow rate mL/min	%CH <sub>4</sub> conversion	%Selectivity <sup>b</sup> of		
			H <sub>2</sub>	C <sub>2</sub>	C <sub>6+</sub>
50	50	3.18	164.16	6.04	6.6
150	50	5.19	91.33	4.48	10.70
250	50	8.64	82.41	2.46	7.38
250	100	2.62	177.10	9.24	20.64

<sup>a</sup>Ru<sub>6</sub>ZL = zeolite supported Ru<sub>6</sub> cluster, C<sub>2</sub>H<sub>5</sub>AlRu<sub>6</sub>H(CO)<sub>18</sub>.

<sup>b</sup>Selectivity was based on carbon number of hydrocarbon and the amount of methane reacted.

Table 4  
CATALYTIC REACTIVITY OF ZEOLITE AND MAGNESIA  
SUPPORTED CATALYSTS FOR METHANE DEHYDROGENATION<sup>a</sup>

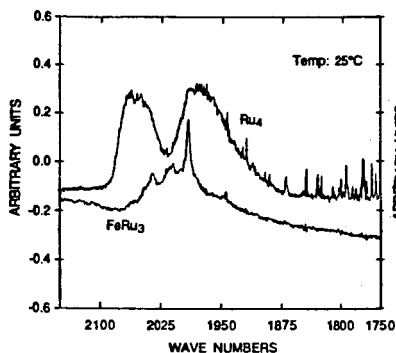
Catalysts	Temp (°C)	Methane	Selectivity <sup>b</sup>	
		Conversion (%)	C <sub>2</sub> (%)	C <sub>6+</sub>
RuMgO	600	21.044	0.1	0.5
Ru <sub>4</sub> MgO	750	4.04	6.9	49.2
FeRu <sub>3</sub> ZL	600	3.07	1.9	18.5
FeRu <sub>3</sub> MgO	600	8.87	0.1	--

<sup>a</sup>Reaction conditions: pressure=150psig, flow rate=20 mL/min, weight of catalyst=2 g, reactor O.D.=3/8in (S.S.).

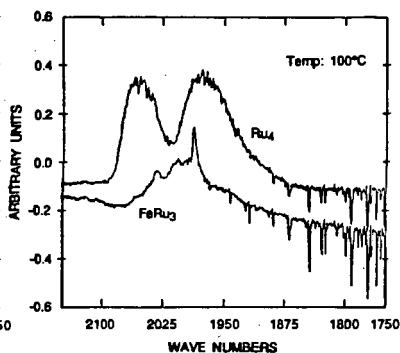
<sup>b</sup>Selectivity to hydrocarbon is based on carbon number.

<sup>c</sup>Not detected.

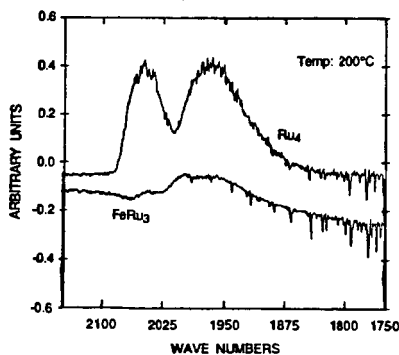




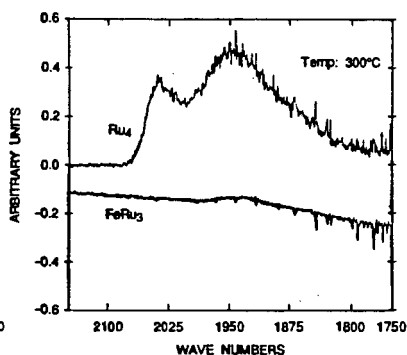
RA-2578-55



RA-2578-55



RA-2578-57



RA-2578-59

FIGURE 1: COMPARISON OF  $\text{Ru}_4$  AND  $\text{FeRu}_3$  CLUSTERS ON  $\text{MgO}$  UNDER  $\text{N}_2$ .

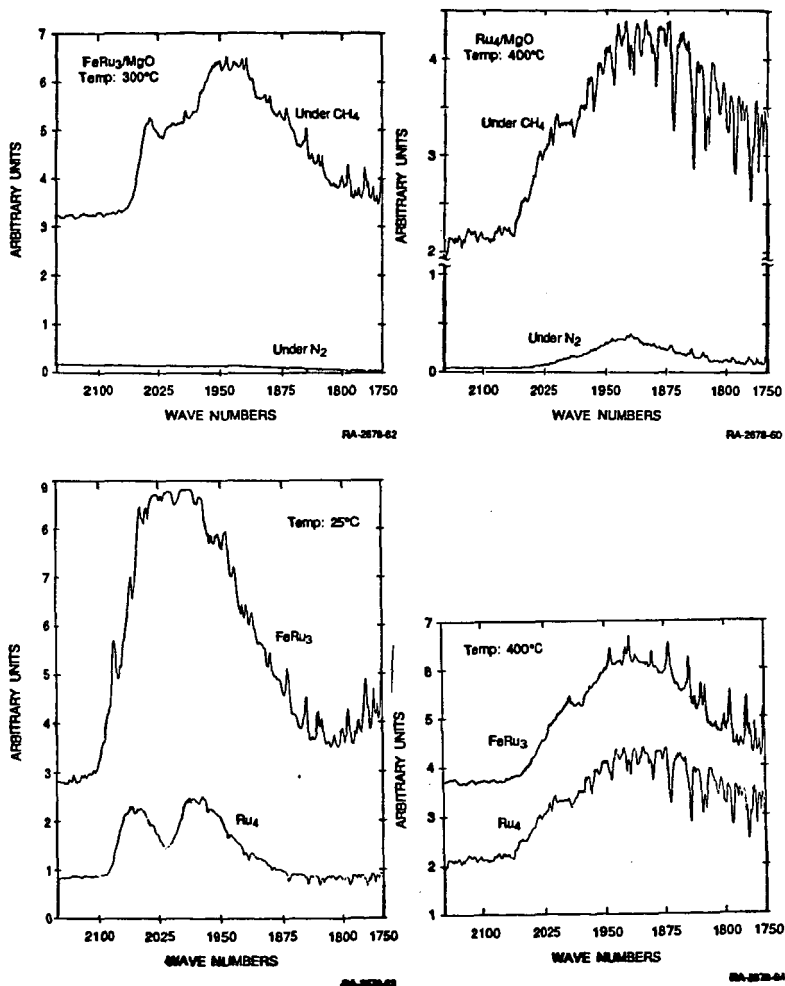


FIGURE 2: COMPARISON OF  $\text{Ru}_4$  AND  $\text{FeRu}_3$  CLUSTERS ON  $\text{MgO}$  UNDER  $\text{CH}_4$ .

Oxidative Coupling of Methane over Perovskite-Type Oxides and Correlation of  
 $T_{\max}$  for Oxygen Desorption with  $C_2$  Selectivity

by

Abolghasem Shamsi\* and Khurram Zahir<sup>21</sup>

United States Department of Energy

Morgantown Energy Technology Center (METC)

P.O. Box 880

Morgantown, WV 26507-0880

ABSTRACT:

Oxidative coupling of methane co-fed with oxygen to  $C_2+$  hydrocarbons has been investigated both in the absence and in the presence of  $La_{0.9}Na_{0.1}MnO_3$  at 1 and 3.6 atm pressures. It was found that residence time, temperature, methane-to-oxygen ratio, and pressure are the major factors affecting the conversion and selectivity both in the empty reactor and in the presence of the catalyst. Significant gas-phase reactions were observed at higher pressure,  $O_2:CH_4$  ratio, and contact time. The results suggest that the activation of methane occurs both in the gas phase and on the surface of the catalyst, and the surface reactions appeared to be important in oxidizing the intermediates  $CH_3$ .,  $C_2H_4$ ,  $C_2H_6$ , and CO to carbon dioxide. Temperature-Programmed desorption studies on a series of perovskite-type catalysts showed that  $T_{\max}$ , the temperature at which maximum  $O_2$  desorbs, correlates very well with the  $C_2$  selectivity for oxidative coupling of Methane; and these results suggest that a strong binding of oxygen to the surface site is essential to selectively produce  $C_2+$  hydrocarbons from methane as opposed to complete oxidation leading to carbon dioxide.

#### BACKGROUND:

Methane is the principal component of natural gas, which is found in porous reservoirs generally associated with crude oil. Some of these abundant reserves of natural gas exist in locations too remote from market areas to be recovered on a commercial basis by present methods. A promising new methane conversion technology uses catalytic oxidative coupling as the first step in the process.<sup>1-3</sup> The oxidative coupling step converts natural gas to olefins, which could be subsequently converted to higher hydrocarbons.<sup>4</sup> A key to developing this technology is optimization of the oxidative-coupling step, such as using novel catalysts. We have shown that by proper cation substitution in perovskite-type oxides, superior catalysts for the oxidative coupling of methane to higher hydrocarbons can be obtained.<sup>5,6</sup> Recent studies showed that gas-phase reactions, especially at higher pressures, play a significant role in the partial oxidation of methane.<sup>7-9</sup> Furthermore, there appears to be a discrepancy between the results obtained by Ito et al.<sup>10</sup> and the results obtained by Yates and Zlotin<sup>7</sup> for empty reactors. Therefore, in order to gain further insight into this catalytic and noncatalytic system, the oxidative coupling of methane was investigated at several reaction conditions, both in the presence and absence of the perovskite-type oxide  $\text{La}_{0.9}\text{Na}_{0.1}\text{MnO}_3$ .

One of the most important factors which govern the catalytic oxidation process is the metal-oxygen bond strength.<sup>11</sup> For metal oxide catalysts, usually three different types of oxygen may be detected, namely, lattice oxygen, adsorbed

oxygen and absorbed oxygen.<sup>12</sup> These activated oxygen species have widely different properties in catalytic oxidation and can affect the activity of a particular catalyst. In the case of metal oxide catalysts, reactivity of these oxygen species depends largely upon the kind of component metal cation present.

Temperature-Programmed Desorption (TPD) is one of the techniques that can be used to obtain useful information on the existence of oxygen species in discrete states and/or over a broad distribution of energies.<sup>12-14</sup> Such information when combined with the results of catalytic reaction studies, carried out under identical conditions, can provide an insight into the catalytic-oxidative conversion of methane to hydrocarbons. In this paper, we report the oxygen-sorptive properties of perovskite-type catalysts in relation to their catalytic activity and selectivity.

#### EXPERIMENTAL:

The details of preparing the perovskite-type oxides have been reported elsewhere.<sup>5</sup> A 0.235m long downflow alumina reactor tube (9.53mm o.d., 6.35mm i.d., calculated heated volume =  $2.0 \text{ cm}^3$ ) with a quartz thermowell was used as a fixed-bed reactor with 0.5 g of catalyst (-28/+48 mesh) held in place by quartz wool. Electronic mass flow controllers were used to feed methane (99.99%), oxygen (99.8%), and helium (99.999%). The reactor was electrically heated to reaction temperatures under a flow of helium. All transfer lines and valves were 316 stainless steel and held at 150 °C. Product analyses were performed by online gas chromatography (GC) and mass spectrometry (MS). The products were sampled but not analyzed until performance stabilized and this

never exceeded 30 minutes. Samples were analyzed for ethane, ethylene, propane, propylene, hydrogen, carbon oxides, formaldehyde, and water.

A thermal conductivity detector was used with a 1m x 3.2mm o.d. stainless steel molecular sieve 5A column and a 3.7m x 3.2mm o.d. stainless steel Porapak Q (80/100 mesh) column at isothermal oven temperatures of 100 and 120 °C, respectively. Results are reported on a carbon-mol % basis (Table 1).

Temperature-programmed studies were performed by passing oxygen (99.8%) over the catalyst and raising the temperature from room temperature to 820 °C with a heating rate of 5 °C/min, and cooling the catalyst to room temperature under oxygen atmosphere. Any excess oxygen not consumed by the catalyst was then flushed out by using high purity He (99.999%). Oxygen desorption was performed by raising the temperature linearly (heating rate = 60 °C/min) with time and using high purity He (30 cm<sup>3</sup>/min) as carrier gas. Products were analyzed by online gas chromatography (GC) and mass spectrometry (MS). For the blank experiment, where no catalyst was present in the reactor, no appreciable traces of oxygen were detected.

#### RESULTS:

The oxidative coupling of methane co-fed with oxygen was studied in an empty alumina reactor with and without dead volume (Table 1). The results showed that extensive conversion of methane and oxygen occurred in the empty reactor, especially at higher pressures and contact times. The heated volume of the reactor was calculated to be 2.0 cm<sup>3</sup> with a contact time of 2.4 seconds at maximum dead volume. However, as the contact time was reduced (< 1 second), by

minimizing the dead volume in the reactor, the contribution from the gas-phase reaction was significantly reduced. Since we were not able to measure the exact volume of the reactor with the minimized dead volume, the contact time is reported as "< 1 second".

Pressure also appears to be an important factor affecting conversion and selectivity both in the gas phase and on the surface of the catalyst. For example, at 1.0 atm pressure and 740 °C (not shown in Table 1), about 1.5 % of the methane and about 1.7 % of the oxygen were converted to products (9%  $C_2H_4$ , 38%  $C_2H_6$ , 3%  $CO_2$ , and 49% CO) in the empty reactor (contact time = 2.4 seconds and  $CH_4:O_2 = 2:1$ ). When the pressure was raised to 3.6 atm, the methane and oxygen conversions increased to 35.7 and 96.8 %, respectively. The product distribution in this case was 11.2%  $C_2H_4$ , 4.6%  $C_2H_6$ , 15.8%  $CO_2$ , and 68.4% CO.

The effects of temperature and pressure on conversions and selectivity to  $C_2+$  hydrocarbons, over  $La_{0.9}Na_{0.1}MnO_3$  catalyst, are shown in Figure 1. At 3.6 atm pressure and temperatures below 780 °C, higher methane and oxygen conversions and higher selectivity to  $C_2+$  hydrocarbons were observed compared to those at 1 atm. However, when the temperature increased the  $C_2+$  selectivity at low pressure (1 atm) increased to a maximum value, while at the higher pressure the  $C_2+$  selectivity slightly decreased. Furthermore, a higher molar ratio of  $C_2H_4:C_2H_6$  was observed at higher pressure. In the presence of the catalyst, the major portion of the carbon oxides was carbon dioxide, indicating that the catalyst played a significant role in the reaction sequences and altered the product distribution.

The dependence of conversion and selectivity on the methane-to-oxygen ratio over  $\text{La}_{0.9}\text{Na}_{0.1}\text{MnO}_3$  was also studied (Figure 2.). Lower conversion of methane and higher selectivity to  $\text{C}_2$ + hydrocarbons were obtained when the methane-to-oxygen ratio was increased. This result indicates that methane and higher hydrocarbon products, at higher oxygen partial pressures and in the presence of the catalyst, were increasingly converted to carbon dioxide.

#### Temperature-Programmed Desorption:

Temperature-Programmed desorption studies on a series of perovskite-type catalysts with general formula  $\text{A}_{1-x}\text{B}_x\text{MnO}_3$  (where A is Gd, Sm, La, or Ho, B is either Na or K and  $x = 0$  or  $0.1$ ) were carried out and the temperature at which maximum oxygen desorbed ( $T_{\text{max}}$ ) was correlated with the  $\text{C}_2$  selectivity. The TPD chromatograms for oxygen desorption are shown in Figure 3 as plots of mass spectrometer signal (desorption rate) for oxygen ( $m/e = 32$ ) versus temperature. All chromatograms are characterized by the appearance of two types of oxygen. The first type, ( $\alpha$ ) oxygen, desorbs at a lower temperature compared to the second type, ( $\beta$ ) oxygen, which desorbs at higher temperature. The values for  $T_{\text{max}}$ , corresponding to the maxima for ( $\alpha$ ) oxygen desorption, are plotted in Figure 4 along with the  $\text{C}_2$  selectivities obtained in the earlier studies.<sup>6</sup> The values for  $T_{\text{max}}$  ranges from 860 °C for  $\text{Gd}_{0.9}\text{Na}_{0.1}\text{MnO}_3$  to 695 °C for  $\text{LaMnO}_3$ , and is sensitive to the presence of alkali metal ion B as well as to substitution at site A.

The results presented in Figure 4 show that  $T_{\text{max}}$  for ( $\alpha$ ) oxygen desorption correlates very well with the  $\text{C}_2$  selectivity. The catalyst  $\text{Gd}_{0.9}\text{Na}_{0.1}\text{MnO}_3$  with



( $\alpha$ ) oxygen desorbing at the highest temperature (865 °C) showed the highest selectivity for  $C_2$  products whereas  $LaMnO_3$  which desorbs at the lowest temperature (695 °C) is the least selective for the conversion of methane to  $C_2$  products.<sup>5</sup> It is interesting to note that optimum conditions (higher  $C_2$  selectivity) for conversion of methane over  $La_{0.9}Na_{0.1}MnO_3$  catalyst correspond to the temperature (820 °C) which matches very nicely with the  $T_{max}$  for that catalyst. For the perovskite-type catalysts examined, it has been speculated earlier that the oxygen binding energy decreases in this order  $(La,Na)MnO_3 > (La,K)MnO_3 > (La,[] )MnO_3$ .<sup>15</sup> Present TPD studies provide an experimental basis for that trend in oxygen binding energies for these compounds and also similar information on other catalysts. For example, when comparing  $LaMnO_3$  with  $La_{0.9}K_{0.1}MnO_3$  and  $La_{0.9}Na_{0.1}MnO_3$ , it becomes apparent that it is the nature of metal-oxygen bond that controls the catalytic activity of oxide catalysts. Therefore we suggest that in catalytic oxidation of methane to higher hydrocarbons, the most important factor may very well be the binding energy of oxygen to a surface site of the catalyst. This observation also agrees well with the earlier claim that some of the common selective oxidation catalysts (e.g.  $V_2O_5$ ,  $MoO_3$  and  $Bi_2MoO_6$ ) did not contain weakly adsorbed oxygen.<sup>13</sup>

#### CONCLUSIONS:

We have shown that by proper cation substitution in perovskite-type oxides, superior catalysts for the oxidative coupling of methane to higher hydrocarbons can be obtained. The results show that surface reactions are important in oxidizing the intermediates  $CH_3\cdot$ ,  $C_2H_4$ ,  $C_2H_6$ , and CO to carbon dioxide. It was found that contact time, temperature, methane-to-oxygen ratio

and pressure were the major factors affecting the conversion and selectivity in the presence and absence of the catalyst. Furthermore, the high activity observed by Yates and Zlotin<sup>7</sup> for the empty reactor could be a result of the higher contact time and possible back pressure (caused by the capillary tube) when compared with the results reported by Ito et al.<sup>10</sup> The activation of methane appeared to be occurring both in the gas phase and on the surface of the catalyst. In the gas phase, methane was possibly activated by diatomic oxygen. The oxidation of methane in the gas phase by diatomic oxygen has been discussed in other reports.<sup>16,17</sup>

The types of oxygen species on the surfaces of the catalyst responsible for the activation of methane are not well defined. However, the activation of methane by surface oxygen species has been proposed by several researchers. Liu et al.<sup>18</sup> have shown  $O^-$  ions; Driscoll et al.<sup>19</sup> have proposed  $[Li^+O^-]$  centers; and Otsuka and Jinno<sup>20</sup> have proposed adsorbed diatomic oxygen, as being responsible for the activation of methane.

From the TPD studies, we can conclude that for the perovskite-type catalysts examined, a strong binding of oxygen to the surface site is essential to selectively produce  $C_2+$  hydrocarbons from methane as opposed to complete oxidation leading to undesirable carbon dioxide. Present results suggest a possibility that TPD technique can be utilized to find more effective catalysts by selecting a proper combination of A and B site substitution in perovskite-type catalysts.

#### REFERENCES:

- (1) Ekstrom, A.; Lapszewicz, J. A. *J. Am. Chem. Soc.* **1988**, 110, 5226.
- (2) Labinger, J. A.; Ott, K. C. *J. Phys. Chem.* **1987**, 91, 2682.
- (3) Zhang, H.-S.; Wang, J.-X.; Driscoll, D.; Lunsford, J. H. *J. of Catal.* **1988**, 112, 366.
- (4) Jezl, J. L.; Michael, G. O.; Spangler, M. J. U.S. Patent **1988**, 4,754,091, June 28.
- (5) France, J. E.; Shamsi, A.; Ahsan, M. Q. *Energy & Fuels* **1988**, 2(2), 235.
- (6) France, J. E.; Shamsi, A.; Headley, L. C.; Ahsan, M. Q. *Energy Progress* **1988**, 2(4), 185.
- (7) Yates, D. J. C.; Zlotin, N. E. *J. of Catal.* **1988**, 111, 317.
- (8) Lane, G.; Wolf, E. E. *J. of Catal.* **1988**, 113, 144.
- (9) Asami, K.; Omata, F.; Fujimoto, K.; Tominaga, H. O. *J. Chem. Soc. Commun.* **1987**, 1287.
- (10) Ito, T.; Wang, J.-X.; Lin, C.-H.; Lunsford, J. H. *J. Am. Chem. Soc.* **1985**, 107, 5062.
- (11) Kung, H. H. *Ind. Eng. Chem. Prod. Res. Dev.* **1986**, 25, 171.
- (12) Seiyama T.; Yamazeo, N.; Eguchi, K. *Ind. Eng. Chem. Prod. Res. Dev.* **1985**, 24, 19.
- (13) Iwamoto M.; Yoda, Y.; Yamazoe, N.; Seiyama, T. *J. Phys. Chem.* **1987**, 82, 2654.
- (14) Falconer J. L.; Schwartz, J. A. *Catal. Rev. Sci. Eng.* **1983**, 25, 141.
- (15) Voorhoeve R. J. H.; Remeika, J. P.; Trimble, L. E.; Cooper, A. S.; Disalvo, F.J.; Gallagher, P. K. *J. Solid State Chem.* **1975**, 14, 395.
- (16) Bone, W. A. *Proc. R. Soc. London, Ser. A* **1932**, 137, 243.

- (17) Walker, R. W. *Reaction Kinetics*; The Chemical Society Burlington House, London, 1975; Vol.1, pp 161-211.
- (18) Liu, H.-F.; Liu, K. Y.; Johnson, R. E.; Lunsford, J. H. *J. Am. Chem. Soc.* 1984, 106, 4117.
- (19) Driscoll, D. J.; Martir, W.; Wang, J.-X.; Lunsford, J. H. *J. Am. Chem. Soc.* 1985, 107, 58.
- (20) Otsuka K.; Jinno, K. ; Morikawa, A. *J. of Catal.* 1986, 100, 353.
- (21) Oak Ridge Associated Universities Postdoctoral Research Fellow

Table 1. Comparison of Activity and Selectivity of Oxidative Coupling of Methane in the Presence and Absence of Catalyst at 845 °C, Alumina Reactor,  $\text{CH}_4/\text{He}/\text{O}_2=20/20/10 \text{ cm}^3/\text{min}$  NPT flow rates.

Catalyst/ Conditions	Conversion (mol%)		Selectivity (carbon-mol%)			
	Methane	Oxygen	$\text{C}_2\text{H}_4$	$\text{C}_2\text{H}_6$	$\text{CO}_2$	CO
Empty, Contact time 2.4 seconds, 1 atm.	29.9	62.9	19.0	5.7	8.8	66.5
Empty, Contact time < 1 second, 1 atm.	1.0	0.5	34.8	51.5	1.2	12.5
Empty, Contact time < 1 second, 3.6 atm.	18.5	37.7	21.8	12.4	8.9	56.9
$\text{La}_{0.9}\text{Na}_{0.1}\text{MnO}_3$ , 0.5 g, Contact time 0.4 second, 1 atm.	19.8	44.5	30.0	17.4	41.5	11.1
$\text{La}_{0.9}\text{Na}_{0.1}\text{MnO}_3$ , 0.5 g, Contact time 2.4 seconds, 1 atm.	37.2	85.1	36.6	13.7	43.2	6.5

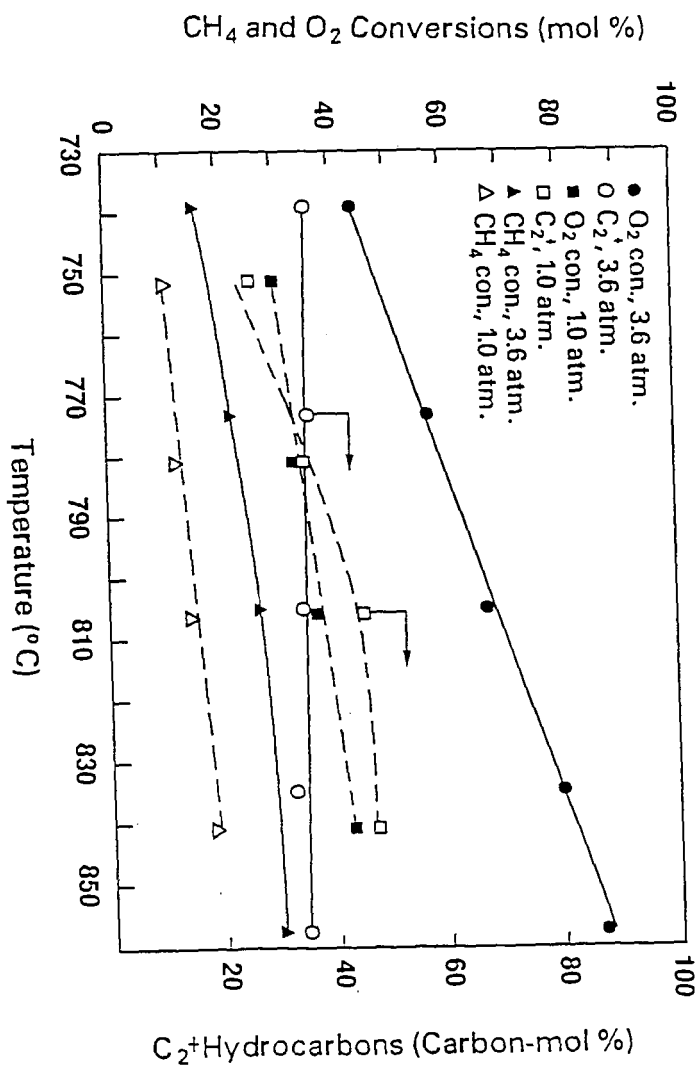
Figure captions:

Figure 1. Dependence of conversion and selectivity on temperature and pressure over  $\text{La}_{0.9}\text{Na}_{0.1}\text{MnO}_3$  Catalyst:  $\text{CH}_4/\text{He}/\text{O}_2 = 20/20/10$  NPT flow rates; contact time = 0.4 seconds; 0.5 g catalyst.

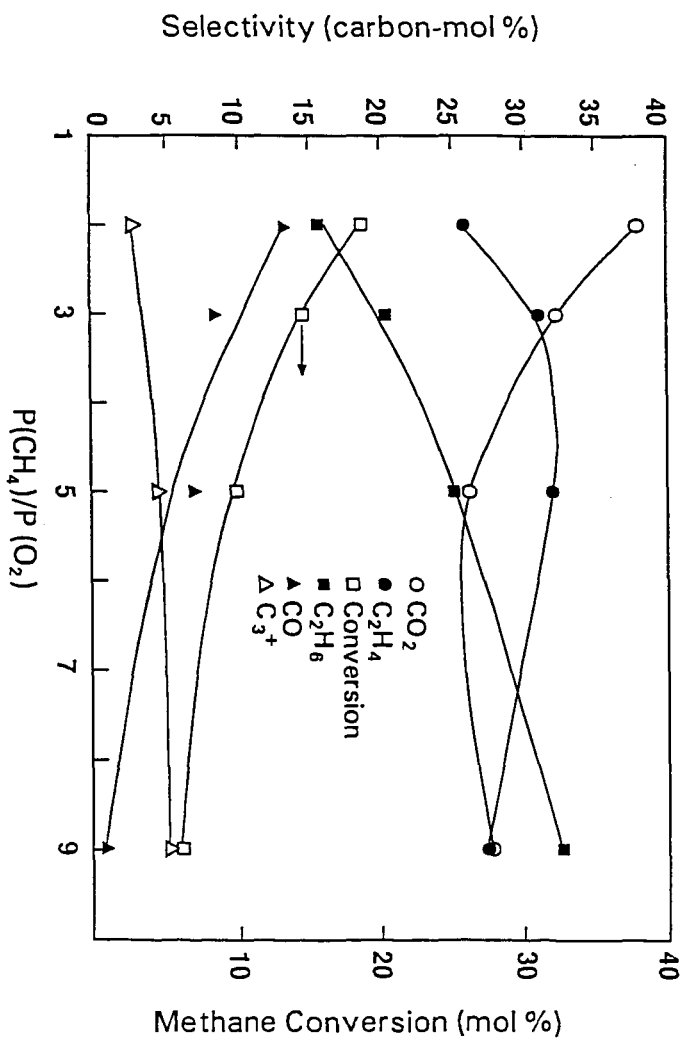
Figure 2. The effect of methane-to-oxygen ratio on conversion and selectivity over  $\text{La}_{0.9}\text{Na}_{0.1}\text{MnO}_3$  in an alumina reactor: 1.0 atm pressure; 830 °C;  $\text{CH}_4/\text{He}/\text{O}_2 = 20/20/10$  NPT flow rates; contact time = 0.4 second; 0.50 g catalyst.

Figure 3. Temperature-programmed desorption of oxygen ( $m/e = 32$ ): Heating rate = 1 °C/sec., He flow rate = 0.5  $\text{cm}^3/\text{sec.}$ , 0.25 g catalyst.

Figure 4. Correlation of  $\text{C}_2$  Selectivity with the temperature at which maximum  $\text{O}_2$  desorbs ( $T_{\text{max}}$ ): 0.25 g catalysts tested at 820 °C,  $\text{CH}_4/\text{O}_2$  ratio = 5.

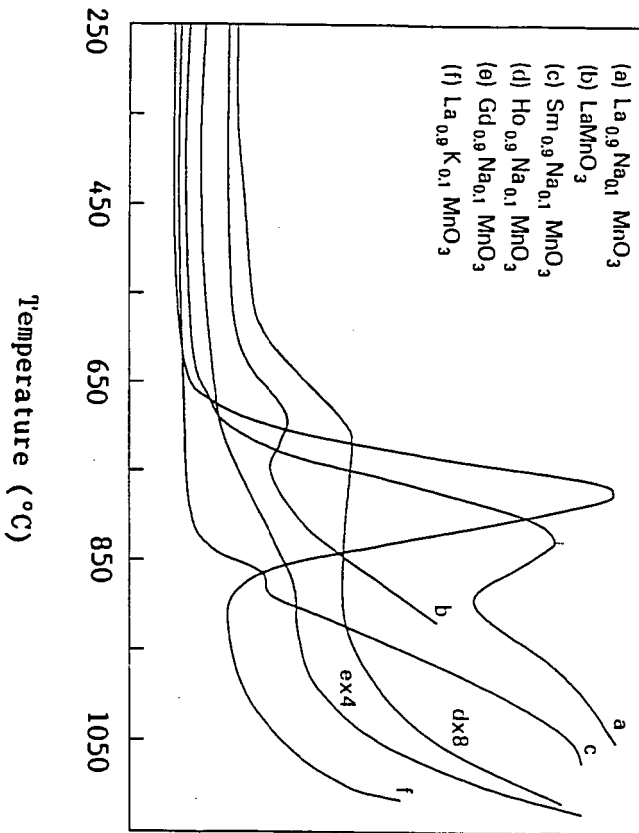


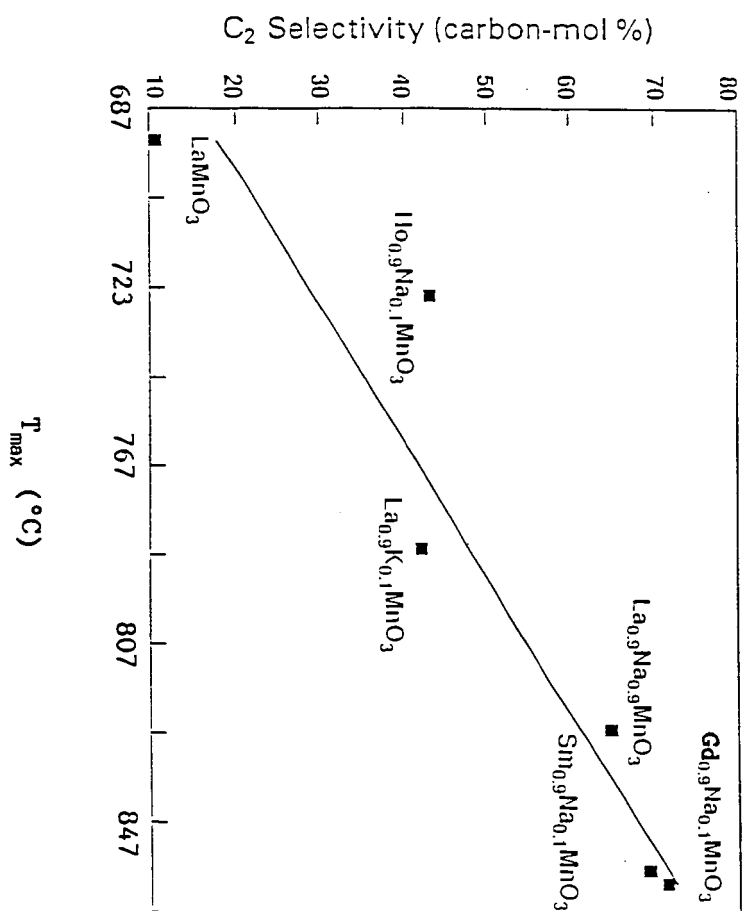
CB9-467-E AA3





Desorption Rate →





## PHOTOCHEMICALLY-DRIVEN BIOMIMETIC OXIDATION OF ALKANES AND OLEFINS

J. A. Shelnutt, D. E. Trudell  
Fuel Science Division 6211

Sandia National Laboratories, Albuquerque, NM 87185

### ABSTRACT

A photochemical reaction for oxidation of hydrocarbons that uses molecular oxygen as the oxidant is described. A reductive photoredox cycle that uses a tin(IV)- or antimony(V)-porphyrin photosensitizer generates the co-reductant equivalents required to activate oxygen. This "artificial" photosynthesis system drives a second catalytic cycle, mimicking the cytochrome  $P_{450}$  reaction, which oxidizes hydrocarbons. An iron(III)- or manganese(III)-porphyrin is used as the hydrocarbon-oxidation catalyst. Methylviologen can be used as a redox relay molecule to provide for electron-transfer from the reduced photosensitizer to the Fe or Mn porphyrin, but appears not to enhance efficiency of the process. The system is long-lived and may be used in time-resolved spectroscopic studies of the photo-initiated reaction to determine reaction rates and intermediates.

### INTRODUCTION

Many alkane and olefin oxidation systems that mimic biological oxidation of hydrocarbons by cytochrome  $P_{450}$  have been reported. Most use an iron, manganese, or ruthenium porphyrin as the analog of the heme (iron porphyrin) functional group of the enzyme.<sup>1-8</sup> In the great majority of these chemistries a single oxygen atom donor, such as iodosylbenzene or hypochlorite, is used as the oxidant rather than molecular oxygen.<sup>1-4</sup> When molecular oxygen is used as the oxidant, as is the case for cytochrome  $P_{450}$ , reducing equivalents must be supplied to reduce the Fe porphyrin causing it to bind and split dioxygen and, subsequently, oxidize the alkane substrate. Several biomimetic systems have been demonstrated using either sodium borohydride, hydrogen/Pt, ascorbate, or zinc metal as the co-reductant.<sup>5-8</sup>

We have been investigating these reactions from the standpoint of stereochemically controlling the reaction at the metal site by designing metalloporphyrins with a shape- and size-selective pocket at the metal center.<sup>9,10</sup> The pockets designed so far are small, and thus require an oxidant, like  $O_2$ , that is small enough to enter the cavity. It is also desirable that the system be stable and operate over many hours. We are interested also in the possibility of photo-initiating the reaction so that reaction intermediates can be followed using time-resolved spectroscopic techniques for kinetic studies. This can be accomplished if the reductant is the product of a photoredox cycle.

Here we describe such a photochemically driven system for oxidation of alkanes and olefins. The system is illustrated in Figure 1. The cycle on the left is the photoredox chemistry that produces the reductant, a long-lived tin(IV)-porphyrin radical anion. In the cycle, a tin(IV)- or antimony(V)-porphyrin absorbs a photon of visible light resulting in the formation of the triplet excited state of the porphyrin. The porphyrin photosensitizer in its excited state is reduced by a sacrificial electron donor such as triethanolamine (TEOA).<sup>11-13</sup> The resulting long-lived  $\pi$  anion of the porphyrin has a

redox potential low enough to reduce either a Fe(III) or Mn(III) porphyrin, which acts as a catalyst for the biomimetic oxidation of hydrocarbons.<sup>13,14</sup> After reduction of the FeP, the photosensitizer anion (SnP<sup>-</sup>) returns to the resting redox state (SnP). Actually, two molecules of the porphyrin anion are required in the biomimetic P<sub>450</sub> cycle as indicated in Figure 1; the first to reduce Fe(II) to Fe(III), allowing O<sub>2</sub> to bind and a second to split dioxygen to form the reactive O=FeP intermediate. In some cases a molecule such as heptylviologen (HV<sup>2+</sup>) is used to relay the electron from the SnP anion to the P<sub>450</sub> cycle. Acetic or benzoic anhydride is sometimes used as an oxygen atom acceptor (replacing H') in the splitting of dioxygen in the hydrocarbon (RH) oxidation cycle.

## RESULTS AND DISCUSSION

A photochemical reaction like that illustrated in Figure 1 was carried out in acetonitrile under an O<sub>2</sub> or air atmosphere. In a typical reaction, 0.24 μmol of Fe(III) tetra(pentafluoro-phenyl)porphyrin (FeTF<sub>5</sub>PP) chloride, 0.45 μmol of Sn(IV) protoporphyrin IX (SnProtoP) dichloride, 1.1 mmol of TEOA, 1.4 μmol of heptylviologen (N,N'-diheptyl-4,4'-dipyridinium dichloride), and 11 μmol of benzoic (or acetic) anhydride, were added to 1 ml of acetonitrile. Hexane (4.7 mmol) was added as a substrate. The samples, contained in a 1-cm path length cuvette, were irradiated with a tungsten lamp for 1-6 hr. Light of wavelengths less than 380 nm was filtered to insure that photosensitization of the reaction was only due to visible light absorption by the porphyrin. 1-, 2-, and 3-Hexanol and 2- and 3-hexanone products were quantified at the end of the run by gas chromatography. Table 1 gives yields and hexanol to hexanone product ratios for typical runs and control experiments.

In the presence of the P<sub>450</sub> catalyst, a generally higher overall yield of products is observed when illumination and other conditions were identical; however, a lower average hexanol to hexanone ratio of 1.3:1 is observed. However, in the absence of the catalyst FeTF<sub>5</sub>PP, photosensitized production of hexanols and hexanones is observed in an average ratio of 2.3:1. In the absence of O<sub>2</sub>, light, photosensitizer, or triethanolamine, there is no significant yield of oxidized hexane.

It is apparent that more than one oxygen activation pathway exists. The excited triplet state of tin porphyrins is known to be quenched in the presence of O<sub>2</sub>,<sup>14</sup> suggesting a possible direct mechanism of O<sub>2</sub> activation by the photosensitizer. We have examined reactions of both singlet O<sub>2</sub> and superoxide anion under our reaction conditions. Chemically-produced superoxide (KO<sub>2</sub>/18-crown-6) is not reactive under our experimental conditions. On the other hand, singlet oxygen, produced by irradiation of free base protoporphyrin (H<sub>2</sub>ProtoP),<sup>15</sup> is reactive in the presence of tertiary amines and gives about the same hexanol to hexanone ratio (2.7, see Table 1) as is observed in the presence of the SnP photosensitizer. Sn-, Sb-, and H<sub>2</sub>ProtoP all have triplet lifetimes of 10 ms or longer, and form singlet O<sub>2</sub> by intermolecular triplet-triplet annihilation. In fact, the photophysical parameters and singlet oxygen sensitizing properties of SnProtoP<sup>14,16</sup> are similar to metal-free porphyrins.<sup>17</sup> The similarity of photosensitizing characteristics of Sn-, Sb-, and H<sub>2</sub>-porphyrins explains the similarity of their properties in the FeP-free reaction (Table 1). However, only the Sn and Sb porphyrins form the stable anions capable of driving the Fe-porphyrin catalyzed reaction.

In the presence of the iron-porphyrin, the alcohol/ketone product

ratio is modified ( $-ol/-one \approx 1$ ) indicating that a competing reaction comes into play. If the FeP-catalyzed reaction is to account for the low product ratio, then this reaction necessarily must give a lower hexanol to hexanone ratio. We can test this hypothesis by determining the product ratio for the  $P_{450}$  cycle when driven by addition of a suitable reductant in the absence of light. Table 1 includes the yield and product ratio for the dark reaction of hexane and  $O_2$  catalyzed by FeTF<sub>2</sub>PP using a Zn/Hg amalgam as the co-reductant.<sup>18</sup> (The ranges of yields and product ratios are for a range of solution conditions. The reaction is run for 2 hr, but is complete in about 10 min in most cases. Although the yields in some cases represent less than one catalyst turnover, the reaction can be continued by adding more amalgam. The FeP or MnP catalyst is required for significant yields of oxidized hexane. In some cases methylviologen is used as a relay molecule, and acetic anhydride is used as an oxygen atom acceptor. The product yield is sensitive to the amount of water in the acetonitrile solvent, and, in addition, acetic acid improved the overall yield and raised the alcohol/ketone product ratio. Presumably, acetic acid aids in the dioxygen lysis step in the reaction.)

Most importantly, when the FeP catalyst is present in the dark reaction the product ratio is one or less. Therefore, the dark reaction appears to compete favorably with the formation of singlet  $O_2$  and the photochemical reaction proceeds as shown in Figure 1. The dark reaction, which also occurs in the presence of light, results in the observed lowering in the alcohol/ketone ratio and higher yield measured for the light-driven reaction in the presence of the FeP catalyst. Also, viologen appears not to aid the reaction, since the yield generally remains unchanged or is slightly lowered in its presence (data not shown).

When cyclohexene is the substrate in the dark reaction, the products cyclohexene oxide (1.0), 2-cyclohexen-1-ol (2.2), and 2-cyclohexen-1-one (1.8) are observed in the ratios (relative product yields are given in parenthesis) observed in other dioxygen-based systems that mimic the cytochrome  $P_{450}$  reaction.<sup>19,20</sup> Also, when Mn tetraphenyl porphyrin is used as the catalyst, imidazole binding as a fifth ligand acts as a promoter for  $P_{450}$  reaction as has been noted in earlier studies.<sup>21</sup> Both of these results support the contention that the reaction is occurring at the porphyrin catalyst under these solution conditions.

The photochemical system produces stable yields of hydrocarbon oxidation products for more than 6 hr as shown in Figure 2. In Figure 2, the yield of products is given in terms of catalyst turnovers (mol product/mol FeP catalyst) as a function of reaction time. Also plotted in Figure 2 is the yield per hour, which only degrades slightly over the 6 hr reaction time. Finally, the alcohol/ketone ratio is a function of reaction time, increasing slightly as the reaction proceeds. The increase in the product ratio and decrease in oxidation rate both could be explained by slow degradation of the FeP-catalyzed cycle.

In summary, a photochemically driven reaction that mimics biological photosynthesis, electron-transfer, and hydrocarbon-oxidation reactions has been described. The reaction occurs at room temperature and uses  $O_2$  as the oxidant. Most importantly, the reaction can be run for hours without significant degradation. This means that the oxidation of low molecular weight alkanes by  $O_2$ , which proceeds at a lower rate than for hexane, can be investigated. Further studies are underway to determine the detailed reaction mechanisms involved in the photochemical reaction. Transient absorption and Raman spectroscopic techniques will also be applied to determine reaction rates.

#### ACKNOWLEDGEMENTS

This work performed at Sandia National Laboratories and supported by the United States Department of Energy Contract DE-AC04-76DP00789.

#### REFERENCES

1. For recent reviews see: (a) Ortiz de Montellano, P. R., Ed. "Cytochrome P-450; Structure, Mechanism, and Biochemistry" (Plenum: New York) **1986**. (b) Guengerich, F. P.; Macdonald, T. L., *Acc. Chem. Res.* **1984**, 17, 9.
2. Groves, J. T.; Nemo, T. E.; Myers, R. S., *J. Am. Chem. Soc.* **1979**, 101, 1032.
3. Groves, J. T.; Quinn, R., *J. Am. Chem. Soc.* **1985**, 107, 4343.
4. Colman, J. P.; Brauman, J. I.; Meunier, T.; Hayashi, T.; Kodadek, T.; Raybuck, S. A., *J. Am. Chem. Soc.* **1985**, 107, 2000.
5. Tabushi, I.; Koga, N., *J. Am. Chem. Soc.* **1979**, 101, 6456.
6. Perree-Fauvet, M.; Gaudemer, A., *J. Chem. Soc. Chem. Commun.* **1981**, 874.
7. Tabushi, I.; Yazaki, A., *J. Am. Chem. Soc.* **1981**, 103, 7371.
8. Fontecave, M.; Mansuy, D., *Tetrahedron* **1984**, 40, 2847.
9. Shelnutt, J. A., Stohl, F. V.; Granoff, B., *Preprints, Fuel Chem. Div., ACS, Los Angeles, CA, September 25-30, 1988*.
10. Quintana, C. A.; Assink, R. A.; Shelnutt, J. A., *Inorg. Chem.* **1989**, in press.
11. Shelnutt, J. A., *J. Am. Chem. Soc.* **1983**, 105, 7179.
12. Shelnutt, J. A., *J. Phys. Chem.* **1984**, 88, 6121.
13. Shelnutt, J. A., U. S. Patent 4,568,435, **1986**.
14. Kalyanasundaram, K.; Shelnutt, J. A.; Grätzel, M., *Inorg. Chem.* **1988**, 27, 2820.
15. (a) Cannistraro, S.; Jori, G.; Van de Vorst, A., *Photobiochem. Photobiophys.* **1982**, 3, 353. (b) Cox, G. S.; Whitten, D. G., *Adv. Exp. Med. Biol.* **1983**, 160, 279.
16. Land, E. J.; McDonagh, A. F.; McGarvey, D. J.; Truscott, T. G., *Proc. Natl. Acad. Sci. USA* **1988**, 85, 5249.
17. Gouterman, M., in "The Porphyrins" Vol. 3, Dolphin, D., ed. (Academic: New York) Chpt. 1, **1978**.
18. Karasevich, E. I.; Khenkin, A. M.; Shilov, E., *J. Chem. Soc., Chem. Commun.* **1987**, 731.
19. Paulsen, D. R.; Ullman, R.; Soane, R. B.; Closs, G. L., *J. Chem. Soc., Chem. Commun.* **1974**, 186.
20. Masui, M.; Tsuchida, K.; Kimata, Y.; Ozaki, S., *Chem. Pharm. Bull.* **1987**, 35, 3078.
21. Battioni, P.; Renaud, J-P.; Bartoli, J. F.; Mansuy, D., *J. Chem. Soc., Chem. Commun.* **1986**, 341.

TABLE 1. Oxidation of hexane by air in acetonitrile.

Catalyst	Reductant System	-ol/-one	Yield <sup>a</sup> (turnovers/hr)
FeTF <sub>3</sub> PP	SnProtoP, hν, TEOA	1.3 <sup>b</sup>	4.3
FeTF <sub>3</sub> PP	SbProtoP, hν, TEOA	1.0	0.8
FeTF <sub>3</sub> PP	hν, TEOA	0.8	0.2
MnTPP	SnProtoP, hν, TEOA	0.9	0.2
FeTF <sub>3</sub> PP	Zn/Hg	0.2-1.1	0.5-1.0 <sup>c</sup>
-	SnProtoP, hν, TEOA	2.3 <sup>b</sup>	1.7
-	H <sub>2</sub> ProtoP, hν, TEOA	2.7	0.6
-	SbProtoP, hν, TEOA	2.2	1.4 <sup>d</sup>
-	hν, TEOA	-	0.0
-	SnProtoP, hν	-	0.0

- a. Yield is in photosensitizer turnovers (mol product/mol photosensitizer) for selected runs. Catalyst concentrations are about one-half of the photosensitizer concentration.
- b. Hexanol/hexanone value is average for all (~20) runs with turnovers > 1.
- c. Total turnovers under various solvent conditions with O<sub>2</sub> as the oxidant.
- d. Light intensity higher than for SbProtoP/FeTF<sub>3</sub>PP run, accounting for higher yield in this case.

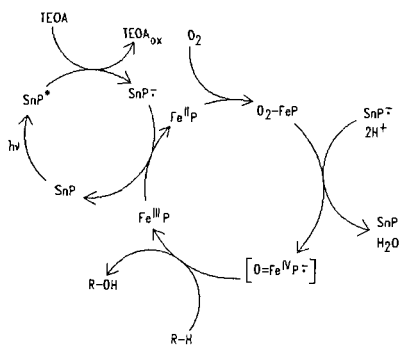


Figure 1. Scheme for photochemical production of co-reductant to drive the oxidation of hydrocarbons by mimicking the cytochrome- $P_{450}$  cycle. The SnP sensitized photoredox cycle is on the left; the  $P_{450}$  catalytic cycle is shown on the right.

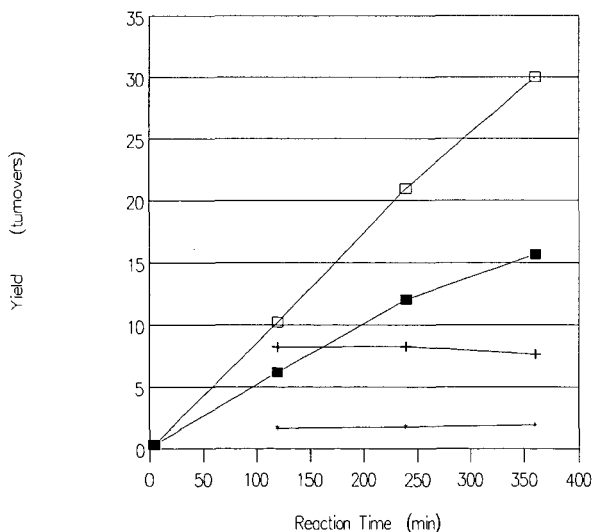


Figure 2. Hexanol and hexanone yields and product ratio as a function of reaction time. Total 1-, 2-, and 3-hexanol yield in catalyst turnovers (□); total 2- and 3-hexanone yield (■); hexanol/hexanone ratio (+); catalyst turnovers/hr (\*).



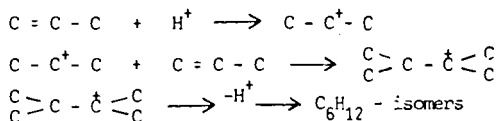
SYMPOSIUM ON NEW CATALYTIC MATERIALS  
PRESENTED BEFORE THE DIVISION OF FUEL CHEMISTRY  
AMERICAN CHEMICAL SOCIETY  
MIAMI MEETING, SEPTEMBER 10-15, 1989

OLIGOMERIZATION OF ISO-BUTENE WITH AN IMPROVED CATALYST

S. Börje Gevert, Peter Abrahamsson and Sven G. Järås  
Department of Engineering Chemistry 1,  
Chalmers University of Technology, Göteborg, S-412 96 Sweden

INTRODUCTION

In conversion processes in oil refining LPG (C<sub>3</sub> and C<sub>4</sub>) are formed as byproducts. When catalytic cracking is used the LPG will have a high content of unsaturated components. The low price of the LPG, compared to gasoline, makes oligomerization of the molecules in LPG worthwhile for the industry. There are mainly two processes used in the refineries for this purpose. In alkylation, liquid sulphuric or hydrofluoric acids are employed and in the other process phosphoric acid on silica or diatomeric earth. In the refining industry the latter process is normally called polymerization, although dimerization is the dominating and most wanted reaction. In the alkylation process iso-butene is reacted with either propane or butane. If using the less strong phosphoric acid, two alkenes must be used as reactants and at a higher temperature. The mounted phosphoric acid catalyst leaks less acid to downstream processing and therefore gives less severe corrosion problems than with alkylation (1). The chemistry of the oligomerization can be shown as:



The formed carbonium ions and hexenes can react further to trimers and higher. The phosphoric acid on silica catalyst is also an important catalyst for the production of petrochemical intermediates like nonene and alkylated aromates.

The traditional method of producing the mounted phosphoric acid on silica is to start from kieselguhr and phosphoric acid. The water content of the phosphoric acid should be low so that the final catalyst contains 65-70% by weight of P<sub>2</sub>O<sub>5</sub>. The mixture is extruded or bricketted, dried, calcined and finally hydrated to a preferred level, usually with steam. There are several proposals in the patent literature to improve the mechanical strength of the final product. One method is to steam treat the mixture before extrusion (2). It is also possible to add bentonite, montmorillonite, halloysite, or other compounds to the mixture before extrusion. The acidity of the catalyst can also be reached by using an aluminum silicate or zeolite instead of the above mentioned acids. The kieselguhr carrier can be replaced by a silica hydrogel (3,4). Recently Bernard et al (5) proposed to extrude the silica carrier before impregnating the phosphoric acid. Little interest has been shown in the development of new or improved catalysts for oligomerization of propene and butene in the recent literature. It is therefore of interest to use modern analytical instruments to explain and improve the catalyst. In this paper, an improved catalyst based on mounted phosphoric acid on silica will be presented.

## EXPERIMENTAL

The used silica carriers were spheres with a diameter of 2.2 mm, received from Shell Corp. in London. In Table 1, more details of pore volumes and pore sizes are presented. The phosphoric acid used was of pro analysi quality from Kebo Lab. (Sweden) and the iso-butene from AGA Gas Ltd. (Sweden).

The catalysts were made by combining the following steps in different sequences: Impregnation with phosphoric acid of 42% by weight of  $P_2O_5$  or other concentrations if indicated. Drying at 170°C for 5 hrs. and calcining in a muffle furnace for 4 hrs. at various temperatures. Some catalysts were steamed at 100°C in 100% steam.

Testing of the activity of the catalysts was done in a 23 cc stainless steel reactor with iso-butene in vapour phase. A constant contact time of 1.00 hr. was maintained in all experiments by measuring and controlling the inlet flow. In Figure 1, a simple flow diagram of the reaction system is presented. Temperature, pressure and gas flow were kept constant at 160°C, 1 atm and 12.5 g of iso-butene per hour, respectively. The yields were determined by measuring the weight of liquid products and the amount of iso-butene feed. The liquid products were analyzed on GC with FID detector and the simulated distillation was made according to ASTM D2887-3. BET pore volume and surface area were measured with Micromeritics Digisorb 2600.

## RESULTS AND DISCUSSION

In Table 2, the BET surface area and pore volumes of the silica spheres used are presented. The pore volume determined with the BET method is considerably different from the pore volumes presented by the manufacturer of the silica spheres (Table 1). The main difference is probably due to macro pores not detected by the BET method.

Impregnation of the silica sphere I with different acid concentrations followed by drying at 170°C, did not effect the initial activity of the final catalyst. However, after 20 hrs. of experiment, catalyst produced by impregnating higher concentrations of phosphoric acid showed a lower conversion (Table 3). In spite of this it is important to use a higher concentration of the acid in order to reach a  $P_2O_5$  concentration of 65-70% in the final catalyst. On the other hand, too high a viscosity, which is found in concentrated phosphoric acid, reduces the impregnation speed.

In Figure 2, the conversion as a function of time is presented for three different catalysts produced from the three different silica spheres by the same procedure. Calcination was done at 425°C. The catalyst produced from silica spheres III, with both larger pores and pore volume compared with silica spheres II, gives the highest activity. The conversion was 78% after 20 hrs. of experiment. The catalyst produced from silica sphere II, gives a better conversion than does the catalyst produced from silica sphere I. Thus the selection of silica carrier should be; large average pores and large pore volumes.

In Figure 3 the effect on activity of calcining at 350°C and 425°C is presented. The higher temperature gives a lower activity and calcining at 350°C gave a catalyst with a conversion of 97,6%. This catalyst also maintained the conversion level in an experiment of over 70 hrs. In a separate experiment silica spheres were calcined at 550°C, before impregnation without affecting the conversion of the final product. Calcining after impregnation effects the bindings between phosphoric acid and the

silanol groups and dehydration of the phosphoric acid. As no effect of calcining at 550°C before impregnation was noted, the silanol groups of the silica remained intact. If only one impregnation is carried out, the activity of the final catalyst drops quickly after a few hours of the experiment (Table 3). When water is added in the feed, or the catalyst is wetted with water, the activity rises again for a short period. This indicates that the phosphoric acid bound to the silica is not as active as free acid in the catalyst. It is probably due to the fact that bound acid does not have the same capacity to retain water as free acid. The high sensitivity of water content in the feed makes the catalyst, which has been impregnated once only, impractical for commercial use.

In Figure 4 the activity of commercial catalyst is plotted as a function of time. The ground catalyst shows a much higher conversion rate (66%) after 20 hrs of experiment than the unground catalyst (18%). In the small reactor used, the unground catalyst will give large wall effects due to the small dimensions of the reactor. The ground catalyst has a lower activity compared to the best of the catalysts produced in this study. In the production of gasoline a dimer or trimer is wanted, while the formation of tetramers is not wanted since they normally fall outside the gasoline boiling range. The selectivity of some catalysts is presented in Table 4. For catalysts with high conversions, the formation of tetramers is also high. The catalyst calcined at 350°C shows an acceptable selectivity (dimer + trimer = 96%) and at the same time conversion 98%. The unground commercial catalyst shows 4.3% tetramers in the liquid while the ground catalyst only shows 2.8%. The higher production of tetramers is probably an effect of large pore diffusion times of the primary dimer in the unground catalyst. The yield of trimers follows the same pattern as the yield of tetramers.

#### CONCLUSIONS

A high activity oligomerization catalyst based on phosphoric acid on silica has been produced by impregnation of silica spheres. A calcining temperature of 350°C is more better than calcining at 450°C or only drying at 170°C. The catalyst has a low sensitivity to water concentration in the feedstock provided it has been impregnated twice with calcination between. The activity of the catalyst produced by impregnation is higher than that of the commercial catalysts used in this study.

#### REFERENCES

1. Eglott, G., Welner, P.C. In Proceedings of the 3rd World Petroleum Congress, The Hague, 1951, Section IV, 201-14.
2. Engel, W.F. U.S. Patent 2 913 506.
3. Morell, J.C. U.S. Patents 3 044 964, 3 050 472, 3 050 473, 3 170 885, 3 213 035.
4. Wilshier, B.G., Smart, P. Western R., Mole T., Behring T. Applied Catalysis, 31 (1987), 339-359.
5. Bernard, J., Le Page, F. Ger. offen 1 954 326.
6. Corner, E.S., Lynch, C.S. U.S. Patent 3 824 149.

Table 1. Silica spheres. Properties according to manufacture.

ID	Pore Volume ml/g	Average Pore Size, Angstroms
I	1.0	300
II	1.0	600
III	1.3	600

Table 2. Silica spheres. Analytical results.

ID	Pore volume BET ml/g	Surface Area m <sup>2</sup> /g	Bulk Density g/cm <sup>3</sup>
I	0.95	79	0.43
II	0.77	62	0.40
III	0.72	60	0.36

Table 3. Conversion expressed as weight percent conversion after 20 hrs. of experiment with iso-butene. Impregnation with different acid concentrations in one step without calcination.

% P <sub>2</sub> O <sub>5</sub>	Conversion
6	20
11	22
21	17
42	6
85	9

Table 4. Selectivities

Catalyst	Time on Stream h	Weight % in Liquid			Conversion Weight %
		di-	tri-	tetra-	
Spheres III, calc 425	3	74.9	22.1	3.0	88.6
Spheres III, calc 425	23	84.0	14.9	1.1	79.6
Spheres III, calc 425	47	84.4	14.6	1.0	79.6
Spheres III, calc 350	27	73.3	22.7	4.0	97.6
Commercial unground	49	68.5	27.2	4.3	16.9
Commercial ground	49	76.5	20.7	2.8	65.4

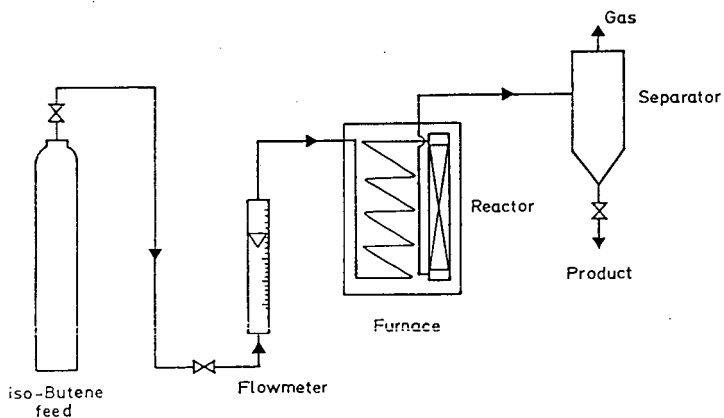


Figure 1. Simple flow diagram of reaction system.

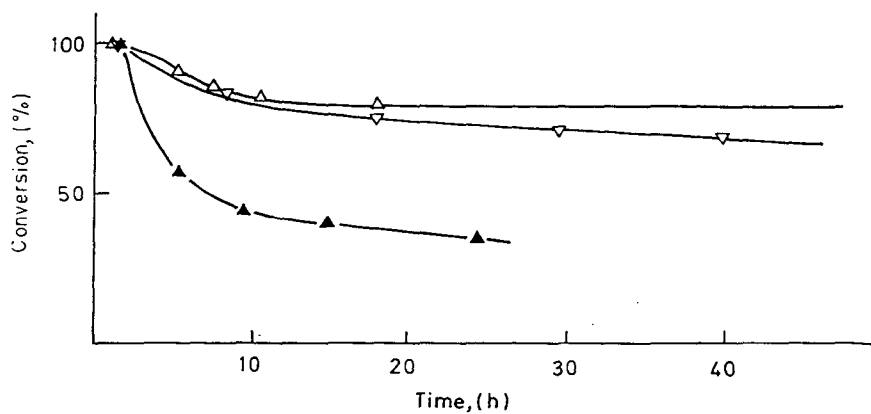


Figure 2. Conversion in weight percent of catalysts prepared with silica spheres  
I ▲, II ▼ and III △. Calcined at 425°C and impregnated twice.

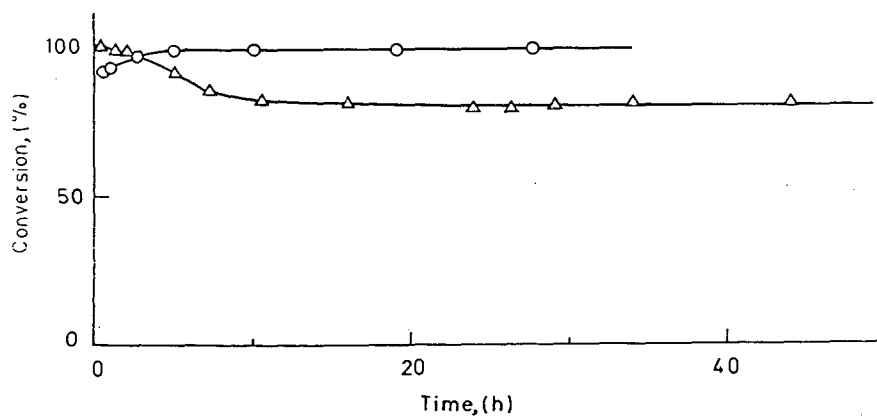


Figure 3. Conversion in weight percent of catalysts calcined at 350°C ○ and 425°C △. Catalysts prepared from sphere III, impregnated with phosphoric acid (42%,  $P_2O_5$ ), calcined, impregnated and dried.

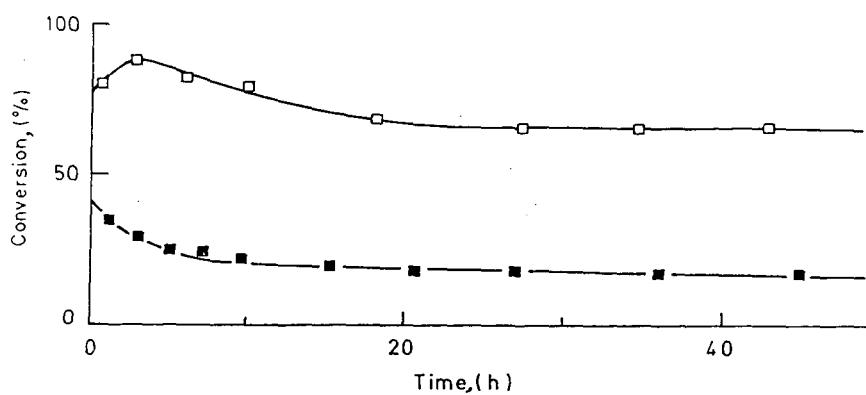


Figure 4. Conversion of commercial catalyst in weight percent. Unground ■ and ground □.

ACTIVATION OF HYDROUS TITANIUM OXIDE-SUPPORTED  
CATALYSTS FOR HYD, HDS, and HDO REACTIONS\*

Robert G. Dosch, Frances V. Stohl  
Sandia National Laboratories  
Albuquerque, NM 87185

and

James T. Richardson  
Department of Chemical Engineering  
University of Houston  
Houston, TX 77204-4792

INTRODUCTION

The objective of our current work is to develop catalysts, based on hydrous titanium oxide (HTO) ion exchangers [1], for use in direct coal liquefaction processing. The ultimate goal of the program is an improved coal liquefaction catalyst produced in quantities that allow testing in a large-scale process development unit such as the Advanced Coal Liquefaction R & D Facility at Wilsonville, Alabama. This paper will give an overview of Sandia's catalyst development program and present results of studies of HTO catalyst preparation and pretreatment procedures.

Catalysts currently employed in process development units for coal liquefaction are hydroprocessing catalysts developed for petroleum refining [2]. They are composed of combinations of the metals Mo or W along with Co, Ni and other promoters dispersed on alumina or silica-alumina supports. When used in liquefaction, these catalysts deactivate rapidly [3], causing decreases in product yield and quality and problems with process operability. Thus the existing generation of supported catalysts cannot adequately meet the demanding requirements for use in coal liquefaction processes.

Past efforts for development of coal liquefaction catalysts have focused on alumina-supported systems and, except for exploratory studies, little attention has been given to systematic development of novel formulations. A particularly promising approach to the development of new catalysts specifically designed for coal liquefaction processes lies in the formulation of multicomponent systems that, in comparison to work on single or bimetallic systems, are essentially unexplored. Use of multimetallic systems offers the possibility of multifunctional catalysts that are needed to perform the many different reactions encountered in coal processing. Because of its versatility for the preparation of multimetallic catalysts, the HTO system is an excellent candidate for further development.

Hydrous titanium oxide ion exchange compounds exhibit a number of properties that make them desirable as substrates for active

\* This work supported by the U. S. Dept. of Energy at Sandia National Laboratories under Contract DE-AC04-76DP00789.



metals: (1) ions of any active metal or mixture of metals can be atomically dispersed over a wide range of concentrations by an easily controlled process; (2) the ion exchange capacity of the materials is large, permitting high loadings of active metals; (3) solution chemistry can be used to provide control of the oxidation state of the active metal; (4) catalyst acidity can be modified by ion exchange; (5) the materials have high surface areas; (6) the ion exchanger substrates are stable in oxidizing and reducing atmospheres, and over a wide pH range in aqueous solution; and 7) the ion exchangers can be prepared as thin films on a wide variety of supports. The latter property offers the potential for tailor-made catalysts for chosen chemical, physical, and mechanical characteristics.

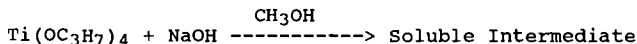
HTO catalysts have been evaluated in several fossil fuel applications including direct coal liquefaction and hydropyrolysis. Initial batch microreactor tests [4] using equal weights of Shell 324M (a NiMo/Al<sub>2</sub>O<sub>3</sub> catalyst that is commonly used in direct coal liquefaction), Ni HTO, Mo HTO, and Pd HTO catalysts with Illinois #6 coal and SRC-II heavy distillate showed that the HTO catalysts, even at low active metals loadings of 1 wt%, are equally effective for conversion of coal to low molecular weight products as Shell 324M, which contains 15 wt% active metals. In addition, for the same oil yield, the HTO catalysts used less hydrogen than the commercial catalyst. HTO catalysts have also been evaluated at the Pittsburgh Energy Technology Center in bench-scale tests with a 1:1 distillate solvent/residuum feed from the Wilsonville Advanced Coal Liquefaction R & D Facility. Results [5] showed that a CoNiMo HTO catalyst gave conversions to cyclohexane solubles, H/C product ratios, and hydrodesulfurization activities that were similar to those obtained with Shell 324M. The CoNiMo HTO catalyst had not been optimized for hydrotreating coal-derived liquids. Studies [6] of hydropyrolysis using a coal coated with a Pd HTO catalyst (0.7 wt% Pd on daf coal basis) showed a 50% increase in tar yield compared to a reaction performed with the addition of ground NiMo/Al<sub>2</sub>O<sub>3</sub> catalyst (3.6 wt% active metals on daf coal basis). These results all indicate that HTO catalysts have potential in coal liquefaction processes.

## EXPERIMENTAL

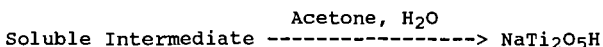
### HTO Catalyst Preparation

Hydrous titanium oxide ion exchangers are amorphous inorganic compounds synthesized in the form of salts of weak acids represented by the empirical formula C(Ti<sub>x</sub>O<sub>y</sub>H<sub>z</sub>)<sub>n</sub>, where C is an exchangeable cation. HTO catalysts can be prepared by a technique that consists of synthesis of sodium hydrous titanate ion exchange material followed by exchanging active metal ions for the sodium. The synthesis involves three steps:

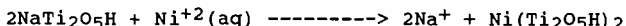
(1) Reaction of tetraisopropyl titanate with an alkali or alkaline earth metal hydroxide in alcohol solution to form a soluble intermediate:



(2) Hydrolysis of the soluble intermediate in acetone/water mixtures to form the HTO exchange material:



(3) Ion exchange of the alkali or alkaline earth metal for active metal ions in aqueous solution to form the catalyst:



Co, Mo, Pd, and NiMo HTO catalysts are prepared by similar procedures. HTO-Si support materials were made by adding tetraethyl orthosilicate to the tetraisopropyl titanate prior to addition of NaOH.

#### Activity Testing

All catalysts were tested as powders and were sulfided in an atmospheric pressure flow reactor prior to activity testing. Sulfiding was carried out at 425°C for 2 h using a 10 mol% H<sub>2</sub>S/H<sub>2</sub> mixture. Some of the catalysts were calcined in air by heating at 50°C/min to 450°C followed by a 10°C/min increase to 500°C with 2 h at this temperature. All activity results are reported on a weight of active metals basis and results are compared to those of Shell 324M.

Hydrogenation (HYD) activities were determined by measuring the rate of hydrogenation of pyrene to dihydropyrene. Experiments were performed at 300°C in 26 cm<sup>3</sup> batch microreactors that were loaded with 100 mg pyrene, 1 g of hexadecane as the solvent, and 500 psig H<sub>2</sub> cold charge pressure. Reaction times were 20 min and catalyst loadings, which were varied depending on the activity of the catalyst, ranged from 10 to 25 mg. The concentrations of pyrene and dihydropyrene in the products were determined using gas chromatography (GC).

Hydrodeoxygenation (HDO) activities were evaluated using the rate of disappearance of dibenzofuran (DBF). Experiments were performed at 300°C in 26 cm<sup>3</sup> batch microreactors that were loaded with 100 mg DBF, 25 mg catalyst, 1 g hexadecane, and 1200 psig H<sub>2</sub> cold charge pressure. Reaction times were 15 min and products were analyzed by GC.

Hydrodesulfurization (HDS) activities were measured in a flow reactor system using thiophene as the model compound. Reaction rates for the HDS of thiophene to butene were determined at 325°C and atmospheric pressure.

#### RESULTS and DISCUSSION

Because the HTOs are new catalytic materials with properties that are significantly different from well-known catalysts such as those supported on alumina, a thorough and systematic approach to their development must be taken. The elements included in this approach are (1) process definition and catalyst requirements; (2) catalyst preparation, pretreatment and characterization; (3) catalyst testing; and (4) catalyst scaleup and processing evaluation. The relationship among the program elements is shown in

Figure 1. The aspects of this program that will be discussed in this paper involve studies of the catalyst preparation and pretreatment procedures that are aimed at enhancing catalyst activity for coal liquefaction.

Seven NiMo HTO catalysts were prepared at an acidification pH of 4. They were evaluated for HYD and HDO activities and the results compared to Shell 324M (Table 1). This series of catalysts was analyzed to determine the effects on catalyst activity of the 500°C calcination procedure, Si addition to the HTO support, and removal of Na from the catalyst. The results show that there is a direct correlation (correlation coefficient = 0.98) between HYD and HDO activities for all the catalysts (HTOs and Shell 324M).

Analysis of the activities of the first three pairs of catalysts (runs 1-6) shows that the calcined catalyst in each pair has significantly greater activity than the noncalcined. The NiMo HTO catalysts without Si gave the lowest activities and the sulfided, calcined catalyst with a Ti:Si ratio of 5 (run 6) gave the highest HYD and HDO activities. These results show that Si addition is beneficial, but that too much Si (Ti:Si=3) causes a decrease in activity. The first six catalysts in Table 1 contained small amounts of Na (0.6 to 1.1 wt %), whereas the catalyst used in run 7 had <0.1 wt%. Comparison of activity results from runs 6 and 7 shows that removal of the Na gives a catalyst with the highest HYD activity; this catalyst has 90% of the HYD activity of Shell 324M. These results are in agreement with studies that show Na can poison catalyst sites. Parameters that are currently being studied to improve the performance of NiMo HTO catalysts include optimizing the Si content, evaluating the effects of the pH used in the acidification step, determining the impacts of different calcining conditions, and analyzing the effects of varying the active metal loadings.

Studies have been performed to determine why Si addition in the support increases catalyst activity. This work was performed with Pd HTO catalysts, which also show an increase in activity with Si addition to the support. Figure 2a shows the effects of the Ti:Si ratio in the support and the acidification pH on the surface areas of Pd HTO catalysts that have been calcined at 300°C in air. The presence of a 6:1 Ti:Si mole ratio results in a 2- to 3-fold increase in surface area with respect to Pd HTO. When the Ti:Si ratio is increased to 2, any discernible enhancement in surface area is limited to materials with the lower pHs. The effect of pH on the surface areas of catalysts prepared on the same supports is more difficult to discern. There appears to be a general trend whereby the surface areas of samples acidified at pH 4 and 5 are slightly enhanced with respect to materials that were not acidified (pH>6) or were treated at pH 2. Increasing the calcination temperature to 500°C (Figure 2b) shows similar trends to those observed at 300°C. As would be expected, the higher temperature resulted in an overall decrease in surface area for all materials. The results of this study on Pd HTO catalysts suggest that it may be possible to increase the activity of the NiMo HTO catalysts by decreasing the calcination temperature, decreasing the Ti:Si ratio to lower values than those shown in Table 1, and using a somewhat higher pH during acidification.

Optimization of the calcination process for these materials is

aimed at maintaining the dispersion of the active metals in the as prepared material while giving a catalyst that is stable under reaction conditions. The usual procedure for preparing alumina supported catalysts involves calcining after the metals have been impregnated onto the support. This procedure has been used in all previous studies of HTO catalysts. However, a different method, calcination of the support prior to ion exchange, may be possible with these materials. The potential benefit of this procedure, which will subsequently be referred to as precalcining, is that the metal is not present during calcination so that it will not sinter, while the possible disadvantage is that the ion exchange capacity of the calcined material may be too low to enable preparation of a good catalyst. The impact of precalcining temperature on the ion exchange capacities of HTOs are shown in Figure 3. The results obtained on two sets of catalysts, one exchanged with Co and the other with Mo, show that the exchange capacity decreases with increasing precalcination temperature. For Co, about 2/3 of the HTO's noncalcined exchange capacity is maintained between 400°C and 700°C. In contrast, Mo exchange shows a sharp decrease due to precalcining at 200°C and a more gradual decrease with increasing precalcination temperature. After a 500°C precalcination, only about 1/4 of the initial Mo exchange occurs. These results suggest that formation of a CoMo HTO catalyst may require two separate exchange steps: the Mo could be exchanged at room temperature followed by calcination and subsequent exchange with Co. Studies are currently underway to compare activities of catalysts prepared using precalcination and calcination after ion exchange.

Studies of HTO calcination after ion exchange are also being performed. Recent work (Figure 4) has shown the effect of calcination temperature on the thiophene HDS activities of two NiMo HTO catalysts. With calcination above 400°C, both catalysts show a significant increase in HDS activity. Differential thermal analyses of these catalysts showed that a thermal event occurred at this temperature. The NiMo HTO catalyst with the lower total metals loading maintains this higher activity up to a calcination temperature of at least 600°C. The NiMo HTO with the higher metals loading shows additional activity enhancement up to a calcination temperature of 500°C and then an activity decrease. The reasons for these phenomena are not yet known. Differential scanning calorimetry and thermal gravimetric analysis techniques are currently being performed in conjunction with activity testing to learn more about calcination and activation procedures for these materials.

#### CONCLUSIONS

Hydrous titanium metal oxide catalysts are extremely versatile materials that have promise as coal liquefaction catalysts. Previous studies have shown that they perform well in both batch and bench-scale coal liquefaction tests. Efforts to improve preparation and activation procedures for these catalysts have identified several promising research areas that either have or may lead to enhancements in catalyst activity. For, example, addition of Si to the support of NiMo HTO catalysts has yielded 2- to 3-fold increases in surface areas and has resulted in a 33% increase in HYD activity

and a doubling of HDO activity compared to an HTO catalyst without Si. In addition, it may be possible to maintain the high atomic dispersion of the metals at reaction conditions by calcining prior to ion exchange of the metal onto the support or reducing the calcination temperature. Current research is addressing these areas.

#### REFERENCES

1. R. G. Dosch, H. P. Stephens, and F. V. Stohl, "Catalysis Using Hydrous Metal Oxide Ion Exchangers," U. S. Patent 4,511,455, April 16, 1985.
2. F. J. Derbyshire, Catalysis in Direct Coal Liquefaction: New Directions for Research, IEA Coal Research Report IEACR/08, London, England, June 1988.
3. F. V. Stohl and H. P. Stephens, I&EC Research 26, 2466, 1987.
4. Stephens, H. P., Dosch, R. G., and F. V. Stohl, Ind. Eng. Chem. Prod. Res. Dev. 24, 15, 1985.
5. Stohl, F. V., Dosch, R. G., and H. P. Stephens, Proc. Direct Liquefaction Contractors' Review Meeting, Pittsburgh, PA, p. 490, Oct. 4-6, 1988.
6. Snape, C. E., Bolton, C., Dosch, R. G., and H. P. Stephens, Preprints Fuel Div. Amer. Chem. Soc. 33(3), 351, 1988.

Table 1. HYD and HDO testing of NiMo HTO catalysts.

Run	Ti:Si <sup>b</sup>	Pretreatment	Wt % Metals		Activity Testing <sup>a</sup>	
			Ni	Mo	HYD	HDO
1	No Si	Sulfide	3.23	12.40	0.134	0.004
2	No Si	Sulfide+calcine	3.23	12.40	0.480	0.037
3	3	Sulfide	3.03	9.69	0.236	0.017
4	3	Sulfide+calcine	3.03	9.69	0.613	0.069
5	5	Sulfide	2.69	9.62	0.227	NA <sup>c</sup>
6	5	Sulfide+calcine	2.69	9.62	0.812	0.080
7	5 (No Na)	Sulfide+calcine	4.08	9.75	0.904	NA
Shell 324M Sulfide			2.80	12.40	1.026	0.112

a k(g<sup>-1</sup>(active metal) sec<sup>-1</sup>)

b Mole ratio

c Not analyzed.

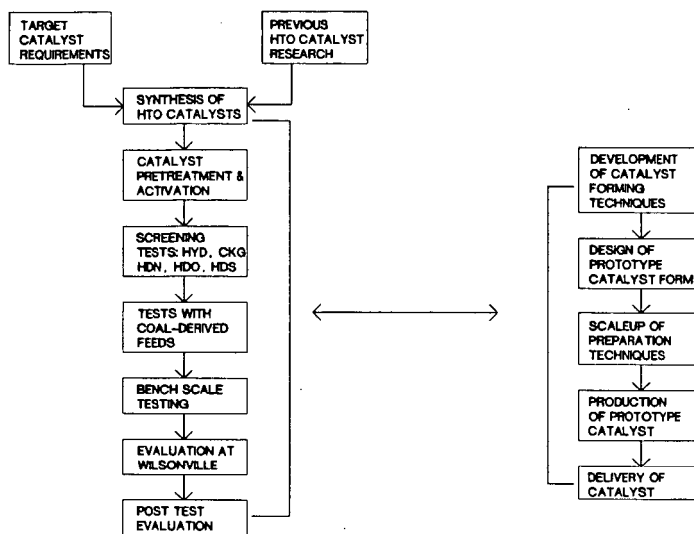


Figure 1. Overview of Sandia's catalyst development program.

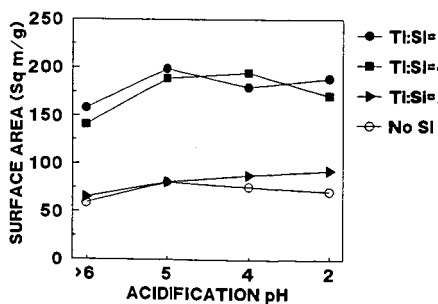


Figure 2a. Calcination at 300 C

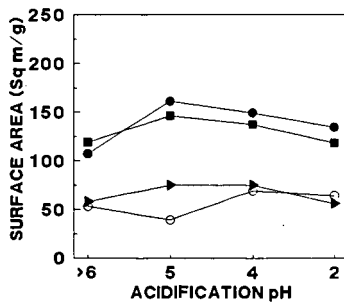


Figure 2b. Calcination at 500 C.

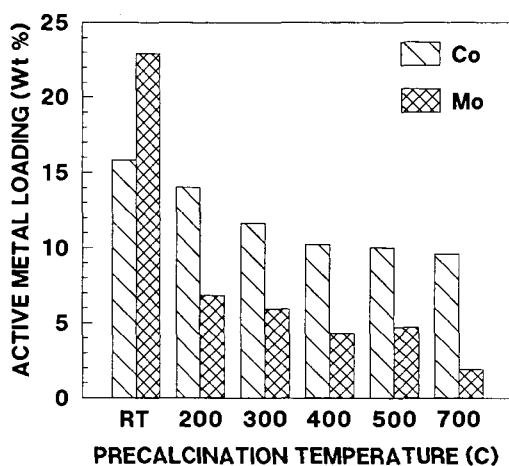


Figure 3. Effects of HTO precalcination temperature on ion exchange capacity.

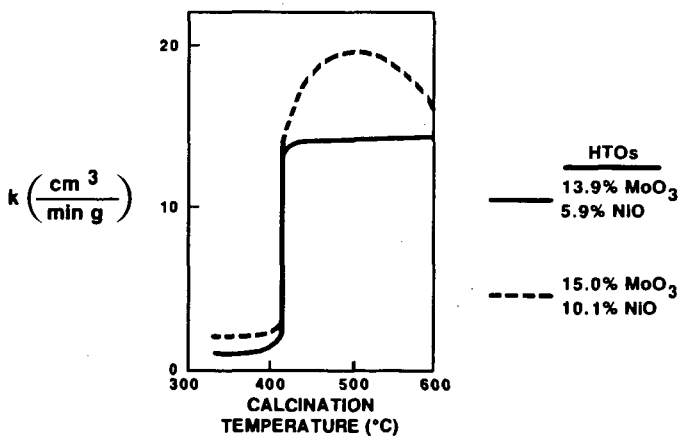


Figure 4. Effects of calcination temperature on thiophene HDS activity for two NiMo HTO catalysts.

## DISPERSED-PHASE CATALYSIS IN COAL LIQUEFACTION

Bruce R. Utz, Anthony V. Cugini, and Elizabeth A. Frommell

Department of Energy  
Pittsburgh Energy Technology Center  
P.O. Box 10940  
Pittsburgh, PA 15236

### ABSTRACT

The specific reaction ("preactivation") conditions for the conversion of catalyst precursors to unsupported catalysts have a direct effect on the catalytic activity and dispersion. The importance of reaction intermediates in decomposition of ammonium heptamolybdate and ammonium tetrathiomolybdate, and the sensitivity of these intermediates to reaction conditions, were studied in coal liquefaction systems. Recent results indicate that optimization of preactivation conditions facilitates the formation of a highly dispersed and active form of molybdenum disulfide for coal liquefaction. The use of the catalyst precursors ammonium heptamolybdate, ammonium tetrathiomolybdate, and molybdenum trisulfide for the conversion of coal to soluble products will be discussed.

### INTRODUCTION

The use of an unsupported dispersed-phase catalyst for direct coal liquefaction is not a novel concept and has been employed with varying success. Dispersed-phase catalysts have been introduced via impregnation techniques (1-4), as water-soluble (5-8) and oil-soluble (9-12) salts, and as finely divided powders (1,2). While some methods of catalyst introduction result in greater dispersion of the catalyst and greater activity for the liquefaction of coal, all of the techniques allow the formation of a finely dispersed inorganic phase. The use of dispersed-phase catalysts in direct coal liquefaction offers several advantages. Since they could be considered "once-through" catalysts, deactivation problems are reduced when compared to supported catalysts, and catalytic activity remains high. Diffusion limitations are minimized because of the high surface area of small catalyst particles. Maximum interaction of coal, vehicle, and gaseous hydrogen can occur on the catalyst surface with a highly dispersed catalyst.

One of the more popular techniques for producing dispersed-phase catalysts involves the use of water- or oil-soluble catalyst precursors. Small amounts of the water-soluble catalyst precursor are added to the coal-vehicle feed and are subsequently converted to a highly dispersed insoluble catalytic phase. The reaction conditions that convert the soluble catalyst precursor to a highly active and dispersed-phase catalyst are critical. The objective of this paper is to identify techniques that will convert a molybdenum catalyst precursor to a highly dispersed MoS<sub>2</sub> phase that has greater activity for coal liquefaction than previously identified dispersed-phase MoS<sub>2</sub> catalysts.



## EXPERIMENTAL

Catalyst screening tests were conducted in 40-mL microautoclave reactors. The liquefaction conditions were the following: temperature, 425°C; reaction pressure, 1000 psig  $H_2$  (pressure at room temperature); residence time, 1 hour; and solvent/coal, 2/1. The coal used was Illinois No. 6, Burning Star Mine (ultimate analysis: C, 71.02 wt%; H, 4.95 wt%; O (diff.), 9.26 wt%; N, 1.41 wt%; S, 3.23 wt%; and ash, 10.12 wt%, on a moisture-free basis), and the vehicle used was tetrahydronaphthalene (tetralin). Rapid heat-up rates were obtained by immersing the microautoclave in a preheated fluidized sand bath at 425°C. The microautoclave reached reaction temperature in 1-2 minutes. Slow heat-up rates were obtained by immersing the microautoclave in the fluidized sand bath at room temperature and gradually heating the sand bath to reaction temperature in 3/4 hour to 1 hour. Catalyst loadings were 1000 ppm, based on the weight of coal. Coal conversion was measured by the solubility of coal-derived products in methylene chloride and heptane using a pressure filtration technique(13).

Molybdenum trisulfide ( $MoS_3$ ) was prepared by acidifying a solution of ammonium tetrathiomolybdate with 24 wt% formic acid (14). All other reagents were ACS grade.

X-ray diffraction studies were conducted with a Rigaku computer-controlled diffractometer equipped with a long fine-focus Cu X-ray tube, a receiving graphite monochromator to provide monochromatic  $Cu-K_\alpha$  radiation, and a scintillation detector.

## RESULTS AND DISCUSSION

Conversion of an aqueous solution of ammonium heptamolybdate [ $(NH_4)_6Mo_7O_{24} \cdot 4H_2O$ ] to an active and high-surface-area catalyst is dependent on a number of factors. Gaseous hydrogen sulfide ( $H_2S$ ) is required to convert ammonium heptamolybdate (AHM), which is essentially an oxide salt, to a series of oxysulfide salts (15) and ultimately to molybdenum disulfide ( $MoS_2$ ), as shown in Figure 1. The ratio of ammonium ion to molybdenum may also be important, since studies have shown that increased  $NH_4/Mo$  ratios result in higher hydrogen consumption for the conversion of petroleum to upgraded products when AHM is used as a dispersed-phase catalyst (7,15). Petroleum upgrading studies demonstrated that the heat-up rate for the conversion of AHM to  $MoS_3$  is extremely important (15). Slower heat-up rates resulted in a gradual transition of AHM to  $MoS_2$  and significantly higher conversions of petroleum to distillate products.

Information on the dispersion of  $MoS_2$  was obtained from X-ray diffraction measurements, which are sensitive to the degree of stacking and dispersion of the  $MoS_2$  layers (Figure 2). The diffraction pattern of single layers of  $MoS_2$  shows the (100) and (110) bands, but no (002) band, as in the middle curve of Figure 2. These crystallites are considered two-dimensional, since there is no growth in the third dimension. When only a very small number of  $MoS_2$  layers are in multilayer stacks, a weak (002) band is present, as in the top curve with the catalyst precursor,  $MoS_3$ . When many multilayer stacks of  $MoS_2$  are present, a strong (002) band can be seen, as in the lower curve. The pattern is that obtained for three-dimensional crystallites. The widths-at-half-maximum can be

used to estimate the size of the  $\text{MoS}_2$  crystallites. The  $\text{MoS}_2$  crystallites formed during a gradual heat-up of AHM, in the absence of coal, are three-dimensional, as shown in the bottom curve of Figure 2. Coal added to AHM under the same reaction conditions prevents the  $\text{MoS}_2$  layers from growing in the third dimension. Since the crystallite size in the plane of the  $\text{MoS}_2$  layers is about the same in both cases (150-200 angstroms), the addition of the coal produces a more highly dispersed, minimally stacked  $\text{MoS}_2$ . All of these results suggest that many factors can affect the extent of dispersion of  $\text{MoS}_2$ . The factors that have been identified include heat-up rate of the catalyst precursor during the conversion to  $\text{MoS}_2$ ; the  $\text{NH}_3/\text{Mo}$  ratio; the  $\text{H}_2\text{S}$  pressure; and other reagents, such as coal, that might affect the transition of AHM to  $\text{MoS}_2$ .

Previous studies by Lopez et al. (16) show that small amounts of ammonium tetrathiomolybdate [  $(\text{NH}_4)_2\text{MoS}_4$  ] are produced during the decomposition of AHM, which represents an intermediate of a minor decomposition pathway. One advantage of using ammonium tetrathiomolybdate (ATTM) as a dispersed-phase catalyst in coal liquefaction is that an external source of  $\text{H}_2\text{S}$  is not required because the catalyst precursor already exists as a water-soluble sulfide salt. It is known that ATTM thermally decomposes to  $\text{MoS}_3$  and subsequently to  $\text{MoS}_2$  (17). Eggertsen et al. (14) examined the reaction conditions for the thermal decomposition of  $\text{MoS}_3$  to  $\text{MoS}_2$  and determined that rapid heat-up (direct introduction of  $\text{MoS}_3$  into a stream of hydrogen at  $450^\circ\text{C}$ ) gave  $\text{MoS}_2$  having a surface area of 85-158  $\text{m}^2/\text{gm}$ , while gradual heat-up (25 min to  $450^\circ\text{C}$ ) resulted in  $\text{MoS}_2$  surface areas of less than  $5\text{m}^2/\text{gm}$ . Naumann and coworkers (17) applied the results of Eggertsen to the catalyst precursor ATTM, since  $\text{MoS}_3$  was considered to be an intermediate in the decomposition of ATTM (Figure 3). The results show that high-surface area  $\text{MoS}_2$  is formed (88  $\text{m}^2/\text{gm}$ ) if the thermal transition of ATTM to  $\text{MoS}_2$  is rapid, and the surface area is low if the thermal transition is gradual.

Studies at PETC examined the conversion of coal to methylene chloride- and heptane-soluble products using ATTM as a catalyst precursor. Experiments were performed using both rapid and gradual heat-up rates for the preparation of the dispersed-phase catalyst and were compared with results using AHM as a catalyst (Figure 4). The results demonstrate that rapid heat-up of ATTM resulted in coal conversions to methylene chloride- and heptane-soluble material that were higher than conversions from experiments done at a slower heat-up, consistent with expectations for surface area studies of pure compounds. Experiments were also performed with  $\text{MoS}_3$ , wherein  $\text{MoS}_3$  was suspended in the same amount of water used for the water-soluble precursor, ATTM. Results show that conversion of coal to methylene chloride- and heptane-soluble products is greater for rapid heat-up experiments and is comparable to those using AHM (Figure 4). Experiments that verify the microautoclave studies were also performed in a 1-liter stirred autoclave, using both batch and continuous modes of operation.

Experiments were also performed with moisture-free solid  $\text{MoS}_3$ . Elimination of water has several advantages. The addition of water causes a decrease in hydrogen partial pressure within the reactor and is more energy intensive because water is being heated. Experimental results presented in Figure 4 demonstrate that the addition of the dry catalyst precursor,  $\text{MoS}_3$ , produced coal conversions comparable to those

obtained with the water-soluble catalyst precursors. Therefore,  $\text{MoS}_3$  may represent an ideal choice in the preparation of dispersed-phase catalysts. The X-ray diffraction pattern of  $\text{MoS}_2$ , from  $\text{MoS}_3$ , showed a very small (002) band, indicating minimal stacking. Minimal stacking infers a well-dispersed, high-surface-area material that provides comparable conversions to the water-soluble catalyst precursors. Scanning electron microscopy (SEM) was not able to detect the presence of  $\text{MoS}_2$ , suggesting that the particle size was less than 1000 angstroms. These results support the existence of highly dispersed  $\text{MoS}_2$ , which has resulted in the high conversion to solvent-soluble products.

#### CONCLUSIONS

Two catalyst precursors have been identified that result in high conversions of coal to solvent-soluble products when heated rapidly to reaction temperature. The use of  $\text{MoS}_3$  and ATTM as catalyst precursors, rather than AHM as a catalyst precursor, offers a number of advantages. Both catalyst precursors are in a sulfided form, and therefore additional  $\text{H}_2\text{S}$  is not required, while AHM requires the addition of  $\text{H}_2\text{S}$  in order to form the oxysulfide intermediates and the final product,  $\text{MoS}_2$ . Both of the sulfided precursors are activated and highly dispersed when heated rapidly to reaction temperature, while AHM requires a gradual heat-up, and therefore activation of AHM is much more energy intensive. The ultimate goal is to identify a dry, highly dispersed, catalyst precursor or catalyst that can be added to a coal-vehicle feed without the addition of water and that results in yields of coal-derived products comparable to those produced using water- or oil-soluble catalyst precursors. Possibly  $\text{MoS}_3$  is the catalyst precursor that satisfies those requirements.

#### ACKNOWLEDGMENTS

The authors thank Raymond Bernarding for conducting the liquefaction experiments and Fred Vinton for preparing the catalyst precursors. The authors would also like to thank Sidney S. Pollack for his assistance in the X-ray diffraction study.

#### DISCLAIMER

Reference in this report to any specific commercial product, process, or service is to facilitate understanding and does not necessarily imply its endorsement or favoring by the United States Department of Energy.

#### REFERENCES

1. Schlesinger, M.D.; Frank, L.V.; Hiteshue, R.W. Bureau of Mines Report No. 6021 (1961).
2. Weller, S.W.; Pelipetz, M.G. Ind. Eng. Chem. 43(5), 1243 (1951).
3. Clark, E.L.; Hiteshue, R.W.; Kandiner, H.J. Chem. Eng. Prog. 48, 14 (1952).

4. Derbyshire, F.J.; Davis, A.; Lin, R.; Stansberry, P.G.; Terrer, M.T. Fuel Proc. Tech. 12, 127 (1986).
5. Moll, N.G.; Quarderer, G.J. Chem. Eng. Prog. 75(10), 46 (1979).
6. Moll, N.G.; Quarderer, G.J. U.S. Patent 4,090,943, May 23, 1978.
7. Lopez, J.; McKinney, J.D.; Pasek, E.A. U.S. Patent 4,557,821, December 10, 1985.
8. Cugini, A.V.; Ruether, J.A.; Cillo, D.L.; Krastman, D.; Smith, D.N.; Balsone, V. Preprints, Div. Fuel Chem., Am. Chem. Soc. 33(1), 6 (1988).
9. Hawk, C.O.; Hiteshue, R.W. Bureau of Mines Bulletin No. 622, 42 (1965).
10. Gatsis, J.G.; Gleim, W.K.T. U.S. Patent 3,252,894, May 1966.
11. Anderson, R.R.; Bockrath, B.C. Fuel, 64, 329 (1984).
12. Aldridge, C.L.; Bearden, R., Jr. U.S. Patent 4,298,454, September 5, 1978.
13. Utz, B.R.; Narain, N.K.; Appell, H.R.; Blaustein, B.D. in "Coal and Coal Products: Analytical Characterization Techniques" (Ed. E.L. Fuller, Jr.), Am. Chem. Soc. Symp. Ser. 205, 225 (1982).
14. Eggertsen, F.T.; Roberts, R.M. J. Phys. Chem. 63, 1981 (1959).
15. Lopez, J.; Pasek, E.A.; Cugini, A.V. U.S. Patent 4,762,812, August 9, 1988.
16. Lopez, J.; Pasek, E.A.; Cugini, A.V. Unpublished results.
17. Naumann, A.W.; Behan, A.S.; Thorsteinson, E.M. Proc. Fourth Int. Conf. Chemistry and Uses of Molybdenum (H.E. Barry and C.N. Mitchell Eds.) 313 (1982).

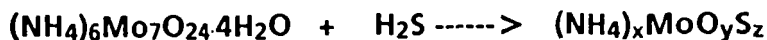


Figure 1. Conversion of Ammonium Heptamolybdate to Molybdenum Disulfide.

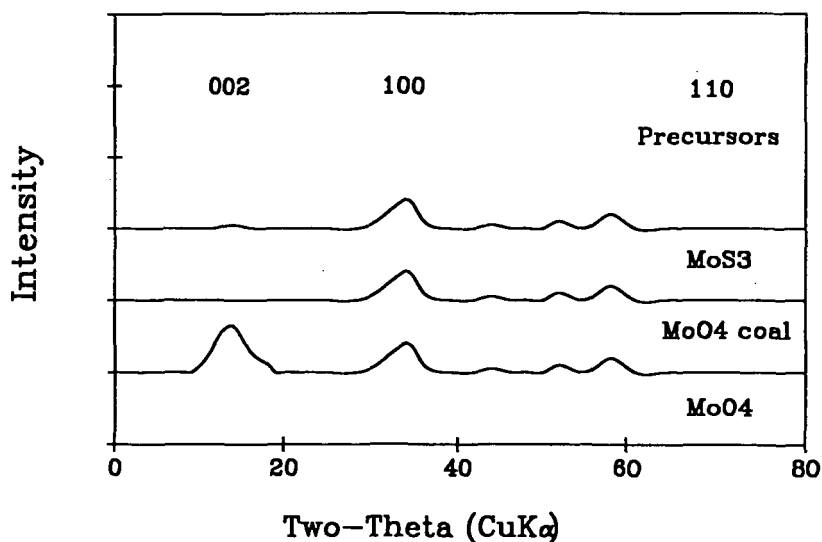


Figure 2. X-Ray Diffraction Patterns for Molybdenum Disulfide (h,k,l) Generated from Mo(VI) Precursors Reacted at Coal Liquefaction Conditions.

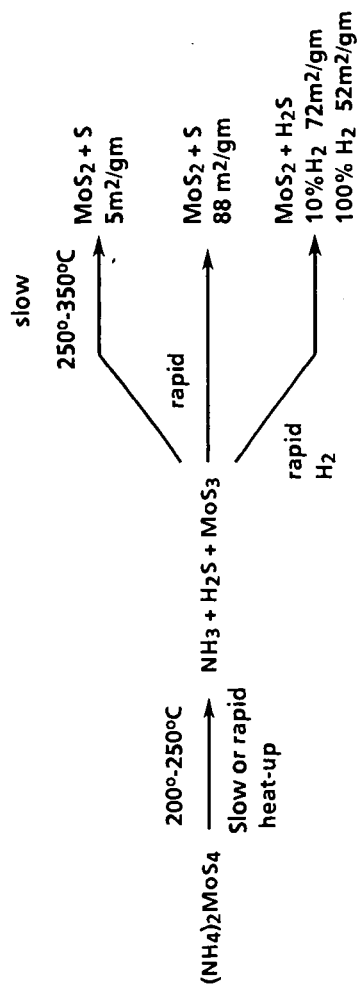


Figure 3. Decomposition of Ammonium Tetrathiomolybdate.

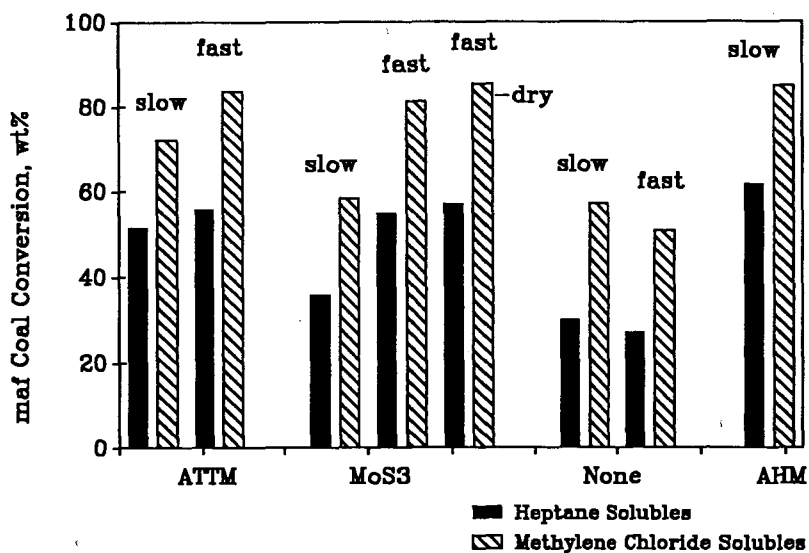


Figure 4. Effect of heat-up rate on coal conversion using presulfided catalyst precursors.

## Characterization of Catalysts from Molybdenum Naphthenate

Honggon Kim\*, Christine W. Curtis\*, Donald C. Cronauer\*\*  
and Daniel J. Sajkowski\*\*

\*Chemical Engineering Department, Auburn University, AL 36849

\*\*Amoco Oil Company, Naperville, Illinois

### INTRODUCTION

Molybdenum naphthenate has been shown to be a highly active catalyst precursor for coal conversion in both coal processing and coal liquefaction (1-3). This catalyst precursor has also been effective for producing highly upgraded end products (4-6). Molybdenum naphthenate, a metal salt of the organic acid, is thermally decomposed releasing the metal at liquefaction conditions. Subsequent reaction of the metal to the sulfide occurs if sulfur is present. This *in situ* sulfided catalyst has been shown to have a different selectivity for hydrogenation and heteroatom removal reactions than commercial hydrotreating catalysts (7) at liquefaction conditions.

Chianelli and coworkers (8-10) have prepared bulk molybdenum sulfides having surface areas up to 50 m<sup>2</sup>/g by reacting MoCl<sub>4</sub> with Li<sub>2</sub>S in a tetrahydrofuran solvent. The precipitated sulfide was then treated with acetic acid to remove residual Li<sub>2</sub>S. It was then treated with H<sub>2</sub>S/H<sub>2</sub> at 400°C. Line broadening analysis of X-ray diffraction peaks suggested that the average size of the crystalline regions was 28Å in the perpendicular direction and 78Å in the lateral direction. Crystallites of these dimensions would, however, give larger surface areas. This discrepancy was resolved by TEM which indicated that the lateral extent of the MoS<sub>2</sub> crystallites was several thousand angstroms (9-10). The authors described the structure as having a "rag morphology" (10).

The purpose of our study was to prepare and characterize the active catalytic species generated from molybdenum naphthenate and excess sulfur under conditions similar to those used in coal liquefaction and coprocessing. Several catalytic hydrogenation reactions were performed using model compounds having structures representative of those present in coal or petroleum residuum. The model systems used were naphthalene, indene, benzofuran, indole, and benzo thiophene dissolved in hexadecane. Molybdenum naphthenate which is oil soluble was added directly into the solvent as was sulfur which was introduced in excess. After reaction, the active catalytic species was recovered from the product solution and characterized by a number of analytical techniques to ascertain its composition and surface properties.



## Experimental

Hydrogenation Reactions.--Hydrogenation reactions were conducted in horizontal stainless steel tubing bomb reactors of ca. 56 cm<sup>3</sup>. The reactor was charged with 11.2g of reactant solution composed of 2 weight percent naphthalene or 1 weight percent of the other model species, molybdenum naphthenate at 3000 ppm Mo per total charge and excess elemental sulfur. Three different amounts of elemental sulfur, 0.067, 0.201, and 0.269g, were charged; these levels corresponded to three, nine, and twelve times the amount of sulfur required to convert Mo to MoS<sub>2</sub>. Reactions were conducted at 380°C for 30 minutes with H<sub>2</sub> introduced at 1250 psig at ambient temperature. The reactors were agitated at 550 cpm. The reactors were quenched in water immediately after reaction.

Chemicals.--The model reactants, naphthalene (99%), indene (99%), benzofuran (99.5%), indole (99%), and benzothiophene (97%), were obtained from Aldrich Chemical Company. Molybdenum naphthenate containing 6 weight percent Mo was obtained from Shepard Chemical Company.

Analysis.--After the reaction, the recovered product solution was separated into a liquid fraction and a black solid. The solid was washed with tetrahydrofuran, dried in a vacuum desiccator for three days and stored in a vial. The total weight of the black solid recovered from three equivalent reactions was approximately 0.19g.

The liquid products were analyzed by gas chromatography using a 30m DB-5 fused silica capillary column of 0.32mm inner diameter from J&W Scientific and FID detection. Para-xylene was used as the internal standard. Selected solid samples were characterized using X-ray diffraction, surface area (BET using N<sub>2</sub>), and scanning and transmission electron microscopy (SEM and TEM). The X-ray diffraction patterns were measured using a Scintag PAD V powder diffractometer using samples mounted on double-sided adhesive tape with curve deconvolution to remove the tape signal. Surface area was measured using a Digisorb-2600. SEM and TEM scans were made using JOEL-840A and Philips-400T instruments.

## Results and Discussion

Reactions Using Molybdenum Naphthenate and Excess Sulfur.--The reactions using molybdenum naphthenate and excess sulfur were performed with naphthalene, indole, benzofuran, indene, and benzothiophene. The product distributions obtained at two different levels of excess sulfur are given for each reactant in Table 1. For naphthalene, the major product was tetralin for both sulfur levels. At the higher sulfur level, slightly more hydrogenation to decalin was observed. The partially saturated hydrocarbon, indene, was readily hydrogenated to indan; however, further hydrogenation to the fully saturated hexahydroindan was limited. Only a small amount, 2%, of hydrogenolysis to methylcyclohexane occurred. The higher sulfur level again showed a higher level of hydrogenation of indene.

The oxygen containing species, benzofuran, was the least reactive of the heteroatomic species used in this study. Benzofuran was completely converted to a product slate containing primarily o-ethylphenol, ethylbenzene, and ethylcyclohexane. The higher sulfur level was detrimental to deoxygenation and nearly doubled the amount of ethylphenol present in the products. Both indole and benzothiophene underwent total heteroatom removal. However, the primary product from indole was ethylcyclohexane, and that from benzothiophene was ethylbenzene. In both cases the higher sulfur levels resulted in slightly higher levels of hydrogenation. However, the effect on indole, because of its high degree of hydrogenation, was small.

Characterization of Catalyst Solids.--Selected samples of reactor solids were analyzed for carbon hydrogen and nitrogen contents. Some samples were also subjected to pyrolysis using a thermogravimetric unit with nitrogen. The results given in Table 2 indicate that adsorbed or trapped hexadecane remained on the catalyst solids; some indole was adsorbed in those two runs. Mass spectrometric analyses confirmed this conclusion.

The results of surface area determinations are given in Table 3. Even though the solids were dried at 250°C under vacuum, not all of the solvent was stripped in all cases. The BET surface area results were low until this material was removed. Final surface areas were in the range of 150 to 200 m<sup>2</sup>/g.

SEM microphotographs taken at X25,000 indicated that the solids were composed of irregular clusters of rounded particles which ranged from about 500 to 2500 Å in diameter. A typical SEM microphotograph is given in Figure 1. Subsequent TEM microphotographs of five selected solid samples (1A, 2A, 4A, 4B, 5A; see Table 3) showed that the solids were similar in appearance and were composed of "needle-shape" crystallites; see Figure 2. The shape was consistent with the "rag morphology" of Chianelli et al. (8-10)

X-ray diffraction analyses indicated that the solids were MoS<sub>2</sub> crystallites as a rhombohedral polymorph, and no excess sulfur was found. A low angle peak at about 13 degree's, after tape correction, corresponded to the diffraction perpendicular to the layers of MoS<sub>2</sub>. From peak width broadening, a spacing of 26 Å (4 layers) was indicated. A peak at 59 degree's, corresponding to the diffraction parallel to the layers, indicated that a lateral dimension of 45 Å existed with additional indications of longer elements.

#### Summary

When molybdenum naphthenate was added as a feed with model compounds for reactions at coal liquefaction conditions, the hydrogenation of naphthalene, indene, benzothiophene, and indole was enhanced by introducing a high level of sulfur. Indole, which had the highest degree of hydrogenation in the product slate, showed the least effect of sulfur level. Benzofuran was the least reactive of the three heteroatomic species having the same molecular skeletal structure. Deoxygenation was

inhibited by the higher amount of sulfur in the system. Molybdenum naphthenate reacted in situ to form rhombohedral MoS<sub>2</sub>. The resulting catalyst particles were of small size, 26A in the perpendicular direction and about 45A, or larger, in the lateral direction. These solids had higher surface areas, 150 to 200 m<sup>2</sup>/g, than previously reported.

#### Acknowledgments

This work was sponsored by DOE under Program DEFG-2285PC80502 and the catalyst analyses were supported by Amoco Oil Co. We also acknowledge the work of J. J. Kolstad, B. L. Meyers, J. B. Hall, J. A. Kaduk, and T. J. Young in the discussion and analytical aspects of this project.

#### REFERENCES

1. Hawk, C., Hiteshue, R. W.; Bureau of Mines Bulletin, 622, 24, (1965).
2. Kottenstette, R. J.; Sandia Report SAND82-2495, March 1983.
3. Curtis, C. W., Cassel, F. N.; Energy & Fuels, 2, 1, (1988).
4. Pellegrino, J. L., Curtis, C. W.; Energy & Fuels, in press (1989).
5. Bearden, R., Jr., Baird, W. C., Jr., Aldridge, C. L.; U. S. Patent 4,424,110, (1984).
6. Aldridge, C. L., Bearden, R., Jr.; U. S. Patent 4,298,454, (1981).
7. Kim, H., Curtis, C. W.; Proceedings of Pittsburgh Conference, 659, September 1988.
8. Chianelli, R. R., Dines, M. B.; Inorg. Chem., 17, 2758, (1978).
9. Chianelli, R. R., Prestridge, E. B., Pecoraro, T. A., DeNeufville, J. P., Science 203, 1107, (1979).
10. Pecoraro, T. A., Chianelli, R. R.; J. Catal. 67, 430, (1981)

Table 1. Catalytic Hydrogenation of Model Compounds Using Molybdenum Naphthenate and Excess Sulfur

## 1. Naphthalene

Sulfur Amount*	Product Distribution (mole %)			
	Naphthalene	Tetralin	Decalin	Butylbenzene
3	1.3±0.2	89.7±0.7	7.9±0.5	1.1±0.1
9	0.9±0.1	87.0±0.2	10.7±0.1	1.1±0.3

## 2. Indene

Sulfur Amount*	Indene	Product Distribution (mole %)			
		Indan	cis-Hexahydro indan	trans-Hexahydro indan	Methyl cyclohexane
3	0	89.1±0.2	7.1±0.2	3.0±0.2	0.7±0.1
12	0	83.7±0.4	9.5±0.4	4.9±0.1	1.9±0.2

## 3. Benzofuran

Sulfur Amount*	Benzofuran	Product Distribution (mole %)					
		Dihydro benzofuran	o-Ethyl phenol	Ethyl benzene	Ethyl cyclohexene	Ethyl cyclohexane	Methyl cyclohexane
3	0	0	15.4±0.4	53.8±0.3	0.2±0.2	30.2±0.2	0.6±0.1
12	0	0	29.5±0.9	35.8±0.6	0.8±0.0	33.1±0.3	0.9±0.1

## 4. Indole

Sulfur Amount*	Indole	Product Distribution (mole %)					
		Indoline	o-Ethyl aniline	Ethyl benzene	Ethyl cyclohexene	Ethyl cyclohexane	Methyl cyclohexane
3	0	0	0	8.9±0.1	0.9±0.1	86.5±0.1	3.8±0.1
12	0	0	0	7.8±0.1	0.9±0.1	88.2±0.1	3.1±0.2

## 5. Benzothiophene

Sulfur Amount*	Benzo thiophene	Product Distribution (mole %)					
		Dihydro benzothiophene	o-Ethylthio phenol	Ethyl benzene	Ethyl cyclohexene	Ethyl cyclohexane	Methyl cyclohexane
3	0	0	0	93.8±0.2	0	5.7±0.2	0.5±0.1
12	0	0	0	89.7±0.2	0	9.4±0.2	0.9±0.1

\* Multiples of the stoichiometric amount of sulfur in MoS<sub>2</sub>

\*\* Each reaction was triplicated.

Table 2. Weight Loss and Carbon & Hydrogen Analyses of Recovered Catalysts

1. Naphthalene

<u>Sulfur Amount</u>	<u>% Loss TGA/N</u>	<u>Carbon</u>	<u>Hydrogen</u>	<u>Nitrogen</u>
3	----	12.6	2.3	----
9	19	14.7	2.6	----

2. Indene

<u>Sulfur Amount</u>	<u>% Loss TGA/N</u>	<u>Carbon</u>	<u>Hydrogen</u>	<u>Nitrogen</u>
3	20	11.0	2.3	----
12	----	----	----	----

3. Benzothiophene

<u>Sulfur Amount</u>	<u>% Loss TGA/N</u>	<u>Carbon</u>	<u>Hydrogen</u>	<u>Nitrogen</u>
3	15	10.1	1.9	----
12	----	----	----	----

4. Indole

<u>Sulfur Amount</u>	<u>% Loss TGA/N</u>	<u>Carbon</u>	<u>Hydrogen</u>	<u>Nitrogen</u>
3	29	24.0	4.3	0.5
12	18	14.1	2.4	0.4

5. Benzofuran

<u>Sulfur Amount</u>	<u>% Loss TGA/N</u>	<u>Carbon</u>	<u>Hydrogen</u>	<u>Nitrogen</u>
3	17	13.4	2.5	----
12	----	----	----	----

Table 3. Areas and Pore Volumes of Recovered Catalysts

1. Naphthalene

<u>Sulfur Amount</u>	<u>% Loss Drying*</u>	<u>Surface Area, M<sup>2</sup>/g</u>	<u>Pore Volume CC/g</u>
3	9.4	158	0.28
9	12.8	96	0.30
	+7.1	141	0.18

2. Indene

<u>Sulfur Amount</u>	<u>% Loss Drying*</u>	<u>Surface Area, M<sup>2</sup>/g</u>	<u>Pore Volume CC/g</u>
3	15.4	198	0.39
12	—	—	—

3. Benzothiophene

<u>Sulfur Amount</u>	<u>% Loss Drying*</u>	<u>Surface Area, M<sup>2</sup>/g</u>	<u>Pore Volume CC/g</u>
3	13.8	214	0.30
12	—	—	—

4. Indole

<u>Surface Amount</u>	<u>% Loss Drying*</u>	<u>Surface Area, M<sup>2</sup>/g</u>	<u>Pore Volume CC/g</u>
3	8.7	35	0.31
	+5.3	103	0.22
12	9.8	161	0.39

5. Benzofuran

<u>Surface Amount</u>	<u>% Loss Drying*</u>	<u>Surface Area, M<sup>2</sup>/g</u>	<u>Pore Volume CC/g</u>
3	16.6	179	0.30
12	—	—	—

\*Drying conditions were 250°C, 16 hours, 20 torr.

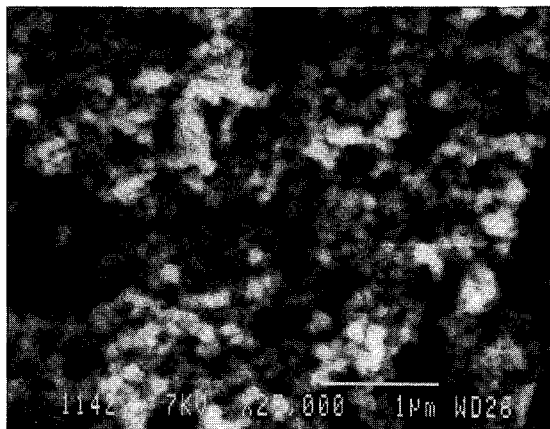


Figure 1 - SEM Photomicrograph of Sample 4B  
(x 25,000)

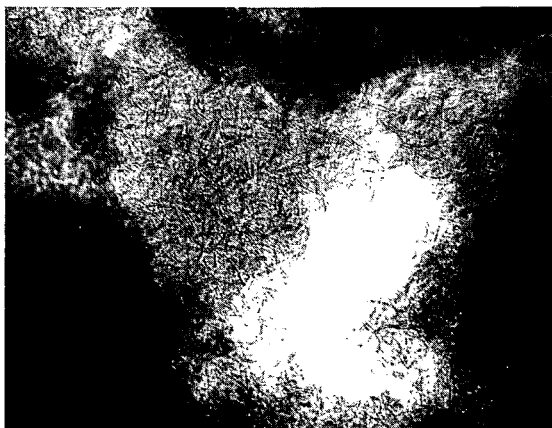


Figure 2 - TEM Photomicrograph of Sample 5A  
(x 800,000)

## Colloidal Coal Hydroliquefaction Catalyst Preparation

Diane R. Milburn, Bruce D. Adkins\*, and Burtron H. Davis

Center for Applied Energy Research  
3572 Iron Works Pike  
Lexington, KY 40511

\*Akzo Chemicals, Inc.  
13000 Bay Park Road  
Pasadena, TX 77507

### Introduction

Typical hydrotreating catalysts, consisting of Mo and W or Ni on aluminoxide, are pelletized and added to and withdrawn from the reactor in batches. The effects of diffusivity on the global reaction rate as well as on dispersion of the active metals are poorly understood.

Current research efforts aimed at cost reduction include dispersion of "disposable" unsupported metals in the feed streams (ref. 1) and impregnation of high surface aerogel supports (ref 2). In the standard incipient wetness impregnation a strongly bridging solvent such as water is used to dissolve the metal salt precursor. On drying, the support is compacted and pore structure of the final product may bear little resemblance to the original starting material. This study involves utilization of commercial colloiddally sized aluminum supports to prepare a homologous series of catalysts to study the effects of solvent and solvent removal on structure of the support and on dispersion of the active phase.

### Experimental

Four impregnation techniques utilizing Degussa Aluminoxide-C (fumed process, 150-200 Å discrete spherical particles) and ammonium molybdate from Fisher Scientific Co. (83% MoO<sub>3</sub>) are described below.

#### Incipient Wetness, (IW)

The Mo salt is dissolved in distilled water and added dropwise to the support. This continues until the support is at "incipient wetness", i.e. the point where unbound moisture is about to become available. The catalyst is dried at ca. 120°C for 12 to 24 hours,



ground with a mortar and pestle and calcined at 500°C for 4 to 6 hours.

Ethanol Slurry, Vacuum Dried, (EtOH-V)

The salt is dissolved in excess ethanol and a slurry is made by adding the support material. The mixture is stirred for several hours and then placed in a vacuum oven at ca. 100°C for 36 to 48 hours. This is followed by grinding as described above.

Ethanol Slurry, Rotary Evaporated, (EtOH-R)

Identical to EtOH-V except that solvent removal is achieved in a rotary evaporating apparatus over a period of 4 to 6 hours.

Critical Point Solvent Evaporation, (CPSE)

A slurry of is made of metal salt, solvent and support material as described for EtOH-V. The slurry is maintained under an inert gas pressure which is higher than the vapor pressure of the solvent at a temperature slightly lower than the critical temperature; the slurry is then heated above the critical point. A very rapid evaporation of the solvent occurs at the critical point (on the order of minutes or less). The catalyst is then removed and calcined as above.

Scanning Electron Microscopy was performed on the samples to observe gross differences in physical structure. The instrument used was an ETEC Omniscan SEM equipped with a PGT-1000 data acquisition and analysis system. Pore structure and surface area measurements were calculated from nitrogen adsorption/desorption isotherms made on a Digisorb 2500 instrument and from combining Hg penetration scans made at three pressure ranges on a Quantachrome Autoscan Porosimeter.

Catalyst Structure

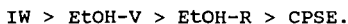
Physical characteristics for five catalysts prepared by the methods described above, for fresh  $\text{Al}_2\text{O}_3$ , and for  $\text{Al}_2\text{O}_3$  which has been wetted and dried as described for the IW sample are summarized in Table 1. The data show that the tap density (determined by measuring the volume of a known weight of material which had been gently tapped in a graduated cylinder) increases significantly in all treatments of the support material except for the case of the CPSE preparation. SEM micrographs indicate that the IW, EtOH-V, and EtOH-R processes yield irregularly shaped particles with a wide distribution of sizes as is typical for a grinding process. In contrast, the sample prepared using the CPSE process is composed of secondary particles which are much more uniform in size and shape.

The BET surface area of  $\text{Al}_2\text{O}_3$  increases when wetted and dried. This is due primarily to the large numbers of interparticle contacts formed during drying; condensation around

an interparticle contact zone essentially adds a contribution to the isotherm volume. Figure 1 shows the comparison of pore volumes calculated from the nitrogen adsorption isotherms for these catalyst samples with fresh Degussa aluminosilicate-C. The CPSE most closely resembles the fresh support material (shown by the dotted line), the wetted alumina and the IW sample show the greatest increase, and the EtOH-V and EtOH-R samples are intermediate in calculated volume increase from fresh  $\text{Al}_2\text{O}_3$ . The mercury porosimetry data for total pore volume indicates that decreasing the severity of compaction during catalyst preparation, either by lowering the bridging strength of the solvent or by increasing the rate of solvent removal, results in an increase in pore volume.

#### Active Phase Dispersion

It is known that the selectivity for octenes in the catalytic dehydration of octanol is a function of the acid/base properties of the catalyst used (ref. 3). This reaction has been used in measuring the dispersion of  $\text{MoO}_3$  on alumina (ref. 4). The selectivity, at constant conversion, for our series of catalysts, for pure  $\text{MoO}_3$  and for pure  $\gamma\text{-Al}_2\text{O}_3$  is shown in figure 2; the line represents selectivity for a series of IW catalysts with increasing  $\text{MoO}_3$  loadings. These data indicate that dispersion of the active phase decreases in the order:



X-Ray diffraction scans suggest that both the IW and CPSE contain little or no crystalline  $\text{MoO}_3$ .

#### Hydrogenolysis Performance

Hydrogenolysis of 1,3,5-trimethylbenzene (tmb) in a plug-flow reactor was used to compare activity for the series of catalysts (ref 5). The catalysts were diluted with an inert  $\alpha\text{-Al}_2\text{O}_3$  (Fisher Scientific,  $0.96\text{m}^2/\text{g}$ ) to minimize the effects of physical differences in the test catalysts by making the reactor beds similar in density, volume and particle size. The catalyst was first reduced in flowing  $\text{H}_2$  overnight at  $450^\circ\text{C}$ ; the reaction mixture was a 10:1 molar mixture of  $\text{H}_2$  and 1,3,5-trimethylbenzene.

For the IW catalyst, hydrogenolysis of 1,3,5-tmb to m-xylene was the dominant reaction; equilibrium between the two had been reached at residence times of 15 minutes. Small amounts of o- and p-xylene as well as 1,2,3- and 1,2,4-tmb were also detected. The EtOH-V and CPSE showed the same product selectivity, although concentrations are shifted downward and the equilibrium between m-xylene and 1,3,5-tmb was not reached until residence times of approximately 1 hour.

The greatest tendency toward hydrogenolysis was seen for the 17%  $\text{MoO}_3$  catalyst. The equilibrium between 1,3,5-tmb and m-

xylene is already established at residence times of 15 minutes, but at longer times the m-xylene production declines and a corresponding increase in benzene and methane is observed. TEM micrographs revealed large  $\text{MoO}_3$  crystallites on the 17%  $\text{MoO}_3$  sample not seen in any of the 12% loading samples. XPS analyses on the two EtOH-V catalysts show the presence of a peak for a more reduced species of Mo in the 17% loading not present in the 12% catalyst reduced under the same conditions. These data suggest that the Mo in excess of one monolayer is apparently more reduced than the supported Mo.

### Conclusions

Choice of solvent and method of solvent removal are critical factors in determining the final structure of a supported catalyst. The use of a less polar solvent and subsequent rapid removal is shown to minimize compaction of the colloidal alumina particles. However, greater metal dispersion and higher hydrogenolysis activity is indicated for catalysts prepared using water. Further investigation is needed to determine the effects of subsequent impregnation, and coimpregnation, of promoters, as well as the removal of water at it's critical point.

### References

1. A. V. Cugini, J. A. Ruether, D. L. Cillo, D. Drastman, D. M. Smith, V. Balsone, ACS Div. Fuel Chem. Preprints, 1988, Vol. 33 #1, pp 6-19.
2. M. Astier, A. Bertrand, D. Bianchi, A. Chenard, G. E. E. Gardes, G. Pajonk, M. B. Taghavi, S. J. Teichner, B. L. Villemin, Preparation of Catalysts, (B. Delmon, P. A. Jacobs and G. Poncelet, eds.), Elsevier Pub. Co., 1976, p. 315.
3. H. Pines and C. N. Pillai, J. Am. Chem. Soc., 82, 2401 (1960).
4. B. H. Davis, J. Catal., 79, 58 (1983).
5. J. Shou and B. H. Davis, Appl. Catal., 1, 277 (1981).

Table 1.  
Physical Properties

	Tap Density (g/cc)	BET Surface Area (m <sup>2</sup> /g) Corrected for Mo	Total Pore Volume (cc/g) Mercury Penetration
Fresh Aluminoxide	0.07	98.32	3.88
Wetted Aluminoxide	0.70	117.39	0.89
IW 12% MoO <sub>3</sub>	0.56	111.01	1.33
EtOH-V 12% MoO <sub>3</sub>	0.34	110.73	2.60
EtOH-V 17% MoO <sub>3</sub>	-	126.01	-
EtOH-R 12% MoO <sub>3</sub>	0.29	108.03	2.17
CPSE 11% MoO <sub>3</sub>	0.05	102.88	7.33

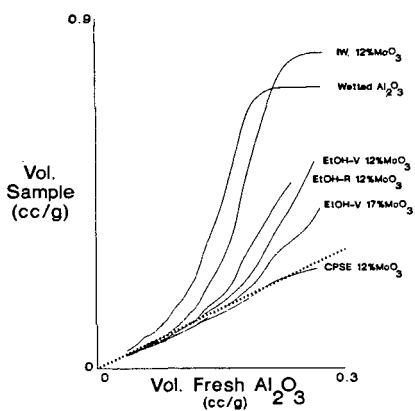


Figure 1. Comparison of pore volumes calculated from nitrogen adsorption isotherms for this catalyst series with fresh Degussa Aluminoside-C.

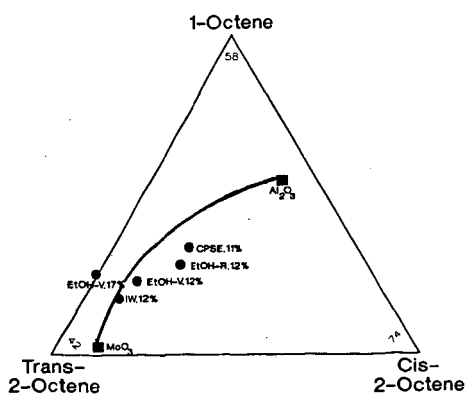


Figure 2. Product selectivity of the dehydration of octanol for pure  $\text{Al}_2\text{O}_3$  and  $\text{MoO}_3$ , a series of  $\text{MoO}_3/\text{Al}_2\text{O}_3$  catalysts prepared by incipient wetness (-), and the series of  $\text{MoO}_3/\text{Al}_2\text{O}_3$  prepared for this study (●).

## EVALUATION OF THE ACTIVITY OF NICKEL IN COPROCESSING USING MODEL SYSTEMS

Honggon Kim and Christine W. Curtis  
Department of Chemical Engineering  
Auburn University, Alabama 36849-5127

The coprocessing of coal with petroleum residuum offers an alternate technology to direct liquefaction by simultaneously upgrading coal, coal liquids and residuum into higher quality products (1-3). Residuum as the solvent contains indigenously the metals, nickel and vanadium, which may be present at a level of a few to several thousand ppm. The objective of this study is to evaluate the catalytic activity of the indigenous Ni in coprocessing by reacting model systems with Ni generated in situ from Ni complexes under coprocessing conditions.

### Experimental

Model Reactants and Nickel Precursors. The model reactants used were naphthalene, indan, indene, benzothiophene, o-cresol, benzofuran, quinoline and indole. All of which were obtained from Aldrich. The nickel sources used were oil-soluble metal salts of organic acids, nickel naphthenate (NiNaph), and nickel octoate (NiOct), and solid complexes, nickel acetylacetonate (NiAcAc) and nickel citrate (NiCit), which were obtained from Air Products, Shepherd Chemical, Strem Chemical and Aldrich.

Reactions and Analyses. Hydrogenation reactions were conducted in 20 cm<sup>3</sup> stainless steel microtubing bomb reactors. For each reaction, 4 grams of 2 weight percent naphthalene and/or 1 weight percent of each of the other reactants in hexadecane were charged. The nickel precursor was introduced at -2850 to 2950 ppm Ni; the Ni to reactant ratio was held constant. The reactions were conducted at 380°C for 30 minutes with 1250 psig H<sub>2</sub> (ambient) while being agitated at 550 cpm.

The liquid products were analyzed by gas chromatography using a 30m fused silica DB-5 column from J & W Scientific with FID detection and p-xylene as the internal standard. Some of the reaction products were identified by GC/MS using a VG 70EHF mass spectrometer and a Varian 3700 gas chromatograph.

### Results and Discussion

The catalytic activity of Ni generated in situ from different nickel precursors were evaluated in the hydrogenation of hydrocarbons and heteroatomic species. The degree to which hydrogenation and heteroatom removal occurred in each reaction is reported in the defined terms of: (1) percent hydrogenation (% HYD) which is the number of moles of hydrogen required to achieve the final product distribution as a percentage of the moles of hydrogen required to achieve the most hydrogenated product; (2) percent hydrogenolysis (% HYG) which is the summation of the mole percents of products resulting from carbon-carbon or carbon-heteroatom bond cleavage; and (3) percent hydrodesulfurization (% HDS), percent hydrodeoxygenation (% HDO) and percent hydrodenitrogenation (% HDN) which are the summation of the mole percents of products not containing sulfur, oxygen, and nitrogen, respectively.

Catalytic Activities of Nickel from Different Precursors. The catalytic activity of in situ generated Ni catalysts produced from several different catalyst precursors were compared using a naphthalene-indan system at 380 and 400°C as shown in Table 1. Three of the Ni precursors, NiOct, NiCit, and NiAcAc, showed

activity for saturating the aromatic rings in both naphthalene and indan while NiNaph did not.

Effect of Sulfur. Since both residuum and coal contain substantial amounts of sulfur, the most likely form of Ni during coprocessing reaction is that of a sulfide. Sulfur was added to the naphthalene reactions to evaluate the catalytic activity of Ni sulfide during coprocessing. As shown in Table 2, elemental sulfur was added from zero to seven times the stoichiometric amount required to form  $\text{Ni}_3\text{S}_2$ , and organic sulfur as benzothiophene was added at a level of 0.1 to 1.0 weight percent. A small amount of sulfur completely inhibited the catalytic activity of Ni giving a % HYD of naphthalene similar to that observed with thermal reactions.

The inhibiting effect of sulfur on the catalytic activity of Ni from NiAcAc and NiCit was examined in naphthalene-indan combined reaction systems. When elemental sulfur was introduced at 0.01g level (2.3 times the amount of sulfur required to form  $\text{Ni}_3\text{S}_2$ ) the naphthalene conversion was reduced from ~98% to 10% and 7%, respectively. No conversion of indan was observed.

Catalytic Activity of Ni for Saturating Aromatic Hydrocarbons. The activity of three different catalysts, NiOct, presulfided powdered  $\text{NiMo}/\text{Al}_2\text{O}_3$  and *in situ* generated  $\text{MoS}_2$  from molybdenum naphthenate, for saturating aromatic hydrocarbons are compared in Table 3. The model systems tested were reaction products observed from the model systems used in this study. Each reaction was reacted with the same amount of total metal, ~ 3000 ppm from each catalyst. Both NiOct and  $\text{NiMo}/\text{Al}_2\text{O}_3$  showed high activity for saturating aromatic rings while  $\text{MoS}_2$  did not. NiOct showed a higher activity for hydrogenating alkylaromatics to alkylalicyclics while presulfided  $\text{NiMo}/\text{Al}_2\text{O}_3$  showed a higher activity for saturating aromatics to alicyclics and for slightly hydrogenolyzing aromatic and hydroaromatic species.

Catalytic Activity and Selectivity of Ni for Hydrogenation of Model Hydrocarbon and Heteroatomic Compounds. The catalytic activity and selectivity of Ni for hydrogenation, hydrogenolysis, and heteroatom removal were evaluated by performing reactions using partially saturated hydrocarbons, aromatics and heteroatom containing species.

Indan and Indene. The Ni catalysts produced from NiOct and NiAcAc showed high activity for saturating the aromatic ring of both indan and indene. The only products observed were saturated species of indan primarily hexahydroindan. No hydrogenolysis was observed.

Benzothiophene. Benzothiophene was not completely desulfurized with either NiOct or NiAcAc, producing ethylbenzene as the major product and dihydrobenzothiophene as the secondary product. Benzothiophene produced 25% HYD and 44% HDS with NiOct in the individual reaction and 26% HYD and 46% HDS in a combined system with naphthalene. The combined system with NiAcAc yielded 31% HYD and 54% HDS. Although NiAcAc yielded slightly higher desulfurization and conversion of benzothiophene, the presence of organic sulfur in benzothiophene appeared to severely poison both of these catalysts. The Ni catalysts did not show the activity previously observed for saturating aromatics in the presence of organic sulfur.

O-Cresol. O-cresol was highly reactive in the presence of NiOct where 98% was converted to methylcyclohexane and fully hydrogenated oxygen-containing hydrocarbons such as trans- and cis-methylcyclohexanol as the major product and methylcyclohexanone as the secondary product. In combined systems with either



naphthalene or indole, the products produced from o-cresol were very similar to those in the individual system. However, when elemental sulfur or benzothiophene was added to the system, the catalytic activity of Ni was completely eliminated. No o-cresol was converted.

Benzofuran. Nearly 100% of benzofuran was converted to alicyclic compounds but less than 17% of the oxygen was removed with NiOct. The major products were trans- and cis-ethylcyclohexanol and ethylcyclohexanone. All of the products produced were saturated yielding ~ 67% HYD. The hydrogenation of benzofuran remained the same when combined with naphthalene while HDO decreased to 7%. The addition of elemental sulfur or benzothiophene at 0.1 weight percent decreased the catalytic activity of Ni for benzofuran and yielded a product distribution similar to that of thermal reactions.

Indole. Indole was totally converted with NiOct or NiAcAc. Neither dihydroindole (indoline) nor o-ethylaniline was observed in the product distribution while small amounts of methylcyclohexane and ethylcyclohexane were observed. Several groupings of unknown chromatographic peaks with broad tailing that is usually characteristic of nitrogen containing compounds were observed. These peaks are postulated to be perhydroindole or o-ethylcyclohexylamine. The addition of sulfur to the reaction system completely eliminated any catalytic activity of NiOct and NiAcAc.

Quinoline. Hydrogenation of quinoline with NiOct or NiAcAc resulted in total conversion of quinoline; however, the reaction products typically seen from quinoline such as 1,2,3,4-tetrahydroquinoline, o-propylaniline, n-propylbenzene and n-propylcyclohexane were not present in the chromatograms (5). A small amount of 5,6,7,8-tetrahydroquinoline as well as a peak representing a substantial amount of decahydroquinoline was observed. Sulfur addition resulted in the elimination of the catalytic activity of the Ni catalyst and yielded a product slate similar to that of a thermal reaction.

Catalytic Reaction of Combined Systems. The effect of other hydrocarbon and heteroatomic compounds on the naphthalene hydrogenation in the presence of NiOct was evaluated. Table 4 shows the effects of these compounds on the hydrogenation of naphthalene. When reacted individually naphthalene yielded 36% tetralin and 64% decalin although the reproducibility was very poor. With the introduction of the other compounds, the reproducibility of naphthalene hydrogenation was improved substantially. None of the additional compounds except for benzothiophene had a significant effect on the naphthalene hydrogenation within the error bounds of the experiments.

Combining naphthalene or a mixture of naphthalene and other compounds with 0.1 weight percent and 1 weight percent benzothiophene severely inhibited the catalytic activity of NiOct. Under these conditions, naphthalene was hydrogenated only to the extent of that observed in thermal reactions.

#### Summary

The catalytic activity of the different Ni precursors for hydrogenating aromatics and partially hydrogenated aromatics ranked in the order of NiAcAc > NiCit > NiOct while NiNaph showed no activity. The reaction pathways observed with oxygen compounds such as o-cresol and benzofuran with NiOct produced methyl and ethyl cyclohexanols and methyl and ethyl cyclohexanones as the major products, respectively. The Ni catalyst from NiOct was highly active for hydrogenating both indole and quinoline but was not effective for removing nitrogen from the rings. Combinations of hydrocarbon and heteroatomic compounds

except for benzothiophene did not affect the hydrogenation of naphthalene in the presence of the Ni catalyst. However, even a small amount of elemental sulfur or benzothiophene completely inhibited the catalytic activity of Ni.

In actual coprocessing systems, a large portion of the nonporphyrinic complexes of Ni are contained in derivatives of naphthenic acid (6) which may be catalytically inactive based on the observed activity of NiNaph in this study. The sulfur content of both coal and residuum can be quite high (7,8). The release of this indigenous sulfur in the coprocessing system would readily poison any nickel released to the coprocessing system and render it inactive.

#### References

1. Moschopedis, S.E., Hawkins, R. W., Fryer, J. W., and Speight, J. G., Fuel, **59**, 647 (1980).
2. Mochida, I., Iwamoto, K., Tahara, T., Korai, Y., Fujitsu, A., and Takeshika, K., Fuel, **61**, 603 (1982).
3. Yan, T. Y., and Espenscheid, W. F., Fuel Processing Technology, **7**, 121 (1983).
4. Yen, T. F., "The Role of Trace Metals in Petroleum", Ann Arbor Science, Ann Arbor, Michigan (1975).
5. Curtis, C. W., and Kim, H., "Interactive Chemistry of Coal-Oil Reactions Using Model Systems", Preceedings of the Fifthe Annual International Pittsburgh Coal Conference, Pittsburgh, PA, Sept., 1988.
6. Fish, R. H., Izquierdo, A., and Komlenic, ACS Division of Petroleum Chemical Preprints, **31(2)**, 613 (1986).
7. Berkowitz, N., "An Introduction to Coal Technology", Academic Press, New York (1979).
8. Speight, J. G., "The Desulfurization of Heavy Oil and Residua", Marcel Dekker Inc., New York (1981).

#### Acknowledgements

We gratefully acknowledge the Department of Energy for support of this work under Grant No. DE-FG2285PC80502.

Table 1. Catalytic Activity of Ni for Hydrogenation of Naphthalene and Indan Combined Using Different Precursors

	Ni Precursor			
	NiNaph	NiOct	NiCit	NiAcAc
<u>Reactions at 380°C</u>				
% HYD of Naphthalene*	2.4	71.3	97.0	98.8
% HYD of Indan*	0	84.0	100.0	100.0
<u>Reactions at 400°C</u>				
% HYD of Naphthalene	2.4	74.4	98.2	98.8
% HYD of Indan	0	85.0	100.0	99.0

Decalin and hexahydroindan were the most hydrogenated products from naphthalene and indan, respectively.

Table 2. Catalytic Activity of Ni for the Hydrogenation of Naphthalene in the Presence of Sulfur

<u>Amount of Elemental Sulfur<sup>a</sup></u>	<u>% HYD of Naphthalene</u>	<u>Amount of Benzothiophene<sup>b</sup></u>	<u>% HYD of Naphthalene</u>
0.0	78 ± 8	0.0	78 ± 8
0.2	0.1	0.1	1.6
0.6	0.2	0.2	0.8
3.5	1.0	0.5	0.8
7.0	0.8	1.0	0.8

<sup>a</sup> Multiples of the stoichiometric amount of sulfur in Ni<sub>3</sub>S<sub>2</sub> (0.0043g).

<sup>b</sup> Weight percent of benzothiophene in hexadecane.

Table 3. Hydrogenation of Aromatic Compounds with Ni Octoate, Presulfided Powder NiMo/Al<sub>2</sub>O<sub>3</sub> and Mo Naphthenate with Excess Sulfur

Reactants Products (mole %)	Catalyst		
	Ni Octoate	Presulfided NiMo/Al <sub>2</sub> O <sub>3</sub>	Mo Naphthenate with Excess Sulfur
- Toluene			
Toluene	5	20	98
Methylcyclohexane	95	79	2
Ethylcyclopentane	0	1	Trace
- Ethylbenzene			
Ethylbenzene	8	18	97
Ethylcyclohexane	91	82	2
Toluene	0	0	1
Methylcyclohexane	1	Trace	Trace
- Propylbenzene			
Propylbenzene	16	20	100
Propylcyclohexane	83	78	0
Butylcyclopentane	0	2	0
Methylcyclohexane	1	Trace	0
- Butylbenzene			
Butylbenzene	11	23	98
Butylcyclohexane	89	75	2
Pentylcyclopentane	0	2	0
Ethylbenzene	0	0	Trace
- Tetralin			
Tetralin	27	13	95
Decalin	73	83	5
n-Butylbenzene	0	2	Trace
others <sup>a</sup>	0	2	0
t-D/c-D <sup>b</sup>	0.45	2.85	1.62
- Naphthalene			
Naphthalene	0	0	2
Tetralin	36	9	92
Decalin	64	87	6
n-Butylbenzene	0	2	Trace
others <sup>a</sup>	0	2	0
t-D/c-D <sup>b</sup>	0.43	2.93	1.39

(a) Unknown products of molecular weight = 138

(b) Approximate weight ratio of trans-decalin to cis-decalin

Table 4. Effect of Other Compounds on Catalytic Hydrogenation of Naphthalene Using  
Ni Octoate without Additional Sulfur

(A)						
Additional Compound <sup>a</sup>	Indan	Indene	O-Cresol	Benzofuran	Quinoline	Indole
Products (mole %)						
Naphthalene	Trace	0	0	0	0	Trace
Tetralin	48	48	50	53	52	58
Decalin	52	52	50	47	48	42
t-D/C- <sup>b</sup>	0.43	0.40	0.42	0.42	0.40	0.40
% Hydrogenation	71.3	71.0	70.1	68.0	69.1	64.5
(B)						
Additional Compound <sup>a</sup>	BZT <sup>c</sup> (1 wt%)	BZT <sup>c</sup> (0.1 wt%)	Indene BZT <sup>c</sup>	O-Cresol BZT <sup>c</sup>	Benzofuran BZT <sup>c</sup>	Indole BZT <sup>c</sup>
Products (mole %)						
Naphthalene	95	88	95	93	90	96
Tetralin	5	12	5	7	10	4
Decalin	0	0	0	0	0	0
% Hydrogenation	1.8	5.0	2.1	3.0	3.8	1.5

(a) Amount of additional compound: 1 weight percent of each in the reactant solution.

(b) Approximate weight ratio of trans-decalin to cis-decalin.

(c) BZT (benzothiophene): 0.1 weight percent of BZT unless noted otherwise.

## FRACTIONATION AND CHARACTERIZATION OF SYNCRUDE SLUDGE POND TAILINGS

Abdul Majid, B.D. Sparks and J.A. Ripmeester  
National Research Council of Canada  
Division of Chemistry  
Ottawa, K1A 0R6, Canada

Two commercial oil sand extraction plants in Alberta generate vast quantities of tailings slurry as a result of the hot water extraction of bitumen from tar sands. The fine grained sludge component of this waste is the most troublesome because of its stability and poor compaction potential. Considerable quantities of organic matter are strongly associated with the fines contained in these clay slimes. This organic matter is believed to be partly responsible for the intractability of the sludge and it could therefore play an important role in determining the nature of slime stability. In this investigation we have isolated organic matter from the mineral fines present in the Syncrude sludge pond tailings. The sludge was first fractionated into recoverable bitumen, sediment and suspension using an oil phase agglomeration technique. The organic matter, associated with the clay fines present in the suspension, was then concentrated by dissolving the mineral matter in HCl/HF. These fractions have been characterized using elemental analysis and solid state  $^{13}\text{C}$  NMR spectroscopy.

### INTRODUCTION

Considerable quantities of organic material, insoluble in common organic solvents, are known to be associated with the clay slimes generated as a result of the hot water extraction of bitumen from tar sands (1-4). Most of this insoluble organic matter (IOM) is strongly associated with the mineral fines (5). The IOM appears to play an important role in the stability and incompressibility of the oil sand slimes (1,3). It is believed that the IOM causes the clay particle surfaces to develop a hydrophobic character, allowing particle bridging, by means of residual bitumen, thereby setting up a weak gel structure. A greater part of the IOM has been reported to consist of humic matter (6,7).

In our previous work we have isolated and characterized this insoluble organic matter from a number of oil sands tailings streams obtained from both Suncor and Syncrude plants (3,6). In this investigation we have attempted to fractionate sludge pond tailings from the Syncrude Canada Ltd. plant in Alberta. The clay fraction containing most of the humic matter was separated from the sludge after removing residual bitumen by means of an oil phase agglomeration technique. The IOM associated with the clay fraction was then concentrated by dissolving the mineral matter in acids (3). These fractions have been characterized using elemental analysis and solid state  $^{13}\text{C}$  NMR spectroscopy.

## EXPERIMENTAL

Residual bitumen from aqueous sludge was recovered as reported in our previous publications (2,4). The general procedure for the fractionation of Syncrude sludge is shown in Figure 1. After removing bitumen from the sludge the aqueous phase was transferred into a 500 ml beaker and the contents were allowed to settle by gravity for one week. The suspension was decanted off and the water evaporated to obtain dry solids. The organic matter associated with the latter solids was concentrated using an acid dissolution scheme reported previously (3). The organic concentrate thus obtained was extracted with 0.5M-NaOH in order to obtain the humic acid fraction.

The procedures for elemental analyses and NMR measurements have been reported previously (3,6).

## RESULTS AND DISCUSSION

About half of the emulsified bitumen present in the sludge was recovered, using Suncor coker feed bitumen as the collector in a grease kettle. This result compares with recoveries of over 90% achieved in our previous work with Suncor sludge and other tailings streams (2,8). In our previous investigations we had used more viscous oils, such as reduced still bottoms, as collectors. It is therefore possible that the poor recovery of bitumen in the present investigation was caused by the lower viscosity of the bitumen compared to reduced still bottoms. The quality and yield of the oil phase solids was also poor compared with our previous investigations.

Partial removal of residual bitumen improved the settling behaviour of the sludge to the extent that about 50% of the solids gravity settled during one week. However, no further improvement in the settling behaviour of the suspension was observed even after an additional month of observation. In previous tests on various tailings streams from tar sands processing (2) complete settling of the solids had been observed after similar treatment. Incomplete removal of organic matter, especially the humic matter associated with the mineral fines could be one reason for this difference. Some compositional differences in the Syncrude Sludge and other tailings streams studied previously could also be responsible. Further work is in progress in order to elucidate this difference; the findings will be reported at a later date.

The organic matter associated with the mineral fraction of the non-settling portion of sludge was concentrated using an acid dissolution scheme reported previously, (3). A major portion of the mineral matter dissolved in HF, as indicated by the low ash content of the resulting organic concentrate.

The elemental compositions of humic matter fractions as well as of the total organic matter associated with the mineral fines are given in the Table I. Elemental analyses were obtained using standard methods. The elemental compositions of a typical sludge pond bitumen and asphaltene sample are included for comparison (3). Carbon analyses were corrected for carbonate carbon to determine the true organic carbon content. No corrections were applied for hydrogen, nitrogen and sulfur analyses. These analyses thus reflect total rather than solely organic content. Oxygen was determined using the standard difference method. The accuracy of these oxygen results is limited owing to the possibility of large errors because of the high mineral content of these samples.

Total organic matter associated with untreated dried sludge, OPS, Solids-I and II, should be similar to the organic matter associated with solids-VI except that the former has a considerably higher ash content than the latter. The elemental compositions of these fractions should therefore be comparable. However, the elemental composition of the organic matter associated with solids-

VI was significantly different to the elemental composition of the total organic matter associated with the other fractions, with the major differences lying in the carbon and oxygen contents of these fractions. The carbon content of the organic matter associated with Solids-VI is approximately double that of the other fractions. This suggests incomplete combustion, and hence underestimation of carbon, in the presence of large amounts of mineral matter. As oxygen was determined by difference underestimation of carbon results in the overestimation of oxygen in these samples. Unusually high H:C ratios for dried sludge, Solids-I and Solids-II indicates a significant contribution from inorganic hydrogen such as of water of hydration of clay minerals associated with these samples. These results demonstrate the importance of ash reduction for the accurate determination of elemental compositions of the organic materials associated with inorganic or mineral matter.

The elemental composition of the organic matter associated with Solids-VI is also different from that of the humic matter fractions. The former has a higher carbon and hydrogen content and lower oxygen content compared to the latter. Organic matter associated with Solid-VI also has a lower ash content than the humic matter and humin fractions. These differences result from the presence of significant (~ 50%) quantities of free bitumen remaining with the organic matter associated with Solids-VI.

The elemental compositions of the humic matter, humic acid and humin fractions was essentially the same except for the nitrogen and sulfur content. Humic acid has a higher nitrogen level compared with the humin fraction, which in turn, has a higher sulfur content than humic acid. Carbon and hydrogen contents of the humic acid were slightly higher than that of the humic acids extracted from oil sands (6). Nitrogen and sulfur contents of humic acid were in the same range as those reported for oil sands humic acid. The oxygen content of all three humic matter fractions appear to be lower than any values published in the literature to date (3,6,9). Small amounts of fluoride were detected only in the Solids-VI and humic matter fractions. The presence of these small amounts of fluoride in the humic matter fractions and its absence in the humic acid and humin fractions, obtained by extraction with NaOH, suggests that the halogen might not have been incorporated into the organic matter during acid dissolution of mineral matter. A more likely scenario is that strongly adsorbed fluoride was washed away during extraction with NaOH.

The average elemental compositions of humic matter fractions from Syncrude sludge have a greater similarity to that of the solvent extractable humic acids from Australian brown coal (10) and benzene/methanol extracts from oil phase solids reported previously (3), than to alkali extractable humic acids. This suggests that a significant portion of the organic matter associated with the mineral solids in Syncrude sludge pond tailings might be of a non-humic nature. Although it is difficult to predict the exact origin of this organic matter, oxidized bitumen or asphaltene complexed to the clay minerals could be one possibility.

<sup>13</sup>C NMR Spectra. The CP/MAS-<sup>13</sup>C NMR spectra of the strongly bound organic matter associated with the mineral fines fraction of Syncrude sludge pond tailings, and a sample of humic acid extracted from these fractions, are shown in Figure 2. The spectra show only bands rather than sharp peaks. However, the resolution is much better than for the spectra of adsorbed organic matter associated with heavy metal minerals reported previously (3). Treatment of Solids-II with 6NHCl dissolved a greater portion of iron and manganese causing carbon enrichment. This resulted in a considerable improvement in resolution, as demonstrated by the spectrum of solids-III compared to the spectrum of Solids-II. The samples of humic acid and humin were dried on a filter paper. While removing the samples with a spatula, fine fragments of filter paper inevitably



contaminated the sample. The signals in the 70-100 ppm region in the spectra of humic acid and humin result from the cellulose-related resonance of this filter paper impurity (11). The interpretation of the  $^{13}\text{C}$  NMR spectra is based on published data on humic substances and coal related materials (3,10-12).

The presence of a broad range of aliphatic compounds in all the spectra is indicated by the resonance in the 10-50 ppm range. The large peak at ~30 ppm results from the presence of a number of repeating polymethylene units in the humic macromolecules. The presence of two sharp shoulders at ~14 and 20 ppm in all spectra except that of Solid-II, indicates the presence of long-chain-terminating methyl groups.

Although carbohydrates have been identified as major components of some sedimentary humic acids (3,13), no noticeable resonances were observed in the 50-100 ppm region. It may be implied that the carbohydrates have been removed during acid treatment.

All spectra show strong resonance in the 110-160 ppm region, characteristic of aromatic carbons and olefinic carbons. However, only the humic acid sample has a distinct signal around 175 ppm which could be assigned to carboxylic, amide or ester carbons. It has been suggested that humic acids are structural equivalents of humin that have been oxidized, resulting in the introduction of carboxyl groups. The absence of carboxyl carbon resonance in the spectrum of the humin fraction is thus understandable. However, the absence of this resonance in the spectra of Solid-II, Solid-III, Solid-VI and humic matter fractions is puzzling, because these fractions contain composite organic matter including humic acid. As humic acid had the lowest ash content of all the fractions, it is possible that the mineral matter associated with the fractions interferes with the detection of carboxyl carbons.

The humic matter and humin spectra were very similar and resemble those obtained for asphaltenes, whereas the humic acid spectrum is similar to spectra published elsewhere for humic materials. Given the very similar nature of the chemical analyses for humic matter, humin and humic acid, it should be considered that the  $^{13}\text{C}$  NMR spectrum may not be representative of all the organic matter present, especially for high ash samples. This could be due to specific interactions of humic fractions with mineral components.

## CONCLUSIONS

1. Partial removal of residual bitumen from Syncrude sludge pond tailings improved its settling behaviour to the extent that about 50% of the solids gravity settled in one week. However, there was no further improvement in the settling of the remaining solids.
2. Insoluble organic matter associated with the mineral matter from the non-settling portion of the sludge was concentrated by dissolving the mineral matter in HCl/HF. This resulted in significant improvements in the elemental analysis results for the insoluble organic matter.
3. The elemental composition of the insoluble organic matter is different from that of oil sands humic acids. Elemental analysis results indicate a similarity of this organic matter to the solvent extractable humic acids from Australian brown coals and benzene/methanol extracts from oil phase solids reported previously. These results suggest that a significant portion of the organic matter associated with clay minerals from Syncrude sludge may be non-humic, possibly oxidized bitumen or asphaltenes.

## ACKNOWLEDGMENTS

We acknowledge the contribution of H. Seguin and V. Clancy for carrying out the elemental analyses. We are also grateful to Dr. R. Schutte for providing the sample of sludge.

## REFERENCES

1. Kessick, M.A., J. Can. Pet. Techn. 77, 49 (1979)
2. Majid, A. and Ripmeester, J.A., J. Sep. Proc. Techn. 4, 20 (1983).
3. Majid, A. and Ripmeester, J.A., Fuel 65, 1726, (1986).
4. Ripmeester, J.A. and Sirianni, A.F., J. Can. Pet. Techn. 2, 131 (1981).
5. Majid, A., Sirianni, A.F. and Ripmeester, J.A., Fuel 61, 477 (1982).
6. Majid, A. and Ripmeester, J.A., ACS-Symposium Series 344, "Metal. complexes in Fossil Fuels: Geochemistry, Characterization and processing" 290 (1987).
7. Ignasiak, T.M.; Zhang, Q.; Kratochvil, B.; Maitra, C.; Montgomery, D.S. and Strausz, O.P., AOSTRA J. Res. 2, 21 (1985).
8. Majid, A., Sirianni, A.F. and Ripmeester, J.A., Canadian Patent No. 1,200,778 (1986).
9. Schnitzer M. and Khan, S.U. "Humic substances in the environment", Marcell Dekker, New York (1972).
10. Verheyen, T.V.; Johns, R.B. and Blackburn, D.T. Geochim. Cosmochim Acta, 46, 269 (1982).
11. Axelsson, D.E., Fuel Processing Technology 16, 257 (1987).
12. Hatcher, P.G. and Orem, W.H. ACS-Symposium Series No. 305, "Organic Marine Geochemistry" 142 (1986).
13. Christman, R.F. and Gjessing, E.T. in, "Aquatic and terrestrial humic materials", Ann Arbor Sci. Pub (1983).

## Figure Captions

Figure 1. Flowsheet for the fractionation of aqueous sludge.

Figure 2. CP/MAS-<sup>13</sup>C NMR spectra of various fractions from Syncrude sludge pond tailings shown in Figure 1.

Table 1. Elemental Analyses (in percentage of dry, ash free basis)

Sample*	Wt. %							Atomic Ratios	
	Ash	C	H	N	S	F	O**	H:C	O:C
Untreated dried Sludge	85.0	37	8.7	0.3	7.3	-	46.7	2.82	0.95
OPS	70.0	45	3.3	-	-	-	51.7	0.88	0.86
Solids-I	87.4	31.8	7.5	-	6.8	-	53.9	2.83	1.27
Solids-II	83.7	35.3	8.7	1.5	5.8	-	48.7	2.95	1.03
Solids-VI	11.8	75.9	7.2	1.0	4.1	0.5	11.3	1.4	0.11
Humic Matter	24.2	71	5.8	1.1	4.8	0.5	16.8	0.99	0.18
Humic Acid	7.6	70.4	5.7	1.4	2.8	-	19.7	0.97	0.21
Humin	28.6	69.1	6.5	0.7	5.6	-	18.1	1.12	0.20
Sludge Pond Bitumen ***	1.0	81.1	8.9	0.6	6.0	-	3.4	1.32	0.03
Asphaltenes from Sludge Pond Bitumen***	5.3	80.2	8.0	1.2	7.9	-	2.7	1.20	0.03

\* Key to sample No. found in Figure 1

\*\* By Difference

\*\*\* Ref. 3

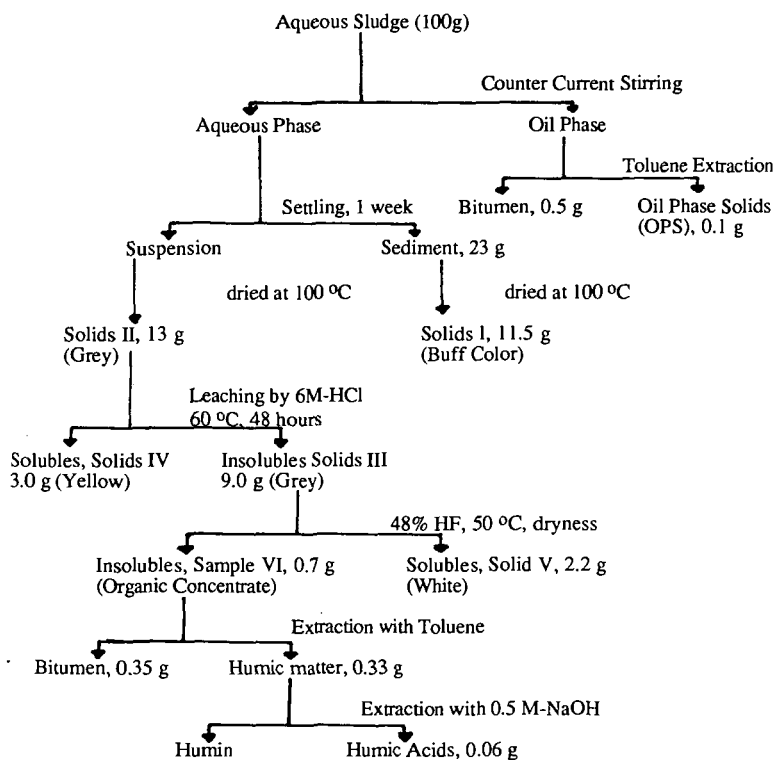


Figure 1. Flow sheet for the fractionation of aqueous sludge.

